Methods for Evaluating and Treating ASR-Affected Structures: Results of Field Application and Demonstration Projects

Volume II: Details of Field Applications and Analysis

Final Report

U.S. Department of Transportation
Federal Highway Administration

Technical Report Documentation Page

1. Report No.	2. Government Accession No.	3. Recipient's Catalog No.
FHWA-HIF-14-0003		

4. Title and Subtitle	5. Report Date
Methods for Evaluating and Treating ASR-Affected Structures: Results of Field Application and Demonstration Projects – Volume II: Details of Field Applications and Analysis	November 2013
	6. Performing Organization Code
7. Author(s)	8. Performing Organization Report No.
Michael D.A. Thomas, Kevin J. Folliard, Benoit Fournier, Patrice Rivard, Thano Drimalas, and Sabrina I. Garber	
9. Performing Organization Name and Address	10. Work Unit No. (TRAIS)
The Transtec Group 6111 Balcones Drive Austin, TX 78731	
	11. Contract or Grant No. DTFH61-06-D-00035
12. Sponsoring Agency Name and Address	13. Type of Report and Period Covered
FHWA Office of Pavement Technology 1200 New Jersey Ave. SE Washington, DC 20590	
	14. Sponsoring Agency Code

15. Supplementary Notes
Contracting Officer's Representative (COR): Gina Ahlstrom, HIAP-10

16. Abstract

As part of the FHWA ASR Development and Deployment Program, nine field trials were conducted across the United States that evaluated mitigation measures applied to concrete structures and pavements already exhibiting ASR-induced distress. The findings from these trials served as the basis for the Volume I report and recommendations. In order to provide a technical underpinning for Volume I and to provide more detailed information on each of the trials (e.g., product types and application rates, treatment methods, monitoring program, etc.), this Volume II report was developed.

This document provides detailed information on each of the ASR field trials, including information and data from visual inspections, petrographic evaluations, laboratory testing, and in-situ field monitoring.

17. Key Word	18. Distribution Statement
Alkali-silica reaction, concrete durability, mitigation, existing structures, laboratory testing, hardened concrete, field investigation.	No restrictions. This document is available to the public through the Federal Highway Administration (FHWA)

19. Security Classif. (of this report)	20. Security Classif. (of this page)	21. No. of Pages	22. Price
Unclassified	Unclassified	338	N/A

Form DOT F 1700.7 (8-72) Reproduction of completed page authorized

SI* (MODERN METRIC) CONVERSION FACTORS

APPROXIMATE CONVERSIONS TO SI UNITS

Symbol	When You Know	Multiply By	To Find	Symbol
		LENGTH		
in	inches	25.4	millimeters	mm
ft	feet	0.305	meters	m
yd	yards	0.914	meters	m
mi	miles	1.61	kilometers	km
		AREA		
in^2	square inches	645.2	square millimeters	mm^2
ft^2	square feet	0.093	square meters	m^2
yd^2	square yard	0.836	square meters	m^2
ac	acres	0.405	hectares	ha
mi^2	square miles	2.59	square kilometers	km^2
		VOLUME		
fl oz	fluid ounces	29.57	milliliters	mL
gal	gallons	3.785	liters	L
ft^3	cubic feet	0.028	cubic meters	m^3
yd^3	cubic yards	0.765	cubic meters	m^3
		NOTE: volumes greater than 1000 L shall be shown in m^3		
		MASS		
oz	ounces	28.35	grams	g
lb	pounds	0.454	kilograms	kg
T	short tons (2000 lb)	0.907	megagrams (or "metric ton")	Mg (or "t")
		TEMPERATURE (exact degrees)		
^oF	Fahrenheit	5 (F-32)/9 or (F-32)/1.8	Celsius	^oC
		ILLUMINATION		
fc	foot-candles	10.76	lux	lx
fl	foot-Lamberts	3.426	$candela/m^2$	cd/m^2
		FORCE and PRESSURE or STRESS		
lbf	poundforce	4.45	newtons	N
lbf/in^2	poundforce per square inch	6.89	kilopascals	kPa

APPROXIMATE CONVERSIONS FROM SI UNITS

Symbol	When You Know	Multiply By	To Find	Symbol
		LENGTH		
mm	millimeters	0.039	inches	in
m	meters	3.28	feet	ft
m	meters	1.09	yards	yd
km	kilometers	0.621	miles	mi
		AREA		
mm^2	square millimeters	0.0016	square inches	in^2
m^2	square meters	10.764	square feet	ft^2
m^2	square meters	1.195	square yards	yd^2
ha	hectares	2.47	acres	ac
km^2	square kilometers	0.386	square miles	mi^2
		VOLUME		
mL	milliliters	0.034	fluid ounces	fl oz
L	liters	0.264	gallons	gal
m^3	cubic meters	35.314	cubic feet	ft^3
m^3	cubic meters	1.307	cubic yards	yd^3
		MASS		
g	grams	0.035	ounces	oz
kg	kilograms	2.202	pounds	lb
Mg (or "t")	megagrams (or "metric ton")	1.103	short tons (2000 lb)	T
		TEMPERATURE (exact degrees)		
^oC	Celsius	1.8C+32	Fahrenheit	^oF
		ILLUMINATION		
lx	lux	0.0929	foot-candles	fc
cd/m^2	$candela/m^2$	0.2919	foot-Lamberts	fl
		FORCE and PRESSURE or STRESS		
N	newtons	0.225	poundforce	lbf
kPa	kilopascals	0.145	poundforce per square inch	lbf/in^2

*SI is the symbol for the International System of Units. Appropriate rounding should be made to comply with Section 4 of ASTM E380.
(Revised March 2003)

Table of Contents

List of Figures

List of Tables

1. INTRODUCTION

As part of the Federal Highway Administration (FHWA) ASR Development and Deployment Program, nine field trials were conducted across the United States that evaluated mitigation measures applied to concrete structures and pavements already exhibiting alkali-silica reaction (ASR) induced distress. The findings from these trials served as the basis for the Volume I report and recommendations. **In order to provide a technical underpinning for Volume I** and to provide more detailed information on each of the trials (e.g., product types and application rates, treatment methods, monitoring program, etc.), **this Volume II report was developed**.

The purpose of this Volume II report is to provide detailed information on each of the ASR field trials, including information and data from visual inspections, petrographic evaluations, laboratory testing, and in-situ field monitoring.

This document is presented in the following chapters, with the first two chapters to describe (1) the Evaluation and Performance Monitoring Methods and (2) the Treatment Technologies used throughout the Program. The remaining chapters devoted to each of the nine field trials, including the state and structure type, are as follows:

- Alabama (bridge arches)
- Arkansas (pavement)
- Delaware (pavement)
- Maine (bridge elements)
- Massachusetts (highway barriers)
- Texas – New Braunfels (precast girders)
- Texas – Houston (bridge columns)
- Rhode Island (bridge walls, retaining wall, and highway barriers)
- Vermont (highway barriers)

1.1 REFERENCES

Thomas, M.D.A., Folliard, K.J., Fournier, B., Rivard, P. and Drimalas, T. 2013. "Methods for Evaluating and Treating ASR-Affected Structures: Results of Field Application and Demonstration Projects – Volume I: Summary of Findings and Recommendations." FHWA-HIF-14-0002, Federal Highway Administration.

2. EVALUATION (DIAGNOSIS) AND PERFORMANCE MONITORING (PROGNOSIS) METHODS

As part of this FHWA ASR Development and Deployment Program, different methods/ approaches were used for the diagnosis and prognosis of ASR in the various projects that were proposed and implemented for field applications.

In coordination with State Departments of Transportation (DOTs), field visits were organized with local DOT representatives for the visual survey of the structure(s) proposed for treatment. Based on the field observations, recommendations were then made for the extraction of cores from selected concrete members in order to perform petrographic examination and mechanical testing (when possible), in order to confirm the contribution of ASR in the deleterious process affecting the structure under investigation. The diagnosis of ASR was then carried out in the laboratory using petrographic examination, particularly the Damage Rating Index (DRI), a method that provides a semi-quantitative assessment of the degree of damage in concrete based on a count of petrographic features of deterioration generally associated with ASR. In one case (structures in Maine), additional cores were extracted and tested using the Stiffness Damage Test (SDT), a test that evaluates the degree/extent of damage in concrete through loading/unloading cycles in compression.

Following the confirmation of ASR as one of the main contributing factors to the deterioration, a treatment scheme was developed and implemented which, depending on the type of structure, its detailing, and condition, included one or several of the following options: chemical treatments (lithium), surface treatment (sealers and/or breathable coating), and strengthening (fiber reinforced polymer [FRP] wrap).

A performance monitoring plan was also developed and implemented to allow quantifying the effects of the various treatments over time; it included regular (once or twice a year) monitoring of expansion, surface cracking, and relative humidity/temperature in treated and untreated (control) sections of the selected structures.

This chapter provides information on the different methods listed above that were used for the diagnosis and prognosis of ASR in the various sites selected for the FHWA ASR Development and Deployment Program.

2.1 DIAGNOSIS - LABORATORY TESTING OF CORES

2.1.1 Damage Rating Index (DRI)

Petrographic examination is a very powerful technique in the diagnosis of the cause of concrete deterioration. ASTM C856 outlines procedures for the petrographic examination of samples of hardened concrete. Interesting information regarding petrographic features of ASR-affected concrete can be found in several publications, including Hobbs 1988, BCA 1992, St. John et al.

1998, CSA 2000, and Walker et al. 2006. Although not necessarily exclusive to ASR, petrographic signs of ASR generally consist of:

- microcracking in aggregates and/or cement paste;
- reaction product "gel";
- reaction rims; and
- loss of the cement paste-aggregate bond.

Grattan-Bellew (1992) and Dunbar and Grattan-Bellew (1995) described a method to evaluate the condition of concrete by counting the number of typical petrographic features of ASR in concrete cores extracted from the structural member under investigation (i.e., showing visual symptoms of deterioration typically associated with ASR).

The concrete core is first cut in two axially and then polished. Different types of polishing equipment can be used for that purpose. The portable hand-polishing device used in this project (see Figure 1), which uses diamond-impregnated rubber disks, was found most suitable as it does not use loose abrasive powders that can fill up cracks/voids in the concrete, and quality polishing is obtained with minimal water supply. A series of diamond-coated rubber disks are used to ensure progressive polishing from coarser to finer sizes (i.e., from disks no. 50 (coarse), 100, 400, 800, 1500 to 3000 (very fine)).

Figure 1. Polishing process of the concrete specimens for the Damage Rating Index.

The polished section is then photographed and a grid is drawn on the surface, which includes a minimum of 200 grid squares, 1 cm by 1 cm (0.4 by 0.4 in.) in size (see Figure 2). Each grid square is then examined under the stereomicroscope to determine the DRI (see Figure 3). The latter represents the normalized value (to 100 cm^2) (16 in^2) of the presence of selected petrographic features after the count of their abundance over the examined surface has been multiplied by weighing factors representing their relative importance in the overall deterioration process. Table 1 gives a list of those features and the weighing factors originally proposed by Dr. Grattan-Bellew from the National Research Council of Canada, which were used in this project.

Figure 2. One cm by one cm (0.4 by 0.4 in.) grid drawn on the surface of a polished concrete section for petrographic examination using the DRI method.

Figure 3. Examination of a polished concrete section under the stereomicroscope for the determination of the Damage Rating Index.

Table 1. Petrographic features and weighing factors for the DRI (from Grattan-Bellew and Mitchell 2006).

Petrographic feature	Abbreviation	Weighing factor
Crack in the coarse aggregate particles	CrCA	x 0.75
Open crack in coarse aggregate	OCrCA	x 4.0
Crack with reaction product in the coarse aggregate particles	Cr + RPCA	x 2.0
Coarse aggregate debonded	CAD	x 3.0
Reaction rims around aggregate particles	RR	x 0.5
Crack in the cement paste	CrCP	x 2.0
Crack with reaction product in the cement paste	Cr+RPCP	x 4.0
Air voids lined or filled with reaction products	RPAV	x 0.50

Figure 4 gives examples of the petrographic features that are quantified as part of the process. The results of the counts of the petrographic features (after their adjustment using the weighing

factors) can then be compiled as in Figure 5, thus illustrating the results of the DRI and the contribution of each petrographic feature to the overall rating. Further details on the experimental procedure for the DRI are given in Fournier et al. (2010).

A

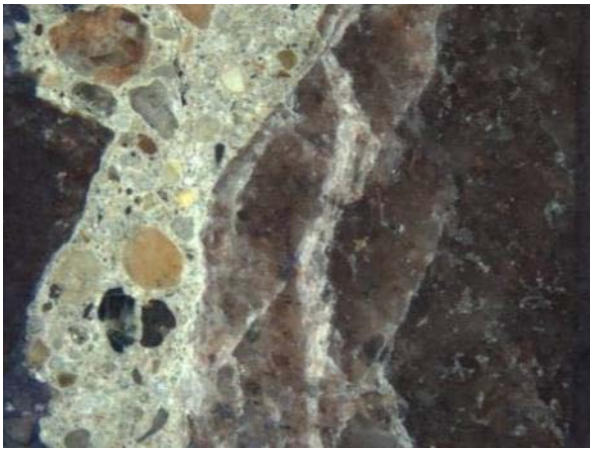

B

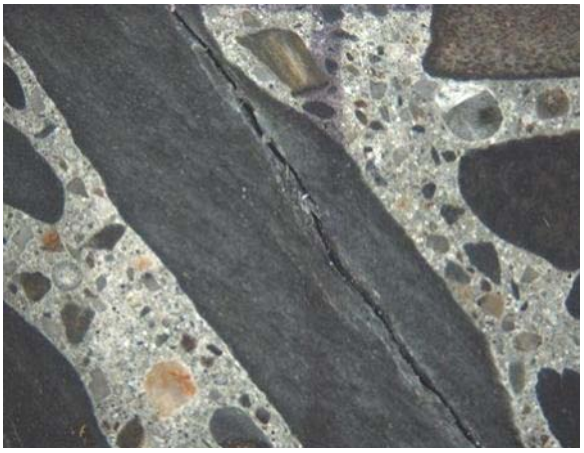

C

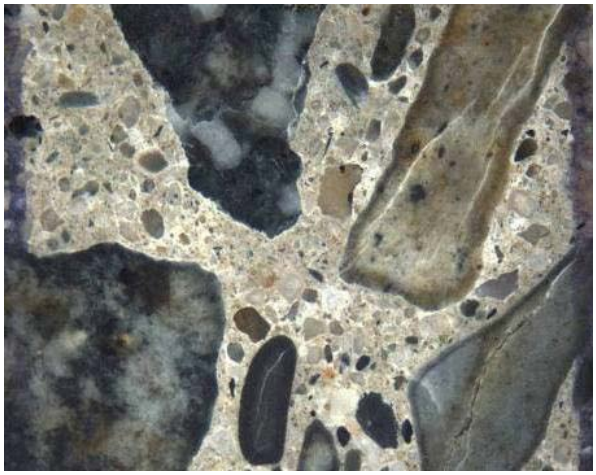

D

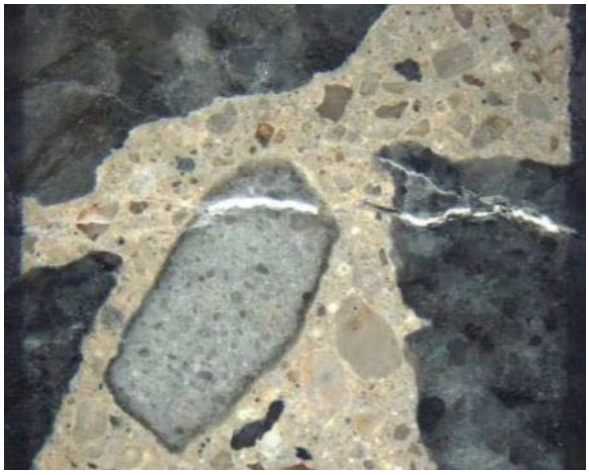

E

F

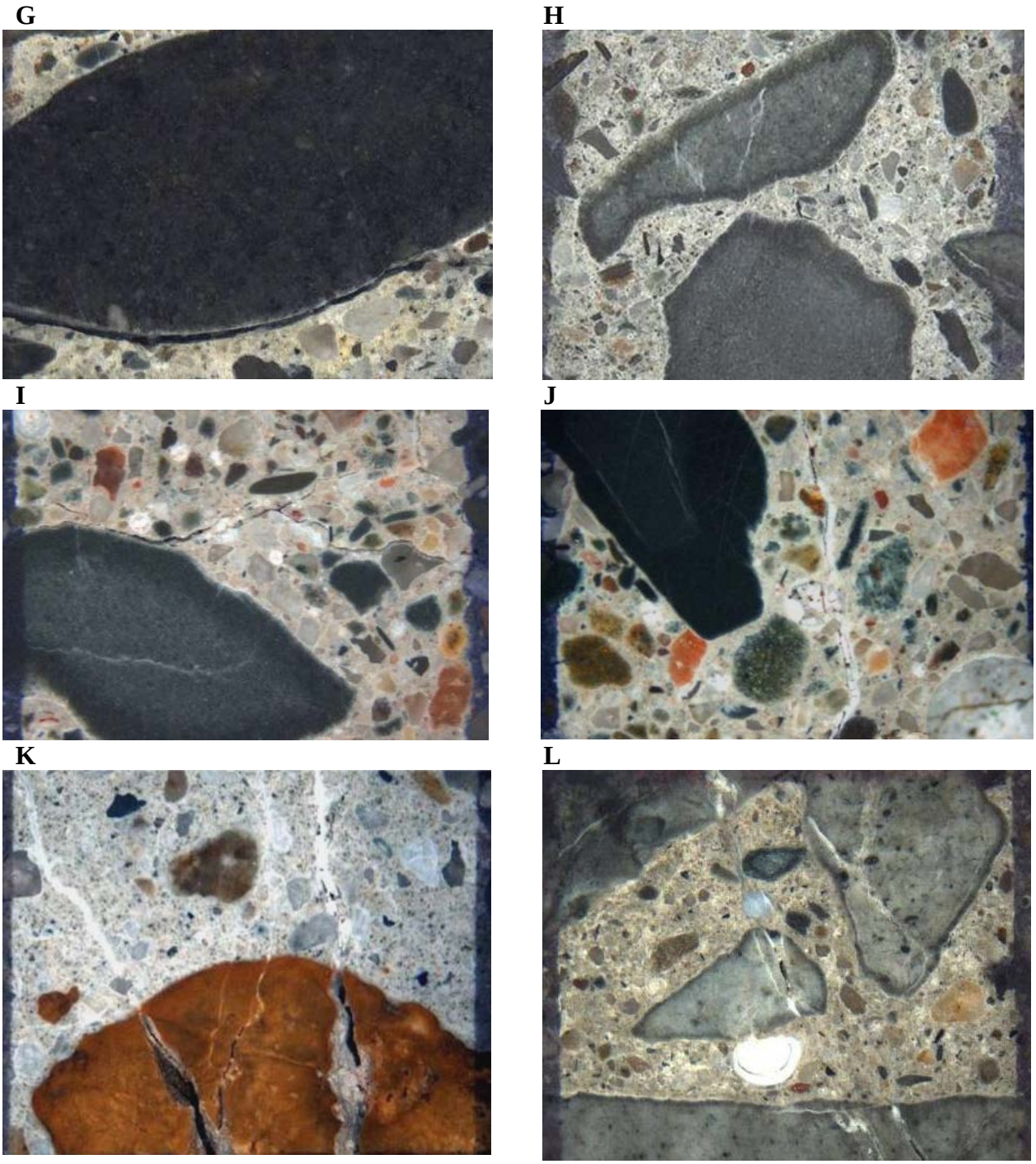

Figure 4. Examples of typical petrographic features of deterioration due to ASR identified on polished concrete sections as part of the Damage Rating Index (DRI).
A&B: Cracks in coarse aggregate particles (A- tight cracks; B- open cracks); C&D: Cracks with reaction products in the coarse aggregate particles; E&F: Cracks with reaction products in fine aggregate particles. G: Debonded coarse aggregate particle; H: Reaction rims around reactive coarse aggregate particles; I: Cracks in the cement paste; J-L: Cracks with reaction products in the cement paste; L: Whitish and glassy alkali-silica reaction products in air voids of the cement paste.

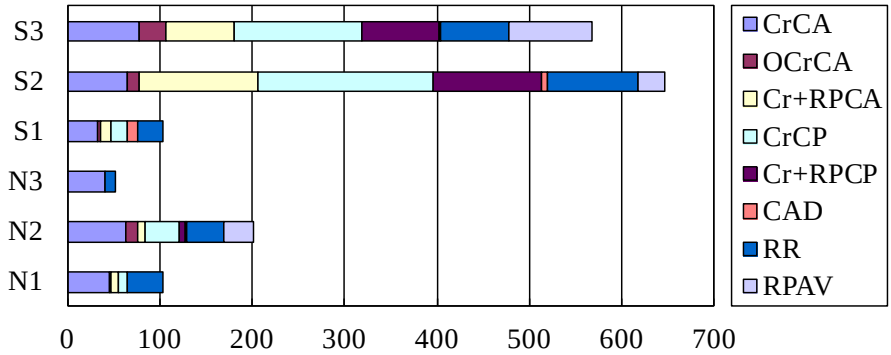

Figure 5. Results of the Damage Rating Index (DRI) for cores extracted from barrier walls of two bridges carrying Interstate 89 over the Dog River near Montpelier, VT. The colored cells give the proportions of each petrographic feature to the DRI value. (See Table 1 for the acronyms.)

The DRI method is a tool for the semi-quantitative assessment of internal damage in concrete due to ASR or other mechanisms. However, the results can be significantly affected by the experience of the petrographer and since there is currently no standard test procedure available, the method can be fairly subjective and the results quite variable from one petrographer to another. Despite that, the DRI method can provide very useful relative information when the examination of sets of cores from various parts of a structure (subjected to different exposure conditions or showing various external features of deterioration) is carried out by the same petrographer. The method also allows identifying the progress of ASR when cores are extracted regularly from the same structural element and examined once again by the same petrographer.

As mentioned before, the DRI method is currently not a standardized method and there are currently no accepted ratings for DRI results. However, Fournier et al. (2009) proposed the classification described in Table 2 for DRI results obtained from a wide range of cores extracted from a large bridge structure affected to different degrees by ASR. The limits between the different groups are not definitive and could vary slightly.

Table 2. Proposed classification of the DRI values as per Fournier et al. (2009).

DRI values	Degree of ASR	General description
0-250	None to trace	Concrete in good condition with no signs of deterioration visible at the macro level (with naked eyes) and limited signs of deterioration at the micro level (under the stereomicroscope at the magnification used for the DRI).
250 - 500	Fair to moderate	Concrete generally in good condition with fair signs of deterioration visible at the macro level (with naked eyes) but fair to moderate signs of deterioration at the micro level (under the stereobinocular microscope at the magnification used for the DRI). These features mainly consist of the following: • Fine cracking in several aggregate particles with a fair to moderate proportion of those being at least partially filled with ASR gel; the aggregate cracks still rarely extend to a significant extent into the cement paste. • Mild to significant cracking is visible in the cement paste under the stereomicroscope; ASR gel can be present in some (but limited proportion) of those cracks.
500 – 800/ 1000	Moderate to severe	Concrete with moderate signs of deterioration visible at the macro level (with naked eyes) and important signs of damage visible at the micro level (under the stereomicroscope at the magnification used for the DRI). These features mainly consist of the following: • Cracks are observed in a large proportion of reactive aggregate particles, a large proportion of those being filled with reaction products. In many cases, cracking in the aggregate particles extends into the cement paste and sometimes connects reactive aggregate particles. • Significant to important cracking is visible in the cement paste (< 0.02 mm, locally up to 0.05 mm [0.8E-4 in., 0.2E-3 in.]); several cracks incorporate ASR gel.
≥ 800/ 1000	Severe to very severe	Concrete with severe signs of deterioration both at the macro (with naked eyes) and micro (under the stereomicroscope at the magnification used for the DRI) levels. • Description similar to previous group but even more severe at the macro level, i.e., cracking visible with naked eyes both in the aggregate particles (numerous white veinlets) and the cement paste (< 0.05 mm with locally up to 0.20 mm [0.2E-3 in., 0.8E-3 in.]).

2.1.2 Stiffness Damage Test (SDT)

Not all mechanical properties of concrete are equally affected by ASR. In most cases, the properties most rapidly affected by ASR are the modulus of elasticity and the direct tensile strength (ISE 1992, Pleau et al. 1989). Several authors have shown that the above are much better indicators of the progression of ASR than compressive strength, which is generally affected only at much higher expansion levels (Thomas et al. 2013).

The Stiffness Damage Test was originally proposed by Chrisp et al. (1989) and adopted shortly after by the Institution of Structural Engineers in the UK (ISE 1992). Recently, the method was modified and used for estimating the expansion attained to date by ASR-affected concrete (Smaoui et al. 2004, Bérubé et al. 2005). The test consists in subjecting a set of concrete specimens, for example 100 mm (4 in.) cores extracted from the concrete member to be evaluated, to five cycles of uniaxial loading/unloading up to a maximum of 5.5 MPa (798 psi) (original method of Crisp and colleagues) or 10 MPa (1450 psi) (Smaoui and colleagues) (see

Figure 6). The latter found that over the five testing cycles, the concrete displays a deformation that generally increases with the expansion reached by the ASR-affected specimens (see Figure 7). Further details on the experimental procedure for stiffness damage testing are given in Fournier et al. (2010).

A number of parameters have been proposed to quantify the degree of damage in the concrete using the SDT, i.e., (1) the energy dissipated (measurement of the surface area) during the first cycle (hysteresis loop), or (2) the energy dissipated during the last four cycles and (2) the accumulated plastic strain over the five load/unload cycles (see Figure 7E). The above parameters were found to progressively increase with increasing internal microcracking and expansion in concrete affected by ASR; however, the energy dissipated parameter was found to best correlate with ASR expansions, and was consequently recommended by Fournier et al. (2010) for assessing the expansion attained to date in concrete affected by ASR.

A

B

C

D

Figure 6. Setup used for the Stiffness Damage Test (SDT).

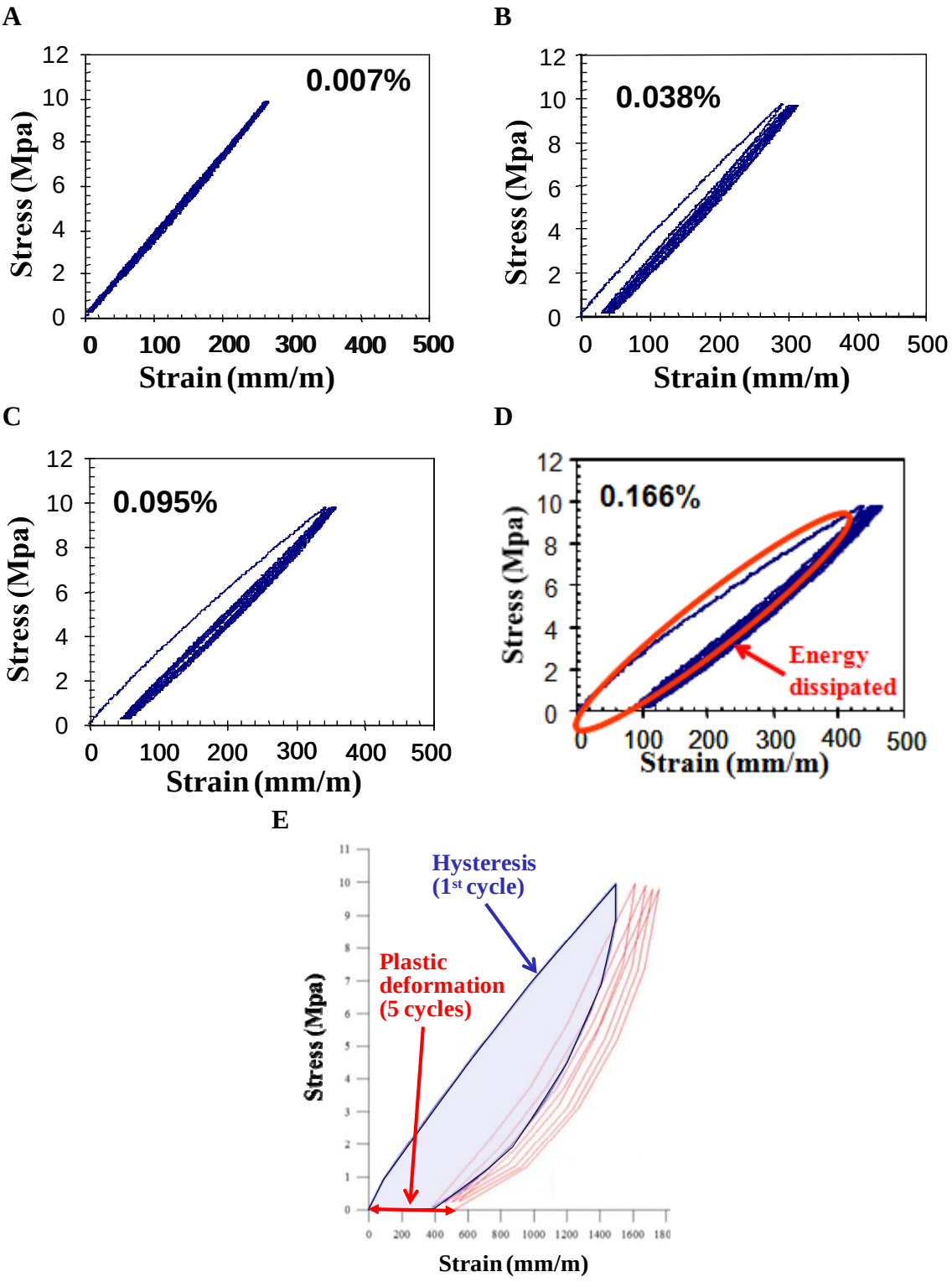

Figure 7. Stress-strain curves, hysteresis, and plastic deformation.
A-D: Stress-strain curves for concrete specimens subjected to 5 loading/unloading cycles in the SDT. The concrete samples had reached expansion levels ranging from 0.007 to 0.166% (from Smaoui et al. 2004).
E: Main parameters used for evaluating concrete condition through SDT: Hysteresis of the 1st loading/unloading cycle and plastic deformation over the 5 cycles.

As for the Damage Rating Index method, there is no standardized method for the SDT, nor rating charts for the results of the SDT. Also, Smaoui et al. (2004) found the results of the SDT to be aggregate-dependent, thus requiring the establishment of a calibration curve suitable to the particular reactive aggregate involved or a similar type. Despite that, the SDT method can provide very useful relative information when sets of cores from various parts of a structure (subjected to different exposure conditions or showing various external features of deterioration) are examined. The method also allows identifying the progress of ASR when adjacent cores are extracted regularly from the same structural element.

It is recommended that, because of the inherent variability in the internal damage of deteriorating concrete members, a set of SDT specimens consist of a minimum of three cores. Moreover, when the number of cores available for mechanical testing is limited, the modulus of elasticity can be determined during stiffness damage testing and a good estimate of the compressive strength obtained by reloading the cores up to failure after the five loading/unloading cycles.

2.2 PERFORMANCE MONITORING IN THE FIELD (PROGNOSIS)

As mentioned before, a program was developed and implemented for the performance monitoring of treated and control sections, which included training of local State DOT personnel so they can continue to track the performance of the structures upon conclusion of the ASR Development and Deployment Program. Monitoring activities included the following:

- Expansion measurements conducted by embedding steel studs at different locations on the treated and control sections, and using a nominal 500-mm (20-in.) gauge to regularly record length changes.
- Severity of cracking over a 500-mm x 500-mm (20-in. x 20-in.) grid drawn on the surface of the treated/control elements. The number of cracks, along with crack widths, were recorded and used to create a Cracking Index (CI).
- Humidity/temperature measurements were carried out by drilling holes to different depths into the concrete. Probes were inserted into the holes and measurements taken upon equilibrium using a handheld reader.
- Three non-destructive methods, i.e., impact-echo, ultrasonic pulse velocity (UPV), and a nonlinear acoustics technique, were applied to monitor internal damage in the concrete members evaluated.

2.2.1 Expansion Monitoring

Expansion monitoring is carried out over a grid (also called crack map since it is also the base for monitoring of cracks – see section 2.2.2) delimited by stainless steel pins embedded into the surface of the concrete member. Three holes are drilled from the corner of each crack map, and a steel pin is glued into each hole with epoxy (see Figure 8). The epoxy used is fast-setting, water resistant and compatible with concrete and plastic materials. Figure 9 shows schematics illustrating the two layouts used in this project for those pins. The 500-mm by 500-mm (20-in. by 20-in.) grid is the preferred layout for expansion monitoring in the various types of structural elements investigated (pavement, retaining wall, abutment, and wing walls) (see Figure 9A). However, in the case of the barrier walls at the Vermont site, the distance from the top of the

barrier to the chamfered base was too short for 500-mm (20-in.) vertical measurement, so the layout shown in Figure 9B was employed; the dimensions of this layout are 150 mm (6 in.) in the vertical direction and 500 mm (20 in.) in the horizontal direction.

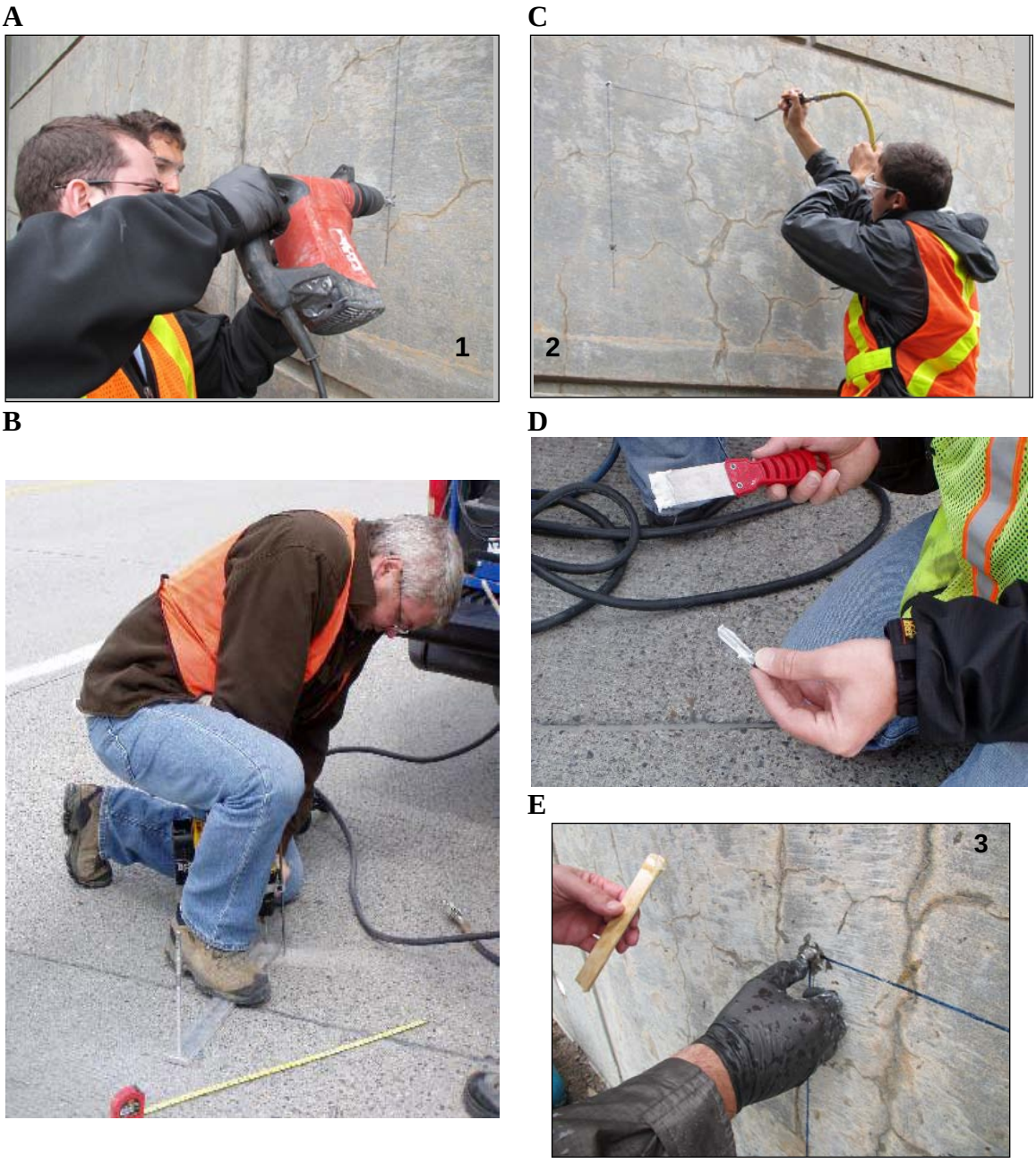

Figure 8. Embedding steel pins for expansion measurements. A&B: Drilling of the holes at the corners of the 500-mm (20-in.) grid (or crack map). C: Cleaning excess drilling debris with compressed air. D: Epoxy spread along the steel pin. E: Inserting the steel pin into the hole, flush with the surface of the concrete.

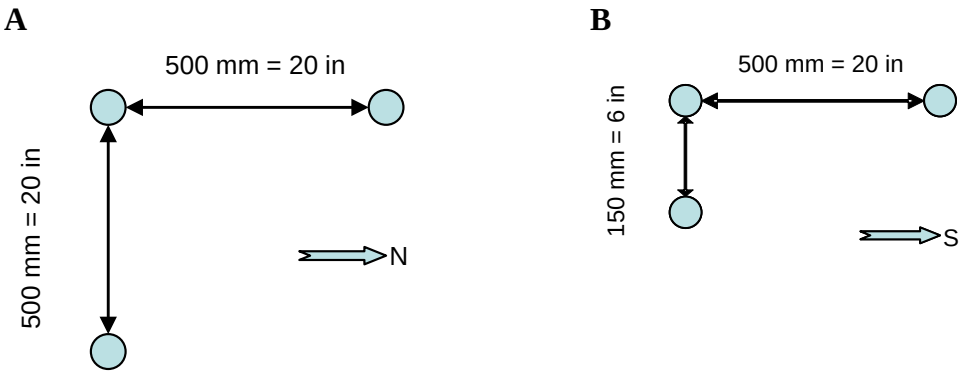

Figure 9. Expansion pins layouts.

DEMEC gauges of 500-mm (approximately 20 in.) or 150-mm (approximately 6 in.) gauge lengths and with a digital output that can measure length changes to within 0.001 mm (or 0.00005 in.) were used at the different sites (see Figure 10).

Figure 10. Expansion measurements using DEMEC gauges. A-C: 500-mm (~ 20 in.) gauge length. D: 150-mm (~ 6 in.) gauge length.

In the case of the circular reinforced concrete columns of the South Parkway bridge over I-395 (Maine), expansion measurements were carried out along the two horizontal lines drawn for crack mapping using a Pi Tape (see Figure 11).

Figure 11. Measurement of the circumferential expansion on concrete columns.

2.2.2 Crack Mapping

Crack mapping is a method of quantifying surface cracking by recording and summing the crack widths measured along a set of lines drawn on the surface of the selected sections (see Figure). Typically, or when possible, the process requires 1000-mm (approximately 40-in.) squares (LCPC 1997) (e.g., on the large columns of the bridge over the Penobscot River, Maine site). However, a 500-mm (approximately 20-in.) square, or crack map, is generally used when the space for drawing the grids is limited and also to favor direct correlations with expansion measurements (see section 2.2.1). Diagonal lines connecting the corners through the crack map are also drawn (see Figure 12B). Hash marks are drawn at 100-mm (approximately 4-in.) intervals along all of the lines (see Figure 12C). Using a handheld magnifying glass and a card used to measure crack widths, the number of cracks and the width of each crack that crosses the line are recorded for each section between hash marks (see Figure 12D & Figure 13).

A Cracking Index (CI) is then calculated and an average crack opening per millimeter (or inch) can be determined. CI data are given in mm/m (or in./yd) as they correspond to the total crack opening, in mm (in.), averaged over a one-meter (or one-yard) length; they are calculated from the measurement of crack widths along a grid system composed of the four lines of the 500-mm (20-in.) square and of the two 700-mm (28-in.) diagonal lines (total of 3.4 m (11 ft) of lines). In general, the higher the CI values, the higher the extent of (surface) damage on the concrete element investigated. Further details on the Cracking Index Method can be obtained from Fournier et al. (2010).

In the case of the reinforced concrete columns of the South Parkway bridge over I-395 (Maine site), crack mapping was carried out by tracing two horizontal lines, one meter apart (~ three feet), along the circumference of the columns. Measurements of the number of cracks and their

opening were carried out along those lines to quantify the extent of cracking in those structural elements (see Figure 14).

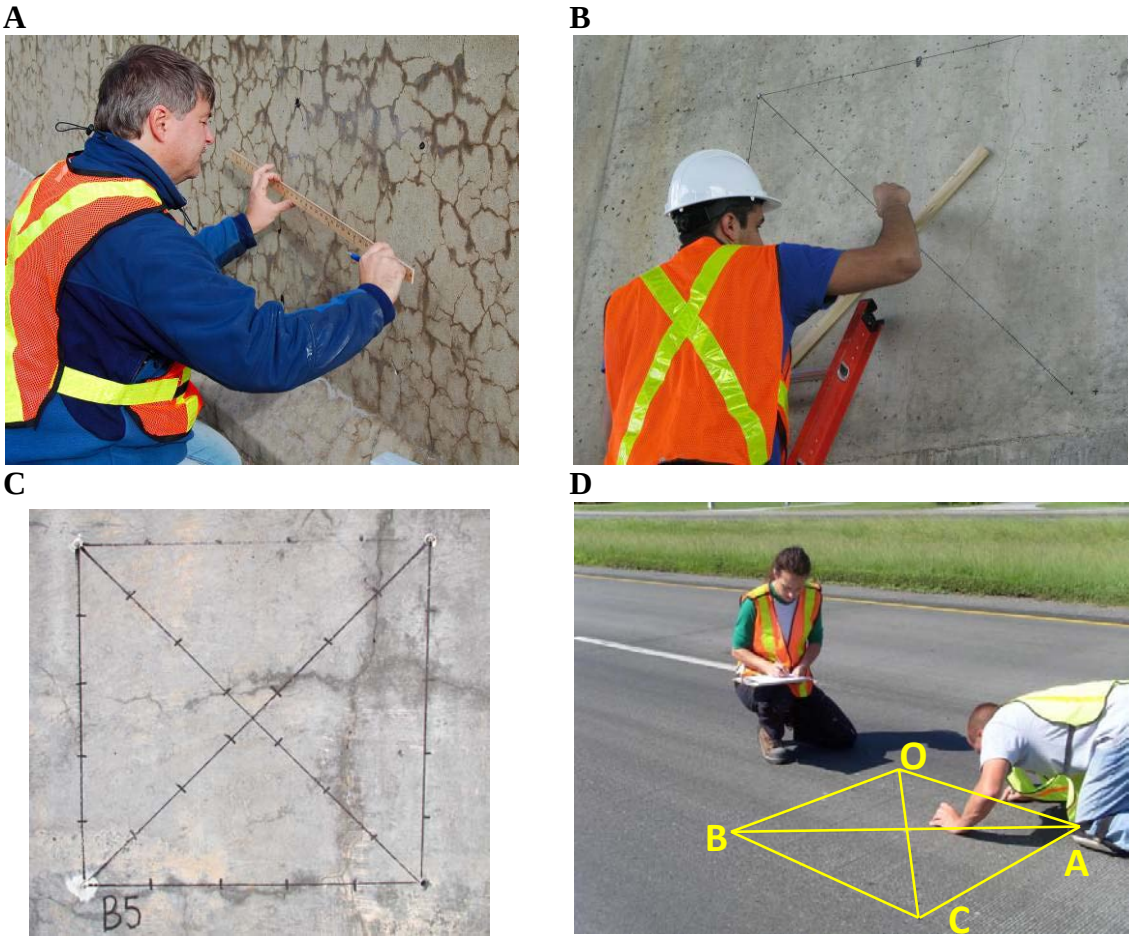

Figure 12. Example of crack mapping grid. A&B: Drawing of the grid. C: 500-mm by 500-mm (20-in. by 20-in.) square drawn on an abutment wall. D: Crack map over a concrete pavement section affected by ASR.

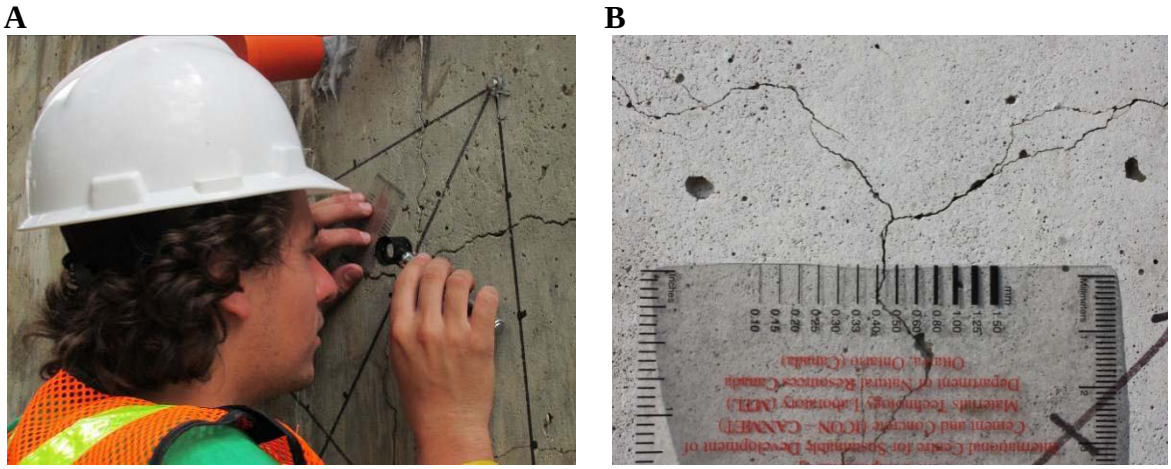

Figure 13. Crack map drawn on a pier; crack widths along crack map are identified and measured.

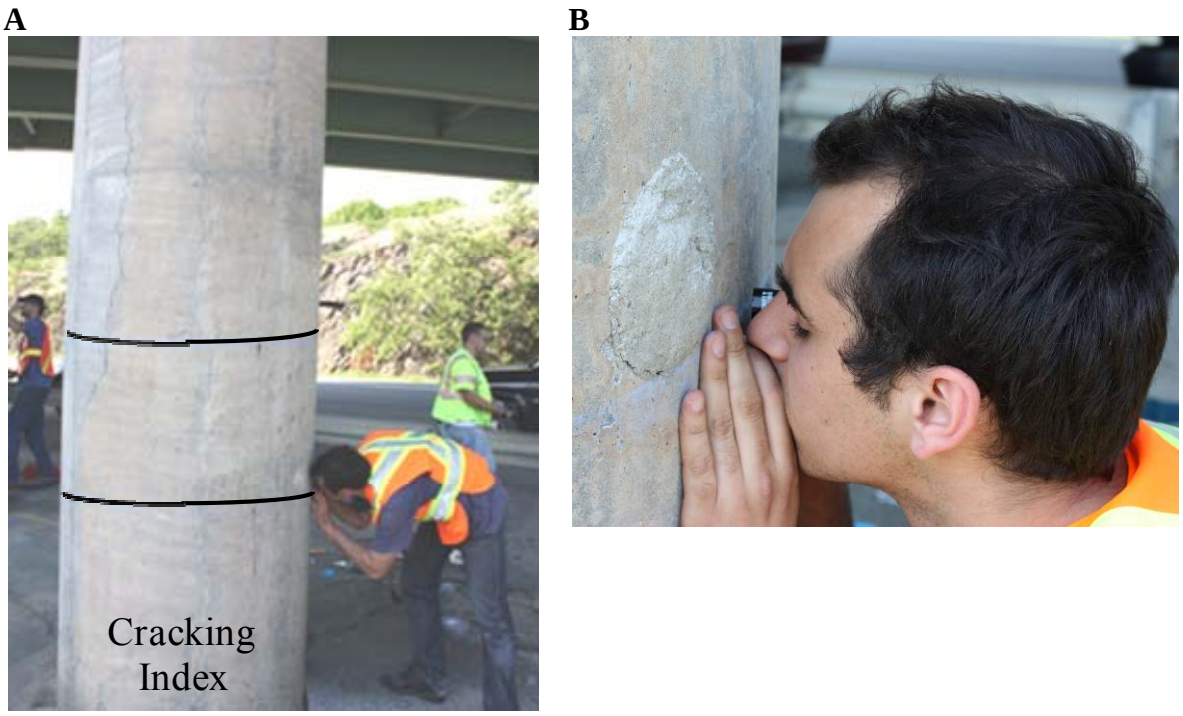

Figure 14. Cracking index measurements on the columns of the South Parkway bridge over I-395 (Maine). The crack mapping operator is measuring crack widths using a magnifying hand lens.

2.2.3 Internal Concrete Temperature and Humidity

Relative humidity and temperature measurements are made at different depths into the concrete in order to help evaluate/interpret the beneficial effect of surface treatments in reducing deleterious expansion due to ASR. A Vaisala HM44 Concrete Humidity Measurement System with accessories for measuring hardened concrete is used to take humidity measurements of the concrete. The HM44 system includes an indicator, probes that measure humidity and temperature, protective covers with rubber stoppers for the probes (used to protect probes while in place for measurements), plastic sleeves, and rubber plugs.

Near each crack map on the selected concrete members, three holes are drilled within six inches of each other for humidity measurements (see Figure 15). The holes are drilled at about a 30-degree angle from the horizontal so that moisture running down the walls will not be encouraged to ingress the hole. Each hole is 16 mm (5/8 in.) in diameter. The holes are drilled to depths of 25 mm (~1 in.), 50 mm (~2 in.), and 75 mm (~3 in.) below the surface.

After drilling, the holes are cleaned of any loose debris using compressed air (same as that illustrated in Figure 8C). A black plastic sleeve is then glued into place with a quick set epoxy (see Figure A). The sleeve extends the entire length of the hole and is open on both ends. The same epoxy used for the steel pins is used. Rubber plugs, shown in Figure 16B, are inserted into the sleeves after the sleeves are epoxied into place to prevent moisture ingress or moisture loss at the hole. The plugs are left in place while the concrete equilibrates. The holes with sleeves and plugs in place are left overnight to equilibrate.

A B

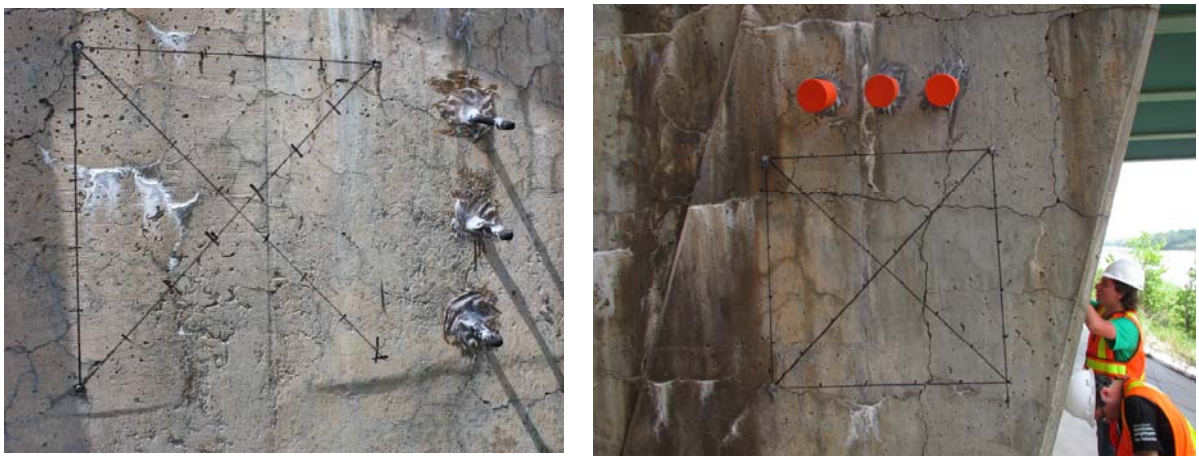

Figure 15. Sleeves and stoppers used for humidity measurements, inserted into three holes drilled at different depths into the selected concrete element.

A B

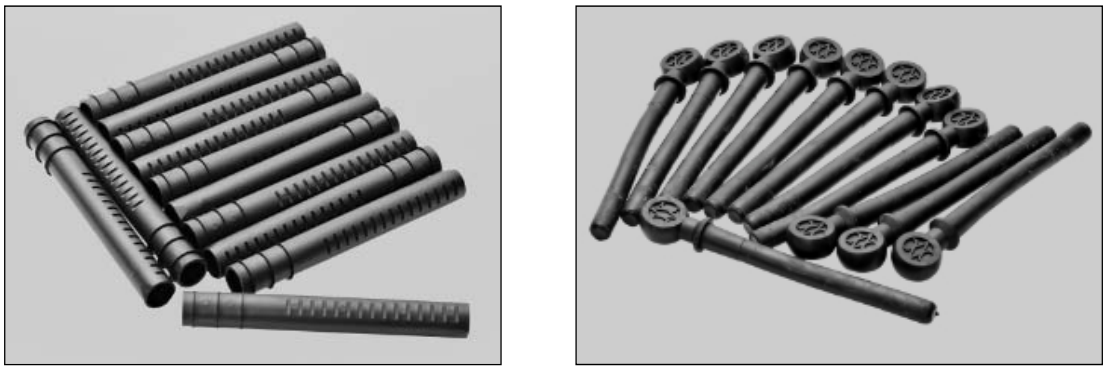

Figure 16. Vaisala kit for the measurement of humidity and temperature within the concrete. Sleeves (A) and stoppers (B) used in humidity holes.

In order to measure, the plugs are removed, the probes are inserted into the sleeves, and the protective covers are placed over the probes (see Figure 17). The covered/protected probes are left in place for one hour to equilibrate with internal concrete conditions. Internal concrete humidity and temperatures are obtained using the indicator, as shown in Figure 17B and Figure 18. Once the measurements are completed, the rubber plugs are re-inserted into the sleeves and sealed using silicone in order to prevent any moisture ingress/loss (see Figure 18D).

A

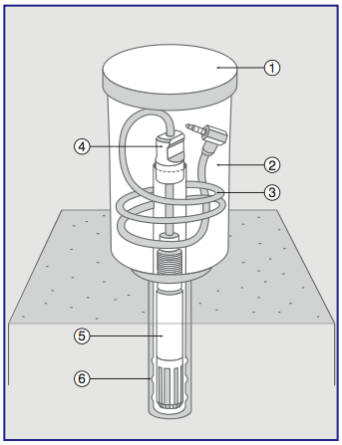

B

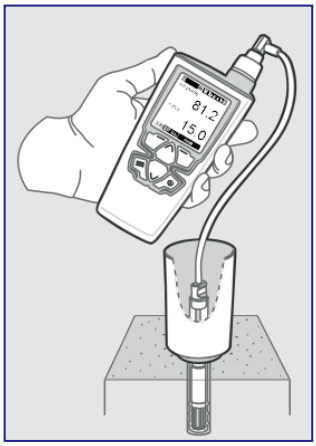

Figure 17. Vaisala kit for the measurement of humidity and temperature within the concrete. Probe that measures humidity and temperature, and protective plastic cover. (A and B) (source: www.vaisala.com)

A

B

C

D

Figure 18. A-C: In-situ humidity and temperature measurements. D: Sealing of the plastic sleeve using the rubber plug with silicone.

2.2.4 Non-Destructive Testing (NDT)

2.2.4.1 General

Various NDT techniques were introduced by ACI 228.2R-98 to evaluate the quality and the integrity of concrete. Among existing techniques, thermography, electrical resistivity, and acoustic-based methods (both linear and nonlinear methods) have been mostly used to evaluate ASR-damage in concrete. Thermography is mostly a qualitative method and is successful at locating surface or subsurface defects (such as honeycomb or delamination) because it measures surface temperature [Carino 2003]; therefore, it is not well suited for detecting diffused damage at greater depths such as ASR damage. Electrical resistivity has been tested to assess ASR damage because ASR gels are thought to modify the electrical properties of concrete; however, Rivard and Saint-Pierre [2009] reported no clear relation between the extent of ASR damage and electrical resistivity, mainly because electrical properties are highly dependent on concrete moisture.

Ground penetrating radar (GPR) provides an alternative approach to ASR monitoring. However, there are two main restrictions to its application [Carino 2003]. The first restriction is that GPR generates pulses of electromagnetic waves which are very sensitive to the dielectric constant of the concrete's pore water content. The second is that when used on reinforced concrete, strong reflections from steel bars can obscure weaker reflections produced by ASR microcracks.

Acoustic methods, which produce stress waves throughout the concrete mass, have been widely used to monitor the integrity of concrete against damage mechanisms. Linear wave attenuation, impact-echo, and ultrasonic pulse velocity (UPV) [Saint-Pierre et al. 2007] are linear acoustic methods that have been commonly used to monitor ASR. However, nonlinear approaches appear to be more sensitive to ASR damage (Van Hauwaert et al. 1998; Kodjo 2008; Kodjo et al. 2009; Van Den Abeele et al. 2000; Van Den Abeele et al. 2001; Payan et al. 2010; Guyer and Johnson 1999; Delsanto and Scalerandi 2003; Sargolzahi et al. 2010; Chen et al. 2010; Chen et al. 2009; Chen et al. 2008). For example, harmonic generation, frequency modulation, and resonance frequency shift are three common methods of nonlinear acoustics. These assessment methods have proven successful in many laboratory applications.

This section provides information on the different methods that were used for the prognosis of ASR in various bridge structures in Maine that were selected for the FHWA ASR Development and Deployment Program.

2.2.4.2 Ultrasonic Pulse Velocity Test

The procedure for measuring the UPV in concrete is presented in detail in ASTM C597-09. The indirect configuration was used for the assessment of all walls (abutment and wing) and large columns of the bridge over the Penobscot River (Veteran's bridge) (see Figure 19A). The circular columns of the 5th Parkway structure were assessed with direct transmission (see Figure 19B). The transducers used for every measurement are compression wave piezoelectric transducers with a central frequency of 50 kHz that correspond to a velocity of 4000 m/s

(approximately 8900 mi/hr) and a wavelength of 80 mm (3 in.). Honey was used as coupling. The equipment system The Andescope ® that was used integrates a signal generator, a data acquisition system, and a computer. The generator excites the transmitting transducer with a tone burst having amplitude of 1000 V. From the recorded signal, the P wave arrival time (the first wave to arrive at the receiving transducer) is detected (see Figure 20) and the velocity can be calculated taking into account the distance between the transducers.

Figure 19. Transmission configurations.
A: Indirect transmission configuration on the wing wall of I-395 over Main Street. B: Direct transmission configuration on South Parkway columns.

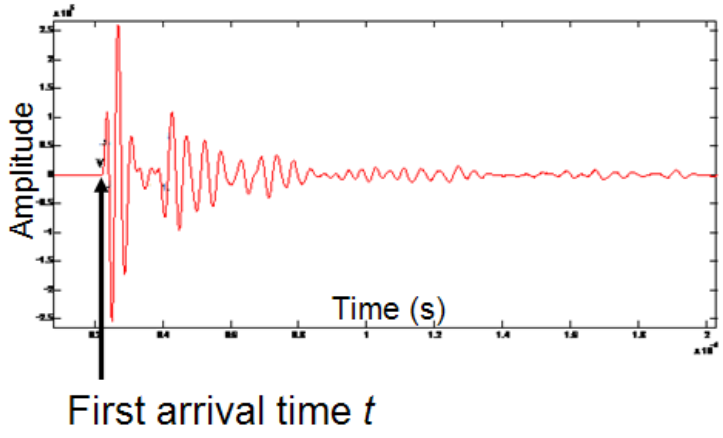

Figure 20. Example of a signal recorded with first arrival time detection.

2.2.4.3 Impact-Echo Test

Impact-echo recording is performed with a hammer to make the impact while a 50-kHz piezoelectric transducer is used to detect the reflected wave from the back of the investigated body (see Figure 21). For each test, 10 ms data points are recorded with the Andescope ® at a sampling rate of 200 kHz. First, a low pass digital filter with a cut-off frequency of 15 kHz is applied on the time domain signal in order to remove the influence of the natural resonant frequency of the transducer. Then, the amplitude spectrum of the time domain signal is processed by a Fast Fourier Transformer (FFT). The frequency of the thickness mode is the frequency that corresponds to the maximum of the spectrum amplitude.

Figure 21. Impact-echo signal recording.

2.2.4.4 Nonlinear Acoustics Testing

This test is performed with a signal generator with an integrated amplifier used to generate a pulse with a duration of 30 µs and a rise time of 6 µs. These pulses excite a Panametrics piezoelectric longitudinal transducer V1012 with a central frequency of 250 kHz. The signal detected by the receiving transducer after propagation in the material is amplified before being sent onto an ADLINK PCI-9820 data acquisition board on the computer for digitization at a sampling rate of 60 MHz. The data acquisition system used is able to record up to 125 signals, 1 ms in length, per second. These signals are stocked on the random access memory (RAM) and then recorded onto a hard drive in separate files after each blast of pulses. While the ultrasonic pulses probe the medium, an impact is applied on the surface of the sample. The impact is produced by a steel ball, set as a pendulum, so the impact energy remains the same (see Figure 22A). The transducers are securely attached to the specimen in order to avoid any displacement when applying the impact. Honey is used for coupling the transducer to the concrete surface.

Due to the height of the measurements points on the Bridge over the Penobscot River, the impact was created with a hammer instead of the pendulum (see Figure 22B).

Figure 22. Nonlinear acoustics recording.
A: Impact generated by a pendulum. B: Impact generated by a hammer at the bridge over the Penobscot River.

While the ultrasonic pulse probes the medium, an impact is applied to the surface of the specimen in order to perturb its elastic properties. For each test performed, unperturbed probe signals are recorded before impact and perturbed probe signals are recorded after impact. The open and/or close cycles of microcracks due to the impact are evaluated by the time delay (Δt) between the signal before impact and the signal after impact. With a signal sampling rate of 60 MHz, the smallest value of Δt that is processed by the cross correlation function is about 10^{-8} s. Keeping the same configuration of transducers, it is assumed that the waves will travel the same path for each test; therefore a change of Δt is to be attributed solely to the degradation of the material.

The signal is first filtered in order to remove the high frequency noise before the cross-correlation process. To increase the sensitivity of the technique, the whole signal is analyzed. To do so, the signal is scanned with consecutive time windows of a specific width which is assumed large enough to take into account enough signal to improve correlation accuracy. For each step *i* of scan, Δt_i is processed. In order to take into account the first arrival waves as well as scattered coda waves (so far part of the signal), the cumulus of all the Δt_i obtained over the whole waveform is calculated. Thus, the sums Δt compared in the results are calculated as follows: sum $\Delta t = \sum_i^N \Delta t_i$, N being the number of windows. The window width and number N are kept identical for each type of specimen during each study. Therefore, the time shift values are

comparable with the same type of specimens. Figure 23 shows the schematic procedure for nonlinear acoustics measurements.

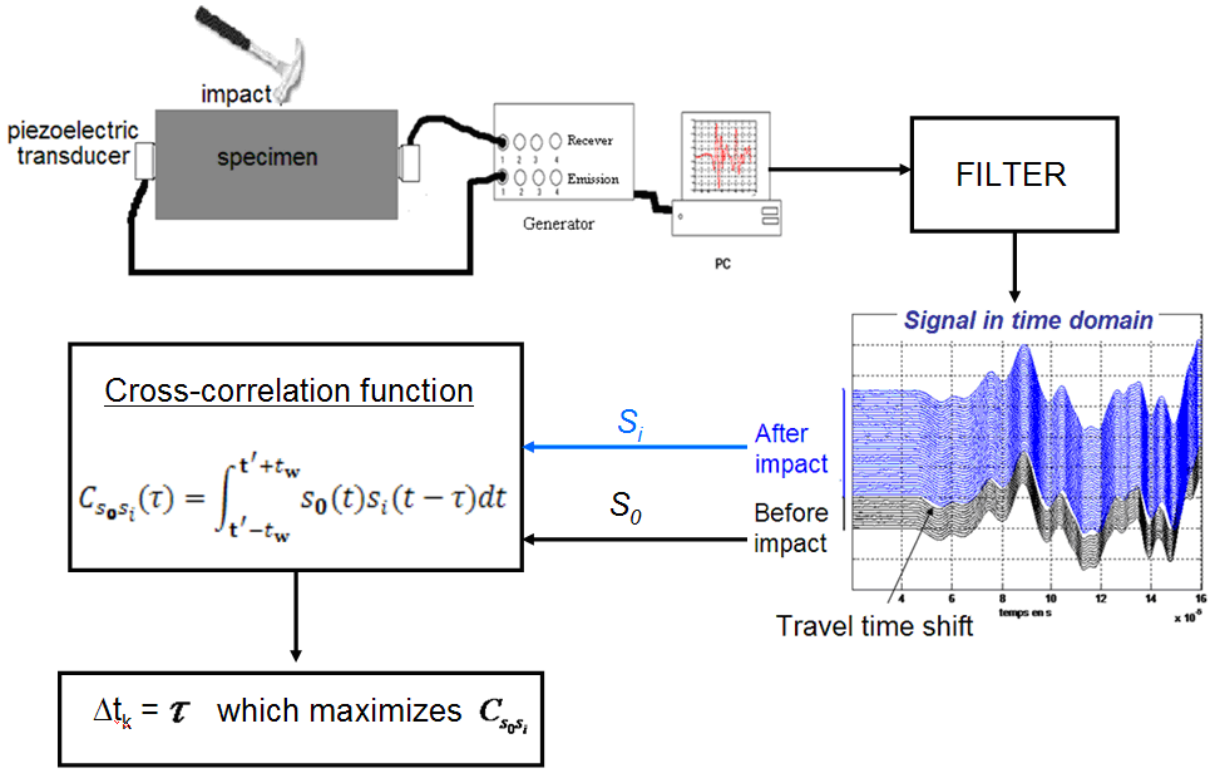

Figure 23. Nonlinear time shift procedure sketch.

2.3 REFERENCES

ACI Committee 228. 1998. "Nondestructive Test Methods for Evaluation of Concrete in Structures." ACI 228.2R-98, American Concrete Institute, Farmington Hills, MI, 62 p.

American Standards for Testing and Materials (ASTM). 2009. "Standard Test Method for Pulse Velocity Through Concrete." ASTM C597-09, ASTM International.

American Standards for Testing and Materials (ASTM). 2003. "Standard Practice for Petrographic Examination of Hardened Concrete." ASTM C856-02, Annual book of ASTM Standards, Section Four, Vol. 04.02 Concrete and Aggregates, ASTM International, 434-450.

Bérubé, M.A., Smaoui, N., Fournier, B., Bissonnette, B. and Durand, B. 2005. "Evaluation of the Expansion Attained to Date by ASR-Affected Concrete – Part III: Application to Existing Structures." *Canadian Journal of Civil Engineering*, 32, 463-479.

British Cement Association (BCA). 1992. "The Diagnosis of Alkali-Silica Reaction – Report of a Working Party." Wexham Springs, Slough, UK, 44 p.

Canadian Standards Association (CSA). 2000. "Guide to the Evaluation and Management of Concrete Structures Affected by Alkali-Aggregate Reaction." CSA A864-00, Canadian Standards Association, Mississauga, Ontario, Canada.

Carino, N.J. 2003. "Non-Destructive Test Methods to Evaluate Concrete Structures." *Proceedings of the 6th International Conference on Durability of Concrete*, CANMET/ACI, Thessaloniki, Greece, 1-78.

Chen, J., Jayapalan, A.R., Kim, J.Y., Kurtis, K.E. and Jacobs, L.J. 2010. "Rapid Evaluation of Alkali-Silica Reactivity of Aggregates Using a Nonlinear Resonance Spectroscopy Technique." *Cement and Concrete Research*, 40(6): 914-923.

Chen, J., Jayapalan, A.R., Kim, J.Y., Kurtis, K.E. and Jacobs, L.J. 2009. "Nonlinear Wave Modulation Spectroscopy Method for Ultra-Accelerated Alkali-Silica Reaction Assessment." *ACI Materials Journal*, 106(4): 340-348.

Chen, J., Jayapalan, A.R., Kurtis, K.E., Kim, J.Y. and Jacobs, L.J. 2008. "Ultra-Accelerated Assessment of Alkali-Silica Reactivity by Nonlinear Ultrasonic Techniques." *Proceedings of the 13th International Conference on Alkali-Aggregate Reaction in Concrete* (ICAAR), Trondheim, Norway.

Chrisp, T.M., Wood, J.G.M. and Norris, P. 1989. "Towards Quantification of Microstructural Damage in AAR Deteriorated Concrete." International Conference on Recent Developments on the Fracture of Concrete and Rocks, Elsevier Applied Science, London, UK, 419-427.

Delsanto, P.P. and Scalerandi, M. 2003. "Modeling Nonclassical Nonlinearity, Conditioning, and Slow Dynamics Effects in Mesoscopic Elastic Materials." *Physics Review. B*, 68(6): 641071-641079.

Dunbar. P.A. and Grattan-Bellew, P.E. 1995. "Results of Damage Rating Evaluation of Condition of Concrete from a Number of Structures Affected by AAR." *Proceedings of CANMET/ACI International Workshop on AAR in Concrete*, Dartmouth, Nova Scotia, CANMET, Department of Natural Resources Canada, 257-265.

Fournier, B., Tremblay, S. and Frenette, J. 2009. "Results of the Petrographic and Stiffness Damage Testing of Concrete Cores from the Princess Margaret Bridge, Fredericton, NB." Gemtec – Consulting Engineers and Scientists, 71p.

Fournier, B., Bérubé, M.A., Folliard, K.J. and Thomas, M.D.A. 2010. "Report on the Diagnosis, Prognosis and Mitigation of Alkali-Silica Reaction (ASR) in Transportation Structures." FHWA-HIF-09-004, Federal Highway Administration.

Grattan-Bellew, P.E. 1992. "Comparison of Laboratory and Field Evaluation of Alkali-Silica Reaction in Large Dams." *Proceedings of the 1st International Conference on Concrete Alkali-Aggregate Reactions in Hydroelectric Plants and Dams*, Fredericton, NB, Canada, 23 p.

Grattan-Bellew, P.E. and Mitchell, L.D. 2006. “Quantitative Petrographic Analysis of Concrete – The Damage Rating Index (DRI) Method, a Review.” *Proceedings of the Marc-André Bérubé Symposium on AAR in Concrete*, CANMET/ACI Advances in concrete technology seminar, Montréal, Canada, 321-334.

Guyer, R.A. and Johnson, P. A. 1999. “Nonlinear Mesoscopic Elasticity: Evidence for a New Class of Materials.” *Physics Today*, 52(4): 30-36.

Hobbs, D.W. 1988. “Alkali-Silica Reaction in Concrete.” Thomas Telford, London, 183 p.

Institution of Structural Engineers (ISE). 1992. “Structural Effects of Alkali-Silica Reaction – Technical Guidance Appraisal of Existing Structures.” London, 45 p.

Kodjo, A. 2008. “Contribution à la Caractérisation des Bétons Endommagés par des Méthodes de l'Acoustique non Linéaire. Application à la Réaction Alcalis-Silice.” *Ph.D. Thesis in French - Université de Sherbrooke/Université Cergy-Pontoise*, 127 p.

Kodjo, A.S., Rivard, P., Cohen-Tenoudji, F. and Gallias, J.L. 2009. “Evaluation of Damages Due to Alkali-Silica Reaction with Nonlinear Acoustics Techniques.” *Proceedings of Meetings on Acoustics (POMA)*, Acoustical Society of America Digital Library, 7(1): 045003-045003-10.

Laboratoire Central des Ponts et Chaussées (LCPC). 1997. “Détermination de l’Indice de Fissuration d’un Parement de Béton.” Méthode no. 47. Ministère de l’équipement, des transports et du logement, Paris.

Payan, C., Garnier, V. and Moysan, J. 2010. “Effect of Water Saturation and Porosity on the Nonlinear Elastic Response of Concrete.” *Cement and Concrete Research* 40, 473-476.

Pleau, R., Bérubé, M.A., Pigeon, M., Fournier, B. and Raphaël, S. 1989. “Mechanical Behavior of Concrete Affected by AAR.” *Proceedings of the 8th International Conference on AAR in Concrete*. Kyoto, Japan, 721-726.

Rivard, P. and Saint-Pierre, F. 2009. “Assessing Alkali-Silica Reaction Damage with Non-Destructive Methods: From the Lab to the Field.” *Construction & Building Materials*, 23(2): 902-909.

Saint-Pierre, F., Rivard, P. and Ballivy, G. 2007. “Measurement of Alkali-Silica Reaction Progression by Ultrasonic Waves Attenuation.” *Cement & Concrete Research*, 37(6): 948-956.

Sargolzahi, M., Kodjo, S.A., Rivard, P. and Rhazi, J. 2010. “Effectiveness of Non-Destructive Testing for the Evaluation of Alkali-Silica Reaction in Concrete.” *Construction and Building Materials*, 24(8): 1398-1403.

Smaoui, N., Bérubé, M.A., Fournier, B., Bissonnette, B. and Durand, B. 2004. “Evaluation of the Expansion Attained to Date by ASR-Affected Concrete – Part I: Experimental Study.” *Canadian Journal of Civil Engineering*, 31, 826-845.

St. John, D., Poole, A.W. and Sims, I. 1998. “Concrete Petrography – A Handbook of Investigative Techniques.” Arnold, London, 474 p.

Thomas, M.D.A., Fournier, B. and Folliard, K.J. 2013. “Alkali-Aggregate Reactivity (AAR) Facts Book.” FHWA-HIF-13-019, Federal Highway Administration, 224 p.

Van Den Abeele, K.E.A., Johnson, P.A. and Sutin, A. 2000. “Nonlinear Elastic Wave Spectroscopy (NEWS) Techniques to Discern Material Damage, Part I: Nonlinear Wave Modulation Spectroscopy (NWMS).” *Research in Nondestructive Evaluation*, 12(1): 17-30.

Van Den Abeele, K.E.A., Sutin, A., Carmeliet, J. and Johnson, P.A. 2001. “Micro-Damage Diagnostics Using Nonlinear Elastic Wave Spectroscopy (NEWS).” *NDT & E International*, 34(4): 239-248.

Van Hauwaert, A., Thimus, J.F. and Delannay, F. 1998. “Use of Ultrasonics to Follow Crack Growth.” *Ultrasonics*, 36(1-5): 209-217.

Walker, H.N., Lane, D.S. and Stutzman, P.E. 2006. “Petrographic Methods of Examining Hardened Concrete: A Petrographic Manual (Revised 2004).” FHWA-HRT-04-150, Federal Highway Administration.

3. TREATMENT TECHNOLOGIES

Following the confirmation of ASR as one of the main contributing factors to the deterioration, a treatment scheme was developed and implemented for each site. Depending on the type of structure, its detailing, and condition, treatment included one or several of the following options: chemical treatments (lithium), surface treatment (sealers and/or breathable coating), or strengthening (fiber reinforced polymer [FRP] wrap).

This chapter provides information on the different methods listed above that were used to treat the ASR-affected structures in the various sites selected for the FHWA ASR Development and Deployment Program.

3.1 CHEMICAL TREATMENT (LITHIUM)

The only chemical treatment used in this project was lithium nitrate (30 percent solution) applied topically; in some cases vacuum-impregnation or electrochemical treatment were used to aid penetration. Two of the structures treated with lithium, the barrier wall near Leominster, MA and the bridge columns in Houston, TX, were treated during the course of previous research through the FHWA Lithium Technology Research Program, but monitoring the treated structures has continued under the FHWA ASR Development and Deployment Program. The concrete pavement near Georgetown, DE and the bridge column near Bangor, ME were treated with lithium under this effort. Further information on the use of lithium to mitigate ASR in existing concrete structures or to prevent ASR in new concrete construction is provided by Folliard et al. (2006) and Thomas et al. (2006).

3.1.1 Topical Applications

Topical applications of lithium were used on the barrier walls (see Figure 24) on State Route 2 near Leominster, MA, a bridge column in Houston, TX, and a concrete pavement (see Figure 24) near Georgetown, DE. In all cases the lithium product used was a 30 percent solution of lithium nitrate ($LiNO_3$). In some cases a proprietary product containing a surfactant (to facilitate penetration) was used; however, comparative testing at The University of New Brunswick (unpublished data) indicated that there was no significant difference between the penetration of 30 percent $LiNO_3$ with or without the surfactant. For topical applications lithium nitrate solution is simply sprayed on the surface of the concrete using a handheld pressure spray applicator (e.g., "garden sprayer") for vertical surfaces and truck-mounted spray bar for horizontal applications. Application rates ranged from 0.06 L/m^2 (1.5 gal/1000 ft^2) to 0.40 L/m^2 (10.0 gal/1000 ft^2) as detailed in the individual site application reports; the higher application rates were achieved by multiple applications at a lower rate.

3.1.2 Vacuum Impregnation

Vacuum impregnation techniques were employed on selected sections of the barrier walls near Leominster, MA and on two of the columns in Houston, TX. In both cases a 30 percent solution

of lithium nitrate was used. In the first case (MA), the barrier wall was simply shrouded and sealed under a plastic membrane, a vacuum applied and then lithium nitrate solution introduced to the area under vacuum. In the second case (TX), a custom-designed steel "vacuum plate" was constructed and the plate was fixed to the surface of the column, a vacuum was drawn under the plate, and then lithium nitrate solution was introduced to the area under vacuum (see Figure 25). More details for the treatments near Leominster, MA and Houston, TX are presented in chapters 8 and 10, respectively.

Figure 24. Topical application of lithium on barrier wall in Massachusetts (left) and concrete pavement in Delaware (right).

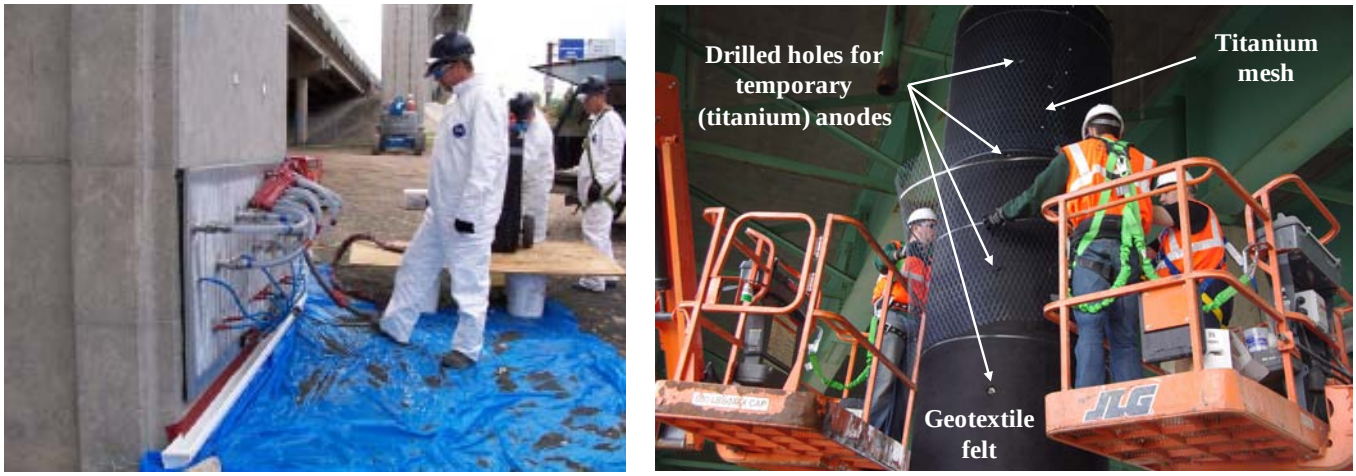

Figure 25. Lithium treatment using vacuum impregnation in Texas (left) and electrochemical migration in Maine (right).

3.1.3 Electrochemical Treatment

Electrochemical lithium treatment was performed on two bridge column in Houston, TX and one column near Bangor, ME (see Figure 25). The principle of the electrochemical technique has been described by Folliard et al. (2006) and Thomas et al. (2006). In both of the field cases described in this report a 30 percent solution of lithium nitrate was used as the initial anolyte and lithium hydroxide (LiOH) was used to buffer the solution during treatment to counteract the acid

produced at the anode. More details for the treatments near Bangor, ME and Houston, TX are presented in chapters 7 and 10, respectively.

3.2 SURFACE TREATMENTS (COATINGS/SEALERS)

With exception of the Bibb Graves Bridge in Alabama, only three surface coatings or sealers were used for the ASR-affected structures that were treated as part of this project; these were a 100 percent silane, a 40 percent water-based silane, and an elastomeric coating (see Figure 26). These products are described below in Sections 3.2.1 and 3.2.2. A carbon-fiber reinforced polymer (CFRP) wrap was used on one of the columns of the bridge near Bangor, ME, and this is described in Section 3.3.1. In addition to the 40 percent water-based silane, a crack-sealing silicone caulk and an epoxy-based "flood-coat" were used on the Bibb Graves Bridge; these products are described in Section 3.3.2. A wider range of sealing/coating products were used for the structures that were treated during previous research projects, such as the FHWA Lithium Technology Research Program, but have been continuously monitored as part of the current project. These include the barrier walls near Leominster, MA and the columns near Houston, TX; the products used are described in Sections 3.3.3 and 3.3.4 below.

Figure 26. Application of 40 percent water-based silane to bridge column in Maine (left) and elastomeric coating to bridge barrier wall in Vermont (right).

3.2.1 100 Percent Silane and 40 Percent Water-Based Silane Sealers

The performance of alkyl alkoxy silanes as "weatherproofing" building materials has been well established (Pfeifer and Scali 1981). Although commercially-available silanes may have a wide range of chemical compositions, the fundamental mechanism of action remains the same; the alkoxy or "silicon functional groups" act to bond to the substrate material (e.g., concrete) by hydrolysis whereas the alkyl or "organofunctional groups" provide hydrophobicity (water repellency) by reducing the surface tension of the substrate. The composition of and the ratio of organofunctional to silicon functional groups strongly influence performance, and while it is possible to predict how a silane will alter the wetting characteristics of a concrete surface it is simpler to measure performance directly by water-absorption test procedures such as that laid out in NCHRP 244 (Pfeifer and Scali 1981). The two silane products used in the current project have

been evaluated using NCHRP 244 and other protocols, and were determined to be effective water-repellants (Wehrle et al. 2010).

Solvents such as water and alcohol are typically used as carriers for silanes. The role of the solvent is to provide a stable solution and to facilitate the dispersion of the active ingredient (the silane) over the surface and its penetration into the surface. Whereas alcohol (e.g., isopropanol or ethanol) has been the preferred carrier due to its low surface tension and miscibility with water, environmental concerns (and legislature) over volatile organic compounds (VOC) have tended to limit the use of alcohol-based silanes recently. Consequently, water-based silanes or solvent-free silanes (with 100 percent active ingredient) are preferred for use nowadays. Note that VOCs result from the solvent carrier and the alcohol liberated by the hydrolysis of the silicon functional groups, so even solvent-free or water-based silanes will emit some level of VOCs (although the amount is significantly reduced compared to silanes with alcohol-based carriers).

One of the silanes used in this study consists of 40 percent active ingredient (reported as alkyl-alkoxy-silane) suspended in water. It contains a fugitive dye and is a milky-white color when applied but is clear when dry. Typical application rates recommended by the manufacturer for concrete are 2.4 to 4.8 m^2/L (100 to 200 ft^2/gal). The second product contains 100 percent active ingredient (reported as alkyl-tri-alkoxy-silane) and is solvent free. Typical application rates recommended by the manufacturer for horizontal concrete surfaces are 2.4 to 8.4 m^2/L (100 to 350 ft^2/gal). Performance data provided by the manufacturers is summarized in Table 3.

Table 3. Selected performance data for silane products.

Property	**40% Water-Based Silane**	**100% Silane**
Solvent	Water	None
Active ingredient	40% alkyl-alkoxy-silane	100% alkyl-tri-alkoxy-silane
VOC (g/L) [lb/gal]	< 350 [~3.0]	390 [~3.3]
NCHRP 244 Series II data		
Reduction in water absorption	85%	86 to 88%
Reduction in chloride ingress (series II)	87%	87 to 88%
Reduction in chloride ingress (series IV)	99%	99%
Alberta DOT Procedures Type 1b		
Initial water repellency	89%	80.7%
After abrasion	89.4%	89.3%
Water absorption (ASTM C642)		
48 hours	0.42%	
50 days	1.2%	

3.2.2 Elastomeric Coating

The elastomeric coating used is described by the manufacturer as a water-dispersed (50 percent solids) and acrylic-based elastomeric coating designed to bridge microcracks and minimize the ingress of carbon dioxide, water, and chlorides while being "water vapor permeable." Typical application rates recommended by the manufacturer are 2.5 m^2/L (100 ft^2/gal) per coat, and two

coats are recommended to provide a total dry-film thickness of 0.4 mm (0.016 in.). The product (with a thickness of 0.4 mm [0.016 in.]) has a reported crack-bridging capacity of 0.75 mm (0.030 in.) when tested statically at -20 °C (-4 °F) .

3.3 OTHER TREATMENTS

3.3.1 FRP Wrap

One of the columns on the bridge carrying South Parkway over I-395 near Bangor, ME was wrapped using a carbon-fiber reinforced polymer (CFRP) wrap (see Figure 27). The product used was a high-strength, unidirectional carbon fiber fabric impregnated with a two-component, high-modulus epoxy resin. Four plies, each with an approximate thickness of 1 mm (0.04 in.), of the material were wrapped around the column. The reported properties of carbon fiber and the impregnated laminate (after curing) are given in Table 4. More details for the treatment near Bangor, ME are presented in chapter 7.

Table 4. Selected (average) properties of carbon fiber and cured CFRP laminate.

Property	Carbon Fiber	Cured Laminate
Tensile Strength (MPa)	3793	849
Tensile modulus (GPa)	234.5	70.6
Elongation (%)	1.5	1.12

Figure 27. Application of FRP to bridge column in Maine.

3.3.2 Materials Used on the Bibb Graves Bridge

Two ASR-affected concrete arches in one span and one unaffected concrete arch in the control span of the Bibb Graves Bridge were treated with the following materials. First the concrete surfaces were sprayed with a water-based, 40 percent silane penetrating sealer (the same product described in section 3.2.1). Larger cracks (≥ 1 mm, 0.04 in.) were then filled with a flexible silicone sealant (caulk). The top surface of the arches was then coated with a two-component epoxy.

3.3.3 Materials Used on Barrier Walls near Leominster, MA

In addition to treating some sections of barrier walls with lithium nitrate (topical and vacuum treatment), other sections were treated with the following materials:

- 40 percent silane in isopropyl alcohol
- 20 percent silane in isopropyl alcohol
- 20 percent silane in water
- lithium silicate-based penetrating sealer

3.3.4 Materials Used on Bridge Columns in Houston, TX

In addition to treating some of the columns with lithium nitrate (vacuum and electrochemical treatment), other sections were treated with the following materials:

- 40 percent silane in isopropyl alcohol
- Silane-siloxane blend, applied via vacuum impregnation
- Sodium silicate, applied via vacuum impregnation

3.4 REFERENCES

American Standards for Testing and Materials (ASTM). 2006. “Standard Test Method for Density, Absorption, and Voids in Hardened Concrete.” ASTM C642-06, ASTM International.

Folliard, K.J., Thomas, M.D.A., Fournier, B., Kurtis, K.E. and Ideker, J.H. 2006. “Interim Recommendations for the Use of Lithium to Mitigate or Prevent Alkali-Silica Reaction (ASR).” FHWA-HRT-06-073, Federal Highway Administration.

Pfeifer, D.W. and Scali, M.J. 1981. “Concrete Sealers for Protection of Bridge Structures.” NCHRP Report 244, Transportation Research Board, Washington, DC.

Thomas, M.D.A., Fournier, B., Folliard, K.J., Ideker, J.H. and Resendez, B. 2006. “The Use of Lithium To Prevent or Mitigate Alkali-Silica Reaction in Concrete Pavements and Structures.” FHWA-HRT-06-133, Federal Highway Administration.

Wehrle, E., Lute, R., Rust, C., Juenger, M.G. and Folliard, K.J. 2010. “Effect of Coatings and Sealers Used to Mitigate Alkali-Silica Reaction and/or Delayed Ettringite Formation in Hardened Concrete.” Final Report, IAC 12-8XXIA008-1, TxDOT.

4. BIBB GRAVES BRIDGE, WETUMPKA, AL

The Bibb Graves Bridge is a reinforced concrete parabolic arch structure with a suspended roadway, with a total of seven arches supporting the roadway as shown in Figure 28. The concrete arch above the roadway in the 5th span is suffering from ASR (see Figure 29) and was treated in November 2010.

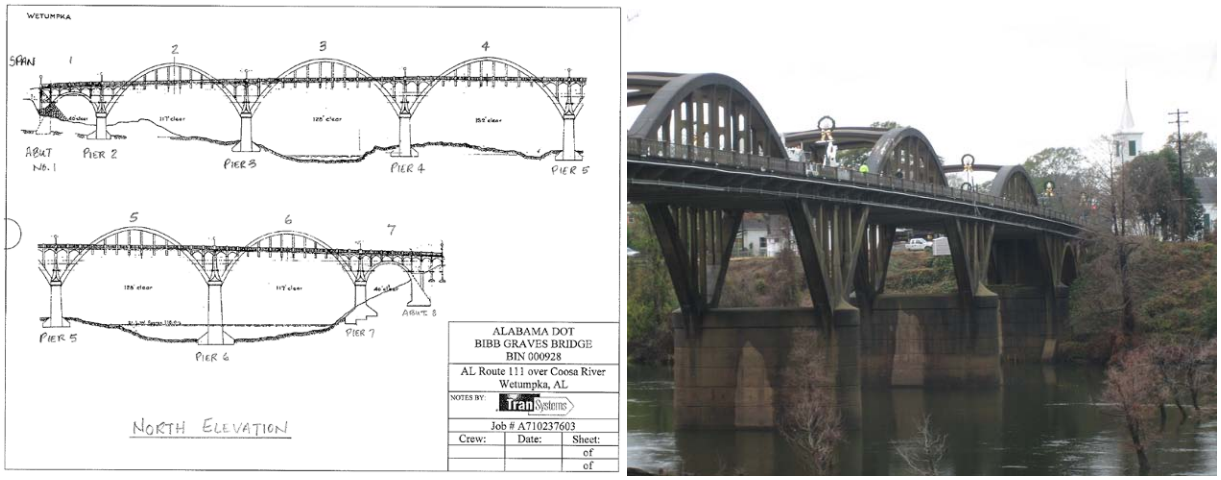

Figure 28. Sketch showing elevation and photograph of Bibb Graves Bridge (north face).

Figure 29. Cracking on top and underside of archway supporting 5th span.

4.1 SUMMARY OF PETROGRAPHIC EVALUATION

Concrete cores were taken from the arches above the roadway in the 4th and 5th spans (numbered from east to west) shortly after the initial site visit in December 2005, under the FHWA Lithium Technology Research Program. Petrographic examination of the concrete (conducted by Dr.

Grattan-Bellew[1]) confirmed that the cracking in the 5th span was due to ASR and that the concrete in the 4th span exhibited no significant signs of ASR. Dr. Grattan-Bellew's report concluded that the aggregate mineralogy and the water-soluble alkalis of the concrete in the two spans was similar and could offer no explanation for why the damage was restricted to the concrete in the arch for the 5th span.

The findings of the petrographic examination of another set of concrete cores extracted from the 4th and 5th spans of the Bibb Graves Bridge in 2010 were reported to the Alabama DOT under the FHWA ASR Development and Deployment Program. The evaluation mainly consisted of the Damage Rating Index (DRI), a method that provides a semi-quantitative assessment of the degree of damage in concrete based on a count of petrographic features of deterioration generally associated with ASR (see Figure 30).

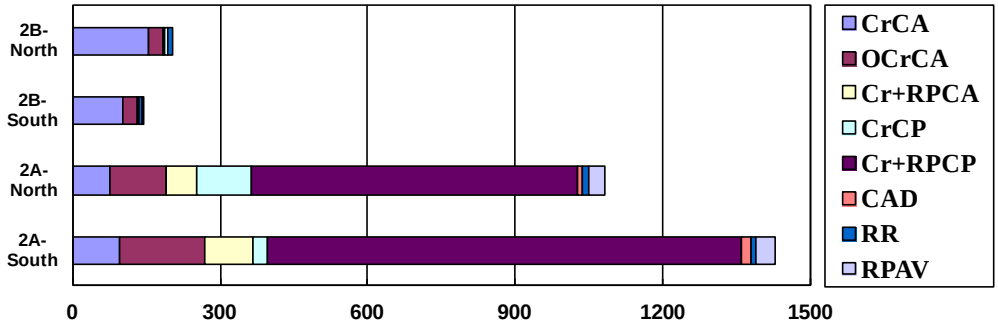

Figure 30. Results of the Damage Rating Index (DRI) for the Alabama cores. The colored cells give the proportions of each petrographic feature to the DRI value. (CrCA: cracking in the coarse aggregate particles; OCrCa: opened cracking in the coarse aggregate particles; Cr+RPCA: cracking in the coarse aggregate particles + reaction product; CrCP: cracking in the cement paste; Cr+RPCP: cracking in the cement paste + reaction product; CAD: coarse aggregate debonded; RR: reaction rim; RPAV: reaction products in air void of the cement paste).

Cores extracted from the 4th span showed no significant signs of deterioration (2B North and South - Figure 30; Figure 31A&B), as indicated by the low DRI values of 141 and 205. On the other hand, cores extracted from the 5th span show several large cracks (up to 1 mm [0.04 in.] in size) that run through the cement paste and the coarse aggregate particles (2A North and South - Figure 30; Figure 31C&D). The DRI values of 1430 and 1081 are indicative of a very high degree of damage in the concrete. Dark reaction rims and extensive cracking were observed for several chert and quartzite coarse aggregate particles. Cracks in the cement paste were often found to be filled with secondary reaction products revealed to be ettringite and alkali-silica gel under the scanning electron microscope (SEM).

[1] Note that Dr. Grattan-Bellew's report refers to the 4th span as arch #3 and the 5th span as arch #4. In the initial visit the arches visible above the roadway were numbered from east to west ignoring the easternmost arch which is below the roadway.

A

B (distance between vertical lines = 1 cm [0.4 in.])

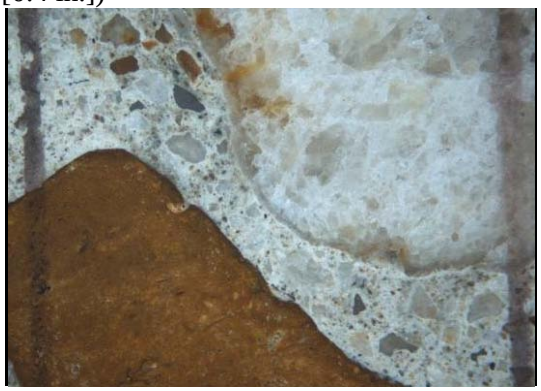

C

D (distance between vertical lines = 1 cm [0.4 in.])

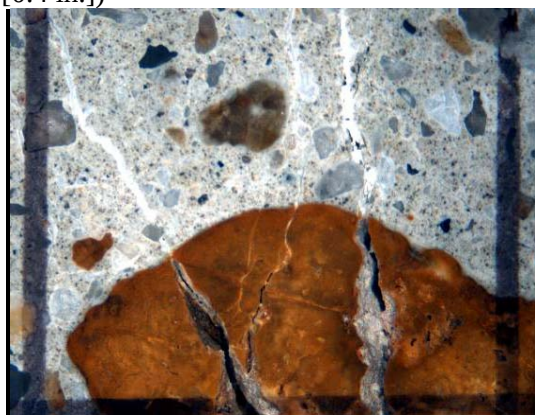

Figure 31. Polished concrete core surfaces. A&B: Core from South span #4 showing very limited cracking in the concrete aggregates and cement paste. C&D: Core from South span #5 showing extensive cracking and secondary reaction products.

4.2 SUMMARY OF APPLICATION REPORT

In November 2010 the following treatment was applied to both ASR-affected arches on the 5th span and the south arch of the 4th span as a control, as shown (see Figure 32):

1. Water-blast all concrete surfaces to clean concrete surfaces and remove loose impediments, efflorescence, ASR gel, algae, etc.
2. Apply silane to all surfaces after a 72-hour drying period. A water-based, 40 percent silane penetrating sealer was applied using a low-pressure garden sprayer.
3. Seal all cracks 0.04 inches (1 millimeter) and wider with a UV-resistant, flexible sealant. The flexible sealant utilized was a structural silicone glazing and weatherproofing sealant, suitable for use for sealing expansion and control joints in precast concrete panels. A bead of sealant was applied onto the crack using a caulk gun, and the bead was then forced into the crack and smoothed by hand.

4. Apply an epoxy flood coat to the top arch surface to seal the cracks on this surface. The epoxy used was a 2-component, 100 percent-solids, low-modulus, highly-penetrating (low-viscosity), epoxy polymer. This two-part epoxy was combined using a 1:1 ratio. Before application, the mixture was blended for three minutes. The epoxy was then applied using a paint roller.
5. Installation of instrumentation for monitoring.

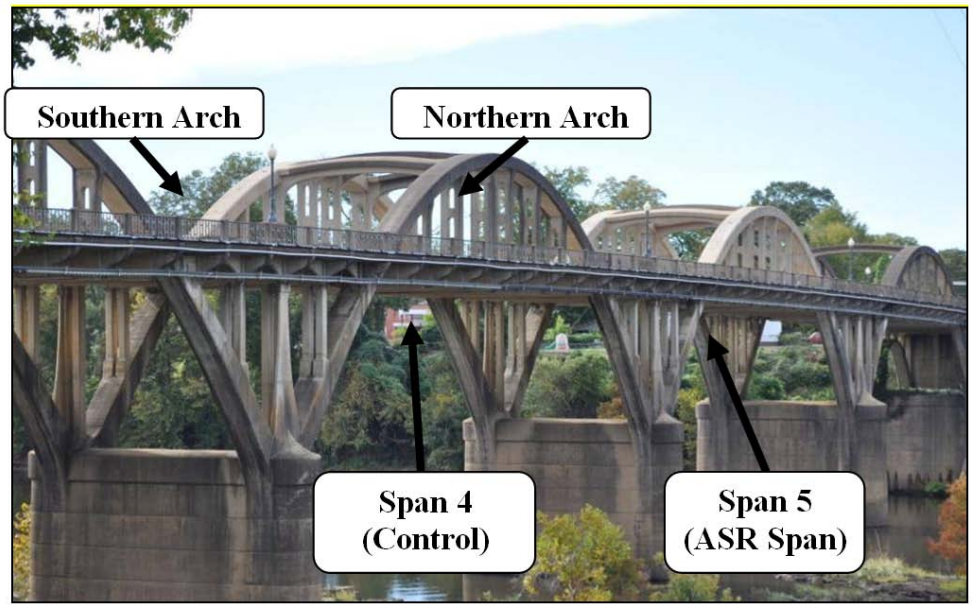

Figure 32. Photograph showing location of treated and control sections.
(Photo courtesy of Warnock and Anton K. Schindler, 2012.)

Note that only the concrete above the roadway was treated. Additional details on the performance monitoring techniques and treatment activities are provided in chapters 2 and 3, respectively.

4.3 MONITORING DATA

Four arches above the roadway were monitored; these were the north and south arches of both the 4th and 5th spans. Both arches of the 5th span are affected by ASR and were treated in November 2010. Neither of the arches of the 4th span exhibited symptoms, but the south arch was treated as a control.

Figure 33 shows the locations of relative humidity measurements; the locations were the same for all four arches. The monitoring locations were labeled to identify the span (4th or 5th), the arch (North or South) and the location within the arch (West-Bottom, West-Top, East-Bottom, East-Top). For example 4-S-EB refers to the 4th span, south arch, eastern side, bottom location (i.e., on the underside of the arch).

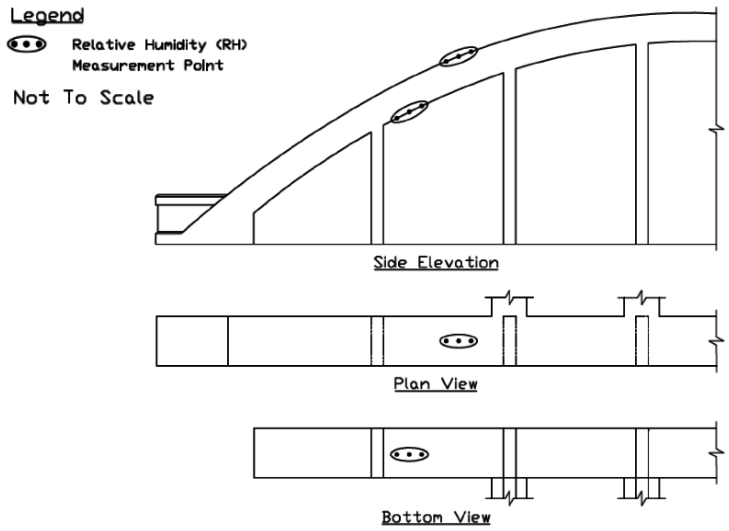

Figure 33. Location of RH measurements. (Courtesy of Warnock and Anton K. Schindler, 2012.)

Figures 34 and 35 show, respectively, the locations for DEMEC gauge (length-change) measurements on the 4th and 5th spans.

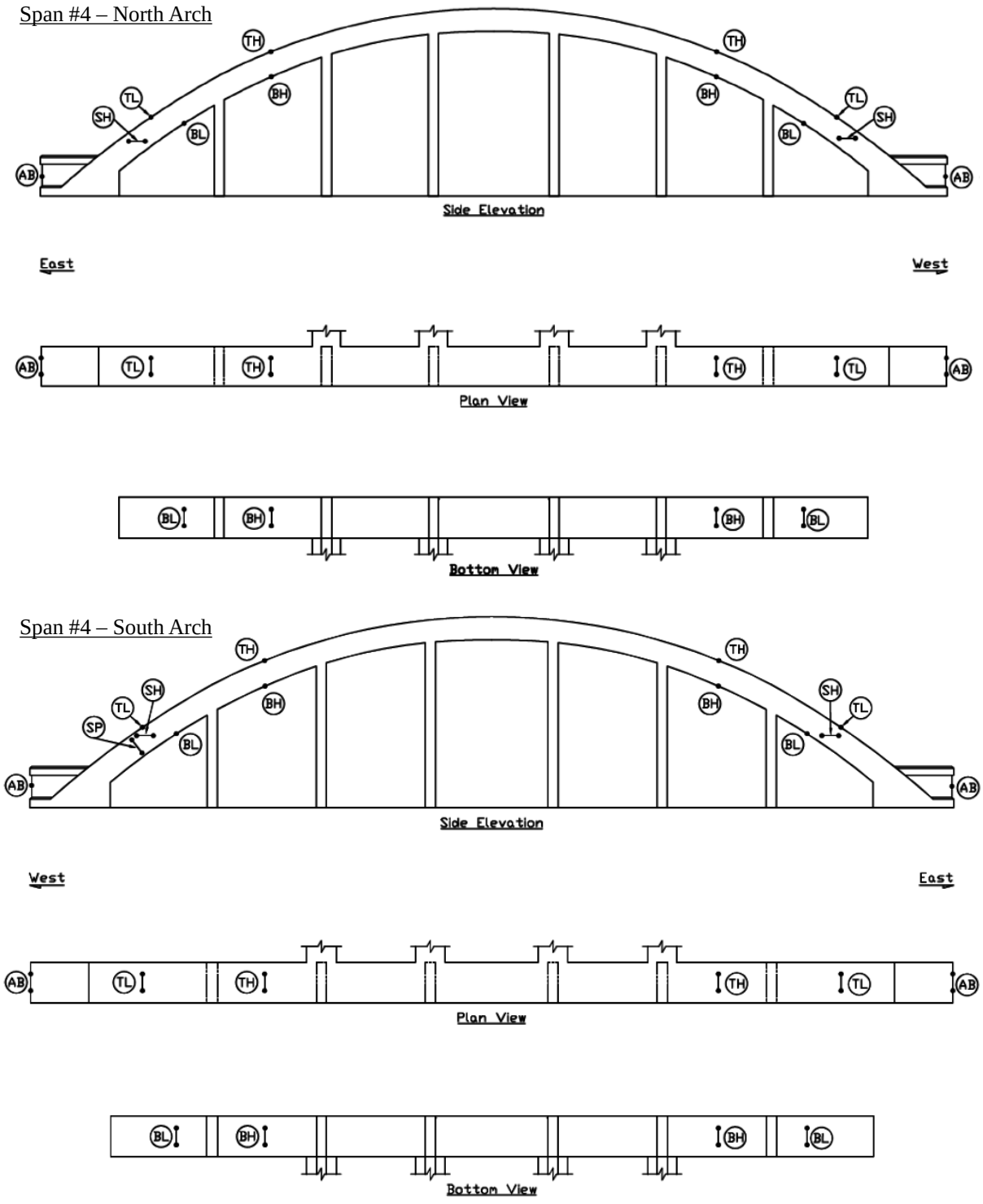

AB – Abutment; SH - Side Horizontal; SP - Side Perpendicular;
BL - Bottom Low; BH - Bottom High; TL - Top Low; TH - Top High

Figure 34. Location of DEMEC gauge measurements on the 4th span. (Courtesy of Warnock and Anton K. Schindler, 2012.)

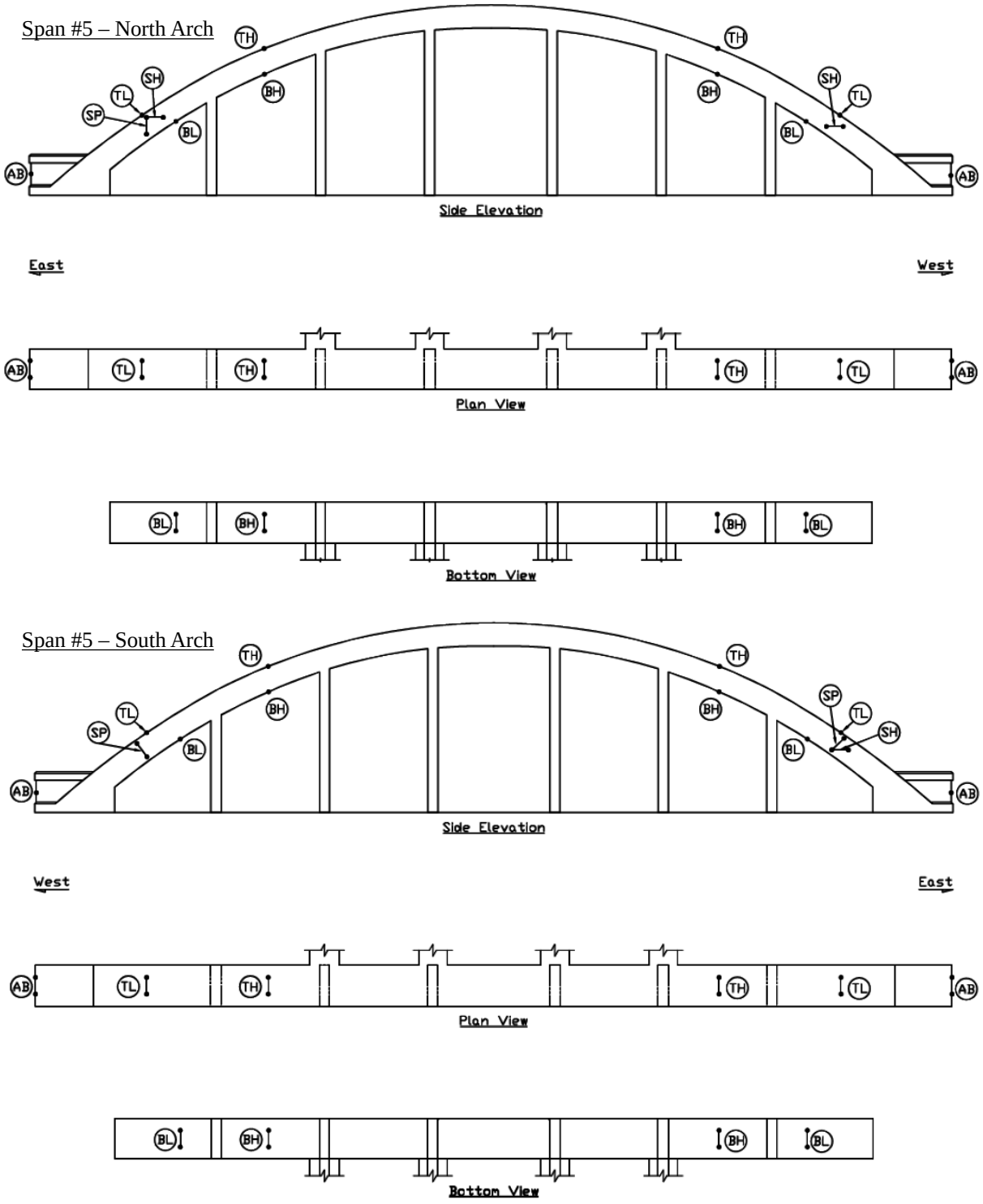

AB – Abutment; SH - Side Horizontal; SP - Side Perpendicular;
BL - Bottom Low; BH - Bottom High; TL - Top Low; TH - Top High

Figure 35. Location of DEMEC gauge measurements on the 5th span. (Courtesy of Warnock and Anton K. Schindler, 2012.)

DEMEC gauge points were fixed in a few locations in December 2005, under the FHWA Lithium Technology Research Program, and length-change measurements were made at these locations in December 2009 and later as part of the FHWA ASR Development and Deployment Program. The remaining DEMEC gauge points and all the sites for RH measurements were fixed in November 2010 at the time of treatment. Measurements of length change and RH have been made since this time at approximately one-month intervals by Auburn University and one-year intervals as part of the FHWA ASR Development and Deployment Program. Only the monthly data are reported here because these readings were taken more frequently and will continue beyond the term of the FHWA ASR Development and Deployment Program[2].

Tables 5 to 20 show the results from the RH probes from February 2011 to May 2013.

Table 5. Relative humidity and temperature measurements – 4th Span South Arch, West Bottom.

	Depth: 25 mm (1 in.)			Depth: 50 mm (2 in.)			Depth: 75 mm (3 in.)		
Date	**Probe**	**°C (°F)**	**RH%**	**Probe**	**°C (°F)**	**RH%**	**Probe**	**°C (°F)**	**RH%**
15/02/2011	4	18.5 (65.3)	83	2	16.8 (62.2)	89.4	7	16.4 (61.5)	86.9
07/04/2011	9	22.2 (72.0)	85.4	5	20.6 (69.1)	92.2	10	20.5 (68.9)	88.3
05/05/2011	9	19.7 (67.5)	87.9	2	18.7 (65.7)	91.5	6	18.7 (65.7)	89.6
03/06/2011	7	35.4 (95.7)	81.7	5	34.7 (94.5)	84.9	6	34.5 (94.1)	82.4
07/07/2011	5	31.7 (89.1)	91.2	7	31.3 (88.3)	92.3	3	31.4 (88.5)	90
10/08/2011	9	29.2 (84.6)	87.8	1	28.2 (82.8)	90.3	8	28 (82.4)	90.1
15/09/2011	10	25.2 (77.4)	92.5	9	26.2 (79.2)	92.9	2	26.4 (79.5)	90.8
18/10/2011	1	26.2 (79.1)	84.3	6	24.9 (76.8)	89.9	7	24.7 (76.5)	83.6
08/11/2011	9	23 (73.4)	86.5	8	21.9 (71.4)	91.3	4	21.8 (71.2)	84.8
14/12/2011	3	16.8 (62.2)	79.5	7	15.1 (59.2)	84.7	7	16.1 (61.0)	83.4
31/01/2012	3	17.7 (63.9)	80	1	15.5 (59.9)	85.5	8	15.1 (59.2)	82.6
08/03/2012	3	24.6 (76.3)	85.6	5	23.1 (73.6)	88.1	9	23.1 (73.6)	85.8
12/04/2012	1	19.7 (67.5)	83.7	2	18.6 (65.5)	91.9	7	18.3 (64.9)	92.5
17/05/2012	9	28.8 (83.8)	84.6	7	27.8 (82.0)	87.1	2	27.7 (81.9)	85.6
08/06/2012	5	27.7 (81.9)	85.8	6	27.3 (81.1)	88.3	9	27.1 (80.8)	87.5
16/07/2012	7	34.7 (94.5)	83.9	6	33.9 (93.0)	88.1	2	33.8 (92.8)	87.3
13/08/2012	2	27.7 (81.9)	89.3	3	28.6 (83.5)	88.5	9	28.6 (83.5)	89
13/09/2012	6	26.6 (79.9)	87.6	10	26.4 (79.5)	88.6	5	26.3 (79.3)	87.2
14/10/2012	5	25.9 (78.6)	86.7	2	25.4 (77.7)	87.4	9	25.3 (77.5)	89.3
19/11/2012	4	16.1 (61.0)	87.2	5	14.3 (57.7)	87.8	6	14.1 (57.4)	87.7
06/12/2012	UT 1.4	20.9 (69.6)	82.3	UT 1.1	20 (68.0)	83.4	UT 1.5	19.9 (67.8)	88
08/01/2013	7	14.2 (57.6)	84.7	4	12.7 (54.9)	86.4	2	12.4 (54.3)	85
05/02/2013	10	16.4 (61.5)	82.2	5	14.1 (57.4)	86.5	4	13.8 (56.8)	87.4
14/03/2013	4	11.8 (53.2)	86.6	7	10.9 (51.6)	83.7	10	10.8 (51.4)	85.1
09/04/2013	6	27.5 (81.5)	81.7	5	26.4 (79.5)	85.6	1	26.3 (79.3)	84.6
14/05/2013	6	24.8 (76.6)	87	2	23.8 (74.8)	88.5	7	23.5 (74.3)	89

[2] The length-change data collected annually during the period 2005 until the time of repair have also been included but have been adjusted to be compatible with the monthly readings taken at the same location since 2010 by Auburn University.

Table 6. Relative humidity and temperature measurements – 4th Span South Arch, West Top.

	Depth: 25 mm (1 in.)			Depth: 50 mm (2 in.)			Depth: 75 mm (3 in.)		
Date	**Probe**	**°C (°F)**	**RH%**	**Probe**	**°C (°F)**	**RH%**	**Probe**	**°C (°F)**	**RH%**
15/02/2011	1	24.2 (75.6)	94.5	2	23 (73.4)	81.2	6	21.6 (70.9)	87.3
07/04/2011	3	29.8 (85.6)	95.1	9	28.2 (82.8)	85.4	5	27 (80.6)	87.8
05/05/2011	2	31.7 (89.1)	95.8	9	31.9 (89.4)	85.5	10	30.6 (87.1)	84.4
03/06/2011	3	47.6 (117.7)	94.9	8	46.7 (116.1)	88.1	4	46.3 (115.3)	85.3
07/07/2011	7	40.9 (105.6)	91.4	5	39.9 (103.8)	90	3	38.8 (101.8)	87.5
10/08/2011	8	39.1 (102.4)	93.7	1	38.2 (100.8)	85.9	9	36.9 (98.4)	85.7
15/09/2011	9	25.7 (78.3)	92.5	2	27.7 (81.9)	90.1	10	28.8 (83.8)	92.9
18/10/2011	3	33 (91.4)	76.7	9	30.6 (87.1)	82	10	29 (84.2)	88.5
08/11/2011	5	28.2 (82.8)	78.2	6	27.3 (81.1)	81.4	3	26.4 (79.5)	84.6
14/12/2011	3	20.7 (69.3)	78.4	9	19 (66.2)	79.7	1	17.7 (63.9)	86.4
31/01/2012	1	22.3 (72.1)	78.5	6	20.3 (68.5)	81	4	19.8 (67.6)	84.8
08/03/2012	7	28.8 (83.8)	89.1	1	27.8 (82.0)	84.1	4	27.4 (81.3)	87.7
12/04/2012	10	28.2 (82.8)	88	4	29.1 (84.4)	86	6	28 (82.4)	88
17/05/2012	3	31.4 (88.5)	80.1	5	29.8 (85.6)	79.4	1	28.6 (83.5)	89
08/06/2012	5	28 (82.4)	81	9	27.7 (81.9)	79.9	6	27.2 (81.0)	89.2
16/07/2012	7	39 (102.2)	78.2	2	37.6 (99.7)	79	10	36.1 (97.0)	85.4
13/08/2012	1	35.5 (95.9)	78	4	32.9 (91.2)	77.8	5	31.4 (88.5)	86.7
13/09/2012	9	30.8 (87.4)	80.2	2	30 (86.0)	77.5	7	29.1 (84.4)	83.4
14/10/2012	7	27 (80.6)	84.5	3	26 (78.8)	75.7	9	25 (77.0)	89.9
19/11/2012	2	15.7 (60.3)	74.1	7	14.1 (57.4)	79.9	3	13.1 (55.6)	85.8
06/12/2012	7	23.7 (74.7)	70.6	4	22.8 (73.0)	80.7	10	21.7 (71.1)	87.2
08/01/2013	3	13.5 (56.3)	80.4	7	12.3 (54.1)	72.2	4	11.2 (52.2)	92.1
05/02/2013	2	18.7 (65.7)	74.1	5	16 (60.8)	89.5	4	14 (57.2)	88.2
14/03/2013	9	15.2 (59.4)	78.8	5	13.1 (55.6)	74.4	2	11.5 (52.7)	87
09/04/2013	5	30.7 (87.3)	78	3	29.4 (84.9)	73.4	2	27.8 (82.0)	83.3
14/05/2013	6	28.2 (82.8)	86.4	2	27 (80.6)	76.8	7	25.4 (77.7)	84.4

Table 7. Relative humidity and temperature measurements – 4th Span South Arch, East Bottom.

	Depth: 25 mm (1 in.)			Depth: 50 mm (2 in.)			Depth: 75 mm (3 in.)		
Date	**Probe**	**°C (°F)**	**RH%**	**Probe**	**°C (°F)**	**RH%**	**Probe**	**°C (°F)**	**RH%**
15/02/2011	6	19.8 (67.6)	80.1	3	17.8 (64.0)	84.7	5	17 (62.6)	84.7
07/04/2011	2	22.3 (72.1)	86.2	6	21.2 (70.2)	86.5	4	20.6 (69.1)	84
05/05/2011	8	20.1 (68.2)	77.4	5	19.3 (66.7)	83.1	10	18.9 (66.0)	82
03/06/2011	4	35 (95.0)	86.1	8	33.4 (92.1)	91	3	34 (93.2)	88.7
07/07/2011	10	32.2 (90.0)	79.8	4	31.7 (89.1)	84.2	8	31.5 (88.7)	87.9
10/08/2011	4	29.8 (85.6)	84.7	2	28.9 (84.0)	90.8	3	28.5 (83.3)	89.2
15/09/2011	8	25.1 (77.2)	92.9	7	26.3 (79.3)	92.9	1	26.8 (80.2)	89.6
18/10/2011	5	26.3 (79.3)	74.3	8	25.8 (78.4)	83.5	4	25.3 (77.5)	80.8
08/11/2011	3	23 (73.4)	74	5	22.1 (71.8)	85	10	21.8 (71.2)	80.6
14/12/2011	2	18.5 (65.3)	68.8	6	16.7 (62.1)	75.4	4	16.3 (61.3)	74.8
31/01/2012	9	18.1 (64.6)	73.3	5	15.6 (60.1)	77.7	10	14.7 (58.5)	78.4
08/03/2012	3	25 (77.0)	80.3	5	23.9 (75.0)	83.1	9	23.6 (74.5)	82.3
12/04/2012	1	20.5 (68.9)	77.2	7	19.8 (67.6)	90.4	2	19.6 (67.3)	87.6
17/05/2012	5	28.8 (83.8)	76.9	1	28.2 (82.8)	80.8	4	27.9 (82.2)	80.6
08/06/2012	2	27.8 (82.0)	80.5	3	27.4 (81.3)	81.8	4	27 (80.6)	81.8
16/07/2012	5	34.3 (93.7)	87	9	34.1 (93.4)	86	10	33.8 (92.8)	84
13/08/2012	10	29.1 (84.4)	80.9	6	29.7 (85.5)	82.4	7	29.7 (85.5)	79.8
13/09/2012	6	26.5 (79.7)	81.1	10	26.2 (79.2)	83.1	5	26.1 (79.0)	84.6
14/10/2012	3	26.2 (79.2)	90	10	25.7 (78.3)	87	7	25.5 (77.9)	88.5
19/11/2012	2	16.1 (61.0)	81.6	3	14.7 (58.5)	85.1	7	14 (57.2)	83.8
06/12/2012	UT 1.3	21.5 (70.7)	77.3	UT 1.8	20.3 (68.5)	78.7	UT 1.7	20.1 (68.2)	78.3
08/01/2013	10	14.3 (57.7)	86.1	9	12.9 (55.2)	80.8	3	12.2 (54.0)	77.8
05/02/2013	2	16.4 (61.5)	79.4	1	14.4 (57.9)	81.7	6	13.7 (56.7)	80.6
14/03/2013	7	13.1 (55.6)	76.7	10	12.2 (54.0)	79.1	4	11.9 (53.4)	80.4
09/04/2013	2	27.8 (82.0)	75.4	7	26.7 (80.1)	78.1	3	26.3 (79.3)	79.3
14/05/2013	9	25 (77.0)	89.9	10	24 (75.2)	82.5	3	23.7 (74.7)	89.1

Table 8. Relative humidity and temperature measurements – 4th Span South Arch, East Top.

Date	Depth: 25 mm (1 in.)			Depth: 50 mm (2 in.)			Depth: 75 mm (3 in.)		
	Probe	°C (°F)	RH%	Probe	°C (°F)	RH%	Probe	°C (°F)	RH%
15/02/2011	9	25.1 (77.2)	96.3	9	22.8 (73.0)	95.5	1	22.7 (72.9)	94.3
07/04/2011	1	31.5 (88.7)	96.4	3	32.6 (90.7)	95	1	31.6 (88.9)	90.2
05/05/2011	4	32.4 (90.3)	96.1	1	32.2 (90.0)	92.4	6	32 (89.6)	88.1
03/06/2011	10	45.8 (114.4)	92.9	2	47.1 (116.8)	93.7	1	47.3 (117.1)	90.4
07/07/2011	8	43.6 (110.5)	90.5	4	43.8 (110.8)	88.8	10	42.7 (108.9)	88.2
10/08/2011	7	41.8 (107.2)	92.2	3	43.1 (109.6)	85.2	6	41.5 (106.7)	91.1
15/09/2011	7	27.2 (81.0)	94.7	8	28.8 (83.8)	92.2	1	29.6 (85.3)	93.1
18/10/2011	2	34.5 (94.1)	80.2	2	34.4 (93.9)	87.3	3	34.1 (93.4)	86.8
08/11/2011	5	29.2 (84.6)	78.6	9	28.5 (83.3)	87.2	2	28.2 (82.8)	87.3
14/12/2011	9	25 (77.0)	83.1	5	23.8 (74.8)	83.8	3	22.7 (72.9)	85.5
31/01/2012	9	21.7 (71.1)	82.4	5	20.3 (68.5)	85.7	3	19.4 (66.9)	85.6
08/03/2012	10	29.5 (85.1)	82.4	6	27.6 (81.7)	88.6	2	27.4 (81.3)	89.3
12/04/2012	3	30.3 (86.5)	86.7	9	30.2 (86.4)	83.5	5	29.7 (85.5)	84.8
17/05/2012	6	34.8 (94.6)	83.5	10	35.1 (95.2)	83.8	4	34.5 (94.1)	88
08/06/2012	2	30 (86.0)	78	3	30.8 (87.4)	84.4	4	30.1 (86.2)	89.3
16/07/2012	9	41.5 (106.7)	84.4	6	42.6 (108.7)	86.7	5	41.3 (106.3)	89.9
13/08/2012	2	36.4 (97.5)	81.3	9	36.9 (98.4)	84.1	3	35.9 (96.6)	89.6
13/09/2012	4	31.4 (88.5)	79.9	1	31.8 (89.2)	84.8	3	31.4 (88.5)	86.4
14/10/2012	5	30.3 (86.5)	82.8	10	30.4 (86.7)	84.2	2	29.4 (84.9)	86.7
19/11/2012	6	17.1 (62.8)	80.7	5	16.2 (61.2)	81.7	4	15.6 (60.1)	91.5
06/12/2012	6	25.8 (78.4)	78.9	2	25.4 (77.7)	80.7	5	25.1 (77.2)	88.1
08/01/2013	2	15 (59.0)	77.5	1	14.1 (57.4)	82.5	10	13.4 (56.1)	90
05/02/2013	1	21.3 (70.3)	80.8	10	20.3 (68.5)	81.3	6	19.2 (66.6)	88.5
14/03/2013	3	19.8 (67.6)	94.9	6	20.6 (69.1)	77.9	1	19.5 (67.1)	86.7
09/04/2013	7	33.5 (92.3)	85.1	1	34.5 (94.1)	81.6	6	33.2 (91.8)	84.5
14/05/2013	3	31 (87.8)	90.3	9	32.2 (90.0)	84.9	10	31.3 (88.3)	89.1

Table 9. Relative humidity and temperature measurements – 4th Span North Arch, West Bottom.

	Depth: 25 mm (1 in.)			Depth: 50 mm (2 in.)			Depth: 75 mm (3 in.)		
Date	**Probe**	**°C (°F)**	**RH%**	**Probe**	**°C (°F)**	**RH%**	**Probe**	**°C (°F)**	**RH%**
15/02/2011	4	13.7 (56.7)	87.5	8	12.4 (54.3)	88.7	9	12.2 (54.0)	85.7
07/04/2011	1	17.5 (63.5)	89.1	6	17.1 (62.8)	88.2	8	17 (62.6)	86.9
05/05/2011	6	16.6 (61.9)	81.2	2	16.4 (61.5)	85.1	3	16.5 (61.7)	86
03/06/2011	7	31.8 (89.2)	82.3	3	32 (89.6)	86.4	2	31.9 (89.4)	87.1
07/07/2011	9	29.8 (85.6)	84.7	7	30.1 (86.2)	85.3	6	30.2 (86.4)	85.8
10/08/2011	5	25.3 (77.5)	84.1	1	25.7 (78.3)	85.5	7	25.7 (78.3)	86.6
15/09/2011	2	26.5 (79.7)	79.8	9	26.9 (80.4)	84.2	8	27 (80.6)	84.9
18/10/2011	6	22.6 (72.7)	76.2	4	22 (71.6)	81	5	21.8 (71.2)	78.3
08/11/2011	9	20.6 (69.1)	74.8	8	20 (68.0)	81.7	3	20 (68.0)	77.1
14/12/2011	5	18.5 (65.3)	68.8	6	16.7 (62.1)	75.4	4	16.3 (61.3)	74.8
31/01/2012	10	11.8 (53.2)	73.1	2	10.5 (50.9)	76.1	1	10.1 (50.2)	84.5
08/03/2012	3	20.6 (69.1)	78.5	4	19.8 (67.6)	81.7	5	19.5 (67.1)	83.3
12/04/2012	3	15.5 (59.9)	74.5	2	15.5 (59.9)	76	7	15.6 (60.1)	79.6
17/05/2012	5	29.1 (84.4)	84.4	1	28.8 (83.8)	82.6	4	28.8 (83.8)	83.2
08/06/2012	5	28.6 (83.5)	76.9	6	28.2 (82.8)	81.6	9	28.1 (82.6)	83.1
16/07/2012	4	33.9 (93.0)	82.1	1	33.6 (92.5)	82.9	3	33.6 (92.5)	84
13/08/2012	10	29.7 (85.5)	81.7	6	29.1 (84.4)	81.5	7	28.9 (84.0)	83.2
13/09/2012	3	27.2 (81.0)	83.7	4	27 (80.6)	83.1	1	26.9 (80.4)	83.1
14/10/2012	9	26.2 (79.2)	84.6	5	25.6 (78.1)	83.7	2	25.5 (77.9)	83.9
19/11/2012	3	15.8 (60.4)	80.5	7	14.3 (57.7)	82.2	2	14.1 (57.4)	80.9
06/12/2012	UT 1.4	20.9 (69.6)	77.5	UT 1.1	20.1 (68.2)	78.3	UT 1.5	19.5 (67.1)	84.2
08/01/2013	1	14.1 (57.4)	80.9	5	12.8 (55.0)	84.4	6	12.5 (54.5)	81.3
05/02/2013	2	17 (62.6)	79.7	1	15.1 (59.2)	84	4	14.7 (58.5)	80
14/03/2013	2	14.3 (57.7)	79.5	9	13.1 (55.6)	83	1	12.8 (55.0)	81.4
09/04/2013	3	27.7 (81.9)	75.2	7	26.7 (80.1)	78.2	2	26.6 (79.9)	80.4
14/05/2013	10	25.6 (78.1)	81.7	3	24.9 (76.8)	87.5	2	24.6 (76.3)	82.9

Table 10. Relative humidity and temperature measurements – 4th Span North Arch, West Top.

Date	Depth: 25 mm (1 in.)			Depth: 50 mm (2 in.)			Depth: 75 mm (3 in.)		
	Probe	°C (°F)	RH%	Probe	°C (°F)	RH%	Probe	°C (°F)	RH%
15/02/2011	6	21.7 (71.1)	84	1	17.5 (63.5)	87.6	6	14.1 (57.4)	89.2
07/04/2011	3	21.1 (70.0)	92.1	2	19.7 (67.5)	90.2	10	18.7 (65.7)	91.9
05/05/2011	4	21.7 (71.1)	88.8	4	22.3 (72.1)	92.4	1	21 (69.8)	89.9
03/06/2011	8	36.4 (97.5)	84	5	35.2 (95.4)	89.2	1	34.7 (94.5)	90
07/07/2011	1	31.2 (88.2)	83.3	2	32.6 (90.7)	88.6	1	31.2 (88.2)	92.1
10/08/2011	9	27.1 (80.8)	80.3	9	28.4 (83.1)	86.3	8	26.8 (80.2)	92.4
15/09/2011	3	27.7 (81.9)	83.9	3	28.6 (83.5)	90.2	5	28.8 (83.8)	89.3
18/10/2011	2	26.1 (79.0)	77.2	2	25.2 (77.4)	85.8	9	23.9 (75.0)	90.2
08/11/2011	6	24.8 (76.6)	75	6	23.1 (73.6)	83.8	2	22.3 (72.1)	86.9
14/12/2011	10	21.1 (70.0)	77.4	7	19.1 (66.4)	87.4	6	18 (64.4)	89.4
31/01/2012	3	16.5 (61.7)	81.3	9	14.2 (57.6)	86.2	9	10.9 (51.6)	89
08/03/2012	3	25.6 (78.1)	84.8	5	24.4 (75.9)	88.3	6	23.2 (73.8)	92.2
12/04/2012	9	20.9 (69.6)	79.3	5	18 (64.4)	90.4	4	17 (62.6)	93.1
17/05/2012	3	30.8 (87.4)	78.9	4	28 (82.4)	89.9	1	26.8 (80.2)	92.4
08/06/2012	6	27.5 (81.5)	78.9	9	26.8 (80.2)	89.5	5	26.2 (79.2)	93.1
16/07/2012	5	37 (98.6)	84.3	6	34.7 (94.5)	89.8	9	33.6 (92.5)	89.5
13/08/2012	1	31.1 (88.0)	84	5	30.6 (87.1)	86.4	9	29.7 (85.5)	90.4
13/09/2012	4	31.1 (88.0)	79.8	1	29.7 (85.5)	85.9	3	28.4 (83.1)	89.4
14/10/2012	5	26.3 (79.3)	86.3	2	26.7 (80.1)	86.7	10	26.5 (79.7)	90.1
19/11/2012	4	14.4 (57.9)	80.6	2	12.7 (54.9)	82.5	7	11.4 (52.5)	88
06/12/2012	UT 9	25.5 (77.9)	83.8	UT 6	23.8 (74.8)	85.6	UT 3	22.9 (73.2)	88
08/01/2013	1	13.1 (55.6)	78.5	2	11.2 (52.2)	80.6	4	9.7 (49.5)	92.7
05/02/2013	4	17.3 (63.1)	74	2	13.9 (57.0)	77.9	5	11.2 (52.2)	92.3
14/03/2013	1	11.9 (53.4)	79.8	6	9.9 (49.8)	79.3	3	8.8 (47.8)	93.1
09/04/2013	2	28 (82.4)	81.1	3	25.7 (78.3)	79.8	5	24.3 (75.7)	92.3
14/05/2013	2	25.9 (78.6)	87.6	7	24.3 (75.7)	89.3	6	23 (73.4)	91.7

Table 11. Relative humidity and temperature measurements – 4th Span North Arch, East Bottom.

Date	Depth: 25 mm (1 in.)			Depth: 50 mm (2 in.)			Depth: 75 mm (3 in.)		
	Probe	°C (°F)	RH%	Probe	°C (°F)	RH%	Probe	°C (°F)	RH%
15/02/2011	3	15 (59.0)	82.8	1	13.3 (55.9)	85	5	12.7 (54.9)	83
07/04/2011	9	17.6 (63.7)	86.7	5	17 (62.6)	83.9	4	16.9 (62.4)	85.2
05/05/2011	10	17 (62.6)	85.5	5	16.5 (61.7)	78.7	9	16.3 (61.3)	80.7
03/06/2011	6	31.6 (88.9)	84.4	4	31.6 (88.9)	82.2	10	31.5 (88.7)	85.1
07/07/2011	5	29.2 (84.6)	88.4	4	29.7 (85.5)	82.5	8	29.7 (85.5)	84.7
10/08/2011	3	25.3 (77.5)	88.1	4	26 (78.8)	83.2	2	26.1 (79.0)	83.2
15/09/2011	7	25.9 (78.6)	86.2	1	26.8 (80.2)	78.2	10	27 (80.6)	82.4
18/10/2011	7	23.5 (74.3)	78.5	8	22.7 (72.9)	74.7	1	22.5 (72.5)	76.3
08/11/2011	10	21.3 (70.3)	78.4	4	20.6 (69.1)	76.1	5	20.1 (68.2)	77.7
14/12/2011	7	19.6 (67.3)	73.3	8	17.6 (63.7)	75	2	16.7 (62.1)	74.2
31/01/2012	4	12.6 (54.7)	75	5	11.2 (52.2)	71.9	6	10.7 (51.3)	73.8
08/03/2012	1	21 (69.8)	80.3	7	20.1 (68.2)	77.6	2	19.7 (67.5)	78
12/04/2012	6	16 (60.8)	84.3	10	16.1 (61.0)	68	1	16 (60.8)	75.3
17/05/2012	9	29 (84.2)	82.3	10	28.6 (83.5)	75.1	3	28.5 (83.3)	80.3
08/06/2012	2	28.8 (83.8)	80.9	3	28.1 (82.6)	74.2	4	27.7 (81.9)	80.9
16/07/2012	3	33.6 (92.5)	82.9	4	33.1 (91.6)	76.7	1	32.8 (91.0)	82.7
13/08/2012	7	30.7 (87.3)	80.9	6	30 (86.0)	74.5	10	29.6 (85.3)	81.9
13/09/2012	10	27.3 (81.1)	84	6	26.9 (80.4)	76	5	26.7 (80.1)	82.1
14/10/2012	4	26.3 (79.3)	84.9	6	26 (78.8)	79.8	1	25.7 (78.3)	88.1
19/11/2012	9	16.4 (61.5)	81.8	10	14.9 (58.8)	90.8	1	14.1 (57.4)	80.9
06/12/2012	UT 1.3	22 (71.6)	81.3	UT 1.7	20.9 (69.6)	75.1	UT 1.8	20.5 (68.9)	79.5
08/01/2013	6	14.6 (58.3)	81	1	13 (55.4)	86.5	5	12.3 (54.1)	83.7
05/02/2013	9	17.6 (63.7)	77.3	3	15.4 (59.7)	83.4	7	14.4 (57.9)	78.8
14/03/2013	4	14 (57.2)	79.4	10	13.1 (55.6)	72.1	7	12.5 (54.5)	72.2
09/04/2013	4	27.7 (81.9)	82.2	10	26.9 (80.4)	78.8	9	26.4 (79.5)	82.6
14/05/2013	4	25.3 (77.5)	81.8	1	24.3 (75.7)	75.9	5	23.7 (74.7)	79.4

Table 12. Relative humidity and temperature measurements – 4th Span North Arch, East Top.

	Depth: 25 mm (1 in.)			Depth: 50 mm (2 in.)			Depth: 75 mm (3 in.)		
Date	**Probe**	**°C (°F)**	**RH%**	**Probe**	**°C (°F)**	**RH%**	**Probe**	**°C (°F)**	**RH%**
15/02/2011	2	23.5 (74.3)	86.1	7	22.9 (73.2)	93.2	10	22.5 (72.5)	91
07/04/2011	7	23 (73.4)	86.6	7	26 (78.8)	96	3	25.4 (77.7)	93.4
05/05/2011	1	24.3 (75.7)	89.3	8	25.6 (78.1)	96.5	7	25.5 (77.9)	89.4
03/06/2011	9	40.4 (104.7)	87	9	47 (116.6)	91.5	1	46.4 (115.5)	89.9
07/07/2011	10	33.9 (93.0)	83.7	3	32.9 (91.2)	92.3	2	32.5 (90.5)	91.4
10/08/2011	6	27.7 (81.9)	76.8	8	27.2 (81.0)	93.2	10	27 (80.6)	93
15/09/2011	5	29.7 (85.5)	84.6	4	29.5 (85.1)	92.5	6	29.5 (85.1)	91.8
18/10/2011	3	31.9 (89.4)	80.5	10	31.1 (88.0)	92.5	9	30.6 (87.1)	89.7
08/11/2011	7	27.3 (81.1)	81.6	2	26.7 (80.1)	86.1	1	26.3 (79.3)	89.6
14/12/2011	6	24.9 (76.8)	81.5	10	24.3 (75.7)	86.7	1	23.6 (74.5)	90.4
31/01/2012	3	16.5 (61.7)	76.4	8	16.4 (61.5)	84.4	7	15.8 (60.4)	89
08/03/2012	1	27.2 (81.0)	85.2	2	27.3 (81.1)	87.6	7	26.7 (80.1)	90.5
12/04/2012	4	26.2 (79.2)	88.6	5	28.6 (83.5)	90.1	9	29 (84.2)	89.9
17/05/2012	5	32.8 (91.0)	87.3	10	33 (91.4)	88.3	6	32.7 (90.9)	89.3
08/06/2012	3	29 (84.2)	94.1	2	28.8 (83.8)	87.6	4	28.8 (83.8)	91
16/07/2012	10	39.3 (102.7)	87.6	2	39.9 (103.8)	92.2	7	39.6 (103.3)	87.7
13/08/2012	4	34 (93.2)	86.9	3	34.7 (94.5)	93.2	2	34.3 (93.7)	90
13/09/2012	7	31.6 (88.9)	77.6	2	32.3 (90.1)	86.4	9	31.9 (89.4)	89.6
14/10/2012	5	26.3 (79.3)	86.3	2	26.7 (80.1)	86.7	10	26.5 (79.7)	90.1
19/11/2012	6	16.4 (61.5)	84.1	3	15.6 (60.1)	84.6	5	14.8 (58.6)	89.3
06/12/2012	UT 1	26.7 (80.1)	79.4	UT 7	25.7 (78.3)	87.2	UT 8	25.4 (77.7)	89.1
08/01/2013	7	15.3 (59.5)	70.1	10	14.6 (58.3)	88.2	3	14.1 (57.4)	87.9
05/02/2013	10	21.6 (70.9)	84.2	6	20.4 (68.7)	88.2	1	19.8 (67.6)	86.8
14/03/2013	2	16 (60.8)	86.7	9	17.5 (63.5)	88.7	5	17.2 (63.0)	90.4
09/04/2013	1	31.2 (88.2)	88.9	7	31.7 (89.1)	81.4	6	31.5 (88.7)	85.9
14/05/2013	9	29.3 (84.7)	93.5	3	30.7 (87.3)	87	10	30.3 (86.5)	87.4

Table 13. Relative humidity and temperature measurements – 5th Span South Arch, West Bottom.

Date	Depth: 25 mm (1 in.)			Depth: 50 mm (2 in.)			Depth: 75 mm (3 in.)		
	Probe	°C (°F)	RH%	Probe	°C (°F)	RH%	Probe	°C (°F)	RH%
15/02/2011	5	17.8 (64.0)	88.1	4	16.1 (61.0)	91.2	7	14.8 (58.6)	92.3
07/04/2011	0:00	21.1 (70.0)	93.2	6	19.9 (67.8)	96.2	7	19 (66.2)	96.7
05/05/2011	1	18.6 (65.5)	96	4	18.1 (64.6)	94.8	7	17.6 (63.7)	97.4
03/06/2011	7	33.3 (91.9)	93.8	6	32.9 (91.2)	92.2	5	32.5 (90.5)	94.8
07/07/2011	7	30.6 (87.1)	94.2	5	30.4 (86.7)	95.1	3	30.5 (86.9)	94.6
10/08/2011	1	28 (82.4)	91.3	8	27.4 (81.3)	94.1	9	27.1 (80.8)	93.7
15/09/2011	9	26.1 (79.0)	94.7	10	26.6 (79.9)	94	7	26.8 (80.2)	94.8
18/10/2011	7	25.2 (77.4)	87.8	8	24.4 (75.9)	94	4	23.8 (74.8)	92.7
08/11/2011	9	22.4 (72.3)	90.6	5	21.5 (70.7)	91.1	3	21 (69.8)	90.6
14/12/2011	10	16.8 (62.2)	86.7	4	15.5 (59.9)	89.1	1	14.3 (57.7)	89
31/01/2012	6	16.7 (62.1)	85.1	10	14.5 (58.1)	89.5	4	13.5 (56.3)	86.2
08/03/2012	9	23.6 (74.5)	89.4	3	22.5 (72.5)	90.6	5	21.5 (70.7)	91.4
12/04/2012	6	17.6 (63.7)	93.4	10	17.3 (63.1)	94.4	3	17.8 (64.0)	93.9
17/05/2012	10	28.5 (83.3)	90.9	6	27.7 (81.9)	93.1	3	27.3 (81.1)	92.7
08/06/2012	7	26.4 (79.5)	90.6	10	26.2 (79.2)	93.9	1	26 (78.8)	94.2
16/07/2012	2	33 (91.4)	92.4	7	32.6 (90.7)	90.5	6	32.4 (90.3)	93.5
13/08/2012	3	30.6 (87.1)	91.4	2	29.8 (85.6)	91.7	9	29.2 (84.6)	93.6
13/09/2012	1	26.6 (79.9)	92.6	3	26.5 (79.7)	92.8	4	26.2 (79.2)	93.8
14/10/2012	5	25.6 (78.1)	91.7	10	25.1 (77.2)	93.1	7	24.6 (76.3)	90.7
19/11/2012	3	15.2 (59.4)	88.7	2	13.8 (56.8)	90.9	7	12.8 (55.0)	89.2
06/12/2012	UT 2.2	21.4 (70.5)	89.1	UT 2.3	20.8 (69.4)	91.2	UT 2.4	20.1 (68.2)	92.1
08/01/2013	2	13.9 (57.0)	87.8	4	12.2 (54.0)	89.2	7	11.1 (52.0)	88.6
05/02/2013	1	16.5 (61.7)	86.6	6	14.8 (58.6)	91.4	2	13.6 (56.5)	89.8
14/03/2013	1	13 (55.4)	91	6	12.1 (53.8)	91.5	3	11.4 (52.5)	90.5
09/04/2013	9	26.8 (80.2)	90.1	10	25.6 (78.1)	92.7	4	24.8 (76.6)	91.4
14/05/2013	7	24.1 (75.4)	89.6	2	23.3 (73.9)	90.7	6	22.6 (72.7)	91.5

Table 14. Relative humidity and temperature measurements – 5th Span South Arch, West Top.

Date	Depth: 25 mm (1 in.)			Depth: 50 mm (2 in.)			Depth: 75 mm (3 in.)		
	Probe	°C (°F)	RH%	Probe	°C (°F)	RH%	Probe	°C (°F)	RH%
15/02/2011	10	23 (73.4)	89	7	21.1 (70.0)	91.6	9	20.6 (69.1)	94.9
07/04/2011	1	27.7 (81.9)	92.7	9	26 (78.8)	91.7	6	25.4 (77.7)	95.9
05/05/2011	6	27.6 (81.7)	93.9	2	27 (80.6)	91.7	3	26.9 (80.4)	93.2
03/06/2011	2	46 (114.8)	97	10	45.4 (113.7)	92.7	10	43.1 (109.6)	92.1
07/07/2011	9	39.7 (103.5)	93	9	39.9 (103.8)	92.3	2	40 (104.0)	91.5
10/08/2011	6	35.5 (95.9)	92.8	10	33.6 (92.5)	90.8	7	33.3 (91.9)	92.8
15/09/2011	6	27.9 (82.2)	96	3	28.9 (84.0)	94.4	5	29.4 (84.9)	92.8
18/10/2011	1	29.5 (85.1)	91.3	7	28.4 (83.1)	87.7	8	27.4 (81.3)	92.8
08/11/2011	1	20.9 (69.6)	93.1	6	26.2 (79.2)	91.9	2	26.4 (79.5)	89.9
14/12/2011	9	16.8 (62.2)	85.5	2	13.9 (57.0)	90.8	6	13.4 (56.1)	92.2
31/01/2012	4	21.4 (70.5)	88.3	6	19.9 (67.8)	89.1	7	18.6 (65.5)	89.9
08/03/2012	6	26.9 (80.4)	91.5	3	25.7 (78.3)	91.1	2	25.6 (78.1)	89.6
12/04/2012	3	27.8 (82.0)	94.3	10	27.3 (81.1)	92.5	9	27.4 (81.3)	89.4
17/05/2012	5	34.4 (93.9)	91.2	10	32.7 (90.9)	90.4	6	32.4 (90.3)	88.3
08/06/2012	3	32.2 (90.0)	89.6	9	29.7 (85.5)	91.4	4	30 (86.0)	89.7
16/07/2012	7	41.8 (107.2)	90.8	10	40.9 (105.6)	90.6	5	40.5 (104.9)	88.8
13/08/2012	9	37.8 (100.0)	91.3	2	36.4 (97.5)	89	3	36.1 (97.0)	87.2
13/09/2012	3	32.9 (91.2)	92	4	32.2 (90.0)	89.3	1	31.6 (88.9)	89.2
14/10/2012	2	30.3 (86.5)	87.8	10	28 (82.4)	89.9	5	27.5 (81.5)	90.8
19/11/2012	3	16.6 (61.9)	89.9	7	15.2 (59.4)	86.7	2	14.9 (58.8)	89.7
06/12/2012	UT 8	23.2 (73.8)	90.5	UT 6	22.7 (72.9)	89.7	UT 1	22.3 (72.1)	91.1
08/01/2013	7	14.8 (58.6)	88.2	4	14.1 (57.4)	91.3	2	13.6 (56.5)	90.6
05/02/2013	10	19 (66.2)	89.9	2	17.4 (63.3)	88.9	1	16.7 (62.1)	91.3
14/03/2013	5	19 (66.2)	89	9	16.9 (62.4)	92.9	2	16.8 (62.2)	89.3
09/04/2013	1	32.6 (90.7)	91.2	7	31.7 (89.1)	87.1	6	31.6 (88.9)	88.5
14/05/2013	9	32 (89.6)	92.7	3	31.5 (88.7)	89.7	10	31.3 (88.3)	89.4

Table 15. Relative humidity and temperature measurements – 5th Span South Arch, East Bottom.

Date	Depth: 25 mm (1 in.)			Depth: 50 mm (2 in.)			Depth: 75 mm (3 in.)		
	Probe	°C (°F)	RH%	Probe	°C (°F)	RH%	Probe	°C (°F)	RH%
15/02/2011	8	18.4 (65.1)	89.5	3	16.6 (61.9)	96.2	10	15.9 (60.6)	93.8
07/04/2011	8	21.5 (70.7)	92.3	4	20.4 (68.7)	96.6	2	19.9 (67.8)	97.5
05/05/2011	7	20.1 (68.2)	95.5	1	19.5 (67.1)	96.1	4	19.2 (66.6)	97.3
03/06/2011	6	34.9 (94.8)	90.8	7	34 (93.2)	94.9	5	33.7 (92.7)	95.2
07/07/2011	4	31 (87.8)	93.6	8	30.8 (87.4)	95.2	10	30.8 (87.4)	94.9
10/08/2011	4	28.7 (83.7)	93.4	3	28.2 (82.8)	93.3	2	27.9 (82.2)	93.9
15/09/2011	2	26.2 (79.2)	93.8	1	27.1 (80.8)	94.5	8	27.3 (81.1)	94.9
18/10/2011	1	26.1 (79.0)	90.8	6	25.4 (77.7)	93.4	5	24.9 (76.8)	90.4
08/11/2011	4	22.6 (72.7)	89.2	8	21.8 (71.2)	94.4	10	21.3 (70.3)	92.5
14/12/2011	8	17.2 (63.0)	88.1	6	16.4 (61.5)	89.3	2	15 (59.0)	90.7
31/01/2012	1	16.9 (62.4)	87.2	8	17 (62.6)	82	2	13.9 (57.0)	91.4
08/03/2012	10	23.7 (74.7)	90.5	1	23.3 (73.9)	90.9	7	22 (71.6)	92.9
12/04/2012	1	19.3 (66.7)	92.8	7	18.8 (65.8)	94.2	2	18.7 (65.7)	94.7
17/05/2012	9	28 (82.4)	91.5	7	27.3 (81.1)	92.1	2	27.1 (80.8)	93.4
08/06/2012	1	27.8 (82.0)	92.1	10	27.2 (81.0)	94.2	7	26.9 (80.4)	93.3
16/07/2012	10	33.3 (91.9)	91.5	5	33.1 (91.6)	93.2	9	33 (91.4)	94
13/08/2012	5	30.7 (87.3)	91.1	1	30 (86.0)	93.3	4	29.6 (85.3)	94
13/09/2012	9	26.8 (80.2)	93.1	7	26.6 (79.9)	92.1	2	26.5 (79.7)	92.5
14/10/2012	2	26 (78.8)	90.9	9	25.7 (78.3)	93.5	3	25.4 (77.7)	93.9
19/11/2012	5	15.7 (60.3)	90	6	14.3 (57.7)	93.5	4	13.6 (56.5)	94.9
06/12/2012	UT 2.1	21.5 (70.7)	90.1	UT 2.6	21.8 (71.2)	85.9	UT 2.5	20.6 (69.1)	93.7
08/01/2013	3	13.9 (57.0)	86.7	10	12.2 (54.0)	93.3	9	11.7 (53.1)	92.6
05/02/2013	4	17.3 (63.1)	87	5	15 (59.0)	90.9	10	14.2 (57.6)	93
14/03/2013	2	13.4 (56.1)	89.3	9	12.6 (54.7)	93.9	5	12.2 (54.0)	95
09/04/2013	4	26.2 (79.2)	89.3	10	25.1 (77.2)	94.7	9	24.8 (76.6)	92.8
14/05/2013	10	24.6 (76.3)	90.5	3	23.7 (74.7)	92.5	9	23.3 (73.9)	94.4

Table 16. Relative humidity and temperature measurements – 5th Span South Arch, East Top.

	Depth: 25 mm (1 in.)			Depth: 50 mm (2 in.)			Depth: 75 mm (3 in.)		
Date	**Probe**	**°C (°F)**	**RH%**	**Probe**	**°C (°F)**	**RH%**	**Probe**	**°C (°F)**	**RH%**
15/02/2011	6	26.3 (79.3)	93.5	8	26.2 (79.2)	90.3	1	26.1 (79.0)	94.9
07/04/2011	7	31.1 (88.0)	94.1	2	30.6 (87.1)	93.1	8	31.1 (88.0)	93.6
05/05/2011	3	32.7 (90.9)	95.2	7	32.9 (91.2)	93.9	3	33.3 (91.9)	96.8
03/06/2011	1	47.9 (118.2)	97	9	48.3 (118.9)	92	9	48.8 (119.8)	90.9
07/07/2011	6	41.5 (106.7)	96.1	2	43 (109.4)	92.1	1	42.6 (108.7)	94.8
10/08/2011	5	39.2 (102.6)	95.3	5	42.2 (108.0)	94.1	10	42.1 (107.8)	93.1
15/09/2011	1	30.1 (86.2)		3	30 (86.0)	95.4	6	30 (86.0)	95.9
18/10/2011	6	33.4 (92.1)	93.5	4	33.2 (91.8)	92.3	5	33.4 (92.1)	85.7
08/11/2011	7	27.9 (82.2)	93.1	7	28 (82.4)	92.6	1	28.2 (82.8)	93.2
14/12/2011	1	20 (68.0)	89.6	5	18.6 (65.5)	89.9	4	19.3 (66.7)	88.6
31/01/2012	2	22.2 (72.0)	88.1	2	20.1 (68.2)	92.4	7	20.1 (68.2)	92.1
08/03/2012	6	27.7 (81.9)	93.3	2	26.9 (80.4)	92.8	4	27.3 (81.1)	92.2
12/04/2012	6	29.2 (84.6)	95	5	30.4 (86.7)	92.1	4	30.7 (87.3)	89.5
17/05/2012	1	36.2 (97.2)	93.6	3	36.9 (98.4)	88.2	4	37 (98.6)	85.9
08/06/2012	2	32.7 (90.9)	95.2	6	33.9 (93.0)	90.3	5	33.4 (92.1)	90.4
16/07/2012	2	45.1 (113.2)	95.3	9	45.4 (113.7)	87.9	6	45 (113.0)	89.3
13/08/2012	5	37.9 (100.2)	94.1	1	38.9 (102.0)	93.6	4	38.8 (101.8)	87.2
13/09/2012	9	33.2 (91.8)	94.8	2	33.2 (91.8)	90.3	7	33.2 (91.8)	87
14/10/2012	3	31.8 (89.2)	90	9	31.8 (89.2)	89.4	7	31.5 (88.7)	85.4
19/11/2012	4	19.3 (66.7)	88.5	5	17.1 (62.8)	92.1	6	17 (62.6)	92
06/12/2012	UT 7	25.4 (77.7)	92.2	UT 9	25.6 (78.1)	92.1	UT 3	25.7 (78.3)	90
08/01/2013	10	16 (60.8)	93.4	1	15 (59.0)	91.9	3	14.9 (58.8)	91.9
05/02/2013	4	21.2 (70.2)	92.7	5	20.3 (68.5)	92	6	20.3 (68.5)	92.5
14/03/2013	6	22.1 (71.8)		1	23.1 (73.6)	91.5	3	23.8 (74.8)	91.3
09/04/2013	2	35.2 (95.4)	92.4	3	36.6 (97.9)	84.7	5	36.2 (97.2)	84.8
14/05/2013	7	34 (93.2)	92.8	2	35 (95.0)	88.8	6	35.1 (95.2)	84.7

Table 17. Relative humidity and temperature measurements – 5th Span North Arch, West Bottom.

Date	Depth: 25 mm (1 in.)			Depth: 50 mm (2 in.)			Depth: 75 mm (3 in.)		
	Probe	°C (°F)	RH%	Probe	°C (°F)	RH%	Probe	°C (°F)	RH%
15/02/2011	4	15.1 (59.2)	76.2	5	13.2 (55.8)	74.3	9	12.6 (54.7)	68.5
07/04/2011	4	20 (68.0)	73.2	5	18.5 (65.3)	76.7	3	18.2 (64.8)	75.7
05/05/2011	9	17.8 (64.0)	68.7	5	17.2 (63.0)	69.3	10	17 (62.6)	70.6
03/06/2011	5	32.7 (90.9)	73.1	3	32.5 (90.5)	75.3	8	32.2 (90.0)	76.3
07/07/2011	8	30.5 (86.9)	71.8	4	30.4 (86.7)	74.4	5	30.3 (86.5)	75.6
10/08/2011	2	26.9 (80.4)	70.7	3	26.6 (79.9)	74	4	26.5 (79.7)	74.8
15/09/2011	1	26.3 (79.3)	69.6	2	26.8 (80.2)	71.7	8	26.9 (80.4)	73.7
18/10/2011	1	24.1 (75.4)	61.4	8	22.7 (72.9)	66.5	7	22.2 (72.0)	66.8
08/11/2011	3	21.5 (70.7)	61.2	9	20.4 (68.7)	67.5	8	20.1 (68.2)	68.2
14/12/2011	3	14.8 (58.6)	60.2	8	13.2 (55.8)	65.7	7	12.3 (54.1)	65.4
31/01/2012	8	14.2 (57.6)	77.9	4	11.6 (52.9)	79	6	10.6 (51.1)	66.1
08/03/2012	9	22.1 (71.8)	81.6	4	20.7 (69.3)	82.5	10	20 (68.0)	74.5
12/04/2012	3	16.2 (61.2)	72.9	6	16.1 (61.0)	80.3	10	16 (60.8)	66.4
17/05/2012	4	29.2 (84.6)	70.4	5	28.2 (82.8)	78.4	1	27.9 (82.2)	72.7
08/06/2012	10	28.6 (83.5)	82.7	1	27.8 (82.0)	78	7	27.4 (81.3)	
16/07/2012	1	34.5 (94.1)	71.2	3	33.8 (92.8)	76.4	4	33.4 (92.1)	75.8
13/08/2012	9	30.5 (86.9)	75.5	3	30 (86.0)	80.7	2	29.5 (85.1)	80.8
13/09/2012	4	26.8 (80.2)	81.5	1	26.4 (79.5)	79.5	3	26.3 (79.3)	87.9
14/10/2012	4	24.4 (75.9)	78.3	1	23.8 (74.8)	77.2	6	23.6 (74.5)	81.2
19/11/2012	9	13.9 (57.0)	76.7	10	12.2 (54.0)	80.4	1	11.6 (52.9)	78.3
06/12/2012	UT 2.3	21.7 (71.1)	66.7	UT 2.4	21.5 (70.7)	72.1	UT 2.2	19.8 (67.6)	70.7
08/01/2013	9	12.9 (55.2)	76.4	5	10.7 (51.3)	77.7	6	10 (50.0)	77.3
05/02/2013	7	16 (60.8)	80.7	3	13.8 (56.8)	87.2	9	12.9 (55.2)	74.3
14/03/2013	3	13.7 (56.7)	80.7	6	12.3 (54.1)	78.4	5	11.7 (53.1)	86.3
09/04/2013	3	26.8 (80.2)	62.7	7	25.3 (77.5)	70.1	2	24.8 (76.6)	72.7
14/05/2013	5	24.6 (76.3)	79.2	1	23.4 (74.1)	74.3	4	22.9 (73.2)	80.4

Table 18. Relative humidity and temperature measurements – 5th Span South Arch, West Top.

	Depth: 25 mm (1 in.)			Depth: 50 mm (2 in.)			Depth: 75 mm (3 in.)		
Date	**Probe**	**°C (°F)**	**RH%**	**Probe**	**°C (°F)**	**RH%**	**Probe**	**°C (°F)**	**RH%**
15/02/2011	3	21.8 (71.2)	89.1	3	18.7 (65.7)	88.1	2	16.9 (62.4)	90.1
07/04/2011	8	24.5 (76.1)	91.7	10	21.3 (70.3)	94	10	23.4 (74.1)	90.8
05/05/2011	5	26.3 (79.3)	96.3	10	25.8 (78.4)	91.3	9	25.1 (77.2)	88.7
03/06/2011	4	42.1 (107.8)	95.1	4	38.7 (101.7)	91.9	2	37.8 (100.0)	91.6
07/07/2011	9	33.3 (91.9)	92.3	6	31.9 (89.4)	90.9	6	33.2 (91.8)	91.7
10/08/2011	10	30 (86.0)	91.1	6	28.4 (83.1)	90.4	6	29.4 (84.9)	91.6
15/09/2011	5	28 (82.4)	93.2	3	28.9 (84.0)	93.5	4	29.1 (84.4)	93.1
18/10/2011	2	29.1 (84.4)	88.1	10	25.6 (78.1)	91.2	3	34.2 (93.6)	89.8
08/11/2011	6	27.6 (81.7)	87.5	7	23 (73.4)	89.8	1	22.3 (72.1)	89.6
14/12/2011	9	20.2 (68.4)	88.7	3	17.8 (64.0)	89.8	8	17.1 (62.8)	90.2
31/01/2012	3	18.4 (65.1)	87.5	9	15.8 (60.4)	90.5	7	14.6 (58.3)	90.8
08/03/2012	1	25.5 (77.9)	91.8	4	24.6 (76.3)	90.7	10	24.1 (75.4)	91.7
12/04/2012	2	23.8 (74.8)	93.7	7	23.7 (74.7)	89.2	1	23 (73.4)	87.6
17/05/2012	2	31.8 (89.2)	86.9	7	29.6 (85.3)	88	9	29 (84.2)	89
08/06/2012	7	28.5 (83.3)	89.3	10	27.7 (81.9)	90.1	1	27.4 (81.3)	90.3
16/07/2012	1	39 (102.2)	89.9	4	37.1 (98.8)	88.4	3	36.2 (97.2)	88.8
13/08/2012	10	34.3 (93.7)	88.3	6	32 (89.6)	89.4	7	31.1 (88.0)	87.3
13/09/2012	5	30.4 (86.7)	90.2	10	29.4 (84.9)	90.2	6	29 (84.2)	91
14/10/2012	6	26.7 (80.1)	91	1	25.4 (77.7)	91	4	24.4 (75.9)	93
19/11/2012	1	14.7 (58.5)	87.8	10	13 (55.4)	91.7	9	12.5 (54.5)	92.5
06/12/2012	6	23.6 (74.5)	89.2	5	22.3 (72.1)	91.5	7	21.4 (70.5)	85.2
08/01/2013	6	13.3 (55.9)	89.8	5	11.4 (52.5)	91.4	9	10.8 (51.4)	92.5
05/02/2013	3	17.8 (64.0)	86.9	7	15 (59.0)	85.5	9	14.1 (57.4)	91.2
14/03/2013	10	16.7 (62.1)	88.8	4	13.7 (56.7)	91.2	7	12.1 (53.8)	84.5
09/04/2013	9	30.3 (86.5)	88.9	10	28.3 (82.9)	90.2	4	27.4 (81.3)	88.1
14/05/2013	4	27.5 (81.5)	89.9	1	25.9 (78.6)	88.7	5	25.1 (77.2)	87.6

Table 19. Relative humidity and temperature measurements – 5th Span South Arch, East Bottom.

	Depth: 25 mm (1 in.)			Depth: 50 mm (2 in.)			Depth: 75 mm (3 in.)		
Date	**Probe**	**°C (°F)**	**RH%**	**Probe**	**°C (°F)**	**RH%**	**Probe**	**°C (°F)**	**RH%**
15/02/2011	7	16 (60.8)	87.1	8	14.4 (57.9)	92.3	10	13.7 (56.7)	97
07/04/2011	5	19.1 (66.4)	91.5	9	18.2 (64.8)	95	4	17.8 (64.0)	95.7
05/05/2011	2	18 (64.4)	93.2	6	17.6 (63.7)	93.3	3	17.3 (63.1)	96.4
03/06/2011	6	32.8 (91.0)	88.3	7	32.4 (90.3)	92.4	10	32.2 (90.0)	93.7
07/07/2011	10	30.1 (86.2)	92.5	3	30.3 (86.5)	94.3	7	30.1 (86.2)	93.4
10/08/2011	5	27.1 (80.8)	93.2	1	27 (80.6)	93.6	7	26.9 (80.4)	95
15/09/2011	10	26.1 (79.0)	94.2	9	26.9 (80.4)	94	7	27.1 (80.8)	93.4
18/10/2011	4	24.9 (76.8)	87.7	6	24 (75.2)	91.6	5	23.4 (74.1)	89
08/11/2011	10	21.7 (71.1)	88.1	4	20.9 (69.6)	90.7	5	20.5 (68.9)	90.1
14/12/2011	10	15.5 (59.9)	87.9	9	16 (60.8)	90.5	5	15.2 (59.4)	90.4
31/01/2012	10	14.4 (57.9)	85.3	2	12.5 (54.5)	89.1	1	11.5 (52.7)	91.7
08/03/2012	9	21 (69.8)	88.8	10	20 (68.0)	92	6	19.6 (67.3)	92.5
12/04/2012	2	16.4 (61.5)	91.5	7	16.9 (62.4)	93.1	1	17 (62.6)	93.8
17/05/2012	2	29.1 (84.4)	87.8	7	28.4 (83.1)	90.7	6	28.1 (82.6)	91.2
08/06/2012	2	29 (84.2)	88.2	5	28.3 (82.9)	93.1	4	27.9 (82.2)	91.2
16/07/2012	4	34.3 (93.7)	90.2	1	34 (93.2)	92.2	3	33.9 (93.0)	90.5
13/08/2012	4	30.5 (86.9)	90.9	5	29.9 (85.8)	92.3	1	29.7 (85.5)	91.5
13/09/2012	9	27.1 (80.8)	91.7	2	26.7 (80.1)	91.8	7	26.4 (79.5)	91.3
14/10/2012	6	26.1 (79.0)	91.6	1	25.6 (78.1)	93.4	4	24.4 (75.9)	93
19/11/2012	1	15.4 (59.7)	87.6	10	14 (57.2)	93	9	13.4 (56.1)	92.4
06/12/2012	UT 2.6	22.4 (72.3)	89.4	UT 2.1	22.3 (72.1)	92.2	UT 2.5	20.8 (69.4)	90.9
08/01/2013	6	13.6 (56.5)	88.5	1	12.3 (54.1)	91.9	5	11.3 (52.3)	92
05/02/2013	9	15.8 (60.4)	86.8	3	13.9 (57.0)	91.7	7	12.9 (55.2)	88.4
14/03/2013	1	14 (57.2)	88.8	9	13.1 (55.6)	92.4	2	12.6 (54.7)	88.6
09/04/2013	1	26.9 (80.4)	88.1	6	25.8 (78.4)	89.7	5	25.1 (77.2)	89.6
14/05/2013	1	23.9 (75.0)	88.7	4	22.9 (73.2)	91	5	22.2 (72.0)	90.5

Table 20. Relative humidity and temperature measurements – 5th Span South Arch, East Top.

	Depth: 25 mm (1 in.)			Depth: 50 mm (2 in.)			Depth: 75 mm (3 in.)		
Date	**Probe**	**°C (°F)**	**RH%**	**Probe**	**°C (°F)**	**RH%**	**Probe**	**°C (°F)**	**RH%**
15/02/2011	5	25 (77.0)	97.7	2	25.4 (77.7)	95	4	24 (75.2)	89.6
07/04/2011	6	25.9 (78.6)	95.8	1	25.8 (78.4)	92.9	2	24.1 (75.4)	88
05/05/2011	8	28.1 (82.6)	97.8	8	27.9 (82.2)	95.9	7	27.3 (81.1)	91.2
03/06/2011	8	43.9 (111.0)	95.8	3	45.4 (113.7)	91.7	2	44.9 (112.8)	84.8
07/07/2011	9	37.1 (98.8)	93.5	2	38.4 (101.1)	92.1	1	37.4 (99.3)	86.7
10/08/2011	7	34.7 (94.5)	93.3	10	34.5 (94.1)	91.7	5	33.5 (92.3)	90.4
15/09/2011	6	29.4 (84.9)		6	29.8 (85.6)	93.7	4	29.7 (85.5)	92.7
18/10/2011	3	33.1 (91.6)	91	9	32.5 (90.5)	92	10	32.8 (91.0)	89
08/11/2011	2	28 (82.4)	92.7	1	27.9 (82.2)	91.7	7	27.7 (81.9)	83.2
14/12/2011	6	22.2 (72.0)	89.4	7	21 (69.8)	91.1	10	21.3 (70.3)	81.6
31/01/2012	5	17.2 (63.0)	90.2	7	16.4 (61.5)	84.2	5	17.5 (63.5)	89.7
08/03/2012	5	26.5 (79.7)	92.7	9	26.5 (79.7)	88.4	7	26.3 (79.3)	86.1
12/04/2012	5	26.5 (79.7)	94.7	4	28.6 (83.5)	88.4	9	29.1 (84.4)	79.8
17/05/2012	9	31.8 (89.2)	89.9	7	32.1 (89.8)	85.6	2	31.8 (89.2)	78.8
08/06/2012	7	27.3 (81.1)	89.4	10	28.2 (82.8)	91.4	1	28.1 (82.6)	87.7
16/07/2012	3	38.6 (101.5)	92	4	39.3 (102.7)	88.2	1	39 (102.2)	84.1
13/08/2012	7	32.6 (90.7)	87.8	10	32.9 (91.2)	89.6	6	32.6 (90.7)	85.8
13/09/2012	6	29.8 (85.6)	92.9	10	30.3 (86.5)	89.8	5	30 (86.0)	84.6
14/10/2012	4	25.3 (77.5)	92.2	1	25.9 (78.6)	91.2	6	25.4 (77.7)	93.3
19/11/2012	9	15.1 (59.2)	91.5	10	14.6 (58.3)	90.7	1	14.1 (57.4)	88.7
06/12/2012	4	25.1 (77.2)	92.5	10	24.8 (76.6)	89	2	24.8 (76.6)	88.1
08/01/2013	9	13.6 (56.5)	92.1	5	13.4 (56.1)	91.3	6	12.5 (54.5)	92.6
05/02/2013	9	18.5 (65.3)	91.5	3	18.7 (65.7)	85.2	7	16.9 (62.4)	79.9
14/03/2013	7	15.5 (59.9)	82.6	4	16.8 (62.2)	88.6	10	15.9 (60.6)	93.6
09/04/2013	4	29.8 (85.6)	89.4	10	30.5 (86.9)	87.8	9	29.6 (85.3)	85
14/05/2013	5	27.7 (81.9)	89.9	1	29 (84.2)	90.5	4	29 (84.2)	80.2

Tables 21 to 28 show the expansion data calculated from the DEMEC gauge readings recorded during the period from February 2011 to May 2013. Note that the length-change measurements were corrected to a temperature of 73 °F (23 °C) using the average temperature measured on the same day for all the RH probes at a depth of 3 inches (approximately 8 centimeters) and assuming a coefficient of thermal expansion of 6.95×10^{-6}/°F (typical for Alabama river gravel).

Table 21. Expansion results (%) – 4th Span South Arch, West Side.

Date	AB	SH	SP	BL	BH	TL	TH
17/11/2010			0.000	0.000		0.000	
02/02/2011		0.000	0.009	-0.012	0.000	-0.007	0.000
07/04/2011		0.006	0.012	-0.007	0.000	-0.009	-0.007
05/05/2011		0.011	0.011	0.000	-0.004	0.000	-0.007
03/06/2011		0.002	0.008	-0.006	-0.006	-0.015	-0.028
07/07/2011		0.013	0.018	0.001	-0.001	-0.010	-0.021
10/08/2011		0.018	0.018	-0.007	-0.001	-0.009	-0.017
15/09/2011		0.014	0.021	0.001	0.002	-0.006	-0.011
18/10/2011		-0.008	0.011	-0.006	-0.007	-0.015	-0.011
08/11/2011		0.007	0.020	-0.003	0.001	-0.009	-0.006
14/12/2011		0.010	0.017	-0.004	0.002	-0.010	0.002
31/01/2012		-0.005	0.014	-0.007	0.001	-0.009	0.007
08/03/2012		0.003	0.015	-0.006	0.000	-0.005	-0.005
12/04/2012		-0.012	0.008	-0.006	-0.002	-0.011	-0.003
17/05/2012		-0.001	0.012	-0.009	-0.003	-0.005	-0.012
08/06/2012		0.004	0.016	-0.003	-0.002	-0.005	-0.010
16/07/2012		-0.007	0.020	-0.015	-0.012	-0.002	-0.001
13/08/2012		-0.003	0.014	-0.011	-0.010	-0.010	0.004
13/09/2012		-0.006	0.018	-0.011	-0.012	-0.008	0.004
14/10/2012		-0.004	0.018	-0.008	-0.009	-0.009	0.006
19/11/2012		-0.010	0.019	-0.010	-0.005	-0.005	0.008
06/12/2012		-0.006	0.019	-0.014	-0.005	-0.011	0.002
08/01/2013		-0.006	0.021	-0.009	0.002	-0.006	0.006
05/02/2013		-0.008	0.022	-0.016	-0.005	-0.010	0.000
14/03/2013		-0.011	0.019	-0.015	-0.006	-0.010	0.009
09/04/2013		-0.014	0.012	-0.019	-0.010	-0.009	0.005
14/05/2013		-0.018	0.010	-0.018	-0.011	-0.013	0.003

Table 22. Expansion results (%) – 4th Span South Arch, East Side.

Months	AB	SH	SP	BL	BH	TL	TH
17/11/2010	0.000			0.000	0.000	0.000	0.000
02/02/2011	0.003			-0.003	-0.005	-0.017	-0.017
07/04/2011	0.004			-0.003	-0.004	-0.022	-0.012
05/05/2011	0.006			-0.006	-0.009	-0.021	-0.012
03/06/2011	-0.001			-0.005	-0.010	-0.027	-0.020
07/07/2011	0.003			0.001	-0.003	-0.027	-0.016
10/08/2011	0.001			0.000	-0.003	-0.035	-0.017
15/09/2011	0.006			0.007	0.003	-0.035	-0.015
18/10/2011	0.006			-0.004	-0.007	-0.033	-0.012
08/11/2011	0.013			-0.002	-0.003	-0.028	-0.011
14/12/2011	0.010			-0.003	-0.002	-0.031	-0.011
31/01/2012	0.010			-0.004	-0.005	-0.033	-0.008
08/03/2012	0.014			-0.004	-0.005	-0.033	-0.011
12/04/2012	0.013			-0.004	-0.004	-0.030	-0.011
17/05/2012	0.012			-0.004	-0.005	-0.031	-0.009
08/06/2012	0.009			0.001	-0.001	-0.036	-0.015
16/07/2012	0.012			-0.004	-0.009	-0.028	-0.012
13/08/2012	0.007			-0.005	-0.006	-0.035	-0.015
13/09/2012	0.007			-0.004	-0.005	-0.040	-0.018
14/10/2012	0.008			-0.001	-0.004	-0.037	-0.016
19/11/2012	0.013			-0.002	-0.001	-0.033	-0.015
06/12/2012	0.012			-0.005	-0.007	-0.034	-0.014
08/01/2013	0.014			-0.002	0.000	-0.039	-0.013
05/02/2013	0.018			-0.008	-0.006	-0.038	-0.015
14/03/2013	0.024			-0.010	-0.006	-0.027	-0.009
09/04/2013	0.015			-0.008	-0.008	-0.035	-0.013
14/05/2013	0.012			-0.009	-0.008	-0.035	-0.014

Table 23. Expansion results (%) – 4th Span North Arch, West Side.

Date	AB	SH	SP	BL	BH	TL	TH
17/11/2010	0.000	0.000		0.000	0.000		0.000
02/02/2011	-0.015	-0.017		-0.007	-0.008		-0.008
07/04/2011	-0.018	-0.016		-0.003	-0.005		-0.011
05/05/2011	-0.020	-0.016		-0.005	-0.008		-0.012
03/06/2011	-0.021	-0.015		-0.003	-0.009		-0.013
07/07/2011	-0.016	-0.010		0.003	-0.001		-0.009
10/08/2011	-0.017	-0.015		0.003	-0.002		-0.011
15/09/2011	-0.012	-0.010		0.007	0.001		-0.005
18/10/2011	-0.018	-0.019		-0.002	-0.005		-0.013
08/11/2011	-0.013	-0.015		-0.001	-0.004		-0.008
14/12/2011	-0.016	-0.019		-0.002	-0.003		-0.011
31/01/2012	-0.014	-0.018		-0.002	-0.004		-0.007
08/03/2012	-0.014	-0.016		-0.003	-0.006		-0.009
12/04/2012	-0.016	-0.017		-0.002	-0.004		-0.010
17/05/2012	-0.016	-0.014		0.000	-0.003		-0.010
08/06/2012	-0.013	-0.011		0.002	-0.001		-0.008
16/07/2012	-0.022	-0.020		-0.009	-0.006		-0.011
13/08/2012	-0.020	-0.019		-0.003	-0.005		-0.010
13/09/2012	-0.017	-0.019		-0.004	-0.008		-0.008
14/10/2012	-0.015	-0.018		0.003	-0.001		-0.009
19/11/2012	-0.013	-0.014		0.000	-0.001		-0.006
06/12/2012	-0.015	-0.016		-0.003	-0.004		-0.011
08/01/2013	-0.014	-0.020		-0.003	-0.002		-0.008
05/02/2013	-0.013	-0.021		-0.006	-0.005		-0.007
14/03/2013	-0.014	-0.022		-0.004	-0.002		-0.010
09/04/2013	-0.015	-0.020		-0.007	-0.008		-0.009
14/05/2013	-0.018	-0.019		-0.007	-0.007		-0.010

Table 24. Expansion results (%) – 4th Span North Arch, East Side.

Date	AB	SH	SP	BL	BH	TL	TH
17/11/2010		0.000		0.000	0.000	0.000	0.000
02/02/2011		0.000		-0.021	-0.009	-0.016	-0.004
07/04/2011		0.003		-0.019	-0.006	-0.022	-0.011
05/05/2011		0.000		-0.019	-0.011	-0.020	-0.011
03/06/2011		-0.003		-0.014	-0.011	-0.025	-0.032
07/07/2011		0.004		-0.005	-0.003	-0.018	-0.025
10/08/2011		0.000		-0.007	-0.003	-0.020	-0.019
15/09/2011		0.003		-0.005	0.000	-0.022	-0.015
18/10/2011		0.000		-0.019	-0.007	-0.015	-0.014
08/11/2011		0.001		-0.021	-0.005	-0.018	-0.010
14/12/2011		0.002		-0.023	-0.006	-0.011	-0.001
31/01/2012		0.002		-0.009	-0.006	-0.016	0.003
08/03/2012		0.004		-0.009	-0.010	-0.014	-0.009
12/04/2012		0.000		-0.008	-0.008	-0.018	-0.007
17/05/2012		0.003		0.004	-0.008	-0.015	-0.018
08/06/2012		-0.001		0.013	-0.004	-0.016	-0.015
16/07/2012		-0.001		0.012	-0.018	-0.020	-0.007
13/08/2012		-0.001		0.007	-0.010	-0.015	0.003
13/09/2012		-0.004		0.006	-0.008	-0.026	0.007
14/10/2012		-0.002		0.012	-0.003	-0.027	0.012
19/11/2012		0.000		0.006	-0.003	-0.022	0.023
06/12/2012		-0.003		0.006	-0.009	-0.020	0.017
08/01/2013		-0.002		-0.004	-0.005	-0.014	0.024
05/02/2013		0.001		-0.018	-0.010	-0.013	0.023
14/03/2013		-0.002		-0.022	-0.009	-0.016	0.028
09/04/2013		0.003		-0.003	-0.012	-0.012	0.020
14/05/2013		-0.003		-0.006	-0.012	-0.016	0.027

Table 25. Expansion results (%) – 5th Span South Arch, West Side.

Date	AB	SH	SP	BL	BH	TL	TH
17/11/2010	0.000		0.000	0.000	0.000	0.000	0.000
02/02/2011	-0.004		-0.021	-0.011	0.000	-0.005	-0.012
07/04/2011	-0.004		-0.016	-0.005	0.010	-0.006	-0.015
05/05/2011	-0.006		-0.018	-0.003	0.009	-0.004	-0.018
03/06/2011	-0.007		-0.015	-0.003	0.009	-0.003	-0.021
07/07/2011	-0.004		-0.004	0.008	0.021	0.000	-0.015
10/08/2011	-0.009		-0.005	0.008	0.018	-0.001	-0.016
15/09/2011	-0.003		0.001	0.012	0.026	0.007	-0.009
18/10/2011	-0.005		-0.001	0.002	0.018	-0.002	-0.012
08/11/2011	-0.003		0.002	0.006	0.025	-0.001	-0.010
14/12/2011	-0.008		-0.003	0.009	0.033	-0.003	-0.003
31/01/2012	-0.007		-0.006	0.007	0.039	-0.005	0.005
08/03/2012	-0.004		-0.009	0.009	0.042	-0.007	0.003
12/04/2012	-0.008		-0.019	0.016	0.047	-0.004	0.006
17/05/2012	-0.006		-0.018	0.020	0.050	0.000	0.006
08/06/2012	-0.004		-0.013	0.026	0.055	0.005	0.005
16/07/2012	-0.005		-0.018	0.019	0.046	0.005	0.005
13/08/2012	-0.007		-0.014	0.025	0.051	-0.001	0.005
13/09/2012	-0.002		-0.008	0.025	0.051	-0.002	0.007
14/10/2012	-0.008		-0.010	0.034	0.059	-0.003	0.008
19/11/2012	-0.008		-0.010	0.035	0.064	0.001	0.015
06/12/2012	-0.009		-0.007	0.033	0.066	-0.004	0.013
08/01/2013	-0.007		-0.010	0.032	0.068	-0.004	0.020
05/02/2013	-0.009		-0.011	0.029	0.069	-0.007	0.018
14/03/2013	-0.010		-0.015	0.041	0.080	0.000	0.026
09/04/2013	-0.006		-0.019	0.030	0.074	-0.006	0.020
14/05/2013	-0.009		-0.018	0.042	0.085	-0.008	0.022

Table 26. Expansion results (%) – 5th Span South Arch, East Side.

Date	AB	SH	SP	BL	BH	TL	TH
17/11/2010	0.000	0.000	0.000	0.000	0.000	0.000	0.000
02/02/2011	-0.014	-0.002	0.000	0.000	0.002	-0.006	-0.015
07/04/2011	-0.011	-0.001	-0.001	0.002	0.005	-0.001	-0.012
05/05/2011	-0.009	-0.002	-0.006	-0.004	0.001	0.001	-0.008
03/06/2011	-0.013	-0.006	-0.012	-0.008	-0.004	-0.005	-0.011
07/07/2011	-0.013	-0.002	-0.005	0.000	0.006	-0.007	-0.015
10/08/2011	-0.016	-0.002	-0.004	0.000	0.005	-0.008	-0.015
15/09/2011	-0.011	0.003	0.002	0.008	0.011	-0.002	-0.010
18/10/2011	-0.009	0.002	0.003	-0.001	0.004	0.002	-0.006
08/11/2011	-0.009	0.005	0.003	0.003	0.008	0.003	-0.006
14/12/2011	-0.010	0.005	0.009	0.010	0.013	0.006	-0.007
31/01/2012	-0.015	0.006	0.013	0.012	0.016	0.009	-0.003
08/03/2012	-0.010	0.006	0.011	0.008	0.015	0.012	-0.006
12/04/2012	-0.009	0.006	0.006	0.008	0.013	0.014	0.000
17/05/2012	-0.010	0.006	0.004	0.008	0.013	0.012	-0.004
08/06/2012	-0.011	0.007	0.006	0.009	0.016	0.010	-0.005
16/07/2012	-0.010	0.001	-0.001	-0.003	0.006	0.012	-0.004
13/08/2012	-0.017	0.003	0.002	0.007	0.013	0.008	-0.008
13/09/2012	-0.016	0.006	0.014	0.004	0.013	0.010	-0.006
14/10/2012	-0.018	0.003	0.011	0.014	0.019	0.008	-0.008
19/11/2012	-0.015	0.012	0.023	0.018	0.024	0.014	-0.004
06/12/2012	-0.016	0.007	0.016	0.012	0.019	0.014	-0.003
08/01/2013	-0.014	0.014	0.025	0.017	0.020	0.018	-0.003
05/02/2013	-0.015	0.012	0.030	0.013	0.019	0.018	-0.001
14/03/2013	-0.010	0.013	0.015	0.020	0.026	0.023	0.004
09/04/2013	-0.011	0.010	0.012	0.012	0.019	0.021	-0.001
14/05/2013	-0.012	0.011	0.011	0.015	0.021	0.017	-0.002

Table 27. Expansion results (%) – 5th Span North Arch, West Side.

Months	AB	SH	SP	BL	BH	TL	TH
17/11/2010	0.000	0.000			0.000	0.000	0.000
02/02/2011	0.002	-0.005			-0.007	0.011	0.001
07/04/2011	0.009	-0.002			-0.008	0.006	0.004
05/05/2011	0.013	-0.002			-0.008	0.011	0.003
03/06/2011	0.015	-0.006			-0.005	0.019	0.002
07/07/2011	0.017	-0.003			0.005	0.017	0.009
10/08/2011	0.015	-0.005			0.003	0.012	0.010
15/09/2011	0.021	-0.001			0.008	0.017	0.017
18/10/2011	0.015	-0.009			-0.003	0.015	0.014
08/11/2011	0.018	-0.003			-0.001	0.015	0.019
14/12/2011	0.011	-0.008			-0.003	0.008	0.022
31/01/2012	0.007	-0.007			-0.006	0.009	0.029
08/03/2012	0.011	-0.008			-0.007	0.011	0.029
12/04/2012	0.015	-0.010			-0.002	0.010	0.033
17/05/2012	0.019	-0.005			0.000	0.012	0.033
08/06/2012	0.025	-0.002			0.003	0.024	0.039
16/07/2012	0.019	-0.009			-0.007	0.024	0.033
13/08/2012	0.016	-0.012			0.000	0.009	0.033
13/09/2012	0.019	-0.009			-0.004	0.017	0.040
14/10/2012	0.021	-0.009			0.008	0.018	0.043
19/11/2012	0.016	-0.011			0.002	0.013	0.047
06/12/2012	0.014	-0.011			-0.004	0.008	0.042
08/01/2013	0.012	-0.009			-0.001	0.009	0.050
05/02/2013	0.011	-0.012			-0.006	0.002	0.047
14/03/2013	0.017	-0.014			0.001	0.008	0.057
09/04/2013	0.022	-0.013			-0.007	0.015	0.053
14/05/2013	0.021	-0.012			-0.002	0.007	0.056

Table 28. Expansion results (%) – 5th Span North Arch, East Side.

Months	AB	SH	SP	BL	BH	TL	TH
17/11/2010	0.000	0.000		0.000	0.000	0.000	0.000
02/02/2011	-0.009	-0.005	0.000	-0.010	-0.009	-0.003	-0.015
07/04/2011	-0.006	0.000	0.006	0.004	0.011	0.009	-0.017
05/05/2011	-0.006	0.003	0.009	0.011	0.009	0.009	-0.019
03/06/2011	-0.008	0.000	0.005	0.014	0.012	0.003	-0.021
07/07/2011	-0.008	0.003	0.009	0.032	0.024	0.001	-0.020
10/08/2011	-0.008	0.006	0.010	0.034	0.025	0.002	-0.018
15/09/2011	-0.003	0.012	0.016	0.044	0.030	0.010	-0.011
18/10/2011	-0.003	0.009	0.008	0.040	0.022	0.017	-0.012
08/11/2011	-0.005	0.013	0.013	0.050	0.030	0.014	-0.012
14/12/2011	-0.005	0.015	0.017	0.058	0.033	0.023	-0.007
31/01/2012	-0.006	0.021	0.022	0.061	0.041	0.027	-0.003
08/03/2012	-0.003	0.022	0.025	0.064	0.043	0.030	-0.003
12/04/2012	-0.004	0.028	0.026	0.072	0.044	0.039	-0.001
17/05/2012	-0.005	0.027	0.031	0.078	0.043	0.034	0.001
08/06/2012	-0.002	0.033	0.034	0.082	0.048	0.037	0.005
16/07/2012	-0.003	0.029	0.031	0.079	0.042	0.036	0.006
13/08/2012	-0.010	0.026	0.032	0.085	0.047	0.033	0.003
13/09/2012	-0.007	0.033	0.036	0.088	0.049	0.034	0.004
14/10/2012	-0.007	0.035	0.040	0.103	0.060	0.036	0.006
19/11/2012	-0.012	0.041	0.046	0.112	0.062	0.044	0.009
06/12/2012	-0.006	0.037	0.046	0.114	0.061	0.048	0.010
08/01/2013	-0.007	0.043	0.051	0.121	0.068	0.054	0.015
05/02/2013	-0.006	0.043	0.049	0.117	0.065	0.056	0.012
14/03/2013	-0.004	0.049	0.057	0.133	0.076	0.062	0.018
09/04/2013	-0.020	0.046	0.058	0.123	0.069	0.057	0.018
14/05/2013	-0.008	0.052	0.060	0.132	0.073	0.059	0.018

4.4 DATA ANALYSES

Figures 36 to 39 show the relative humidity data plotted against time for each location. Each relative humidity is the average for the three different depths (one, two, and three inches) at that location. The data were averaged as there was no consistent difference between the RH readings at the different depths for a given location. The ambient RH is a 28-day running average for data obtained from a weather station in Montgomery, AL. These data indicate that the treatment has had little impact on the internal relative humidity of the concrete during the 2.5 years that have elapsed since the treatment was implemented. For the "West Bottom" location the treated north arch of ASR-affected the 5th span has a significantly lower RH than the other arches, but the treated south arch of the same span is the highest. In the three other locations, the RH for the treated arches of the ASR-affected the 5th span is generally higher than or equal to that of the treated or untreated arches of the 4th span. There is no consistent difference in the internal RH for the treated versus untreated arches of the 4th span which does not show signs of ASR.

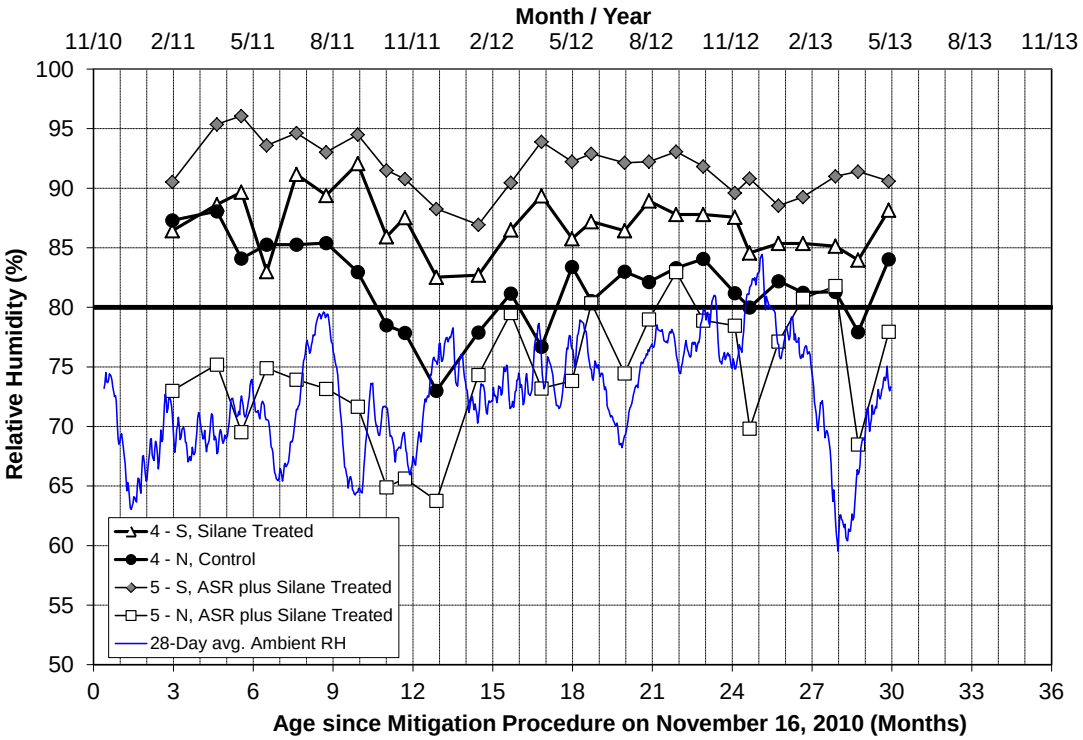

Figure 36. Relative humidity readings (average for 3 depths) for West Bottom location.

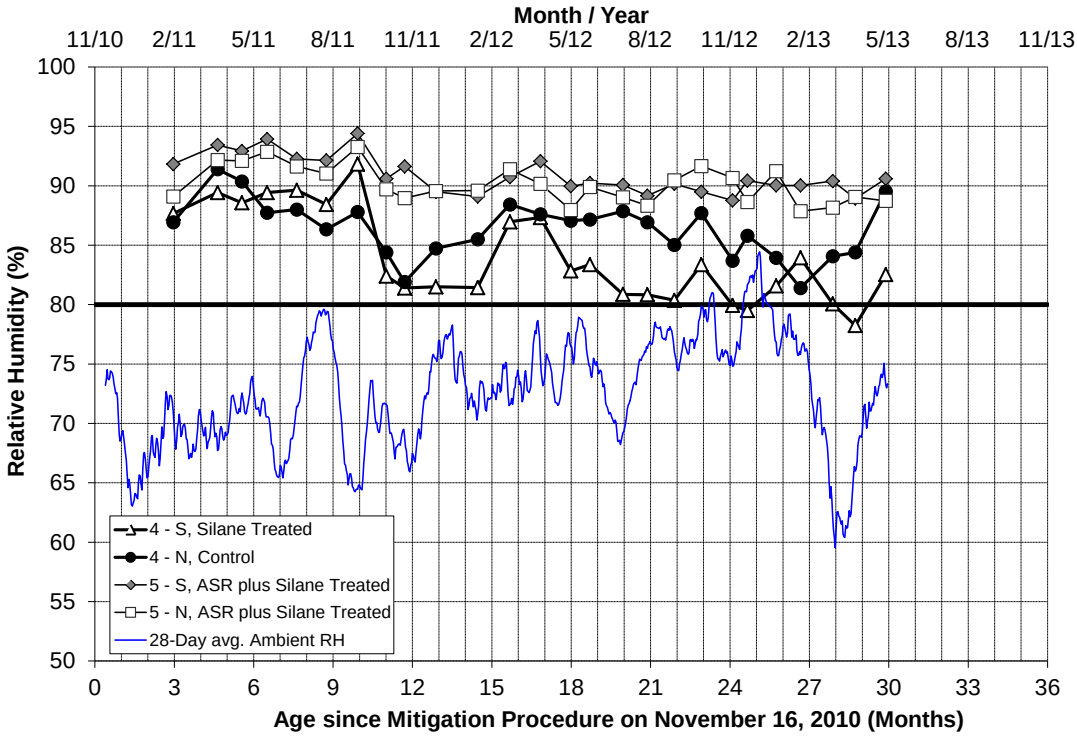

Figure 37. Relative humidity readings (average for 3 depths) for West Top location.

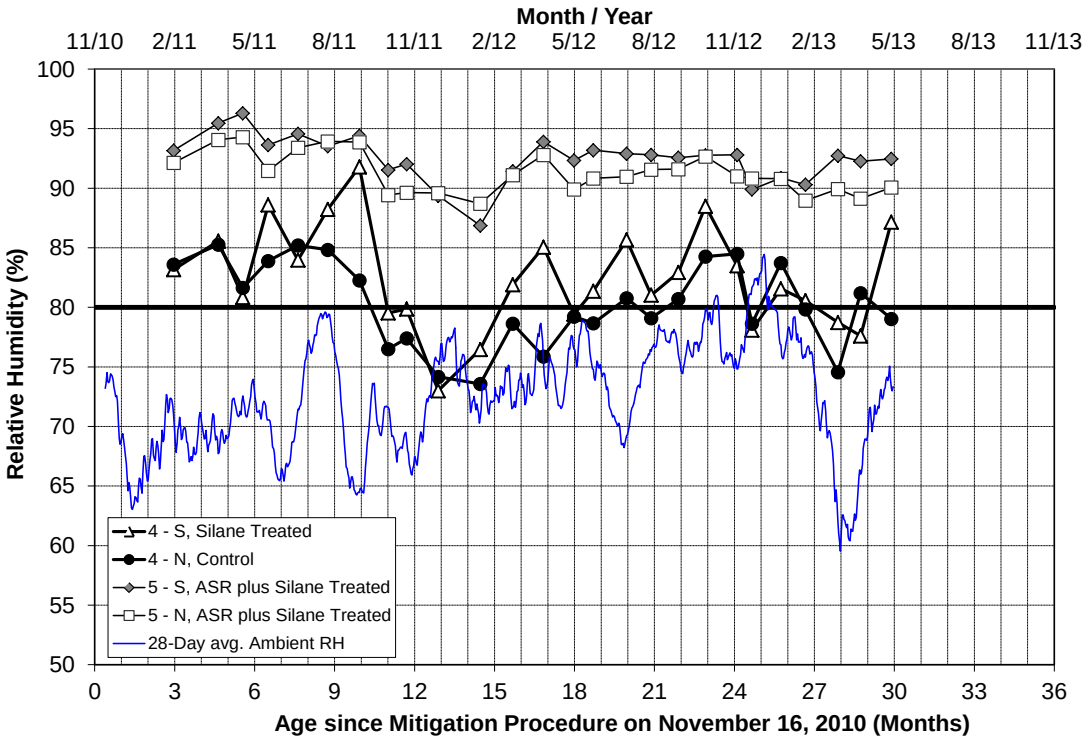

Figure 38. Relative humidity readings (average for 3 depths) for East Bottom location.

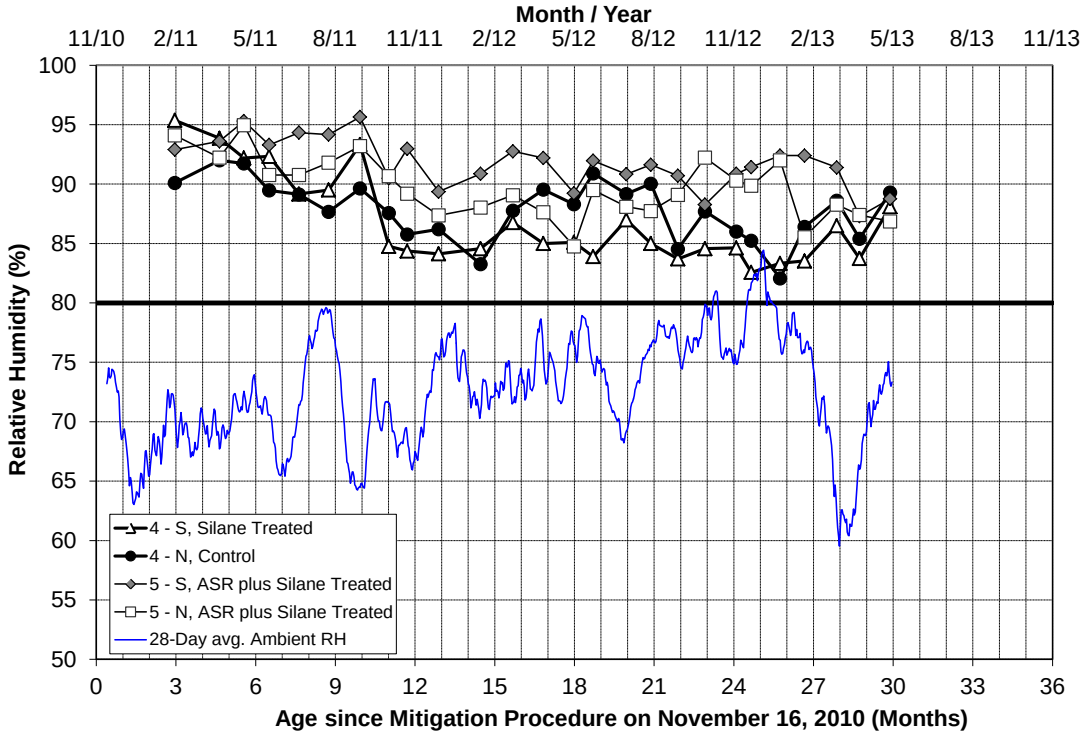

Figure 39. Relative humidity readings (average for 3 depths) for East Top location.

Figures 40 to 42 show the calculated expansion plotted against time for the three locations where data were available since December 2005. The data collected annually at three different times

between 2005 and 2010 were corrected to supplement the data collected monthly since 2010. These data indicate significant expansion of the ASR-affected concrete in the 5th span between 2005 and the time of treatment. Generally, the concrete in this span appears to continue to expand after treatment and the rate does not appear to be significantly affected by the treatment, at least during the 2.5 years that have elapsed since treatment. Additional readings are required to confirm the post-treatment expansion rate. Little significant expansion has been observed before or after treatment for the concrete in the 4th span (unaffected by ASR).

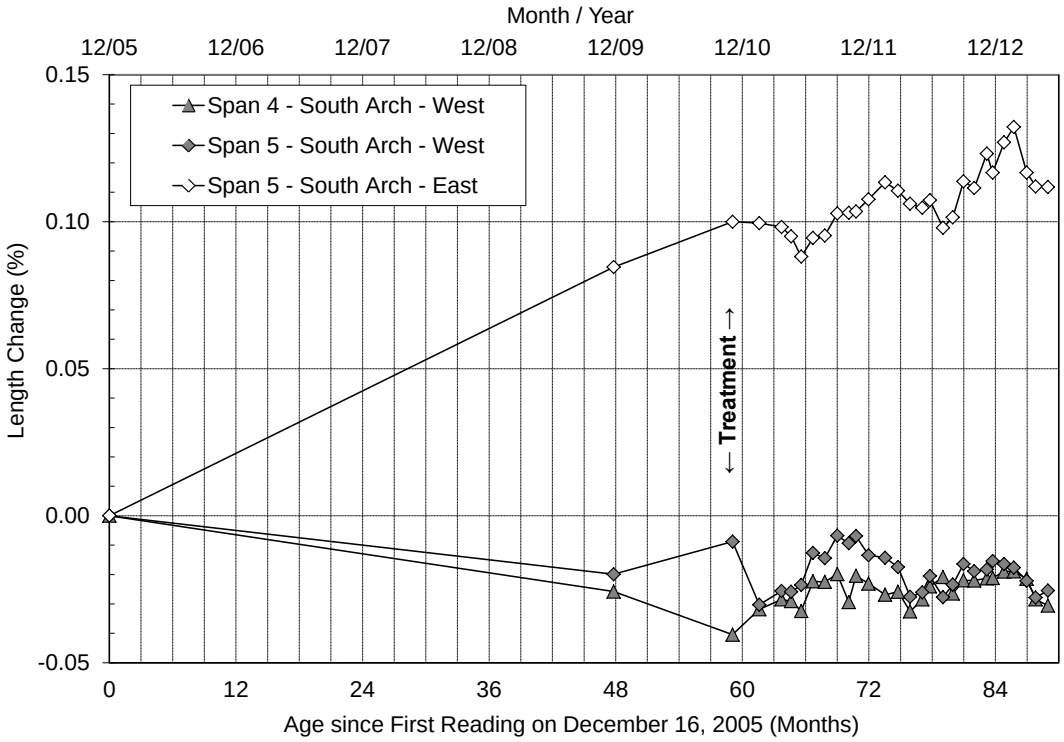

Figure 40. Expansion data for location "Side Perpendicular" (SP).

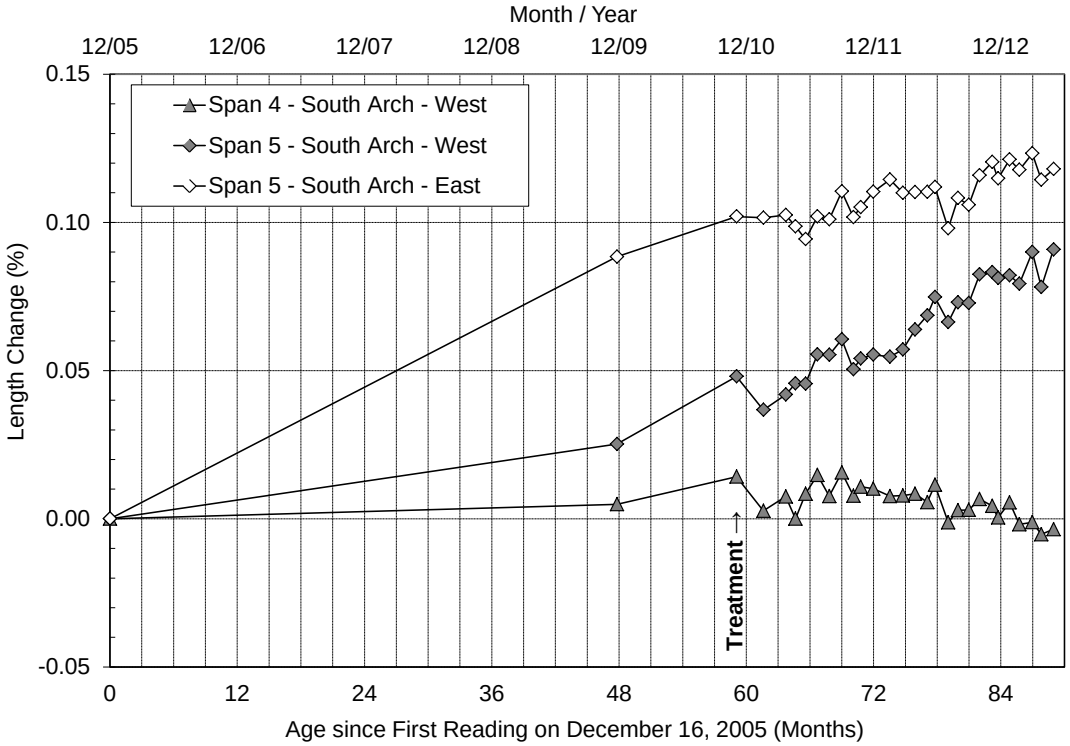

Figure 41. Expansion data for location "Bottom Low" (BL).

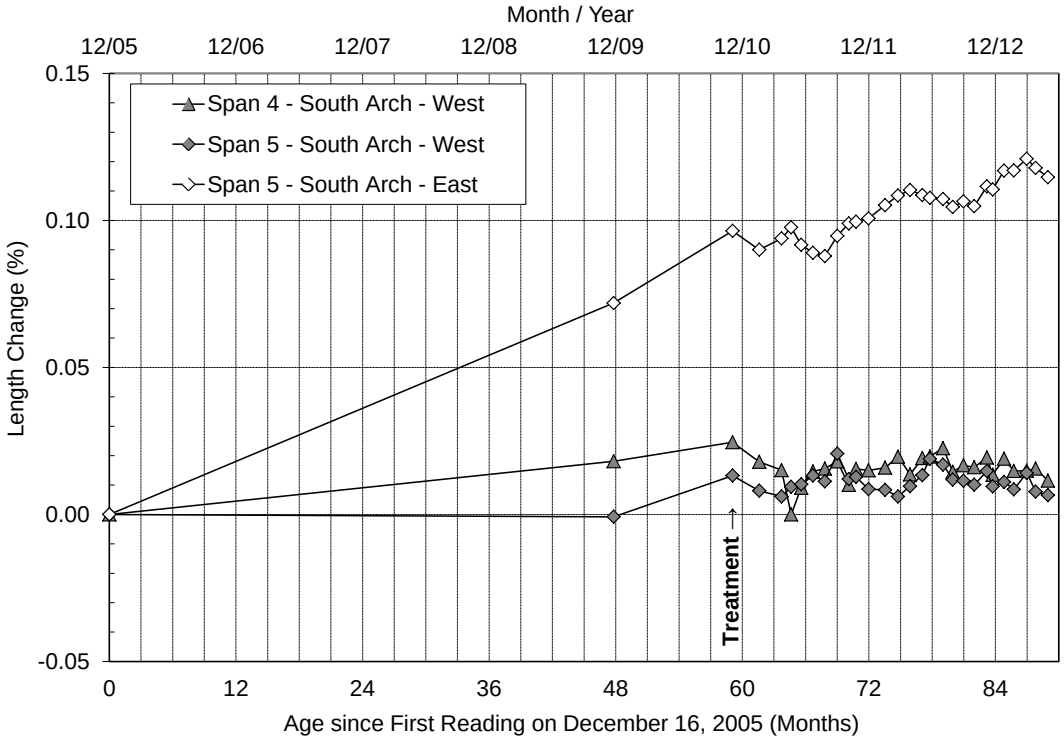

Figure 42. Expansion data for location "Top Low" (TL).

4.5 SUMMARY

The results from field survey and laboratory investigations in 2005 and 2010 confirmed that ASR was a contributing factor in the deterioration of one of the arches at the Bibb Graves Bridge in Wetumpka, AL.

A treatment plan involving a combination of crack-filling, silane (hydrophobic) sealer and epoxy coating was implemented in November 2010. In addition to the above treatment, a performance monitoring plan was also developed and implemented to allow quantifying the effects of the various treatments over time. Specific areas were identified for expansion measurements and temperature/humidity readings.

The relative humidity data indicate that the treatment has not had a significant impact in terms of reducing the internal humidity within the concrete. In addition, expansion data indicate that the ASR-affected concrete arches supporting the 5th span are continuing to expand at most locations where gauge pins have been installed. New cracks have formed and existing cracks have widened since implementation of the treatment. These cracks allow for the ingress of rain water, which maintains a high humidity within the concrete and permits the alkali-silica reaction to continue unabated. Given the rate of expansion of the concrete and appearance of new cracks to provide for moisture ingress, any attempt to dry the concrete would probably require the provision of external cladding over the concrete. Further attempts to "seal" the concrete with coatings are likely to prove to be ineffective.

The ASR damage to the concrete arches is quite advanced and, since the arches are directly exposed to precipitation, attempts to reduce the internal humidity do not appear to have been successful. Successful drying of the concrete arches may be possible by cladding or covering the affected arches to protect them from rainfall. Given the extent of ASR, it is recommended that a structural analysis is conducted to determine the structural adequacy of the affected arches supporting the 5^{th} span. It may be necessary to provide additional shoring (possibly a truss beneath the roadway supported on the existing piers) to support this span.

4.6 REFERENCES

Grattan-Bellew, P.E. 2005. "Petrographic Investigation of Concrete Cores from Arches #3 and #4 of a Bridge in Alabama." Materials & Petrographic Research G-B Inc., 13 p.

5. CONCRETE PAVEMENT, PINE BLUFF, AR

In November 2011, a 19.3 km (12 mi) long section of pavement on I-530 near Pine Bluff, AR was visually inspected to assess whether the observed distress was potentially triggered by ASR. The pavement is a jointed plain concrete pavement (JPCP), with joint spacing of approximately 4.6 m (15.0 ft) and a nominal thickness of 280 mm (11 in.) Distress was quite common in much of the pavement, with a range of distress from minimal to moderate to severe. Figure 43 shows some of the typical features of distress observed in various pavement sections. Evidence was found of map cracking, joint cracking and failure, and efflorescence/gel staining. There was some significant longitudinal cracking in isolated pavement sections, including the left photo in Figure 43; however, it is highly unlikely that this longitudinal cracking was caused by ASR and more likely that the cracking was caused by construction/design factors.

Figure 43. Typical distress observed from visual inspection of pavement.

At the time of this initial site visit and survey, locations were identified for extracting cores for petrographic evaluation. Based on the combined results from this initial site survey and the petrographic evaluation (described in the next section), it was decided to include a subset of this 19.3 km (12 mi) long section of pavement on I-530 near Pine Bluff as a candidate for the FHWA Development and Deployment Program, with focus on the use of silane to attempt to reduce internal relative humidity. Silane has been shown to work well in relatively small elements and/or those elements that can be easily treated, such as highway barriers. It was unknown at the time of this field trial whether topically coating the exposed surface of a concrete pavement would effectively reduce internal relative humidity when moisture is available through the base and subbase for the pavement. This was the only pavement included in the FHWA Development and Deployment Program, but given the limited time available for monitoring within this program, the benefits, if any, of applying silanes to pavements will be realized in the future.

5.1 SUMMARY OF PETROGRAPHIC EVALUATION

A total of five concrete cores extracted from Pine Bluff Bypass concrete pavement in 2011 were evaluated petrographically, and a report was provided to the Arkansas State Highway and Transportation Department (AHTD). The evaluation mainly consisted of the Damage Rating Index (DRI), a method that provides a semi-quantitative assessment of the degree of damage in concrete based on a count of petrographic features of deterioration generally associated with alkali-silica reaction (ASR).

Damage Rating Indices ranging from 254 to 489 were obtained for the cores Ark-1 to Ark-5 (Figure 44), thus suggesting low to moderate degree of deterioration/damage due to ASR. Signs of ASR were found in chert particles of the coarser fraction of the sand in the concrete. Typical petrographic features of ASR correspond to cracking with ASR gel and reaction rims in the chert particles within the fine aggregate portion, as well as cracking in the cement paste with reaction products associated to the reactive chert particles (Figure 45). Tight/closed cracks were observed in several coarse aggregate particles, consisting of granitic gneiss; this cracking is thought to be associated to the aggregate processing operations and not to ASR.

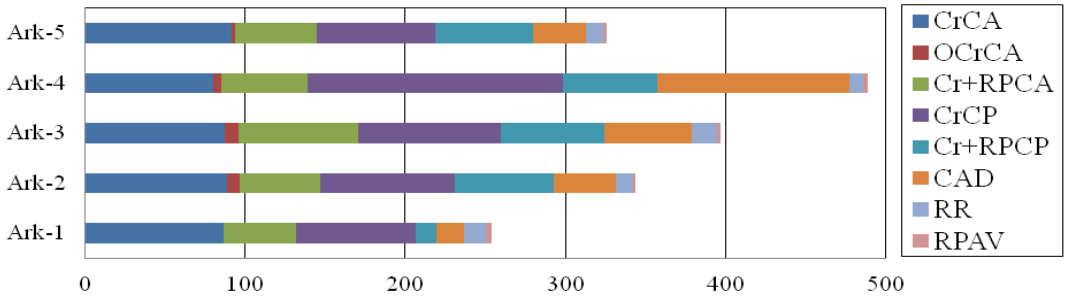

Figure 44. Results of the Damage Rating Index (DRI) for the Arkansas cores. The colored cells give the proportions of each petrographic feature to the DRI value. (CrCA: cracking in the coarse aggregate particles; OCrCa: opened cracking in the coarse aggregate particles; Cr+RPCA: cracking in the coarse aggregate particles + reaction product; CrCP: cracking in the cement paste; Cr+RPCP: cracking in the cement paste + reaction product; CAD: coarse aggregate debonded; RR: reaction rim; RPAV: reaction products in air void of the cement paste).

A

B (distance between vertical lines = 1 cm [0.4 in.])

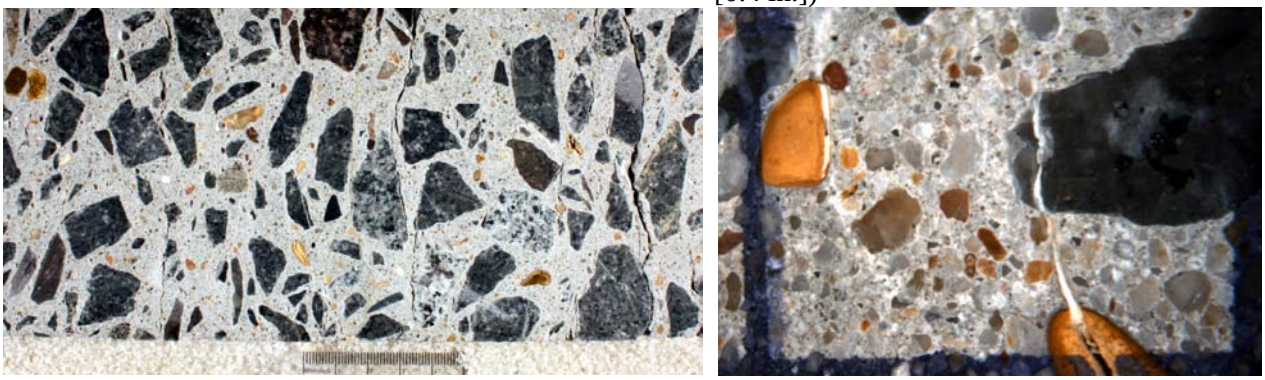

Figure 45. A: Polished core showing macrocracks parallel to the surface. B: Visible cracking and secondary reaction products in cracks of the fine aggregate particles of the cement paste.

5.2 SUMMARY OF APPLICATION REPORT

After determining that ASR was, in fact, the primary cause of distress of the pavement, a field trial was initiated to evaluate the effectiveness of two different silane-based sealers in reducing internal relative humidity and future potential for ASR-induced expansion. A second visual inspection of the entire 19.3 km (12 mi) section of pavement on I-530 near Pine Bluff was performed on May 14, 2012 through the use of a rolling lane closure. The purpose of this scan was to identify continuous sections of pavements that exhibited similar levels of distress (preferably minor and moderate), thereby allowing for an untreated control, plus two silane-treated sections within a region of similar distress. Two sections of pavement, each approximately 549 m (1800 ft) long and northbound, were found to meet this criteria (see Figure 46):

- **Section 1: Mild ASR distress** – This section begins just after mile marker 39 and north of Oakwood Road at mile marker 39.2. A small amount of cracking was seen in the mild section. This cracking was typically observed in or near the wheel paths of the panels. Some shading was noticed at the joints. Overall, however, the 120 panels that make up the mild section showed little to no major distresses within the panels and at the joints.

- **Section 2: Moderate ASR distress** – This section begins just north of the Shannon Petty overpass, which separates the two test sections, and ends just south of the exit to State Highway 190 at mile marker 37. This pavement section also featured edge drains. Significantly more distress was noted in the moderate section. Typical distresses include spalling and cracking at the joints, as well as random cracking and longitudinal cracks in or near the wheel paths.

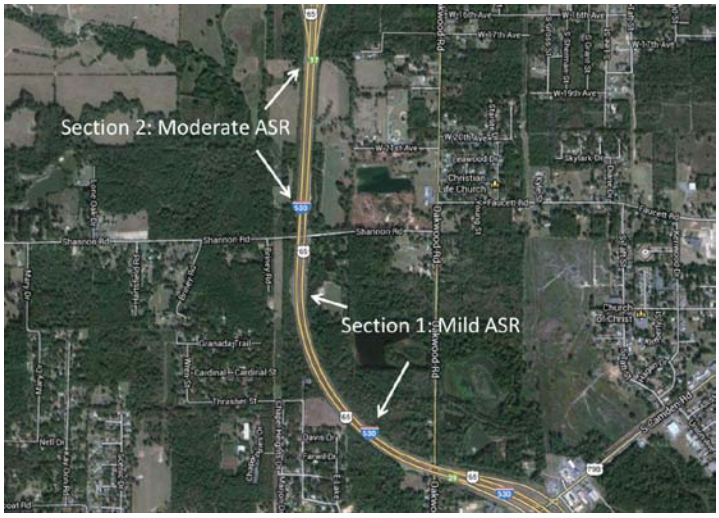

Figure 46. Google map image showing location of the two test sections, separated by the Shannon Petty overpass.

It should be noted that the southbound lanes showed similar distress patterns; however, the northbound lanes were chosen for trial implementation because the cores taken for petrographic analysis were taken from the northbound lanes, and it was also believed that traffic control would be easier and safer for the northbound lanes. It was decided that only the traveling lane (i.e., the

outside lane) in each trial section would be instrumented, measured, and treated with the two silane-based products. There were two primary reasons for this decision. First, only one day was available for the team to instrument the pavement and take initial measurements. Second, lane-closures, required for the safety of the team, would be necessary only for the outside lane, which meant the public could still travel safely and efficiently in the passing lane (i.e., inside lane).

Each trial section consisted of a total of 120 slabs (or panels). The panels were numbered from "1" to "120" in order, starting just after mile marker 39 and heading north. Panel 120 marked the end of the mild section and is located just before the bridge over Shannon-Petty Road. Numbering started again with "1" for the first panel in the moderate section, which is located about 73 m (240 ft) after the terminal joint at the end of the bridge.

For both the mild and moderate sections, panels 1 through 40 served as untreated control sections. Panels 41 through 80 were treated topically with 100 percent silane at an approximate application rate of 3.1 m^2/L (125 ft^2/gal). Panels 81 through 120 were treated topically with 40 percent silane (water-based) at an approximate application rate of 3.1 m^2/L (125 ft^2/gal). Figure 47 shows aerial images (from Google maps) of Test Section 1 (mild ASR) and Test Section 2 (moderate ASR), including the locations of the control and silane-treated sections.

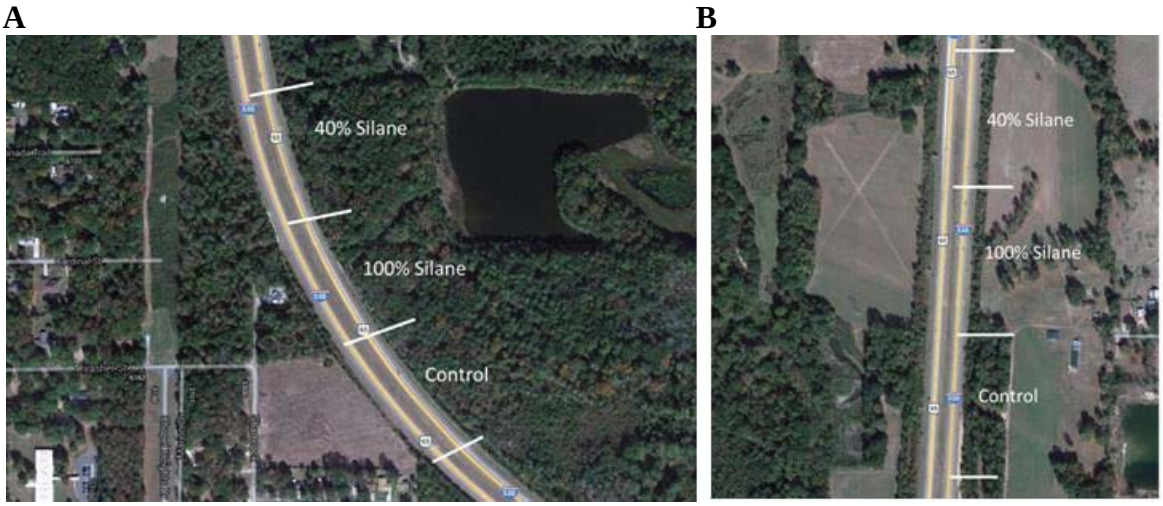

Figure 47. Google map image showing location of the control and silane-treated portions within each of the two test sections. A: Test Section 1 (mild ASR). B: Test Section 2 (moderate ASR).

Within each test section every 10th panel was marked, and panels 10, 20, 30, 50, 60, 70, 90, 100, and 110 were instrumented for expansion measurements, both in the longitudinal and transverse directions (see Figure 48A), and panels 10, 30, 50, 70, and 90 were instrumented for internal concrete temperature and humidity measurements (see Figure 48B). In each of the panels being monitored for internal relative humidity, holes were drilled at varying depths to allow for the measurement of relative humidity 25 mm (1 in.) and 75 mm (3 in.) from the pavement surface.

A B

Figure 48. A: Length change measurements on pavement surface using DEMEC gauge. B: Internal relative humidity and temperature measurements using the Vaisala HM44 humidity measurement system.

The two silane-based products were applied using two truck-mounted tank sprayers, operated by AHTD. Prior to treating the pavement surface, each truck/sprayer was calibrated in order to deliver the target application rate of 3.1 m^2/L (125 ft^2/gal). Figure 49 shows one of the trucks used to apply the silane to the test section.

Figure 49. Photograph of ATHD maintenance truck, equipped with truck-mounted, tank sprayer. The truck/sprayer was pre-calibrated in order to deliver the target application rate of 3.1 m^2/L (125 ft^2/gal).

Figure 50 shows photographs of the pavement sections taken shortly after the application of the two silane products, with the 100 percent silane on the left and the 40 percent silane on the right. The 100 percent silane was applied as a clear liquid and appeared to dry within an hour. The surface seemed somewhat slippery when walked on while still wet. After drying, walking on the pavement gave no indication of lasting slippery conditions. The 40 percent silane was applied as white liquid, and as it dried, it became clear. However, the surface of the pavement remained wet for an extended time and was very slippery while wet. To ensure the traveling public's safety, the lane-closure was kept in place for 48 hours after the application of the 40 percent silane. Fortunately, this section of pavement is not heavily congested, and as such, the lane closures did not result in significant delays or traffic congestion. Reports by AHTD several weeks after silane treatment confirm that the sections did not show any signs of being slippery once the lane-closures were removed, even after several rainfall events.

Figure 50. Photograph of pavement sections treated topically with 100 percent silane (left) and 40 percent silane (right). The slow drying of the 40 percent silane section resulted in a slick surface that required lane closures for about 48 hours.

In addition to monitoring expansion, internal relative humidity, and temperature, photographs were taken of the various test panels at each visit; select photos of these panels are provided in the following section. Additional details on the performance monitoring techniques and treatment activities are provided in chapters 2 and 3, respectively.

5.3 MONITORING DATA

This section summarizes the data obtained from expansion, temperature, and internal relative humidity measurements from the instrumented panels. In addition, photographs taken prior to silane treatment and approximately seven months after the treatment are presented. It should be noted that because this project was initiated towards the end of the FHWA Development and Deployment Program, only limited monitoring data are available (initial measurements prior to treatment and measurements approximately seven months after treatment). As such, it is not possible to draw conclusions or cite trends based on the limited dataset.

Table 29 and Table 30 show the internal relative humidity and temperature data for pavement sections in Section 1 (mild ASR distress) and Section 2 (moderate ASR distress), respectively. Table 31 and Table 32 show the length change measurement results for instrumented panels within Section 1 and Section 2, respectively. The data were not corrected for temperature (thermal) effects. Lastly, Figure 51 through Figure 56 show photographs taken within each test/treatment section prior to treatment and approximately seven months after treatment.

Table 29. Relative humidity and temperature measurements – Section 1 (mild ASR distress).

Slab # (Treatment)	Depth	Data	May 2012	December 2012
10 (Control)	25 mm (1 in.)	°C (°F)	20.7 (69.3)	14.3 (57.7)
		RH%	27.6	83.5
	75 mm (3 in.)	°C (°F)	21.0 (69.8)	14.7 (58.5)
		RH%	67.4	85.6
30 (Control)	25 mm (1 in.)	°C (°F)	19.9 (67.8)	13.4 (56.1)
		RH%	40.6	72.90
	75 mm (3 in.)	°C (°F)	21.0 (69.8)	14.8 (58.6)
		RH%	62.1	89.4
50 (100% Silane)	25 mm (1 in.)	°C (°F)	21.7 (71.1)	13.5 (56.3)
		RH%	53.4	92.1
	75 mm (3 in.)	°C (°F)	21.6 (70.9)	14.5 (58.1)
		RH%	68.7	93.9
70 (100% Silane)	25 mm (1 in.)	°C (°F)	20.2 (68.4)	15.0 (59.0)
		RH%	55.7	90.5
	75 mm (3 in.)	°C (°F)	21.1 (69.9)	15.1 (59.2)
		RH%	70.7	86.2
90 (40% Silane water-based)	25 mm (1 in.)	°C (°F)	20.3 (68.5)	15.2 (59.4)
		RH%	75.6	89.4
	75 mm (3 in.)	°C (°F)	20.7 (69.3)	15.2 (59.4)
		RH%	78.5	91.2
110 (40% Silane water-based)	25 mm (1 in.)	°C (°F)	-	14.2 (57.6)
		RH%	-	93.9
	75 mm (3 in.)	°C (°F)	-	15.5 (59.9)
		RH%	-	90.4

Table 30. Relative humidity and temperature measurements – Section 2 (moderate ASR distress).

Slab # (Treatment)	Depth	Data	May 2012	December 2012
10 (Control)	25 mm (1 in.)	°C (°F)	22.2 (71.9)	14.5 (58.1)
		RH%	87.7	90.7
	75 mm (3 in.)	°C (°F)	21.0 (71.4)	16.4 (61.5)
		RH%	86.90	91.1
30 (Control)	25 mm (1 in.)	°C (°F)	23.7 (74.7)	14 (57.2)
		RH%	91.3	89.4
	75 mm (3 in.)	°C (°F)	22.7 (72.9)	16.6 (61.9)
		RH%	74.8	91.4
50 (100% Silane)	25 mm (1 in.)	°C (°F)	24.8 (76.6)	14.6 (58.3)
		RH%	67.9	83.8
	75 mm (3 in.)	°C (°F)	24.0 (75.2)	16.9 (62.4)
		RH%	73.6	93.0
70 (100% Silane)	25 mm (1 in.)	°C (°F)	26.6 (79.9)	16.5 (61.7)
		RH%	90.6	90.8
	75 mm (3 in.)	°C (°F)	24.2 (75.6)	16.0 (60.8)
		RH%	77.9	90.0
90 (40% Silane water-based)	25 mm (1 in.)	°C (°F)	26 (78.8)	16.0 (60.8)
		RH%	57.5	91.3
	75 mm (3 in.)	°C (°F)	25.4 (77.7)	16.5 (61.7)
		RH%	88.9	91.3

Table 31. Expansion results (%) – Section 1 (mild ASR distress).

Slab # (Treatment)	Measurement	Length change (from May 2012 to December 2012)
10 (Control)	Longitudinal	-0.07
	Transverse	-0.11
20 (Control)	Longitudinal	-
	Transverse	-0.11
30 (Control)	Longitudinal	-0.09
	Transverse	0.01
50 (100% Silane)	Longitudinal	-0.21
	Transverse	0.02
60 (100% Silane)	Longitudinal	0.11
	Transverse	-0.03
70 (100% Silane)	Longitudinal	0.00
	Transverse	-0.03
90 (40% Silane water-based)	Longitudinal	0.00
	Transverse	0.00
100 (40% Silane water-based)	Longitudinal	-0.12
	Transverse	0.02
110 (40% Silane water-based)	Longitudinal	-0.02
	Transverse	0.03

Table 32. Expansion results (%) – Section 2 (moderate ASR distress)

Slab # (Treatment)	Measurement	Length change (from May 2012 to December 2012)
10 (Control)	Longitudinal	0.06
	Transverse	0.00
20 (Control)	Longitudinal	0.00
	Transverse	0.00
30 (Control)	Longitudinal	0.04
	Transverse	-0.05
50 (100% Silane)	Longitudinal	-0.01
	Transverse	0.02
60 (100% Silane)	Longitudinal	0.05
	Transverse	0.00
70 (100% Silane)	Longitudinal	-
	Transverse	-0.22
90 (40% Silane water-based)	Longitudinal	0.49
	Transverse	0.02
100 (40% Silane water-based)	Longitudinal	-0.01
	Transverse	0.02
110 (40% Silane water-based)	Longitudinal	-0.02
	Transverse	-

A – Control Section 10 (May 2012)

B – Control Section 30 (May 2012)

C – Control Section (December 2012)

D – Control Section (December 2012)

Figure 51. Visual evaluations of Section 1 (control). A: May 2012. B: May 2012. C: December 2012. D: December 2012.

A – 100% Silane Section 60 (May 2012)

B – 100% Silane Section 70 (May 2012)

C – 100% Silane Section (December 2012)

D – 100% Silane Section (December 2012)

Figure 52. Visual evaluations of Section 1 (100 percent silane). A: May 2012. B: May 2012. C: December 2012. D: December 2012.

A – 40% Silane (May 2012)

B – 40% Silane (May 2012)

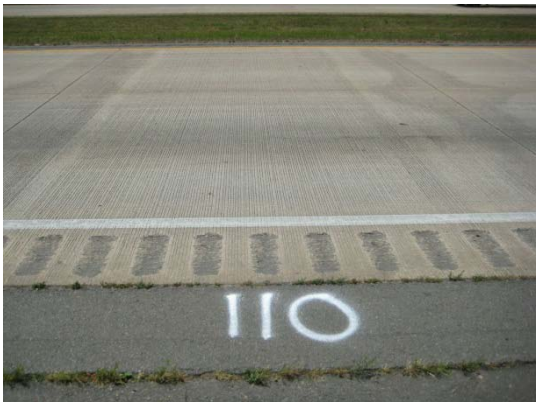

C – 40% Silane (December 2012)

D – 40% Silane (December 2012)

Figure 53. Visual evaluations of Section 1 (40 percent silane). A: May 2012. B: May 2012. C: December 2012. D: December 2012.

A – Control Section (May 2012)

B – Control Section (May 2012)

C – Control Section (December 2012)

D – Control Section (December 2012)

Figure 54. Visual evaluations of Section 2 (control). A: May 2012. B: May 2012. C: December 2012. D: December 2012.

A – 100% Silane Section (May 2012)

B – 100% Silane Section (May 2012)

C – 100% Silane Section (December 2012)

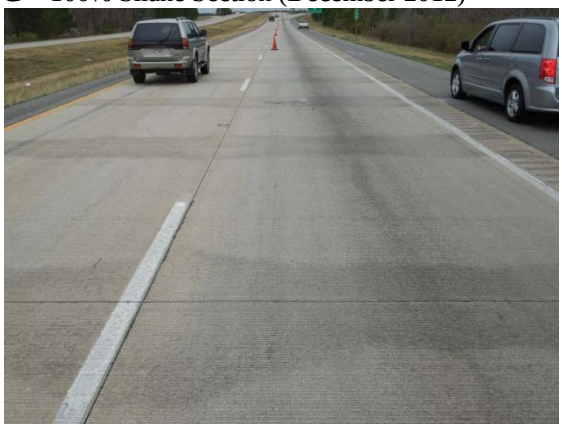

D – 100% Silane Section (December 2012)

Figure 55. Visual evaluations of Section 2 (100 percent silane). A: May 2012. B: May 2012. C: December 2012. D: December 2012.

A – 40% Silane Section (May 2012)

B – 40% Silane Section (May 2012)

C – 40% Silane Section (December 2012)

D – 40% Silane Section (December 2012)

Figure 56. Visual evaluations of Section 2 (40 percent silane). A: May 2012. B: May 2012. C: December 2012. D: December 2012.

5.4 DATA ANALYSES

Because only limited monitoring was possible within the time constraints of this project, there is insufficient data to perform a detailed analysis or to draw even tentative conclusions. It is expected that with long-term monitoring and with the benefit of the baseline and post-treatment data generated to date, the effects of silane treatments on ASR-affected pavement sections will be better understood and quantified.

5.5 SUMMARY

Through the use of an FHWA protocol (Fournier et al. 2010) for evaluating ASR-affected structures, it was determined that ASR was the primary cause of distress within the pavement near Pine Bluff, AR. Components of the protocol that were employed included:

- Visual survey and evaluation
- Petrographic evaluation of extracted cores (including the application of the Damage Rating Index [DRI])
- In-situ expansion measurements of field elements
- Internal relative humidity measurement

Through a detailed, petrographic evaluation of five cores extracted from various pavement sections, it was determined that ASR is playing a substantial role in the observed pavement distress. More time and monitoring is needed to determine whether silanes are effective in (1) reducing internal relative humidity in pavement slabs, and (2) reducing the future potential for ASR-induced expansion and cracking.

5.6 REFERENCES

Fournier, B., Bérubé, M.A., Folliard, K.J. and Thomas, M.D.A. 2010. "Report on the Diagnosis, Prognosis and Mitigation of Alkali-Silica Reaction (ASR) in Transportation Structures." FHWA-HIF-09-004, Federal Highway Administration.

6. CONCRETE PAVEMENT, GEORGETOWN, DE

In June 2009, 16 lane miles (26 lane kilometers) of concrete pavement along US 113 in Georgetown, DE were treated with a topical application of lithium nitrate after it had been determined that the concrete was suffering damage due to alkali-silica reaction (ASR). The pavement was overlaid with hot mix asphalt in May/June 2011 which prevented any long-term monitoring (e.g., visual rating, crack survey, length-change, or relative humidity measurements) of the treated pavement. Cores were taken to determine the depth of lithium penetration.

6.1 SUMMARY OF PETROGRAPHIC EVALUATION

A one-mile (approximately two-kilometer) section of the pavement was visited in May 2008, and cores were extracted from selected locations for petrographic analysis and stiffness-damage testing. The findings of the petrographic examination of two concrete cores extracted from the concrete pavement of Route 113 (Delaware) were presented in 2008 to the Delaware DOT.

The evaluation mainly consisted of the Damage Rating Index (DRI), a method that provides a semi-quantitative assessment of the degree of damage in concrete based on a count of petrographic features of deterioration generally associated with ASR. Damage Ratings of 65 and 395 were obtained, thus indicating an extent of ASR/damage in the concrete ranging from very low to moderate (see Figure 57). Core 113-05 showed significant signs of ASR both in the coarse (gneiss) and the fine (chert) aggregates (see Figure 58). The main signs of reactivity were cracking both in the coarse aggregate particles and in the cement paste. In many cases, alkali-silica gel was observed in the cracks (both in the cement paste and the aggregate particles). A few air voids contained deposits of alkali-silica gel, while deposits of ettringite were found lining a large proportion of the air voids in the concrete. A low degree of ASR and deterioration was observed in core 113-07 (see Figure 58). A large proportion of the air voids in the cement paste, especially in the bottom part of the core, were lined with secondary deposits of ettringite.

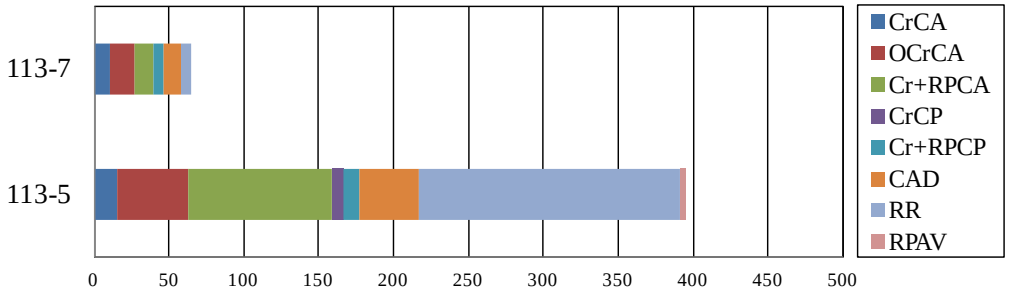

Figure 57. Results of the Damage Rating Index (DRI) for the Delaware cores. The colored cells give the proportions of each petrographic feature to the DRI value. (CrCA: cracking in the coarse aggregate particles; OCrCa: opened cracking in the coarse aggregate particles; Cr+RPCA: cracking in the coarse aggregate particles + reaction product; CrCP: cracking in the cement paste; Cr+RPCP: cracking in the cement paste + reaction product; CAD: coarse aggregate debonded; RR: reaction rim; RPAV: reaction products in air void of the cement paste).

A (distance between vertical lines = 1 cm [0.4 in.])

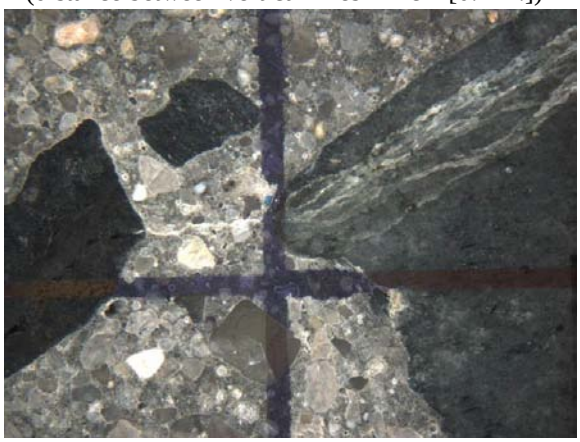

B (distance between vertical lines = 1 cm [0.4 in.])

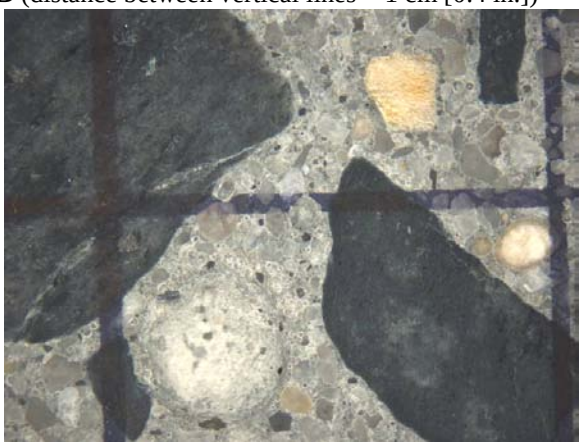

Figure 58. Micrograph from the polished cores.
A: Section 113-05 showing microcracking in a reactive coarse aggregate particle extending into the cement paste (filled with ASR gel). B: Section 113-07 showing cracking in an aggregate particle but limited overall damage (core 113-07).

6.2 SUMMARY OF APPLICATION REPORT

Areas of the pavement were diamond ground and shot-blasted. As a result, four surface textures were evaluated: original texture (transverse tine), shot-blasted (original texture), shot-blasted (diamond ground), and diamond ground.

In June 2009 the following treatment was applied to a total of 16 lane miles (26 lane kilometers) of pavement using a moving-lane closure:

- Water sprayed on the surface at a rate of 1 gal/1000 ft² (0.041 L/m^2) of pavement
- Lithium-nitrate solution (30 percent $LiNO_3$) sprayed on the surface at a rate of 1.5 gal/1000 ft² of pavement (0.061 L/m^2)
- Water sprayed on the surface at a rate of 1 gal/1000 ft² (0.041 L/m^2) of pavement
- A third application of water (same rate as the previous water applications) was used only when lithium salts were observed to precipitate on the surface of the pavement as the solution evaporated (the precipitation of lithium salts can create a slippery surface which is hazardous to vehicular traffic).

Additional details on the performance monitoring techniques and treatment activities are provided in chapters 2 and 3, respectively.

6.3 MONITORING DATA

At the time of treatment a total of 13 treated panels and 4 control panels were selected along the north and southbound lanes of the pavement for monitoring. Monitoring included visual observations, crack mapping, length-change measurements, and determining the internal relative humidity. Baseline measurements were made the day after treatment. The treated pavement was overlaid with hot mix asphalt (HMA) in May/June 2011 and no further monitoring was possible.

Coring locations were also selected during treatment, and cores were taken during the fall of 2009. A number of cores were tested to determine the depth of lithium penetration; these results are presented in Figure 59.

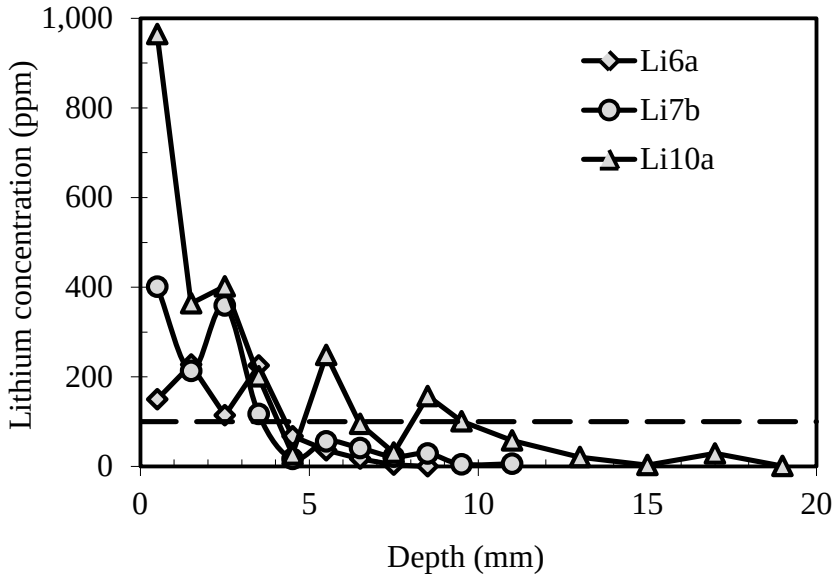

Figure 59. Lithium-concentration profiles.
Core locations: Li6a from section where the surface had been remediated by shot-blasting and diamond-grinding; Li7b and Li10a from section with the original surface texture; Li10a from section with the highest petrographic damage rating. The broken horizontal line shows the approximate lithium concentration (~ 100 ppm) required to mitigate expansion.

Originally it was planned to subject some of the core samples to other tests, including the petrographic Damage Rating Index (DRI) and the Stiffness Damage Test (SDT), but these tests were discontinued once it was learned that the pavement would be overlaid with HMA.

6.4 DATA ANALYSES

A decision was made to overlay the pavement with hot mix asphalt two years after the topical lithium application, and it is not possible to conclusively determine whether the treatment had any impact on the progression of ASR as further monitoring was not possible. However, coring and testing to determine the depth of lithium penetration (Figure 59) indicates that lithium did not penetrate the concrete to any significant depth. The maximum depth of penetration measured was approximately 12 mm (0.5 in.). The amount of lithium required to effectively suppress expansion due to ASR varies depending on the nature of reactive aggregate and the amount of

alkali (sodium and potassium) available in the concrete. However, previous estimates have indicated that a lithium concentration in the range of 100 to 300 ppm (by mass of concrete) would be sufficient in typical cases. The data in Figure 59 indicate that such levels of lithium are only achieved very close to the surface (i.e., within 3 to 10 mm [0.1 to 0.4 in.]). It is highly unlikely that such low depths of lithium penetration would have any impact on the future rate of deterioration of the concrete pavement due to ASR.

6.5 SUMMARY

Although the decision to overlay the concrete pavement with HMA prevented long-term monitoring of the "post-treatment" performance of the concrete, the very low depths of lithium penetration measured indicate that the treatment was unlikely to have had a significant benefit.

7. BRIDGE STRUCTURES, BANGOR/BREWER, ME

On April 8th, 2009, a field visit to a series of bridge structures along I-395 in Bangor/Brewer, ME was conducted in the company of representatives from the Maine DOT (see Figure 60).

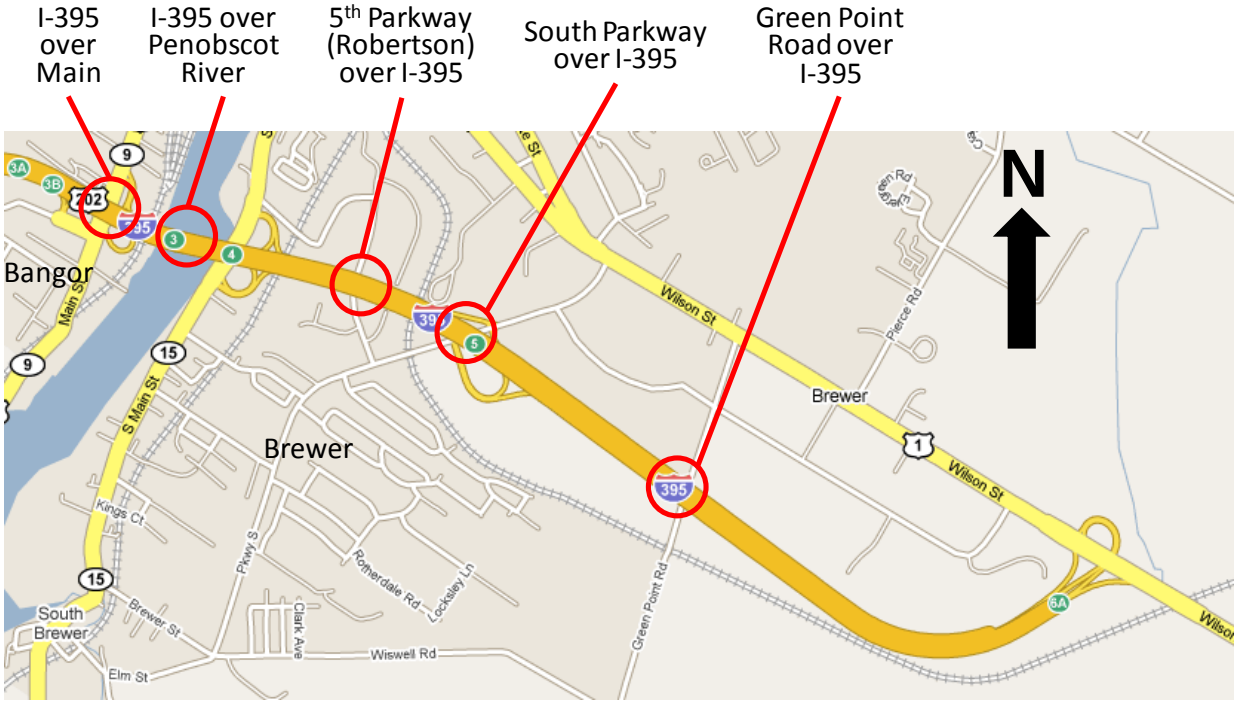

Figure 60. Google map showing location of the structures at the site.

The first structure corresponds to a highway bridge on I-395 over Main Street on the west side of the Penobscot River (see Figure 61A). The section of the abutment walls sheltered from direct exposure to rain and sun showed very limited visible cracking, while the exposed portions of the abutments and the wing walls showed moderate to severe map cracking (see Figure 61B). The second structure corresponds to the major I-395 bridge over the Penobscot River (see Figure 61C). Once again, cracking was mostly found on the sections of the piers exposed to an "excess" of moisture (in addition to ambient moisture), most commonly on external piers and sections of piers under leaking joints (see Figure 61D). The third structure in the corridor corresponds to the 5th Parkway bridge (Robertson Road) over I-395 (see Figure 61E). The concrete elements under the bridge deck, protected from the rain, show cracking of low severity, while the exposed portions of the abutment and wing walls show moderate to severe map cracking (see Figure 61F).

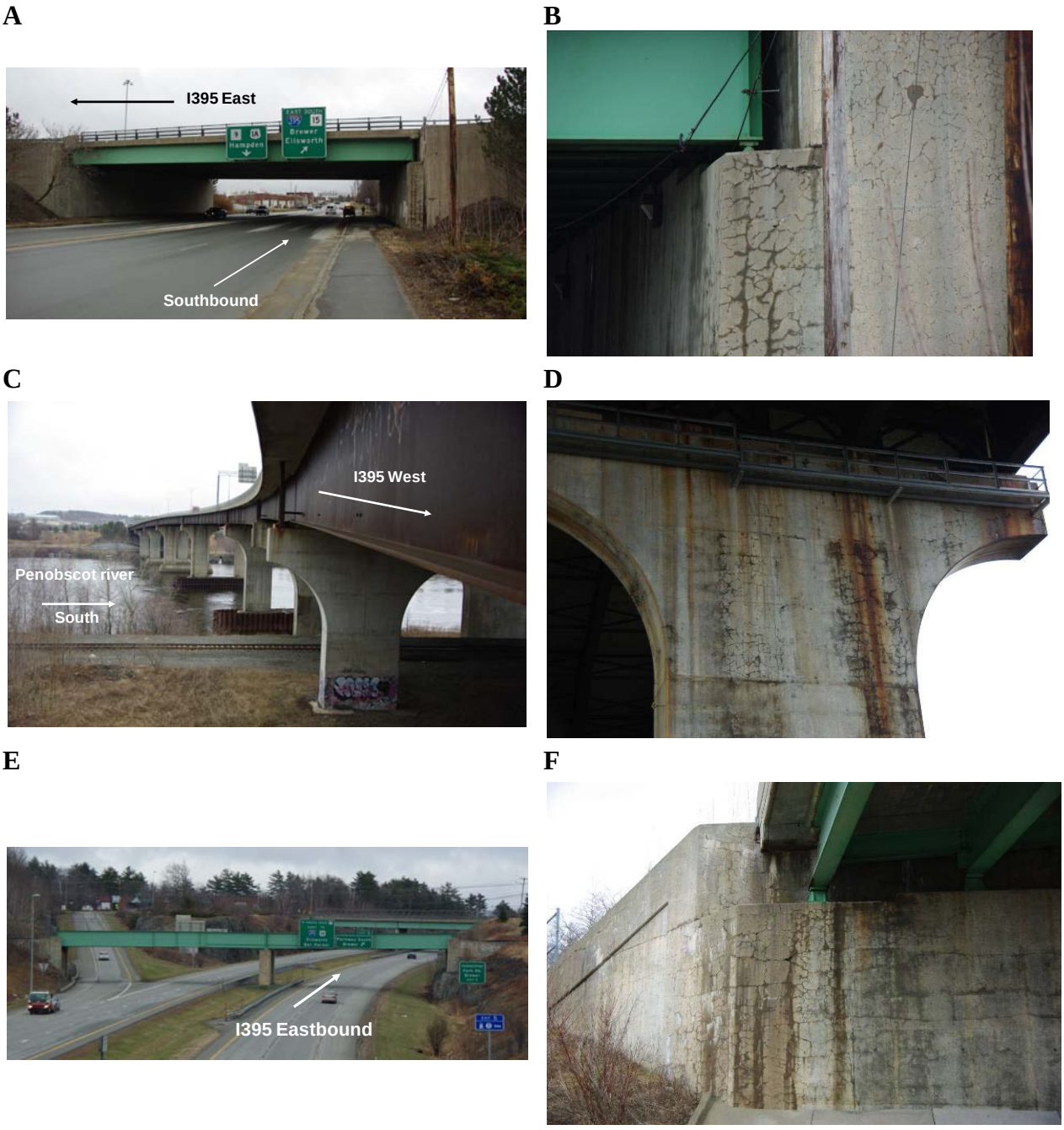

Figure 61. I-395 bridge and 5th Parkway bridge.
A: General view of the I-395 bridge over Main Street. B: Typical (moderate) map cracking affecting the exposed portions of the abutment and wing walls of the I-395 bridge over Main Street. C: General view of the I-395 bridge over the Penobscot River. D: Cracking in a pier of the bridge over the Penobscot River. E: General view of the 5th Parkway bridge over I-395. F: Moderate to severe cracking and localized exudations affecting the abutment and wing walls of the 5th Parkway bridge; also, effect of moisture on the severity of cracking on the exposed and protected (under bridge deck) portions of the bridge.

The fourth structure in the corridor corresponds to the South Parkway bridge over I-395; the activities on that bridge focused on the six columns located under the central span of the bridge (see Figure 62A). The external columns (exposed to moisture) show moderate map and aligned

(vertical) cracking (see Figure 62B), while those under the bridge deck, i.e., protected from rain, show very limited cracking. The fifth structure investigated corresponds to the Green Point Road bridge over I-395 (see Figure 62C). Portions of the abutment walls under the bridge deck, protected from direct excess of moisture (rain), show limited cracking while the exposed portions of the abutment and wing walls show moderate map cracking (see Figure 62D).

Figure 62. Bridges over I-395.
A: General view of the South Parkway bridge over I-395. B: External column (east side) showing moderate to severe aligned (vertical) cracking. C: General view of the Green Point Road bridge over I-395. D: Moderate cracking and localized exudations affecting the abutment and wing walls of the Greenpoint Road bridge; also, effect of moisture on the severity of cracking on the exposed and protected (under bridge deck) portions of the bridge.

Following the visit, locations for the extraction of cores for petrographic examination were proposed. A subsequent site visit was conducted on June 15th and 16th, and a total of 20 cores

were extracted from the different structures by Maine DOT personnel. Maine DOT completed the extraction of additional cores on June 17th.

7.1 SUMMARY OF PETROGRAPHIC EVALUATION AND STIFFNESS DAMAGE TESTING

Findings of the petrographic examination of 24 concrete cores extracted from six bridge structures along I-395 in Bangor, ME in 2009 were reported to Maine DOT. The evaluation mainly consisted of the Damage Rating Index (DRI), a method that provides a semi-quantitative assessment of the degree of damage in concrete based on a count of petrographic features of deterioration generally associated with alkali-silica reaction (ASR). Damage Rating Indices ranging from 133 to 882 were obtained for the various cores, thus suggesting low to severe degree of deterioration/damage due to ASR (see Table 33).

Table 33. Results of the Damage Rating Index (DRI).

Structure	Sample	Location of coring and condition of the area from where the core was extracted	DRI
I-395 over Main Street	I395 MS-1	In the abutment wall, sheltered (no cracking).	**133**
	I395 MS-2	In the abutment wall, exposed (moderate cracking)	**195**
	I395 MS-3	In the wing wall, exposed (moderate cracking)	**528**
I-395 over the Penobscot River	I395 PR-1a	In the abutment wall, sheltered (map/pattern cracking due to leaking joint)	**530**
	I395 PR-1b	In the same abutment wall, sheltered (no visible cracking).	**208**
	I395 PR-2	In the wing wall, exposed (severe map cracking).	**764**
	I395 PR-3	First row of piers; external pier partially exposed (light map cracking).	**230**
	I395 PR-4a	First row of piers; middle pier, sheltered (light map/pattern cracking).	**198**
	I395 PR-4b		**196**
	I395 PR-5	2nd row of piers; south pier, west face (no cracking).	**228**
	I395 PR-6	2nd row of piers; south pier, west face (no cracking).	**200**
	I395 PR-7	2nd row of piers; north pier, east face (facing the river) (no cracking).	**240**
	I395 PR-8	2nd row of piers; north pier, west face (Longitudinal cracking).	**201**
5th Parkway (Robertson) over I-395	I395 5th-1	In the abutment wall, sheltered (no visible cracking).	**279**
	I395 5th-2	In the abutment wall, exposed (severe vertical and horizontal cracking).	**882**
	I395 5th-3	In the wing wall, exposed (moderate map cracking).	**427**
South Parkway over I-395	I395 SP-1	In the first column on the east side of the bridge, exposed (regularly-spaced vertical cracks connected by map cracking).	**531**
	I395 SP-2	In the second column (from the east side of the bridge), sheltered (light vertical cracking).	**203**
	I395 SP-3	In the third column (from the east side of the bridge), sheltered (light vertical cracking).	**152**
Green Point Road over I-395	I395 GPR-1	In the abutment wall, sheltered (light map cracking).	**499**
	I395 GPR-2	In the abutment wall, exposed (moderate map cracking).	**479**
Route 1A over I-395	I395 R1A-1	In the abutment wall, sheltered (no visible cracking).	**258**
	I395 R1A-2	In the abutment wall, exposed (vertical cracks connected by map cracking).	**627**
	I395 R1A-3	In the wing wall, exposed (moderate map cracking).	**636**

The extent of ASR/damage was found to vary significantly as a function of the exposure conditions of the structural elements examined (see Figure 63). The concrete specimens examined typically incorporated a reactive greywacke/argillite coarse aggregate. Several concrete specimens (especially those exposed to moisture) showed typical signs of ASR consisting of cracking in the coarse aggregate particles and in the cement paste, often filled with alkali-silica reaction products, reaction rims around reactive aggregate particles, and air voids filled with secondary reaction products (see Figure 64). The extent of the petrographic signs of ASR are, once again, very much a function of the exposure conditions of the concrete, cores extracted from those parts of the structures that are exposed to rain and excess moisture generally showing significantly higher DRI values.

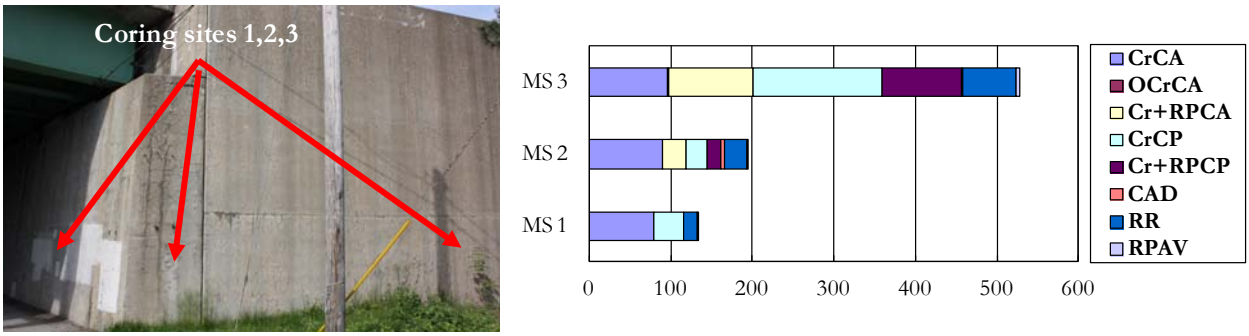

Figure 63. Results of the Damage Rating Index (DRI) for three cores extracted from various areas of I-395 over Main Street in Bangor, ME.

MS1: abutment wall under the bridge deck, sheltered (no cracking); MS2: exposed portion of the abutment wall (map cracked); MS3: exposed portion of the wing wall (map cracked). The colored cells give the proportions of each petrographic feature to the DRI value. (CrCA: cracking in the coarse aggregate particles; OCrCa: opened cracking in the coarse aggregate particles; Cr+RPCA: cracking in the coarse aggregate particles + reaction product; CrCP: cracking in the cement paste; Cr+RPCP: cracking in the cement paste + reaction product; CAD: coarse aggregate debonded; RR: reaction rim; RPAV: reaction products in air void of the cement paste).

A (distance between vertical lines = 1 cm [0.4 in.])

B (distance between vertical lines = 1 cm [0.4 in.])

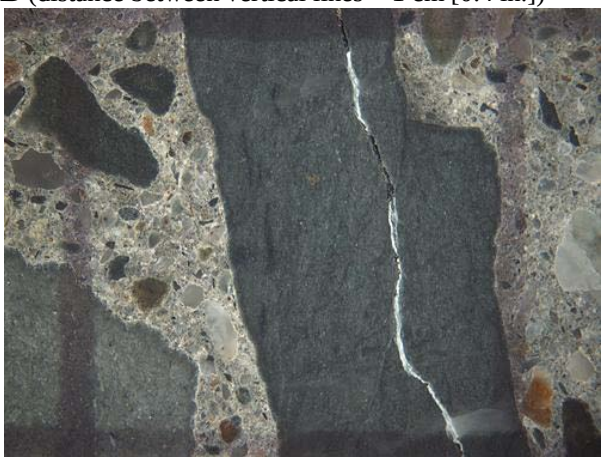

Figure 64. Polished concrete surfaces, cores extracted from bridge structures along I-395 in Bangor, Maine. A&B: Cracking in coarse aggregate particles (greywacke) extending into the cement paste; secondary (ASR) products are observed in the cracks both in the particles and the cement paste. Dark reaction rims are observed surrounding the reactive aggregate particles.

Additional (3-inch [approximately 8-cm]) cores were extracted from the exposed and sheltered sections of two bridge structures, and subjected to the Stiffness Damage Test (SDT) (see chapter 2 for details on the method). Table 34 presents the results of the SDT. Although there is currently no chart available to allow a proper analysis of the extent of deterioration in ASR-affected concrete specimens through the SDT, the results of the various SDT parameters gave a very similar diagnostic to that obtained with the DRI, i.e., significantly higher first cycle hysteresis and plastic deformation over the five cycles, and lower modulus of elasticity values, i.e., related to higher internal damage, for ASR-affected concrete cores extracted from the exposed portions of the structures compared to the sheltered ones. Figure 65 illustrates this typical difference.

Table 34. Results of stiffness damage testing on cores extracted from two bridge structures.

SDT parameters	Cores	Main Street Site 1	Main Street Site 3	5th Parkway Site 1	5th Parkway Site 2
First cycle hysteresis (J/m^3)	A	896	2339	919	2757
	B	724	2415	665	2154
	C	906	---	565	4386
	Average	**842**	**2377**	**717**	**3099**
Plastic deformation over the five cycle (μstrain)	A	149	194	122	265
	B	54	263	129	129
	C	147	---	47	472
	Average	**117**	**229**	**99**	**289**
Average modulus of elasticity of the cycles 1 and 2 (Gpa)	A	24	14	25	12
	B	30	13	21	14
	C	18	---	26	9
	Average	**24**	**13**	**24**	**12**

In summary, the petrographic evaluation and the SDT testing confirmed the presence of ASR in all structures that were cored. The extent of ASR and associated damage was found to range from low to high, a significant variation in the damage being observed from one location to another as a function of the exposure conditions of the structural element examined. Many of the concrete components sheltered from direct exposure to rain and sun showed limited to no visible cracking or hairline cracking, which is consistent with the low DRI/SDT values for cores taken from these locations. In the case of the exposed portions of the abutments and the wing walls, petrographic signs of ASR ranging from moderate to high were generally observed.

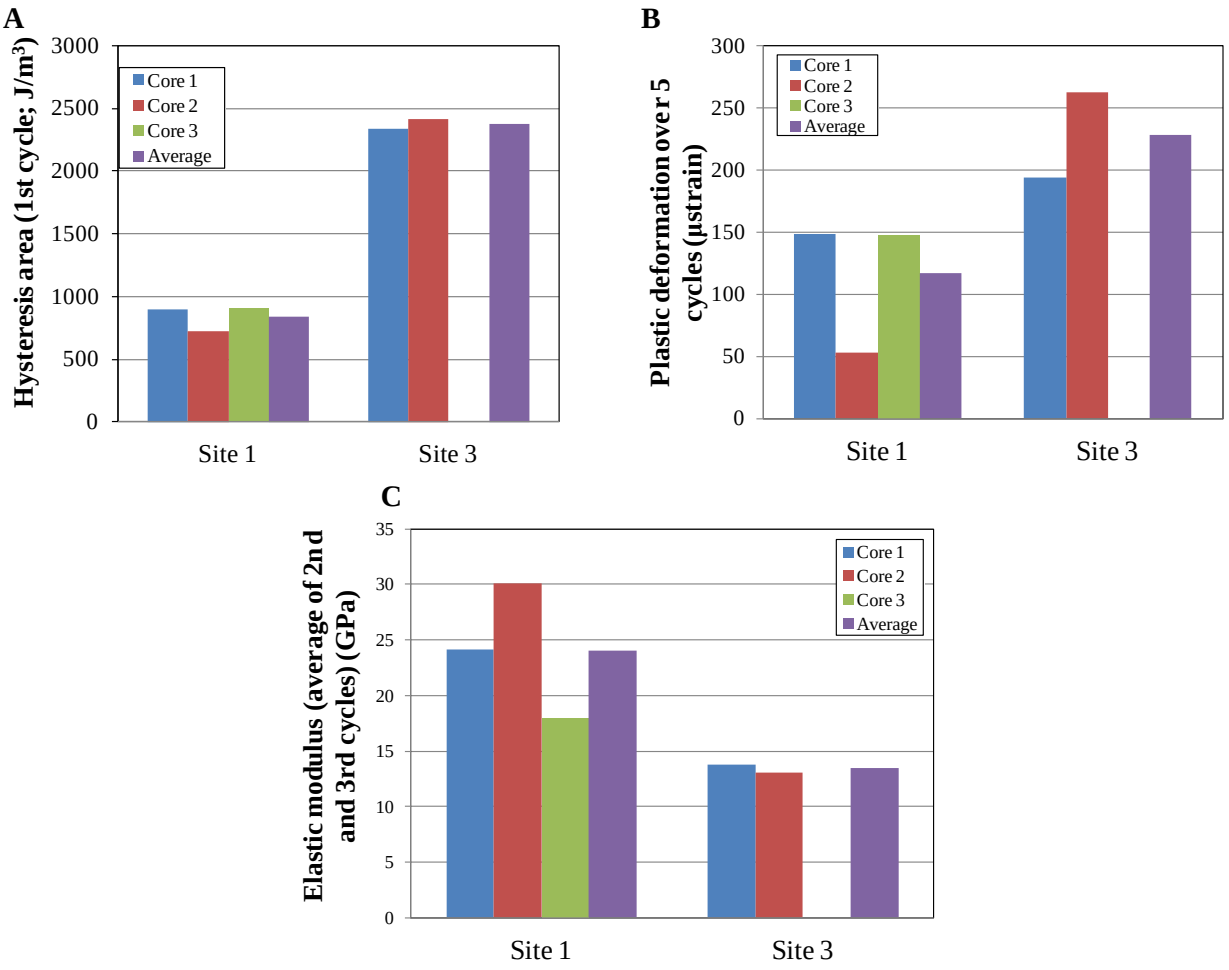

Figure 65. Results of the SDT for cores extracted from the bridge structure on I-395 over Main Street. Results are compared for sets of cores extracted from exposed and sheltered portions of the bridge structure. A: Hysteresis area, 1st cycle. B: Plastic deformation, 5 cycles. C: Modulus of elasticity, average of 2nd & 3rd cycles.

7.2 SUMMARY OF APPLICATION REPORT

Based on the results of the field inspection and laboratory testing (diagnosis), it was thus decided that the five ASR-affected bridge structures along Interstate 395 (I-395) in Bangor/Brewer, ME made a suitable test section. The bridge elements selected for treatments include bridge abutment and wing walls, and reinforced concrete columns and pier caps, all of which exhibited typical signs of distress associated with ASR.

A treatment plan involving the application of different types of surface treatment products (sealers, elastomeric coating), an electrochemical lithium treatment, and strengthening (fiber reinforced polymer (FRP) wrap) on various elements of five structures on I-395 was implemented in 2010. In addition, a performance monitoring plan was developed and implemented to allow quantifying the effects of the various treatments over time. Details on the

performance monitoring techniques and treatment activities are provided in chapters 2 and 3, respectively.

Within each of the bridge elements, specific areas were identified for implementation of a Performance Monitoring Package (PMP), including crack mapping, expansion measurements, and temperature/humidity readings. Figure 66 shows a performance monitoring area consisting of a 500-mm (20-in.) by 500-mm (20-in.) grid layout for length-change and crack mapping measurements; the latter was used for all bridge elements; however, a one-meter (40 in.) by one-meter (40 in.) grid was used for crack mapping purposes in the case of the large concrete columns of the I-395 bridge over the Penobscot River.

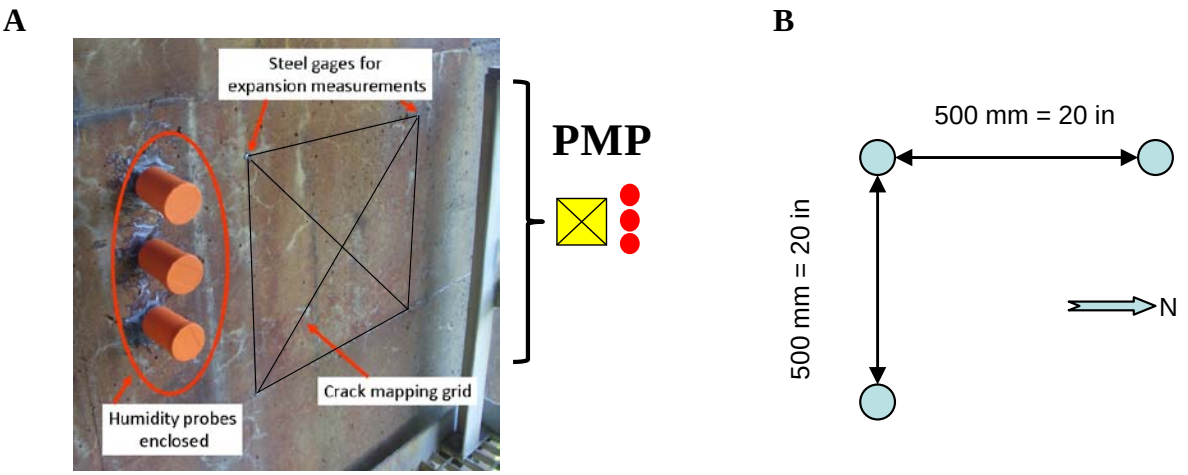

Figure 66. Performance monitoring area.
A: Area within a section of a pier instrumented with a crack mapping grid, expansion pins, humidity sleeves, and plugs for data collection (PMP = Performance Monitoring Package). B: Expansion pin layout.

The structures were then treated during the summer and fall of 2010. Three sealers were selected for application on separate sections of the above structures. The products correspond to a 100 percent silane, a 40 percent silane (water-based), and one elastomeric coating. Details on these products are given in chapter 3. In addition to the above surface treatments, two columns of the South Parkway bridge over I-395 were selected for lithium impregnation (electrochemical procedure) and strengthening (through the use of fiber reinforced polymer (FRP) wrap). In addition to the "conventional" performance monitoring package (PMP), non-destructive testing methods were used for the diagnosis/prognosis of ASR in the various bridge structures. The methods used consisted of the Ultrasonic Pulse Velocity (UPV), impact-echo, and nonlinear acoustics. Details on the non-destructive methods are provided in chapter 2. Table 35 and Figure 67 to Figure 71 give the details of the treatments and monitoring plan for each of the sites (bridges) selected.

Table 35. Treatment plan details. Presentation of the performance monitoring sites.

Structure	Condition of the section	Monitoring site number					
		Control	Elastomeric coating	40% silane	100% silane	FRP wrap	Lithium electro.
I-395 over Main Street	Sheltered	1	3	---	---		
	Exposed	2	4	---	---		
I-395 over the Penobscot River	Sheltered	4	---	2	3		
	Exposed	5	---	1	---		
5th Parkway bridge over I-395	Sheltered	7	3	2	6		
	Exposed	8	4	1	5		
South Parkway bridge over I-395	Sheltered	4,5	---	3	--	---	2
	Exposed	1	---	---	---	6	---
Green Point Road bridge over I-395	Sheltered	2	7	6	3		
	Exposed	1	8	5	4		

A

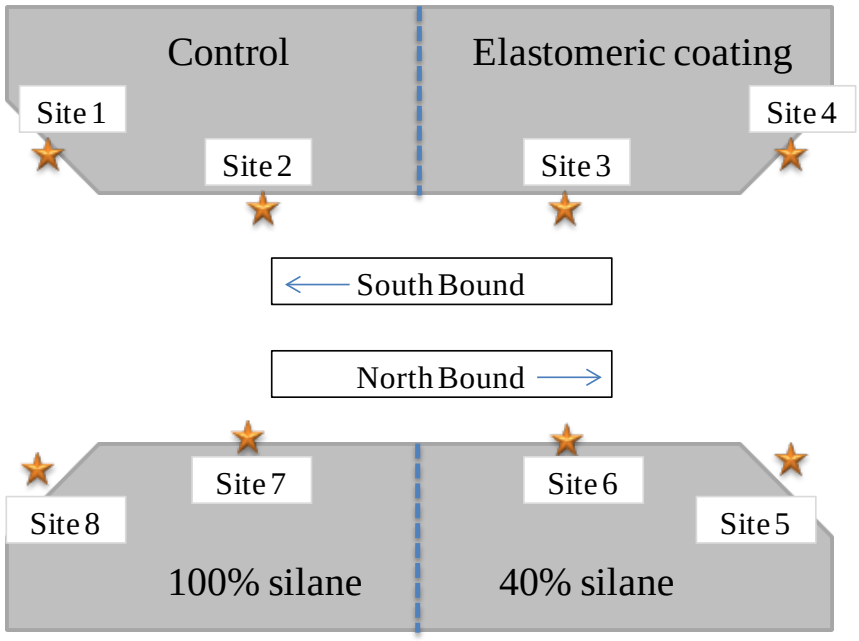

B

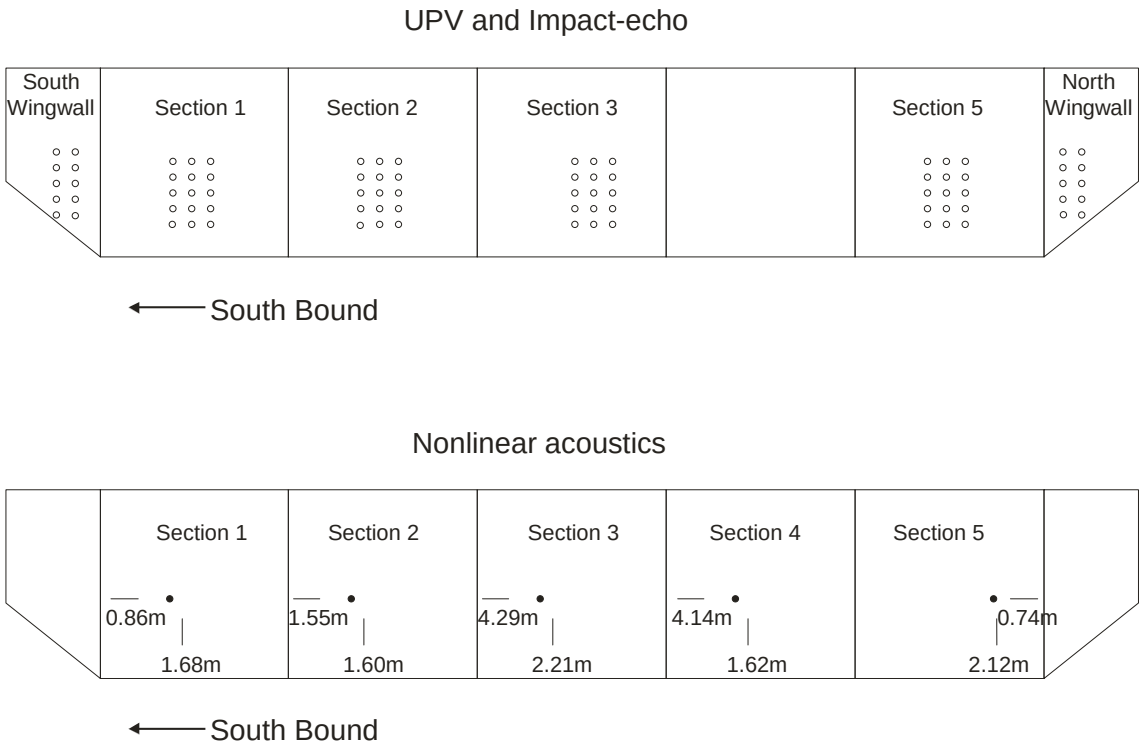

Figure 67. Treatment and monitoring plans for the I-395 bridge over Main Street. A: Performance monitoring package (PMP). B: Sketch of the UPV, impact-echo and nonlinear acoustics measurement patterns.

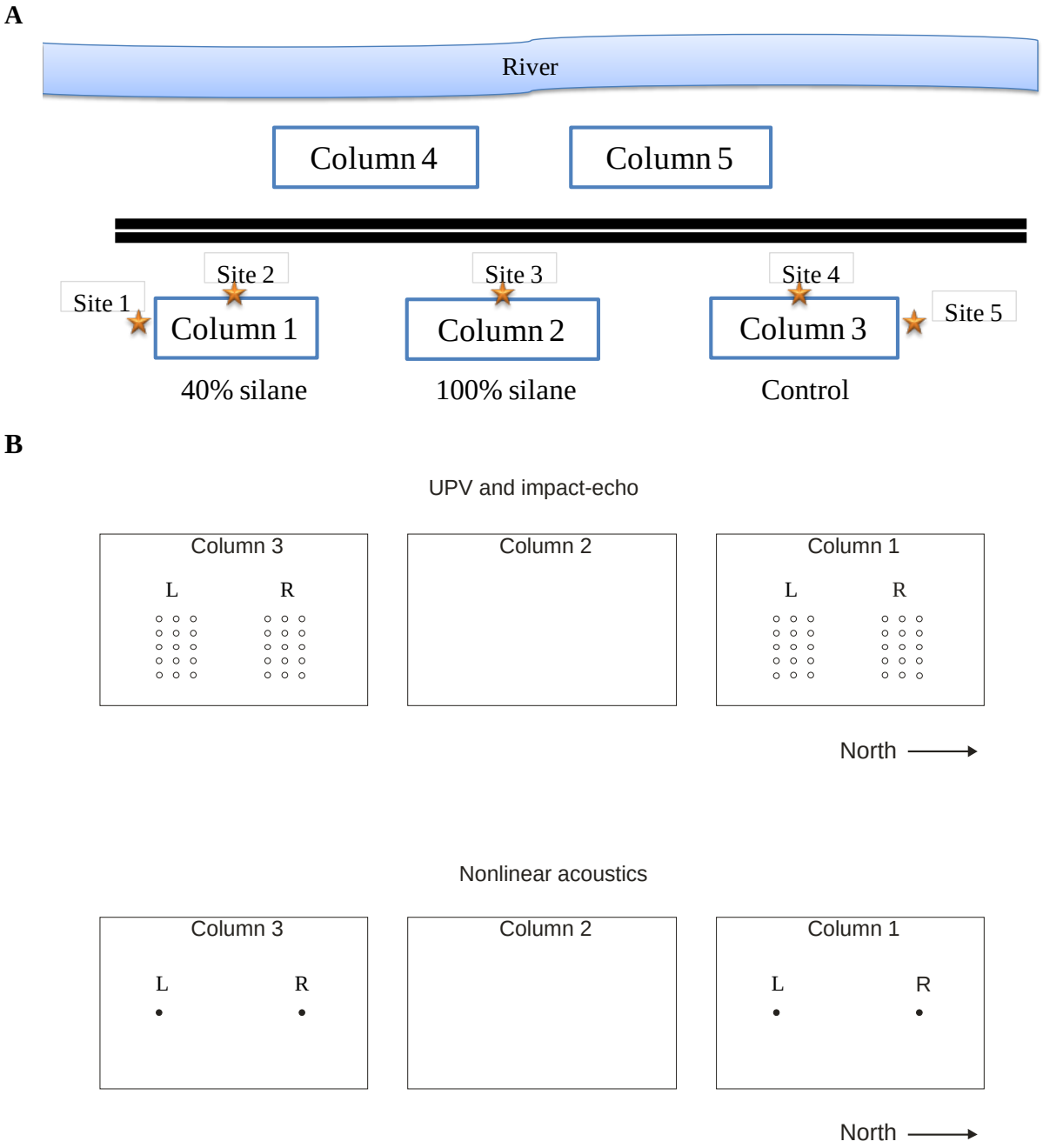

Figure 68. Treatment and monitoring plans for the I-395 bridge over the Penobscot River. A: Performance monitoring package (PMP). B: Sketch of the UPV, impact-echo and nonlinear acoustics measurement patterns.

A

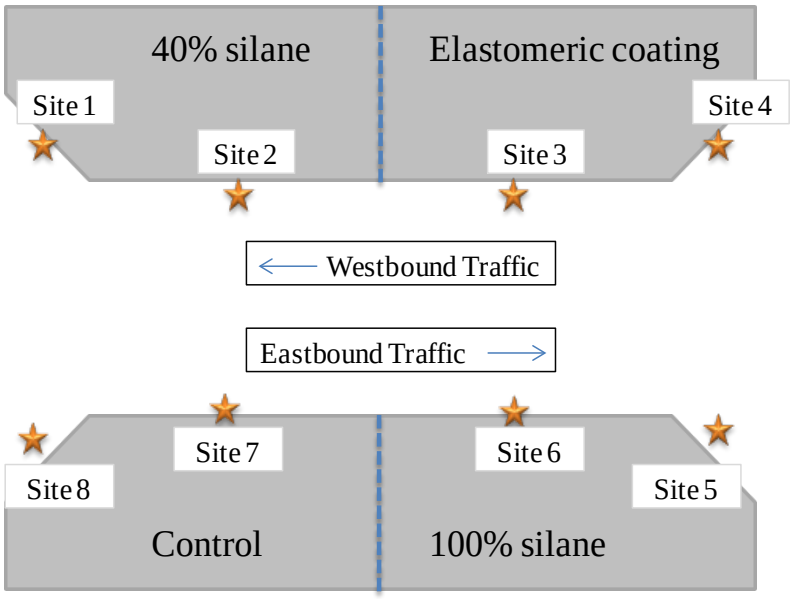

B

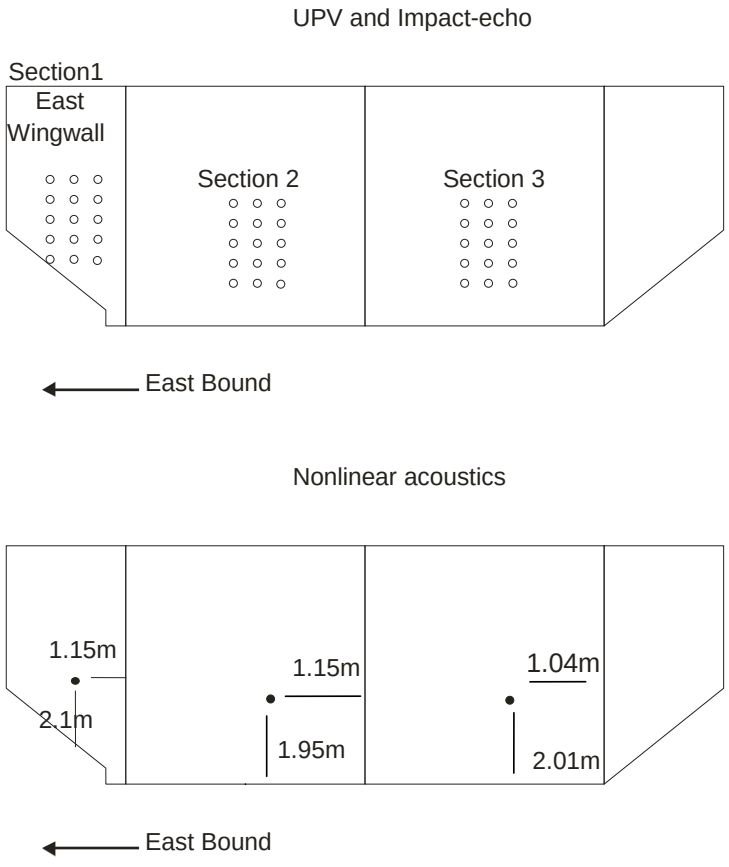

Figure 69. Treatment and monitoring plans for the 5th Parkway (Robertson Road) bridge over I-395. A: Performance monitoring package (PMP). B: Sketch of the UPV, impact-echo and nonlinear acoustics measurement patterns.

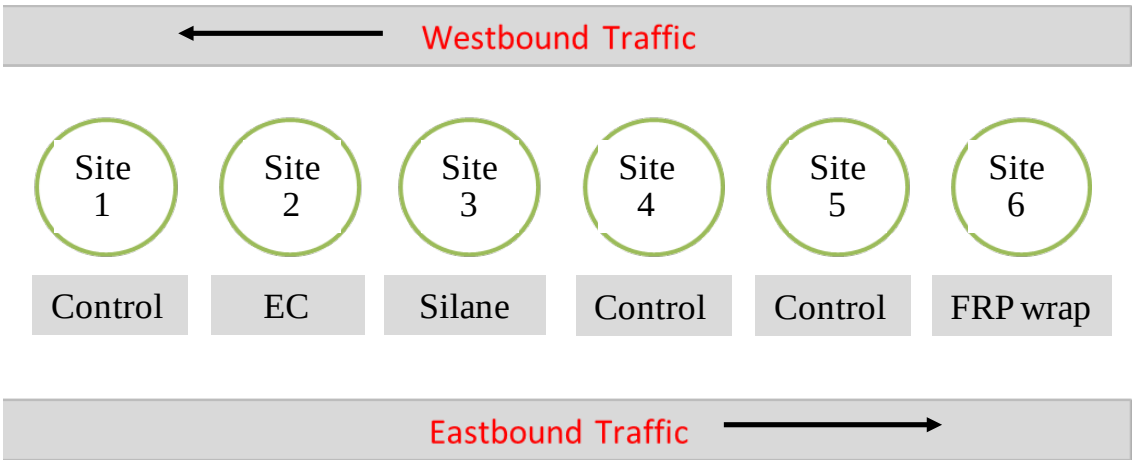

Figure 70. Treatment and monitoring plans for the South Parkway bridge over I-395.

A

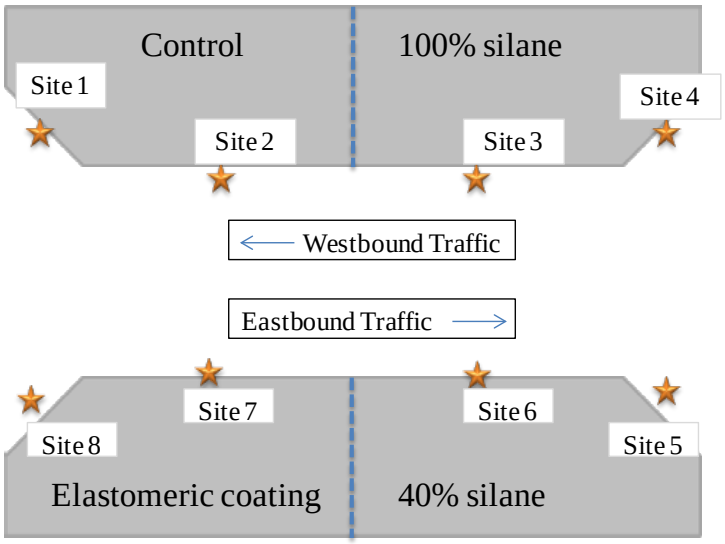

B

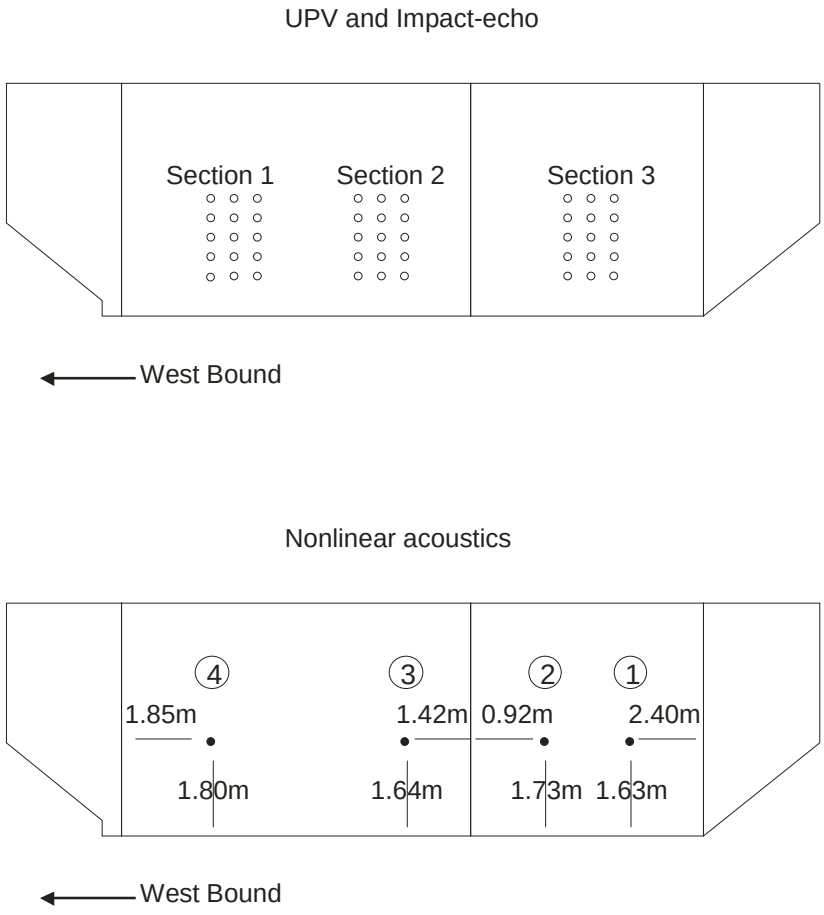

Figure 71. Treatment and monitoring plans for the Green Point Road bridge over I-395. A: Performance monitoring package (PMP). B: Sketch of the UPV, impact-echo and nonlinear acoustics measurement patterns.

The 100 percent silane product was applied using a handheld pressurized container and spray nozzle. It was sprayed onto the surface of bridge abutment and wing walls, as well as on one part of a pier, in a left-to-right-to-left pattern. This product was sprayed onto the surface as a clear liquid and dried as a clear coating. The 40 percent silane (water-based) product was applied in the same way that the 100 percent silane product was applied. The 40 percent silane was sprayed on as a white liquid. While it dried, it became a clear coating. The elastomeric coating product was applied like paint. Rollers and paint brushes were used instead of spray nozzles. Like the above silane products, one coat of material was applied as evenly as possible so that the entire area was covered. The 40 percent silane and 100 percent silane materials were applied at a rate of about 3.7 m^2/L (150 ft^2/gallon), while the elastomeric coating was applied with coats at a rate of 2.5 m^2/L (100 ft^2/gallon). Figure 72 gives examples of the surface treatment procedures, while Figure 73 illustrates some of the treated bridge structures with the corresponding performance monitoring sites.

Figure 72. Application of surface treatments.
A: 40 percent silane (left) and elastomeric coating on the abutment wall of 5th Parkway bridge over I-395. B: Elastomeric coating on the abutment wall of the I-395 bridge over Main Street. C: 40 percent silane on Column No. 3 of the South Parkway bridge over I-395. D: 100 percent silane on Pier No. 2, I-395 bridge over the Penobscot River.

A

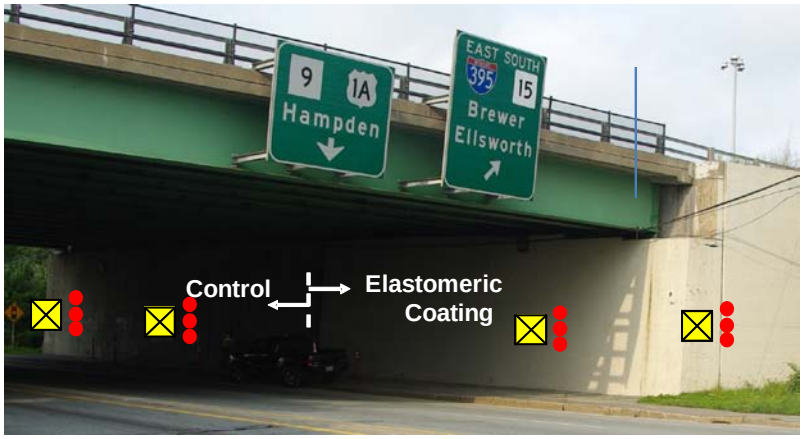

B

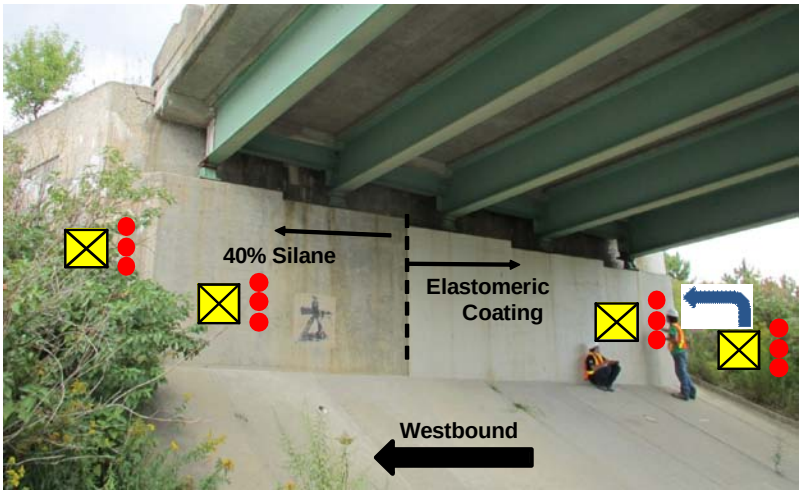

C

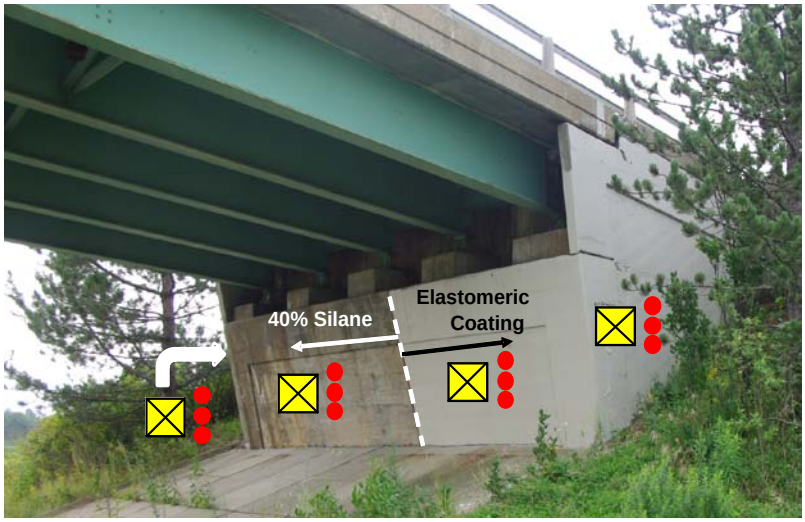

Figure 73. Examples of treatment and monitoring plans for different structures on the I-395 corridor in Bangor/Brewer, Maine.
A: I-395 bridge over Main Street. B: 5th Parkway (Robertson Road) bridge over I-395. C: Green Point Road bridge over I-395.

The six columns at mid-span of the South Parkway bridge over I-395 provided an opportunity to evaluate additional types of remedial actions on a series of 7-m (23-ft) tall columns exhibiting different levels of ASR. Column No. 6, which exhibited the highest degree of deterioration (moderate-to-severe cracking – see Figure 62B and Figure 70) was encapsulated using four layers of carbon fiber reinforced polymer (CFRP) strengthening wrap. The column was first cleaned, and then a structural epoxy paste adhesive was applied for filling in bug holes and hairline cracks before applying CFRP strengthening. Following the application of the above paste, a high strength, high modulus epoxy was rolled onto the surface of the column, followed by four layers of carbon fiber fabric (see Figure 74A). The CFRP wrap is gently rolled between every layer to remove any air pockets that may have been encapsulated during the application, each layer being bound to each other using the high-strength epoxy mentioned before (see Figure 74B). Details on the application techniques and processes are given in chapter 3.

A **B**

Figure 74. Application of strengthening (FRP wrap).
A: An epoxy resin is rolled onto the surface first covered with a special paste. B: CFRP wrap applied onto the surface of the column.

Electrochemical (lithium) migration technique was applied on column No. 2 of the South Parkway bridge over I-395 (moderate degree of cracking) (see Figure 70). The treatment involved the installation of a temporary anode system consisting of a series of titanium anodes placed into holes drilled in a grid pattern in the upper 6-m (20-ft) portion of the column and a titanium mesh layer sandwiched between layers of geotextile felt that covered the concrete surface of the column (see Figure 75A). Both the temporary anode system and the embedded reinforcing steel, which acts as a cathode, were then connected to an AC/DC rectifier, which, once energized, applies a low voltage DC potential between the anode and the cathode to migrate lithium into the concrete from the electrolyte (30 percent lithium nitrate solution) that is pumped onto the surface of the concrete column through a temporary irrigation system (see Figure 75B and Figure 75C). The lithium impregnation system was sealed with polyethylene sheets to prevent evaporation or dry out over the eight-week treatment period.

Figure 75. Titanium mesh.
A: Installation of the titanium mesh over a layer of geotextile felt. One can see holes that were drilled into the column, in a grid pattern, in which the titanium anodes were inserted to ensure connection between the reinforcing steel (cathode) and the titanium mesh. B: The titanium mesh, sandwiched between layers of geotextile felt, is sealed with polyethylene sheets. The electrolyte (30 percent-$LiNO_3$ solution) is pumped onto the surface of the concrete column through a temporary irrigation system. C: AC/DC rectifier and irrigation system.

7.3 MONITORING DATA

This section summarizes the data obtained from expansion, crack mapping, internal relative humidity measurements, as well as non destructive test methods (ultrasonic pulse velocity, impact-echo and nonlinear acoustics) from the five structures under investigation. Data are presented for the period between May 2010 and June 2013.

Table 36 presents the measured temperature and relative humidity values obtained from the performance monitoring sites of the I-395 bridge over Main Street. For the various monitoring sites (see Figure 67A), data are reported at 25-millimeter (~1 inch), 50-millimeter (~2 inches), and 75-millimeter (~3 inches) depths below the surface. Actually, one will note that many data are missing from the different survey times. This is due to the fact that several holes were either filled with water or humid (condensation) to the point that no reliable data could be obtained from those holes during the field surveys.

Table 36. Relative humidity and temperature measurements - I-395 bridge over Main Street.

Section	Site	Depth	Data	May 2010 23 °C (74 °F)* Before treatment	June 2011 22 °C (71 °F)*	August 2012 20 °C (68 °F)*	June 2013 19 °C (66 °F)*
Control	1	25 mm (1 in.)	T °C (°F)	-	23.1 (73.6)	24.8 (76.6)	-
			RH%	-	87.0	94.4	-
		50 mm (2 in.)	T °C (°F)	-	22 (71.6)	24.8 (76.6)	-
			RH%	-	87.5	90.8	-
		75 mm (3 in.)	T °C (°F)	-	21.8 (71.2)	24.8 (76.6)	30.8 (87.4)
			RH%	-	91.2	92.3	71.4
	2	25 mm (1 in.)	T °C (°F)	25.2 (77.36)	19.8 (67.6)	22 (71.6)	19.8 (67.6)
			RH%	72.7	79.9	71.3	83.7
		50 mm (2 in.)	T °C (°F)	23.5 (74.3)	18.8 65.8	21.8 (71.2)	19.4 (66.9)
			RH%	76.9	86.2	77.9	87.3
		75 mm (3 in.)	T °C (°F)	22.2 (72)	18.3 (64.9)	21.7 (71.1)	18.9 (66.0)
			RH%	85.1	90.2	87.8	89.9
Elastomeric coating	3	25 mm (1 in.)	T °C (°F)	24.6 (76.3)	23.5 (74.3)	22.1 (71.8)	20.2 (68.4)
			RH%	86.7	85.6	84.4	76.1
		50 mm (2 in.)	T °C (°F)	23.3 (73.9)	20.3 (68.5)	21.9 (71.4)	18.5 (65.3)
			RH%	87.8	90.6	90.9	86.3
		75 mm (3 in.)	T °C (°F)	22.3 (72.1)	19.6 (67.3)	21.8 (71.2)	18.3 (64.9)
			RH%	89.5	90.5	92.1	88.9
	4	25 mm (1 in.)	T °C (°F)	-	29.3 (84.7)	-	-
			RH%	-	91.1	-	-
		50 mm (2 in.)	T °C (°F)	-	28 (82.4)	-	-
			RH%	-	94.0	-	-
		75 mm (3 in.)	T °C (°F)	-	27.2 (81)	-	27.1 (80.8)
			RH%	-	90.6	-	88.5

*That temperature corresponds to the daily average obtained from http://www.wunderground.com

Table 37 presents the length change values obtained from the performance monitoring sites on the I-395 Bridge over Main Street. Data are reported for a 500-millimeter (20-inch) gauge length in both the horizontal and vertical directions. The data were not corrected for thermal effects.

Table 37. Expansion results (%) - I-395 bridge over Main Street.

Section	Site	Location	May 2010 23 °C (74 °F)* Before treatment	June 2011 22 °C (71 °F)*	August 2012 20 °C (68 °F)*	June 2013 19 °C (66 °F)*
Control	1	Vertical	"0" reading	0.074	0.081	0.086
		Horizontal	"0" reading	-	-	-
	2	Vertical	"0" reading	0.040	0.025	0.028
		Horizontal	"0" reading	0.032	0.055	0.061
Elastomeric coating	3	Vertical	"0" reading	0.066	0.039	0.045
		Horizontal	"0" reading	0.022	0.076	0.088
	4	Vertical	"0" reading	0.071	0.055	0.054
		Horizontal	"0" reading	0.011	0.018	0.024

*That temperature corresponds to the daily average obtained from http://www.wunderground.com

Table 38 presents the results of Cracking Index measurements obtained from the performance monitoring sites of the I-395 Bridge over Main Street. CI data are given in mm/m (or in./yd) as they correspond to the total crack opening, in mm (in.), averaged over a one-meter (or one-yard) length; they are calculated from the measurement of crack widths along a grid system composed of the four lines of a 500-mm (20-in.) square and of the two 700-mm (28-in.) diagonal lines (total of 3.4 m (about 11 ft) of lines). In general, the higher the CI values, the higher the extent of (surface) damage on the concrete element investigated.

Table 38. Cracking Index measurements - I-395 bridge over Main Street.

Section	Site	May 2010 23 °C (74 °F)* mm/m (in./yd) Before treatment	June 2011 22 °C (71 °F)* mm/m (in./yd)	August 2012 20 °C (68 °F)* mm/m (in./yd)	June 2013 19 °C (66 °F)* mm/m (in./yd)
Control	1	1.59 (0.057)	-	2.86 (0.103)	1.73 (0.062)
	2	-	-	0.43 (0.015)	0.13 (0.005)
Elastomeric coating	3	0.12 (0.004)	0.40 (0.014)	0.00 (0.000)	0.00 (0.000)
	4	0.31 (0.011)	-	0.00 (0.000)	0.00 (0.000)

*That temperature corresponds to the daily average obtained from http://www.wunderground.com

As illustrated in Figure 67B, measurements on the abutment wall sections were performed following a grid of 3 x 5 points. A grid of 2 x 5 was used for the wing walls. Due to the particular shape of the wing walls on Main Street, only UPV was performed on those walls. The horizontal spacing between points was 500 mm (20 in.), and the vertical spacing was 300 mm (12 in.). UPV was performed on every horizontal pair of points (10 recordings per grid for the abutment walls and 5 recordings per grid for the wing walls), while impact-echo was performed on every points of the grid. Table 39 gives the values of UPV, while Table 40 provides data from impact-echo measurements.

Table 39. Results of UPV - I-395 bridge over Main Street.

Section	2010		2012		2013	
	Average UPV m/s (ft/s)	Standard deviation	Average UPV m/s	Standard deviation	Average UPV (m/s)	Standard deviation
1	Bad signals	-	2499 (8199)	234	3546 (11634)	448
2	2948 (9672)	-	3832 (12572)	301	4161 (13652)	530
3	3974 (13038)	-	3300 (10827)	450	3774 (12382)	514
4	2505 (8219)	-	2384 (7822)	210	3245 (10646)	526
SWW	no recording	-	2878 (9442)	262	2701 (8862)	193
NWW	2553 (8376)	-	2697 (8848)	101	3021 (9911)	117

Table 40. Results of impact-echo - I-395 bridge over Main Street.

Section	2010		2012		2013	
	Average frequency (Hz)	Standard deviation	Average frequency (Hz)	Standard deviation	Average frequency (Hz)	Standard deviation
1	1075	58	1108	194	1157	140
2	1137	108	1156	85	1250	153
3	1179	104	1094	28	1173	131
5	974	280	949	71	1007	96
SWW	Not assessed	-	Not assessed	-	Not assessed	-
NWW	Not assessed	-	Not assessed	-	Not assessed	-

Nonlinear acoustics measurements were not performed on the wing walls because the surface damage was too rough. Only one measurement per section was performed, typically around the center of the wall section (see Figure 67B). The results of nonlinear acoustics (ΔT) are provided in Table 41.

Table 41. Results of nonlinear acoustics - I-395 bridge over Main Street.

Sections	ΔT ($x10^{-8}$ s)		
	2010	2012	2013
1	52	136	Noisy signals
2	9	70	22
3	24	25	43
4	Not assessed	73	18
5	36	118	63

Table 42 presents the measured temperature and relative humidity values obtained from the performance monitoring sites of the I-395 bridge over the Penobscot River. For the various monitoring sites (see Figure 68A), data are reported at 25-millimeter (~1 inch), 50-millimeter (~2 inches), and 75-millimeter (~3 inches) depths below the surface.

Table 42. Relative humidity and temperature measurements - I-395 bridge over the Penobscot River.

Section	Site	Depth	Data	May 2010 23 °C (74 °F)* Before treatment	June 2011 22 °C (71 °F)*	August 2012 20 °C (68 °F)*	June 2013 19 °C (66 °F)*
40 percent silane (water-based)	1	25 mm (1 in.)	T °C (°F)	25.6 (78.1)	-	25.2 (74.4)	22.5 (72.5)
			RH%	83.4	-	92.9	91.1
		50 mm (2 in.)	T °C (°F)	24.5 (76.1)	-	24.5 (76.1)	22.3 (72.1)
			RH%	88.7	-	93.2	87.1
		75 mm (3 in.)	T °C (°F)	23.5 (74.3)	-	26.6 (79.9)	22.2 (72.0)
			RH%	90.8	-	92.3	91.2
Control	5	25 mm (1 in.)	T °C (°F)	28.5 (83.3)	-	30.1 (86.2)	23.7 (74.7)
			RH%	68.5	-	88.9	83.7
		50 mm (2 in.)	T °C (°F)	25.8 (78.4)	-	30.1 (86.2)	23.4 (74.1)
			RH%	77.5	-	85.4	86.5
		75 mm (3 in.)	T °C (°F)	22.8 (73.0)	-	29.6 (85.3)	22.7 (72.9)
			RH%	86.8	-	87.0	88.8

*That temperature corresponds to the daily average obtained from http://www.wunderground.com

Table 43 present the length change values obtained from the performance monitoring sites on the I-395 Bridge over the Penobscot River. Data are reported for a 500-millimeter (20-inch) gauge length in both the horizontal and vertical directions. The data were not corrected for thermal effects.

Table 43. Expansion results (%) - I-395 bridge over the Penobscot River.

Section	Site	Location	May 2010 23 °C (74 °F)* Before treatment	June 2011 22 °C (71 °F)*	August 2012 20 °C (68 °F)*	June 2013 19 °C (66 °F)*
40 percent silane (water-based)	1	Vertical	"0" reading	0.053	0.017	0.022
		Horizontal	"0" reading	0.032	0.053	0.052
	2	Vertical	"0" reading	0.051	0.008	0.011
		Horizontal	"0" reading	0.019	0.012	0.011
100 percent silane	4	Vertical	"0" reading	0.044	0.010	0.004
		Horizontal	"0" reading	0.024	0.027	0.041
Control	5	Vertical	"0" reading	0.042	0.018	0.014
		Horizontal	"0" reading	0.020	0.041	0.036
	6	Vertical	"0" reading	0.064	0.032	0.034
		Horizontal	"0" reading	0.020	0.032	0.029

*That temperature corresponds to the daily average obtained from http://www.wunderground.com

Table 44 gives the results of Cracking Index measurement values obtained from the performance monitoring sites of the I-395 Bridge over the Penobscot River. CI data are given in mm/m (or in./yd) as they correspond to the total crack opening, in mm (in.), averaged over a one-meter (or one-yard) length; they are calculated from the measurement of crack widths along a grid system composed of the four lines of a 500-mm (20-in.) square and of the two 700-mm (28-in.) diagonal lines (total of 3.4 m (about 11 ft) of lines).

Table 44. Cracking Index measurements - I-395 bridge over the Penobscot River.

Section	Site	May 2010 23 °C (74 °F)* mm/m (in./yd) Before treatment	June 2011 22 °C (71 °F)* mm/m (in./yd)	August 2012 2 0°C (68 °F)* mm/m (in./yd)	June 2013 19 °C (66 °F)* mm/m (in./yd)
40 percent silane (water-based)	1	1.95 (0.070)	1.88 (0.068)	1.68 (0.060)	1.56 (0.056)
	2	1.09 (0.039)	1.31 (0.047)	1.35 (0.048)	0.94 (0.034)
100 percent silane	3	0.92 (0.033)	0.99 (0.036)	-	0.55 (0.020)
Control	4	1.25 90.045)	1.33 (0.048)	1.04 (0.037)	0.92 (0.033)
	5	2.04 (0.073)	2.37 (0.085)	2.72 (0.098)	1.41 (0.051)

*That temperature corresponds to the daily average obtained from http://www.wunderground.com

The lower part of columns 1 and 3 were assessed. The same grid type was used as for other structures (15 x 3) (see Figure 68B). The letters "l" and "r" refer to the left and right sections of the column respectively. UPV results are given in Table 45, while Table 46 provides data from impact-echo measurements.

Table 45. Results of UPV - I-395 bridge over the Penobscot River.

Site	2010		2012		2013	
	Average UPV m/s (ft/s)	Standard deviation	Average UPV (m/s)	Standard deviation	Average UPV m/s (ft/s)	Standard deviation
Column 1r	4065 (13337)	-	3754 (12316)	554	3893 (12772)	182
Column 1l	4320 (14173)	-	3896 (12782)	79	3730 (12238)	316
Column 3r	4329 (14203)	-	3799 (12464)	361	3136 (10289)	417
Column 3l	4274 (14022)	-	3710 (12172)	40	3064 (10052)	283

Table 46. Results of impact-echo - I-395 bridge over the Penobscot River.

Column	2010		2012		2013	
	Average frequency (Hz)	Standard deviation	Average frequency (Hz)	Standard deviation	Average frequency (Hz)	Standard deviation
Column 1r	1374	0	1075	92	1098	101
Column 1l	1396	302	1159	100	1204	133
Column 3r	1460	102	1155	78	1182	125
Column 3l	1150	127	1135	67	1118	89

Unlike UPV and impact-echo, nonlinear acoustics measurements were taken at about 4 m (13 ft) above the ground (see Figure 68B). Table 47 provides the results of ΔT.

Table 47. Results of nonlinear acoustics - I-395 bridge over the Penobscot River.

Column	ΔT ($x10^{-8}$ s)		
	2010	2012	2013
Column 1r	53	111	26
Column 1l	45	82	98
Column 3r	73	115	65
Column 3l	26	56	28

A seismic tomography was performed on columns 1 and 3 during 2012. Seismic tomography enables the mapping of sections in order to image the distribution of the concrete condition in 2D. The different zones visible on the investigated sections correspond to the variations in the propagation velocity of compression waves through the concrete. These waves, generated by a mechanical impact, are the first waves to be recorded by the receiver (accelerometers), so they are also called primary waves or P-waves. The variations of velocity, calculated from the different signals recorded by every receiver, are related to the mechanical properties of the concrete (primarily the stiffness), as well as the presence of large defects such as cracks or voids. Therefore, zones of lower speeds correspond to lower quality or damaged concrete. The aim of a tomography is thus to identify problematic areas in a concrete body. Additional information on seismic tomography applied to ASR can be found in Rivard et al. (2010).

Forty-eight accelerometers were placed around the column along a horizontal plane located about 79 in. (201 cm) above the ground (see Figure 76). Impacts were generated with a hammer. This configuration enables imaging a horizontal cross-section of the column.

Figure 76. Seismic tomography on Column 1 of the I-395 bridge over the Penobscot River.

Table 48 presents the measured temperature and relative humidity values obtained from the performance monitoring sites of the 5th Parkway bridge over I-395. For the various monitoring sites (see Figure 69A), data are reported at 25-millimeter (~1 inch), 50-millimeter (~2 inches), and 75-millimeter (~3 inches) depths below the surface. Also, one will note that many data are missing from the different survey times. This is due to the fact that several holes were either filled with water or humid (condensation) to the point that no reliable data could be obtained from those holes during the field surveys.

Table 48. Relative humidity and temperature - 5th Parkway (Robertson Road) bridge over I-395.

Section	Site	Depth	Data	May 2010 23 °C (74 °F)* Before treatment	June 2011 22 °C (71 °F)*	August 2012 20 °C (68 °F)*	June 2013 19 °C (66 °F)*
40 percent silane (water-based)	1	25 mm (1 in.)	T °C (°F)	27.4 (81.3)	-	29.6 (85.3)	-
			RH%	92.6	-	90.8	-
		50 mm (2 in.)	T °C (°F)	25.3 (77.5)	-	28.1 (82.6)	26.4 (79.5)
			RH%	92.4	-	92.4	89.6
		75 mm (3 in.)	T °C (°F)	24.5 (76.1)	-	27.6 (81.7)	-
			RH%	87.2	-	93.2	-
Elastomeric coating	4	25 mm (1 in.)	T °C (°F)	23.2 (73.8)	27.1 (80.8)	29.8 (85.6)	-
			RH%	91.9	90.0	86.0	-
		50 mm (2 in.)	T °C (°F)	22.6 (72.7)	26.3 (79.3)	28.2 (82.8)	-
			RH%	87.9	93.0	86.8	-
		75 mm (3 in.)	T °C (°F)	22.3 (72.1)	25.4 (77.7)	27.5 (81.5)	-
			RH%	89.8	94.3	88.5	-
100 percent silane	5	25 mm (1 in.)	T °C (°F)	25.3 (77.5)	-	-	29.2 (84.6)
			RH%	85.9	-	-	91
		50 mm (2 in.)	T °C (°F)	22.0 (71.6)	-	25.4 (77.7)	28.7 (83.7)
			RH%	92.0	-	93.2	89.8
		75 mm (3 in.)	T °C (°F)	21.4 (70.5)	26.3 (79.3)	24.7 (76.5)	-
			RH%	91.3	89.2	91.9	-
Control	8	25 mm (1 in.)	T °C (°F)	18.1 (64.6)	24.2 (75.6)	23.5 (74.3)	22.9 (73.2)
			RH%	92.1	89.7	93.4	82.6
		50 mm (2 in.)	T °C (°F)	16.1 (61.0)	22.6 (72.7)	22.8 (73.0)	20.7 (69.3)
			RH%	79.0	89.1	90.4	90.7
		75 mm (3 in.)	T °C (°F)	15.7 (60.3)	21.9 (71.4)	22.3 (72.1)	20.0 (68.0)
			RH%	92.5	92.7	93.3	90.1

*That temperature corresponds to the daily average obtained from http://www.wunderground.com

Table 49 presents the length change values obtained from the performance monitoring sites on the 5th Parkway bridge over I-395. Data are reported for a 500-millimeter (20-inch) gauge length in the horizontal and vertical directions. The data were not corrected for thermal effects.

Table 50 gives the results of Cracking Index measurement values obtained from the performance monitoring sites of the 5th Parkway bridge over I-395. CI data are given in mm/m (or in./yd) as they correspond to the total crack opening, in mm (in.), averaged over a one-meter (or one-yard) length; they are calculated from the measurement of crack widths along a grid system composed of the four lines of a 500-mm (20-in.) square and of the two 700-mm (28-in.) diagonal lines (total of 3.4 m (about 11 ft) of lines). In general, the higher the CI values, the higher the extent of (surface) damage on the concrete element investigated.

Table 49. Expansion results (%)- 5th Parkway (Robertson Road) bridge over I-395.

Section	Site	Location	May 2010 23 °C (74 °F)* Before treatment	June 2011 22 °C (71 °F)*	August 2012 20 °C (68 °F)*	June 2013 19 °C (66 °F)*
40 percent silane (water-based)	1	Vertical	"0" reading	0.032	0.001	0.012
		Horizontal	"0" reading	-0.008	0.015	0.009
	2	Vertical	"0" reading	0.039	0.061	0.078
		Horizontal	"0" reading	0.036	0.049	0.051
Elastomeric coating	3	Vertical	"0" reading	-0.001	0.031	0.056
		Horizontal	"0" reading	0.016	0.046	0.056
	4	Vertical	"0" reading	0.028	0.009	0.025
		Horizontal	"0" reading	0.015	-0.004	0.009
100 percent silane	5	Vertical	"0" reading	0.104	0.133	0.152
		Horizontal	"0" reading	0.009	0.015	0.022
	6	Vertical	"0" reading	0.100	0.127	0.158
		Horizontal	"0" reading	0.059	0.115	0.133
Control	7	Vertical	"0" reading	0.038	0.007	0.002
		Horizontal	"0" reading	0.009	0.013	0.007
	8	Vertical	"0" reading	0.044	0.056	0.068
		Horizontal	"0" reading	0.044	0.090	0.115

*That temperature corresponds to the daily average obtained from http://www.wunderground.com

Table 50. Cracking Index measurements - 5th Parkway (Robertson Road) bridge over I-395.

Section	Site	May 2010 23 °C (74 °F)* mm/m (in./yd) Before treatment	June 2011 22 °C (71 °F)* mm/m (in./yd)	August 2012 20 °C (68 °F)* mm/m (in./yd)	June 2013 19 °C (66 °F)* mm/m (in./yd)
40 percent silane (water-based)	1	1.82 (0.065)	2.08 (0.075)	1.98 (0.071)	1.68
	2	0.93 (0.033)	1.29 (0.046)	1.12 (0.040)	1.27
Elastomeric coating	3	1.82 (0.065)	-	0.00 (0.000)	0.00 (0.000)
	4	4.12 (0.148)	-	0.00 (0.000)	0.00 (0.000)
100 percent silane	5	3.97 (0.143)	4.29 (0.154)	4.24 (0.152)	2.72 (0.098)
	6	3.99 (0.143)	4.21 (0.151)	4.39 (0.158)	3.27 (0.117)
Control	7	0.78 (0.028)	1.00 (0.036)	0.90 (0.032)	0.72 (0.026)
	8	1.92 (0.069)	2.37 (0.085)	1.97 (0.071)	2.68 (0.096)

*That temperature corresponds to the daily average obtained from http://www.wunderground.com

The configuration used for Robertson Road is similar to the previous bridges, but no measurements were taken on the west wing wall (see Figure 69B). Results of UPV are given in Table 51, while Table 52 provides data from impact-echo measurements.

Nonlinear acoustics measurements were performed on the east wing wall as well as on sections 2 and 3 of the abutment (see Figure 69B). Results of ΔT are provided in Table 53.

Table 51. Results of UPV - 5th Parkway (Robertson Road) bridge over I-395.

Section	2010		2012		2013	
	Average UPV m/s (ft/s)	Standard deviation	Average UPV m/s (ft/s)	Standard deviation	Average UPV m/s (ft/s)	Standard deviation
EWW	2735 (8973)	-	2667 (8750)	173	2483 (8146)	233
2	3020 (9908)	-	3682 (12080)	361	3390 (11122)	137
3	4663 (15299)	-	3432 (11260)	674	3540 (11614)	336

Table 52. Results of impact-echo - 5th Parkway (Robertson Road) bridge over I-395.

Section	2010		2012		2013	
	Average frequency (Hz)	Standard deviation	Average frequency (Hz)	Standard deviation	Average frequency (Hz)	Standard deviation
EWW	Not assessed		1038	118	1177	81
2	1239	117	1227	180	1327	64
3	1323	83	1258	214	1333	63

Table 53. Results of nonlinear acoustics - 5th Parkway (Robertson Road) bridge over I-395.

Section	ΔT (x10^{-8} s)		
	2010	2012	2013
EWW	525	76	148
2	66	42	5
3	30	93	3

Table 54 presents the measured temperature and relative humidity values obtained from the performance monitoring sites of the South Parkway bridge over I-395. For the various monitoring sites (see Figure 70A), data are reported at 25-millimeter (~1 inch), 50-millimeter (~2 inches), and 75-millimeter (~3 inches) depths below the surface.

Table 55 gives the length change values obtained from the performance monitoring sites on the South Parkway bridge over I-395. Data are reported for a 500-millimeter (20-inch) gauge length in the horizontal and vertical directions. The data were not corrected for thermal effects.

Table 54. Relative humidity and temperature measurements - South Parkway bridge over I-395.

Section	Site	Depth	Data	May 2010 23 °C (74 °F)* Before treatment	June 2011 22 °C (71 °F)*	August 2012 20 °C (68 °F)*	June 2013 19 °C (66 °F)*
Control 1	1	25 mm (1 in.)	T °C (°F)	27.5 (81.5)	28.7 (83.7)	24.9 (76.8)	17.6 (63.7)
			RH%	60.4	74.8	74.3	85.2
		75 mm (3 in.)	T °C (°F)	24.5 (76.1)	26.0 (78.8)	23.6 (74.5)	17.5 (63.5)
			RH%	79.0	83.5	84.8	80.5
40 percent silane (water-based)	3	25 mm (1 in.)	T °C (°F)	19.2 (66.6)	25.5 (77.9)	24.3 (75.7)	17.4 (63.3)
			RH%	86.0	77.5	93.1	68.7
		75 mm (3 in.)	T °C (°F)	19.2 (66.6)	21.2 (70.2)	23.7 (74.7)	17.5 (63.5)
			RH%	89.0	84.8	87.2	78.3
Control 2	4	25 mm (1 in.)	T °C (°F)	19.0 (66.2)	25.5 (77.9)	24.7 (76.5)	18.0 (64.4)
			RH%	84.4	82.3	81.4	74.7
		75 mm (3 in.)	T °C (°F)	19.0 (66.2)	24.7 (76.5)	24.3 (75.7)	17.9 (64.2)
			RH%	88.1	81.5	84.0	80
Control 3	5	25 mm (1 in.)	T °C (°F)	-	25.7 (78.3)	26.0 (78.8)	19.0 (62.2)
			RH%	-	89.8	84.0	91.1
		75 mm (3 in.)	T °C (°F)	-	25.1 (77.2)	26.0 (78.8)	19.0 (62.2)
			RH%	-	81.6	87.0	87

*That temperature corresponds to the daily average obtained from http://www.wunderground.com

Table 55. Expansion results (%) - South Parkway bridge over I-395.

Section	Site	Location	May 2010 23 °C (74 °F)* Before treatment	June 2011 22 °C (71 °F)*	August 2012 20 °C (68 °F)*	June 2013 19 °C (66 °F)*
Control	1	Lower	"0" reading	-0.017	0.137	0.167
		Upper	"0" reading	-0.007	0.034	0.153
Lithium electrochemical	2	Lower	"0" reading	0.074	0.269	0.210
		Upper	"0" reading	0.069	0.166	0.225
40 percent silane (water-based)	3	Lower	"0" reading	0.014	0.090	0.119
		Upper	"0" reading	0.000	0.038	0.038
Control	4	Lower	"0" reading	-0.019	0.038	0.128
		Upper	"0" reading	0.052	0.106	0.136
Control	5	Lower	"0" reading	0.019	0.085	0.085
		Upper	"0" reading	0.012	0.103	0.178

*That temperature corresponds to the daily average obtained from http://www.wunderground.com

Table 56 gives the results of Cracking Index values obtained from the performance monitoring sites of the South Parkway bridge over I-395. CI data are given in mm/m (or in./yd) as they correspond to the total crack opening, in mm (in.), averaged over a one-meter (or one-yard) length. In the case of the reinforced concrete columns of the South Parkway bridge over I-395, crack mapping was carried out by tracing two horizontal lines, one meter apart (approximately three feet), along the circumference of the columns. Measurements of the number of cracks and their opening were carried out along those lines to quantify the extent of cracking in those structural elements.

Table 56. Cracking Index measurements - South Parkway bridge over I-395.

Section	Site	May 2010 23 °C (74 °F)* mm/m (in./yd) Before treatment	June 2011 22 °C (71 °F)* mm/m (in./yd)	August 2012 20 °C (68 °F)* mm/m (in./yd)	June 2013 19 °C (66 °F)* mm/m (in./yd)
Control	1	3.8 (0.136)	-	2.68 (0.096)	2.38 (0.085)
Lithium electrochemical	2	1.38 (0.050)	1.2 (0.043)	0.83 (0.030)	0.89 (0.032)
40 percent silane (water-based)	3	0.63 (0.023)	0.64 (0.023)	0.63 (0.023)	0.56 (0.020)
Control	4	0.58 (0.021)	0.63 (0.023)	0.71 (0.026)	0.69 (0.025)
Control	5	0.86 (0.031)	0.78 (0.028)	1.35 (0.048)	1.17 (0.042)
FRP wrap	6	-	-	-	-

*That temperature corresponds to the daily average obtained from http://www.wunderground.com

Due to the circular shape of the columns, only UPV was performed on that site. Wave velocities were measured through direct transmission, so P-waves probed the surface and inside concrete. Four measurements were done: two parallel and two perpendicular to the highway. Columns 1 to 5 were assessed. Nonlinear acoustics testing was not conducted on this site. Table 57 gives the results of UPV for the five columns.

Table 57. Results of UPV - South Parkway bridge over I-395.

Column	2010		2012		2013	
	Average speed m/s (ft/s)	Standard deviation	Average speed m/s (ft/s)	Standard deviation	Average speed m/s (ft/s)	Standard deviation
1	3781 (12405)	-	4057 (13310)	23	4042 (13261)	8
2	4123 (13527)	-	4350 (14272)	20	4176 (13701)	53
3	4341 (14242)	-	4377 (14360)	52	4104 (13465)	8
4	4263 (13986)	-	4386 (14390)	44	4168 (13675)	33
5	4217 (13835)	-	4186 (13734)	103	3945 (12943)	32

Table 58 presents the measured temperature and relative humidity values obtained from the performance monitoring sites of the Green Point Road bridge over I-395. For the various monitoring sites (see Figure 71A), data are reported at 25-millimeter (~1 inch), 50-millimeter (~2 inches), and 75-millimeter (~3 inches) depths below the surface. Also, one will note that many data are missing from the different survey times. This is due to the fact that several holes were either filled with water or humid (condensation) to the point that no reliable data could be obtained from those holes during the field surveys.

Table 59 presents the length change values obtained from the performance monitoring sites on the Green Point Road bridge over I-395. Data are reported for a 500-millimeter (20-inch) gauge length in both the horizontal and vertical directions. The data were not corrected for thermal effects.

Table 58. Relative humidity and temperature measurements - Green Point Road bridge over I-395.

Section	Site	Depth	Data	May 2010 23 °C (74 °F)* Before treatment	June 2011 22 °C (71 °F)*	August 2012 20 °C (68 °F)*	June 2013 19 °C (66 °F)*
Control	1	25 mm (1 in.)	T °C (°F)	21.1 (70.0)	23.3 (73.9)	24.2 (75.6)	21.9 (71.4)
			RH%	63.2	76.3	74.2	70.8
		50 mm (2 in.)	T °C (°F)	19.0 (66.2)	-	24.0 (75.2)	21.3 (70.3)
			RH%	92.8	-	93.2	93.1
		75 mm (3 in.)	T °C (°F)	19.0 (66.2)	22.4 (72.3)	23.7 (74.7)	20.9 (69.6)
			RH%	92.7	92.5	95.6	91.5
100% silane	4	25 mm (1 in.)	T °C (°F)	23.1 (73.6)	26.6 (79.9)	27.0 (80.6)	-
			RH%	89.7	93.0	92.6	-
		50 mm (2 in.)	T °C (°F)	21.9 (71.4)	-	26.6 (79.9)	-
			RH%	92.1	-	91.3	-
		75 mm (3 in.)	T °C (°F)	21.5 (70.7)	25.1 (77.2)	26.2 (79.2)	-
			RH%	87.6	94.6	93.1	-
40% silane (water-based)	5	25 mm (1 in.)	T °C (°F)	19.6 (67.3)	-	27.0 (80.6)	25.8 (78.4)
			RH%	89.4	-	85.1	86.4
		50 mm (2 in.)	T °C (°F)	19.1 (66.4)	23.7 (74.7)	25.4 (77.7)	24.9 (76.8)
			RH%	91.9	92.3	90.8	90.6
		75 mm (3 in.)	T °C (°F)	19.2 (66.6)	23.6 (74.5)	24.6 (76.3)	24.9 (76.8)
			RH%	77.1	93.7	92.8	89
Elastomeric coating	8	25 mm (1 in.)	T °C (°F)	18.8 (65.8)	-	23.6 (74.5)	22.1 (71.8)
			RH%	94.4	-	93.3	89.2
		50 mm (2 in.)	T °C (°F)	17.6 (63.7)	24.3 (75.7)	23.2 (73.8)	20.6 (69.1)
			RH%	93.5	92.1	92.9	91.8
		75 mm (3 in.)	T °C (°F)	17.3 (63.1)	22.4 (72.3)	22.5 (72.5)	19.9 (67.8)
			RH%	92.4	90.5	91.5	89.4

*That temperature corresponds to the daily average obtained from http://www.wunderground.com

Table 60 gives the results of Cracking Index measurement values obtained from the performance monitoring sites of the Green Point Road bridge over I-395. CI data are given in mm/m (or in./yd) as they correspond to the total crack opening, in mm (in.), averaged over a one-meter (or one-yard) length. They are calculated from the measurement of crack widths along a grid system composed of the four lines of a 500-mm (20-in.) square and of the two 700-mm (28-in.) diagonal lines (total of 3.4 m (about 11 ft) of lines). In general, the higher the CI values, the higher the extent of (surface) damage on the concrete element investigated.

Table 59. Expansion results (%) - Green Point Road bridge over I-395.

Section	Site	Location	May 2010 23 °C (74 °F)* Before treatment	June 2011 22 °C (71 °F)*	August 2012 20 °C (68 °F)*	June 2013 19 °C (66 °F)*
Control	1	Vertical	"0" reading	-	-	-
		Horizontal	"0" reading	0.012	0.040	0.041
	2	Vertical	"0" reading	0.068	0.106	0.125
		Horizontal	"0" reading	0.091	0.161	0.174
100 percent silane	3	Vertical	"0" reading	0.050	0.078	0.079
		Horizontal	"0" reading	0.041	0.116	0.132
	4	Vertical	"0" reading	0.123	0.218	0.259
		Horizontal	"0" reading	0.000	0.047	0.055
40 percent silane (water-based)	5	Vertical	"0" reading	0.056	0.078	0.103
		Horizontal	"0" reading	-0.014	-0.004	-0.002
	6	Vertical	"0" reading	0.057	0.074	0.080
		Horizontal	"0" reading	0.017	0.058	0.072
Elastomeric coating	7	Vertical	"0" reading	0.041	0.091	0.097
		Horizontal	"0" reading	0.016	0.041	0.047
	8	Vertical	"0" reading	0.037	0.011	0.049
		Horizontal	"0" reading	0.051	0.071	0.056

*That temperature corresponds to the daily average obtained from http://www.wunderground.com

Table 60. Cracking Index measurements - Green Point Road bridge over I-395.

Section	Site	May 2010 23 °C (74 °F)* mm/m (in./yd) Before treatment	June 2011 22 °C (71 °F)* mm/m (in./yd)	August 2012 20 °C (68 °F)* mm/m (in./yd)	June 2013 19 °C (66 °F)* mm/m (in./yd)
Control	1	5.35 (0.192)	6.30 (0.226)	5.02 (0.180)	4.89 (0.176)
	2	1.57 (0.056)	1.89 (0.068)	1.64 (0.059)	2.17 (0.078)
100 percent silane	3	3.32 (0.119)	3.73 (0.134)	4.02 (0.144)	3.54 (0.127)
	4	4.97 (0.179)	5.36 (0.193)	4.83 (0.173)	4.08 (0.147)
40 percent silane (water-based)	5	4.41 90.158)	5.01 (0.180)	3.99 (0.143)	3.05 (0.110)
	6	1.69 (0.061)	2.26 (0.081)	2.25 (0.081)	1.64 (0.059)
Elastomeric coating	7	3.19 (0.115)	-	0.00	0.00
	8	8.45 (0.304)	-	0.00	0.00

*That temperature corresponds to the daily average obtained from http://www.wunderground.com

The same configuration as that used for the 5th Parkway (Robertson Road) bridge over I-395 was adopted; however, the wing walls were not assessed due to the high level of damage (see Figure 71B). UPV results are given in Table 61, while Table 62 provides data from impact-echo measurements.

Nonlinear acoustics measurements were not performed on the wing walls but only on the abutment walls (see Figure 71B). Table 63 provides the ΔT calculated for all sections of the Green Point Road bridge.

Table 61. Results of UPV - Green Point Road bridge over I-395.

Section	2010		2012		2013	
	Average UPV m/s (ft/s)	Standard deviation	Average UPV m/s (ft/s)	Standard deviation	Average UPV m/s (ft/s)	Standard deviation
1	3715 (12188)	-	3703 (12149)	233	3660 (12008)	287
2	4148 (13609)	-	3997 (13114)	174	3970 (13025)	77
3	3797 (12457)	-	3463 (11362)	400	3700 (12139)	461

Table 62. Results of impact-echo - Green Point Road bridge over I-395.

Section	2010		2012		2013	
	Average Frequency (Hz)	Standard deviation	Average Frequency (Hz)	Standard deviation	Average Frequency (Hz)	Standard deviation
1	1309	115	1390	176	1201	134
2	1464	96	1555	154	1351	118
3	1386	37	1388	175	1213	99

Table 63. Results of nonlinear acoustics - Green Point Road bridge over I-395.

Section	ΔT ($x10^{-8}$ s)		
	2010	2012	2013
1	101	56	113
2	60	115	127
3	65	81	88
4	111	111	93

7.4 DATA ANALYSES

Considering that ASR was found to be a contributing factor to the deterioration observed in the structures selected for treatment along I-395 in Bangor, ME, it is important to keep in mind the main objectives of this investigation:

- Main objective: evaluate the long term efficacy of various types of treatments to control the progress of deterioration in ASR-affected concrete members;
- Secondary objectives: further analyze this efficacy as a function of:
  - Different types of elements (treated vs. control, different types of structural elements – abutment and wing walls, reinforced concrete columns),
  - Different exposure conditions (for instance in relation to the exposure conditions, e.g., direct exposure to rain, availability of moisture from backfill material (wing walls), direct exposure to sun (UV degradation of the sealer), etc.),
  - Different types of treatment products (penetrating sealers, surface coating).
  - Other treatment approaches (chemical treatment, strengthening)

Because of the timing of the applications (summer of 2010), performance monitoring data are available for a period of only 3 years. Consequently, in general, it is too early to be able to draw any definite conclusions from the monitoring data accumulated so far. However, observations can be made from some of the data accumulated to date.

Increasing RH values with increasing depth are obtained at Site 2 (control) located on the abutment wall section, but protected under the bridge deck (see Figure 67A for site locations); the RH values were found to vary over time but with no specific increasing or decreasing trend (see Figure 77A). On the other hand, RH values for Site 3, treated in 2010 with elastomeric coating and also under the bridge deck, showed a drop in RH values in 2013 (see Figure 77B). It is yet to be seen if this "trend" will continue in 2014.

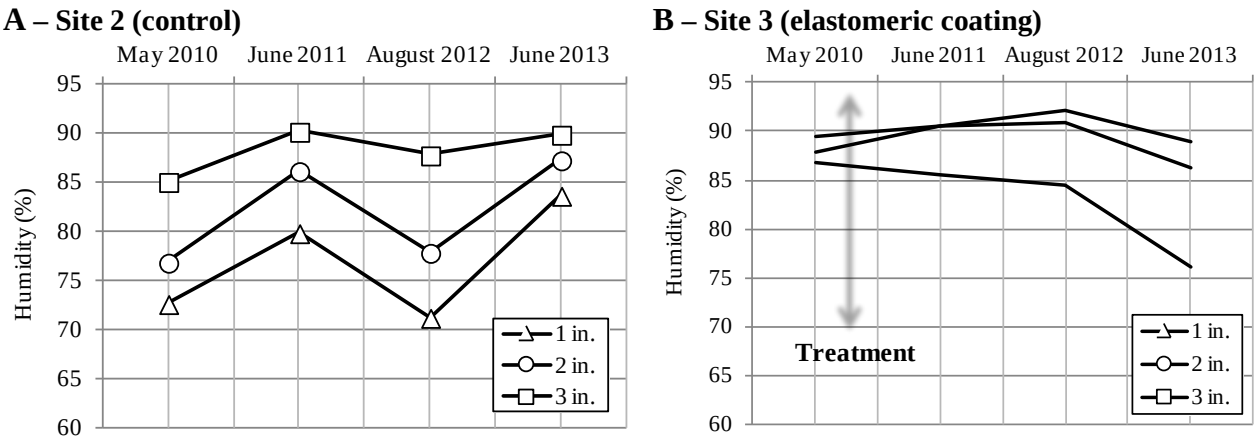

Figure 77. Values of relative humidity as a function of depth over the 2010-2013 monitoring period (I-395 over Main Street).
A: Site 2 – no treatment (control) (not exposed – under bridge deck). B: Site 3 – treated with the elastomeric coating (not exposed – under bridge deck).

Length change data often show a significant increase between the 2010 (initial or "0") and the 2011 readings. Such a "jump" was actually visible for either control or treated sites. The reason(s) for such an increase is (are) unclear; however, it is unlikely to be related to ASR and probably due to the stabilization of the gauge studs at the measuring sites between the two readings. It is consequently more realistic to look at the progress in length changes after the 2011 reading to analyze the possible progress of ASR and the effects of the treatments on expansion.

Following the initial 2010-2011 "jump" in the readings, limited additional expansions, and even some "shrinkage" were measured at the different sites (see Figure 78), with the exception, perhaps, of the horizontal direction at Site 3 (not exposed), treated with elastomeric coating, which seems to display progressive expansion (see Figure 78B). The latter was somewhat unexpected considering that Site 3 is well protected from rainfall (under the bridge deck), showed a decreasing trend for RH values in 2013 (see Figure 77B), and no significant cracking was observed after the treatment (Cracking Index values of 0.0 both in 2012 and 2013 – see Figure 79). Further monitoring will be necessary to confirm that trend.

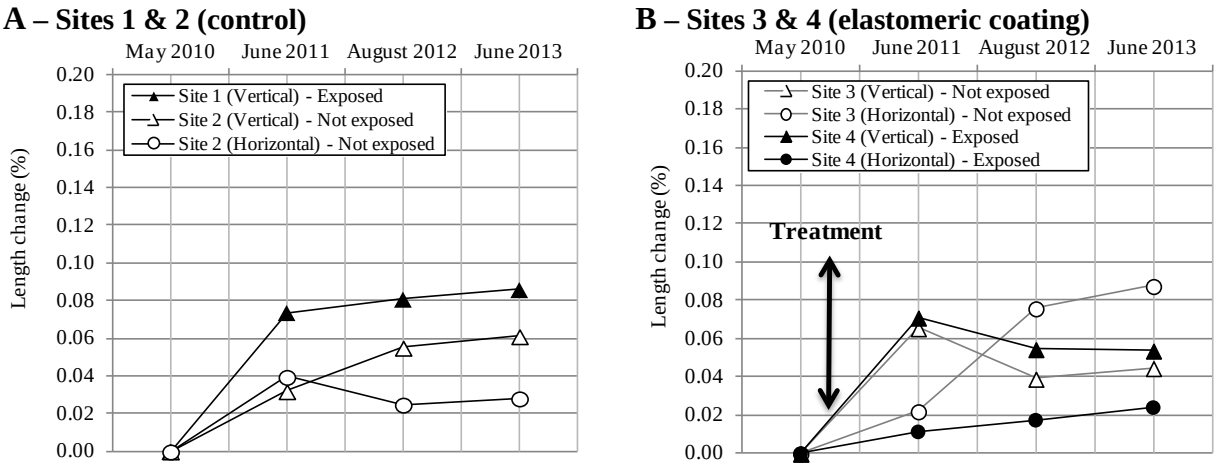

Figure 78. Values of length changes over the 2010-2013 monitoring period (I-395 bridge over Main Street). A: Site 2 – no treatment (control) (not exposed – under bridge deck). B: Site 3 – treated with the elastomeric coating (not exposed – under bridge deck).

Figure 79 illustrates the results of the Cracking Index measurements over the 2010-2013 monitoring period. As expected, higher CI values were observed for Site 1 (exposed to moisture) than Site 2 (protected from moisture under the bridge deck). This can be seen clearly from Figure 80 that illustrates the crack maps both in 2010 and 2013. The above figures suggest an increase in the severity of cracking with time at Site 1 (see Figure 80A and Figure 80B); however, such a trend is unclear from the CI data. This might be partially due to the fact that operators performing the CI have changed over time, which is a source of variability in the test.

It is to be noted that in the case of the sections treated with the elastomeric coating, CI values of "0" were obtained for the measurements carried out in 2012 and 2013 (see Figure 79), i.e., following the application of the coating. The product has generally been efficient in bridging the cracks present in the treated concrete member (see Figure 80E and Figure 80F).

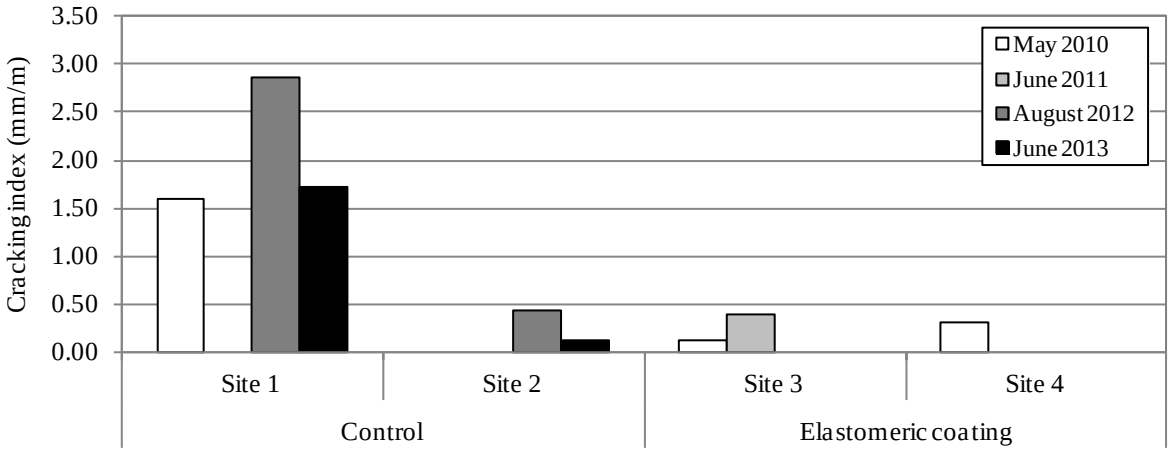

Figure 79: Values of Cracking Index over the 2010-2013 monitoring period (I-395 bridge over Main Street).

A – Control (Site 1: exposed) 2010

B – Control (Site 1: exposed) 2013

C – Control (Site 2: not exposed) 2010

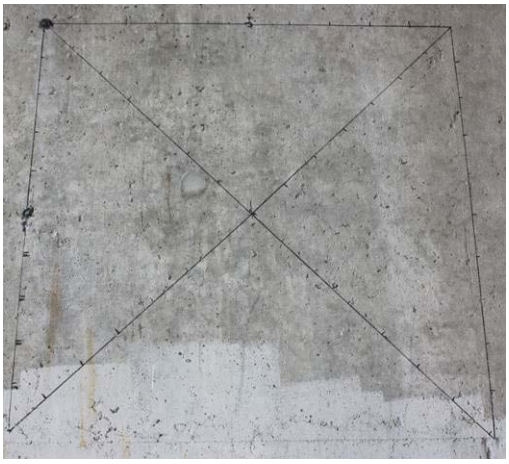

D – Control (Site 2: not exposed) 2013

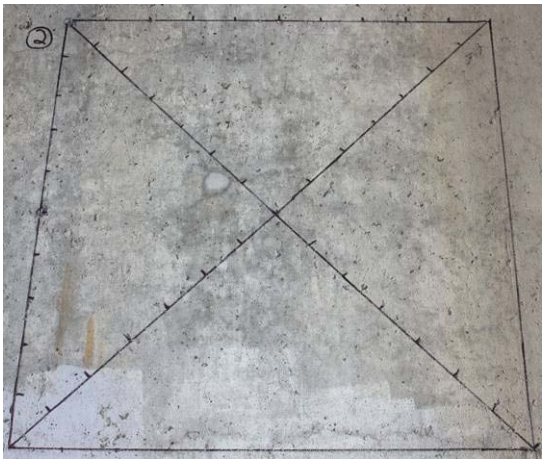

E – Elastomeric coating (Site 4: exposed) 2010

F – Elastomeric coating (Site 4: exposed) 2013

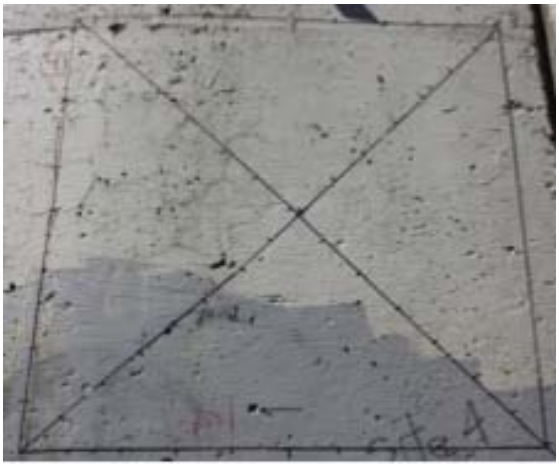

Figure 80. Examples of crack map sections before (2010) and after (2013) treatments (I-395 bridge over Main Street).

The evolution of the velocities with time can be seen in Figure 81. The values of UPV show high variations from one section to another, as well as over time. Standard deviations are fairly high for nearly every section in 2012 and 2013, which might partly explain the absence of a conclusive trend. Sections 2 and 3, protected from the sun and rain, show the highest velocities (lower damage). Both wing walls (i.e. SWW and NWW) typically show velocities below 3000 m/s (9843 ft/s) and appear to be the most deteriorated sections. However, the surface concrete condition of the north wing wall seems to improve with time (velocities increasing from 2553 m/s (8376 ft/s) to 3021 m/s (9911 ft/s)). The latter was treated with the elastomeric coating in 2010.

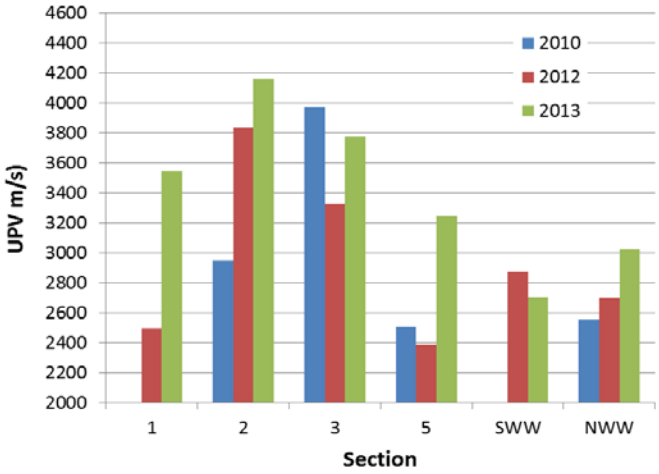

Figure 81. Evolution of UPV with time (I-395 bridge over Main Street).

Figure 82 illustrates the evolution of the peak frequencies with time. According to the impact-echo results, section 5 is significantly more deteriorated (lower frequencies) than the other sections, and the level of damage is still fairly constant with time (despite the treatment with the elastomeric coating). The concrete condition does not seem to vary significantly between the other sections. There are slight increases with time of the frequencies in sections 1 and 2 (control sections but somewhat protected under the bridge deck), which would suggest that the concrete quality is improving. Some fluctuations were observed in section 3.

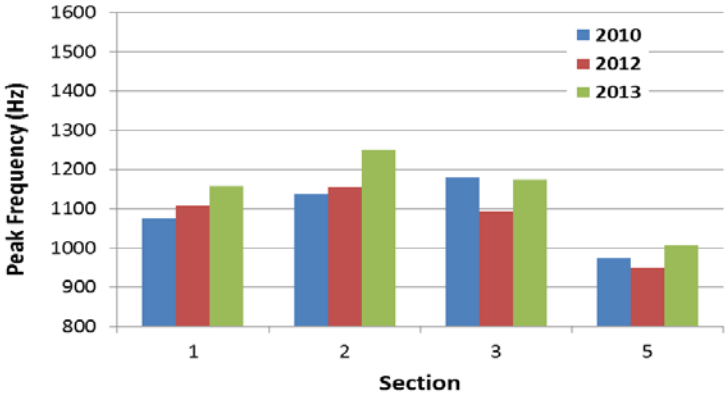

Figure 82. Evolution of peak frequency with time (I-395 bridge over Main Street).

The evolution of ΔT (nonlinear acoustics) with time is shown in Figure 83. No general trend can be drawn from the nonlinear acoustics measurements. Damage in section 1 seems to increase significantly from 2010 to 2012. Signals were however too noisy in 2013 to be recorded. Middle (not exposed) sections (2 to 4) seem to be less deteriorated (higher ΔT) than side (exposed to rain and sun exposure) sections. The 2012 campaign yielded significantly higher ΔT. For the time being, no explanation can be provided.

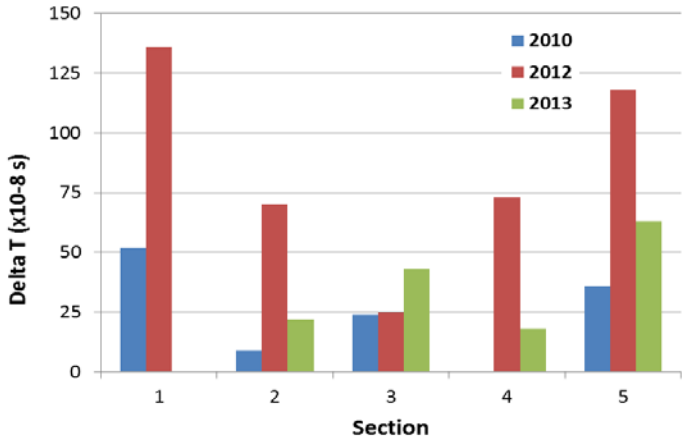

Figure 83. Evolution of ΔT with time (I-395 bridge over Main Street).

Visual observations of concrete condition seem to indicate that cracking is somewhat progressing in the portions of the bridge abutment and wing walls exposed to excess moisture (rainfall) and sun exposure, although not evident from Cracking Index measurements. On the other hand, sections of the above structural elements protected from rainfall and sun exposure are still somewhat unaffected (no or less cracking). Those observations are confirmed by non-destructive test data, which indicates that middle wall sections (2, 3, and 4) are less damaged than wing walls and side (exposed) portions of the abutment walls (1 and 5). On one hand, NDT results suggest that the condition of the concrete in sections 1, 2 (not exposed), and 5 (treated with elastomeric coating) has slightly improved between 2010 and 2013. On the other hand, in section 3 (under the deck), damage seems to increase slightly during this period.

At this stage, monitoring data do not clearly highlight increasing or decreasing expansion trends for either treated or untreated sections of the abutment walls. However, a drop in internal RH values was observed in 2013 for Site 3, from a section treated in 2010 with elastomeric coating, although located under the bridge deck and largely protected from direct rainfall. It is yet to be seen if this "trend" will continue in 2014. Also, in the case of the sections treated with the elastomeric coating, CI values of "0" were obtained following the application of the coating (i.e., in 2012 and 2013), thus indicating that the product has generally been efficient in bridging the cracks present in the treated concrete member.

Increasing RH values with increasing depth were also measured in 2010 at Sites 1 and 5 located on the external portions (but somewhat protected under the bridge deck) of the large columns of the I-395 bridge over the Penobscot River (see Figure 68A for site locations); however, fairly similar RH values were measured at all depths for the treated and untreated columns in 2012 and 2013 (see Figure 84).

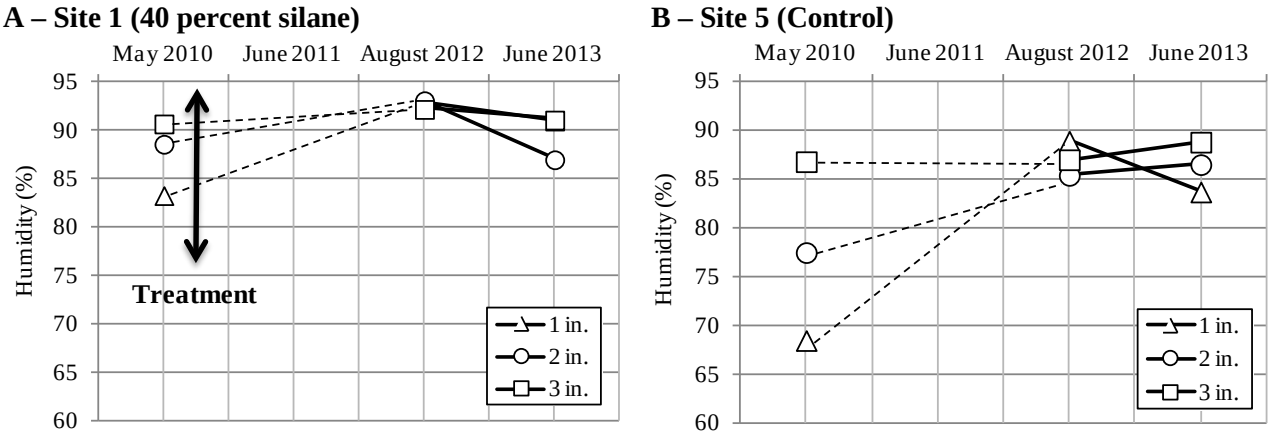

Figure 84. Values of relative humidity as a function of depth over the 2010-2013 monitoring period (I-395 bridge over the Penobscot River).
A: Site 1 – treated with 40 percent silane (± exposed). B: Site 5 – no treatment (control) (± exposed). The dotted lines cover periods over which no data were obtained.

Length change data often show a significant increase between the 2010 (initial or "0") and the 2011 readings. Such a "jump" was visible for both control and treated monitoring sites. The reason(s) for such an increase is (are) unclear; however, it is unlikely to be related to ASR and probably due to the stabilization of the gauge studs at the measuring sites between the two readings. It is consequently more realistic to look at the progress in length changes after the 2011 reading to analyze the possible progress of ASR and the effects of treatments on expansion.

Limited additional expansion and even some "shrinkage" were measured at the different sites after the 2010-2011 "jump" in readings (see Figure 85). In the case of the monitoring sites on the large columns of the bridge over the Penobscot River, Sites 1 and 5 are located on the sides of the columns. They are marked as “exposed” in Figure 85A and Figure 85C; however, they are still somewhat protected from direct rainfall by the bridge deck (see Figure 86).

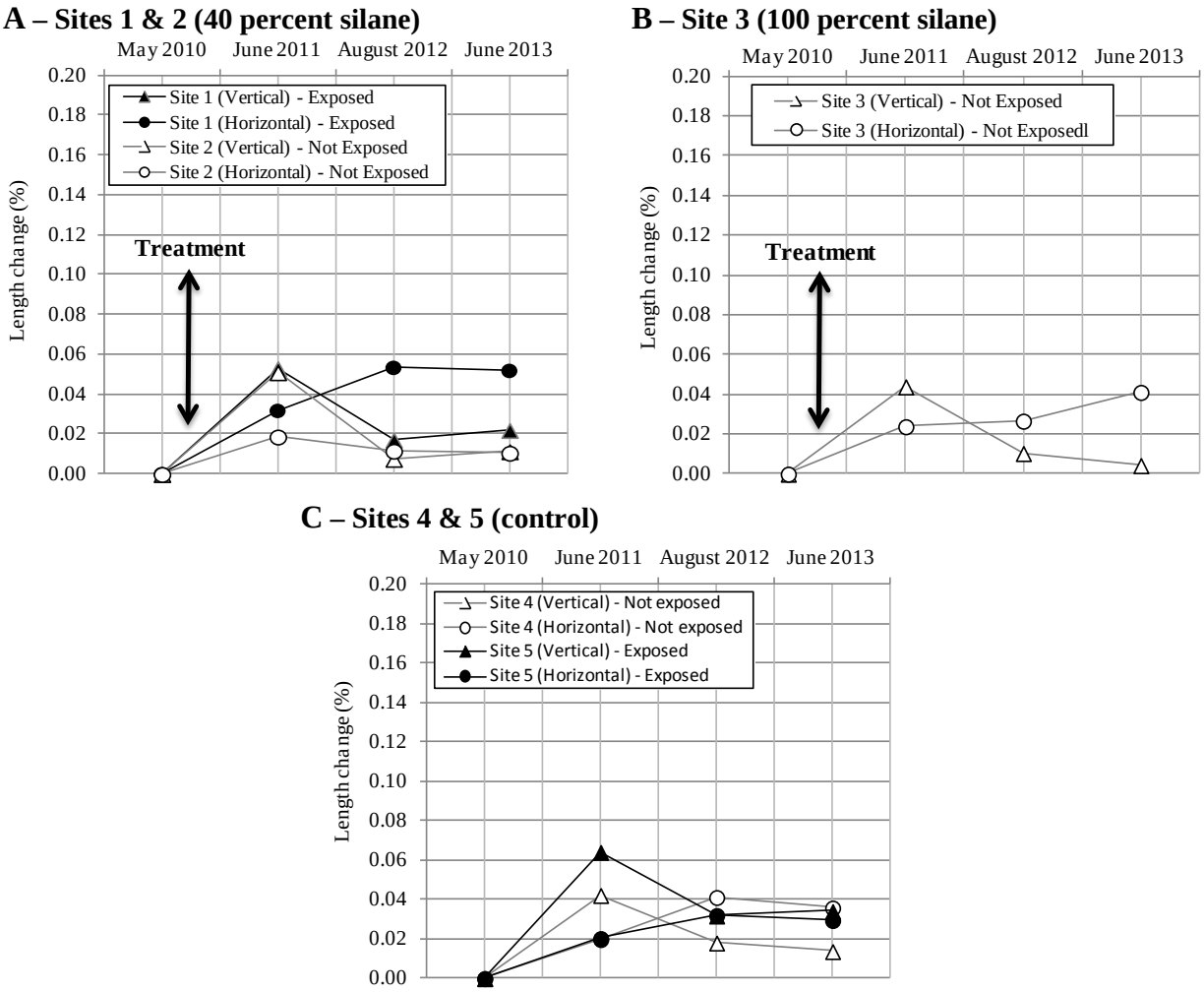

Figure 85. Values of expansion over the 2010-2013 monitoring period (I-395 bridge over the Penobscot River).
A: Sites 1 & 2 – treated with 40 percent silane (± exposed). B: Site 3 – treated with 100% silane (not exposed). C: Sites 4 & 5 – no treatment (control) (± exposed).

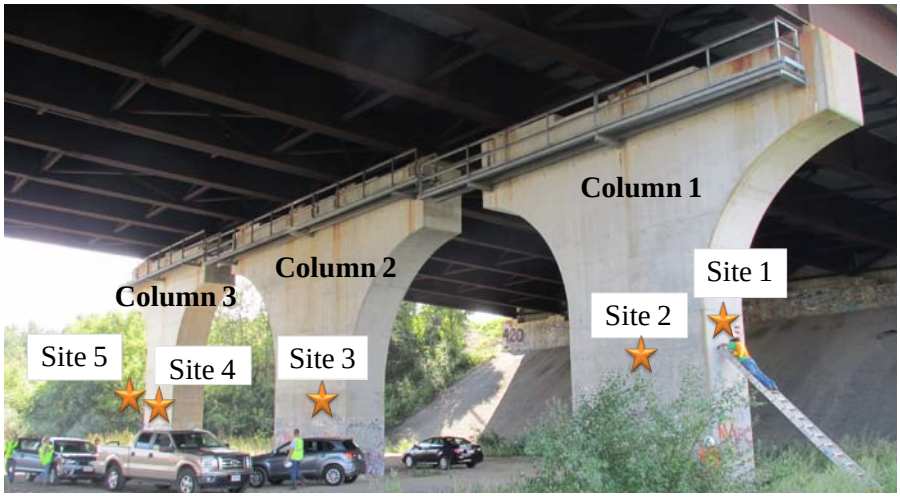

Figure 86. Monitoring (PMP) sites for the I-395 bridge over the Penobscot River.

Figure 87 illustrates the results of the Cracking Index measurements over the 2010-2013 monitoring period. Slightly higher CI values are observed for Sites 1 and 5 (exposed to moisture) than the other sites (2, 3, and 4) protected from moisture under the bridge deck (see Figure 87). Cracking is still fairly mild, as can be seen in Figure 88 and Figure 89 which illustrate crack maps both in 2010 and 2013. No clear increasing trends can be seen from the CI data, with perhaps the exception of Site 5 (control – no treatment), despite a lower CI value, still unexplained, obtained in 2013. The variability in the CI data might be partially due to the fact that operators performing the CI have changed over time, which is a source of variability in the test.

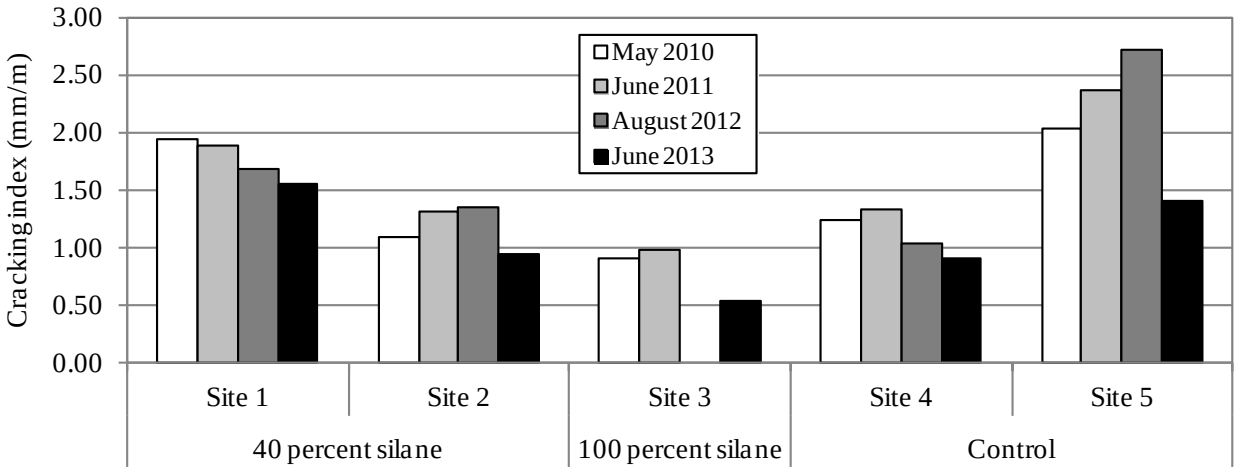

Figure 87. Values of Cracking Index over the 2010-2013 monitoring period (I-395 bridge over the Penobscot River).

Figure 88. Enlargement of a section of the crack map at Site 1 (external and somewhat exposed to moisture) showing light cracking on column No. 1 of the I-395 bridge over the Penobscot River (2012).

A – 40 percent silane (Site 1: exposed) 2010

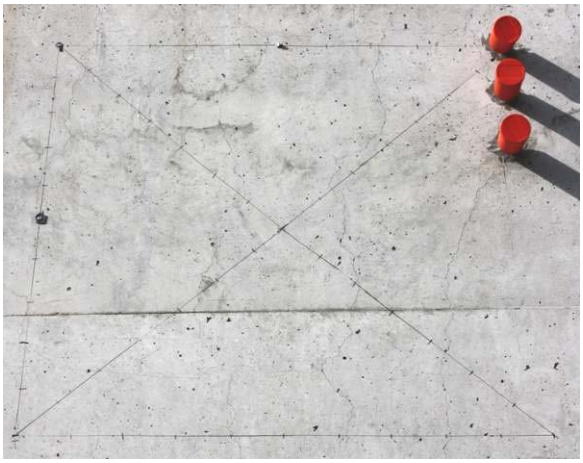

B – 40 percent silane (Site 1: exposed) 2013

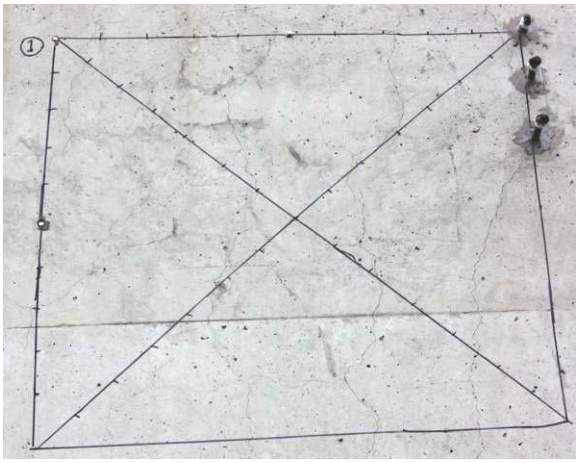

C – 100 percent silane (Site 3: not exposed) 2010

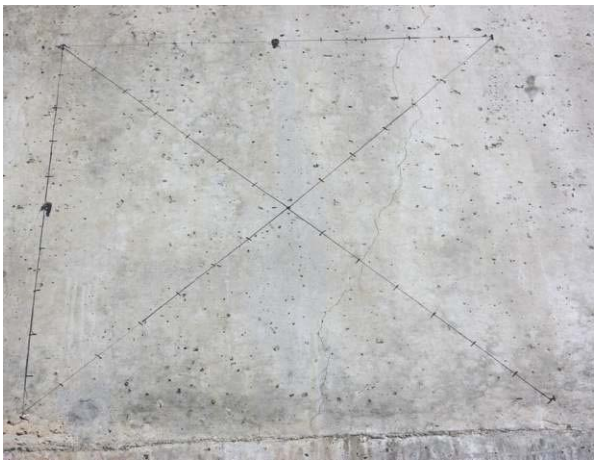

D – 100 percent silane (Site 3: not exposed) 2013

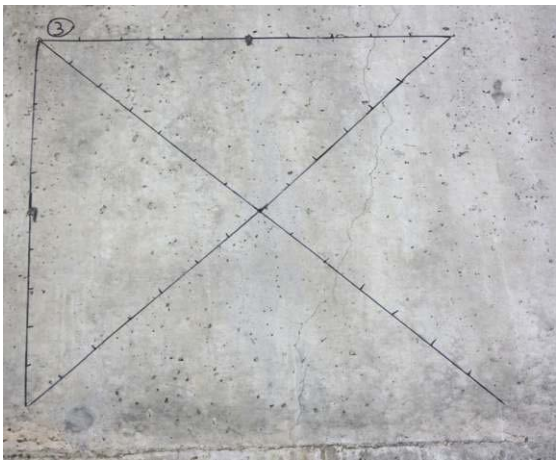

E – Control (Site 5: exposed) 2010

F – Control (Site 5: exposed) 2013

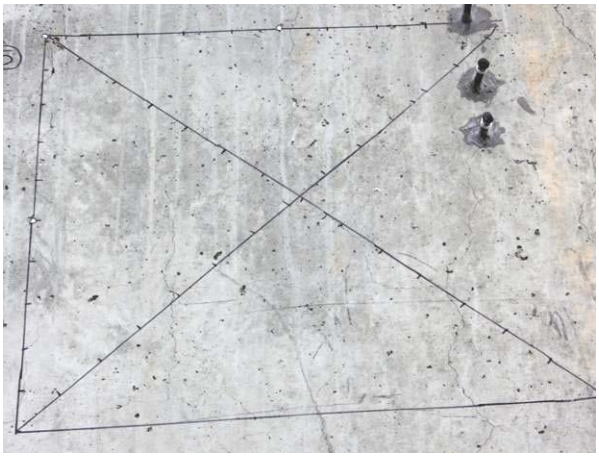

Figure 89. Examples of crack map sections before (2010) and after (2013) treatments (I-395 bridge over the Penobscot River).

Figure 90 illustrates the evolution of the average UPV with time. A global trend can be seen from 2010 to 2013: average velocities significantly decreased in column 3 and in the left portion of column 1 ("1l") (see Figure 68 and Figure 86 for location). For column 3, the velocities were high in 2010 (above 4200 m/s [13780 ft/s]) and they dropped to 3100 m/s (10171 ft/s) in 2013. The decrease is lower in the left portion of column 1, with a drop from 4320 m/s (14173 ft/s) in 2010 to 3730 m/s (12238 ft/s) in 2013. It seems that the velocities have not changed much in the right portion of column 1 ("1r"), lying between 3754 m/s (12316 ft/s) and 4065 m/s (13337 ft/s). These results suggest that ASR is still creating damage in the bottom part of the columns, especially in column 3 which is the most exposed to the wetting/drying cycles.

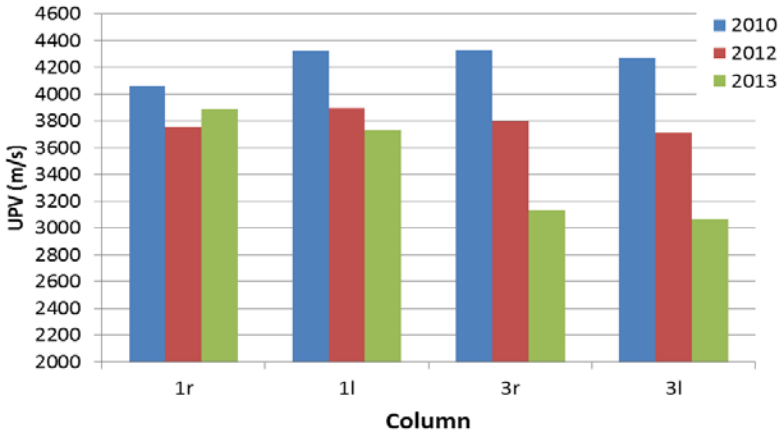

Figure 90. Evolution of UPV with time (I-395 bridge over the Penobscot River).

Figure 91 illustrates the evolution of the peak frequencies (impact-echo) with time. In 2010, the peak frequencies were very high (above 1300 Hz) in column 1 (left and right) and in the right section of column 3, suggesting that the condition of the concrete inside these columns was very good. Lower frequency (1150 Hz) was measured for the left side of column 3. Peak frequencies measured in 2012 and 2013 were much lower (drop from 14 percent to 21 percent). Between 2012 and 2013, only slight changes were observed in all columns, suggesting that the condition of inner concrete has not changed significantly.

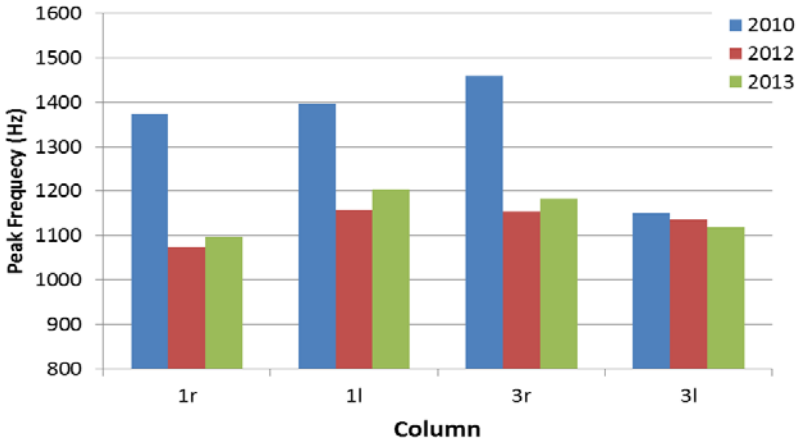

Figure 91. Evolution of peak frequencies with time (I-395 bridge over the Penobscot River).

The evolution of ΔT with time is shown in Figure 92. The 2012 campaign yielded the highest ΔT (higher damage) for the left section of column 1 and for both sections of column 3. The interpretation of the variation of ΔT is not easy to make. There is no general trend to be drawn from the nonlinear acoustics data. Let us recall that the measurements were performed in areas above sections assessed with UPV and impact-echo.

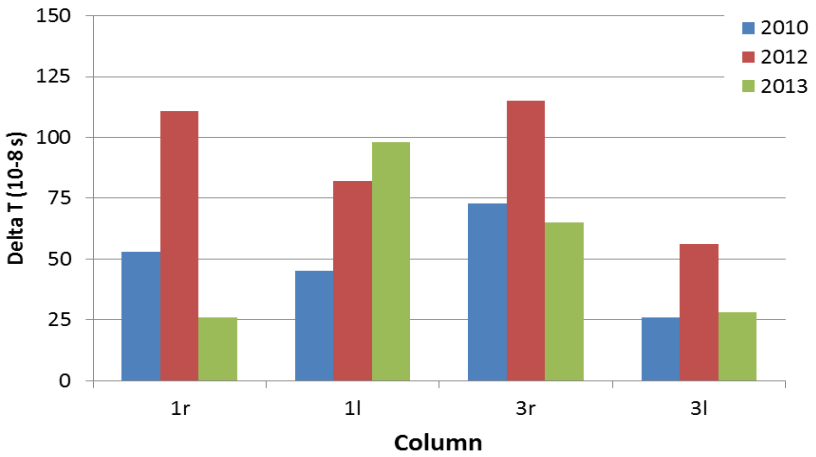

Figure 92. Evolution of ΔT with time (I-395 bridge over the Penobscot River).

Figure 93 shows the speed mapping of the cross-section of column 1. The color scale on the right of the cross-section corresponds to the speed, expressed in km/s. The average calculated speed is 4500 m/s (14764 ft/s), with a minimum of 2200 m/s (7218 ft/s) and a maximum of 5500 m/s (18045 ft/s). Figure 94 illustrates the speed mapping for column 3. The average calculated speed is 4300 m/s (14108 ft/s), with a minimum of 3500 m/s (11483 ft/s) and a maximum of 5500 m/s (18045 ft/s).

In both cases, the inner concrete seems to be in good condition (blue tints). Cracks (red and yellow) are primarily surficial. The very high speeds that were calculated (> 5000 m/s (16404 ft/s)) can be attributed to the presence of reinforcing bars. It must be pointed out that tomography relies on the assumption the P-waves travel through a direct path from the impact to the receiver. However, P-waves tend to follows the fastest paths, such as rebars, where speed can reach up to 6000 m/s (19685 ft/s).

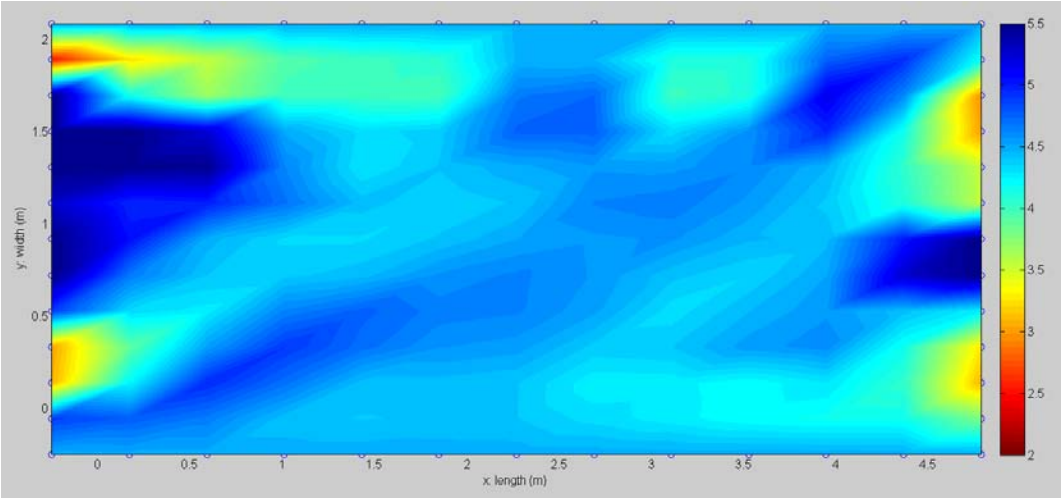

Figure 93. P-wave speed distribution in column 1 (horizontal cross-section at 79 in. [201 cm] above ground).

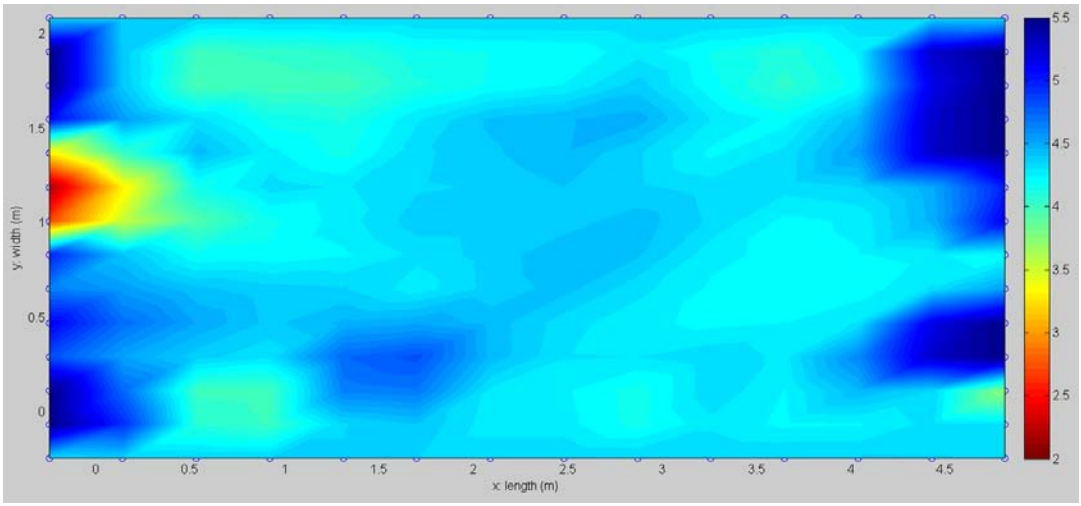

Figure 94. P-wave speed distribution in column 3 (horizontal cross-section at 79 in. [201 cm] above ground).

Visual observations of concrete condition, as well as Cracking Index (CI) data, indicate that cracking is affecting significantly more the external portions of the large reinforced concrete columns, i.e., those exposed to excess moisture from rainfall, as well as sun exposure. CI data actually show some progress in the extent of cracking for monitoring Site 5 (despite an unexpected and unexplained drop in 2013), which correspond to the external (exposed) side of column No. 3 (see Figure 86 for location). Also, cracking is developing in the upper portions of the columns due to moisture available from leaking joints (see Figure 61D). On the other hand, there is no evidence of progressing expansion from the length change data gathered at this stage for the various monitoring sites.

The above observations are once again confirmed by non-destructive test data. According to seismic tomography and impact-echo test results, the internal concrete of those heavily reinforced concrete columns seems to be in relatively good condition. However, UPV results

suggest that the surficial damage is increasing at the bottom of the columns, especially in column 3 which is more exposed to the sun, wind, and rain.

Fairly similar internal concrete RH values (1 to 3 in. [3 to 8 cm] deep) were obtained between the control and treated (40 percent silane) concrete, which do not allow any specific conclusion regarding the potential beneficial effect of the silane treatment on the progress of ASR at this stage.

In the case of the 5th Parkway bridge over I-395 (see Figure 95), no specific trends for decreasing/increasing RH values in the surficial portions (1 to 3 in. [3 to 8 cm] deep) of the exposed sections (i.e., Sites 1, 4, 5, and 8) of the abutment wall were obtained over the monitoring period completed to date. Also, RH values were often similar at all depths, thus suggesting a limited effect of the treatments so far.

Length change data often show a significant increase between the 2010 (initial or "0") and the 2011 readings. Such a "jump" was actually visible for both control and treated monitoring sites. The reason(s) for such an increase is (are) unclear; however, it is unlikely to be related to ASR and probably due to the stabilization of the gauge studs at the measuring sites between the two readings. It is consequently more realistic to look at the progress in length changes after the 2011 reading to analyze the possible progress of ASR and the effects of the treatments on expansion.

Somewhat confusing trends are observed from the expansion data available to date. On one hand, limited "additional" expansion, and even some "shrinkage," was measured following the 2010-2011 "jump" in readings for the following sites:

- 1 (40 percent silane (water-based); exposed) (see Figure 96A),
- 4 (elastomeric coating; exposed) (see Figure 96B),
- 5 (100 percent silane, exposed, horizontal direction) (see Figure 96C), and
- 7 (control, not exposed) (see Figure 96D).

On the other hand, expansive behavior was observed for the following sites:

- 2 (40 percent silane (water-based); not exposed) (see Figure 96A),
- 3 (elastomeric coating; not exposed) (see Figure 96B),
- 5 (100 percent silane, exposed, vertical direction) (see Figure 96C),
- 6 (100 percent silane, not exposed) (see Figure 96C), and
- 8 (control, exposed) (see Figure 96D).

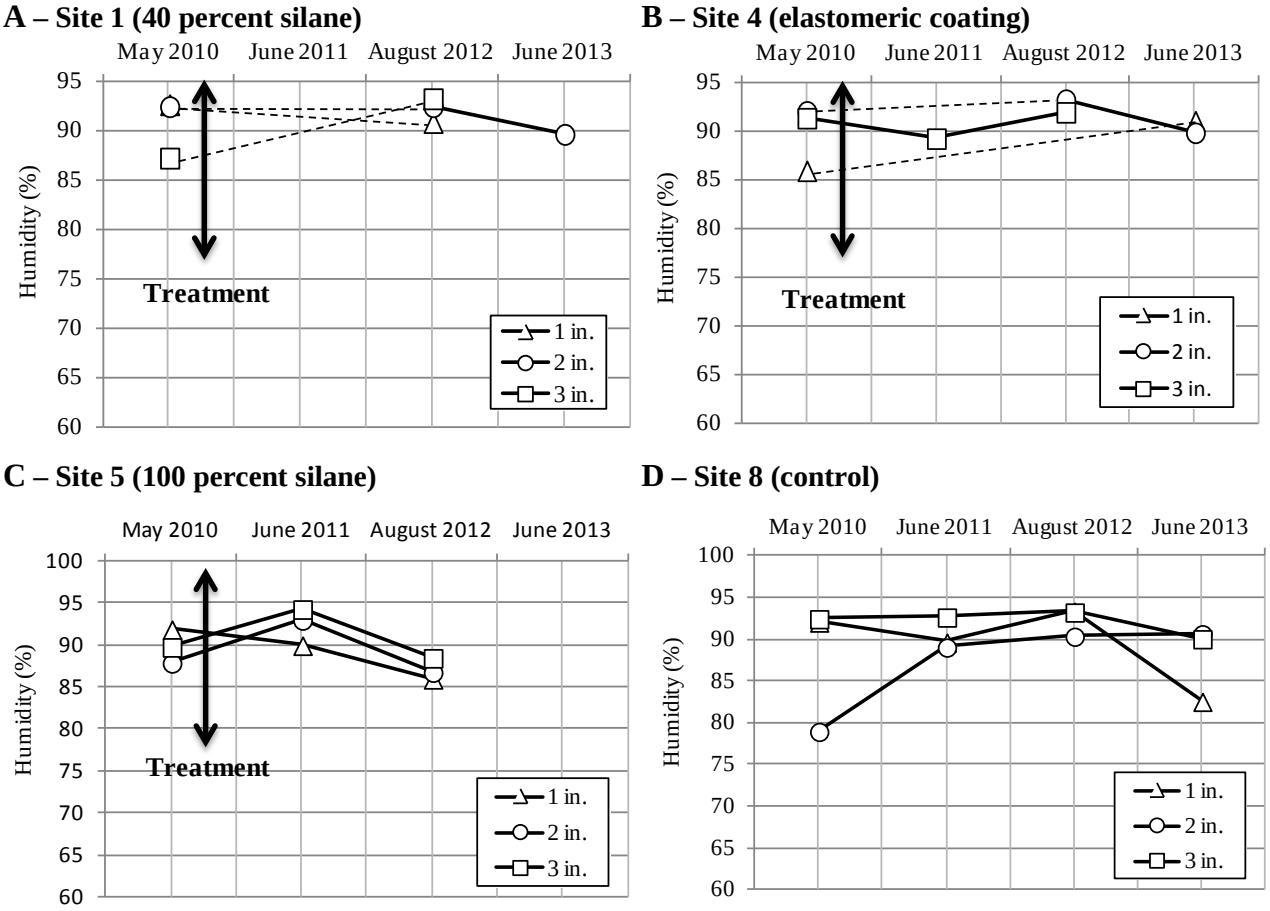

Figure 95. Values of relative humidity as a function of depth over the 2010-2013 monitoring period (5th Parkway bridge over I-395).
A: Site 1 – treated with 40 percent silane (exposed). B: Site 4 – treated with elastomeric coating (exposed). C: Site 5 – treated with 100 percent silane (exposed). D: Site 8 - no treatment (control) (exposed). The dotted lines cover periods over which no data were obtained.

The length change data suggests that an expansive process is taking place in non-exposed abutment wall sections treated with penetrating sealers and the elastomeric coating, while exposed portions of the same structural elements show limited expansion/shrinkage after treatment. Actually, fairly similar relative humidity values were measured at all depths (25 mm [1 in.] to 75 mm [3 in.]) in exposed abutment wall sections after treatment (see Figure 95). On the other hand, as expected, an expansive process is observed for control abutment wall sections exposed to moisture, while the non-exposed portion of the wall shows a fairly stable behavior. Continuing monitoring at the site will be necessary to confirm the above trends and the potential beneficial effects of the treatments.

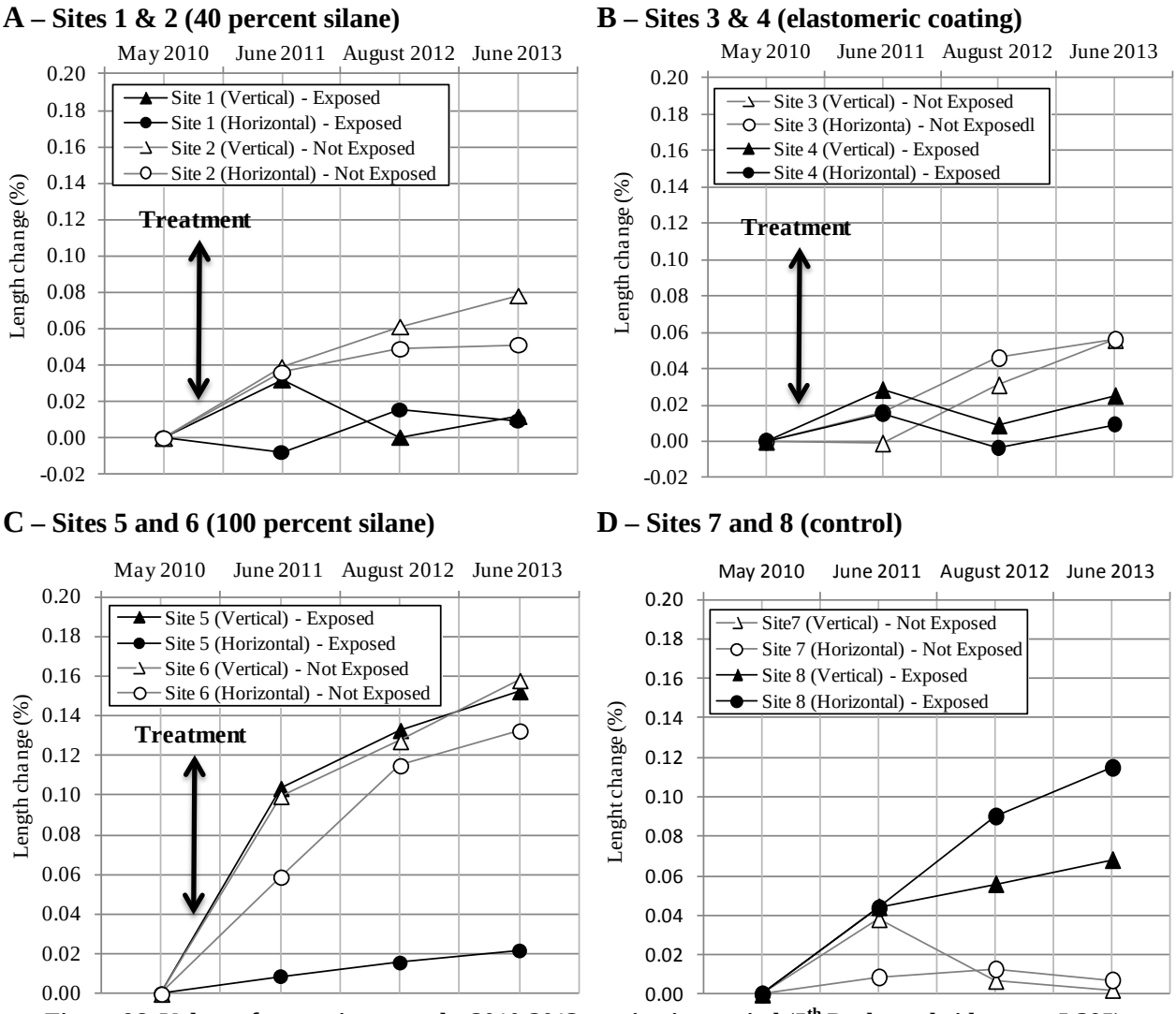

Figure 96. Values of expansion over the 2010-2013 monitoring period (5th Parkway bridge over I-395). Different treatment and sites (exposed vs. not exposed)
A: Sites 1 & 2 – treated with 40 percent silane. B: Sites 3 & 4 – treated with elastomeric coating. C: Sites 5 & 6 – treated with 100 percent silane. D: Sites 7 & 8 - no treatment (control).

Figure 97 illustrates the results of the Cracking Index measurements over the 2010-2013 monitoring period. Significantly higher CI values are obtained for Sites 4 to 6 (exposed to moisture) compared to the other sites protected from moisture under the bridge deck (Sites 2, 3, and 7; see crack maps in Figure 98 and Figure 99).

No clear increasing trends with time can be seen from the CI data; however, a drop in CI value was obtained in 2013 for Sites 5 and 6, perhaps suggesting a beneficial effect of the 100 percent silane treatment (although not evident from the pictures in Figure 98A and Figure 98B that seem to show increasing damage over the monitoring period).

It is to be noted that in the case of Sites 3 and 4, treated in 2010 with the elastomeric coating, CI values of "0" were obtained for the measurements carried out in 2012 and 2013, i.e., following the application of the coating (see Figure 99A and Figure 99B).

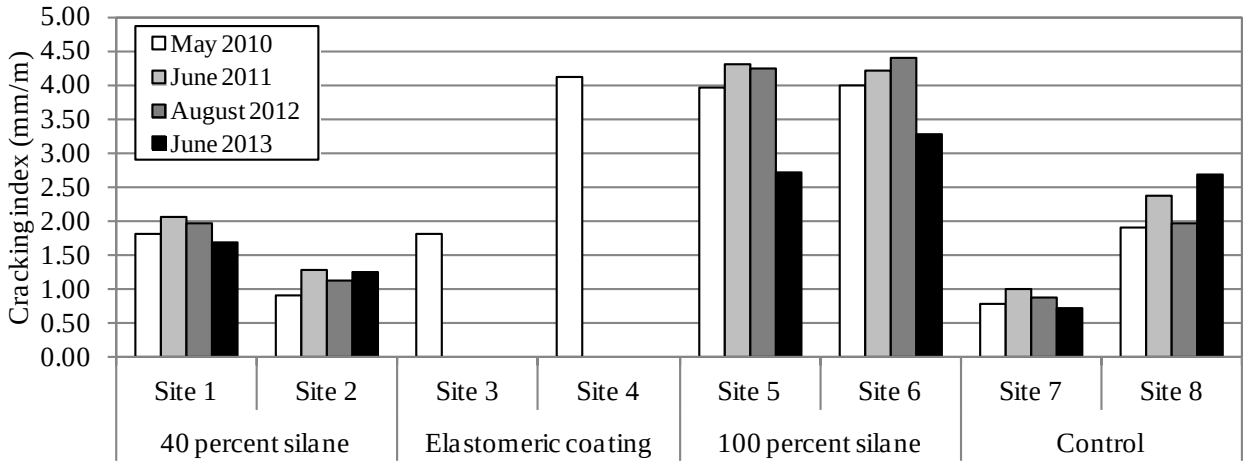

Figure 97. Values of cracking index over the 2010-2013 monitoring period (5th Parkway (Robertson Road) over I-395).

A – 100 percent silane (site 5: exposed) 2010

B – 100 percent silane (site 5: exposed) 2013

Figure 98. Examples of crack map sections before (2010) and after (2013) treatments (5th Parkway (Robertson Road) bridge over I-395).

A – Elastomeric coating (Site 4: exposed) 2010

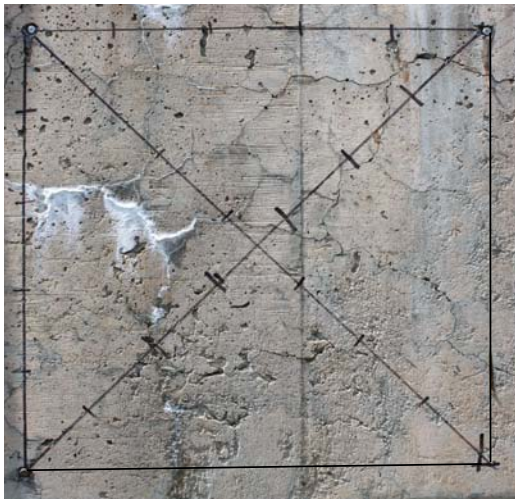

B – Elastomeric coating (Site 4: exposed) 2013

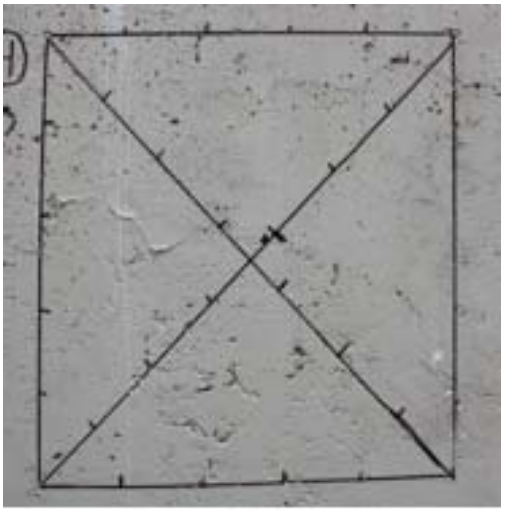

C – 40 percent silane (Site 1 : exposed) 2010

D – 40 percent silane (Site 1 : exposed) 2013

E – Control (Site 8: exposed) 2010

F – Control (Site 8: exposed) 2013

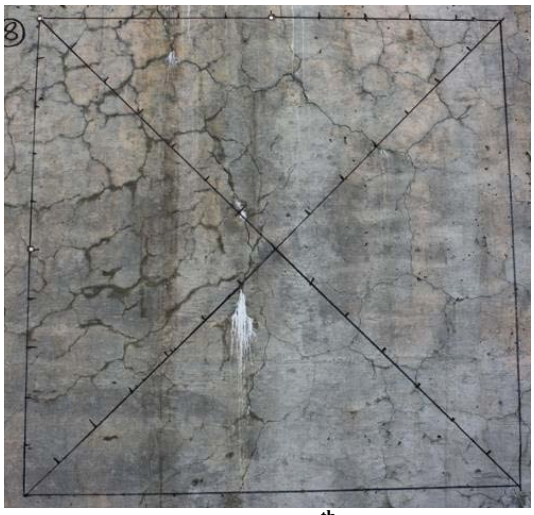

Figure 99. Examples of crack map sections before (2010) and after (2013) treatments (5th Parkway (Robertson Road) bridge over I-395).

Figure 100 illustrates the evolution of UPV with time. The east wing wall (exposed to moisture) shows the highest damage (velocities below 2800 m/s) (see Figure 69B for location), and the level of damage slightly increases with time (despite treatment with 100 percent silane in 2010). Section 2 (treated with 100 percent silane but protected under the bridge deck) shows variable velocities with time, with average velocities lying between 3020 m/s (9908 ft/s) in 2010 and 3682 m/s (12080 ft/s) in 2012. The 2010 UPV value for section 3 might be questionable: a value of 4663 m/s (15299 ft/s) was recorded, which appears to be very high. Then, there were only slight variations between 2012 and 2013 (control section protected under the bridge deck). Actually, no trend for expansion was noticed in that zone over the same period (see Figure 96D – Site 7).

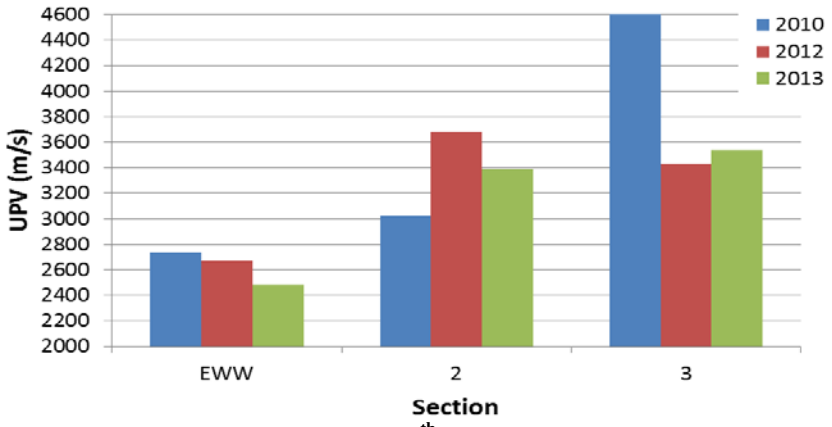

Figure 100. Evolution of UPV with time (5th Parkway (Robertson Road) over I-395).

Figure 101 shows the evolution of the peak frequency with time (impact-echo). Like UPV, impact-echo results suggest that the east wing wall is the most deteriorated section. However, unlike UPV results, the level of damage seems to lower between 2012 and 2013, as well as the standard deviation. It must be mentioned that no recording was made in 2010. The frequencies in other sections (protected under the bridge deck) show some variable fluctuations with time, and it might be inferred that the level of damage in the concrete has not varied significantly with time.

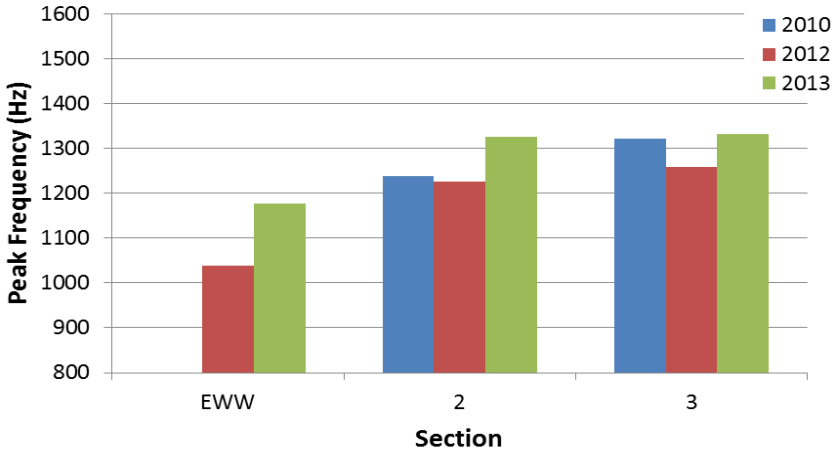

Figure 101. Evolution of peak frequencies with time (5th Parkway (Robertson Road) over I-395).

Figure 102A shows the evolution of ΔT with time. There was a very high value (525 $X10^{-8}$ s) recorded on the east wing wall in 2010. This value is questionable. In order to better appraise the evolution of ΔT, this value is not shown in Figure 102B. It can be seen that damage seems to decrease in section 2, while it significantly increases on the east wing wall (exposed to moisture but treated with 100 percent silane in 2010). The ΔT value increases and then drops with time in section 3.

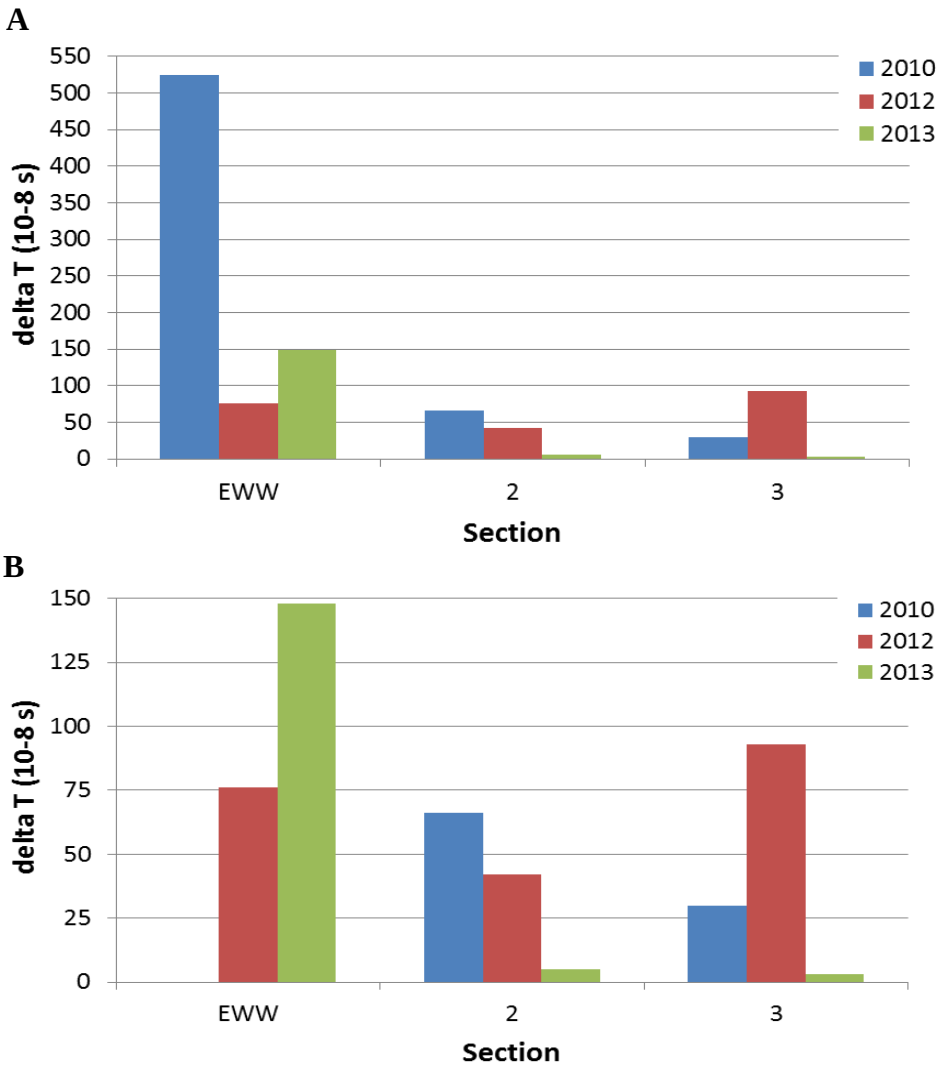

Figure 102. Results of nonlinear acoustics measurements.
A: Evolution of ΔT with time. B: Evolution of ΔT with time (Robertson without 2010 EWW result).

Visual observations of concrete condition indicate that cracking is largely affecting portions of the bridge abutment and wing walls exposed to excess moisture (rainfall) and sun exposure. Those observations are confirmed by Cracking Index and non-destructive test data. The three non-destructive methods indeed showed that the east wing wall is the most deteriorated section. Results from UPV and nonlinear acoustics (which both primarily assess surficial concrete condition) suggest the level of cracking of the wing wall is actually increasing with time. This is somewhat visible from pictures of the monitoring sites as well. On the other hand, and according to the impact-echo results, the deeper concrete condition seems to improve with time.

The length change data from monitoring sites suggests that an expansive process is taking place in non-exposed abutment wall sections treated with penetrating sealers and the elastomeric coating as well as the control section exposed to moisture (which is logical), while exposed portions of the treated structural elements show limited expansion and even some shrinkage after treatment. Also, fairly uniform relative humidity values, around 90 percent, were measured at all depths (25 mm [1 in.] to 75 mm [3 in.]) and as a function of time in exposed abutment wall sections after treatment. All of the above behaviors will require further investigations and continued monitoring to confirm a potential beneficial contribution of the treatments.

Finally, in the case of the sections treated with the elastomeric coating, CI values of "0" were obtained following the application of the coating (i.e., in 2012 and 2013), thus indicating that the product has generally been efficient in bridging the cracks present in the treated concrete member.

Increasing RH values with increasing depth are generally obtained at all sites (exposed (Site 1) and non-exposed (Sites 3 and ~5) columns) (see Figure 70A for site locations); the difference is, however, relatively less important at Site 5 where relatively close RH values were obtained both at 25 mm (1 in.) and 75 mm (3 in.) (see Figure 103C).

In the case of exposed control column No. 1, the RH values remained relatively similar (i.e., between 80 and 85 percent) over time at 3-inch (75-mm) depth, while RH values progressively increased over time in the surficial (1-in. [25-mm]) portion of the concrete to reach a level similar to that of the 3-inch (75-mm) RH value in 2013 (see Figure 103A). A trend for decreasing RH values at both depths was observed over time for the 40 percent silane treated column (Site 3 – see Figure 103B) and the non-exposed control column 5 (see Figure 103C).

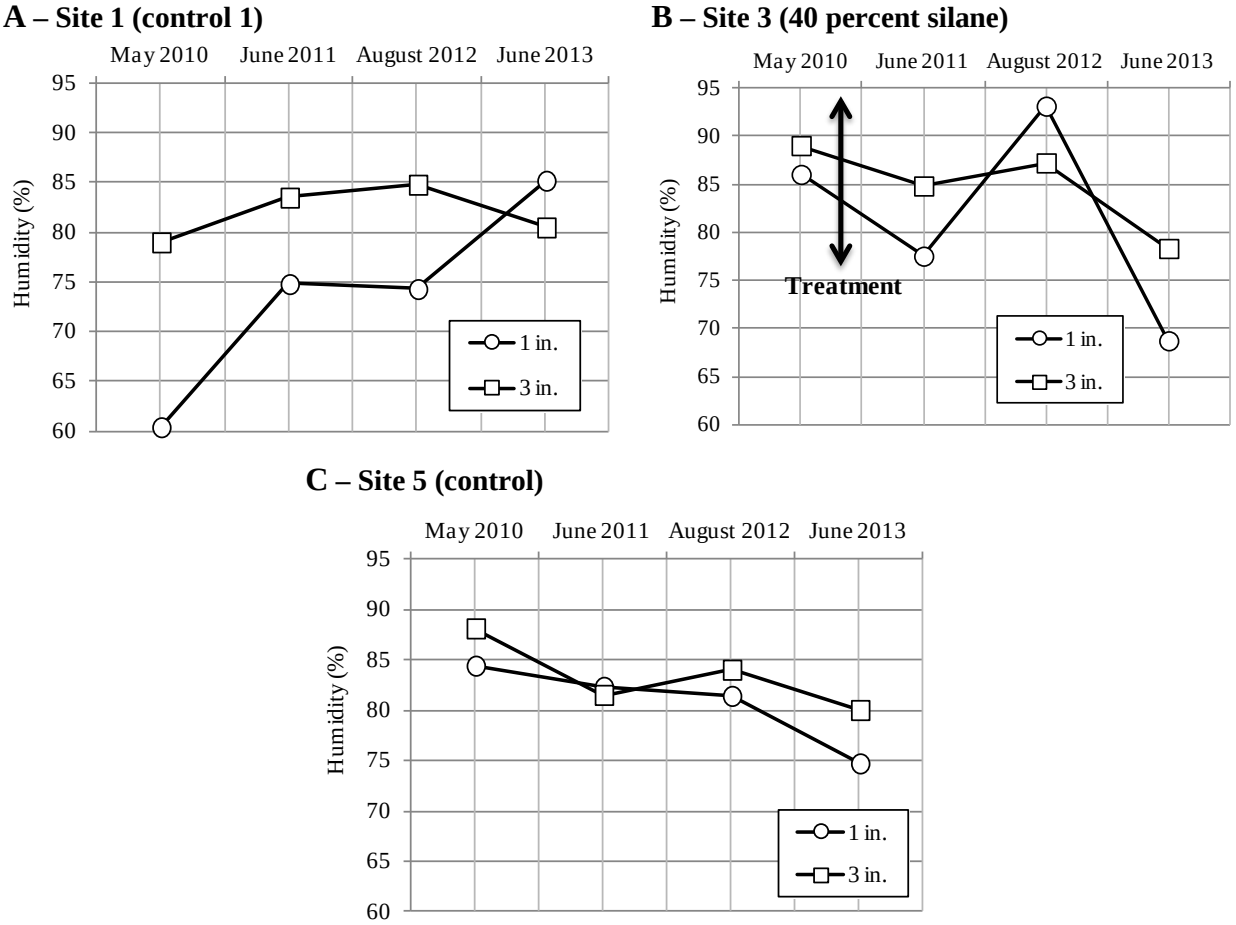

Figure 103. Values of relative humidity as a function of depth over the 2010-2013 monitoring period (South Parkway bridge over I-395).
A: Site 1 – no treatment (control) (exposed). B: Site 3 - treated with 40 percent silane (not exposed). C: Site 5 – no treatment (control) (± exposed).

Circumferential expansion measurements were taken along two lines separated by about 1 m (39 in.). Figure 104 illustrates the results of the above measurements. The precision of the measurements is, however, limited, so the "expansion" values should be considered as indicative only.

According to the data obtained to date, expansive trends are observed for all columns. The highest expansions of about 0.22 percent were obtained for column 2, which has been subjected to electrochemical treatment with lithium nitrate; the column is the second from the side and is somewhat protected from direct rainfall by the bridge deck (see Figure 104B). Expansions ranging from 0.08 to 0.18 percent were obtained for the various control columns in 2013 (see Figure 104A), which vary in their exposure conditions. An expansive trend is also observed for column 3, treated with 40 percent silane, which reached between 0.04 and 0.12 percent in 2013 (see Figure 104C); that column is well protected from direct rainfall under the bridge deck.

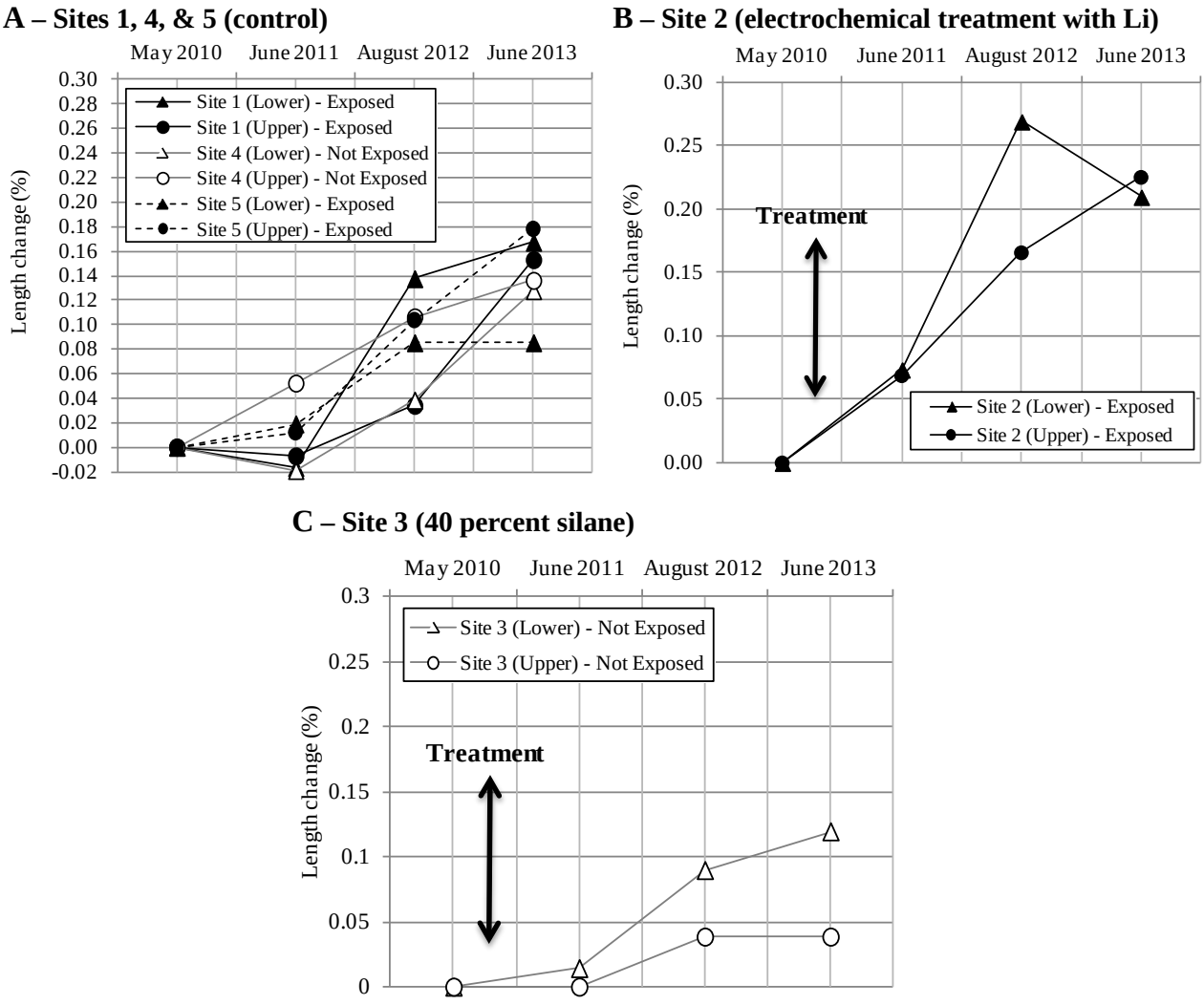

Figure 104. Values of expansion over the 2010-2013 monitoring period (South Parkway bridge over I-395). Different treatment on reinforced concrete columns (exposed vs. not exposed). A: Sites 1, 4, & 5 – no treatment (control). B: Site 2 – electrochemical treatment with lithium. C: Site 3 – treated with 40 percent silane.

Figure 105 illustrates the results of the Cracking Index measurements over the 2010-2013 monitoring period. Crack width measurements were taken along two lines separated by about 1 meter (39 inches), and the cracking indices were calculated from those readings. The same two lines were also used for expansion measurements.

The highest CI values (ranging from about 2.5 to 3.8 mm/m [0.089 to 0.136 in./yd]) were obtained for column (Site) 1 (control), exposed to moisture (see Figure 105). That column also shows a significant expansive behavior (see Figure 104A) and the highest RH values measured in 2013 (see Figure 103). However, for some unknown reasons, the CI measurements show a decreasing trend from 2010 to 2012-2013. This might be partially due to the fact that operators performing the CI have changed over time, which is a source of variability in the test. Column 1 displays moderate vertical cracking, as illustrated in Figure 106A and Figure 106B. Column 6,

on the opposite side of the set of columns, was also displaying significant cracking back in 2010 (see Figure 106C), and was since then wrapped with fiber reinforced plastics (see Figure 106D).

The lowest CI values were obtained for the silane treated column (Site 3) and the control column (Site 4). Both columns are well protected from excess moisture (under the bridge deck), but still display a light vertical cracking pattern (Figure 107). Silane-treated column 3 shows the lowest expansive rate (see Figure 104), as well as a global trend for reduction in internal humidity (RH) (from 2010 to 2013 – see Figure 103B). On the other hand, control column 4 shows a steady increasing expansive behavior (see Figure 104A) but still fairly low CI values.

Similar CI values were measured for control column 5 (see Figure 108A and Figure 108B), as well as column 2 (Li treatment) (see Figure 108C and Figure 108D). Both columns show significant rates of expansion according to current length change measurements (see Figure 104A).

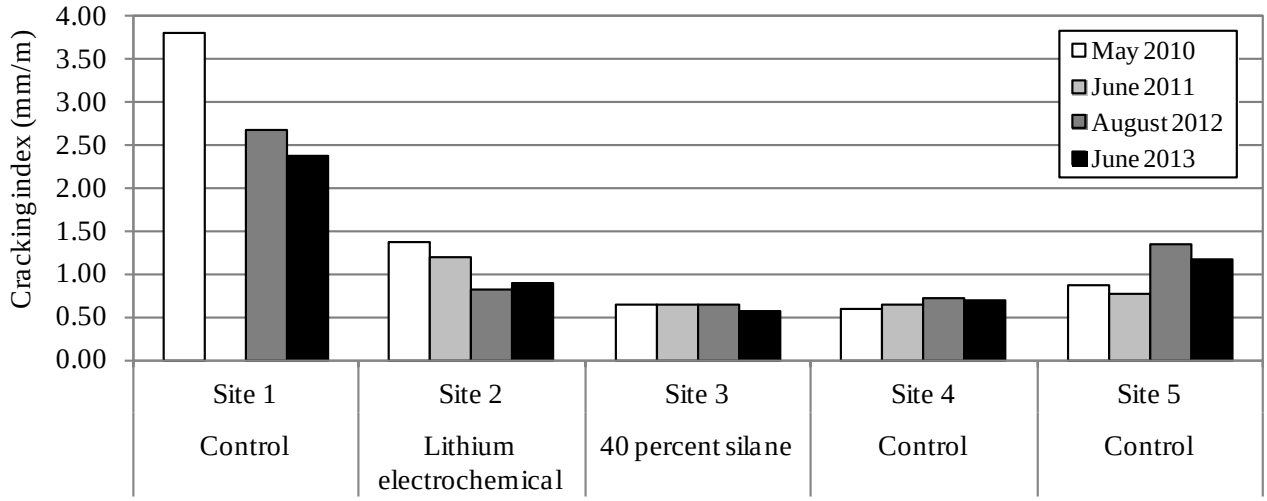

Figure 105. Values of cracking index over the 2010-2013 monitoring period (South Parkway bridge over I-395).

A – Control (Site 1: exposed) 2012

B – Control (Site 1: exposed) 2012

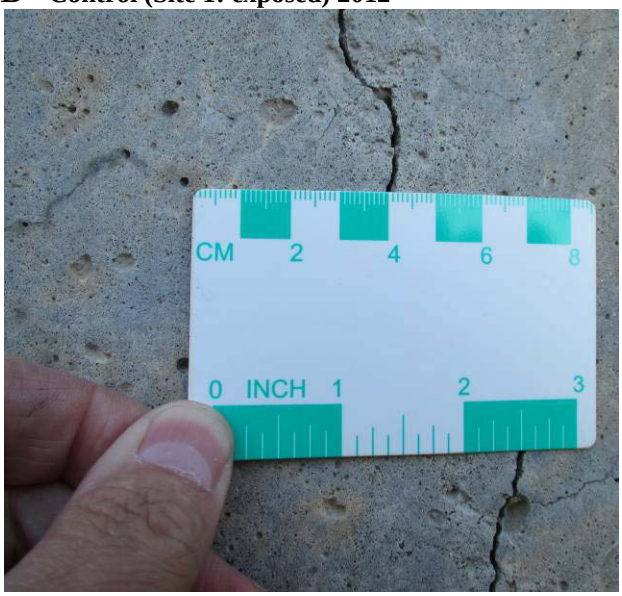

C – Control (Site 6: exposed) 2010

D – Control (Site 6: exposed) 2012

Figure 106. Condition of concrete columns of the South Parkway bridge over I-395. A&B: Site (column) 1. C&D: Site (column) 6.

A – 40 percent silane (Site 3: not exposed) 2012

B – 40 percent silane (Site 3: not exposed) 2012

C – Control (Site 4: not exposed) 2012

D – Control (Site 4: not exposed) 2012

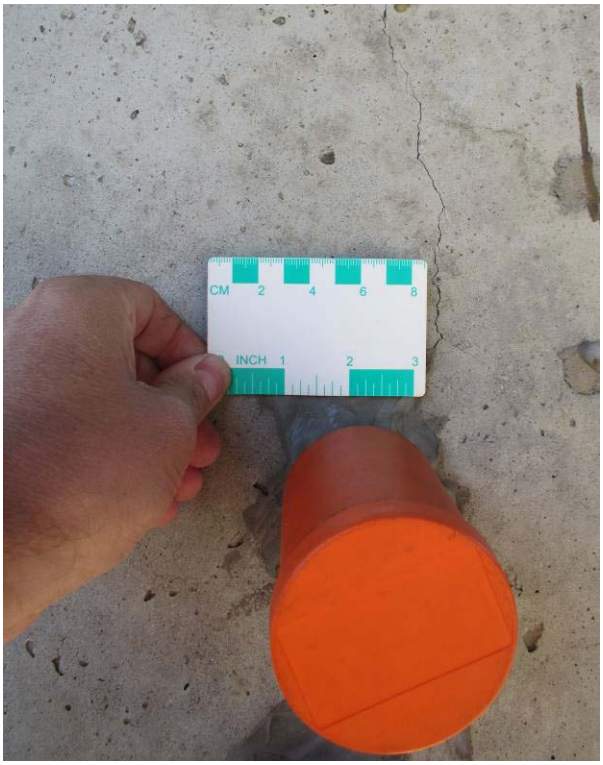

Figure 107. Condition of concrete columns of the South Parkway bridge over I-395. A&B: Site (column) 3. C&D: Site (column) 4.

A – Control (Site 5: ~ exposed) 2012

B – Control (Site 5: ~ exposed) 2012

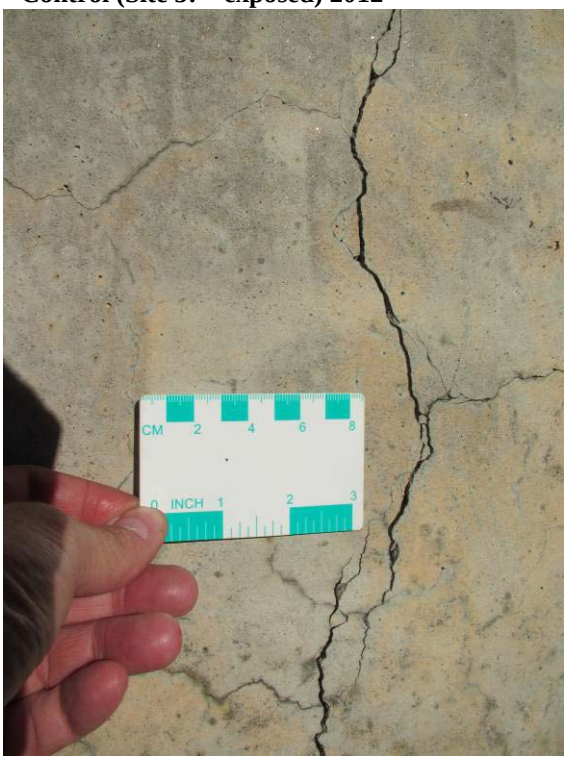

C – Lithium electrochemical (site 2: exposed) 2012

D – Lithium electrochemical (site 2: exposed) 2012

Figure 108. Condition of concrete columns of the South Parkway bridge over I-395. A&B: Site (column) 5. C&D: Site (column) 2.

Figure 109 shows the evolution of UPV with time. Inferring that UPV is related to the amount of global damage (since recording was performed through direct transmission), columns that are located on the sides (i.e., subjected to rainfall and sun exposure) are slightly more deteriorated compared with those located in the middle (i.e., protected from excess moisture). The evolution of velocities with time does not show a progress in damage, with the exception of column 5 (control) that shows decreasing UPV values with time with a drop from 4217 m/s (13835 ft/s) to 3945 m/s (12943 ft/s). Otherwise, the values measured in other columns varied from one survey to another within a range of about 300 m/s (984 ft/s). It must be pointed out that the velocities measured in 2012 were generally higher than those measured in 2010 and 2013. One should also note that the standard deviations are fairly low (except for column 5 in 2012).

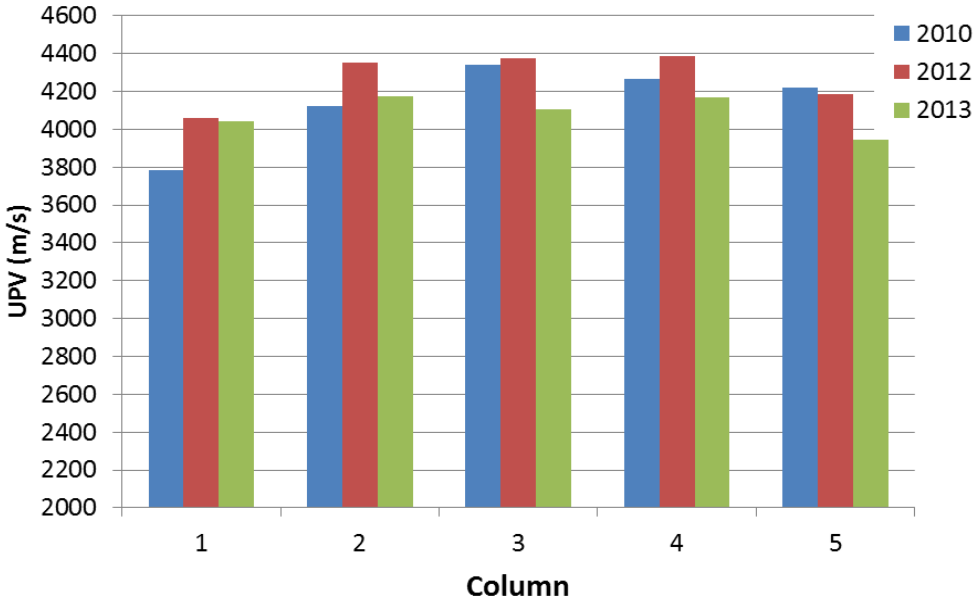

Figure 109. Evolution of UPV with time (South Parkway bridge over I-395).

Once again, visual observations of concrete condition, as well as Cracking Index (CI) data, indicate that cracking is affecting significantly more the concrete columns (or portions of) that are exposed to excess moisture from rainfall, as well as sun exposure. The above observations are once again confirmed by non-destructive test data, side (exposed) columns being more damaged than middle (under bridge deck) columns. Global damage in column 5 seems to increase slightly with time, while it slightly decreased over the monitoring period in column 1.

NDT data indicate that after a slight increase in velocities in 2012 (lower damage), velocity slightly dropped in 2013 in columns 2, 3, and 4, suggesting that the concrete is slowly decaying. Actually, expansion data, which correspond to circumferential length changes and should be interpreted with care (because of lower degree of precision), also suggest an expansive behavior for most columns, the highest expansion rates being obtained for the Li-treated (2) and the control columns (1, 4, and 5). The lowest expansion rate is obtained for the silane-treated column, which is protected from direct rain exposure under the bridge deck.

The RH values obtained for the different exposed sites instrumented on the Green Point Road bridge were found to range between 90 and 95 percent, and be quite stable in that range over the

2010–2013 period (see Figure 110). The main exception to the above trend is the control Site 1, where the RH values in the first inch (3 cm) of concrete were found to land in the 65–75 percent range over the monitoring period complete to date (see Figure 110A).

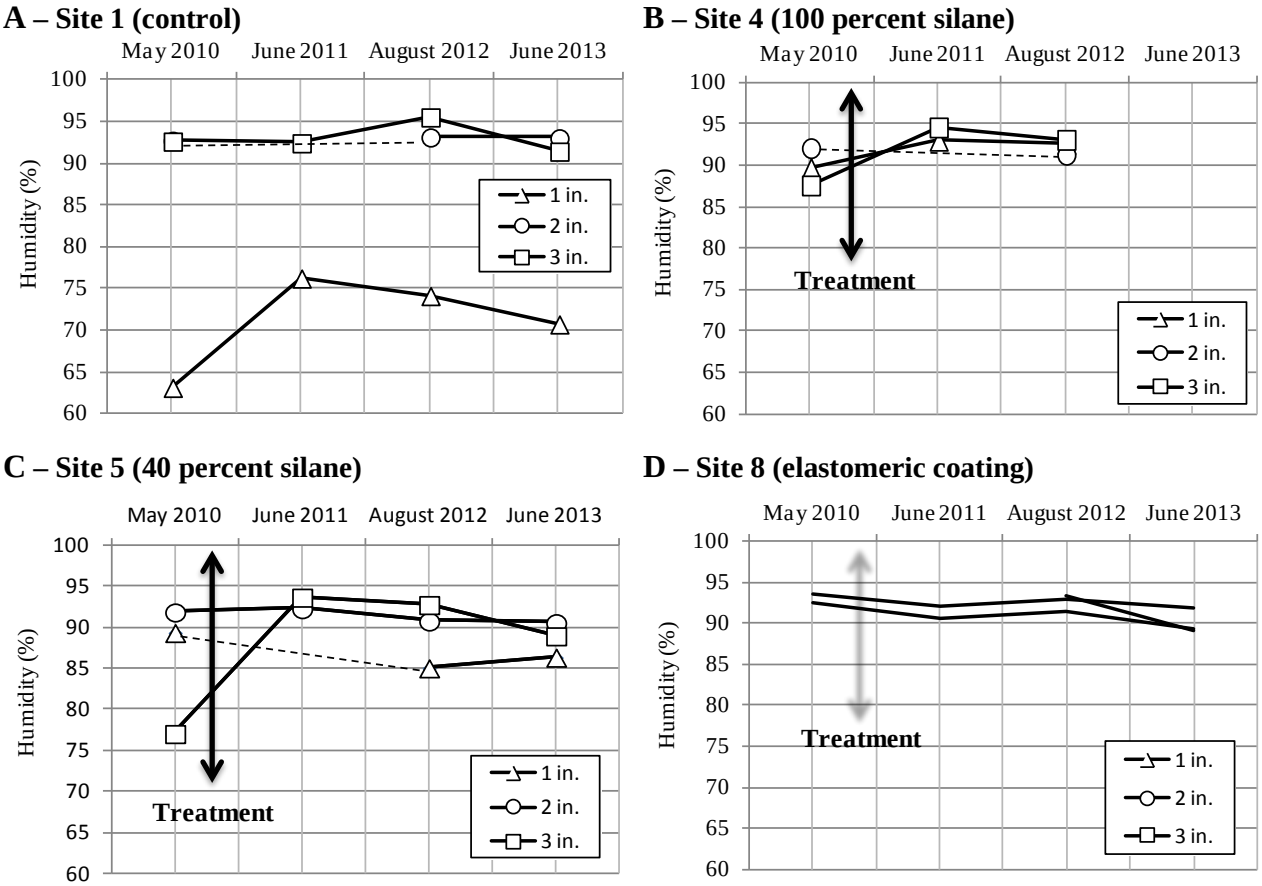

Figure 110. Values of relative humidity as a function of depth over the 2010-2013 monitoring period (Green Point Road bridge over I-395).
A: Site 1 – no treatment (control) (exposed). B: Site 4 - treated with 100 percent silane (exposed). C: Site 5 - treated with 40 percent silane (exposed). D: Site 8 – treated with elastomeric coating (exposed). The dotted lines cover periods over which no data were obtained.

Fairly high expansions were obtained over the 2010-2013 monitoring period for several sites of the Green Point Road bridge over I-395 (see Figure 111).

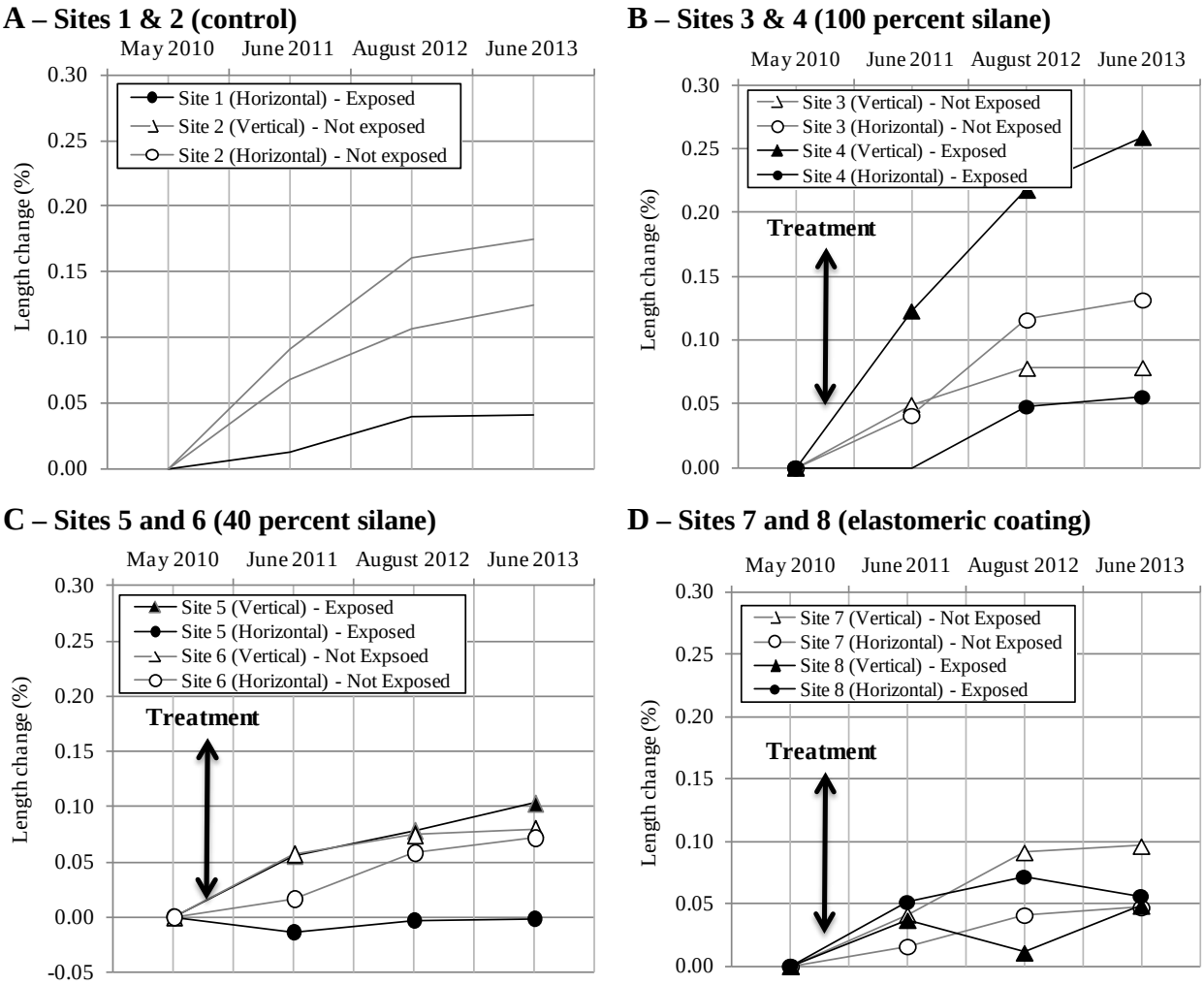

Figure 111. Values of expansion over the 2010-2013 monitoring period (Green Point Road bridge over I-395). Different treatment and sites (exposed vs. not exposed).
A: Sites 1 & 2 – no treatment (control) B: Sites 3 & 4 - treated with 100 percent silane. C: Sites 5 & 6 – treated with 40 percent silane. D: Sites 7 & 8 – treated with elastomeric coating.

Similarly to the 5th Parkway bridge, somewhat confusing trends were observed from the expansion data available at this stage. On one hand, limited additional expansion, and even some "shrinkage," was measured after the 2010-2011 "jump" in readings for the following sites:

- 1 (control, exposed, horizontal direction) (see Figure 111A),
- 4 (100 percent silane, exposed, horizontal direction) (see Figure 111B),
- 5 (40 percent silane (water-based); exposed, horizontal direction) (see Figure 111C), and
- 8 (elastomeric coating; exposed) (see Figure 111D).

On the other hand, expansive behavior was observed at the following sites:

- 2 (control, not exposed) (see Figure 111A),
- 3 (100 percent silane, not exposed) (see Figure 111B),
- 4 (100 percent silane, exposed, vertical direction) (see Figure 111B),
- 6 (40 percent silane (water-based); not exposed) (see Figure 111C),
- 5 (40 percent silane (water-based); exposed, vertical direction) (see Figure 111C), and

- 7 (elastomeric coating; not exposed) (see Figure 111D).

Once again, and similarly to Green Point Road bridge over I-395, the above data suggests that an expansive behavior is taking place in non-exposed concrete abutment wall sections following their treatment with penetrating sealers and the elastomeric coating, while exposed portions of the same structural elements show limited expansion/shrinkage after treatment. Actually, similar relative humidity values were measured at all depths (25 mm [1 in.] to 75 mm [3 in.]) in exposed abutment wall sections after treatment (see Figure 109). In the case of the control (non-treated) sections, an expansive behavior is observed in the non-exposed portion of the wall. Continuing monitoring at the site will be necessary to confirm all of the above trends and the potential beneficial effects of the treatments.

Figure 112 illustrates the results of the Cracking Index measurements over the 2010-2013 monitoring period. Significantly higher and similar CI values are obtained for sections of the bridge exposed to moisture, i.e., Sites 1, 4, and 5, compared to the other sites protected from moisture under the bridge deck (e.g., Sites 2, 6, and 7) (see Figure 112). A trend for decreasing CI values is observed for the exposed sites treated with 100 percent (Site 4) and 40 percent (Site 5) silane over the 2011-2013 period; however, the visual appearance of the concrete sections did not seem to improve significantly over that same period (see Figure 113). In the case of Sites 7 and 8, treated in 2010 with the elastomeric coating, CI values of "0" were obtained for the measurements carried out in 2012 and 2013, i.e., following the application of the coating (see Figure 114).

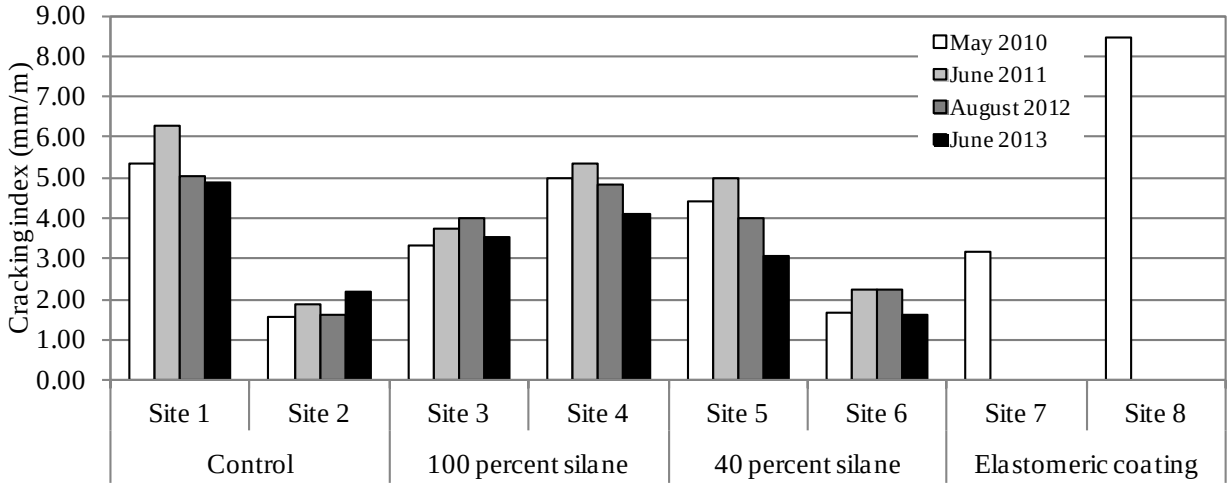

Figure 112. Values of cracking index over the 2010-2013 monitoring period (Green Point Road bridge over I-395).

A – 100 percent silane (Site 4: exposed) 2010

B – 100 percent silane (Site 4: exposed) 2013

C – 40 percent silane (Site 6: not exposed) 2010

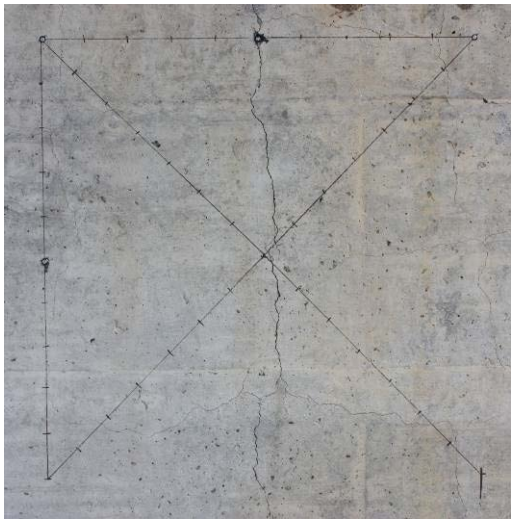

D – 40 percent silane (Site 6: not exposed) 2013

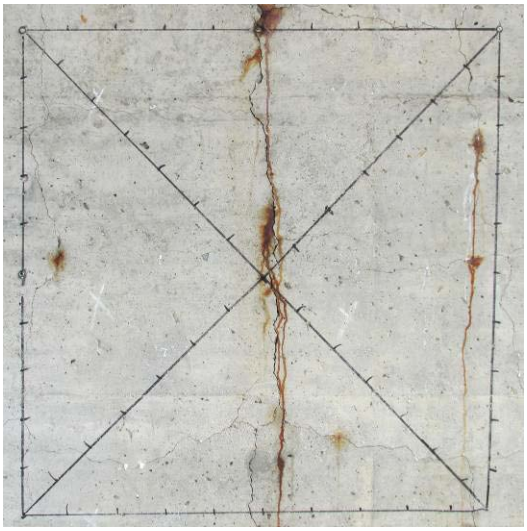

E – 40 percent silane (Site 5: exposed) 2010

F – 40 percent silane (Site 5: exposed) 2013

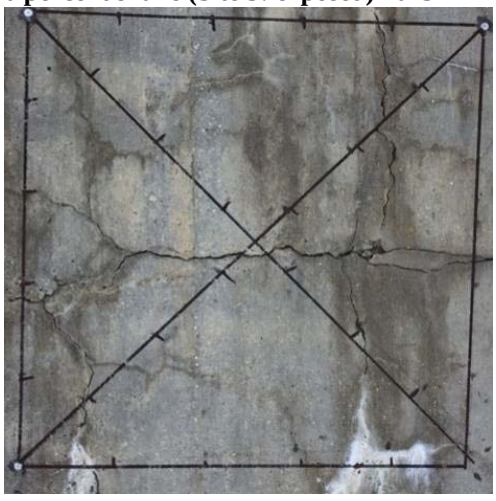

Figure 113. Examples of crack map sections before (2010) and after (2013) treatments (Green Point Road bridge over 1-395).

A – Elastomeric coating (Site 7: ~ exposed) 2010

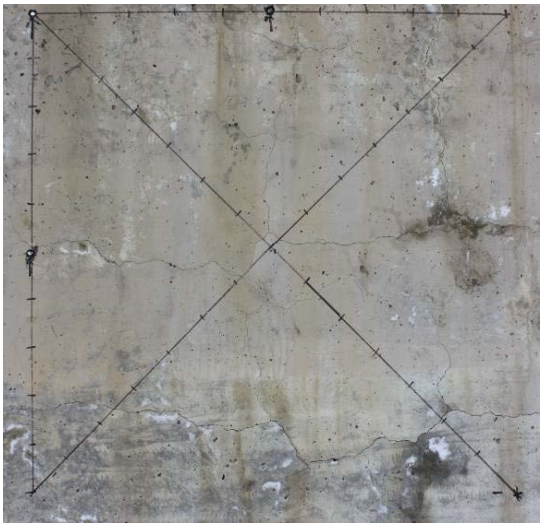

B – Elastomeric coating (Site 7: ~ exposed) 2013

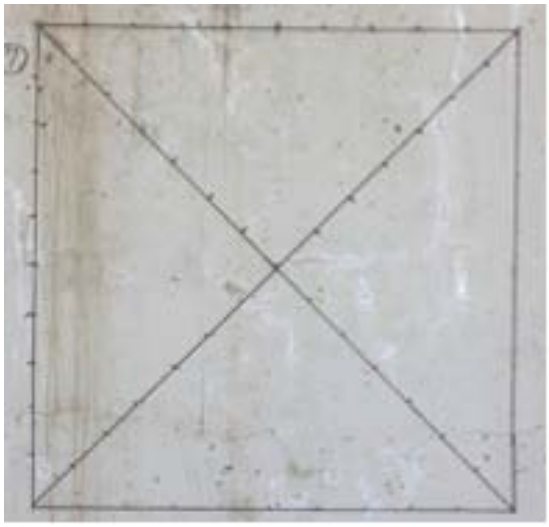

C – Control (Site 1: exposed) 2010

D – Control (Site 1: exposed) 2013

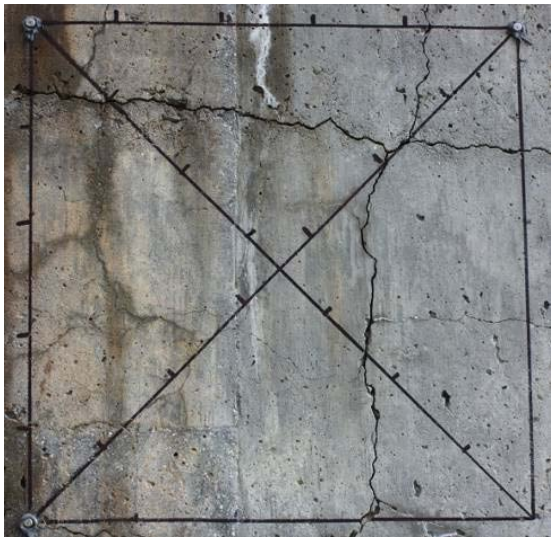

Figure 114. Examples of crack map sections before (2010) and after (2013) treatments (Green Point Road bridge over 1-395).

Figure 115 shows the evolution of the velocities with time. Section 2, which is located in the central portion of the abutment wall, and consequently well protected from excess moisture by the bridge deck, shows the highest velocities (from 3970 to 4148 m/s (13025 to 13609 ft/s)), indicating the lowest amount of damage. However, the UPV shows a slight decreasing trend with time. Damage is slightly higher in sections close to the wing walls (sections 1 and 3). UPV values are fairly constant over time for section 1 (very slight decrease from 3715 to 3660 m/s (12188 to 12008 ft/s)). Variations are slightly higher for section 3, with velocities of 3463 m/s (11362 ft/s) in 2012 to 3700 m/s (12139 ft/s) in 2013. Standard deviations for both are fairly high (400 and 461), suggesting numerous surface cracks.

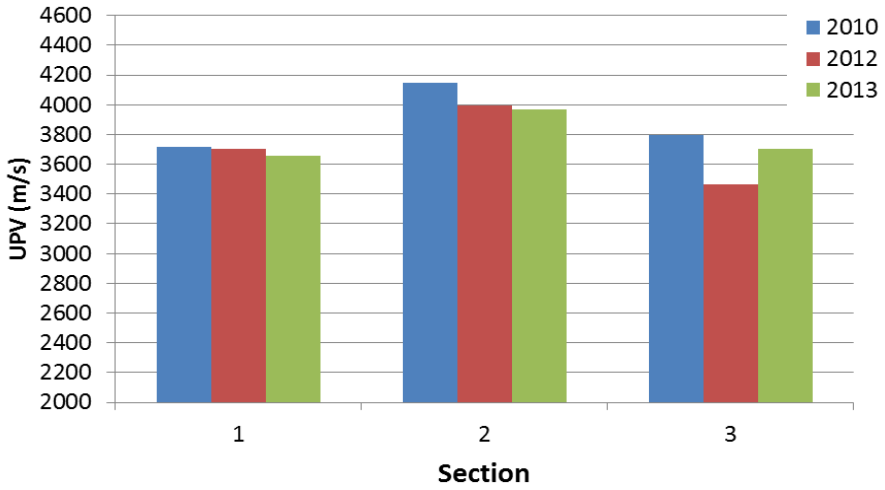

Figure 115. Evolution of UPV with time (Green Point Road bridge over I-395).

Figure 116 shows the evolution of the peak frequencies with time (impact-echo). An improvement in the internal concrete condition for all three sections is suggested from the data obtained in 2012, but the frequencies dropped significantly in 2013 (13-14 percent). From 2010 to 2013 the concrete condition seems to decay in all sections.

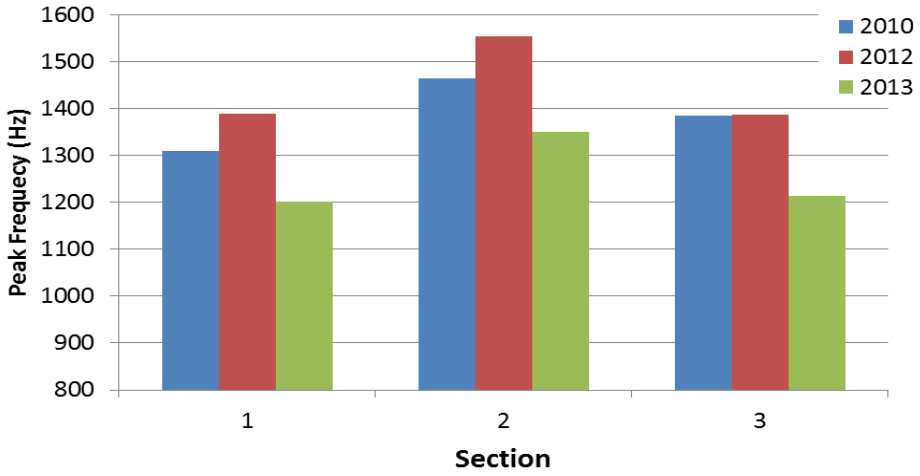

Figure 116. Evolution of peak frequencies with time (Green Point Road bridge over I-395).

Figure 117 shows the evolution of ΔT with time. No conclusive trend can be drawn from these results. The damage observed in the middle sections (2 and 3) was lower in 2010 compared with other sections, but it seems to increase with time. Fluctuations were measured for sections 1 and 4.

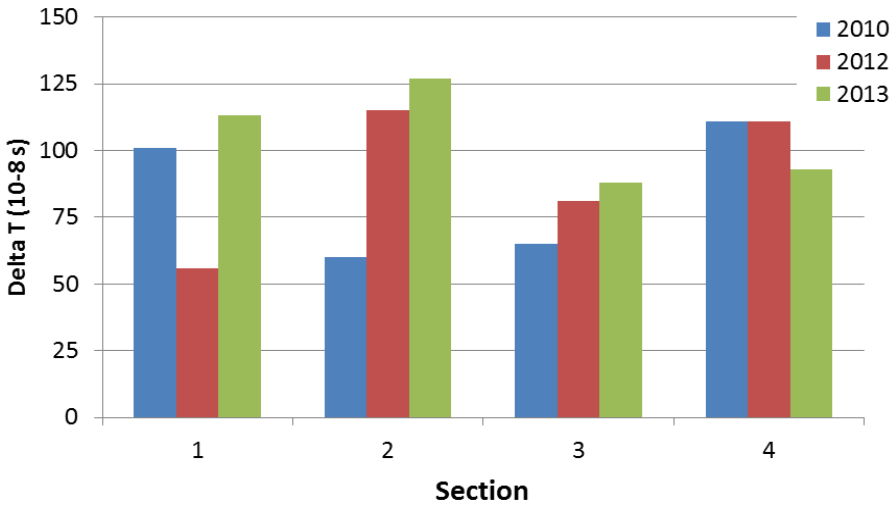

Figure 117. Evolution of ΔT with time (Green Point Road bridge over I-395).

Visual observations of concrete condition indicate that cracking is largely affecting portions of the bridge abutment and wing walls exposed to excess moisture (rainfall) and sun exposure. Those observations are confirmed by Cracking Index and, to some extent, by non-destructive test data. UPV and impact-echo measurements tend to suggest that there is a slight decay of the concrete condition (surface and inside) between 2010 and 2013 for all of the investigated sections. Nonlinear acoustics measurements are in agreement with this trend for sections 2 and 3 (middle or non-exposed sections). The difference in the concrete condition from the exposed and non-exposed portions of the bridge is visible from pictures of the monitoring sites (crack maps).

The length change data from monitoring sites suggests that an expansive process is taking place in non-exposed abutment wall sections treated with penetrating sealers and the elastomeric coating, as well as (to some extent) the control section exposed to moisture (which is logical), while exposed portions of the treated structural elements show limited expansion and even some shrinkage after treatment. Also, fairly uniform relative humidity values, around 90-95 percent, were measured at all depths (25 mm [1 in.] to 75 mm [3 in.]) and as a function of time in exposed abutment wall sections after treatment. All of the above behaviors will require further investigations and continued monitoring to confirm a potential beneficial contribution of the treatments.

Finally, in the case of the sections treated with the elastomeric coating, CI values of "0" were obtained following the application of the coating (i.e., in 2012 and 2013), thus indicating that the product has generally been efficient in bridging the cracks present in the treated concrete member.

7.5 SUMMARY

The results from field survey and laboratory investigations confirmed that ASR was an important contributing factor in the deterioration of a series of bridge structures along I-395 in Bangor/Brewer, ME. The petrographic evaluation and the SDT testing confirmed the presence of ASR in all structures that were cored, typically related to the use of reactive greywacke/argillite

coarse aggregates. Based on the above investigations, it was thus decided that the five ASR-affected bridge structures along Interstate 395 (I-395) in Bangor/Brewer, ME made a suitable test section. The bridge elements selected for treatments include bridge abutment and wing walls, and reinforced concrete columns.

A treatment plan involving the application of different types of surface treatment products (sealers, elastomeric coating) on the barrier wall sections was implemented in 2010. In addition to the above treatments, a performance monitoring plan was also developed and implemented to allow quantifying the effects of the various treatments over time. Within selected abutment wall sections and reinforced concrete columns, specific areas were identified for implementation of a Performance Monitoring Package (PMP), including crack mapping, expansion measurements, and temperature/humidity readings. In addition to the above, non-destructive testing methods were used for the diagnosis/prognosis of ASR in the various bridge structures. The methods used consisted of Ultrasonic Pulse Velocity (UPV), impact-echo, and nonlinear acoustics.

The structures were treated during the summer and fall of 2010. Three sealers were selected for application on separate sections of the above structures. The products correspond to a 100 percent silane, a 40 percent silane (water-based), and one elastomeric coating. In addition to the above surface treatments, two (circular) reinforced concrete columns were selected for lithium impregnation (electrochemical procedure) and strengthening (through the use of fiber reinforced polymer (FRP) wrap).

With only two years of monitoring data accumulated, it is currently too early to draw definite conclusions on the efficacy of the above treatments at reducing the deleterious effects of ASR on the barrier walls treated. However, interesting trends seemed to develop. Globally, visual observations of concrete condition, Cracking Index measurements, and results from non-destructive testing all indicate that internal/external cracking is largely affecting portions of the bridge abutment and wing walls as well as reinforced concrete columns exposed to excess moisture (rainfall) and sun exposure, and that cracking/internal damage has generally progressed over the 2010-2013 monitoring period in those sections exposed to severe environmental conditions.

Length change data from monitoring sites suggests that an expansive process is taking place in several structural members of the bridges, for instance non-exposed abutment wall sections treated with penetrating sealers and the elastomeric coating, as well as control sections exposed to moisture; on the other hand, in many cases, exposed portions of the treated abutment walls show limited expansion and even some shrinkage after treatment. These behaviors, somewhat surprising, will require further investigations and continued monitoring to confirm or disprove a potential beneficial contribution of the treatments.

7.6 REFERENCES

Rivard P., Ballivy, G., Gravel, C. and Saint-Pierre, F. 2010. “Monitoring of an Hydraulic Structure Affected by ASR: A Case Study.” Special issue *Cement & Concrete Research*, 40, 676-680.

8. HIGHWAY BARRIERS, LEOMINSTER, MA

In mid-2004, under the FHWA Lithium Technology Research Program, a section of highway barriers in Leominster, MA on State Route 2 was visually inspected, and upon extracting cores and performing a petrographic evaluation in early 2005, it was confirmed that alkali-silica reaction (ASR) was the primary cause of observed distress (see Figure 118). Cracking was observed on a relatively long section of barriers, approximately 6.4 km (4 mi) along Route 2. For some barrier sections, ASR-induced cracking led to subsequent freezing and thawing damage along the haunch of the barriers, as shown in Figure 119.

Figure 118. Typical example of cracking and staining observed on highway barriers on Route 2 in Leominster, MA.

Figure 119. Example of freezing and thawing damage at bottom (haunch) of barrier.

Because of the widespread nature of ASR in this barrier section, and because the freezing and thawing damage appeared to be a substantial risk once the concrete was cracked, it was decided to evaluate several treatment options aimed at trying to slow down the progression of ASR and increase the service life of the barriers. In 2005, under the FHWA Lithium Technology Research Program, a series of these barriers was treated with lithium nitrate (applied topically and by vacuum impregnation), lithium silicate, and silanes. Later in 2005, the Massachusetts Highway

Department (MassDOT) treated significantly longer sections of barriers on both sides of the FHWA test section with silane. In 2010, under the FHWA ASR Development and Deployment Program, most of the barriers were treated with an elastomeric paint, applied over existing silane, in the MassDOT section. This field trial in Leominster, MA is unique in that it combined the resources of two FHWA projects, and between the two projects over eight years of monitoring data are available. This chapter summarizes the treatments applied to the barriers and the results of the monitoring program, with primary focus on the barriers treated under the two FHWA programs.

8.1 SUMMARY OF PETROGRAPHIC EVALUATION

Cores were taken from three highway barrier walls along Route 2, near Leominster (Massachusetts), and the petrographic examination of the concrete was conducted by Dr. Grattan-Bellew in 2005. The author reported evidence of significant deterioration of the concrete due to ASR, in the form of cracks filled with gel in the coarse aggregate particles and in the cement paste and air voids, as well as reaction rims around occasional aggregate particles in all three cores. The coarse aggregate (greywacke) appeared to be the reactive component in the concrete. Tremblay (2011) reported the findings of the petrographic examination of another set of concrete cores extracted from the same sections of Jersey barrier walls, in 2010. The evaluation mainly consisted of the Damage Rating Index (DRI), a method that provides a semi-quantitative assessment of the degree of damage in concrete based on a count of petrographic features of deterioration generally associated with ASR. Damage Rating Indices ranging from 339 to 690 were obtained for the cores (Figure 120), thus suggesting fair to moderate/severe degree of deterioration/damage due to ASR. Petrographic features of ASR were found to be related to the coarse aggregate (greywacke) particles. Typical features of ASR correspond to cracking with ASR gel and reaction rims in the greywacke particles, as well as reaction (ASR) products in cracks and air voids of the cement paste (Figure 121).

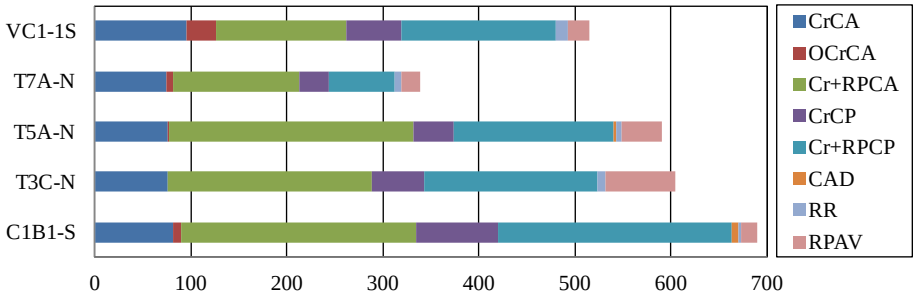

Figure 120. Results of the Damage Rating Index (DRI) for the Massachusetts cores. The colored cells give the proportions of each petrographic feature to the DRI value. (CrCA: cracking in the coarse aggregate particles; OCrCa: opened cracking in the coarse aggregate particles; Cr+RPCA: cracking in the coarse aggregate particles + reaction product; CrCP: cracking in the cement paste; Cr+RPCP: cracking in the cement paste + reaction product; CAD: coarse aggregate debonded; RR: reaction rim; RPAV: reaction products in air void of the cement paste).

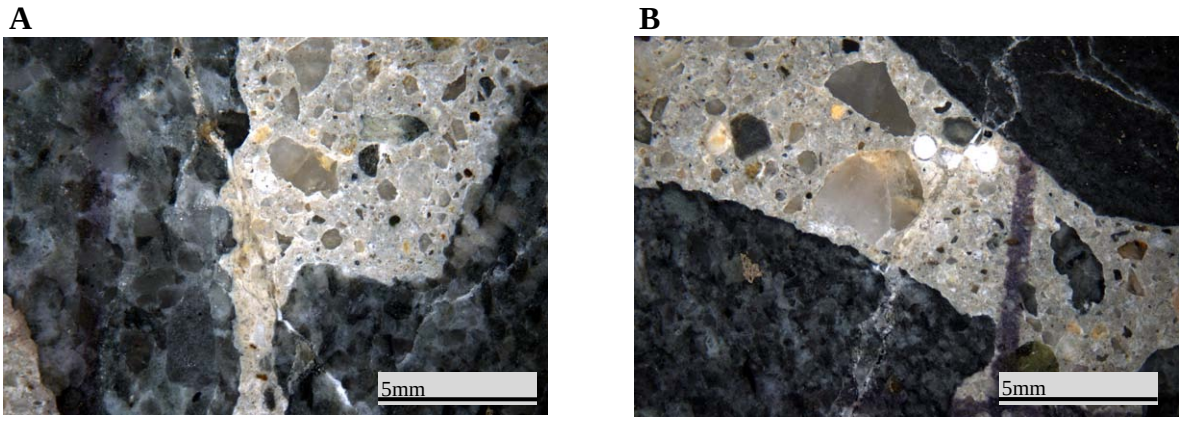

Figure 121. Polished concrete core surfaces.
A&B: Cracking in coarse aggregate particles (greywacke) extending into the cement paste; secondary (ASR) products are observed in the cracks both in the particles and the cement paste.

8.2 SUMMARY OF APPLICATION REPORT

This section describes the application of various products to the highway barriers on Route 2 in Leominster, MA. The first treatment was in 2005 under the FHWA Lithium Technology Research Program and is shown in Figure 122 as the "original test section." Also shown in Figure 122 is the "extended test section," which refers to the sections, on both sides of the original test section, treated by MassDOT (with 40 percent silane) in 2005 and again in 2010 under the FHWA ASR Development and Deployment Program. This section focuses primarily on the FHWA treatments in 2005 and 2010.

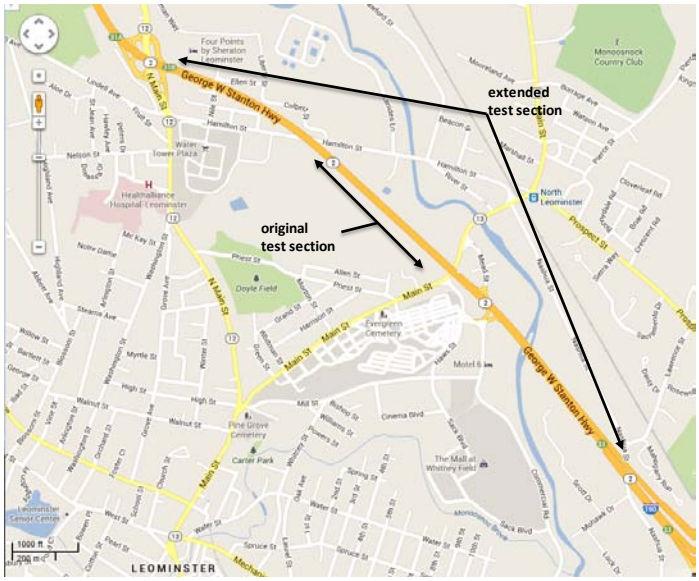

Figure 122. Location of highway barriers treated on Route 2 in Leominster, MA. Note that the "original test section" refers to the section treated in 2005 under the FHWA Lithium Technology Research Program; the "extended test section" refers to the section treated by MassDOT in 2005 and again in 2010 under the FHWA Development and Deployment Program.

After conducting a visual survey of the entire 6.4 km (4 mi) section of ASR-affected barriers in 2004 and 2005, it was determined that these barriers along Route 2 generally exhibited similar levels of distress. Under the FHWA Lithium Technology Research Program, it was decided in 2005 to evaluate a range of different mitigation measures aimed at trying to slow down the rate of ASR-induced expansion and cracking and to, in turn, reduce the potential for freezing and thawing damage along the bottom of the barriers. In order to establish representative treatment sections, three median barriers, each approximately 3 m (10 ft) in length, were selected for each treatment. A barrier was skipped between each treatment to distinguish the different treatments from each other. Table 64 describes the specific details of each treatment, and Figure 123 to Figure 125 show the layout of the various test sections, including the locations where monitoring were performed.

Table 64. Details of treatments applied in 2005 under FHWA Lithium Technology Research Program.

Treatment	Treatment Description	Application Rate
C1	Control section 1	
C2	Control section 2	
C3	Control section 3	
T1	Single topical application of lithium nitrate	30%-lithium nitrate solution applied at 0.12 l/m^2 (1 gal/345 ft^2)
T2	Two topical applications of lithium nitrate	30%-lithium nitrate solution applied twice at 0.12 l/m^2 (1 gal/345 ft^2)
T3	Four topical applications of lithium nitrate	30%-lithium nitrate solution applied four times at 0.12 l/m^2 (1 gal/345 ft^2)
T4	Two topical applications of lithium nitrate and double topical application of silane	30%-lithium nitrate solution applied twice at 0.12 l/m2 (1 gal/345 ft^2); 40% silane (isopropyl alcohol-based) applied twice at 0.33 l/m^2 (1 gal/125 ft^2)
T5	Single topical application of silane	40% silane, isopropyl alcohol-based applied at 0.33 l/m^2 (1 gal/125 ft^2)
T6	Single topical application of silane	20% silane, isopropyl alcohol-based applied at .33 l/m^2 (1 gal/125 ft^2)
T7	Single topical application of silane	20% silane, water-based applied at .33 l/m^2 (1 gal/125 ft^2)
T8	Single topical application of lithium silicate sealer	Applied at .33 l/m^2 (1 gal/125 ft^2)
VA	Short-term vacuum impregnation of lithium nitrate on both sides	30%-lithium nitrate solution applied by vacuum for 15 minutes.
VB	Short-term vacuum impregnation of lithium nitrate on both sides + topical silane application on both sides	30%-lithium nitrate solution applied by vacuum for 15 minutes.; 20% silane, water based applied topically at 0.33 l/m^2 (1 gal/125 ft^2)
VC	Long-term vacuum impregnation of lithium nitrate on one side and short term on the other side	30%-lithium nitrate solution applied by vacuum for 7.5 hours on one side of barrier; 30%-lithium nitrate solution applied by vacuum for 15 minutes on other side of barrier
VD	2 short-term vacuum impregnations of lithium nitrate on both sides of the barrier	30%-lithium nitrate solution applied twice by vacuum for 15 minutes each on both sides of barrier

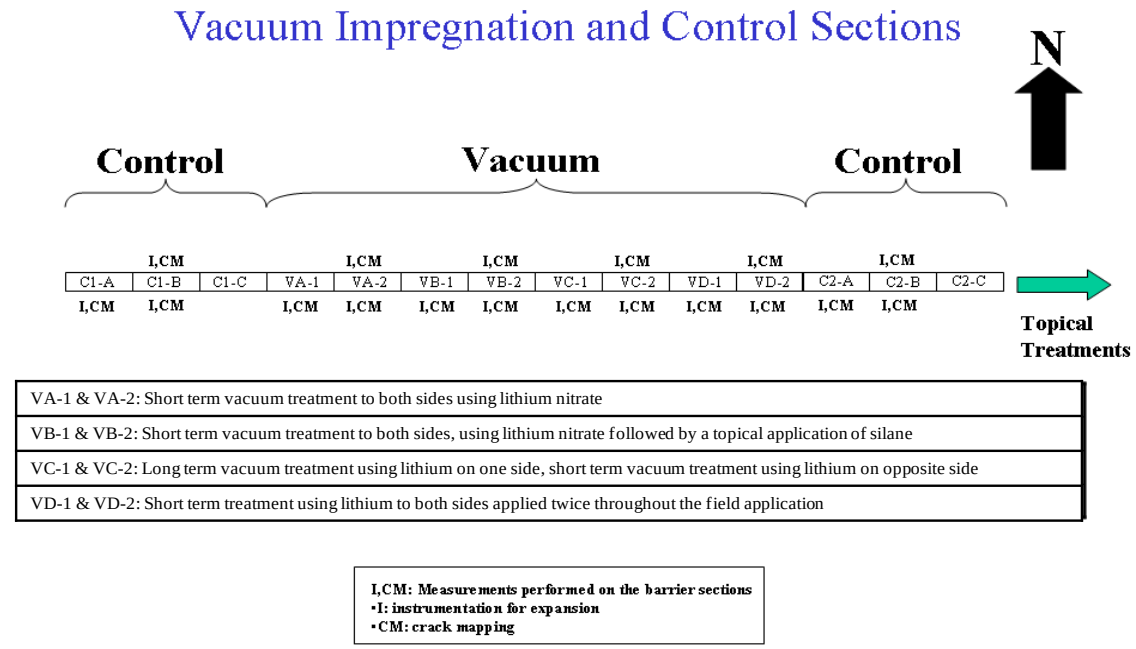

Figure 123. Treatment and monitoring plan for vacuum impregnation and control sections.

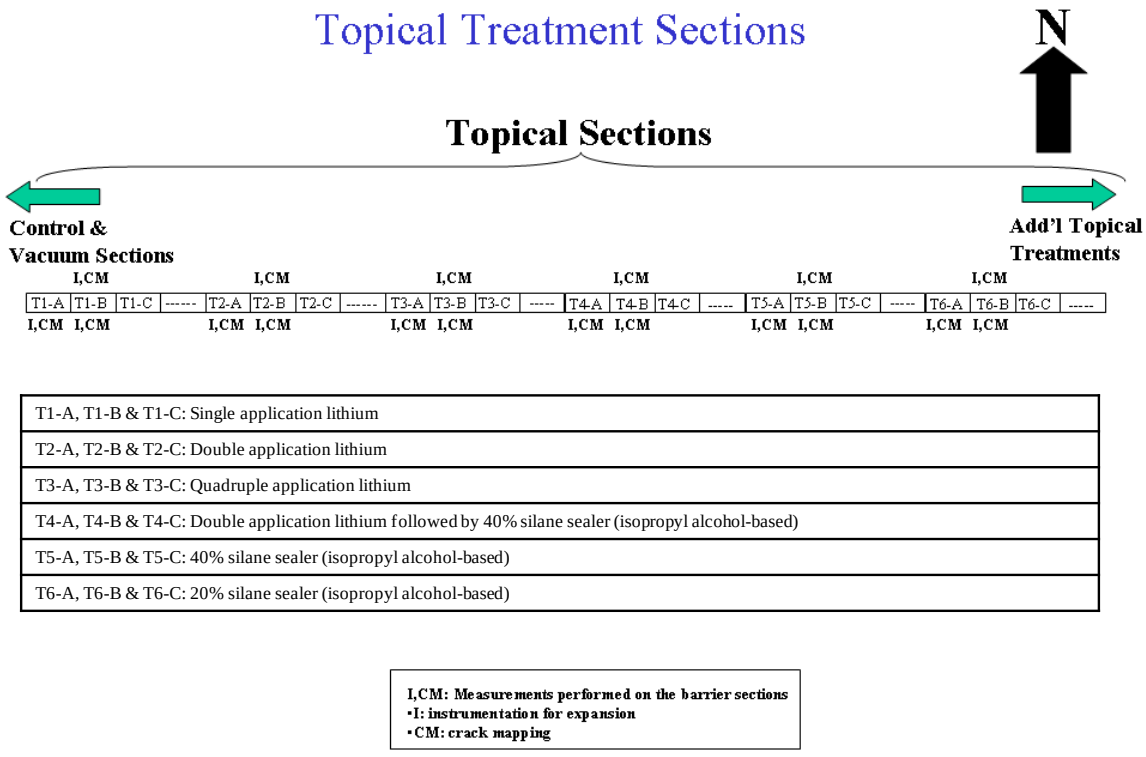

Figure 124. Treatment and monitoring plan for topical treatment sections.

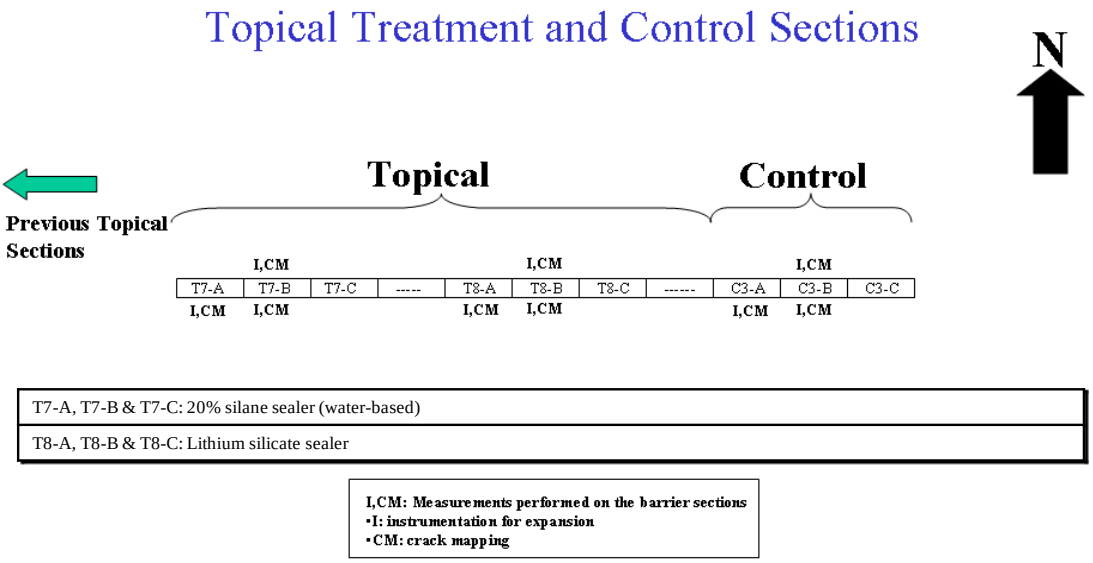

Figure 125. Treatment and monitoring plan for topical treatment and control section.

A handheld pump sprayer was used to apply the silanes, lithium nitrate, and lithium silicate, as shown in Figure 126 at application rates described in Table 1. Figure 127 shows the vacuum setup shortly after 30 percent lithium nitrate solution was introduced to the system. This vacuum pressure was applied for either a short term (15 minutes) or long term (7.5 hours).

Figure 126. Silane product applied with a handheld pump sprayer.

Figure 127. Vacuum impregnation of 30 percent lithium nitrate solution into highway barrier. This photograph was taken shortly after the solution was entered into the system under vacuum. Once a full vacuum was obtained, the vacuum was held for either 15 minutes (short term) or 7.5 hours (long term).

A few months after the first treatment phase was completed, as just described, MassDOT treated the remaining section of the distressed barrier section with 40 percent silane (water-based), thus completing the "extended test section," as depicted in Figure 122. This treatment was done separate from any FHWA efforts, and specific details of the treatment are not presented herein. As described next, some of these MassDOT-treated sections were monitored by the FHWA ASR Development and Deployment Program research team and some additional treatments were subsequently applied over these treated barriers.

In 2010, it was decided that the FHWA ASR Development and Deployment research team would initiate additional treatments on the barriers previously treated by MassDOT in 2005 with silane. Most of the barrier sections outside of the "original test section" were sprayed with an elastomeric paint with the goal of reducing the potential for frost damage from the lower portions of barriers heavily affected by ASR. For this study, four representative 10-barrier sections within this extended test section were selected to evaluate the performance of repeated applications of silane and the effects of applying elastomeric paint over a surface previously treated with silane, as shown in Table 65. Figure 128 shows the elastomeric paint being spray-applied to the barriers. The "original test section" did not receive any treatments in this program so that the original treatments from 2005 could be evaluated. Additional details on the performance monitoring techniques and treatment activities are provided in chapters 2 and 3, respectively.

Table 65. Details of treatments applied in 2010 under the FHWA ASR Development and Deployment Program.

Treatment	Treatment Description	Details
1X Si	Control section	Previously treated with 40% silane in 2005. No additional treatments under this program.
2X Si	Topical application of 40% silane (solvent-based)	Applied at 3.1 m^2/L (125 ft^2/gal), over surface previously treated with silane in 2005.
2X Si + Elast	Topical application of 40% silane (solvent-based), followed by application of elastomeric paint (Elast)	Silane applied at 3.1 m^2/L (125 ft^2/gal), over surface previously treated with silane in 2005. Elastomeric paint was spray-applied at 2.5 m^2/L (100 ft^2/gal)
1X Si + Elast	Application of elastomeric paint	Elastomeric paint was spray-applied at 2.5 m^2/L (100 ft^2/gal), over surface previously treated with silane in 2005.

Figure 128. Elastomeric paint sprayed in 2010 onto barrier sections previously treated with 40 percent silane in 2005 by MassDOT.

8.3 MONITORING DATA

This section summarizes the data obtained from expansion, internal relative humidity, and crack mapping measurements from the instrumented barriers along Route 2 in Leominster, MA. For barriers treated with lithium nitrate using vacuum impregnation, the results of lithium concentration profiling are presented. Lastly, photographs of each crack mapping region taken prior to treatment and over the course of the monitoring period are presented.

Figures 129 to 132 summarize the vertical expansion results for the various barriers that were monitored over the course of about eight years. The data were not corrected for temperature (thermal) effects. Note that horizontal expansion was much less than vertical expansion, due to

external restraint and internal steel reinforcement, and they are not presented herein. Figure 129 shows the results of topical application of lithium nitrate, where the only time that expansion was reduced was when lithium treatment was followed up with an application of silane. The control and lithium nitrate-treated barriers expanded considerably during the course of the monitoring period, whereas the barrier treated with lithium nitrate and subsequently silane showed no expansion and in fact has exhibited shrinkage since the time of treatment in 2005. Figure 130 shows the expansion results for topical applications of various silanes, as well as lithium silicate. The results show that all of the barriers treated with silane, regardless of the silane content or whether the product was water-based or solvent-based, exhibited reductions in expansion compared to untreated barriers. The barrier treated with lithium silicate exhibited expansions similar to that of the control barriers. Figure 131 shows the expansion results for barriers treated by vacuum with lithium nitrate solution. Once again, the barrier that exhibited the least expansion was the barrier that was treated with silane (after vacuum treatment with lithium nitrate). Lastly, Figure 132 shows the expansion results since 2010 for barriers that were initially treated with silane by MassDOT in 2005, some of which were then treated again using silane and/or elastomeric paint in 2010. Because these barriers were treated only three years ago, it is difficult to identify trends in performance.

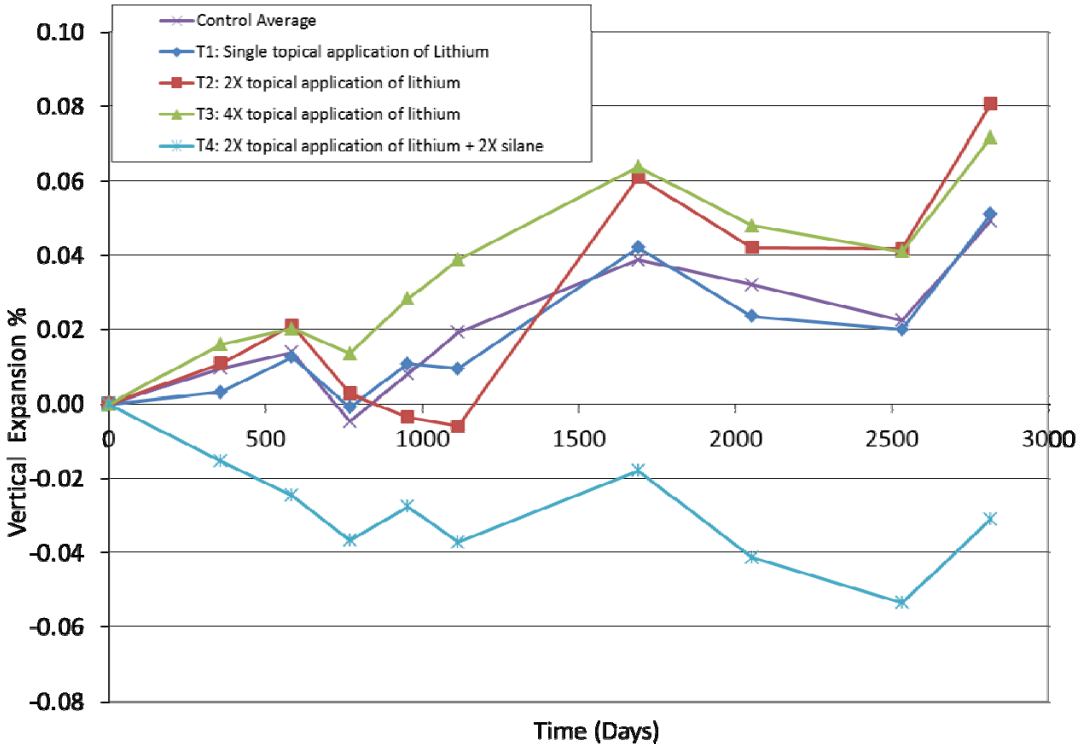

Figure 129. Average vertical expansion for highway barriers in Leominster, MA, comparing effects of topical treatment of lithium nitrate (with and without subsequent treatment with silane). The expansion of the control barriers is based on the average of three control sections (North and South sides of barriers). The expansion values for the treated sections are based on the average expansion for the North and South faces of the instrumented barrier in each test section.

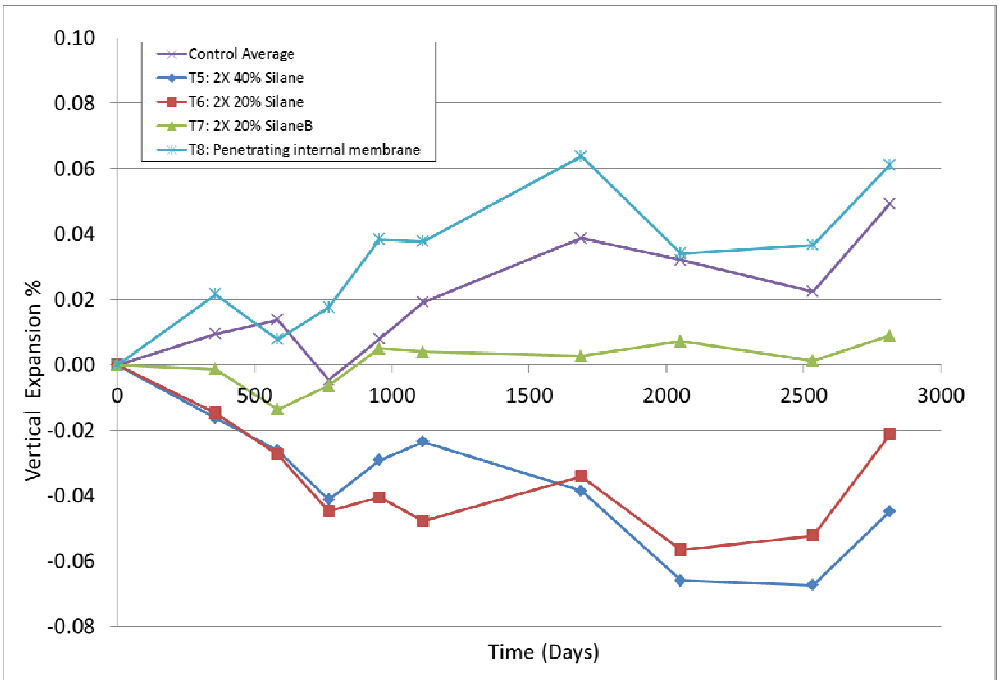

Figure 130. Average vertical expansion for highway barriers in Leominster, MA, comparing effects of topical treatment of various silane products and lithium silicate. The expansion of the control barriers is based on the average of three control sections (North and South sides of barriers). The expansion values for the treated sections are based on the average expansion for the North and South faces of the instrumented barrier in each test section.

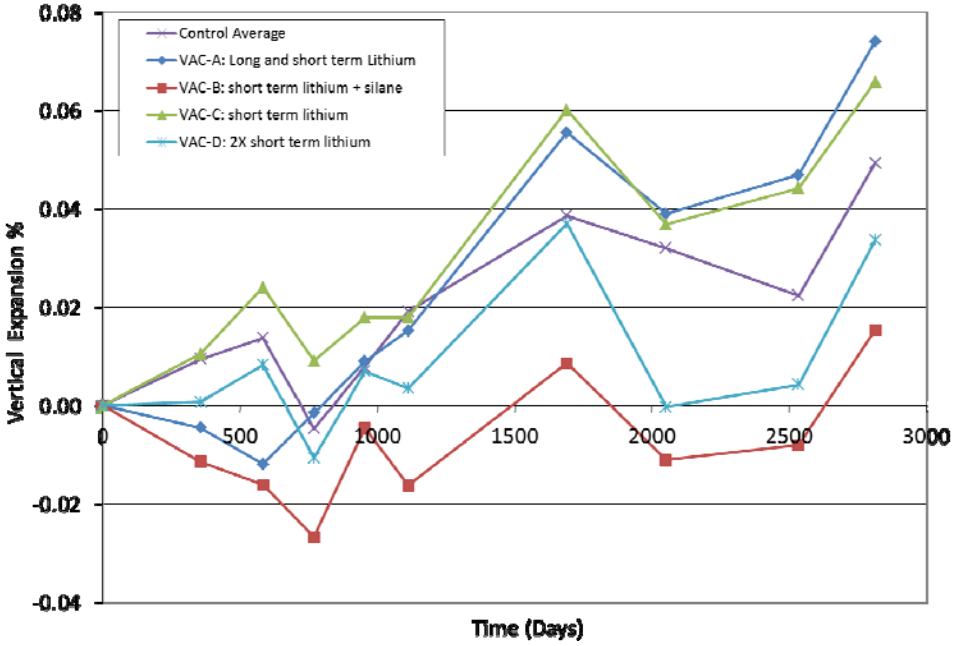

Figure 131. Average vertical expansion for highway barriers in Leominster, MA, comparing effects of vacuum treatment with lithium nitrate, as well as a combination of applying lithium under vacuum, followed by topical application of silane. The expansion of the control barriers is based on the average of three control sections (North and South sides of barriers). The expansion values for the treated sections are based on the average expansion for the North and South faces of the instrumented barrier in each test section.

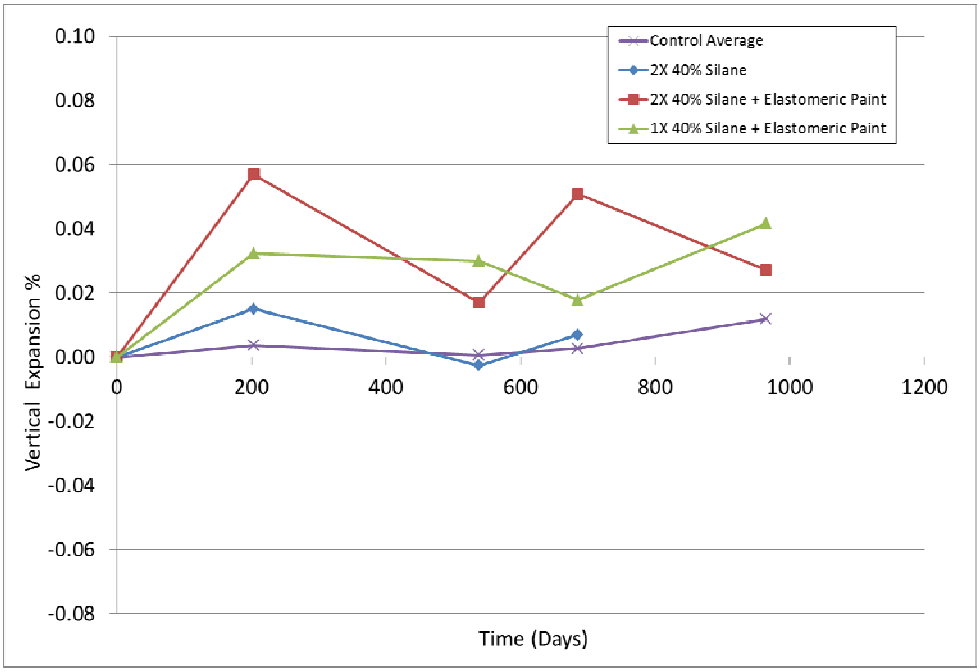

Figure 132. Average vertical expansion for highway barriers in Leominster, MA, comparing effects of a second silane treatment (five years after the first treatment) and the effects of applying elastomeric paint over barriers previously treated with silane. The expansion of the control barriers is based on the average of three control sections (North and South sides of barriers) from the time of the 2010 treatment. The expansion values for the treated sections are based on the average expansion for the North and South faces of the instrumented barrier in each test section.

Figure 133 shows the results of relative humidity measurements for the barriers treated with silane in 2005, compared to the control barrier. The values shown are based on the composite average relative humidity values recorded at depths of 25 mm (1 in.), 50 mm (2 in.), and 75 mm (3 in.). Figure 134 shows similar data for barriers that were treated in 2010. As can be seen in these two figures, the variability in relative humidity measurements is significantly higher than expansion measurements, making it more difficult to identify trends in performance.

Figure 135 to Figure 137 show the average calculated Cracking Index (CI) values based on crack mapping measurements from the South face of each of the instrumented barriers. The results shown are based on map cracking on the South-facing side of each instrumented barrier. Barriers that were treated with elastomeric paint were no longer crack mapped because the paint covered most all of the visible cracking (with the exception of large cracks that the elastomeric paint was unable to bridge). In general, there is quite a bit of scatter in the data, due to inherent difficulties in visually assessing cracked concrete in field elements. Also, crack mapping is quite sensitive to the user (or crack mapping operator), and over the course of eight years of monitoring, it was not possible to have one individual take all measurements.

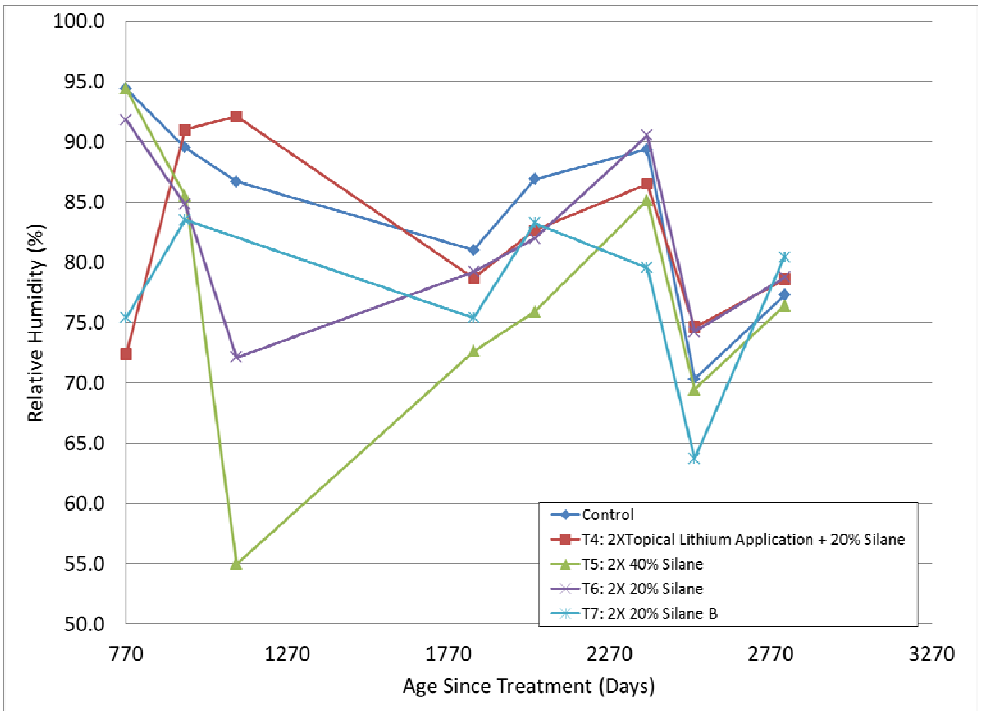

Figure 133. Average relative humidity values for highway barriers in Leominster, MA, comparing effects of silane applied in 2005. All values shown are based on the composite average relative humidity values recorded at depths of 25 mm (1 in.), 50 mm (2 in.), and 75 mm (3 in.).

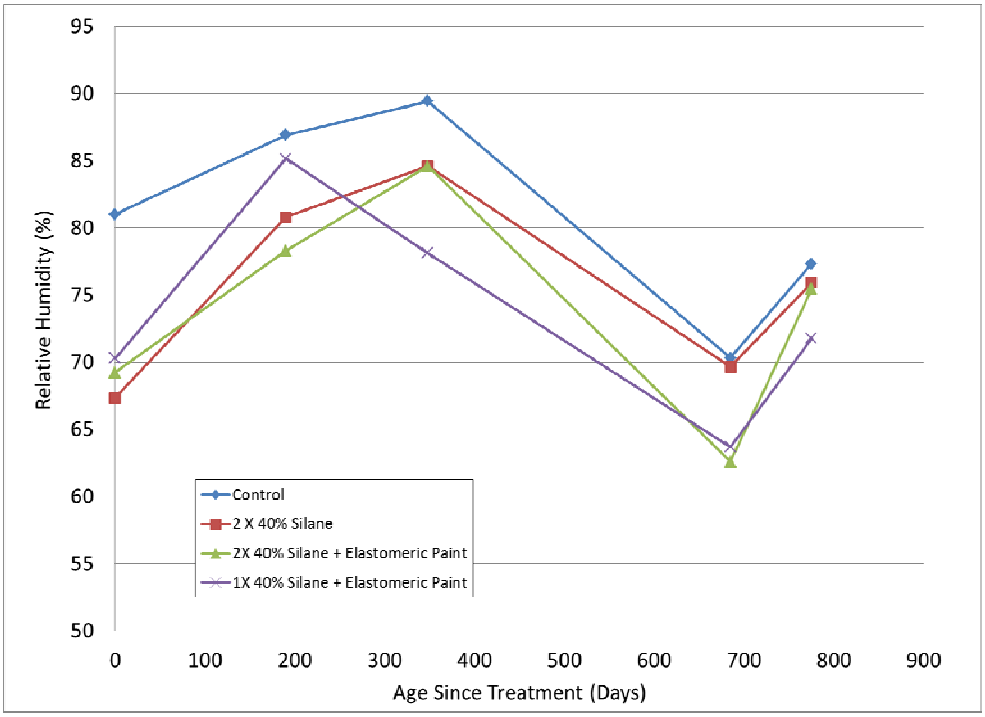

Figure 134. Average relative humidity values for highway barriers in Leominster, MA, comparing effects of a second silane treatment (five years after the first treatment) and the effects of applying elastomeric paint over barriers previously treated with silane. All values shown are based on the composite average relative humidity values recorded at depths of 25 mm (1 in.), 50 mm (2 in.), and 75 mm (3 in.).

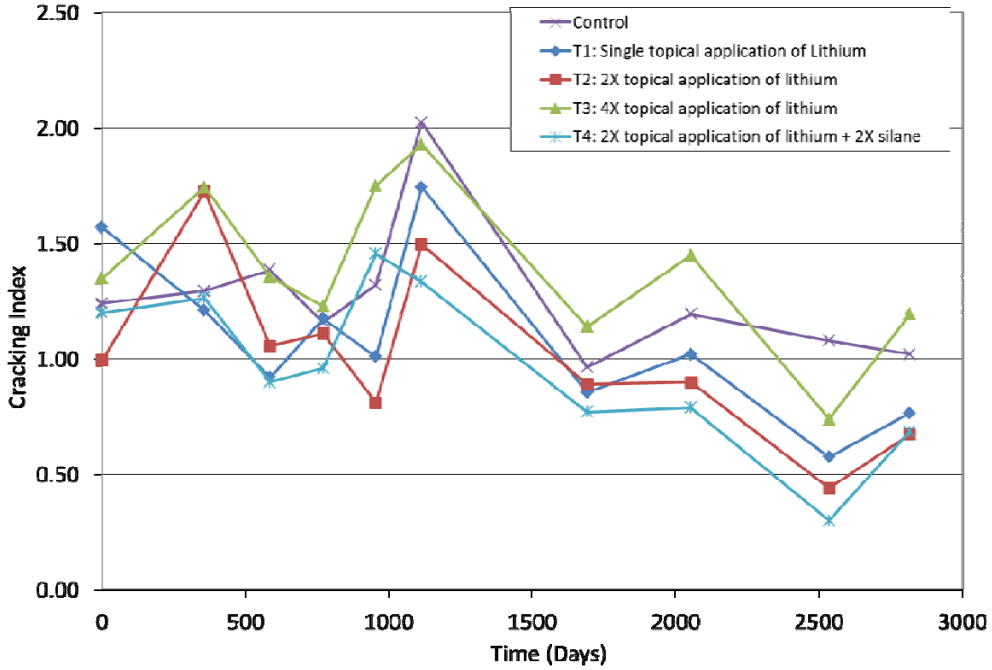

Figure 135. Calculated Cracking Index (CI) (mm/m) values for highway barriers in Leominster, MA, comparing effects of topical treatment of lithium nitrate (with and without subsequent treatment with silane). The CI calculations are based on crack mapping performed on the South face of each instrumented barrier.

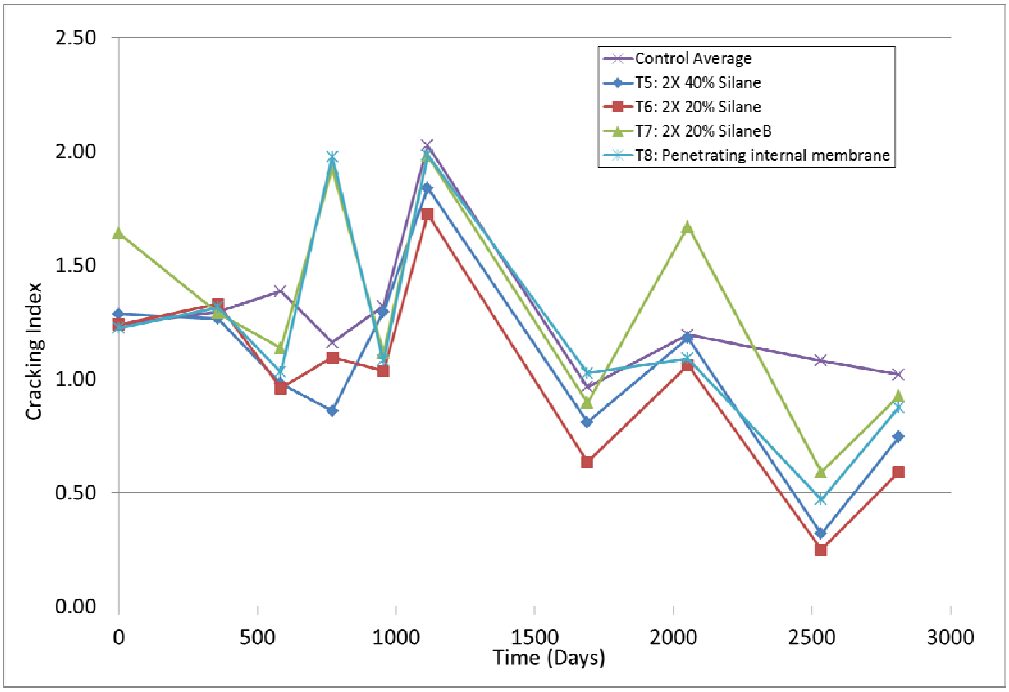

Figure 136. Calculated Cracking Index (CI) (mm/m) values for highway barriers in Leominster, MA, comparing effects of topical treatment of various silane products and lithium silicate. The CI calculations are based on crack mapping performed on the South face of each instrumented barrier.

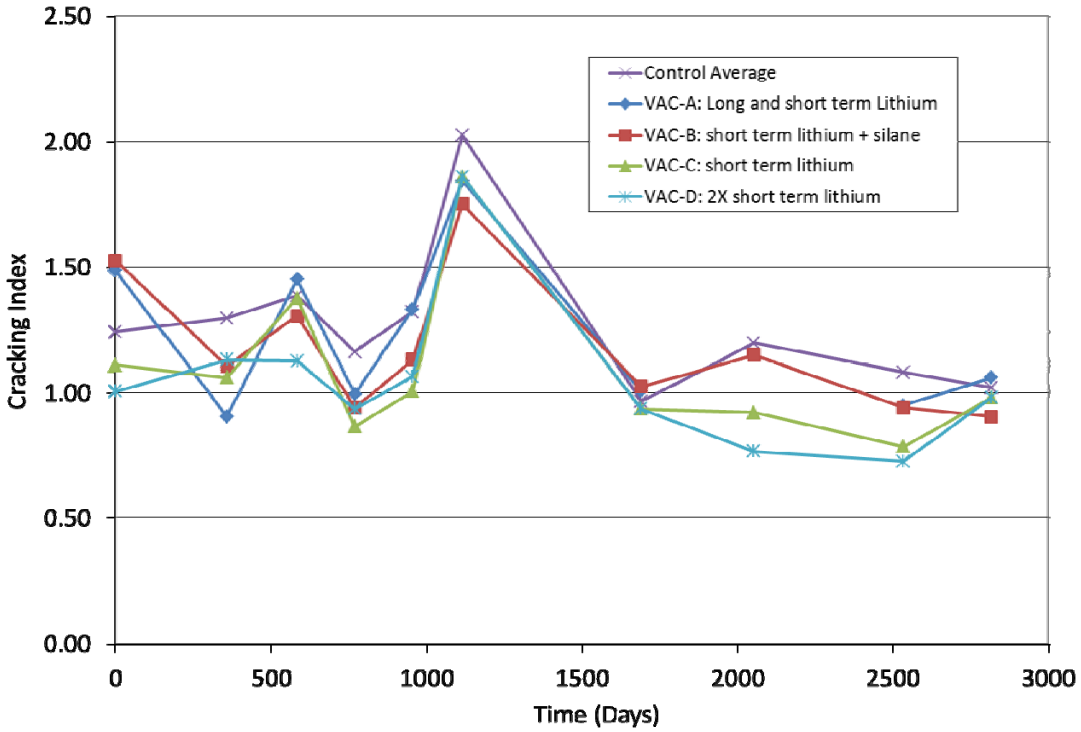

Figure 137. Calculated Cracking Index (CI) (mm/m) values for highway barriers in Leominster, MA, comparing effects of vacuum treatment with lithium nitrate, as well as a combination of applying lithium under vacuum, followed by topical application of silane. The CI calculations are based on crack mapping performed on the South face of each instrumented barrier.

Before evaluating lithium profile data (presented next), it is important to consider much lithium is typically needed to control expansion due to ASR. Assume that a plain concrete mixture containing 3 kg/m^3 Na_2O_e and has been shown to require approximately 13.8 L/m^3 of 30 percent lithium nitrate solution in order to sufficiently suppress expansion when tested with a specific aggregate. This dosage of $LiNO_3$ solution contains 504 g of Li, and assuming that half of this lithium gets bound in early hydration products (as well documented in literature), approximately 250 g of lithium per m^3 will remain in the concrete to combat ASR. If one assumes a concrete density of 2350 kg/m^3 the concentration of lithium ions in pore solution would be approximately 100 ppm, and this concentration would be enough to control expansion when used as an admixture. In short, 100 ppm is a reasonable threshold lithium concentration in concrete needed to suppress expansion due to ASR.

Figure 138 shows the measured lithium profiles for cores extracted from barriers (VC) that were vacuum impregnated with lithium nitrate for over seven hours. Cores were extracted from these barriers as they received the most long-term, aggressive vacuum treatment, and it was assumed that the maximum lithium penetration would be found in these barriers. The results show that the depth of lithium penetration was minimal, with lithium only present in a concentration above the 100 ppm threshold in the outer 2-4 mm (0.08-0.16 in.). Lithium profiling was not conducted on the other barriers treated with lithium (topically or by vacuum), but it is expected that the depths of penetration would be less than the penetration shown in Figure 138.

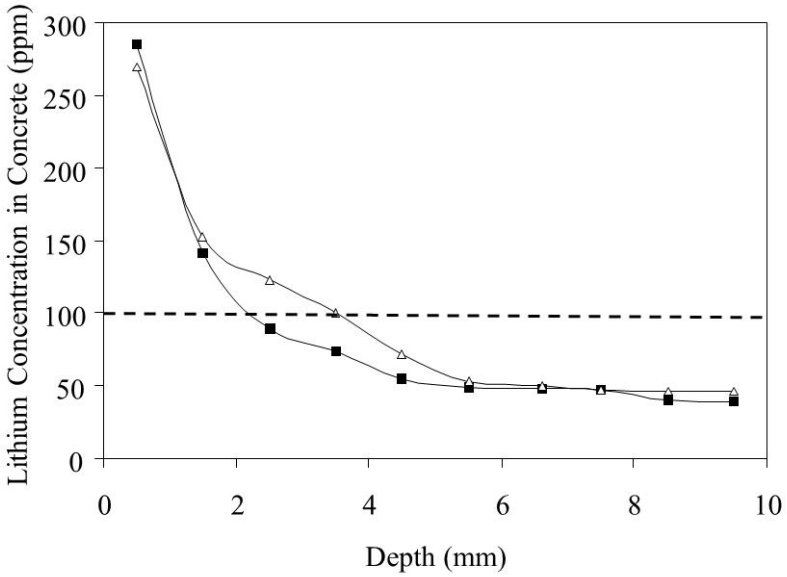

Figure 138. Depth of lithium penetration for Massachusetts highway barrier (vacuum impregnated with lithium nitrate). Plots are duplicate samples extracted from barrier that had been vacuum impregnated with lithium nitrate for 7.25 hours). Dashed line (100 ppm) indicates concentration of lithium estimated to suppress ASR-induced expansion.

Photographs were regularly taken of each of the map cracking areas as a means of documenting the visual changes that occurred during the monitoring period. Figure 139 to Figure 168 show a series of photographs from 2008 to 2013 of the South-facing side of each instrumented barrier, with the exception of barriers that have been treated with elastomeric paint. These painted sections are not included herein because the elastomeric paint essentially covers almost all of the cracks prior to treatment.

A – C1A - 2008

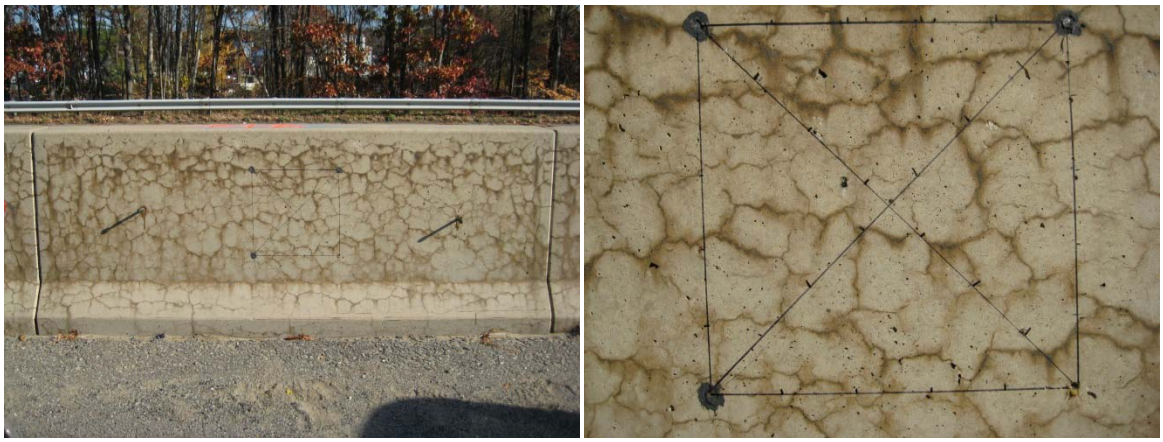

B – C1A - 2010

C – C1A - 2013

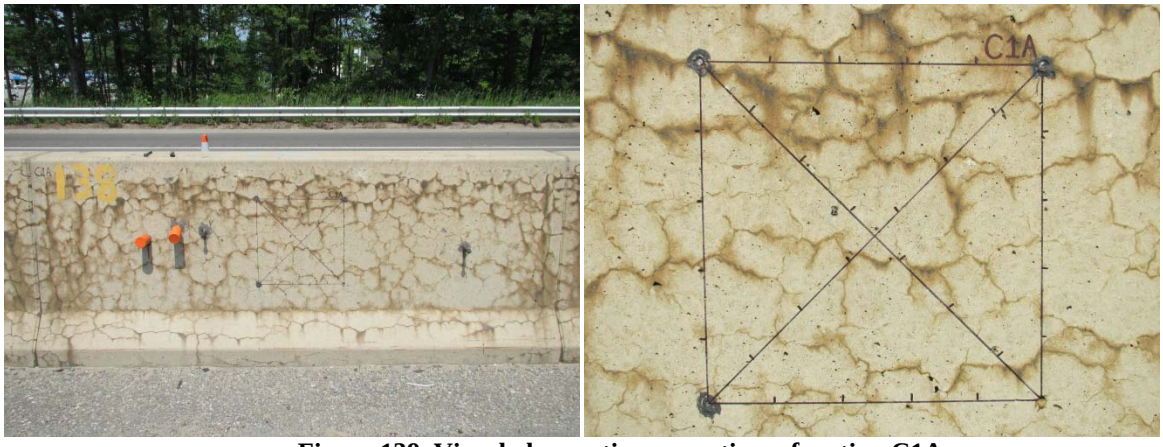

Figure 139. Visual observations over time of section C1A.

A – C1B – 2008

B – C1B - 2010

C – C1B - 2013

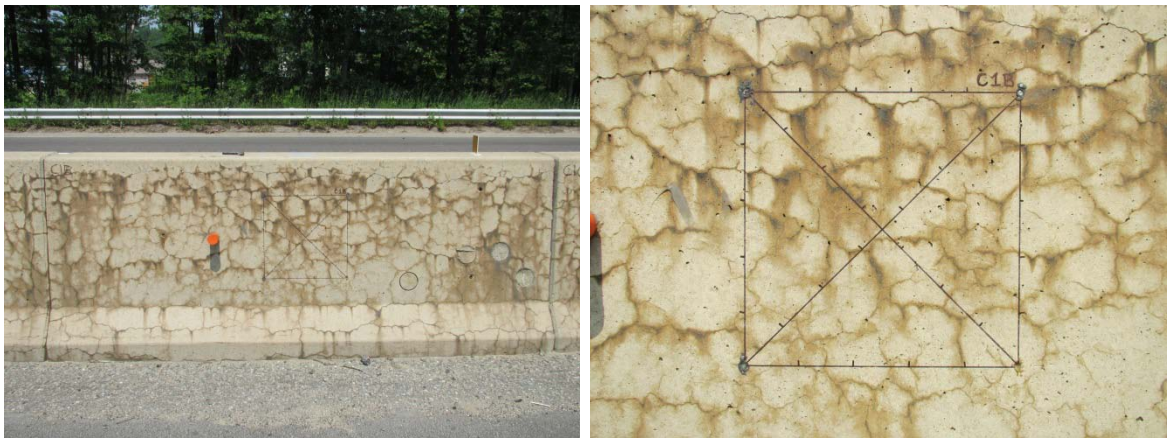

Figure 140. Visual observations over time of section C1B.

A – C2A - 2008

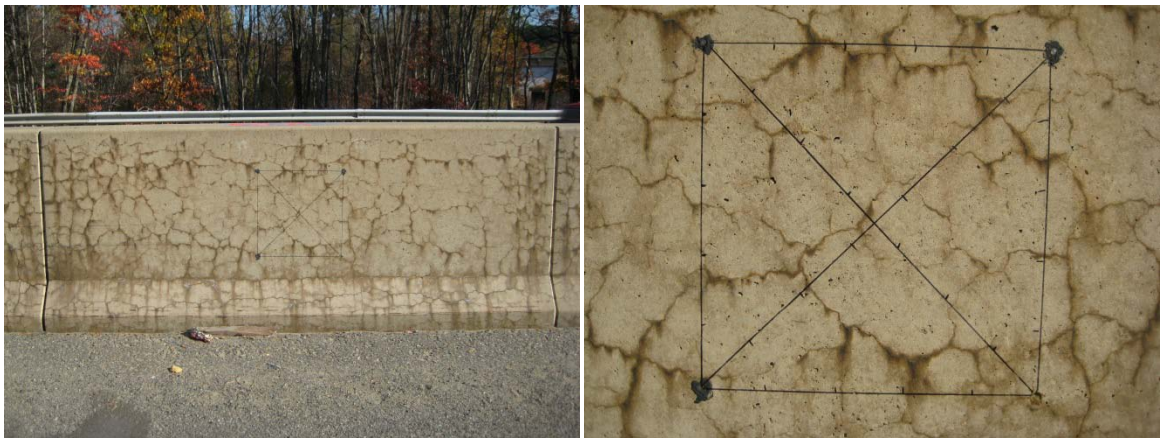

B – C2A - 2010

C – C2A - 2013

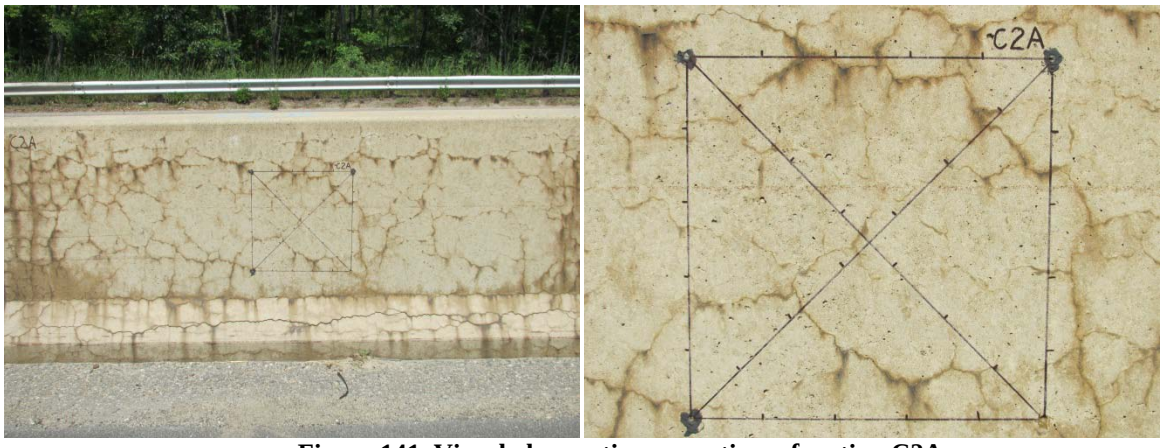

Figure 141. Visual observations over time of section C2A.

A – C2B - 2008

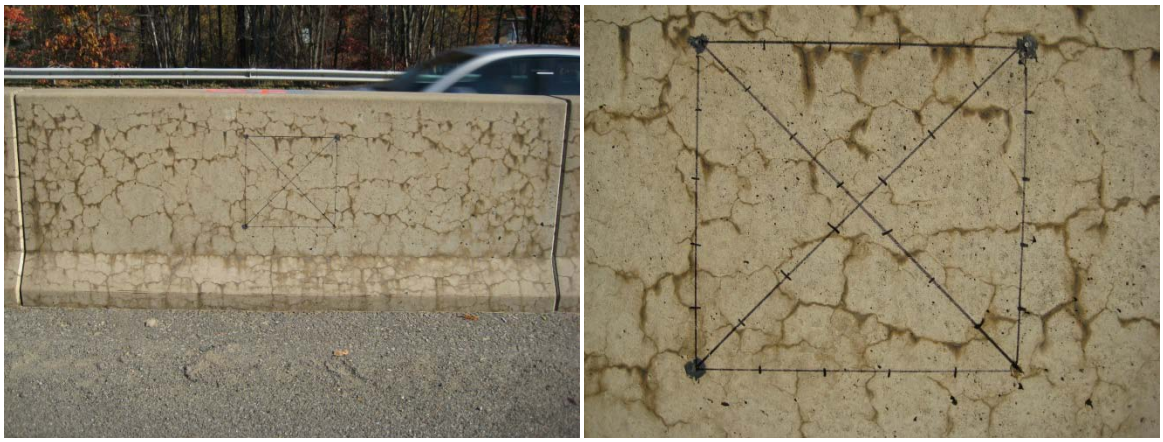

B – C2B - 2010

C – C2B - 2013

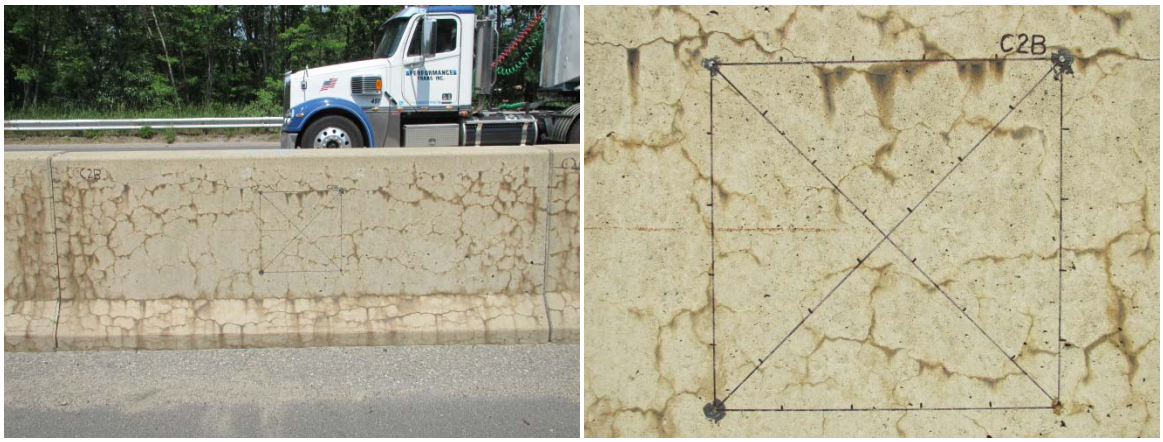

Figure 142. Visual observations over time of section C2B.

A – C3A - 2008

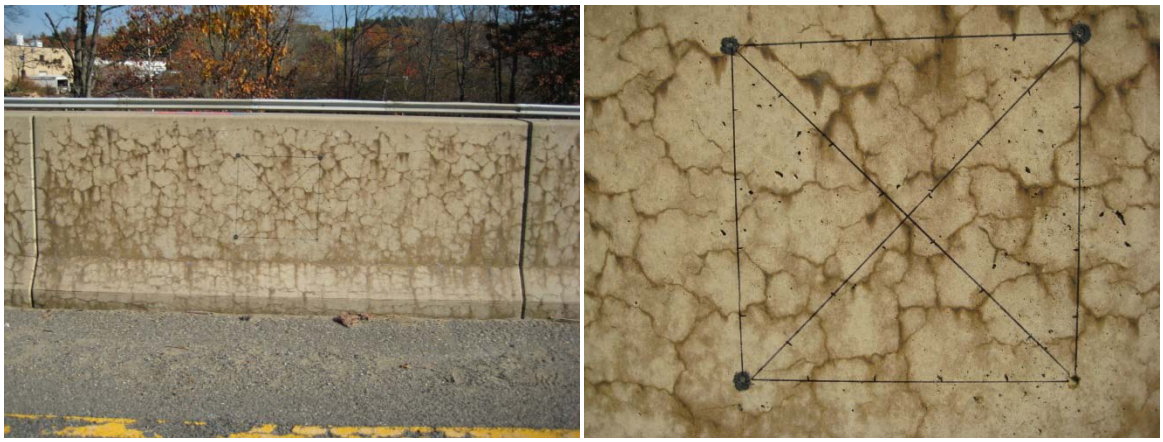

B – C3A - 2013

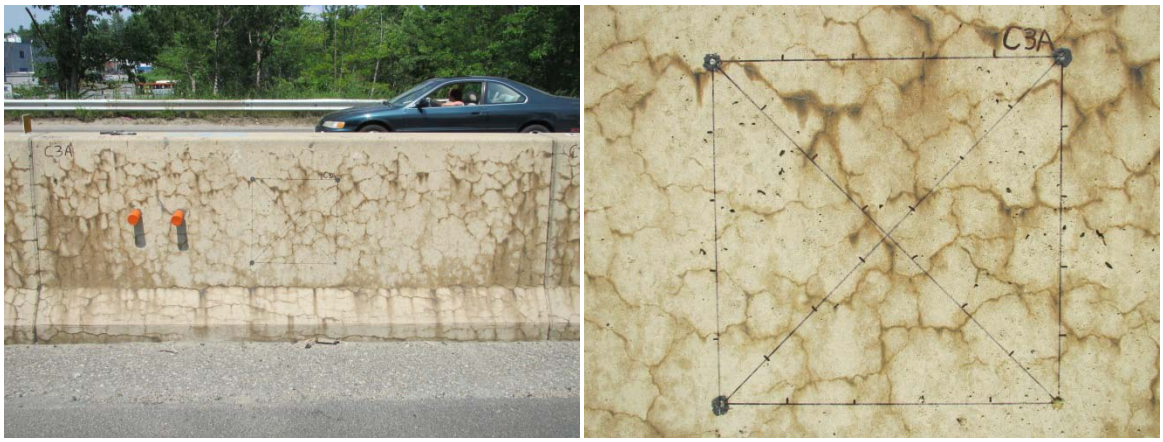

Figure 143. Visual observations over time of section C3A.

A – C3B - 2008

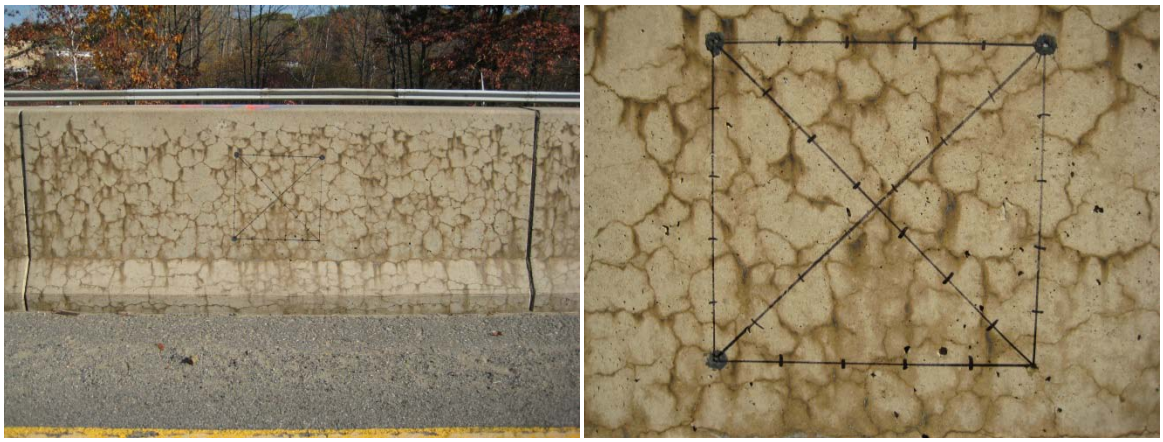

B – C3B - 2013

Figure 144. Visual observations over time of section C3B.

A - T1A - 2008

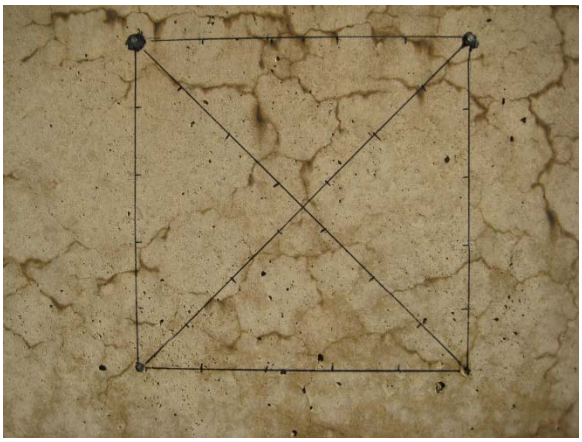

B – T1A - 2010

C – T1A - 2013

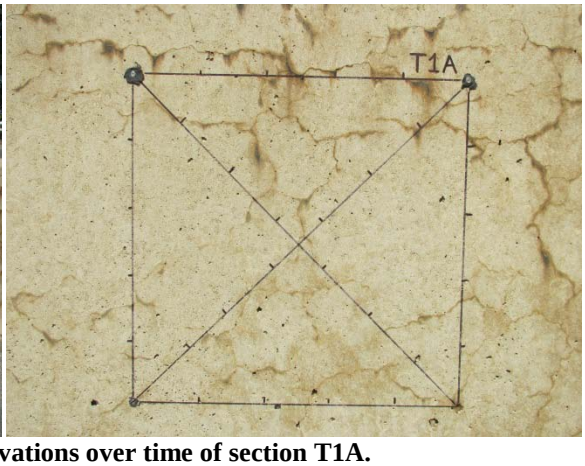

Figure 145. Visual observations over time of section T1A.

A – T1B - 2008

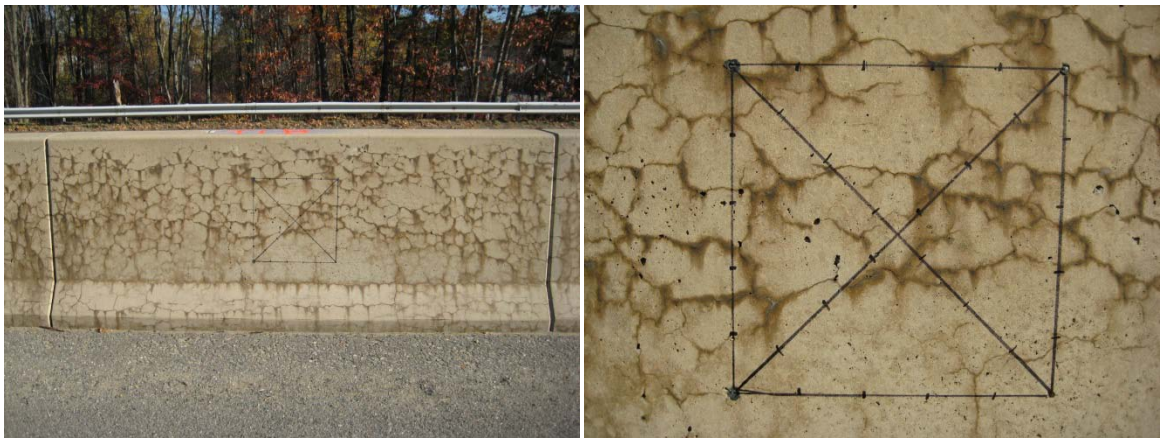

B – T1B - 2010

C – T1B - 2013

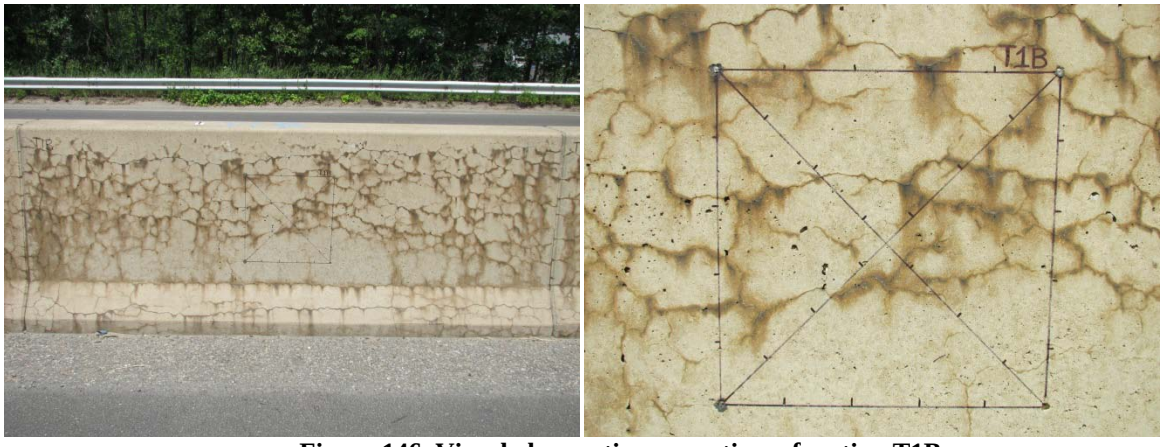

Figure 146. Visual observations over time of section T1B.

A – T2A - 2008

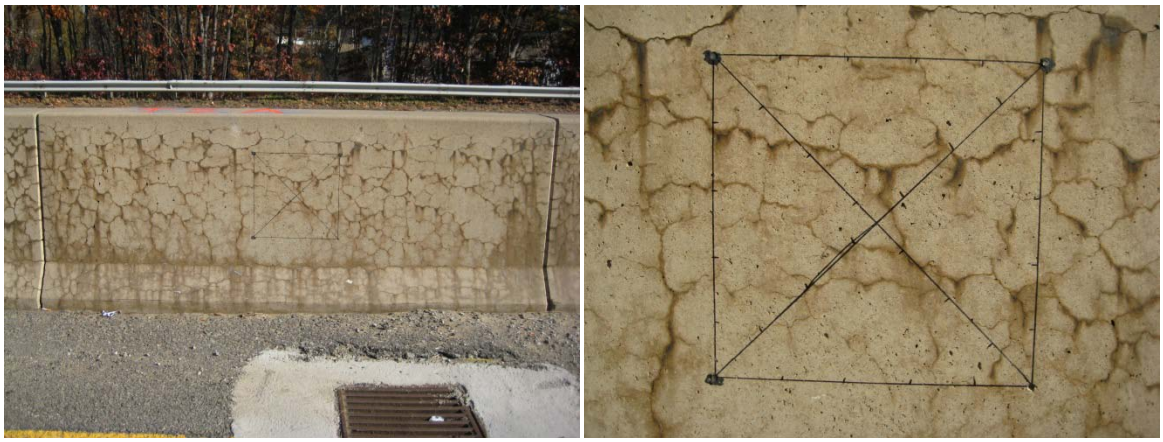

B – T2A - 2010

C – T2A - 2013

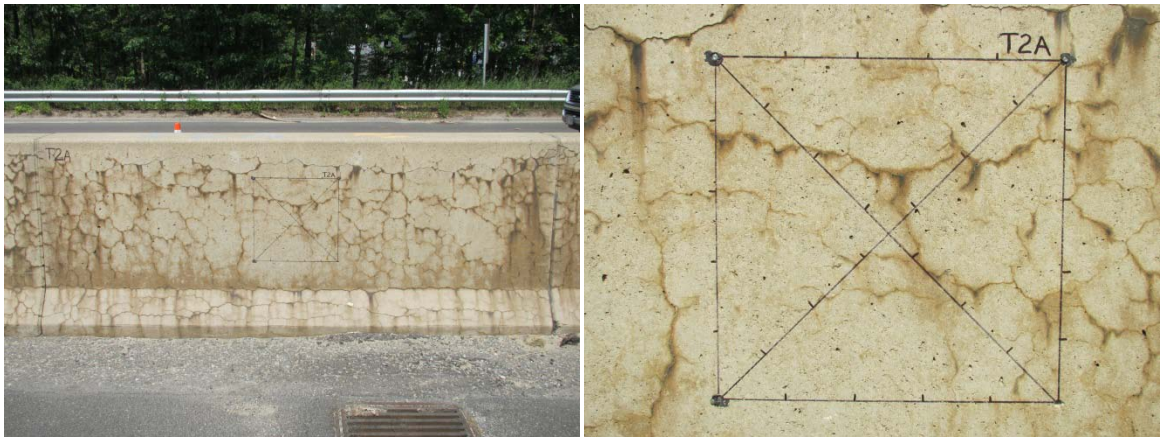

Figure 147. Visual observations over time of section T2A.

A – T2B - 2008

B – T2B - 2010

C – T2B - 2013

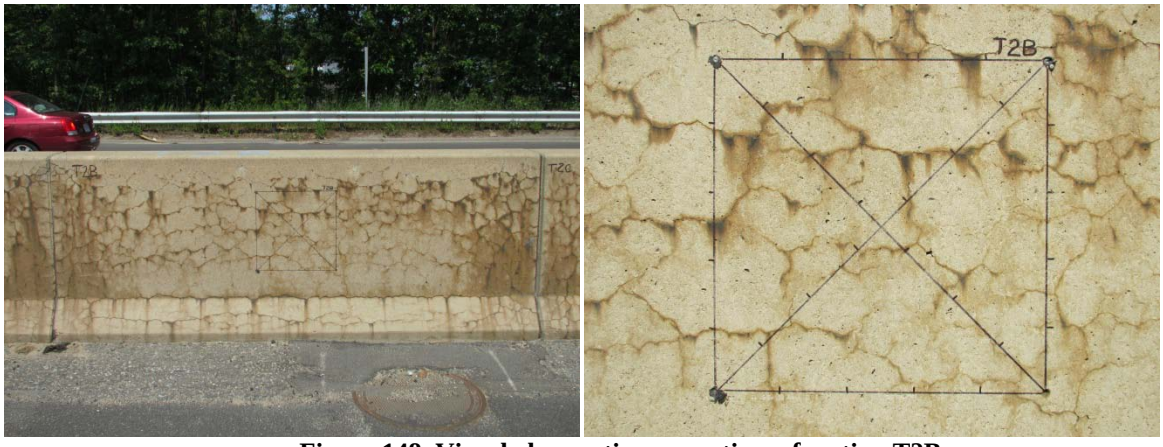

Figure 148. Visual observations over time of section T2B.

A – T3A - 2008

B – T3A - 2010

C – T3A - 2013

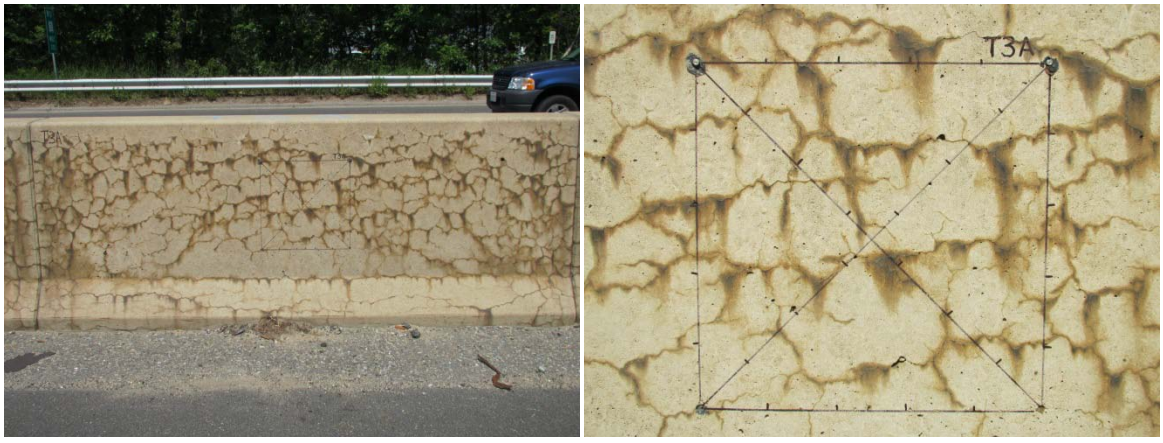

Figure 149. Visual observations over time of section T3A.

A – T3B - 2008

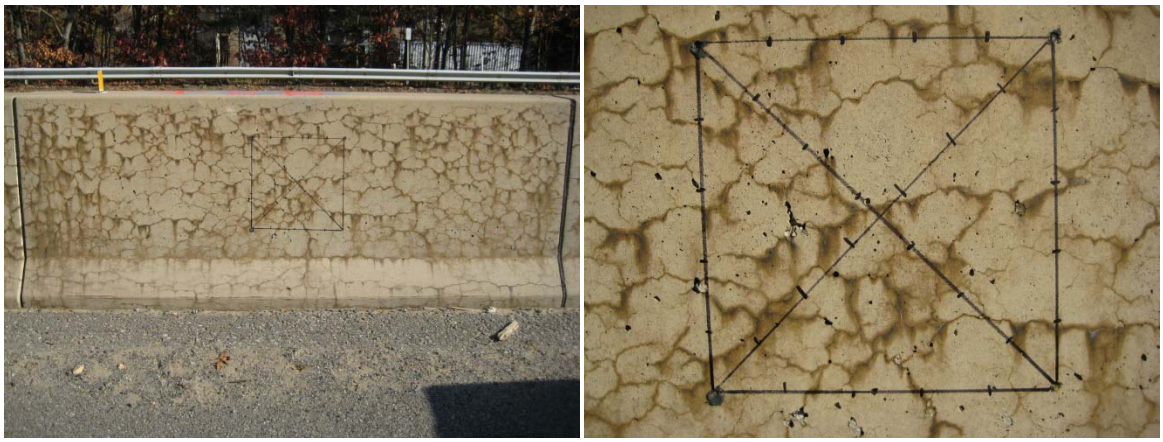

B – T3B - 2010

C – T3B - 2013

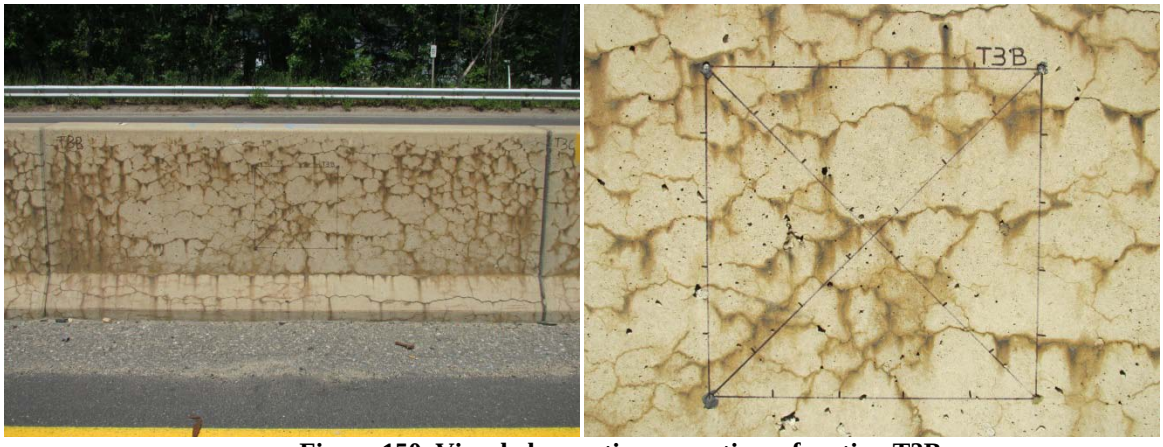

Figure 150. Visual observations over time of section T3B.

A – T4A - 2008

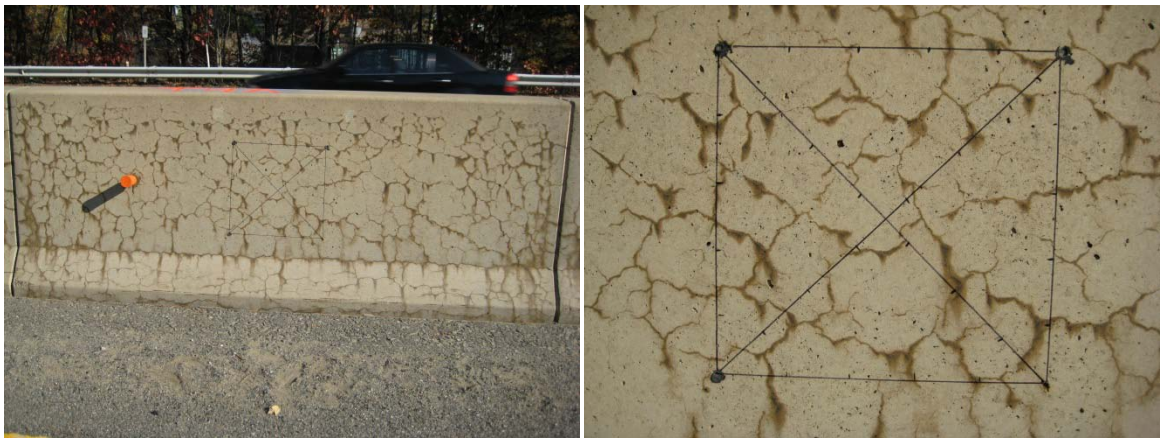

B – T4A - 2010

C – T4A – 2013

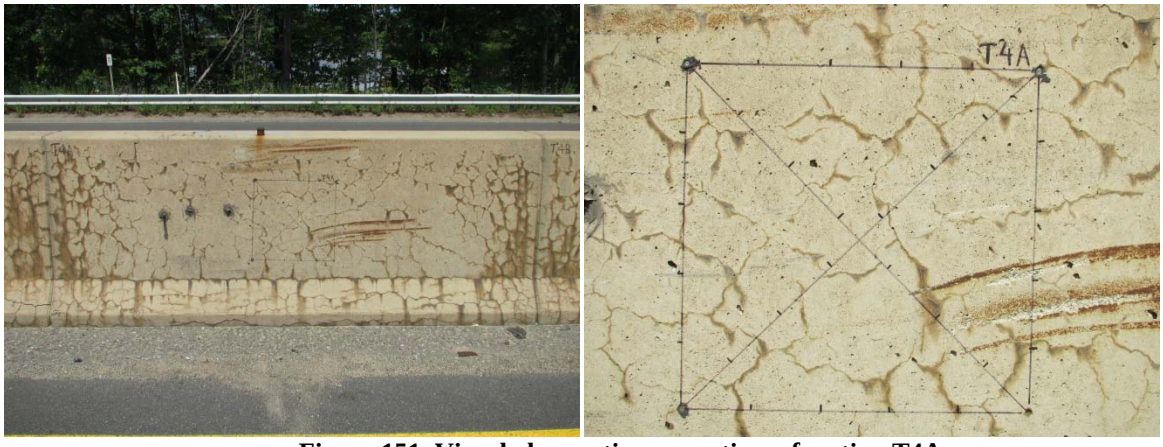

Figure 151. Visual observations over time of section T4A.

A – T4B - 2008

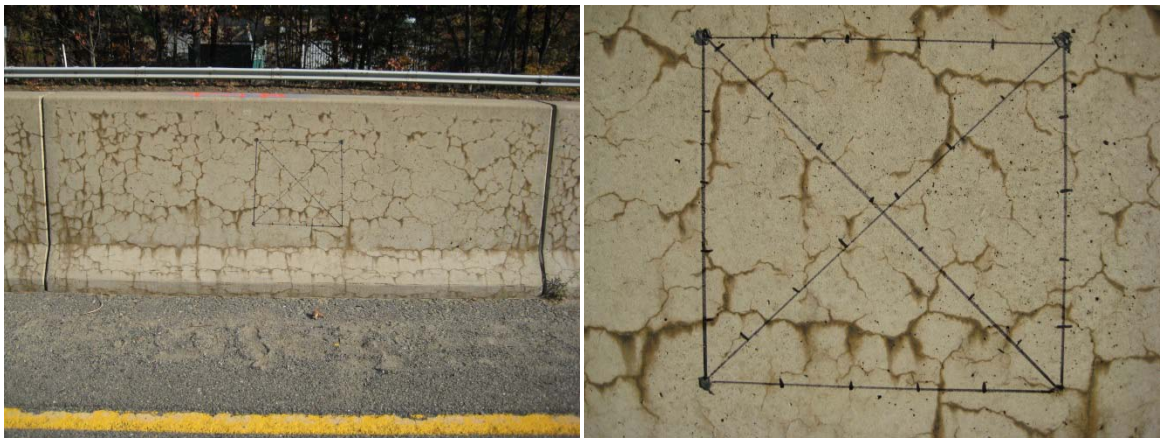

B – T4B - 2010

C – T4B - 2013

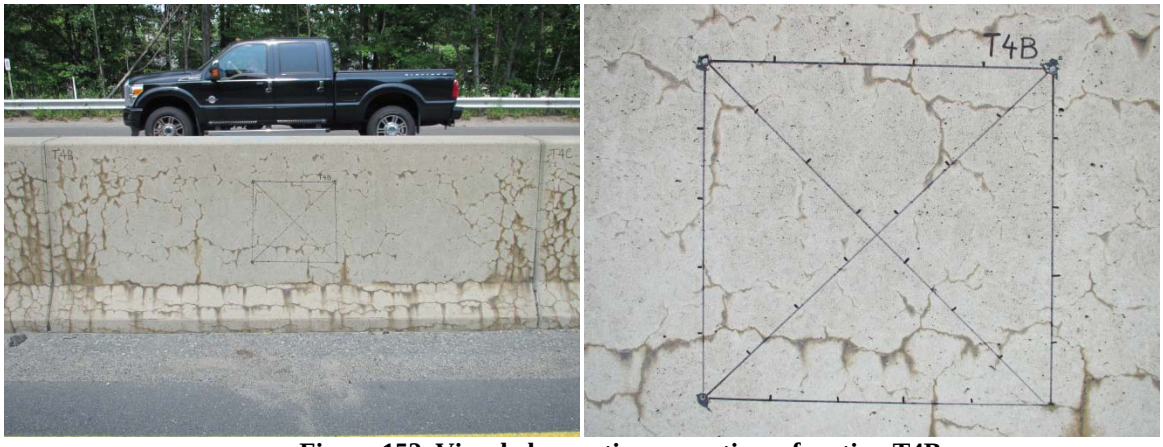

Figure 152. Visual observations over time of section T4B.

A – T5A - 2008

B – T5A - 2010

C – T5A - 2013

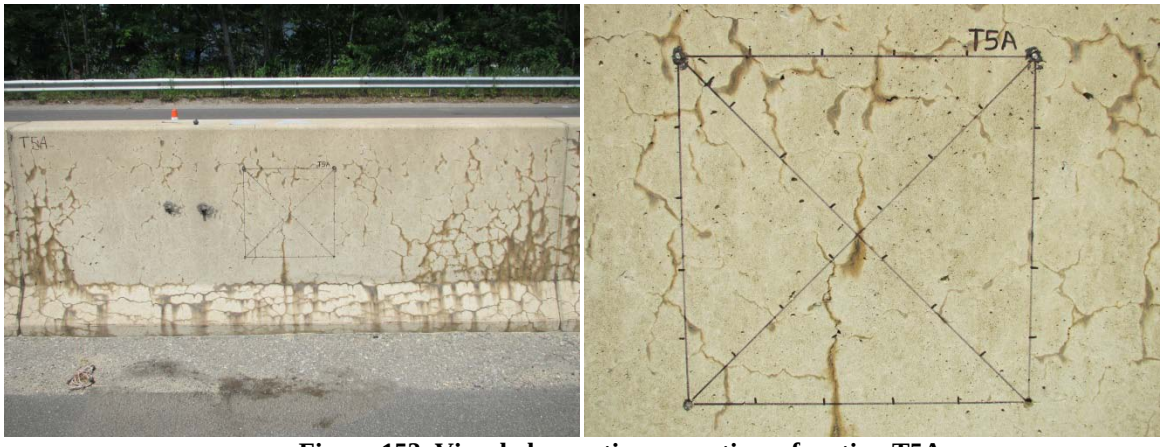

Figure 153. Visual observations over time of section T5A.

A – T5B - 2008

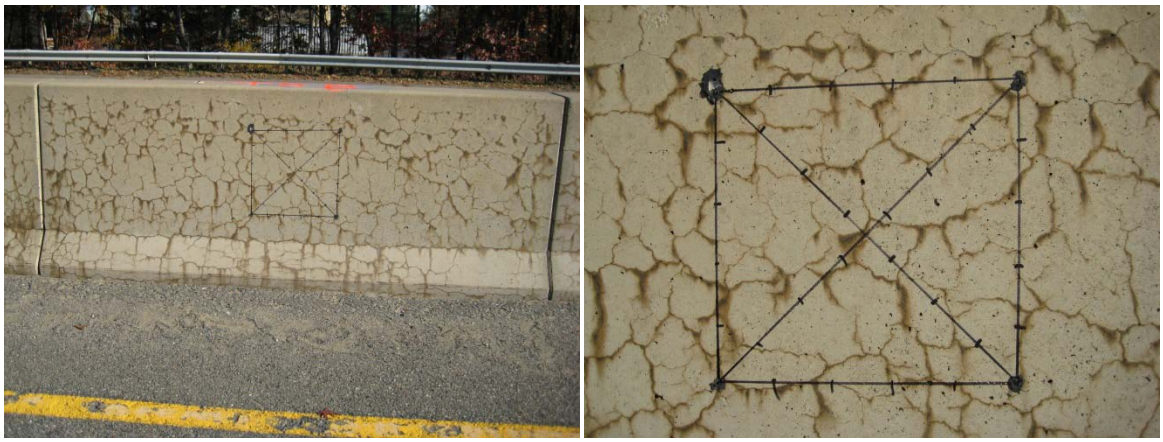

B – T5B - 2010

C – T5B - 2013

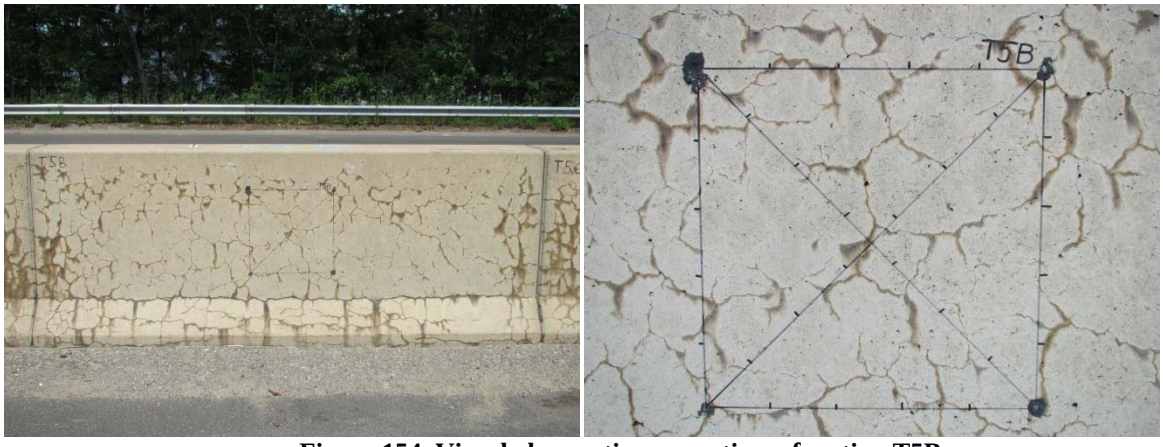

Figure 154. Visual observations over time of section T5B.

A – T6A - 2008

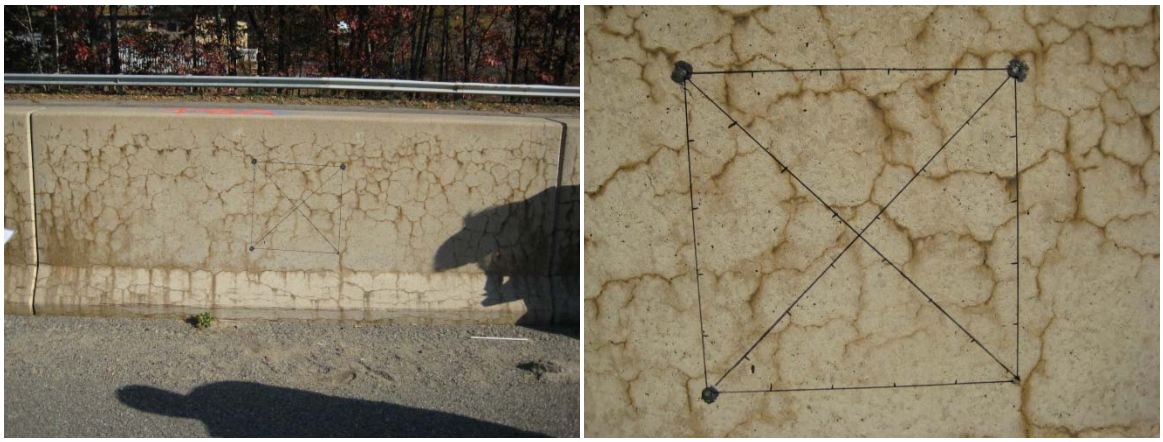

B – T6A - 2010

C – T6A - 2013

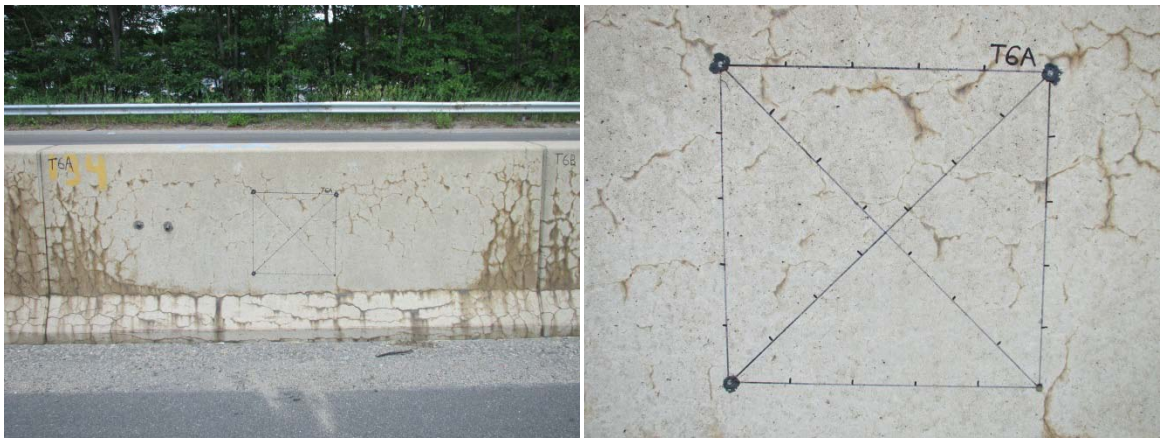

Figure 155. Visual observations over time of section T6A.

A – T6B - 2008

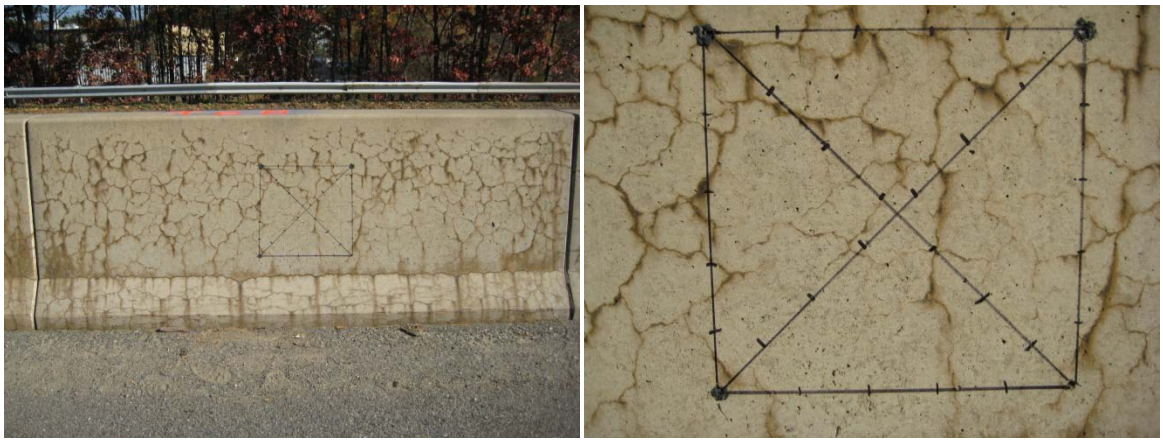

B – T6B - 2010

C – T6B - 2013

Figure 156. Visual observations over time of section T6B.

A – T7A - 2008

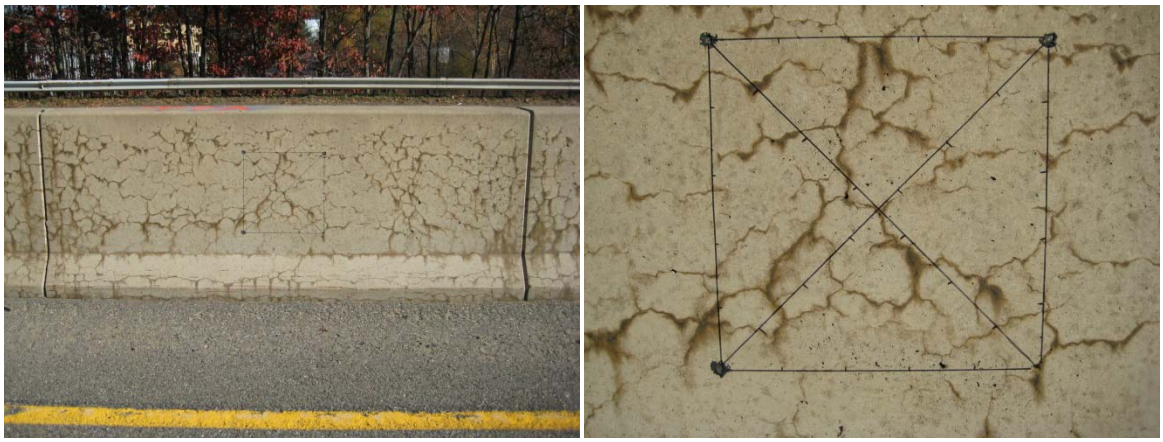

B – T7A - 2010

C- T7A - 2013

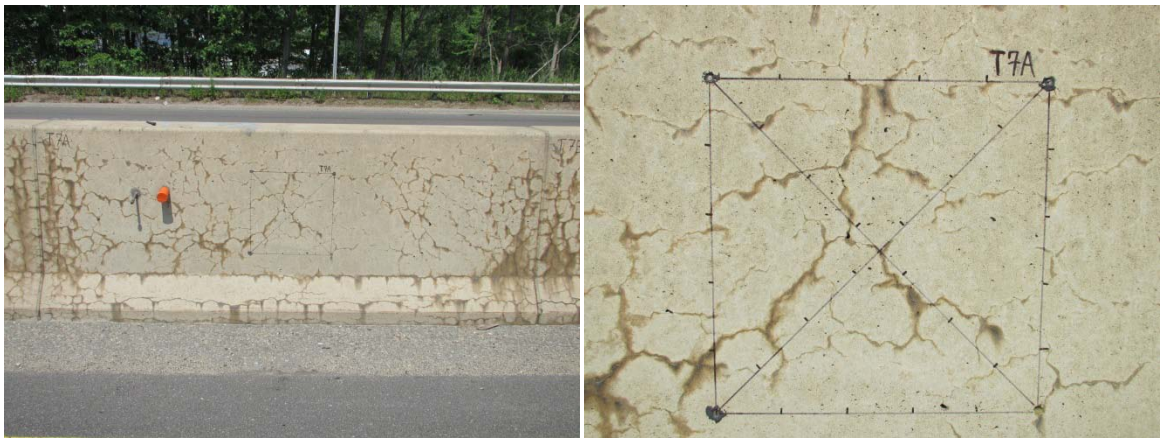

Figure 157. Visual observations over time of section T7A.

A - T7B - 2008

B – T7B - 2010

C – T7B -2013

Figure 158. Visual observations over time of section T7B.

A – T8A - 2008

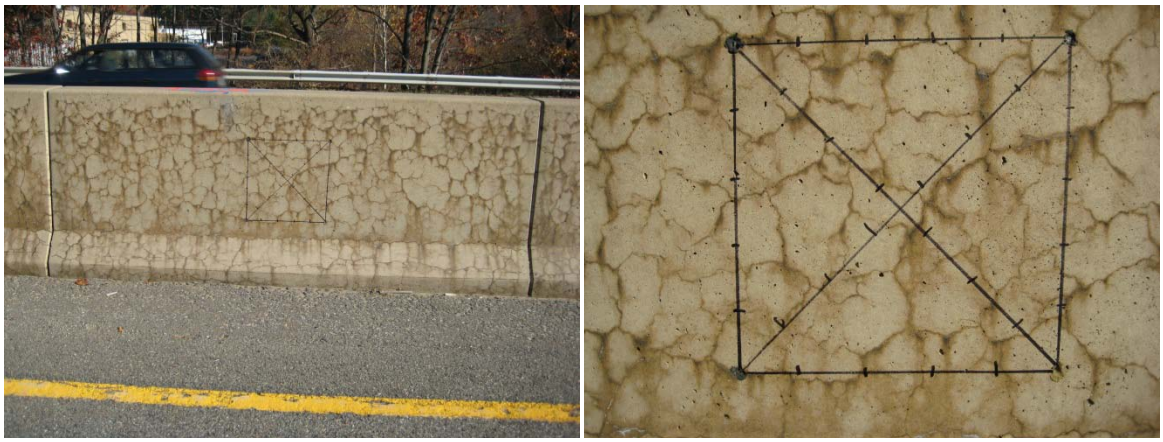

B – T8A - 2010

C – T8A - 2013

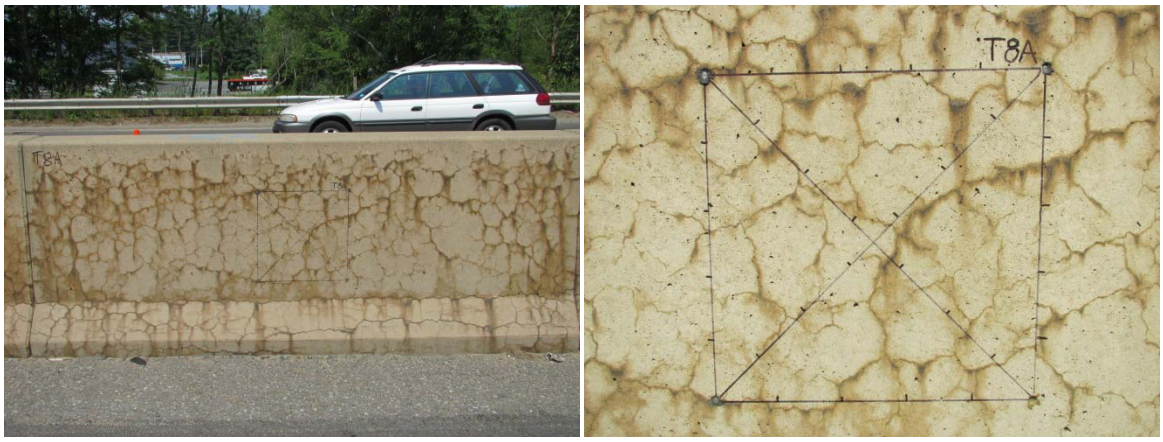

Figure 159. Visual observations over time of section T8A.

A – T8B – 2008

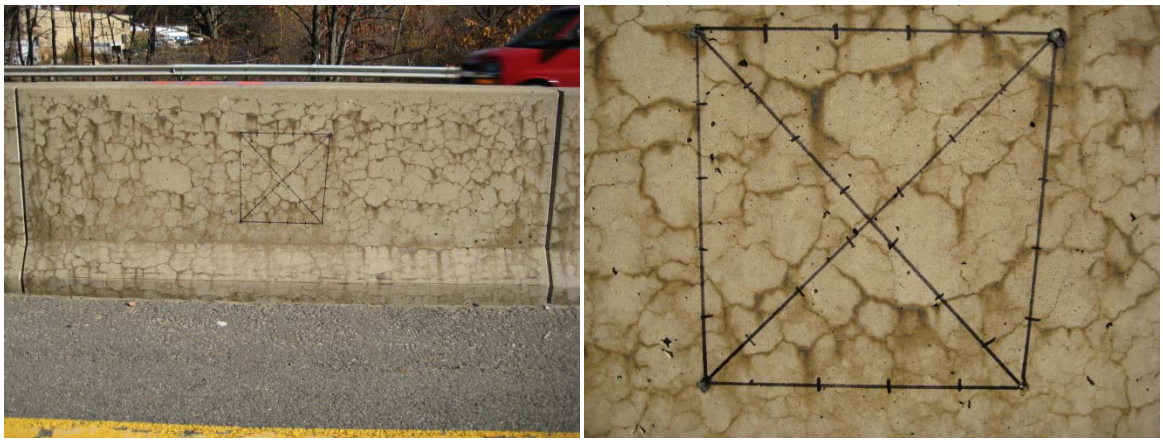

B – T8B - 2010

C – T8B - 2013

Figure 160. Visual observations over time of section T8B.

A – VA1 - 2008

B – VA1 - 2010

C – VA1 - 2013

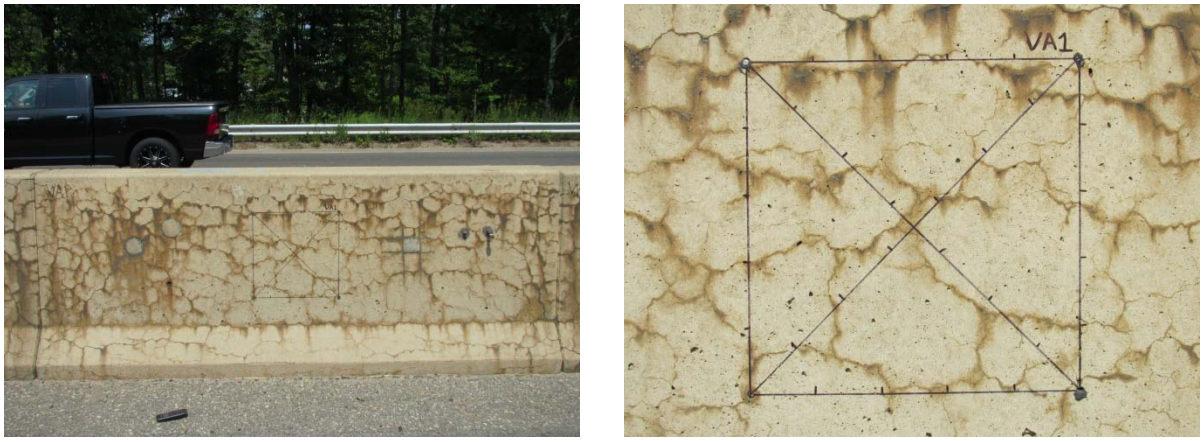

Figure 161. Visual observations over time of section VA1.

A –VA2 - 2008

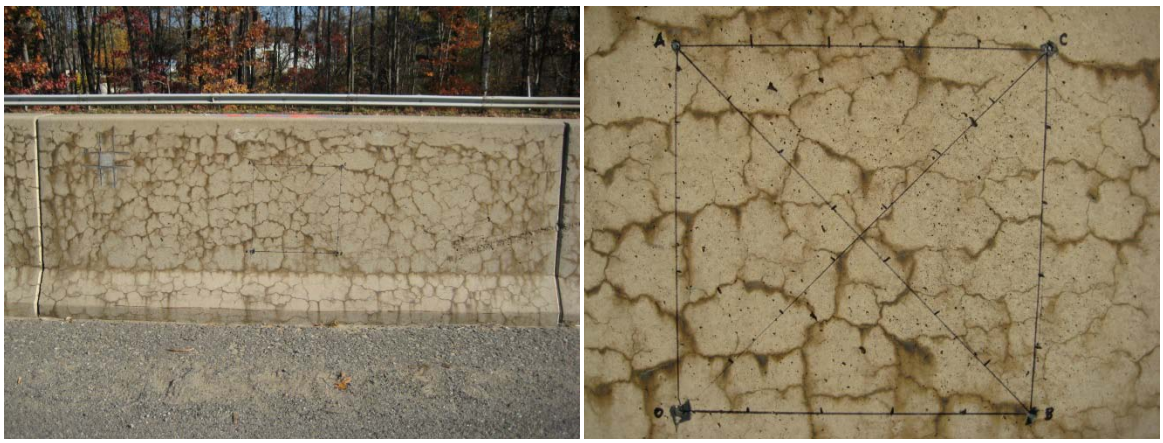

B – VA2 - 2010

C - VA2 - 2013

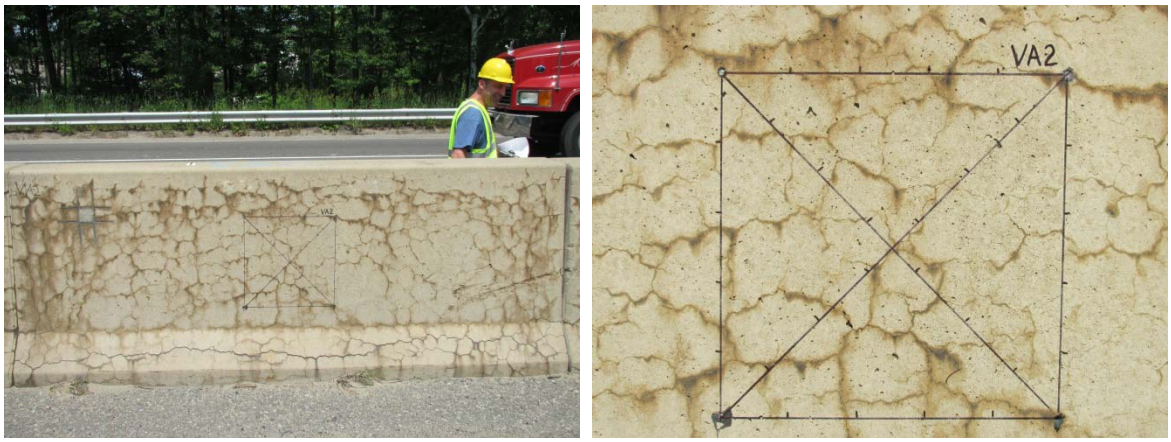

Figure 162. Visual observations over time of section VA2.

A - VB1 - 2008

B – VB1- 2010

C – VB1- 2013

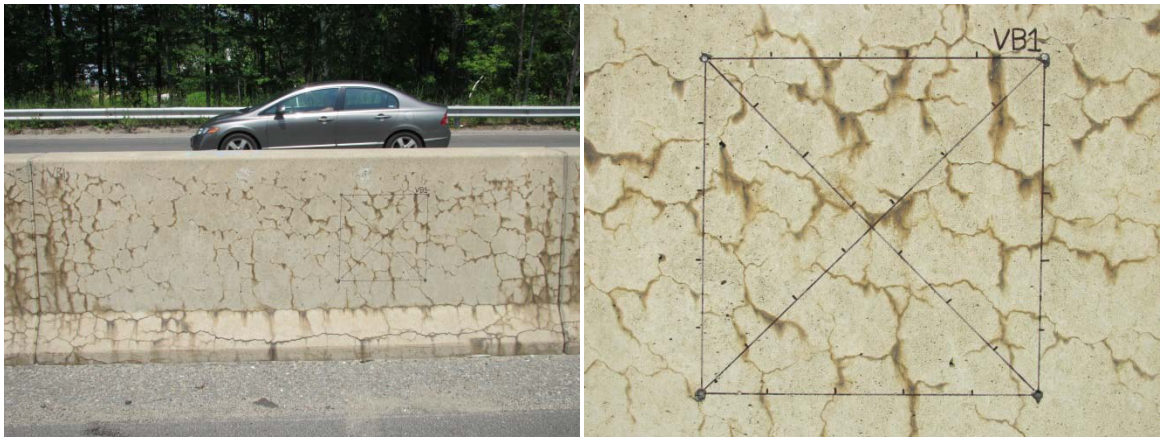

Figure 163. Visual observations over time of section VB1.

A – VB2 - 2008

B – VB2 - 2010

C – VB2 - 2013

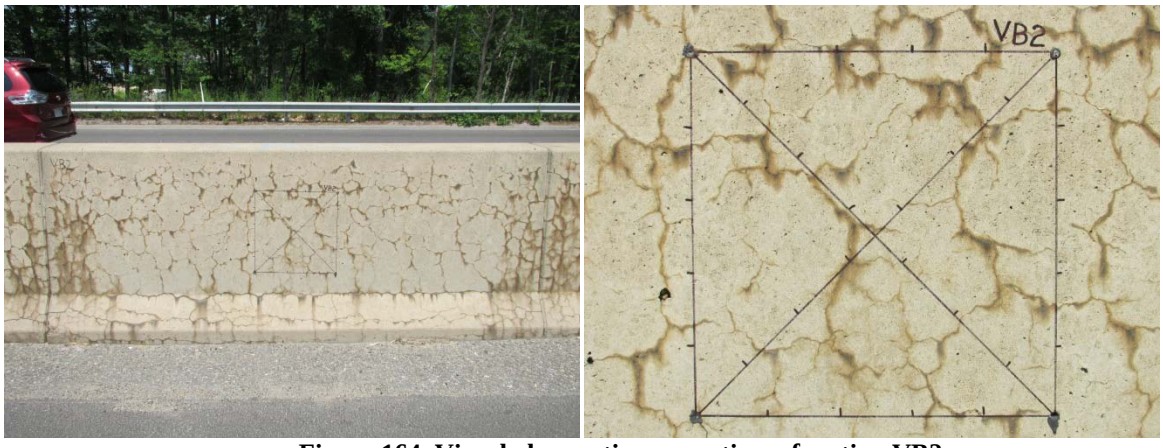

Figure 164. Visual observations over time of section VB2.

A - VC1 - 2008

B – VC1 - 2010

C – VC1 - 2013

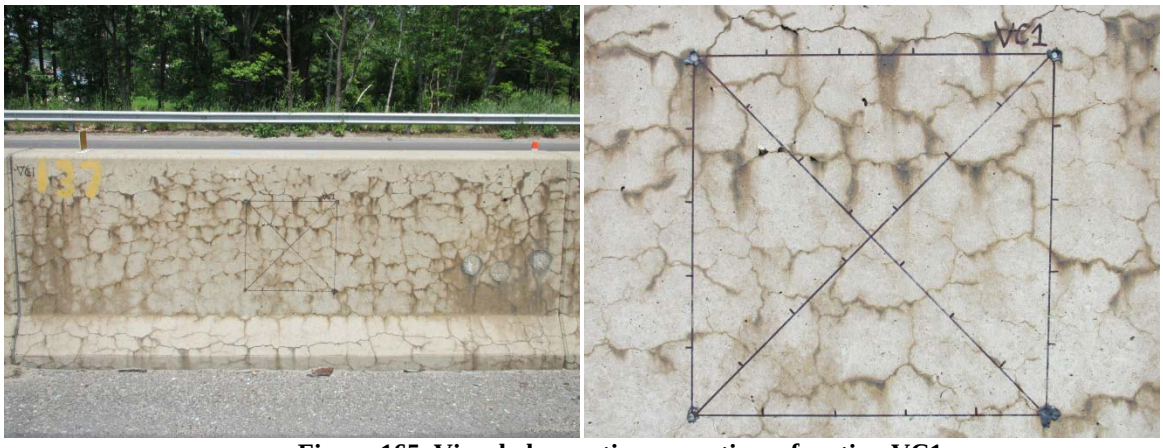

Figure 165. Visual observations over time of section VC1.

A - VC2 - 2008

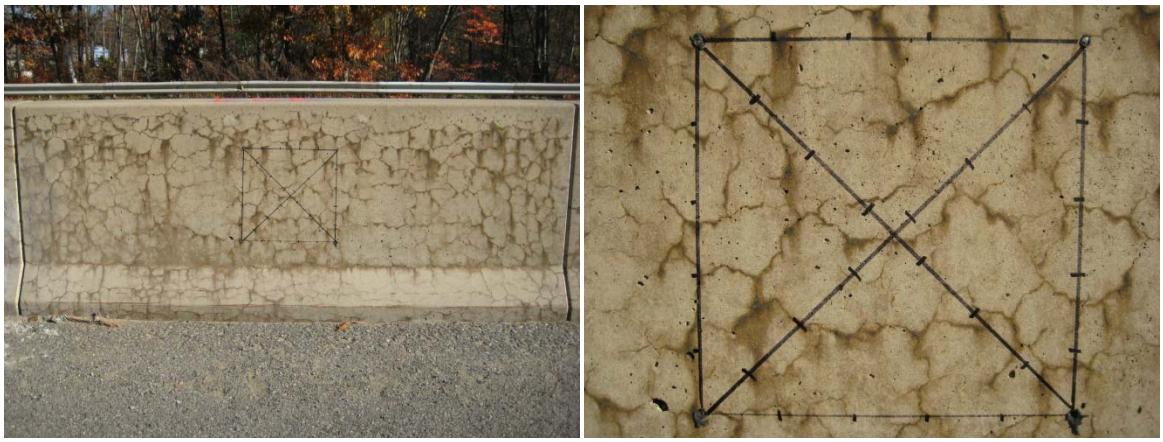

B – VC2 - 2010

C – VC2 - 2013

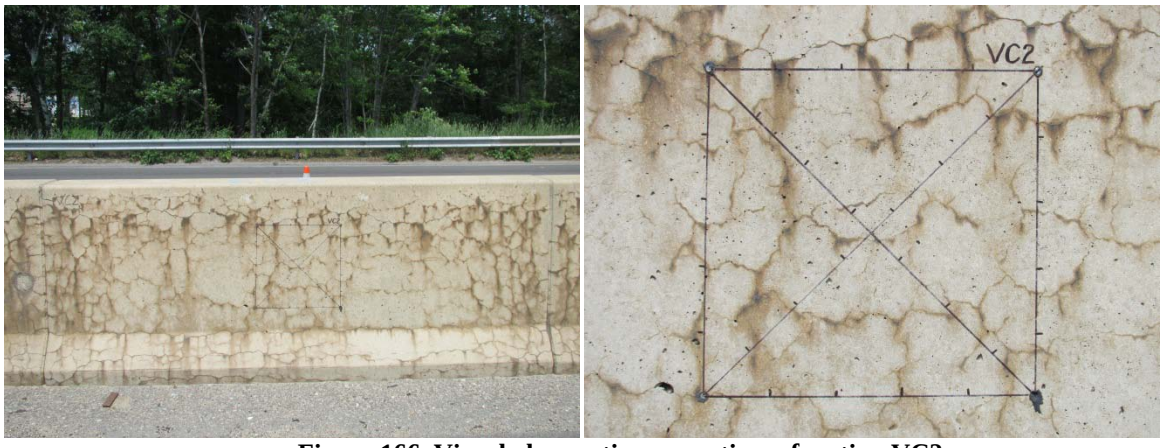

Figure 166. Visual observations over time of section VC2.

A - VD1 - 2008

B – VD1 - 2010

C – VD1 - 2013

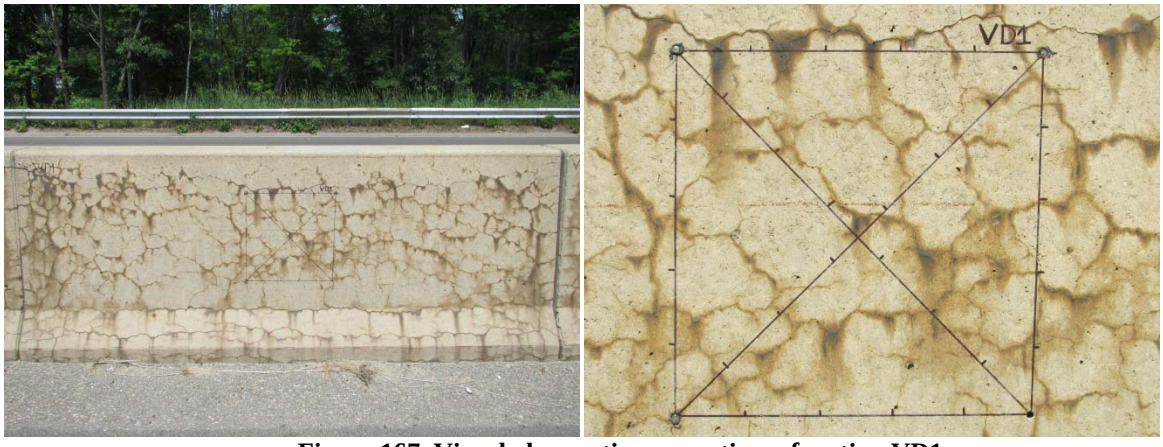

Figure 167. Visual observations over time of section VD1.

A - VD2 - 2008

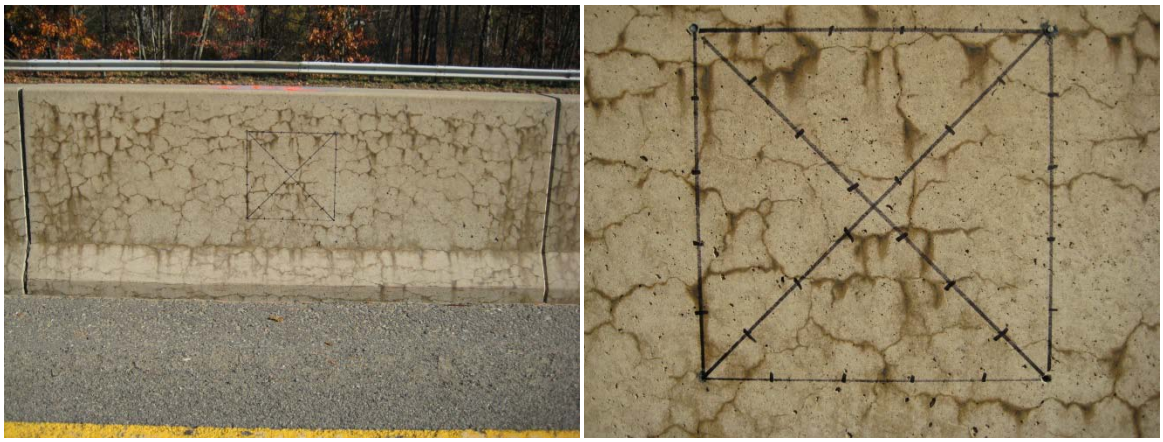

B – VD2 - 2010

C – VD2 - 2013

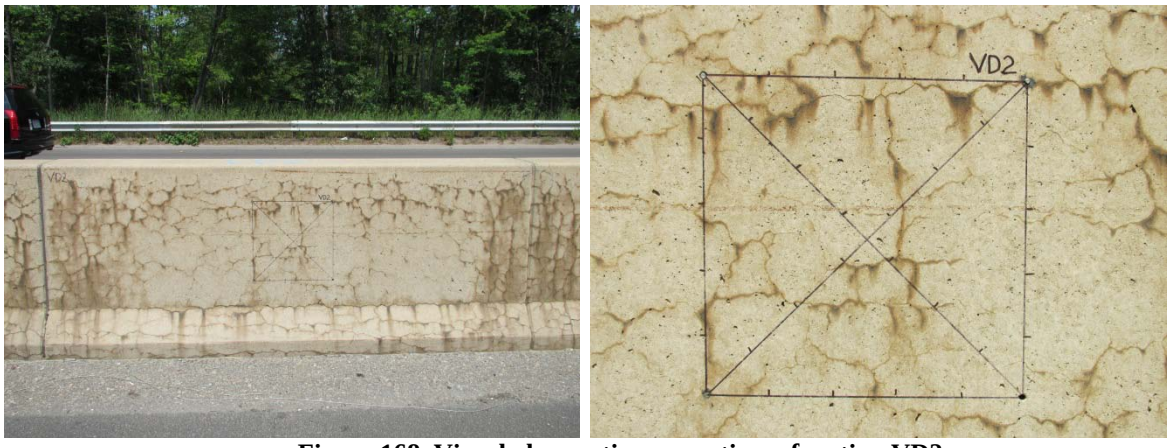

Figure 168. Visual observations over time of section VD2.

8.4 DATA ANALYSES

This section discusses and analyzes the results obtained over an eight-year period. Because some of the barriers were treated over eight years ago and have been monitored regularly during this time frame, some clear trends can be identified. For a subset of the barriers treated during this project in 2010, it is likely too premature to identify any trends or draw any conclusions.

The overall results from this study show that treating highway barriers with silane-based products is quite effective in reducing the future potential for ASR-induced expansion. This statement is backed by the expansion results previously shown in Figure 129 to Figure 131. The results clearly show that applying silane, whether it be water-based or solvent-based and whether it be composed of 20- or 40-percent silane, significantly reduces expansion. Most of the silane-treated barriers exhibited essentially no expansion during the monitoring period, and in fact, most exhibited a net shrinkage during the course of the monitoring period. Of note is that barriers that were treated with lithium nitrate (topically or by vacuum) only showed reductions in expansion and visible cracking when the lithium nitrate application was followed with treatment by silane, further highlighting the beneficial effects of silane treatment on highway barriers.

The effects of silane treatment not only manifest themselves in substantial reductions in expansion but also in visual improvements in the barriers themselves, as illustrated in Figure 169. This photograph shows barriers treated with silane (on right) adjacent to barriers that were not treated (on left). Additional photos showing similar trends are shown in Figure 139 to Figure 168. The observed reductions in expansion and visible cracking imparted by silane application are consistent with previous field trials on highway barriers in Quebec, Canada (Bérubé et al. 2002).

Figure 169. Significant reduction in visible cracking for the barriers treated with 40 percent silane (right), compared to untreated barriers (left).

The application of lithium nitrate, either topically or by vacuum, showed no tangible benefits in terms of reducing expansion or cracking. This is likely attributed to the overall lack of penetration of the lithium nitrate into the highway barriers, as previously shown in Figure 138. The results show that the depth of lithium penetration was minimal, with lithium only present in a concentration above the 100 ppm threshold in the outer 2–4 mm (0.08-0.16 in.). Lithium profiling was not conducted on the other barriers treated with lithium (topically or by vacuum), but it is expected that the depths of penetration would be less than the penetration shown in Figure 138. Given the lack of lithium penetration, it is not surprising that no beneficial effects of the treatment were observed. The barriers treated with lithium silicate also showed no reductions in expansion or visible cracking, most likely due to limited penetration of the product into the barriers.

The measurement of internal relative humidity was found to be quite challenging during the course of this field trial. Some of the challenges included:

- Limited lane time was available during each monitoring visit, due to Route 2 being heavily traveled. Typically, lane closures of only five or six hours were possible for a given day.
- Relative humidity sleeves and plugs, which were left in place between visits, often were found to be damaged, perhaps due to snow plows or snow drifts in the winter months or just the inherent harshness of the exposure conditions (freezing and thawing, exposure to deicing salts, etc.). Some additional holes were drilled during the course of the project and new sleeves/plugs were inserted, but this issue of damaged sleeves/plugs was quite common.
- An unusually high number of relative humidity holes were found to be wet at the time humidity measurements were to be taken. This moisture can come from within the concrete, from precipitation or tire splash, or from condensation within the measuring hole.

Because of the above factors, it is not possible to draw conclusions on the effects of the various treatments on internal relative humidity. However, in general, the internal relative humidity values for barriers treated with silane were lower than that of the controls, albeit the results may not be statistically significant.

The crack mapping results show quite a bit of scatter in the data, due to inherent difficulties in visually assessing cracked concrete in field elements. Also, crack mapping is quite sensitive to the user (or crack mapping operator), and over the course of eight years of monitoring, it was not possible to have one individual take all measurements. It is possible that future monitoring of these barriers, including crack mapping, will yield data that will capture the differences in overall cracking between control barriers and barriers that were treated with silanes. In addition, the crack mapping “square” serves other purposes, such as setting the corners for expansion measurements (both horizontal and vertical) and providing a consistent benchmark for taking photographs. Figures 139 to 168 make use of the cracking mapping regions as the focal point for photographs taken on each day of monitoring.

Because it has only been about three years since selected barriers were coated with elastomeric paint, it is too premature to determine its efficacy in reducing relative humidity, ASR-induced expansion, and especially freezing and thawing damage, the latter being the primary motivation for applying this breathable, flexible paint over sections previously treated with silane.

8.5 SUMMARY

Through the use of an FHWA protocol (Fournier et al. 2010) for evaluating ASR-affected concrete, it was determined that ASR was a significant cause of expansion and cracking observed in highway barriers on Route 2 in Leominster, MA. Components of the protocol that were employed included:

- Visual survey and evaluation
- Petrographic evaluation of extracted cores (including the application of the Damage Rating Index [DRI])
- In-situ expansion measurements of field elements
- Internal relative humidity measurement

This field trial spanned two separate FHWA projects (Lithium Technology Program and ASR Development and Deployment Program), and as such, up to eight years of monitoring data are available. With this extensive database, it is possible to make several conclusions:

- Topically applying silane-based products to various highway barriers was found to significantly reduce expansion, as well as visible cracking. In fact, most barriers treated with silanes (water- and solvent-based, with silane contents from 20 to 40 percent) exhibited a net shrinkage during the course of the monitoring program. These results, coupled with results from other studies where silanes were applied to highway barriers (Bérubé et al. 2002), demonstrate that highway barriers are ideal candidates for silane treatment when ASR is deemed to be of concern. In addition, silanes and other breathable coatings that reduce the relative humidity content in concrete are also helpful in reducing the ingress of water and deicing salts, thus improving the frost resistance and scaling resistance of concrete.
- Lithium nitrate, applied either topically or by vacuum, showed no tangible benefits in terms of reducing expansion or cracking. This is likely attributed to the overall lack of penetration of the lithium nitrate into the highway barriers. The results show that the depth of lithium penetration was minimal, with lithium only present in a concentration above the 100 ppm threshold in the outer 2–4 mm (0.08- 0.16 in.) of barriers that were vacuum-impregnated for over seven hours with lithium nitrate. Given the lack of lithium penetration, it is not surprising that no beneficial effects of the treatment were observed. The barriers treated with lithium silicate also showed no reductions in expansion or visible cracking, most likely due to limited penetration of the product into the barriers.
- The results from crack mapping and internal relative humidity were somewhat inconclusive in this study, but it is expected that further monitoring may yield discernible differences in behavior between the various treated barriers.

- Because it has only been about three years since selected barriers were coated with elastomeric paint, it is too premature to determine its efficacy in reducing relative humidity, ASR-induced expansion, and especially freezing and thawing damage, the latter being the primary motivation for applying this breathable, flexible paint over sections previously treated with silane.

8.6 REFERENCES

Bérubé, M.A., Chouinard, D., Pigeon, M., Frenette, J., Rivest, M. and Vézina, D. 2002. "Effectiveness of Sealers in Counteracting Alkali-Silica Reaction in Highway Median Barriers Exposed to Wetting and Drying, Freezing and Thawing, and Deicing Salts." *Canadian Journal of Civil Engineering*, 29(2): 329-337.

Fournier, B., Bérubé, M.A., Folliard, K.J. and Thomas, M.D.A. 2010. "Report on the Diagnosis, Prognosis, and Mitigation of Alkali-Silica Reaction (ASR) in Transportation Structures." FHWA-HIF-09-004, Federal Highway Administration.

Grattan-Bellew, P.E. 2005. "Petrographic Evaluation of Concrete Concrete Cores from Massachusetts Jersey Barrier Project." Materials & Petrographic Research G-B Inc.

Tremblay, S. 2011. "Étude de l'efficacité d'adjuvants à base de lithium afin de contrôler la réaction alcalis-silice dans le béton frais et dans les structures existantes incorporant cet adjuvant." Mémoire de maîtrise, Département de géologie et de génie géologique, Université Laval, Québec, 347 p.

9. BRIDGE BEAMS, NEW BRAUNFELS, TX

The Texas Department of Transportation (TxDOT) identified several precast beams (or girders) that exhibited significant cracking that visually looked similar to that observed in ASR, even though the mixtures were cast under stringent ASR specifications, including limits on total alkali loading for plain cement mixtures and minimum required dosage of Class F fly ash. As a result, TxDOT was concerned about their current ASR specifications. Four of these beams had previously been rejected for use by TxDOT and were being stored at two different precast yards before being moved to outdoor storage along State Highway Loop 337 (TX SH Loop 337) in New Braunfels, TX for further monitoring (see Figure 170). TxDOT engineers began monitoring these beams for expansion, and it was decided that the FHWA ASR Development and Deployment Program efforts would take over the monitoring of the beams (expansion and internal relative humidity), starting in November 2010, and expand the program to monitor the efficacy of silane-based products on portions of the distressed beams. Figure 171 shows a photograph taken between beams 1 and 2, showing how the beams are supported off of the ground by railroad ties. Figure 172 shows the typical cracking that was observed on these beams, prior to treating portions of them with silane.

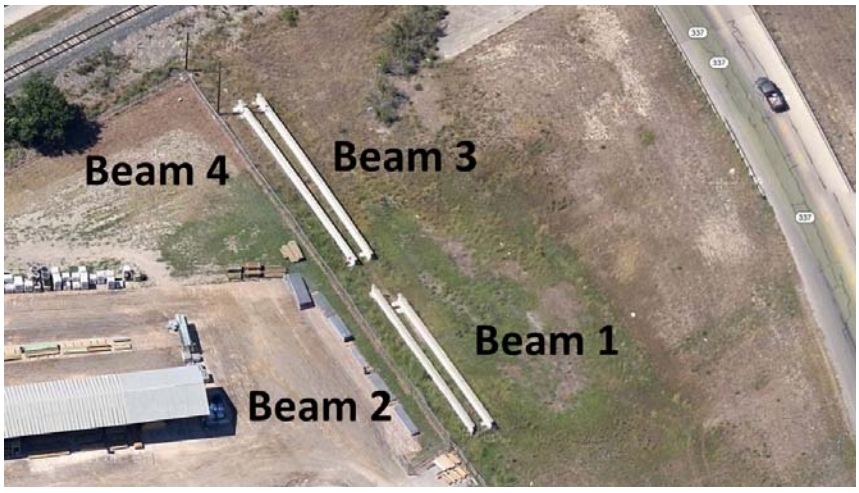

Figure 170. Google satellite image showing the location of the precast beams.

Figure 171. Beams 1 and 2 resting on railroad ties.

Figure 172. Typical cracking observed on the precast beams.

This project is somewhat different from the others under the FHWA ASR Development and Deployment Program – the primary focus was placed more on determining if the observed deterioration was due to ASR by following protocols for diagnosing ASR in field structures, developed under the same FHWA efforts (Fournier et al. 2010). While these efforts were underway, portions of each of the four beams were treated with silane to evaluate the efficacy of the products in reducing internal relative humidity and reducing future expansion (if ASR were, in fact, the dominant cause of distress).

This section summarizes the evaluation of these four precast beams, which were cast between 2003 and 2006, and includes a summary of petrographic evaluations, laboratory testing using the same aggregate sources, and monitoring techniques and preliminary results.

9.1 SUMMARY OF PETROGRAPHIC EVALUATION

Petrographic examination was carried out on six concrete cores extracted from the four precast beams and stored outdoors in New Braunfels, Texas. The evaluation mainly consisted of the Damage Rating Index (DRI), a method that provides a semi-quantitative assessment of the

degree of damage in concrete based on a count of petrographic features of deterioration generally associated with alkali-silica reaction (ASR).

Very low Damage Rating Indices ranging from 36 to 66 were obtained for the New Braunfels cores (Figure 173). Actually, the cores showed no significant signs of ASR or noticeable deterioration. As shown in Figure 174, the petrographic features identified essentially consisted of non-ASR related and very limited internal cracking within some coarse aggregate particles (mainly limestone/dolostone and some chert), a few reaction rims (surrounding some chert particles), and only a few air voids lined with ASR gel (adjacent to chert particles). No cracking was noticed in the cement paste, at least at the magnification used for the test (16x).

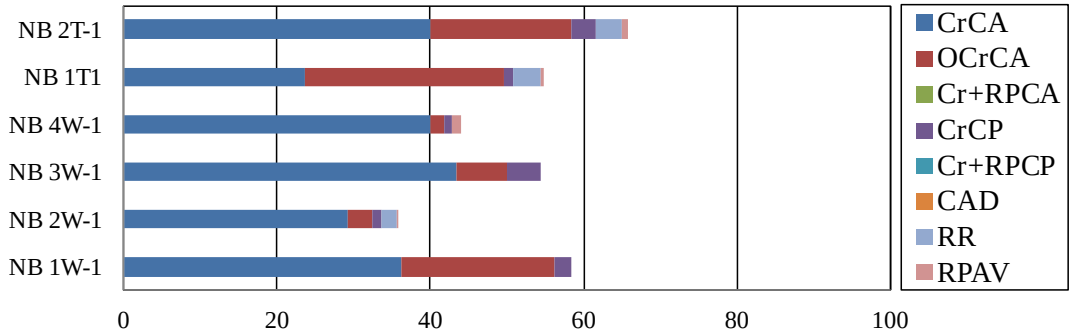

Figure 173. Results of the Damage Rating Index (DRI) for the Texas cores. The colored cells give the proportions of each petrographic feature to the DRI value. (CrCA: cracking in the coarse aggregate particles; OCrCa: opened cracking in the coarse aggregate particles; Cr+RPCA: cracking in the coarse aggregate particles + reaction product; CrCP: cracking in the cement paste; Cr+RPCP: cracking in the cement paste + reaction product; CAD: coarse aggregate debonded; RR: reaction rim; RPAV: reaction products in air void of the cement paste).

A (Core 1W-1)

B (Core 3W-1)

Figure 174. Typical micrographs of the polished core sections showing carbonate (mainly) and chert coarse aggregate particles (¾ inch [2 cm] nominal size) in a dark grey cementitious matrix. There is no visible evidence of cracking both in the aggregate particles (coarse and fine) as well as in the cementitious matrix at the magnification used for the DRI (16x).

9.2 SUMMARY OF APPLICATION REPORT

Table 66 provides information on the four beams selected for treatment and monitoring. Three of the beams chosen consisted of cement-only mixtures and one beam contained 20 percent cement replacement (by mass of total cementitious material) with Class F fly ash. In general, the older beams showed more extensive cracking, as shown in Figure 172, than the younger beams.

Table 66. Details of the beams treated in New Braunfels, TX.

Beam	Cast Date	Length m (ft)	Cement Type	Fly Ash
1	12/18/2003	29.2 (98.2)	Type III	-
2	4/14/2004	33.0 (108.1)	Type III	-
3	3/10/2006	36.5 (119.7)	Type III	20% Class F
4	3/7/2006	36.5 (119.7)	Type III	-

The beams were then treated in December 2010. Figure 175 and Figure 176 provide details of the treatment and performance monitoring instrumentation. Each of the four beams was divided in half, and half of the beam served as an untreated control while the other half was topically treated with 40 percent silane (alcohol-based). The silane was applied with a handheld pressurized container and spray nozzle, as shown in Figure 177, with a coverage rate of 3.7 m^2/L (150 ft^2/gal).

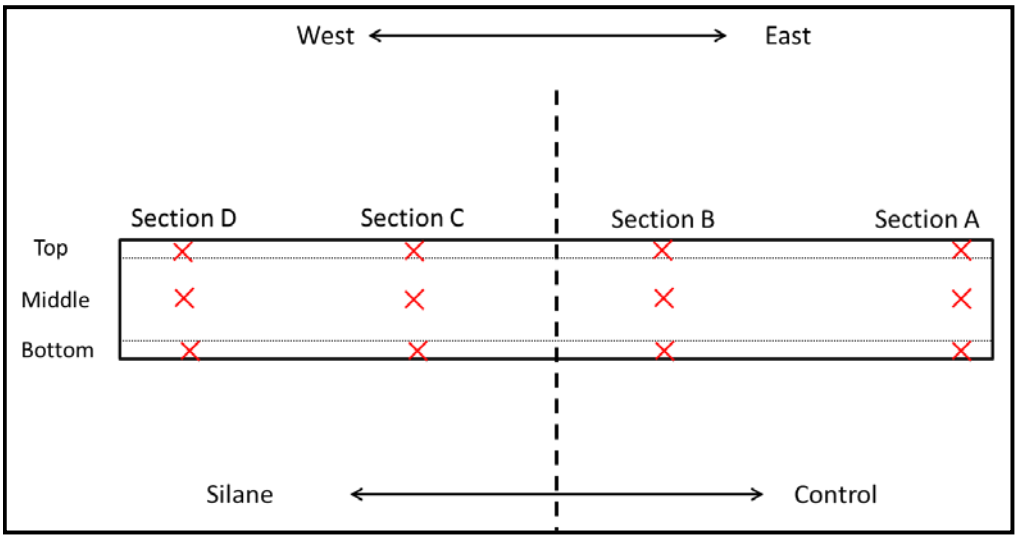

Figure 175. Treatment and expansion monitoring plan for each beam.

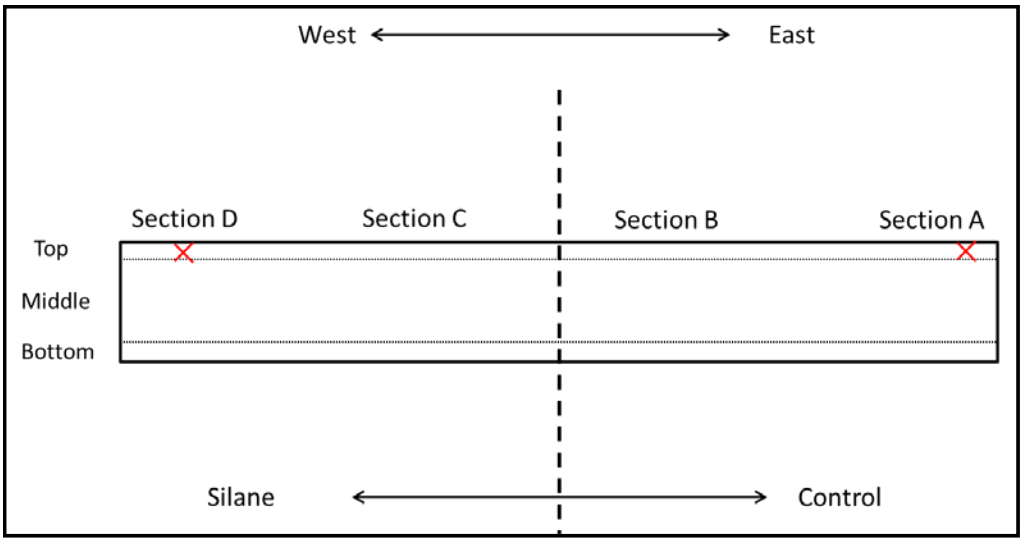

Figure 176. Treatment and internal relative humidity monitoring plan for each beam.

Figure 177. Topical silane application on the precast beams

TxDOT initially instrumented the beams for expansion monitoring and took initial measurements. As depicted in Figure 178, horizontal and vertical length change measurements were made in the top, middle, and bottom of the beams. Note that only the south side of each beam was instrumented for expansion. Each beam has a total of 12 expansion monitoring areas, with 6 areas on the silane treated side and 6 areas on the control side. Figure 178 shows Station D of beam 3 and the three areas for expansion monitoring.

In February 2011, humidity probes (Vaisala HM44) were installed on the beams as indicated in Figure 176. In each of the regions depicted in Figure 176 as relative humidity measurement points, holes were drilled at varying depths to allow for the measurement of relative humidity 25 mm (1 in.), 50 mm (2 in.), and 75 mm (3 in.) from the concrete surface. Additional details on the performance monitoring techniques and treatment activities are provided in chapters 2 and 3, respectively.

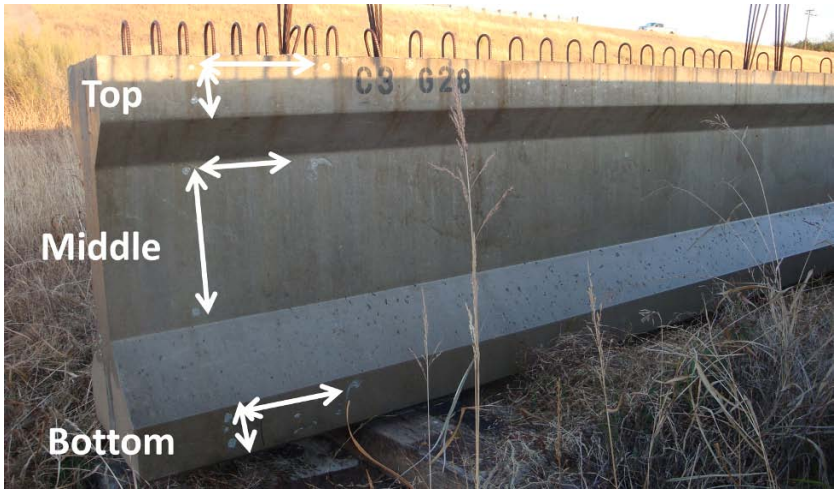

Figure 178. Section D on Beam 3 showing the expansion measurement locations.

9.3 MONITORING DATA

This section summarizes the data obtained from expansion and internal relative humidity measurements from the four bridge beams. In addition, the results of laboratory testing and exposure block testing of the aggregates used in the beams are presented, as well as the results of testing replicate blocks that use the same materials and mixture proportions as the beams that were treated and are being monitored. Some of the ASR laboratory expansion testing (AASHTO T 303 and ASTM C1293) and exposure block testing was initiated by TxDOT prior to the treatment of the New Braunfels beams, so long-term data, through almost five years, are available for the exposure blocks. However, it should be noted that because of the timing of the silane application, only limited expansion and relative humidity data are available after treatment (about 17 months).

Table 67 shows the measured temperature and relative humidity for each of the beams at varying depths from the exposed concrete surface. Table 68 shows the results of length change measurements made between April 2011 and August 2012. The data were not corrected for temperature (thermal) effects. Due to the limited time available for measuring these beams, it is not possible to draw conclusions or identify trends in behavior.

Table 67. Relative humidity and temperature measurements – New Braunfels Beams.

Beam	Depth	Data	April 2011	December 2011	August 2012
1 Control	25 mm (1 in.)	°C (°F)	22.9 (73.2)	19.1 (66.4)	37.8 (100.0)
		RH%	63.4	71.1	66.6
	50 mm (2 in.)	°C (°F)	22.9 (73.2)	18.9 (66.0)	36.9 (98.4)
		RH%	72.1	74.6	74.4
	75 mm (3 in.)	°C (°F)	22.9 (73.2)	19.1 (66.4)	36.6 (97.9)
		RH%	80.4	69.0	79.9
1 Silane	25 mm (1 in.)	°C (°F)	23.2 (73.8)	23.5 (74.3)	23.2 (73.8)
		RH%	63.5	71.7	57.8
	50 mm (2 in.)	°C (°F)	19.6 (67.3)	19.5 (67.1)	19.7 (67.5)
		RH%	72.5	72.6	67.1
	75 mm (3 in.)	°C (°F)	38.7 (101.7)	37.0 (98.6)	36.3 (97.3)
		RH%	76.7	69.3	73.4
2 Control	25 mm (1 in.)	°C (°F)	23.8 (74.8)	23.7 (74.7)	24.0 (75.2)
		RH%	64.5	70.5	68.1
	50 mm (2 in.)	°C (°F)	19.2 (66.6)	19.2 (66.6)	19.0 (66.2)
		RH%	73.2	74.0	70.7
	75 mm (3 in.)	°C (°F)	37.9 (100.2)	36.9 (98.4)	36.5 (97.7)
		RH%	73.2	69.5	76.4
2 Silane	25 mm (1 in.)	°C (°F)	23.9 (75.0)	23.5 (74.3)	23.6 (74.5)
		RH%	65.5	69.9	62.5
	50 mm (2”)	°C (°F)	19.0 (66.2)	19.5 (67.1)	20.1 (68.2)
		RH%	72.7	73.5	69.7
	75 mm (3 in.)	°C (°F)	38.6 (101.5)	37.4 (99.3)	37.3 (99.1)
		RH%	73.9	80.3	62.4

Table 67 (cont'd). Relative humidity and temperature measurements – New Braunfels Beams.

Beam	Depth	Data	April 2011	December 2011	August 2012
3 Control	25 mm (1 in.)	°C (°F)	24.2 (75.5)	23.8 (74.8)	23.7 (74.7)
		RH%	64.4	74.6	61.3
	50 mm (2 in.)	°C (°F)	20.0 (68.0)	19.8 (67.6)	19.4 (66.9)
		RH%	71.1	78.4	71.4
	75 mm (3 in.)	°C (°F)	40.5 (104.9)	38.8 (101.8)	38.3 (100.9)
		RH%	62.7	82.4	66.9
3 Silane	25 mm (1 in.)	°C (°F)	24.2 (75.6)	23.6 (74.5)	23.4 (74.1)
		RH%	61.9	73.3	55.4
	50 mm (2 in.)	°C (°F)	20.1 (68.2)	19.6 (67.3)	19.7 (67.5)
		RH%	59.4	78.6	59.2
	75 mm (3 in.)	°C (°F)	42.3 (108.1)	39.2 (102.6)	39.5 (103.1)
		RH%	66.2	78.9	71.2
4 Control	25 mm (1 in.)	°C (°F)	26.4 (79.5)	26.0 (78.8)	25.7 (78.3)
		RH%	69.9	72.5	-
	50 mm (2 in.)	°C (°F)	20.1 (68.2)	75.8 (168.4)	19.7 (67.5)
		RH%	72.3	-	-
	75 mm (3 in.)	°C (°F)	-	-	39.3 (102.7)
		RH%	79.8	76.5	-
4 Silane	25 mm (1 in.)	°C (°F)	26.7 (80.1)	26.1 (79.0))	25.9 (78.6)
		RH%	64.8	76.3	60.4
	50 mm (2 in.)	°C (°F)	20.0 (68.0)	19.6 (67.3)	19.7 (67.5)
		RH%	70.9	78.6	67.9
	75 mm (3 in.)	°C (°F)	41.2 (106.2)	39.8 (103.6)	39.6 (103.3)
		RH%	75.5	79.4	75.8
3 Control North	25 mm (1 in.)	°C (°F)	26.8 (80.2)	-	-
		RH%	58.2	-	-
	50 mm (2 in.)	°C (°F)	25.3 (77.5)	-	-
		RH%	64.7	-	-
	75 mm (3 in.)	°C (°F)	24.5 (76.1)	-	-
		RH%	70.6	-	-

Table 68. Expansion results (%) – New Braunfels Beams.

Beam	Section	Measurement	Length change, % (from April 2011 to August 2012)
1	A	Top Flange Vertical	0.09
		Top Flange Horizontal	0.02
		Web Vertical	0.02
		Web Horizontal	0.00
		Low Vertical	0.01
		Low Horizontal	0.00
	B	Top Flange Vertical	0.02
		Top Flange Horizontal	0.01
		Web Vertical	-0.01
		Web Horizontal	0.01
		Low Vertical	0.16
		Low Horizontal	0.01
	C (Silane)	Top Flange Vertical	0.03
		Top Flange Horizontal	0.00
		Web Vertical	0.00
		Web Horizontal	0.02
		Low Vertical	0.02
		Low Horizontal	-0.01
	D (Silane)	Top Flange Vertical	0.02
		Top Flange Horizontal	0.02
		Web Vertical	0.01
		Web Horizontal	0.00
		Low Vertical	0.01
		Low Horizontal	-
2	A	Top Flange Vertical	-
		Top Flange Horizontal	0.00
		Web Vertical	-
		Web Horizontal	0.01
		Low Vertical	-
		Low Horizontal	0.01
	B	Top Flange Vertical	0.06
		Top Flange Horizontal	0.02
		Web Vertical	-
		Web Horizontal	0.01
		Low Vertical	0.06
		Low Horizontal	0.00
	C (Silane)	Top Flange Vertical	-
		Top Flange Horizontal	0.02
		Web Vertical	0.01
		Web Horizontal	0.02
		Low Vertical	0.01
		Low Horizontal	0.02
	D (Silane)	Top Flange Vertical	0.03
		Top Flange Horizontal	0.03
		Web Vertical	0.02
		Web Horizontal	0.04
		Low Vertical	-
		Low Horizontal	0.02

Table 68 (cont'). Expansion results (%) – New Braunfels Beams.

Beam	Section	Measurement	Length change, % (from April 2011 to August 2012)
3	A	Top Flange Vertical	0.01
		Top Flange Horizontal	0.02
		Web Vertical	-
		Web Horizontal	0.02
		Low Vertical	0.02
		Low Horizontal	0.01
	B	Top Flange Vertical	0.03
		Top Flange Horizontal	-0.01
		Web Vertical	-0.01
		Web Horizontal	0.01
		Low Vertical	0.01
		Low Horizontal	-0.03
	C (Silane)	Top Flange Vertical	0.02
		Top Flange Horizontal	0.02
		Web Vertical	0.00
		Web Horizontal	0.00
		Low Vertical	0.04
		Low Horizontal	-
	D (Silane)	Top Flange Vertical	0.01
		Top Flange Horizontal	0.03
		Web Vertical	0.01
		Web Horizontal	0.02
		Low Vertical	0.01
		Low Horizontal	0.01
4	A	Top Flange Vertical	-
		Top Flange Horizontal	0.02
		Web Vertical	0.01
		Web Horizontal	0.02
		Low Vertical	0.03
		Low Horizontal	0.01
	B	Top Flange Vertical	0.03
		Top Flange Horizontal	0.02
		Web Vertical	0.00
		Web Horizontal	0.02
		Low Vertical	0.03
		Low Horizontal	0.01
	C (Silane)	Top Flange Vertical	0.04
		Top Flange Horizontal	0.02
		Web Vertical	0.01
		Web Horizontal	0.01
		Low Vertical	0.03
		Low Horizontal	0.01
	D (Silane)	Top Flange Vertical	0.03
		Top Flange Horizontal	0.00
		Web Vertical	-0.01
		Web Horizontal	0.02
		Low Vertical	0.02
		Low Horizontal	0.02

In conjunction with the monitoring of the beams before and after silane treatment, laboratory testing was conducted to evaluate the reactivity of both the coarse and fine aggregates used in the distressed beams. For each of the aggregate sources, AASHTO T 303 (accelerated mortar bar test) and ASTM C1293 (concrete prism test) were conducted. Figure 179 shows the results of the AASHTO T 303 tests, showing that both aggregates were found to exceed the typical 0.10 percent expansion limit at 14 days.

Figure 180 shows the results for ASTM C1293 for the coarse aggregate used in the beam (in combination with a non-reactive fine aggregate) and the fine aggregate used in the beam (in combination with a non-reactive coarse aggregate). Both aggregates exhibited less expansion than the commonly applied 0.04 percent expansion at one year. Replicate concrete mixtures to two of the distressed beams (beams 3 and 4) were tested under ASTM C1293 conditions. It should be noted that the actual mixture was used, as opposed to the conventional method of boosting alkalies in the concrete prism test. The results for the replicate mixtures, with and without fly ash, show that the expansion limits are below the 0.04 percent expansion limit at one year, and in fact, very little expansion is observed at all (see Figure 181).

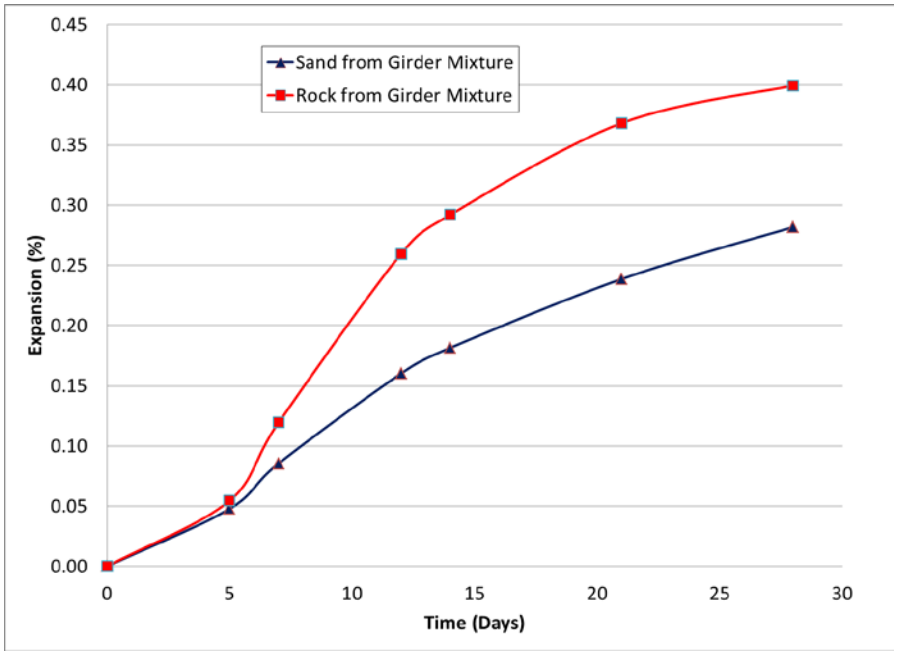

Figure 179. AASHTO T 303 (accelerated mortar bar test) results for fine and coarse aggregates used in bridge beams.

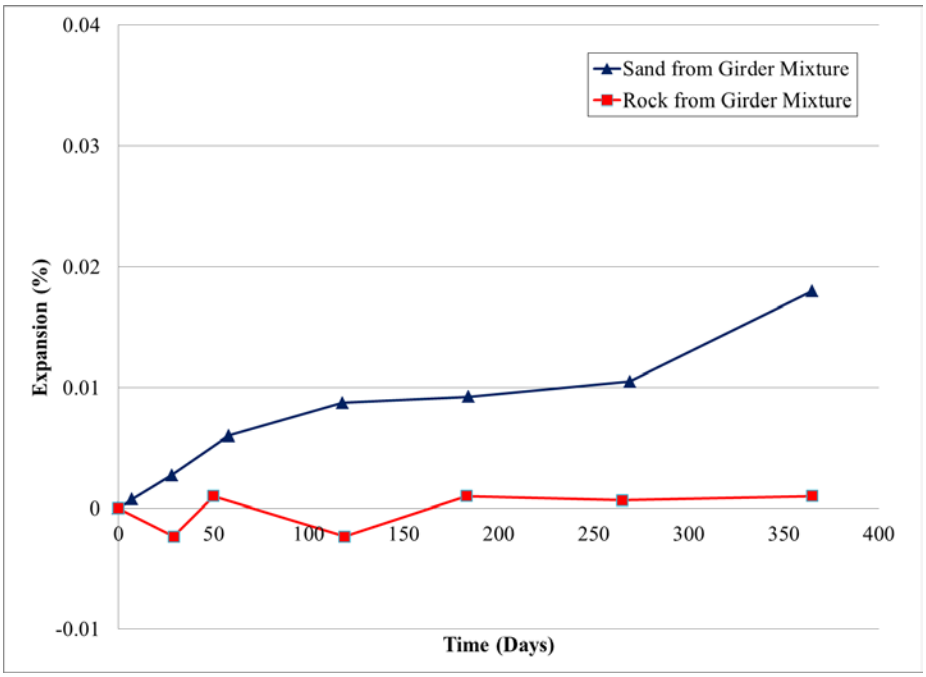

Figure 180. ASTM C1293 (concrete prism test) results for fine and coarse aggregates used in bridge beams.

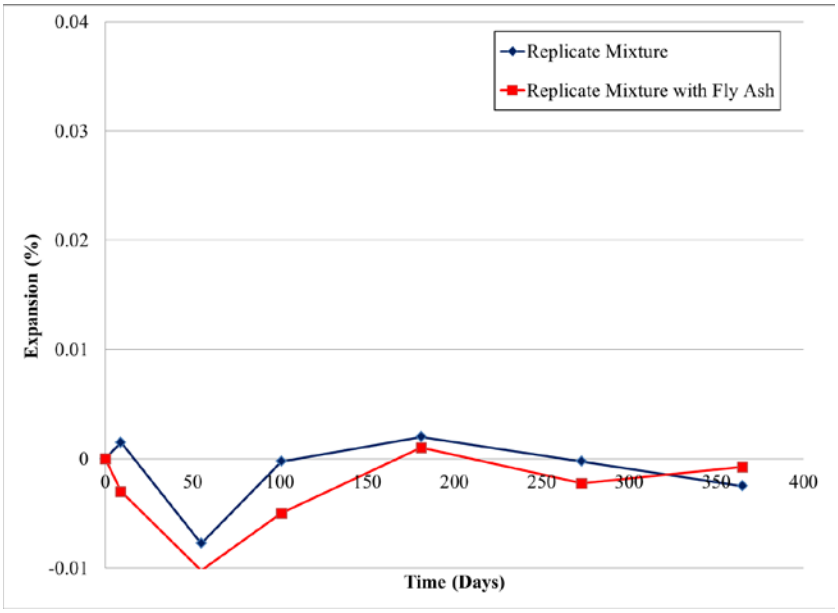

Figure 181. ASTM C1293 (concrete prism test) results for replicate mixtures to the beams (with and without fly ash).

Exposure blocks replicating the materials and mixture proportions used in distressed beam 3 (containing 20 percent Class F fly ash) and distressed beam 4 (plain concrete mixture) were also cast and monitored. Figure 182 shows that neither of these exposure blocks has exhibited significant expansion after approximately five years on the outdoor exposure site in Austin, TX. Interestingly, although the blocks have exhibited negligible expansion, visible cracking is evident on both replicate blocks, and this distress looks quite similar to the type of cracking

observed in the bridge beams. Figure 183 shows photos of both replicate blocks after approximately five years stored outdoors in Austin, TX.

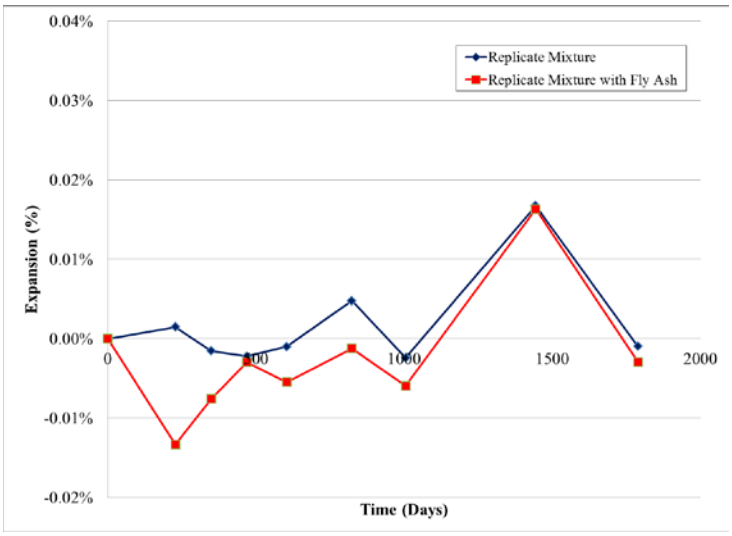

Figure 182. Outdoor exposure block expansion results for blocks replicating beams 3 and 4. (Note: blocks have been stored outdoors in Austin, TX for approximately five years.)

Figure 183. Visible cracking of replicate exposure blocks to beam 3 (with fly ash), on the left, and beam 4 (without fly ash), on the right. It is important to note that both blocks cracked about 1.5 – 2 years after casting without exhibiting measurable expansion.

9.4 DATA ANALYSES

When analyzing the results from the laboratory and field studies described herein, it is important to keep in mind the two main objectives of this investigation:

- Determine if ASR is a cause of distress in the damaged bridge beams in New Braunfels, TX, following the FHWA protocol for diagnosing structures potentially affected by ASR (Fournier et al. 2010).
- Evaluate the efficacy of silane in reducing the internal relative humidity in distressed bridge beams.

With regard to the first objective, the results from both the laboratory and exposure site show clearly that ASR is not a major cause of distress for these bridge beams. First, a detailed petrographic evaluation yielded little evidence of ASR-induced expansion and cracking. Damage Rating Index (DRI) values were between 36 and 66, well below values known to be typical of ASR-induced damage. Second, ASTM C1293 results showed that both aggregates used in the beams passed the one-year expansion limit of 0.04 percent. Expansions in AASHTO T 303 for the two aggregates used in the beams were above the typical 0.10 percent expansion limit at 14 days (or 28 days). However, when data are available for a given aggregate from both ASTM C1293 and AASHTO T 303, the ASTM C1293 data governs, as per AASHTO PP 65-11. Thus, based on the petrographic evaluation and expansion tests, it is a logical conclusion to state that ASR does not appear to be the culprit behind the distress of the four bridge beams.

Further evidence that ASR is not a key factor is that the replicate blocks have exhibited essentially zero expansion but are showing visible cracking. This cracking mimics the cracking pattern observed on all four of the bridge beams. Lastly, the actual bridge beams were cast under stringent TxDOT specifications that limited alkali loadings to 2.1-2.4 kg/m^3 (3.5-4 lbs/yd^3) of Na_2O_e for plain concrete mixtures and required a minimum of 20 percent Class F fly ash. Based on significant experience with Texas aggregates, in general, and these two aggregates, specifically, it would be highly unusual to expect significant ASR-induced expansion with such low alkali loadings and/or with the use of 20 percent Class F fly ash. The underlying mechanism of distress for these precast beams is currently under investigation under a separate TxDOT project.

The second goal of this field trial was to evaluate the efficacy of silane, in this case a 40-percent, alcohol-based silane, in reducing the internal relative humidity in concrete. Although ASR was not found to be the root cause of distress, it is still of significant interest to quantify the ability of silane to reduce humidity in bridge beams. Further, although determining the actual governing cause of cracking in precast beams was beyond the scope of this project, reducing internal humidity could potentially help to reduce the future potential for cracking if the mechanism is driven by moisture availability (like many durability-related issues are). Given the short duration of the monitoring program, it is too premature to accurately quantify the effects of silane on internal relative humidity. However, based on monitoring for a period of about 17 months since the application of silane, the beam sections treated with silane tend to exhibit consistently lower internal relative humidities than control, untreated sections. The reduction (based on averaging the internal relative humidities for the three measurement depths) after 17 months was approximately 5-7 percent RH for sections treated with silane, compared to control sections. Again, it should be noted that more time is needed to better quantify the effects of silane treatment on internal relative humidity of bridge beams. Given the small section size of the beams and the ability to treat all sides of the beam with silane, it is expected that the overall reduction in internal relative humidity will become more pronounced with time and additional wetting and drying cycles.

9.5 SUMMARY

Through the use of an FHWA protocol (Fournier et al. 2010) for evaluating ASR-affected structures, it was determined that ASR was not a significant cause of distress in the four bridge beams that were evaluated, treated, and monitored. Components of the protocol that were employed included:

- Visual survey and evaluation
- Petrographic evaluation of extracted cores (including the application of the Damage Rating Index [DRI])
- Accelerated laboratory testing (AASHTO T 303, ASTM C1293) – as per AASHTO PP 65-11
- In-situ expansion measurements of field elements
- Internal relative humidity measurement

The diagnosis that ASR was not the culprit in the observed bridge beam cracking has given TxDOT more confidence that existing specifications aimed at preventing ASR are indeed effective. Further, by ruling out ASR as the underlying mechanism, TxDOT has now been able to focus on other potential causes of cracking, including volume changes due to shrinkage (autogenous and drying).

Although the monitoring period was limited, the effects of silane treatment on internal relative humidity are beginning to become apparent. On average, beam sections that were treated topically with silane are yielding relative humidity values that are about 5 to 7 percent lower than beam sections that were not treated with silane. Based on experience with treating other ASR-affected elements with silane, it is anticipated that the difference in humidity between the silane-treated and control sections will become more pronounced with additional exposure to wetting and drying cycles.

9.6 REFERENCES

American Association of State Highway and Transportation Officials (AASHTO). 2008. "Standard Method of Test for Accelerated Detection of Potentially Deleterious Expansion of Mortar Bars Due to Alkali-Silica Reaction." AASHTO T 303, AASHTO, 6 p.

American Association of State Highway and Transportation Officials (AASHTO). 2011. "Standard Practice for Determining the Reactivity of Concrete Aggregates and Selecting Appropriate Measures for Preventing Deleterious Expansion in New Concrete Construction." AASHTO PP 65-11, AASHTO, 24 p.

American Standards for Testing and Materials (ASTM). 2008. "Standard Test Method for Determination of Length Change of Concrete Due to Alkali-Silica Reaction." ASTM C1293, ASTM International.

Fournier, B., Bérubé, M.A., Folliard, K.J. and Thomas, M.D.A. 2010. “Report on the Diagnosis, Prognosis, and Mitigation of Alkali-Silica Reaction (ASR) in Transportation Structures.” FHWA-HIF-09-004, Federal Highway Administration.

10. BRIDGE COLUMNS, HOUSTON, TX

With collaboration from the Texas Department of Transportation (TxDOT), a set of bridge columns in Houston, TX were identified as possibly suffering from ASR-induced expansion and cracking. The initial evaluation and treatment at this site was conducted in January 2006 under the FHWA Lithium Technology Research Program by the same research team leading the efforts under FHWA ASR Development and Deployment Program. After viewing various columns, cores were extracted from damaged sections. Petrographic evaluations confirmed that ASR was occurring to a range of degrees in the various cores, and residual expansion testing showed the potential for future expansion.

Based on these preliminary visual inspection and laboratory data, it was decided to select a total of 12 columns for treatment and monitoring – one set of six columns (Columns 31, 32, 33, 34, 35, and 36) was selected to visually represent moderate-to-severe damage, and a second set of six columns (Columns 41, 42, 43, 44, 45, and 46) was selected to represent slight-to-moderate-damage. The bridge columns selected for the treatment and monitoring are located at the interchange of I-10 and I-45, just to the west of downtown Houston, with the 12 selected columns being those that support the high-occupancy vehicle (HOV) ramp. Figure 184 shows an aerial view of the columns selected for treatment and monitoring.

Figure 184. Google satellite image showing the location of the bridge columns selected for treatment and monitoring.

This field trial is unique for several reasons. First, the concrete used in the columns contained recycled concrete aggregate (RCA) as the coarse aggregate fraction. RCA is currently used quite infrequently in structural concrete, thus, this is a unique occurrence. Second, other bridge structures in Texas had previously suffered from ASR and/or delayed ettringite formation (DEF), as well as thermal cracking. Much of the observed deterioration has now been addressed by TxDOT through improved test methods, specifications, and standard practices aimed at

preventing ASR, DEF, and thermal cracking, but these bridge columns and other structures in Texas were constructed prior to such stringent durability requirements. As such, part of the charter for this project was to determine the mechanism of deterioration for these columns, knowing that multiple durability mechanisms can affect the same structure. Lastly, the columns were quite large, with a tapered cross-section with average cross section of 2 m x 2 m (6.6 ft x 6.6 ft) and heights as high as 20 m (66 ft). This represented unique challenges in terms of access, treatment, and monitoring.

Figure 185. Typical column at Houston, TX test site.

This chapter summarizes the treatment and monitoring of the 12 bridge columns. Treatments evaluated included the application of lithium nitrate (by vacuum and electrochemical means) and various coatings/sealers aimed at reducing internal relative humidity.

10.1 SUMMARY OF PETROGRAPHIC EVALUATION

Cores were extracted from Columns 34 and 43 and evaluated petrographically by Dr. Paddy Grattan-Bellew in early 2006. Damage Rating Index (DRI) values were calculated to be 43 and 27 for Columns 34 and 43, respectively. These are relatively low DRI values indicative of low levels of ASR distress. However, it should be noted that the DRI approach used herein was not developed to address concrete containing recycled concrete aggregate. Also, the DRI approach used in 2006 has since been refined and essentially standardized, with revised DRI classification values (Fournier et al. 2009). For these reasons, it is difficult to directly apply the DRI scores in this case; however, a general observation is that only minor ASR-induced expansion and cracking was evident from polished sections examined at a magnification of up to 16x.

Although the petrographic evaluation, using polished sections, did not find substantial ASR-induced damage at up to 16x magnification, there were signs of ASR activity and products

within the RCA particles. However, there was no significant microcracking observed in the paste surrounding the RCA particles. There were also signs of particles that underwent or are undergoing dissolution or becoming "gelified," although there are no visible cracks (at 16x magnification) radiating away or extending from these particles. There were trace amounts of sulfates found in some voids (acicular deposits, most likely ettringite), but not enough to be of concern from a durability perspective. There were no visible signs of distress mechanisms associated with internal sulfate attack or DEF, such as gapping around aggregate particles or nests of ettringite in small pores (although these DEF-specific features are typically more evident in thin section petrography).

For a more detailed microstructural investigation, thin sections from the two extracted cores were prepared and analyzed under a scanning electron microscope (SEM). Through examining several thin sections, symptoms of ASR were clearly observed, such as those shown in Figure 186. There was no evidence within any of the thin sections of classic DEF symptoms, such as gapping around aggregates, ettringite backfilling into gaps around aggregates and open voids, or small nests of ettringite in micropores.

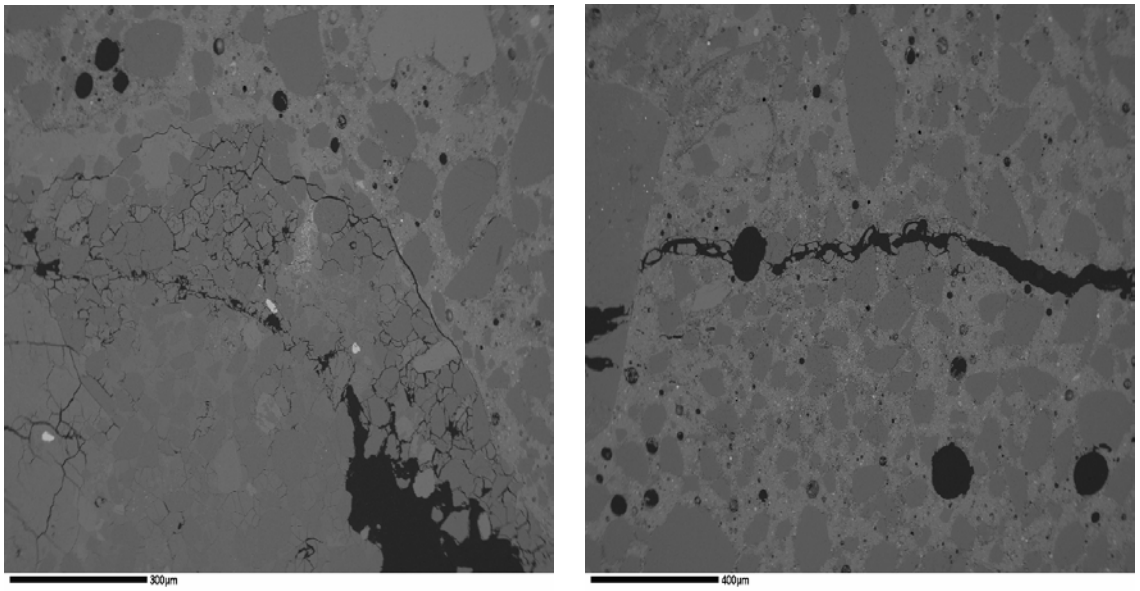

A **B**

Figure 186. SEM micrographs of thin sections from Houston columns, showing (A) dissolution of siliceous aggregate, and (B) gel-filled cracks emanating from site of reaction.

10.2 SUMMARY OF APPLICATION REPORT

This section describes the various treatments that were performed on the Houston columns. The treatments were performed over a several-month period in early 2006. As previously stated, the 12 columns were divided into 2 groups. Columns 31-36 were considered to be moderately to severely damaged, while columns 41-46 were considered to be slightly to moderately damaged. Each of these two sets of columns also consisted of columns of similar dimensions and exposure conditions. Within each set of six columns, one column was left as an untreated control, four columns were treated under the FHWA Lithium Technology Research Program (under the

guidance of the same research team that continued monitoring the site as part of the FHWA Development and Deployment Program), and one column was treated separately as per the instructions of TxDOT engineers, who worked closely with the FHWA team throughout the process. TxDOT selected the application of sodium silicate (Column 31) and silane-siloxane blend (Column 41). Table 69 shows the various treatments performed on the columns. Treatments were only applied to the lower 8.0 m (26.3 ft) portions of each column due to difficulties in accessing portions of the column above this nominal height. Figure 187 and Figure 188 show a subset of the columns that were treated. Details on the performance monitoring techniques and treatment activities are provided in chapters 2 and 3, respectively.

Table 69. Houston columns and selected treatments.

Column #	Visual distress rating (slight, moderate, severe)	Treatment
31	Moderate to severe	Sodium silicate vacuum impregnation over blasted surface
32	Moderate to severe	Topical silane over original painted surface
33	Moderate to severe	Lithium vacuum impregnation
34	Moderate to severe	Topical silane over blasted surface
35	Moderate to severe	Electrochemical lithium impregnation
36	Moderate to severe	Control
41	Slight to moderate	Silane-siloxane blend vacuum impregnation over blasted surface
42	Slight to moderate	Topical silane over original painted surface
43	Slight to moderate	Control
44	Slight to moderate	Topical silane over blasted surface
45	Slight to moderate	Lithium vacuum impregnation
46	Slight to moderate	Electrochemical lithium impregnation

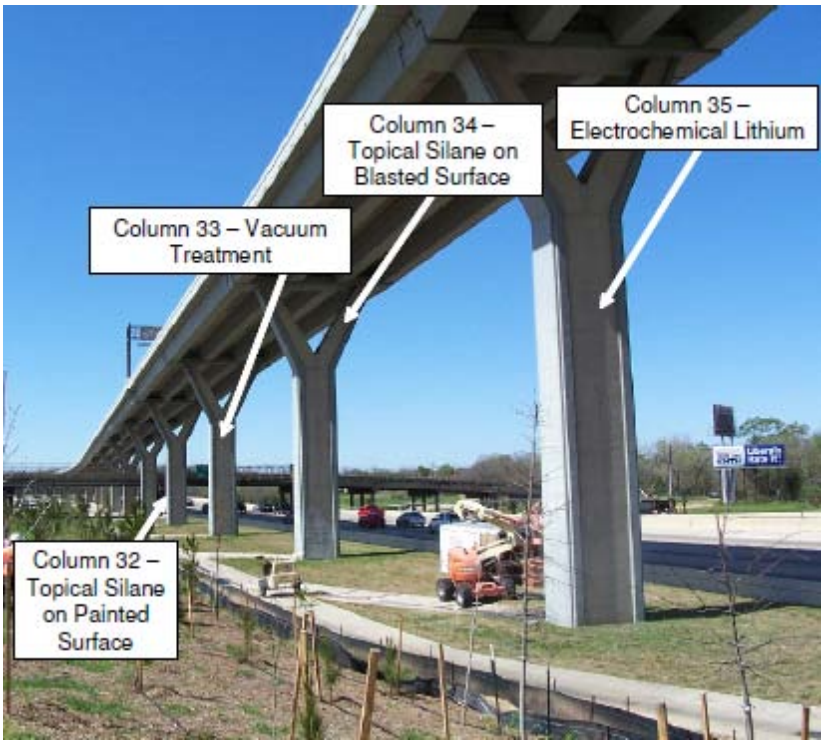

Figure 187. Columns 32-35 in Houston, TX, along with their treatments.

Figure 188. Columns 42-46 in Houston, TX, along with their treatments.

For the electrochemical method, the columns were first blasted to remove the existing paint, after which an anode (a 30 percent lithium nitrate solution absorbed into a sprayed cellulose layer at the surface of the concrete) was electrically coupled to the embedded reinforcing steel, which acts as a cathode, and lithium nitrate solution was driven into the columns using 40V over the course of six to eight weeks. Figure 189 shows the method used for the electrochemical treatment of Columns 35 and 46.

A **B** **C**

Figure 189. Summary of electrochemical treatment of Houston columns.
A: Irrigation tubes, wood splices, and metal strips are placed on the column. The metal strips are attached to titanium mesh that runs inside holes drilled into the sides of the column. B: A cellulose layer is being applied to the side of the column. C: Plastic sheeting is placed on all sides of the column. The gutters under the sheeting collect excess lithium to be reused.

Shortly after the completion of the electrochemical treatment, cores were extracted from several columns to determine the depth of lithium penetration. Lithium ion concentrations were then measured using acid digestion and subsequent analysis using ion chromatography.

The lithium vacuum impregnation treatment was applied to Columns 33 and 45. Surface preparation for the treatment involved media blasting of the columns to a height of 7.6 m (25 ft) to remove paint. Lithium nitrate was applied at a rate of approximately 1.63 L/m^2 (1 gal/25 ft^2) on all four sides of each column to a height of 7.6 m (25 ft). Figure 190 shows the lithium vacuum impregnation on Column 45. The same vacuum technique was used to attempt to increase the penetration of lithium silicate (Column 31) and a silane-siloxane blend (Column 41).

Figure 190. Lithium vacuum treatment on Column 45.

A 40-percent, alcohol-based silane was applied by spray to Columns 32, 34, 42, and 44. In order to investigate whether paint removal prior to silane treatments is necessary and beneficial, it was decided to apply silane to Columns 32 and 42 over the existing paint, while Columns 34 and 44 were media blasted prior to the silane application. A target application rate of 3.1 m^2/L (125 ft^2/gallon) was used to apply the 40 percent silane to each of the columns.

As depicted in Figure 191, horizontal and vertical length change measurements were made through the use of embedded gauge studs and a DEMEC gauge. Figure 191 shows that the measurement points also serve as the corners for the map cracking square monitored on two faces (North and West faces for Columns 31-36 and Southeast and Southwest faces for Columns 41-46) of each of the 12 test columns. In addition to measuring length change and performing map cracking measurements for each monitoring visit, the internal relative humidity of each of the columns was measured using the Vaisala HM44 humidity measurement system, shown in the upper portion of the photograph in Figure 191. Most internal relative humidity data generated for these columns were for a measurement depth of 50 mm (2 in.), and for select columns, additional holes were drilled and humidity measurements were taken at depths of 25 mm (1 in.) and 75 mm (3 in.).

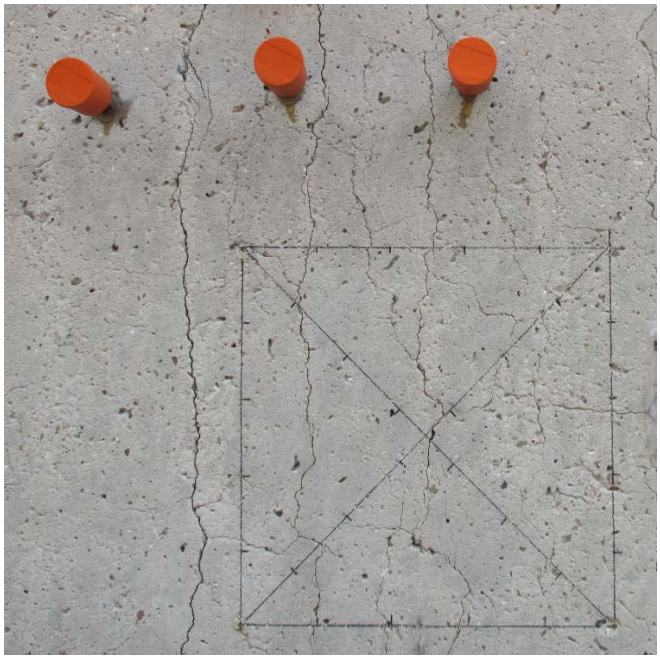

Figure 191. Example of monitoring performed on each column. Relative humidity probes, measuring internal relative humidity values at depths of 25 mm (1 in.), 50 mm (2 in.), and 75 mm (3 in.) from the concrete surface, are shown on the top of the photograph, and the map cracking region is shown at the bottom. Both horizontal and vertical length change measurements are taken using embedded gauge studs at the corners of the map cracking square.

10.3 MONITORING DATA

This section summarizes the data obtained from expansion and internal relative humidity measurements from the 12 columns included in this trial. For select columns, the results of lithium concentration profiling are presented. In addition, the results of residual expansion testing are presented that are aimed at determining whether there is future potential for expansion due to ASR and/or DEF. Lastly, photographs of each crack mapping region taken prior to treatment and over the course of seven years are presented.

Figure 192 (Columns 31-36) and Figure 193 (Columns 41-46) show the average expansion, based on horizontal expansions only, for each of the columns. The data were not corrected for temperature (thermal) effects. Vertical expansions were found to be minimal, due to restraint provided by the primary reinforcement, as well as the dead (and live) load on the columns. Figure 194 (Columns 31-36) and Figure 195 (Columns 41-46) show the average relative humidity values recorded at a depth of 50 mm (2 in.) for each of the columns. Figure 196 (Columns 31-36) and Figure 197 (Columns 41-46) show the average calculated Cracking Index (CI) values based on crack mapping measurements from both faces that are being monitored for each column. For each of the above graphs, data are shown from the date of treatment (day zero) up to the last date of monitoring (about 2500 days).

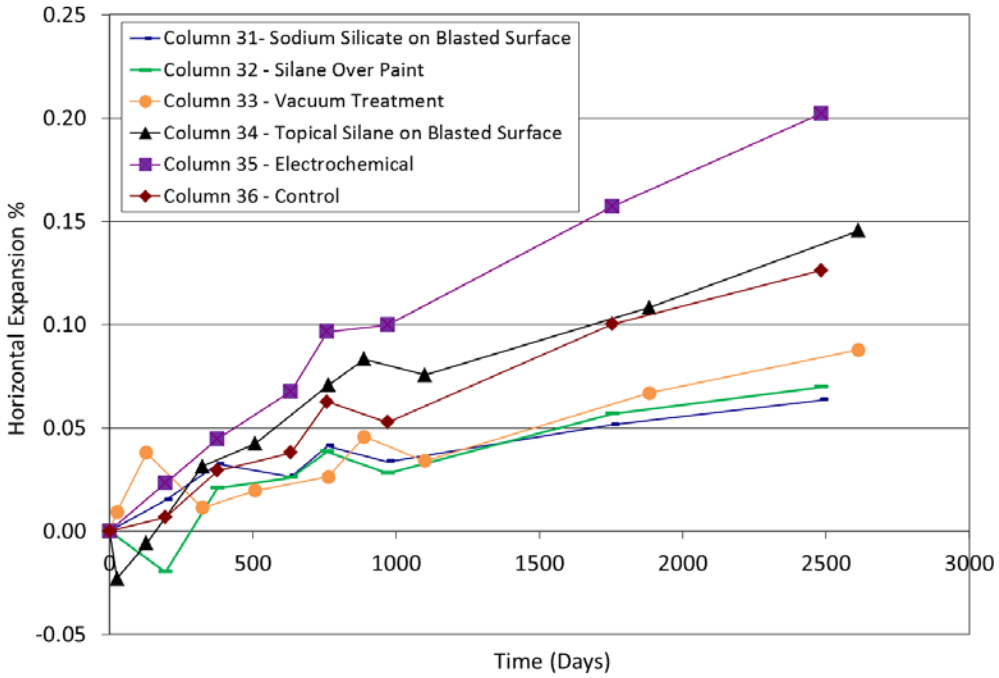

Figure 192. Average expansion of Columns 31-36. (Measurements are average values of horizontal expansions measured on the North and West face of each column.)

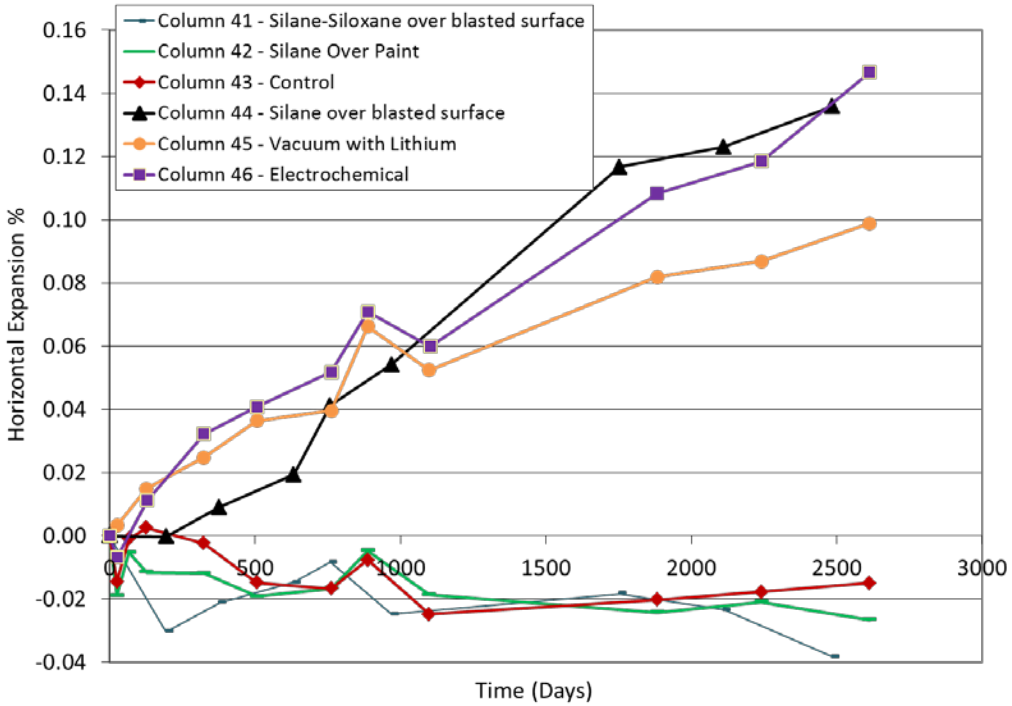

Figure 193. Average expansion of Columns 41-46. (Measurements are average values of horizontal expansions measured on the Southeast and Southwest face of each column.)

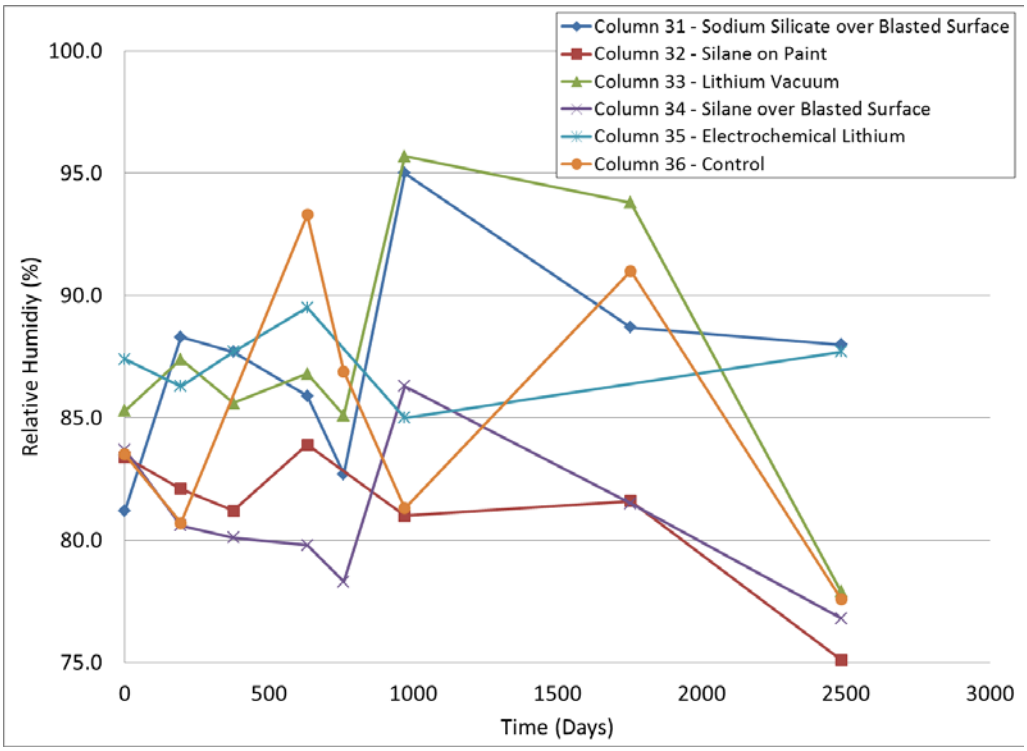

Figure 194. Average internal relative humidity of Columns 31-36. (Measurements are average values of relative humidity values measured at a distance of 50 mm (2 in.) from the exposed/treated concrete surface.)

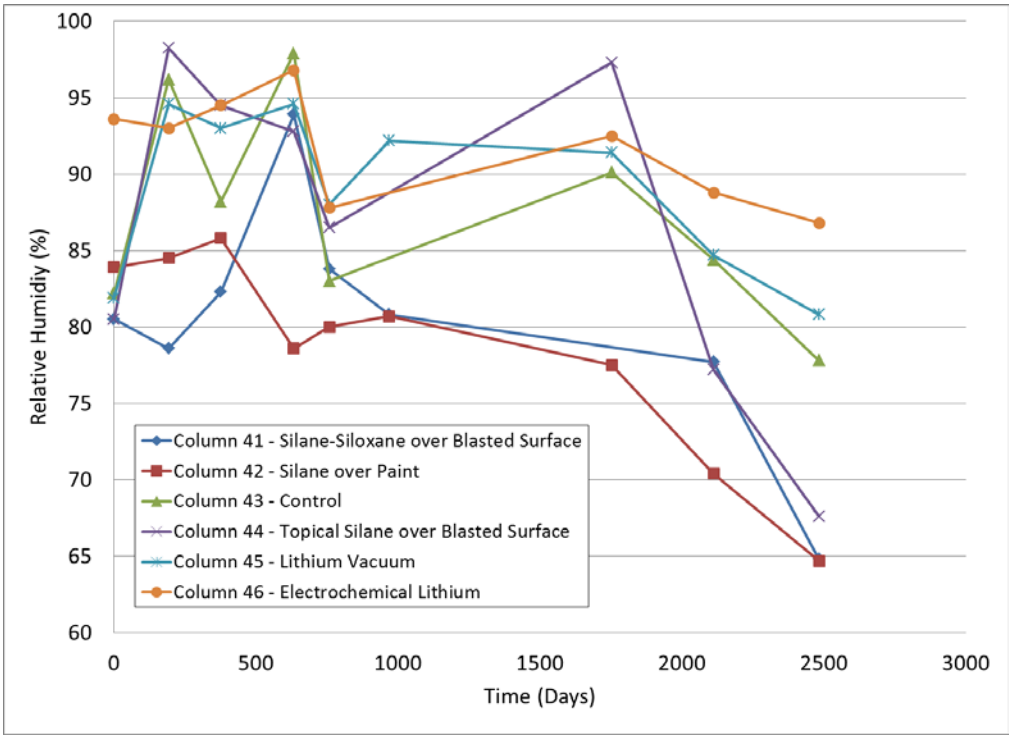

Figure 195. Average internal relative humidity of Columns 41-46. (Measurements are average values of relative humidity values measured at a distance of 50 mm (2 in.) from the exposed/treated concrete surface.)

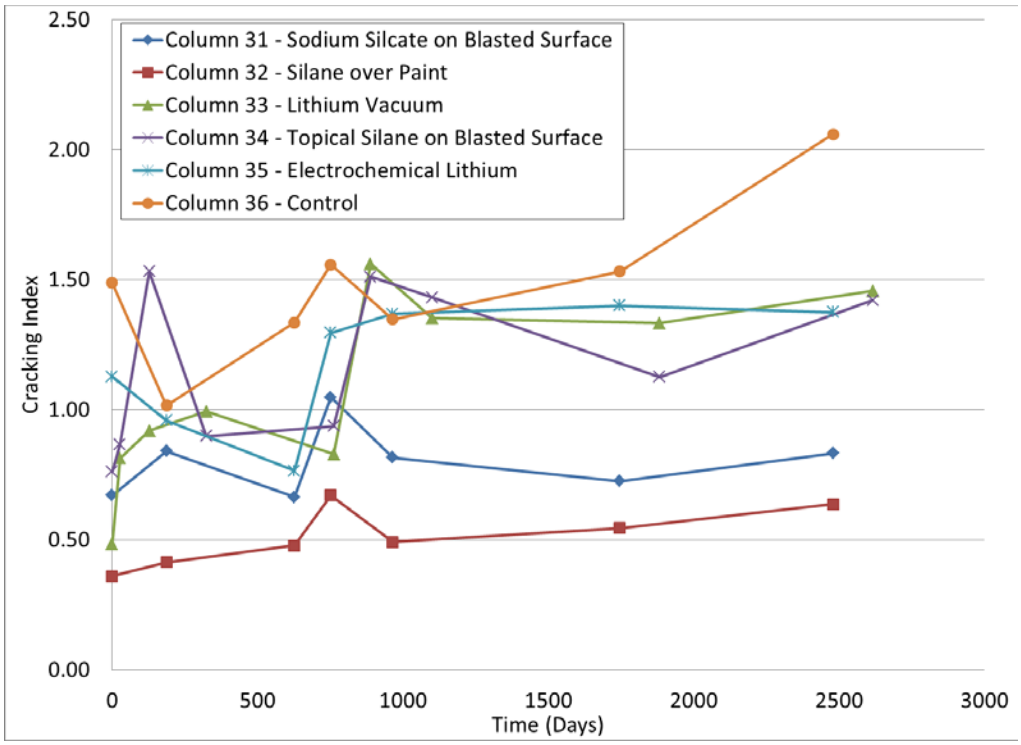

Figure 196. Average calculated Cracking Index (CI) (mm/m) for Columns 31-36. (Calculations are based on the average of CI values obtained from the North and West faces of each column.)

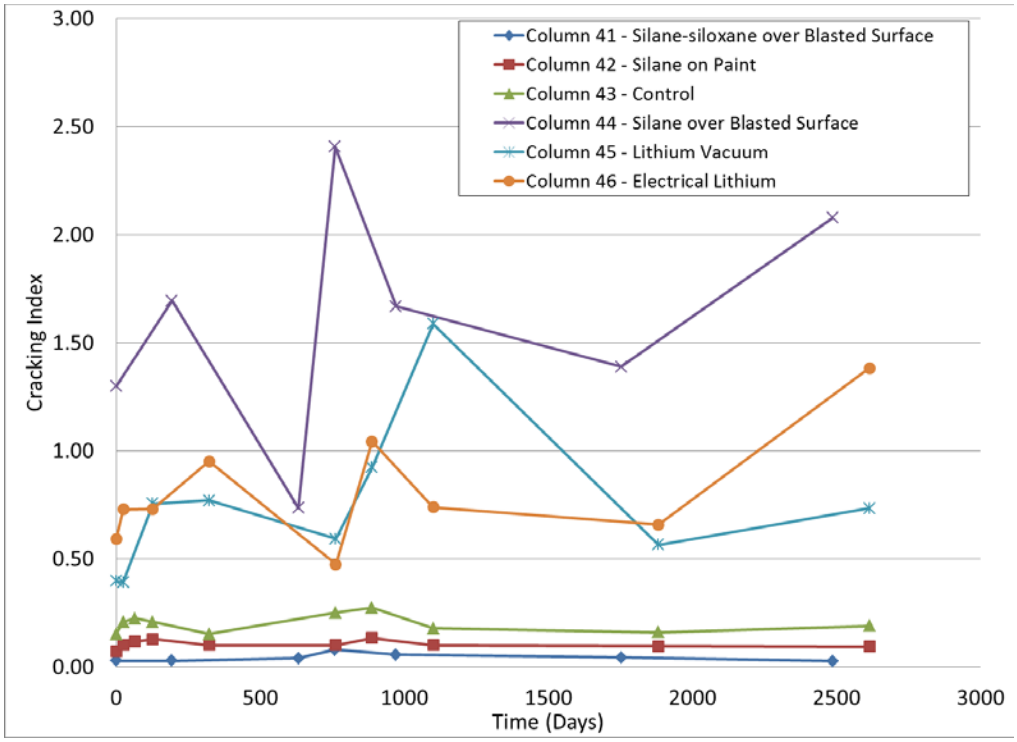

Figure 197. Average calculated Cracking Index (CI) (mm/m) for Columns 41-46. (Calculations are based on the average of CI values obtained from the Southeast and Southwest faces of each column.)

When evaluating lithium profile data (presented next), it is important to consider much lithium is needed to control expansion due to ASR. Assume that a plain concrete mixture containing 3 kg/m^3 Na_2O_e and has been shown to require approximately 13.8 L/m^3 of 30 percent lithium nitrate solution in order to sufficiently suppress expansion when tested with a specific aggregate. This dosage of $LiNO_3$ solution contains 504 g (1 lb) of Li, and assuming that half of this lithium gets bound in early hydration products (as well documented in literature), approximately 250 g of lithium per m^3 will remain in the concrete to combat ASR. If one assumes a concrete density of 2350 kg/m^3 the concentration of lithium ions in pore solution would be approximately 100 ppm, and this concentration would be enough to control expansion when used as an admixture. In short, 100 ppm is a reasonable threshold lithium concentration in concrete needed to suppress expansion due to ASR.

Figure 198 shows the measured lithium profiles for cores extracted from columns to which lithium nitrate was applied electrochemically (Column 46) and through vacuum impregnation (Columns 33 and 45). Profiling was conducted to a depth of 50 mm (2 in.) for cores extracted over reinforcing steel and about 58 mm (2.3 in.) for cores extracted between reinforcing steel. Using the aforementioned 100 ppm lithium concentration threshold, requisite concentrations were measured to a depth of about 8-10 mm (0.3-0.4 in.) from the surface treated with lithium. For the electrochemical treatment, lithium concentrations of about 300 ppm, well above the 100 ppm threshold, were measured to the depth of the reinforcing steel at 50 mm (2 in.). For cores extracted between reinforcing steel, the lithium concentration was found to be at or just above the 100 ppm lithium concentration down to the depth of the deepest measurement.

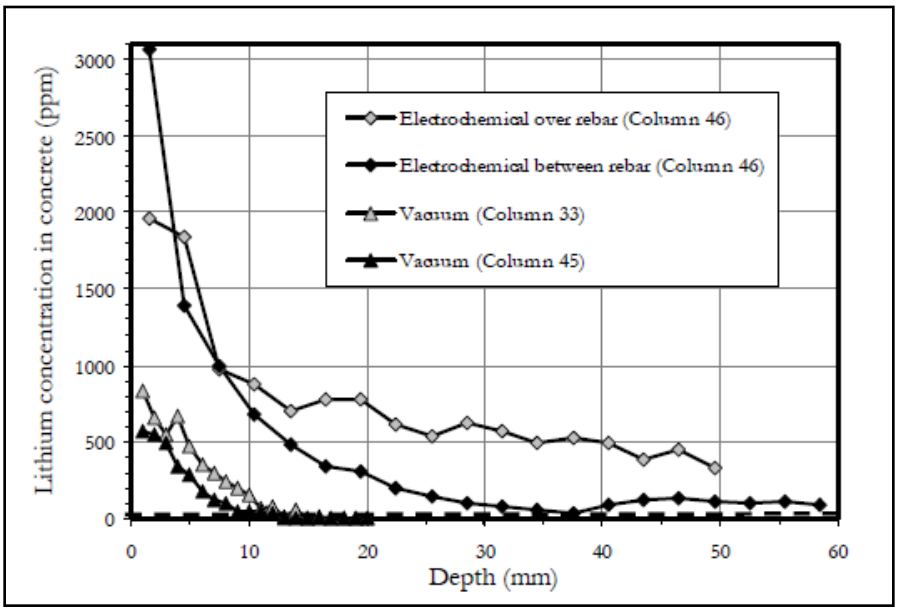

Figure 198. Lithium concentration profile measured in cores after electrochemical (Column 46) or vacuum impregnation (Columns 33 and 45).

Figure 199 shows the results of additional analyses performed on the core extracted over the reinforcing steel in Column 46. In addition to measuring the lithium concentration (previously shown in Figure 198), the sodium and potassium concentrations were also measured. The data show that sodium and potassium concentrations were found to be elevated in the region closest

to the reinforcing steel. The potential mechanism(s) responsible for this and possible implications on durability are discussed next in the data analyses section.

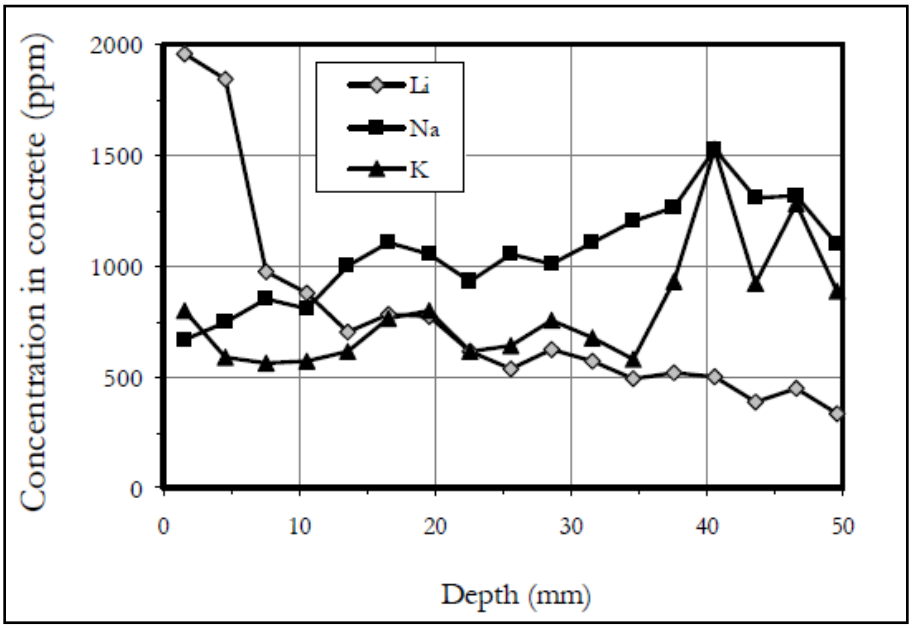

Figure 199. Lithium, sodium, and potassium concentration profiles for core extracted over reinforcing steel in Column 46 after electrochemical lithium treatment.

A protocol for the diagnosis and prognosis of structures affected by ASR and/or DEF, developed by Thomas et al. (2008), was followed as part of the investigation on the underlying causes of distress and future potential for expansion. As part of this protocol, small cores (50 mm [2 in.] diameter) were extracted from several of the bridge columns (Columns 34, 42, 43, 45, and 46) and were subjected to two different testing regimes – (1) cores are immersed in 1 N NaOH solution at 80 °C (176 °F), and (2) cores are immersed in lime water at 23 °C (73 °F). The former test aims to estimate the remaining potential for ASR-induced expansion, based on the remaining reactive silica within the aggregates. This testing regime drives ASR, through high temperatures and essentially an unlimited supply of alkalies in the soak solution, but because of the high temperature and high pH of the soak solution, DEF is suppressed. The latter testing regime, storage in lime water at room temperature, promotes DEF through the leaching of alkalies from the core samples, which also suppresses ASR. The results of these tests show that the potential for ASR-induced expansion exists as residual expansions between 0.05 and 0.20 were measured for cores stored in 1 N NaOH at 80 °C (176 °F) after six months. Negligible expansions were observed in cores stored in lime water at 23 °C (73 °F) for over six months, which is typically a signal that the potential for DEF-induced expansion is low.

Photographs were regularly taken of each of the map cracking areas as a means of documenting the visual changes that occurred during the seven-year monitoring period. Figures 200 to 223 show these photographs for both faces of each column that are being monitored (North and West faces for Columns 31-36; Southeast and Southwest faces for Columns 41-46).

A – Column 31 – West Face 2006

B – Column 31 – West Face 2009

C – Column 31 – West Face 2011

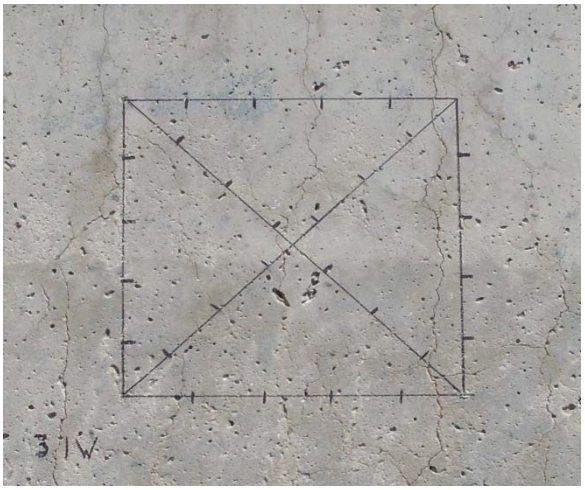

D – Column 31 – West Face 2013

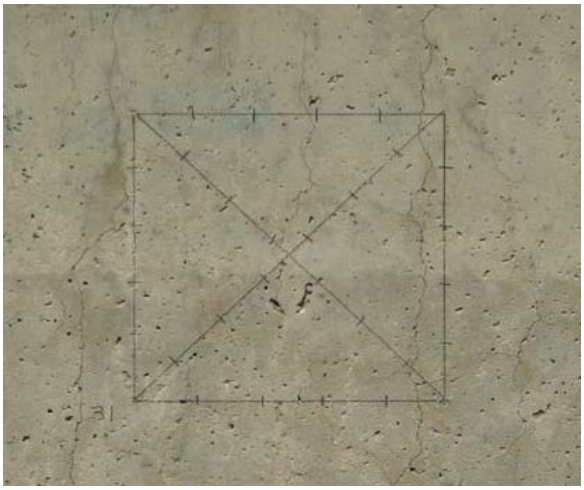

Figure 200. Visual observation of Column 31 West face.

A – Column 31 – North Face 2006

B – Column 31 – North Face 2009

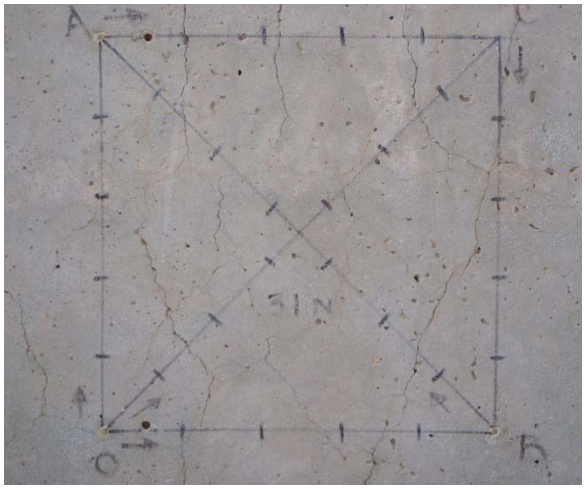

C – Column 31 – North Face 2011

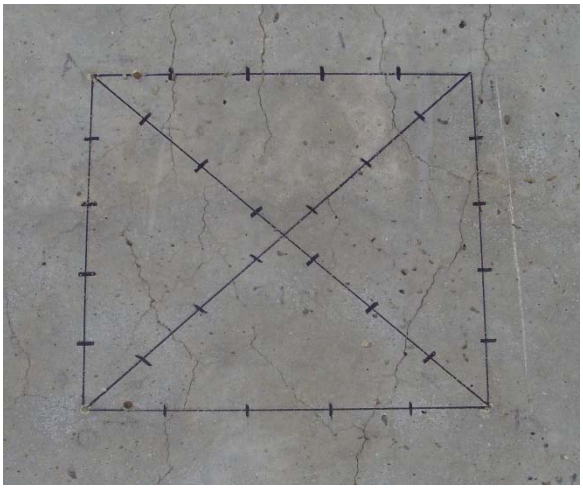

D – Column 31 – North Face 2013

Figure 201. Visual observation of Column 31 North face.

A – Column 32 – West Face – 2006

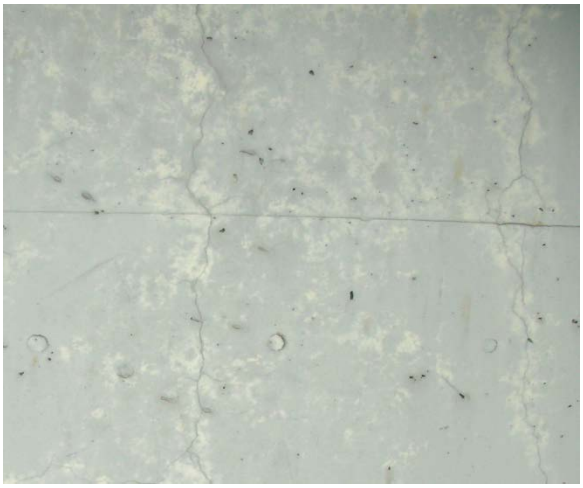

B – Column 32 West Face - 2009

C – Column 32 – West Face 2011

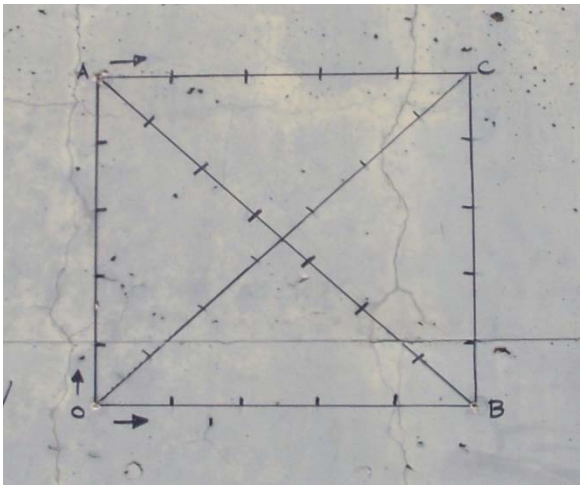

D – Column 32 – West Face 2013

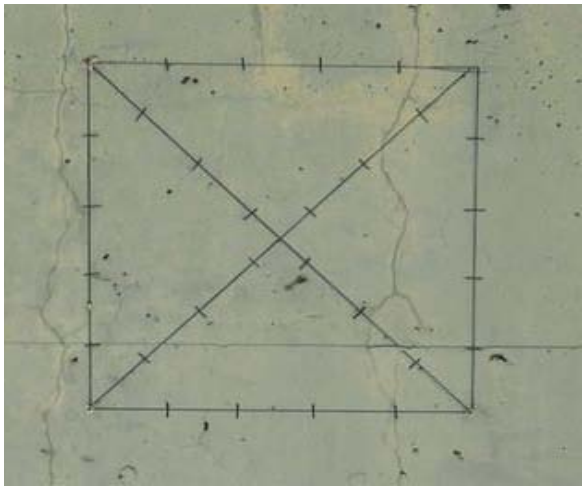

Figure 202. Visual observation of Column 32 West face.

A – Column 32 – North Face 2006

B – Column 32 – North Face 2009

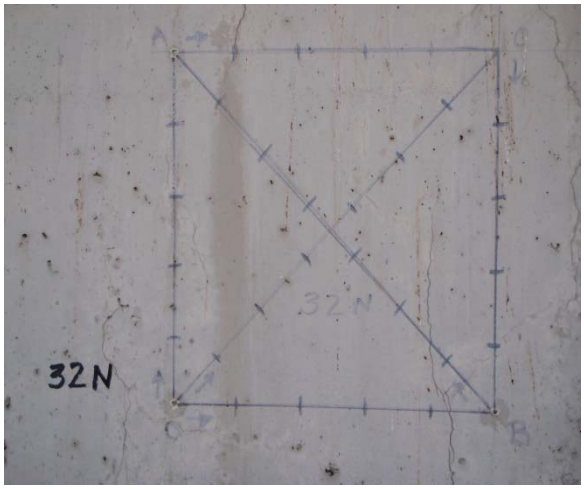

C - Column 32 – North Face – 2011

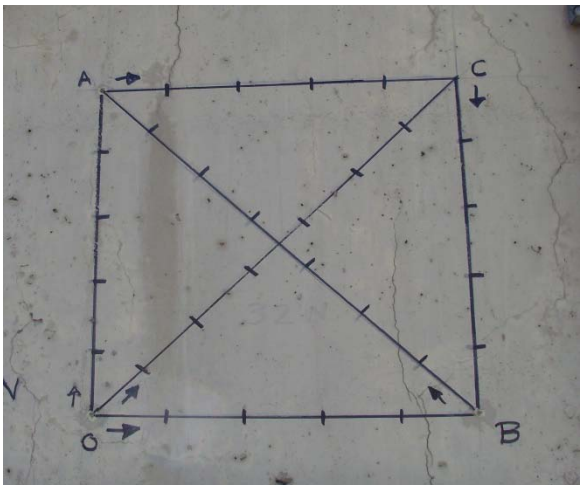

D – Column 32 – North Face 2013

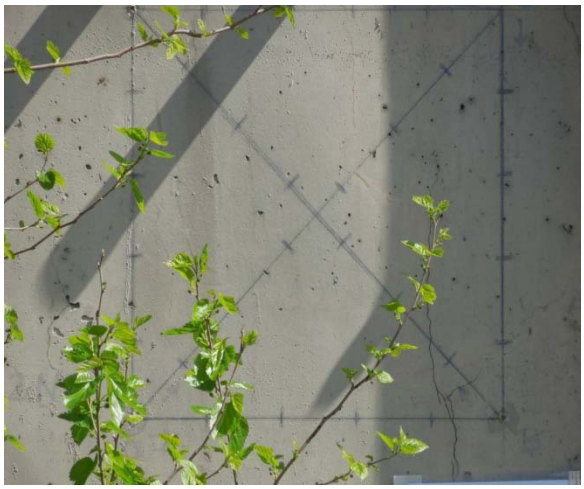

Figure 203. Visual observation of Column 32 North face.

A – Column 33 – West Face 2006

B – Column 33 – West Face 2009

C - Column 33 – West Face 2011

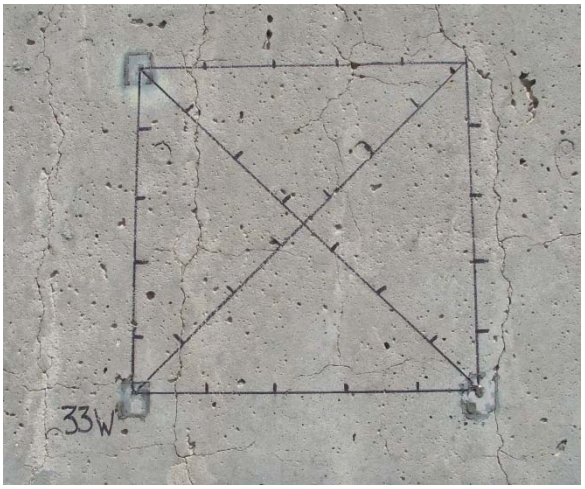

D – Column 33 – West Face 2013

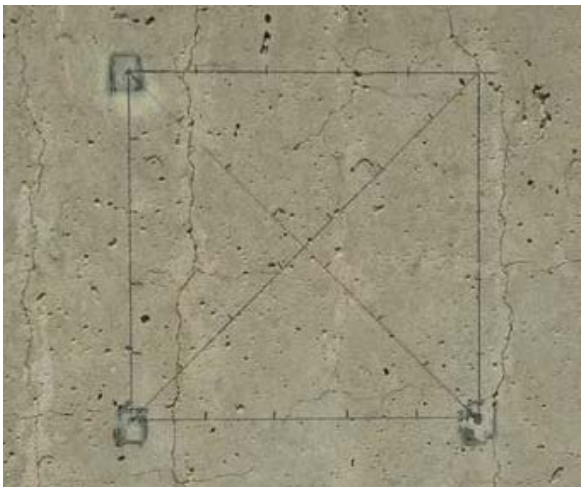

Figure 204. Visual observation of Column 33 West face.

A – Column 33 – North Face 2006

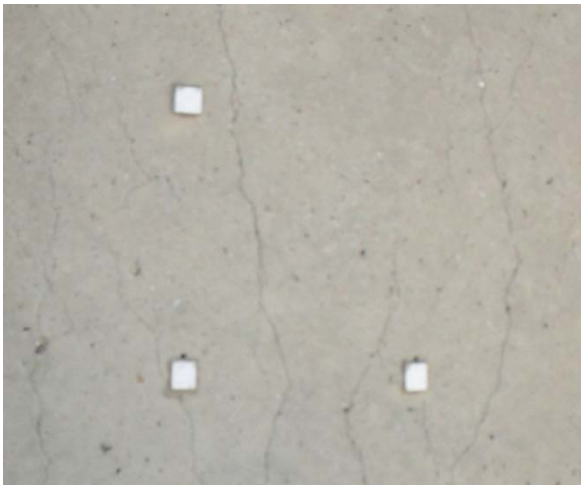

B – Column 33 – North Face 2009

C – Column 33 – North Face 2011

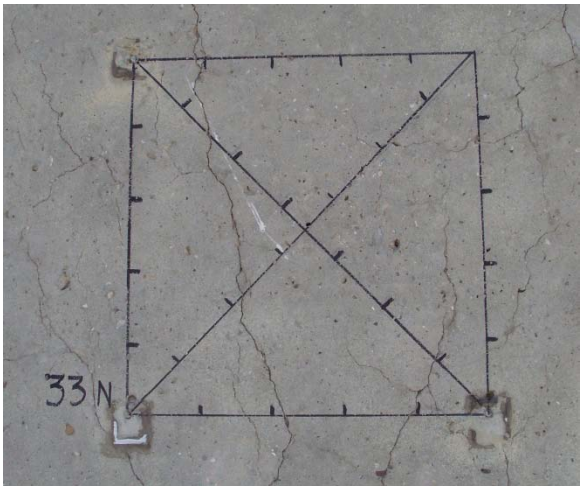

D – Column 33 North Face 2013

Figure 205. Visual observation of Column 33 North face.

A – Column 34 – West Face 2006

B – Column 34 West Face 2009

C – Column 34 – West Face 2011

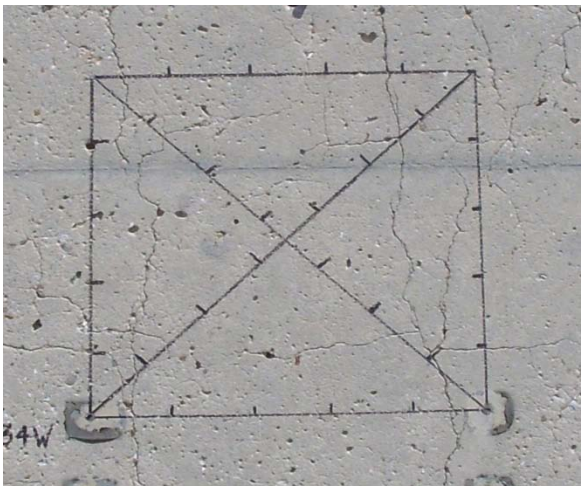

D – Column 34 West Face 2013

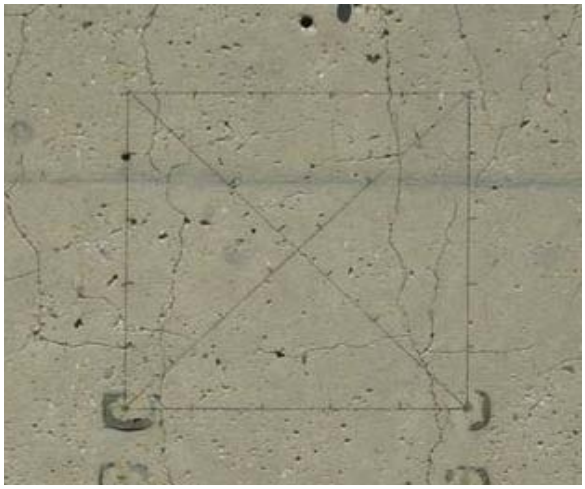

Figure 206. Visual observation of Column 34 West face.

A – Column 34 North Face 2009

B – Column 34 North Face 2011

C – Column 34 North Face 2013

Figure 207. Visual observation of Column 34 North face.

A – Column 35 West Face 2006

B – Column 35 West Face 2009

C – Column 35 West Face 2011

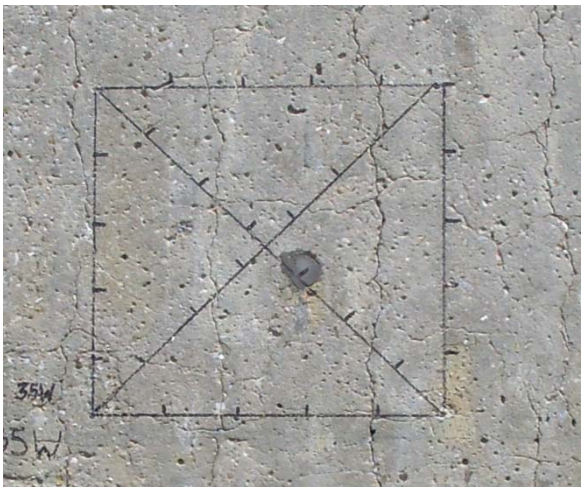

D – Column 35 West Face 2013

Figure 208. Visual observation of Column 35 West face.

A - Column 35 – North Face 2006

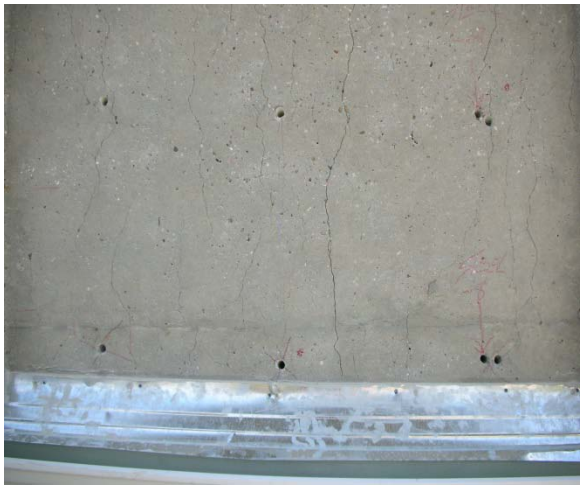

B – Column 35 North Face 2009

C - Column 35 – North Face 2011

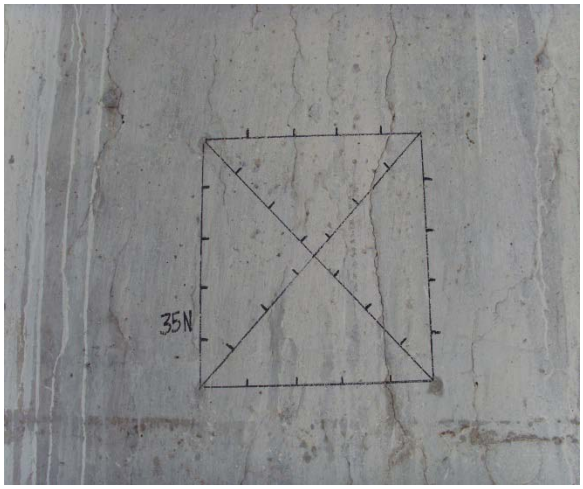

D – Column 35 North Face 2013

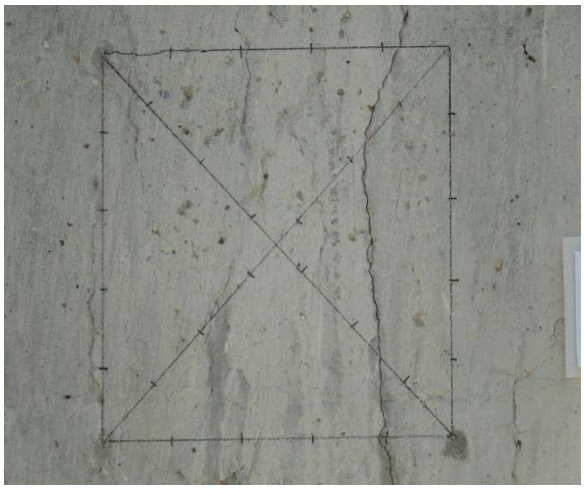

Figure 209. Visual observation of Column 35 North face.

A – Column 36 West Face – 2009

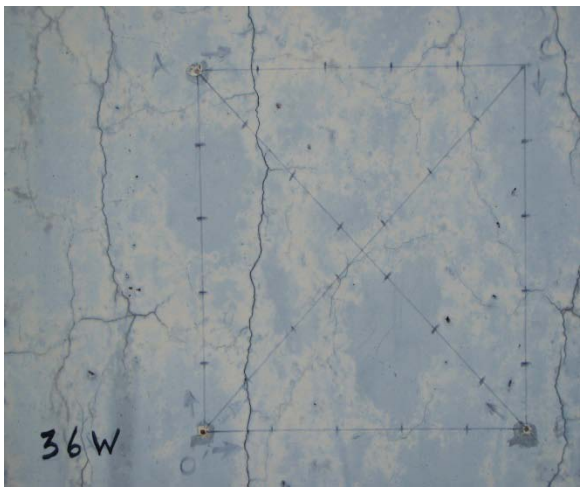

B – Column 36 West Face 2011

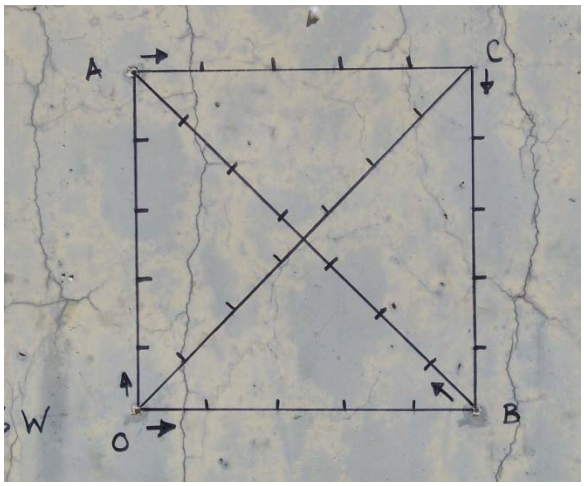

C – Column 36 West Face 2013

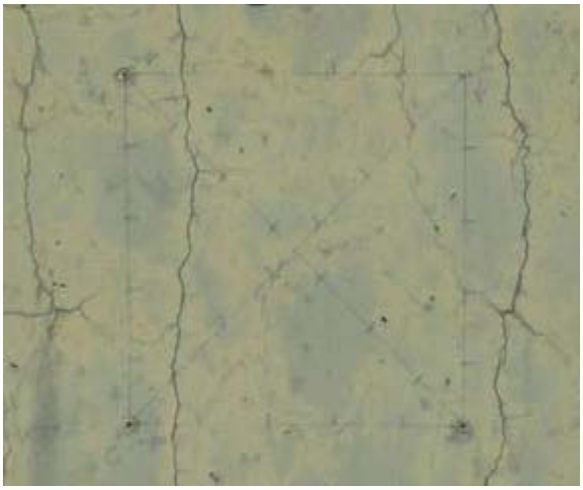

Figure 210. Visual observation of Column 36 West face.

A – Column 36 North Face 2009

B – Column 36 North Face 2011

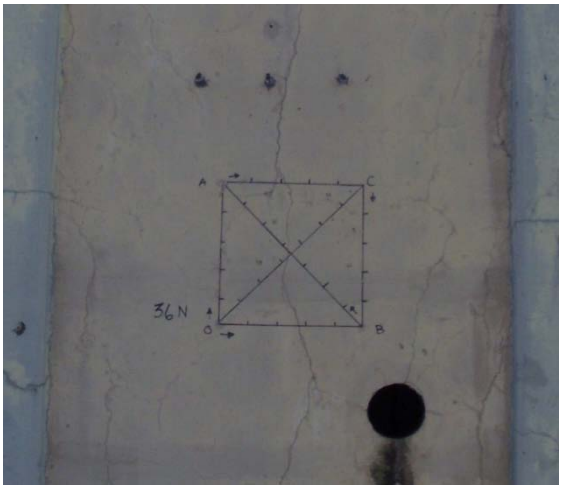

C – Column 36 North Face 2013

Figure 211. Visual observation of Column 36 North face.

A – Column 41 – SW Face – 2009

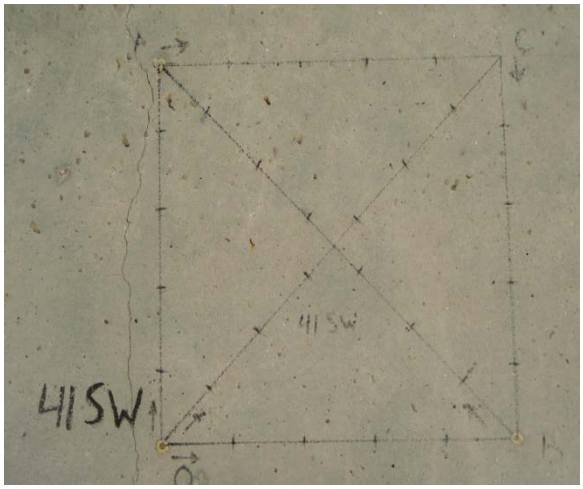

B – Column 41 – SW Face 2011

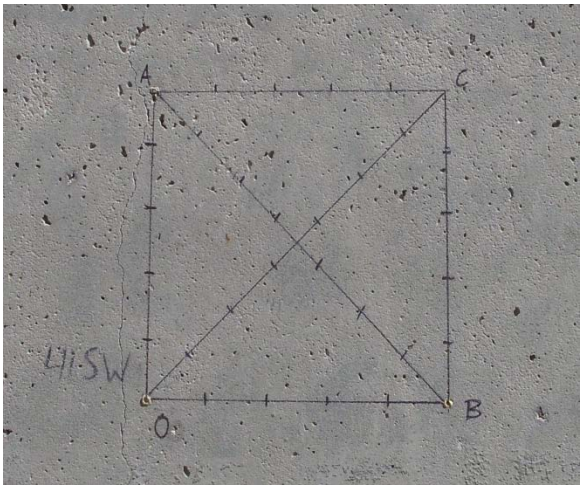

C – Column 41 - SW Face 2013

Figure 212. Visual observation of Column 41 Southwest face.

A – Column 41 SE Face 2009

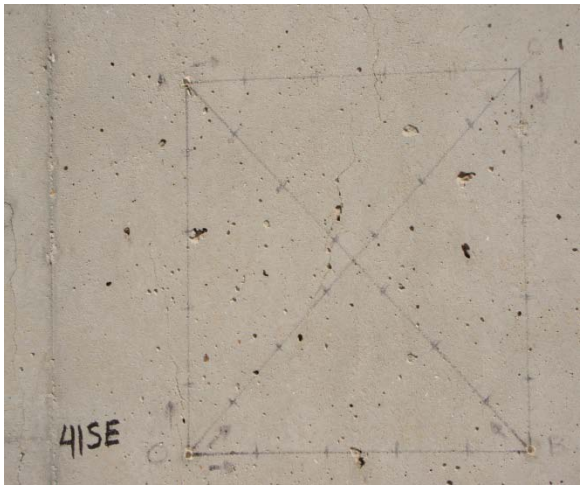

B – Column 41 SE Face 2011

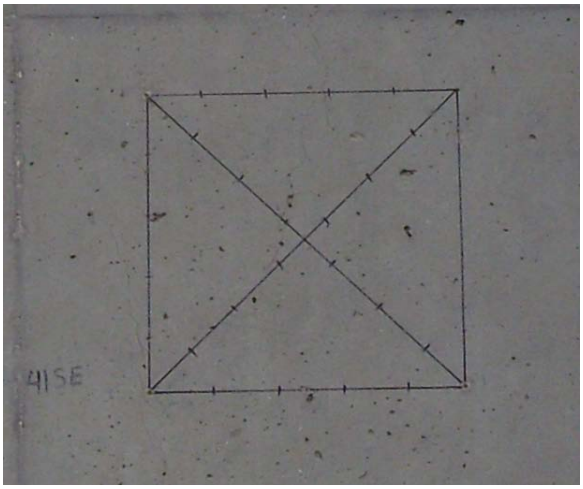

C – Column 41 SE Face 2013

Figure 213. Visual observation of Column 41 Southeast face.

A – Column 42 – SW Face 2006

B – Column 42 – SW Face 2009

C – Column 42 SW Face – 2011

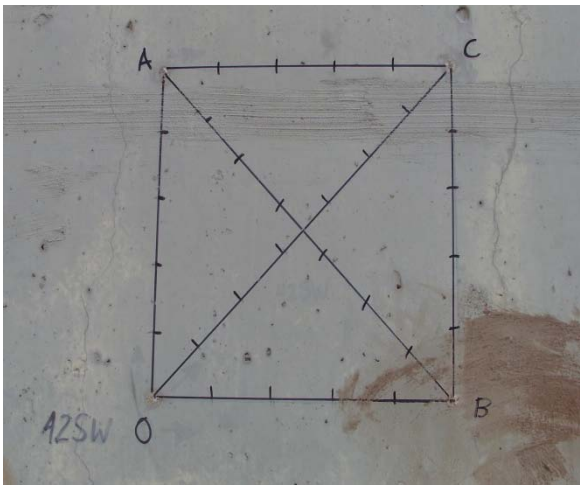

D – Column 42 SW Face - 2013

Figure 214. Visual observation of Column 42 Southwest face.

A – Column 42 SE Face – 2009

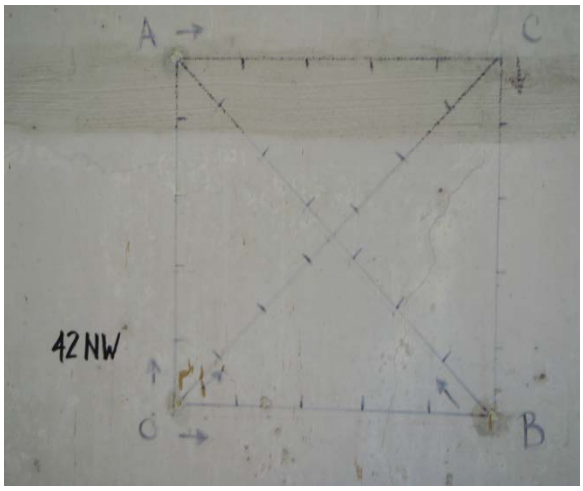

B - Column 42 SE Face 2011

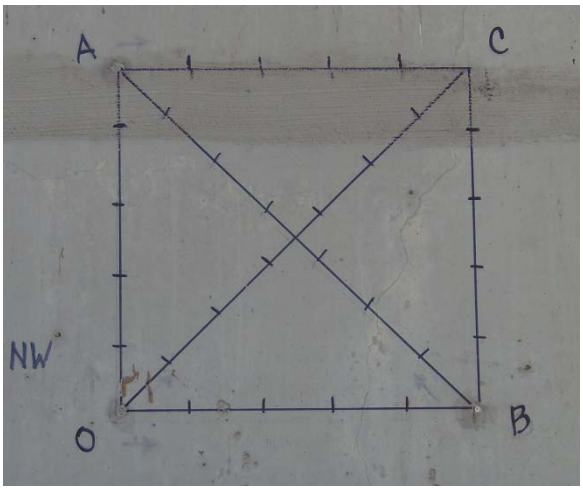

Figure 215. Visual observation of Column 42 Southeast face.

A – Column 43 SW Face 2006

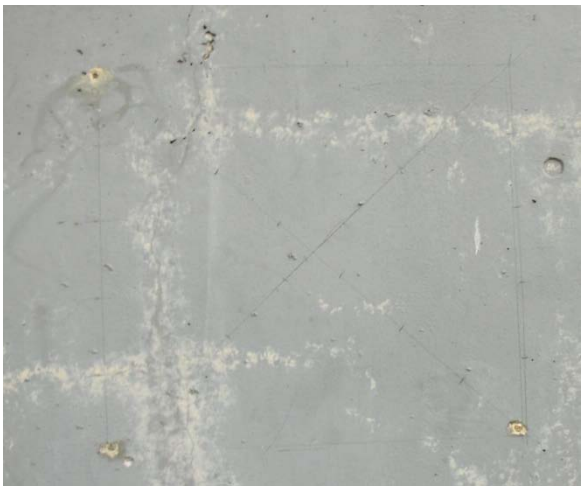

B – Column 43 SW Face 2009

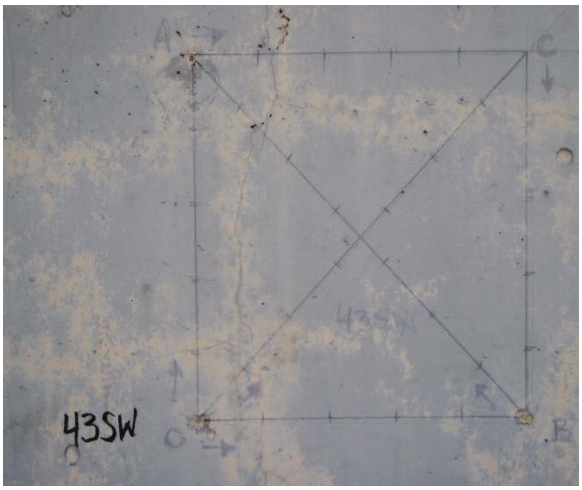

C – Column 43 SW Face 2011

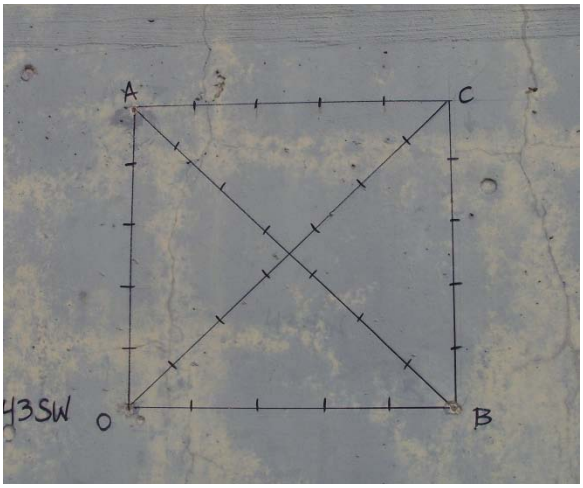

D – Column 43 SW Face 2013

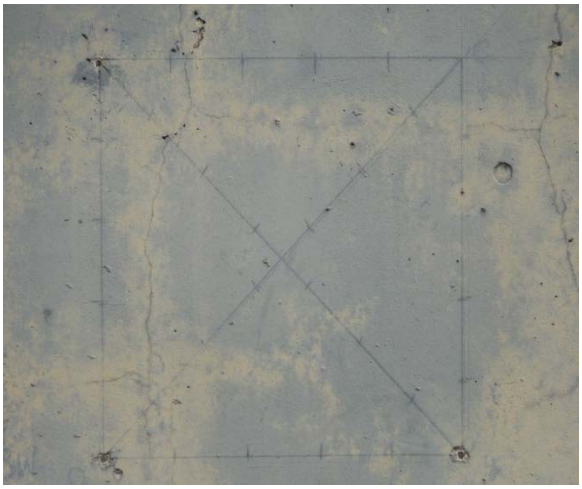

Figure 216. Visual observation of Column 43 Southwest face.

A – Column 43 SE Face 2006

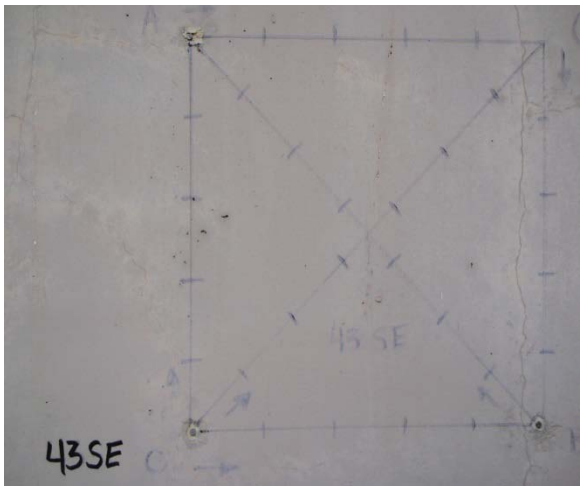

B – Column 43 SE Face 2009

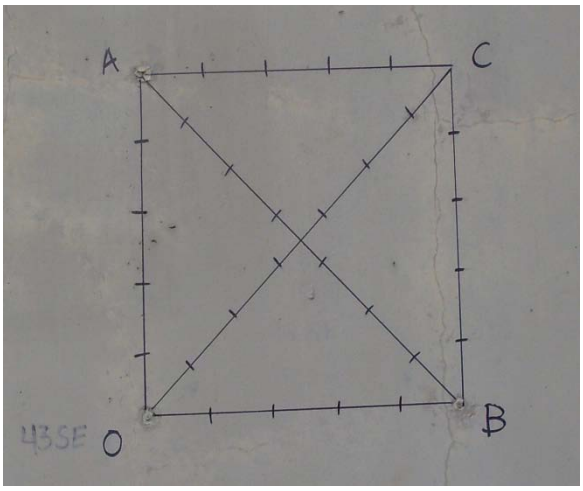

C – Column 43 SE Face 2013

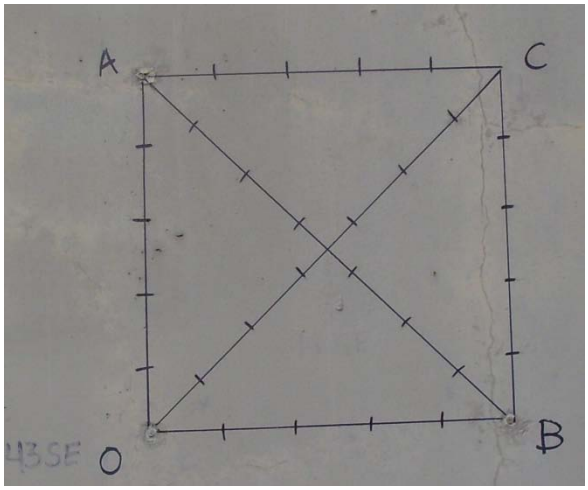

Figure 217. Visual observation of Column 43 Southeast face.

A – Column 44 SW Face 2009

B – Column 44 SW Face 2011

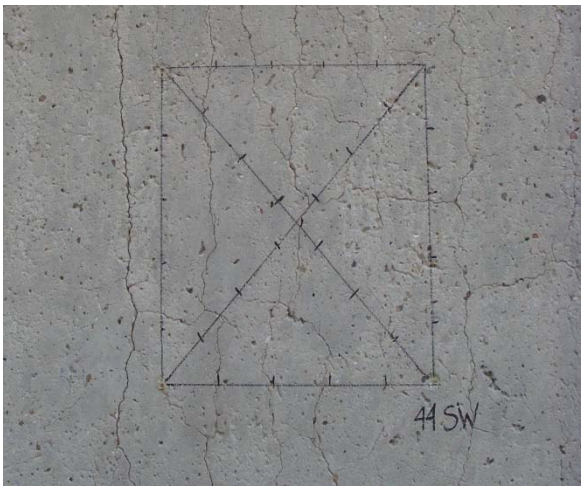

C – Column 44 SW Face 2013

Figure 218. Visual observation of Column 44 Southwest face.

A – Column 44 SE Face 2009

B – Column 44 SE Face 2011

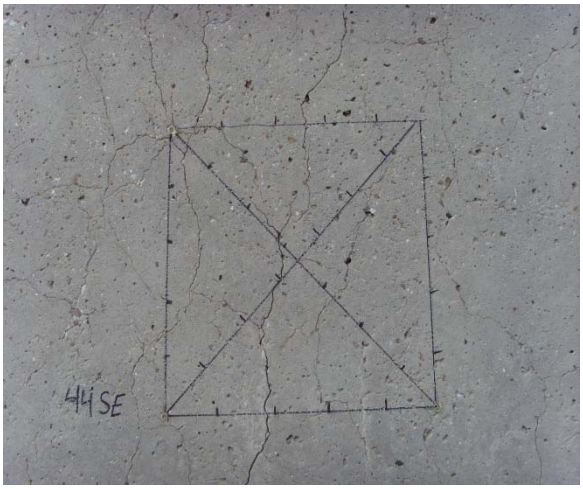

C – Column 44 SE Face 2013

Figure 219. Visual observation of Column 44 Southeast face.

A – Column 45 SW Face 2009

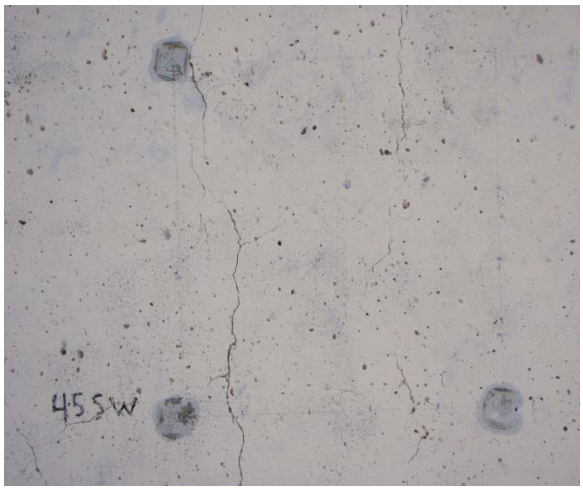

B – Column 45 SW Face 2011

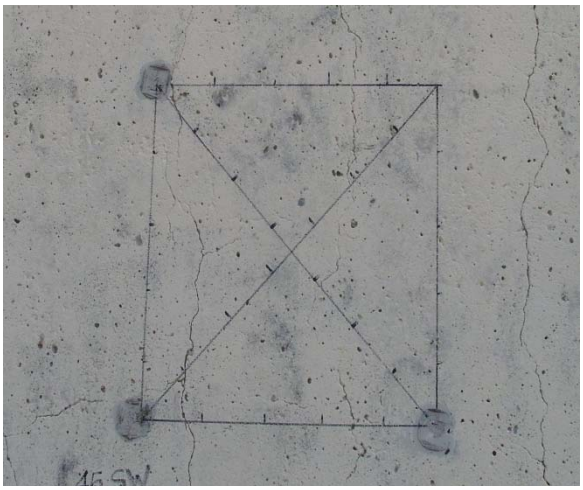

C – Column 45 SW 2013

Figure 220. Visual observation of Column 45 Southwest face.

A – Column 45 SE Face 2009

B – Column 45 SE Face 2011

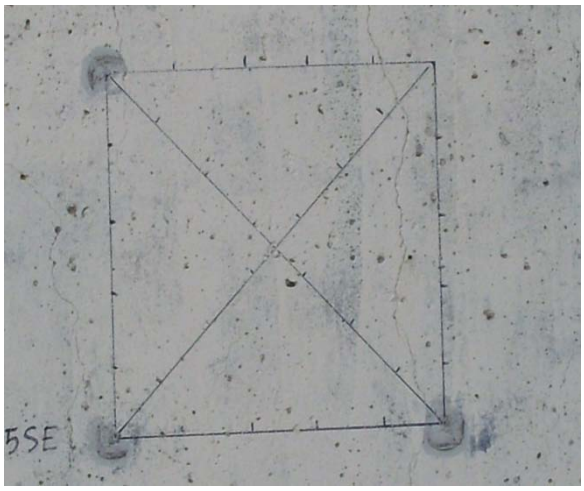

C – Column 45 SE Face 2013

Figure 221. Visual observation of Column 45 Southeast face.

A – Column 46 SW Face 2009

B – Column 46 SW Face 2011

C - Column 46 SW Face 2013

Figure 222. Visual observation of Column 46 Southwest face.

A – Column 46 SE Face 2009

B – Column 46 SE Face 2011

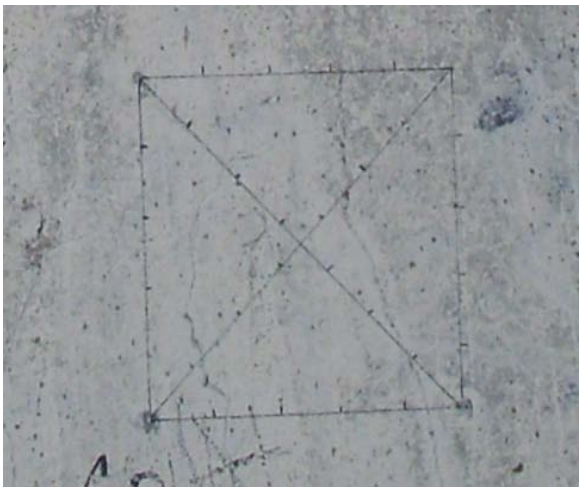

C – Column 46 – SE Face 2013

Figure 223. Visual observation of Column 46 Southeast face.

10.4 DATA ANALYSES

The results of expansion measurements taken over a seven year period, as previously shown in Figures 192 and 193, show some significant differences between the various test columns. Columns 31-36, those deemed to be the most distressed prior to treatment, generally showed continued expansion during the monitoring period, ranging from about 0.07 to 0.21 percent expansion, with an average expansion of about 0.12 percent. However, there were some differences in expansion between the various columns, with expansions being the lowest for the columns treated with silane over paint, sodium silicate over a blast surface, and lithium nitrate applied by vacuum impregnation. The average measured expansion was highest for Column 34,

which was treated electrochemically with lithium nitrate. The column that had its paint removed first, prior to silane treatment, expanded slightly more than the control column, which expanded by about 0.12 percent. The expansions measured for Columns 41-46 fell into two distinct groupings: three of the columns (44 – silane over blasted surface, 45 – lithium (vacuum), and 46 – lithium (electrochemical)) expanded about 0.12 percent during the monitoring period, while the other three columns (41 – silane/siloxane blend (vacuum), 42 (silane over paint), and 43 (control)) exhibited no measurable expansion and, in fact, showed slight shrinkage during the monitoring period.

What is most interesting and difficult to explain is that Column 42, the untreated control in the mild to moderate distress set, did not expand at all during the monitoring period. For reference, the other control column (Column 36) from the more distressed column set expanded about 0.12 percent during the same period. The reasons for the difference in behavior between the two control columns is not known, but conceivably, differences in materials, mixture proportions, construction methods, and exposure conditions may have led to this vastly different behavior. More discussion on some of these potential parameters, especially materials and mixture proportions, is provided later in this section.

When analyzing the overall expansion results, some interesting trends and/or observations emerge. First, columns in which silane was applied over the existing paint showed the lowest expansion in both sets of columns. This is surprising in that common practice is to remove existing paint prior to the application of silane (or similar coatings/sealers). However, the results of this investigation, as well as previous TxDOT research (Wehrle 2010), are consistent in that applying silane over existing appearance paint reduced both the potential for future expansion and the internal relative humidity. Paint removal is quite expensive and requires strict environmental standards in containing the removed paint, debris, dust, or liquid, and as such, it is quite advantageous to be able to apply coatings/sealers over the existing paint. However, the results included in this report and Wehrle (2010) do not automatically translate to all applications of silane over paint. The specific combination of paint and coating/sealer should be evaluated first to ensure that the underlying paint is breathable, that the silane is able to penetrate sufficiently, and that the combination reduces internal relative humidity or water uptake in accelerated tests, such as the NCHRP 244 Series II cube test (Pfeifer and Scali 1981), as described in detail by Wehrle (2010).

The two columns that were electrochemically treated with lithium exhibited relatively high expansions, at or near the maximum for each column set. This may be attributable to inherent differences between the columns in terms of materials, mixture proportions, and construction operations. But it is also worth discussing the results of the lithium profiling for these columns. Lithium was driven all the way to the reinforcing steel (depth of 50 mm or 2 in.) in a concentration estimated to be sufficient enough to suppress ASR-induced expansion. This is the most encouraging lithium penetration data generated under recent FHWA efforts and certainly suggests that electrochemical methods hold promise for treating ASR-affected structures with lithium compounds. However, one “side effect” of this process must be addressed. Figure 199 shows the sodium and potassium profiles, alongside the lithium profiles. Lithium ions were clearly driven to the reinforcing steel, as was the intention, but because the steel serves as a cathode in the electrochemical process, hydroxyl ions are produced at the surface of the

reinforcing steel. To maintain charge neutrality and to offset the production of hydroxyl ions at the reinforcing steel surface, sodium and potassium ions from within the concrete migrated towards the steel surface. This increase in the hydroxyl ion concentration and subsequent increase in alkali (sodium and potassium) concentration near the surface of the reinforcing steel could potentially exacerbate ASR-induced expansion and cracking in this region. More work is needed to determine if this redistribution of sodium and potassium towards the reinforcing steel has any adverse effects on long-term durability. There is insufficient data from this field trial alone to make this determination.

The expansion results for the columns treated with lithium nitrate by vacuum impregnation varied between the two column sets. In the first set of more distressed columns, the column treated with lithium by vacuum exhibited one of the lower expansions, but in the second set (Columns 41-46), the same treatment resulted in some of the higher expansions within the set. Aside from the other possible reasons for varying column behavior in this field trial, it is likely that the lithium nitrate would penetrate more easily under vacuum through the more heavily cracked column. The columns vacuum impregnated with a silane-siloxane blend or sodium silicate product showed relatively low expansions within both column sets.

When comparing the expansion of columns treated by silane over paint to the expansion of columns treated by silane after first removing paint, applying silane over paint resulted in lower expansions, which is in agreement with Wehrle (2010). The reasons for this are not known at this time, but one possible explanation may be that paint removal (either through sand blasting or wet media blasting) might adversely affect the surface of the concrete, potentially inducing microcracking or allowing for easier access of moisture. This is just postulation, but it is worth considering this as a potential issue in terms of transport mechanisms active at or near the concrete surface. Also, as discussed later, crack mapping becomes a bit more difficult on a surface that has been abraded, especially if a rough texture exists.

The two columns that were vacuum treated with products selected by TxDOT exhibited relatively low expansions within both column sets. The silane-siloxane blend, applied by vacuum, would be expected to penetrate deeper into concrete and enhance its ability to prevent liquid water from entering concrete while allowing vapor inside the concrete to escape. The sodium silicate product would not necessarily be expected to reduce internal relative humidity (this was confirmed from RH measurements), but perhaps the hardening of the concrete surface due to the sodium silicate application provides additional, physical resistance to expansion.
Significant data were collected on internal relative humidity from the test columns, as was summarized in Figures 194 and 195. Although relative humidity measurements tend to fluctuate more widely than expansion measurements, some trends were evident. Columns treated topically by silane (over paint or with paint removed), or by vacuum with a silane-siloxane blend showed consistently lower relative humidities than the other test columns, and after seven years of monitoring, all columns treated with silane or silane-siloxane blends exhibited expansion below the 80 percent threshold often cited as a target below which ASR-induced expansion slows considerably. Columns treated with either lithium nitrate or sodium silicate generally exhibited similar relative humidities as the untreated columns.

The results of extensive crack mapping, as shown in Figures 196 and 197, tend to follow similar trends as expansion, although there is quite a bit of noise in the data. Crack mapping is quite user sensitive and because this site was monitored over seven years under two different projects, several different individuals performed the measurements. Care was taken in keeping the measurement method consistent from individual to individual. Generally, the columns that expanded the most during the course of the monitoring showed parallel increases in CI values. Further, the three columns from the second set (41-46) that showed no expansion during the monitoring period also showed no increase in cracking in the same period. Some other factors that are worth noting is that crack mapping can be more challenging and variable when evaluating a rough surface, such as that created by paint removal. Also, there was some surface etching due to the electrochemical lithium treatment, and that also made it more difficult to track surface conditions of those columns. Nevertheless, as a whole, crack mapping was found to be a useful tool for tracking the progression of visible cracking. In addition, the crack mapping "square" serves other purposes, such as setting the corners for expansion measurements (both horizontal and vertical) and providing a consistent benchmark for taking photographs. Figures 200 to 223 make use of the cracking mapping regions as the focal point for photographs taken on each day of monitoring.

The application of lithium nitrate by vacuum impregnation increased its depth of penetration, with a penetration of about 8-12 mm (0.3-0.4 in.) of a concentration of lithium sufficient to reduce expansion. This penetration depth is higher than for typical topical applications of lithium nitrate, which tend to penetrate to depths of 1-5 mm (0.04-0.2 in.). However, it seems unlikely that this increase in penetration depth can justify the need for the additional equipment and expertise needed for such vacuum applications.

The overall results of this field trial, including both the laboratory and field monitoring components, suggest that ASR is the significant cause of expansion and cracking of the columns treated and monitored in Houston, TX. This is based on microstructural investigations, including the evaluation of polished and thin sections, residual expansion tests, and the overall progression of expansion and cracking in most of the columns. No symptoms of DEF were observed in any of the cores examined, and there does not appear to be the potential for future expansion due to DEF (based on the lack of expansion of small cores stored in lime water at room temperature). This was an important finding as ASR and DEF had been implicated as working in tandem in various structures in Texas (Folliard et al. 2006).

Through collaboration with TxDOT engineers, it was learned that these columns were cast in the late 1990s and the bridge was open to traffic in 2000. Based on typical practice in the late 1990s, the mixture proportions would have included a cement content of approximately 395-423 kg/m^3 (658-705 lbs/yd^3), with some columns potentially containing 20 percent Class C fly ash as replacement for portland cement. Based on the materials used at the time, ASR would likely be observed when using reactive aggregates in such mixtures. Although the fly ash would help to reduce the potential for ASR, typically more than 20 percent Class C fly ash is needed to suppress most of the reactive aggregates used in TxDOT applications. Lastly, the coarse aggregate used in these columns was a recycled concrete aggregate, and it is not known if the original concrete contained reactive aggregates.

A number of bridge structures in Texas also exhibited early-age thermal cracking during the time this bridge was constructed, which was prior to the implementation of specifications aimed at preventing ASR, DEF, and thermal cracking. Cracking of these test columns was reportedly noticed within the first few years after the bridge was open to traffic. It is quite possible that the columns, because of their relatively high cement content and large cross-sectional area, suffered from early-age thermal cracking. Using free software (ConcreteWorks) developed under TxDOT funding, analyses were performed to estimate the maximum temperature at the center of the columns and the maximum thermal gradient between the center and the surface of the concrete. Based on a variety of analyses based on casting at different times of the year, it was estimated that maximum temperatures would be in the range of 79-82 °C (175-180 °F) and that the maximum thermal gradient would be approximately 29-32 °C (85-90 °F). The maximum temperatures estimated would theoretically be enough to potentially cause DEF, but it depends on the length of time the concrete was above the nominal DEF threshold of 70 °C (158 °F). Further, if the concrete did contain 20 percent fly ash, it may be enough fly ash to chemically suppress DEF. The thermal gradients predicted were well above the typical gradient limit imposed for mass concrete of 20 °C (68 °F), and it is possible that such large temperature gradients could have led to early-age thermal cracking, especially shortly after formwork removal.

Figure 224 shows a photograph of the West face of Column 36. The larger vertical cracks could be caused by early-age thermal cracking as evidence of such cracking has been observed in bridges cast at the same time in the same general region of Texas. Once the thermal cracking occurs, water more easily can penetrate the columns, which can help promote ASR. This column is typical in that larger vertical cracks are visible, with branching or even map cracking emanating from the vertical cracks. A characteristic “buff” color can be observed around the cracks, which is typically associated with ASR-induced damage, and staining is evident.

Although it cannot be stated with a degree of certainty, it is possible that some of the test columns have been affected by thermal cracking, followed by cracking caused by ASR. This may also help to explain why some columns have performed differently from others. For example, Columns 41-43 showed no expansion or active cracking during the course of the monitoring period. It could be possible that these columns were less susceptible to thermal cracking, perhaps due to the use of fly ash or due to changes in ambient conditions while these three columns were cast. Following this line of thought, ASR may be much slower or not yet active in these columns as they were not exposed to the increased moisture ingress caused by more extensive thermal cracking that may have occurred in other columns.

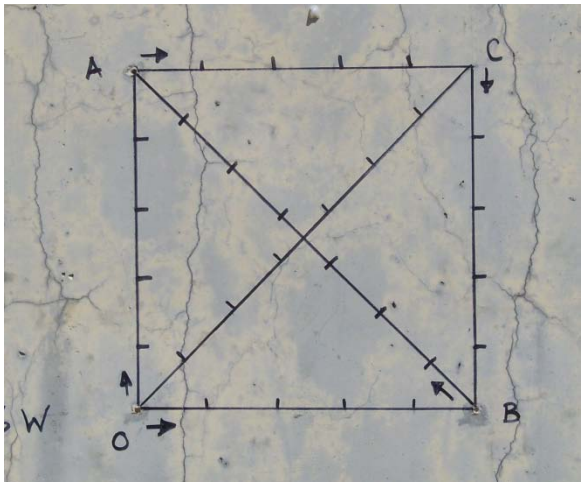

Figure 224. Extensive cracking evident on the West face of Column 36, possibly caused by early-age thermal cracking, followed by ASR.

10.5 SUMMARY

Through the use of an FHWA protocol (Fournier et al. 2010) for evaluating ASR-affected structures, it was determined that ASR was a significant cause of distress in various bridge columns in Houston, TX. Components of the protocol that were employed included:

- Visual survey and evaluation
- Petrographic evaluation of extracted cores (including the application of the Damage Rating Index [DRI])
- SEM analysis of thin section
- Residual expansion measurements
- In-situ expansion measurements of field elements
- Internal relative humidity measurement

Various treatments were applied to the test columns. In general, silanes and silane/siloxane blends were found to be effective in reducing internal relative humidity and reducing the potential for future expansion. The application of lithium nitrate through vacuum impregnation resulted in limited depths of penetration (8-12 mm, 0.3-0.5 in.), but electrochemical methods were able to drive lithium all the way to the reinforcing steel. However, it was also found that internal alkalies (sodium and potassium) were drawn to the surface of the steel because the steel serves as a cathode in the electrochemical process, resulting in the formation of hydroxyl ions. As such, it is possible that ASR may be exacerbated in the concrete adjacent to the reinforcing steel, due to the local increase in hydroxyl, sodium, and potassium concentrations. More research is needed to determine if the potential benefits of increased lithium penetration outweigh the potential negative effects of increased pore solution pH near the embedded reinforcing steel.

10.6 REFERENCES

Concrete Durability Center. ConcreteWorks. http://www.texasconcreteworks.com.

Folliard, K.J., Barborak, R., Drimalas, T., Du, L., Garber, S., Ideker, J., Ley, T., Williams, S., Juenger, M., Thomas, M.D.A. and Fournier, B. 2006. "Preventing ASR/DEF in New Concrete: Final Report." CTR 4085-5, Center for Transportation Research (CTR), The University of Texas at Austin.

Fournier, B., Tremblay, S. and Frenette, J. 2009. "Results of the Petrographic and Stiffness Damage Testing of Concrete Cores from the Princess Margaret Bridge, Fredericton, NB." Gemtec – Consulting Engineers and Scientists, 71 p.

Fournier, B., Bérubé, M.A., Folliard, K.J. and Thomas, M.D.A. 2010. "Report on the Diagnosis, Prognosis, and Mitigation of Alkali- Silica Reaction (ASR) in Transportation Structures." FHWA-HIF-09-004, Federal Highway Administration.

Pfeifer, D.W. and Scali, M.J. 1981. "Concrete Sealers for Protection of Bridge Structures." NCHRP Report 244, Transportation Research Board, 138 p.

Thomas, M.D.A., Folliard, K.J., Drimalas, T. and Ramlochan, T. 2008. "Diagnosing Delayed Ettringite Formation in Concrete Structures." *Cement and Concrete Research*, 38(6): 841-847.

Wehrle, E. 2010. "The Effects of Coatings and Sealers Used to Mitigate Alkali-Silica Reaction and/or Delayed Ettringite Formation in Hardened Concrete." M.S. Thesis, The University of Texas at Austin, Austin, TX.

11. CONCRETE STRUCTURES, WARWICK, RI

In May 2011, a field visit to a series of concrete structures around the State was conducted in the company of representatives from the Rhode Island Department of Transportation (RIDOT), including structures along Post Road and Post Road Extension, in Warwick, RI, near Providence (see Figure 225).

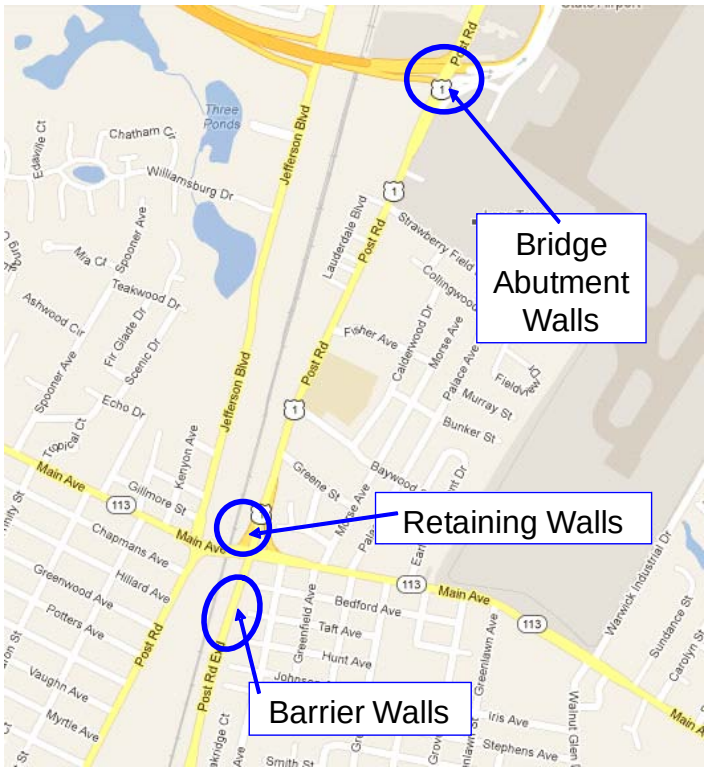

Figure 225. Google map showing location of the structures at the site.

The retaining wall is located adjacent to the southbound lane of traffic north of the Post Road Extension/Post Road and Main Avenue intersection. The structure shows a large scale map cracking pattern of overall moderate severity (see Figure 226A and Figure 226B). The barrier walls are located south of the same intersection (see Figure 226C and Figure 226D). The walls show severe longitudinal cracking in the chamfered base, and a light to moderate map cracking pattern in the upper part. The bridge abutment walls are at the intersection of Post Road and Airport Connector Road. The sections of the abutment walls sheltered from direct exposure to rain and sun show very limited visible cracking, while the exposed portions of the abutments and the wing walls show moderate map cracking (see Figure 226E and Figure 226F).

Figure 226. Structures on Post Road.
A: General view of the retaining wall on Post Road (southbound). B: Typical (moderate) map cracking affecting the wall. C: General view of the barrier walls on Post Road (southbound). D: Typical longitudinal cracking in the chamfered base of the barrier walls. E: General view of the bridge structure on Post Road (southbound view). F: Moderate cracking and localized exudations affecting the abutment and wing walls of the bridge.

11.1 SUMMARY OF PETROGRAPHIC EVALUATION

In October 2011, RIDOT cored the selected structures along Post Road and Post Road Extension. Table 70 lists the cores and the corresponding structures. Petrographic analysis was conducted on those cores.

Table 70. Cores provided for petrographic examination.

Core number	Location	Condition	Length cm (in.)
RI-1	Post Rd. Ext. S.B. - Greenwood Ramp Retaining Wall 8-3-2011	Core in 1 section	31.0 (12.2)
RI-2	Post Rd. Ext. S.B. - Greenwood Ramp Retaining Wall East Face 8-3-2012	Core in 1 section	26.1 (10.3)
RI-3	Post Rd. Ext. S.B. - Barriers 8-4-2011	Core in 1 section	5.2 (2.0)
RI-4	Post Rd. Ext. S.B. - Barriers 8-4-2011	Core in 1 section	12.9 (5.1)
RI-5	Post Rd. Ext. E.B. - Bridge Airport Connector 8-4-2011	Core in 1 section	24.7 (9.7)
RI-6	Post Rd. Ext. S.B. - Barriers 8-4-2011	Core in 1 section	18.2 (7.2)

Findings of the petrographic examination of the six concrete cores extracted by the Rhode Island DOT from bridge abutments, retaining wall, and barrier walls along the Post Road Ext. near Providence (Warwick), RI were reported to RIDOT. The evaluation mainly consisted of the Damage Rating Index (DRI), a method that provides a semi-quantitative assessment of the damage in concrete based on a count of petrographic features of deterioration generally associated with alkali-silica reaction (ASR).

Overall, cores RI-1/RI-2 (retaining wall; DRIs of 129 and 157) and RI-5/RI-6 (bridge; DRIs of 230 and 296) showed low to mild degree of deterioration/ASR-related damage. On the other hand, cores RI-3 and RI-4 (barrier walls; DRIs ranging from 285 to 546) showed moderate to high degree of deterioration/ASR-related damage (see Figure 227); aggregate particles in those cores show a wide variety of petrographic compositions (quartzite, granitic gneiss, sandstone). The highest contributors to the DRI for this set of cores are *Cracks in the cement paste with or without reaction product (CrCP – Cr+RPCP), Cracks in the aggregate particles (CrCA),* and *Air voids filled with reaction product (RPAV)* (see Figure 228). Silica gel was observed in this set of cores, mostly in cracks in the cement paste but also in aggregate particles and filling cement paste air voids.

In summary, the petrographic evaluation confirmed the presence of ASR in all structures that were cored. The extent of ASR and associated damage was found to range from low to moderate, a significant variation in the damage being observed from one location to another, as well as a function of the exposure conditions of the structural element examined.

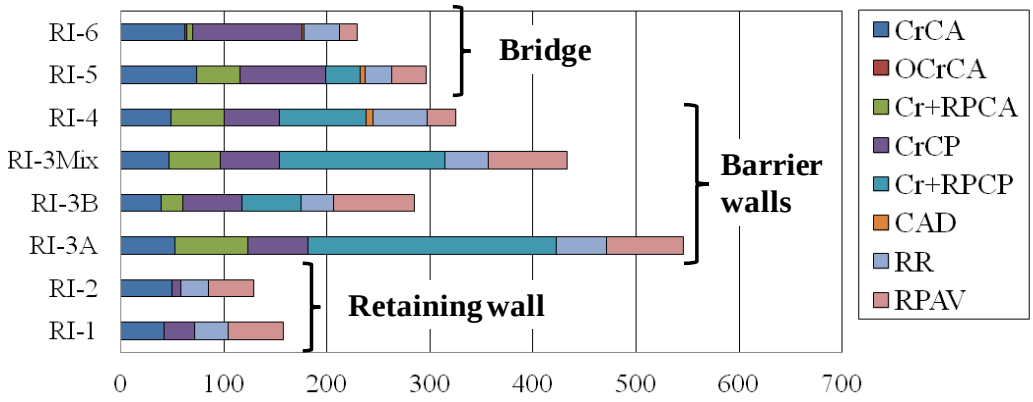

Figure 227. Results of the Damage Rating Index (DRI) for the Rhode Island cores. The colored cells give the proportions of each petrographic feature to the DRI value. (CrCA: cracking in the coarse aggregate particles; OCrCa: opened cracking in the coarse aggregate particles; Cr+RPCA: cracking in the coarse aggregate particles + reaction product; CrCP: cracking in the cement paste; Cr+RPCP: cracking in the cement paste + reaction product; CAD: coarse aggregate debonded; RR: reaction rim; RPAV: reaction products in air void of the cement paste).

A (distance between vertical lines = 1 cm [0.4 in.])

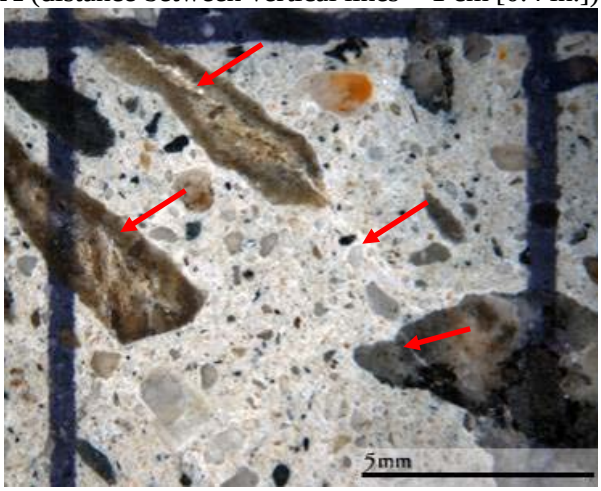

B (distance between vertical lines = 1 cm [0.4 in.])

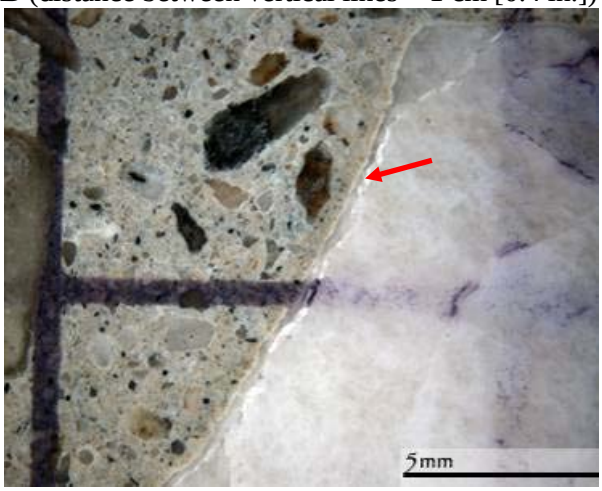

Figure 228. Polished concrete surfaces (cores extracted from the barrier walls along Post Road near Providence (Warwick), RI).
A&B: Cracking in coarse aggregate particles extending into the cement paste; secondary (ASR) products are observed in the cracks both in the particles and the cement paste. Dark reaction rims are observed surrounding the reactive aggregate particles.

11.2 SUMMARY OF APPLICATION REPORT

Based on the results of the field inspection and laboratory testing (diagnosis), which confirmed that ASR was the primary cause of distress at the different structures, a treatment plan involving the application of different types of surface treatment products (sealers, elastomeric coating) on various elements of the three structures on Post Road was implemented in 2012. In addition to the above treatments, a performance monitoring plan was developed and implemented to allow quantifying the effects of the various treatments over time. Details on the performance monitoring techniques and treatment activities are provided in chapters 2 and 3, respectively.

Within each of the structural elements, specific areas were identified for crack mapping, length-change, and humidity/temperature measurements. Figure 229A shows a performance monitoring area consisting of a 500-mm (20-in.) by 500-mm grid layout for length-change and crack mapping measurements; the latter was used for the bridge abutment walls and the retaining wall. In the case of the barrier walls, the distance from the top of the barrier to the chamfered base being too short for 500-mm (20-in.) vertical measurements, the layout shown in Figure 229B was rather employed. The dimensions of this layout are 150 mm (6 in.) in the vertical direction and 500 mm (20 in.) in the horizontal direction. This layout was used for vertical length-change measurements, while a 500 x 500 mm (20 in.) grid system was still used for the determination of the Cracking Index (see Figure 236).

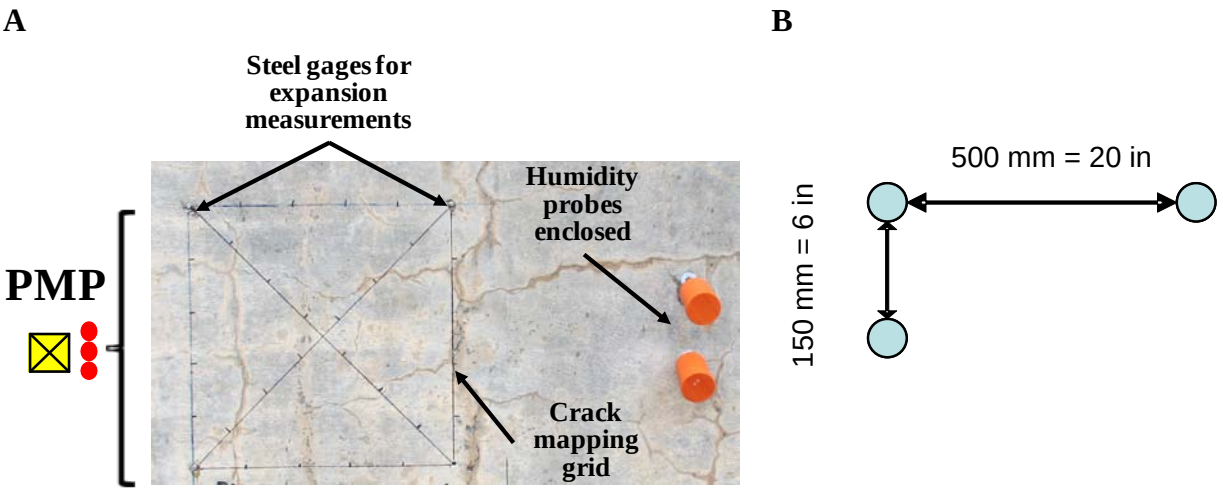

Figure 229. Performance monitoring area.
A: Area within a section of the retaining wall on Post Road instrumented with a crack mapping grid, expansion pins, and humidity sleeves and plugs for data collection (Performance Monitoring Package, PMP).
B: Expansion pin layout used in the case of the barrier walls.

The structures were treated during the summer of 2012. Three sealers were selected for application on separate sections of the above structures. The products correspond to a 100 percent silane, a 40 percent silane (water-based), and one elastomeric coating. Details on these products are given in chapter 3. Figure 230 and Table 71 give the details of the treatments and monitoring plan for each of the sites selected.

A – Retaining wall along Post Road

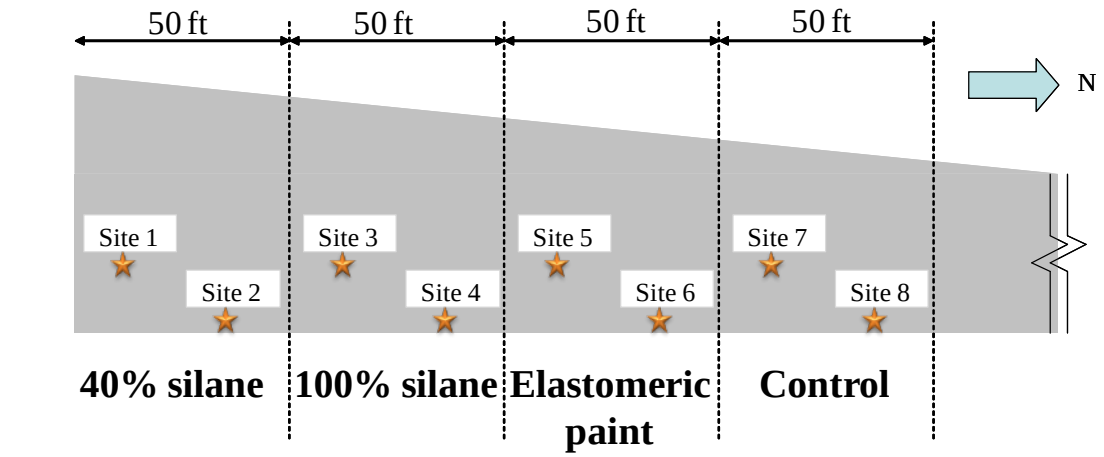

B – Barrier walls along Post Road

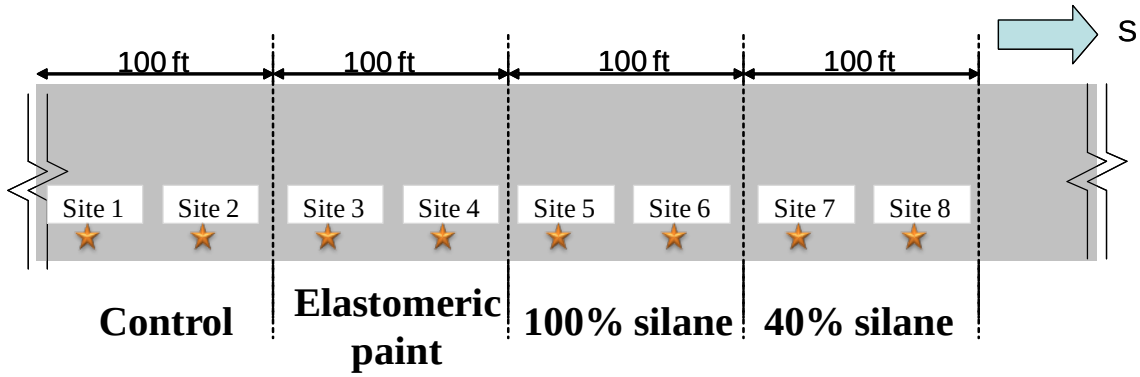

C – Bridge structure along Post Road

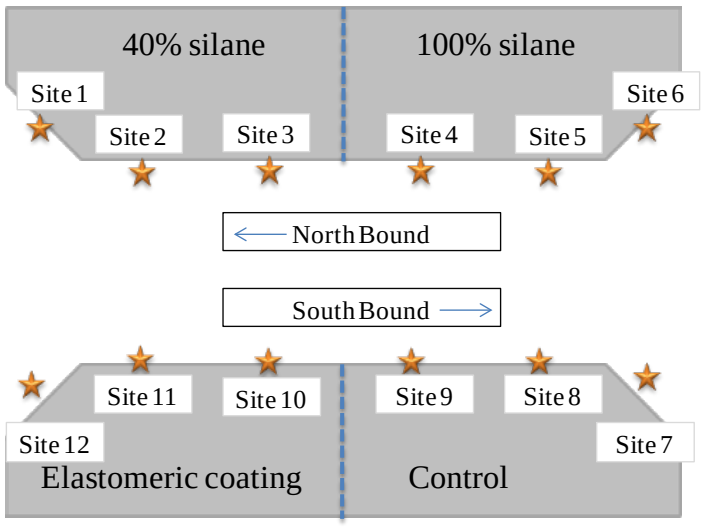

Figure 230. Treatment plan and monitoring sites (PMP) for the structures along Post Road in Warwick, RI.

Table 71. Treatment plan details and sites for performance monitoring.

Structure	Condition of the section	Monitoring site number (PMP)			
		Control	Elastomeric coating	40% silane	100% silane
Retaining wall	Sheltered	---	---	---	---
	Exposed	7,8	5,6	1,2	3,4
Bridge	Sheltered	9	10	3	4
	Exposed	7,8*	11*,12	1,2*	5*,6
Barrier walls	Sheltered	---	---	---	---
	Exposed	1,2	3,4	7,8	5,6

*Those sections are considered as partially exposed.

The 100 percent silane product was applied using a handheld pressurized container and spray nozzle. It was sprayed onto the surface of the different elements in a left-to-right-to-left pattern. This product was sprayed onto the surface as a clear liquid and dried as a clear coating.

The 40 percent silane (water-based) product was applied in the same way that the 100 percent silane product was applied. The 40 percent silane was sprayed on as a white liquid. While it dried, it became a clear coating.

The elastomeric coating product was applied like paint. Rollers and paint brushes were used instead of spray nozzles. Like the above silane products, one coat of material was applied as evenly as possible so that the entire area was covered.

The 40 percent silane and 100 percent silane materials were applied at a rate of about 3.7 m^2/L (150 ft^2/gal), while the elastomeric coating was applied with coats at a rate of 2.5 m^2/L (100 ft^2/gal).

Figure 231 gives examples of the surface treatment procedures, while Figure 232 illustrates some of the treated structures with the corresponding performance monitoring sites.

A

B

C

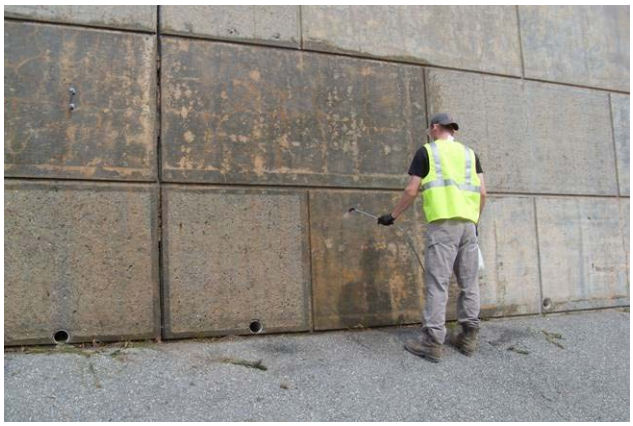

D

Figure 231. Application of surface treatments.
A: 40 percent silane (left) on the abutment wall of the bridge structure. B: Elastomeric coating on the wing wall of the bridge structure. C: 100 percent silane on the retaining wall. D: 100 percent silane on the barrier walls.

A

B

Figure 232. Examples of treatment and monitoring plans for different structures on Post Road in Warwick, RI.
A: Retaining wall. B: Barrier walls (elastomeric coating and PMP).

11.3 MONITORING DATA

This section presents the data obtained from internal relative humidity, length change, and crack mapping measurements from the three structures investigated over the period covered from June 2012, i.e., just before the treatments, to June 2013. It is to be noted that the average daily temperatures at the time of measurements ranged from 12 ^{o}C (53 ^{o}F) in October 2012 to 34 ^{o}C (93 ^{o}F) in June 2013.

Table 72 to Table 74 present the measured temperature and relative humidity for each of the performance monitoring sites. For the abutment walls of the bridge structure and the retaining wall, data are reported at 25-mm (~1 in.) and 75-mm (~3 in.) depths below the surface. In the case of the barrier walls, however, only the 25-mm (1-in.) hole was drilled because the width of the barrier wall was not wide enough to warrant a deeper hole. Also, one should note that some data are missing from the October 2012 and June 2013 field surveys. This is due to the fact that

some of the holes were filled with water or humid (condensation) to the point that no reliable readings could be taken from those holes.

Table 72. Relative humidity and temperature measurements - bridge abutment walls.

Section	Site	Depth	Data	June 2012	October 2012	June 2013
40% silane (water-based)	1	25 mm (1 in.)	°C (°F)	16.9 (62.4)	13.5 (56.3)	30.1 (86.2)
			RH%	93.3	96.1	90,0
		75 mm (3 in.)	°C (°F)	16.8 (62.2)	14.2 (57.6)	28.7 (83.7)
			RH%	91	92.1	90.6
	2	25 mm (1 in.)	°C (°F)	14.9 (58.8)	12.3 (54.1)	30.2 (86.4)
			RH%	92.3	87.7	76.7
		75 mm (3 in.)	°C (°F)	15.1 (59.2)	14.1 (57.4)	28.3 (82.9)
			RH%	93.8	93.3	83.3
	3	25 mm (1 in.)	°C (°F)	14.4 (57.9)	12.9 (55.2)	-
			RH%	92	96.7	-
		75 mm (3 in.)	°C (°F)	14.4 (57.9)	14.3 (57.7)	27.2 (81.0)
			RH%	92.5	93.1	91,0
100% silane	4	25 mm (1 in.)	°C (°F)	14.5 (58.1)	12.4 (54.4)	28.2 (82.8)
			RH%	93.5	92.6	81.8
		75 mm (3 in.)	°C (°F)	14.4 (57.9)	14.6 (58.3)	27 (80.6)
			RH%	92.3	90.2	80.4
	5	25 mm (1 in.)	°C (°F)	15.4 (59.7)	13.2 (55.8)	29.3 (84.7)
			RH%	93.7	93.4	80.5
		75 mm (3 in.)	°C (°F)	15.7 (60.3)	15.8 (60.4)	27.5 (81.5)
			RH%	88.5	92.6	86.1
	6	25 mm (1 in.)	°C (°F)	19.4 (66.9)	17.3 (63.1)	-
			RH%	92.7	91.3	-
		75 mm (3 in.)	°C (°F)	18.7 (65.7)	17.3 (63.1)	-
			RH%	91.8	91.3	-

Note: Some of the data are missing from the June 2013 field survey. Some of the holes were filled with water or humid (condensation) to the point that no reliable reading could be taken from those.

Table 72 (cont'd). Relative humidity and temperature measurements - bridge abutment walls.

Section	Site	Depth	Data	June 2012	October 2012	June 2013
Control	7	25 mm (1 in.)	°C (°F)	19 (66.2)	29.7 (85.5)	-
			RH%	87.5	84.6	-
		75 mm (3 in.)	°C(°F)	19.2 (66.6)	31.0 (87.8)	-
			RH%	91.1	86.6	-
	8	25 mm (1 in.)	°C (°F)	16.7 (62.1)	26.7 (80.1)	-
			RH%	88.4	90.6	-
		75 mm (3 in.)	°C (°F)	16.5 (61.7)	25.7 (78.3)	29.5 (85.1)
			RH%	88.2	78,0	74.3
	9	25 mm (1 in.)	°C (°F)	14.5 (58.1)	14.0 (57.2)	30.7 (87.3)
			RH%	90.4	94,0	81.9
		75 mm (3 in.)	°C (°F)	14.7 (58.3)	15.3 (59.5)	27.4 (81.3)
			RH%	93.1	87.3	82.7
Elastomeric coating	10	25 mm (1 in.)	°C (°F)	14.6 (58.3)	13.5 (56.3)	28.1 (82.6)
			RH%	85.6	84.6	78.9
		75 mm (3 in.)	°C (°F)	14.4 (57.9)	15.4 (59.7)	26.5 (79.7)
			RH%	88.5	91,0	88,0
	11	25 mm (1 in.)	°C (°F)	14.6 (58.3)	12.9 (55.2)	-
			RH%	81.5	89.6	-
		75 mm (3 in.)	°C (°F)	14.2 (57.6)	14.3 (57.7)	27.1 (80.8)
			RH%	93.2	88.7	83.8
	12	25 mm (1 in.)	°C (°F)	16.0 (60.8)	13.2 (55.8)	33.3 (91.9)
			RH%	94.3	94.2	89.5
		75 mm (3 in.)	°C (°F)	16.1 (61.0)	13.6 (56.5)	31.5 (88.7)
			RH%	90.5	90,0	83.8

Table 73. Relative humidity and temperature measurements - barrier walls.

Section	Site	Depth	Data	June 2012	October 2012	June 2013
Control	1	25 mm (1 in.)	°C (°F)	13.6 (56.5)	12.7 (54.9)	29.5 (85.1)
			RH%	87.6	79.2	87.5
	2	25 mm (1 in.)	°C (°F)	14.1 (57.4)	12.6 (54.7)	29.5 (85.1)
			RH%	92.5	87,0	89.5
Elastomeric coating	3	25 mm (1 in.)	°C (°F)	15.1 (59.2)	12.8 (55.0)	30.1 (86.2)
			RH%	92.5	92.7	89.1
	4	25 mm (1 in.)	°C (°F)	14.2 (57.6)	-	-
			RH%	90,0	-	-
100% silane	5	25 mm (1 in.)	°C (°F)	13.6 (56.5)	12.7 (54.9)	29.3 (84.7)
			RH%	87.5	81.9	82.7
	6	25 mm (1 in.)	°C (°F)	14.1 (57.4)	13.0 (55.4)	29.6 (85.3)
			RH%	94.1	82.3	85,0
40% silane (water-based)	7	25 mm (1 in.)	°C (°F)	14.1 (57.4)	12.9 (55.2)	29.3 (84.7)
			RH%	95.5	77.3	81.2
	8	25 mm (1 in.)	°C (°F)	13.7 (56.7)	12.8 (55.0)	-
			RH%	91.4	84.7	-

Note: Some of the data are missing from the June 2013 field survey. Some of the holes were filled with water or humid (condensation) to the point that no reliable reading could be taken from those.

Table 74. Relative humidity and temperature measurements - retaining wall.

Section	Site	Depth	Data	June 2012	October 2012	June 2013
40% silane (water-based)	1	25 mm (1 in.)	°C (°F)	17.1 (62.8)	-	-
			RH%	94.8	-	-
		75 mm (3 in.)	°C (°F)	17.1 (62.8)	-	38.2 (100.8)
			RH%	95.6	-	84.7
	2	25 mm (1 in.)	°C (°F)	17.6 (63.7)	-	-
			RH%	95.9	-	-
		75 mm (3 in.)	°C (°F)	17.2 (63.0)	-	-
			RH%	95.8	-	-
100% silane	3	25 mm (1 in.)	°C (°F)	17 (62.6)	-	-
			RH%	98.4	-	-
		75 mm (3")	°C (°F)	17.3 (63.1)	-	38.9 (102.0)
			RH%	97.8	-	80.5
	4	25 mm (1 in.)	°C (°F)	17.2 (63.0)	-	-
			RH%	95.7	-	-
		75 mm (3 in.)	°C (°F)	17 (62.6)	-	-
			RH%	91.6	-	-
Elastomeric coating	5	25 mm (1 in.)	°C (°F)	17.1 (62.8)	-	-
			RH%	97	-	-
		75 mm (3 in.)	°C (°F)	17.7 (63.9)	-	37.8 (100.0)
			RH%	93.1	-	73.6
	6	25 mm (1 in.)	°C (°F)	16.7 (62.1)	-	-
			RH%	95.6	-	-
		75 mm (3 in.)	°C (°F)	17.5 (63.5)	-	37.0 (98.6)
			RH%	91.5	-	83.1
Control	7	25 mm (1 in.)	°C (°F)	16.1 (61.0)	13.2 (55.8)	-
			RH%	93	85.6	-
		75 mm (3 in.)	°C (°F)	16.9 (62.4)	13.3 (55.9)	-
			RH%	90.8	82.2	-
	8	25 mm (1 in.)	°C (°F)	15.8 (60.4)	-	-
			RH%	93.1	-	-
		75 mm (3 in.)	°C (°F)	17.2 (63.0)	-	38.5 (101.3)
			RH%	92.1	-	83.7

Note: Some of the data are missing from the October 2012 and June 2013 field surveys. Some of the holes were filled with water or humid (condensation) to the point that no reliable reading could be taken from those.

Table 75 to Table 77 give the results of length change measurements made between June 2012 and June 2013. With the June 2012 measurements serving as the "0" reading, no "expansion" data can be calculated for that time. Expansion data are reported for a 500-millimeter (~20-in.) gauge-length in the horizontal direction for all structures, as well as the vertical direction in the case of the retaining wall and the bridge abutment walls. In the case of the barrier walls, vertical expansions are given for a 150-mm (~6-in.) gauge length. The data were not corrected for temperature (thermal) effects.

Table 75. Expansion results (%) - bridge abutment walls.

Section	Site	Location	June 2012 13°C (55°F)*	October 2012 12°C (53°F)*	June 2013 34°C (93°F)*
40% silane (water-based)	1	Vertical	"0" reading	-0.016	-0.003
		Horizontal	"0" reading	-0.011	0.012
	2	Vertical	"0" reading	0.000	0.010
		Horizontal	"0" reading	-0.001	0.008
	3	Vertical	"0" reading	0.004	0.008
		Horizontal	"0" reading	-0.001	0.012
100% silane	4	Vertical	"0" reading	0.001	0.012
		Horizontal	"0" reading	0.001	0.008
	5	Vertical	"0" reading	0.000	0.004
		Horizontal	"0" reading	0.005	0.017
	6	Vertical	"0" reading	0.001	0.008
		Horizontal	"0" reading	-0.009	0.006
Control	7	Vertical	"0" reading	0.001	0.013
		Horizontal	"0" reading	-0.002	0.018
	8	Vertical	"0" reading	0.000	0.016
		Horizontal	"0" reading	0.015	0.039
	9	Vertical	"0" reading	-0.001	0.004
		Horizontal	"0" reading	0.000	0.005
Elastomeric coating	10	Vertical	"0" reading	0.002	0.009
		Horizontal	"0" reading	0.002	0.012
	11	Vertical	"0" reading	-0.001	0.009
		Horizontal	"0" reading	-0.011	0.005
	12	Vertical	"0" reading	-0.025	-0.003
		Horizontal	"0" reading	0.000	0.031

*The temperature corresponds to the daily average obtained from http://www.wunderground.com

Table 76. Expansion results (%) - barrier walls.

Section	Site	Location	June 2012 16°C (61°F)	October 2012 12°C (53°F)	June 2013 34°C (93°F)
Control	1	Vertical	"0" reading	-0.006	0.002
		Horizontal	"0" reading	0.006	0.021
	2	Vertical	"0" reading	-0.007	-0.003
		Horizontal	"0" reading	0.006	0.016
Elastomeric coating	3	Vertical	"0" reading	-0.008	-0.013
		Horizontal	"0" reading	0.007	0.021
	4	Vertical	"0" reading	-0.013	-0.027
		Horizontal	"0" reading	-0.004	-0.005
100% silane	5	Vertical	"0" reading	-0.018	-0.008
		Horizontal	"0" reading	-0.003	0.009
	6	Vertical	"0" reading	-0.008	-0.001
		Horizontal	"0" reading	-0.009	0.003
40% silane (water-based)	7	Vertical	"0" reading	-0.008	-0.004
		Horizontal	"0" reading	0.001	0.016
	8	Vertical	"0" reading	-0.004	0.001
		Horizontal	"0" reading	-0.001	0.006

*The temperature corresponds to the daily average obtained from http://www.wunderground.com

Table 77. Expansion results (%) - retaining wall.

Section	Site	Location	June 2012 13°C (55°F)*	October 2012 12°C (53°F)*	June 2013 34°C (93°F)*
40% silane (water-based)	1	Vertical	"0" reading	-0.001	0.014
		Horizontal	"0" reading	-0.006	0.006
	2	Vertical	"0" reading	-0.012	0.002
		Horizontal	"0" reading	0.003	0.011
100% silane	3	Vertical	"0" reading	-0.008	0.006
		Horizontal	"0" reading	0.001	-0.001
	4	Vertical	"0" reading	-0.009	0.004
		Horizontal	"0" reading	-0.003	0.006
Elastomeric coating	5	Vertical	"0" reading	-0.009	0.004
		Horizontal	"0" reading	-0.028	-0.015
	6	Vertical	"0" reading	-0.015	-0.003
		Horizontal	"0" reading	-0.018	0.008
Control	7	Vertical	"0" reading	0.001	0.030
		Horizontal	"0" reading	0.002	0.019
	8	Vertical	"0" reading	-0.012	0.027
		Horizontal	"0" reading	-0.001	0.013

*The temperature corresponds to the daily average obtained from http://www.wunderground.com

Table 78 to Table 80 show the results of Cracking Index measurements made between June 2012 and June 2013. CI data are given in mm/m (or in./yd) as they correspond to the total crack opening, in mm (in.), averaged over a one-meter (or one-yard) length; they are calculated from the measurement of crack widths along a grid system composed of the four lines of a 500-mm (20-in.) square and of the two 700-mm (28-in.) diagonal lines (total of 3.4 m (11 ft) of lines). In general, the higher the CI values, the higher the extent of (surface) damage on the concrete element investigated.

Table 78. Cracking Index measurements - bridge abutment walls.

Section	Site	June 2012 mm/m (in./yd)	October 2012 mm/m (in./yd)	June 2013 mm/m (in./yd)
40% silane (water-based)	1	0.69 (0.025)	0.48 (0.017)	0.56 (0.020)
	2	0.71 (0.026)	0.57 (0.020)	0.57 (0.020)
	3	0.12 (0.004)	0.09 (0.003)	0.11 (0.004)
100% silane	4	0.34 (0.012)	0.24 (0.009)	0.28 (0.010)
	5	0.63 (0.023)	0.65 (0.023)	0.73 (0.026)
	6	0.63 (0.023)	0.48 (0.017)	0.63 (0.023)
Control	7	1.64 (0.059)	1.52 (0.055)	1.74 (0.063)
	8	1.54 (0.055)	1.48 (0.053)	1.68 (0.060)
	9	0.23 (0.008)	0.25 (0.009)	0.30 (0.011)
Elastomeric coating	10	0.35 (0.013)	0.00 (0.000)	0.00 (0.000)
	11	0.37 (0.013)	0.00 (0.000)	0.00 (0.000)
	12	0.87 (0.031)	0.00 (0.000)	0.00 (0.000)

Table 79. Cracking Index measurements - retaining wall.

Section	Site	June 2012 mm/m (in./yd)	October 2012 mm/m (in./yd)	June 2013 mm/m (in./yd)
40% silane (water-based)	1	1.16 (0.042)	0.25 (0.009)	0.36 (0.013)
	2	0.73 (0.026)	0.1 (0.004)	0.39 (0.014)
100% silane	3	0.83 (0.030)	0.48 (0.017)	0.58 (0.031)
	4	0.77 (0.028)	0.42 (0.015)	0.54 (0.019)
Elastomeric coating	5	1.18 (0.042)	0.00 (0.000)	0.00 (0.000)
	6	0.74 (0.027)	0.00 (0.000)	0.00 (0.000)
Control	7	1.19 (0.043)	0.45 (0.016)	0.73 (0.026)
	8	0.96 (0.034)	0.36 (0.013)	0.68 (0.024)

Table 80. Cracking Index measurements -barrier walls.

Section	Site	June 2012 mm/m (in./yd)	October 2012 mm/m (in./yd)	June 2013 mm/m (in./yd)
Control	1	0.79 (0.028)	0.99 (0.036)	0.68 (0.024)
	2	0.52 (0.019)	0.48 (0.017)	0.60 (0.022)
Elastomeric coating	3	1.01 (0.036)	-	0.00 (0.000)
	4	12.65 (0.454)	-	0.00 (0.000)
100% silane	5	0.85 (0.031)	0.82 (0.029)	0.77 (0.028)
	6	0.27 (0.010)	0.40 (0.014)	0.44 (0.016)
40% silane (water-based)	7	0.69 (0.025)	0.86 (0.031)	0.90 (0.031)
	8	0.28 (0.010)	0.36 (0.013)	0.72 (0.026)

Figure 233 to Figure 236 show examples of crack map sections for the bridge abutment walls, retaining wall, and barrier walls.

A – Bridge 40% silane (site 3: not exposed) 2013

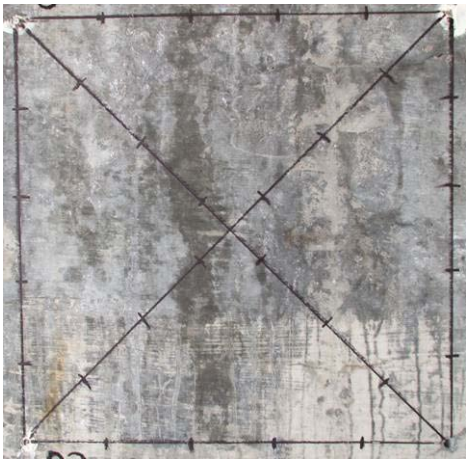

B – Bridge 40% silane (site 1: exposed) 2013

C – Bridge 100% silane (site 4: not exposed) 2013

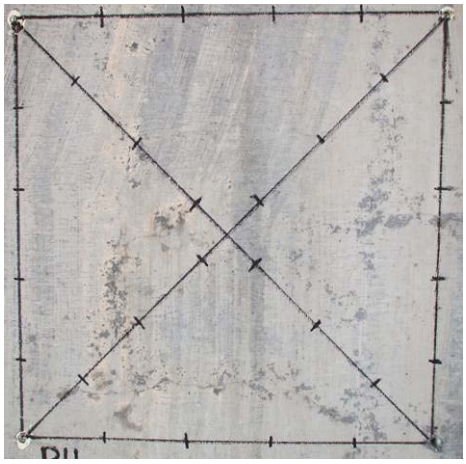

D – Bridge 100% silane (site 6: exposed) 2013

E – Bridge Control (site 8: not exposed) 2013

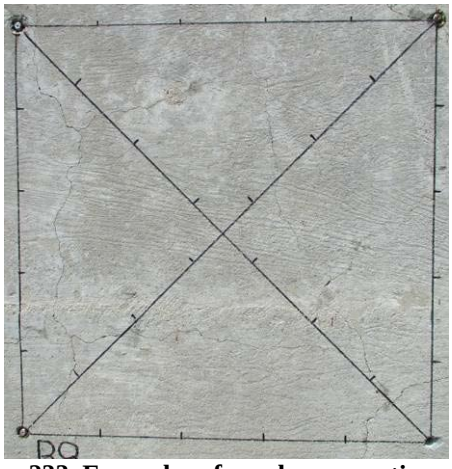

F – Bridge Control (site 7: exposed) 2013

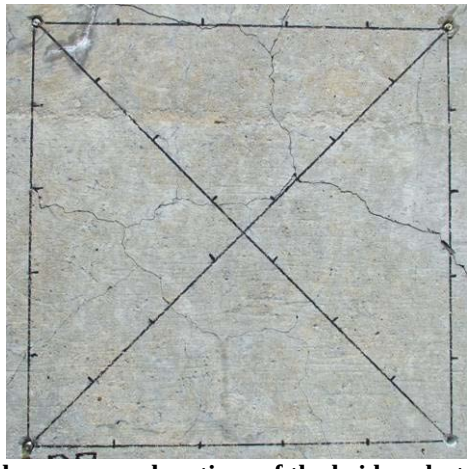

Figure 233. Examples of crack map sections for exposed and non-exposed sections of the bridge abutment walls.

A – 40% silane (site 1: exposed) 2012

B – 40% silane (site 1: exposed) 2013

C – 100% silane (site 6: exposed) 2012

D – 100% silane (site 6: exposed) 2013

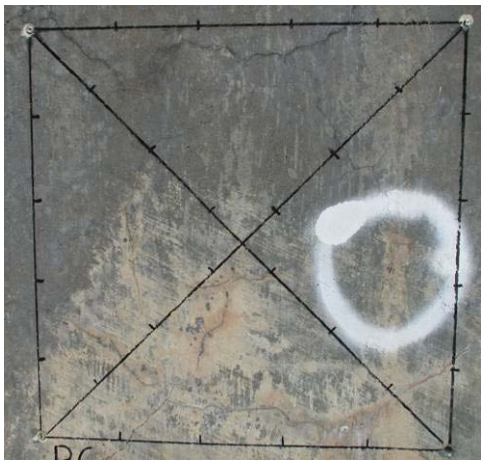

E – Control (site 7: exposed) 2012

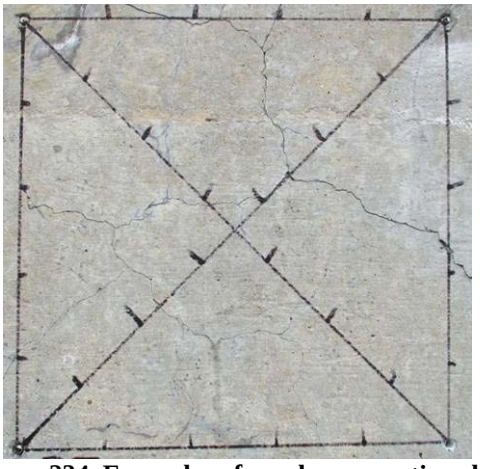

F – Control (site 7: exposed) 2013

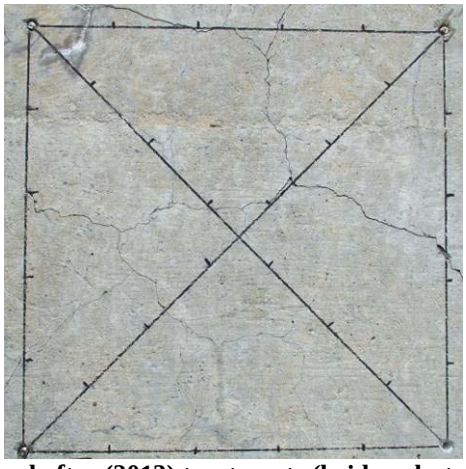

Figure 234. Examples of crack map sections before (2012) and after (2013) treatments (bridge abutment walls).

A – 40% silane (site 1: exposed) 2012

B – 40% silane (site 1: exposed) 2013

C – 100% silane (site 4: exposed) 2012

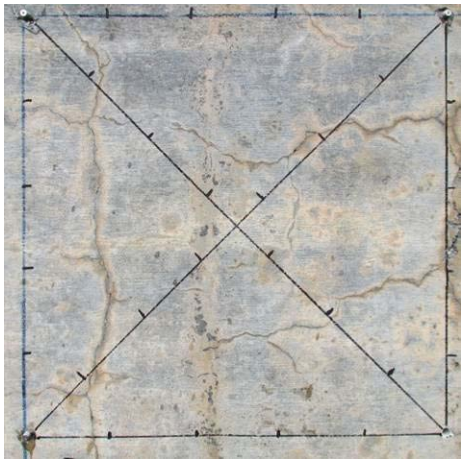

D – 100% silane (site 4: exposed) 2013

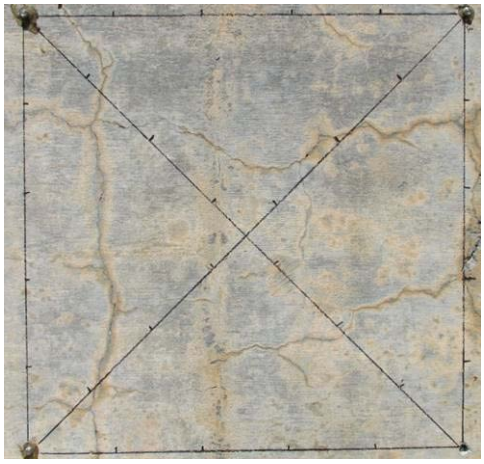

E – Control (site 7: exposed) 2012

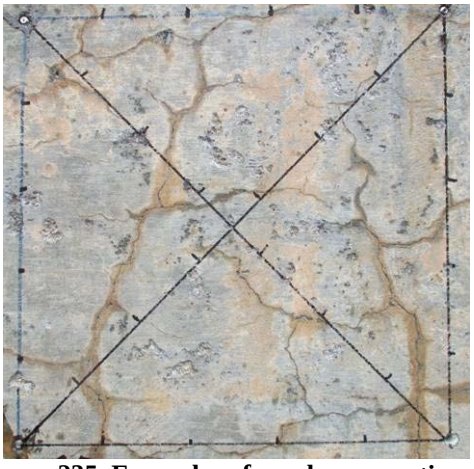

F – Control (site 7: exposed) 2013

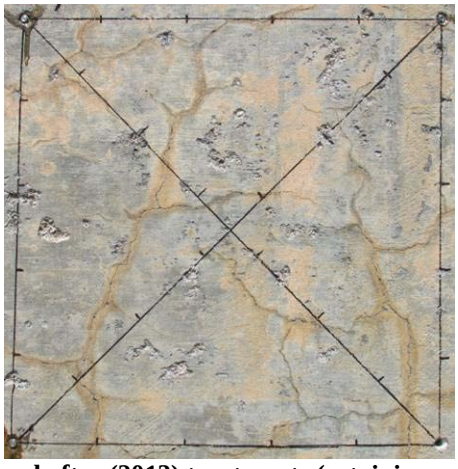

Figure 235. Examples of crack map sections before (2012) and after (2013) treatments (retaining wall).

A – Control (site 2: exposed) 2012

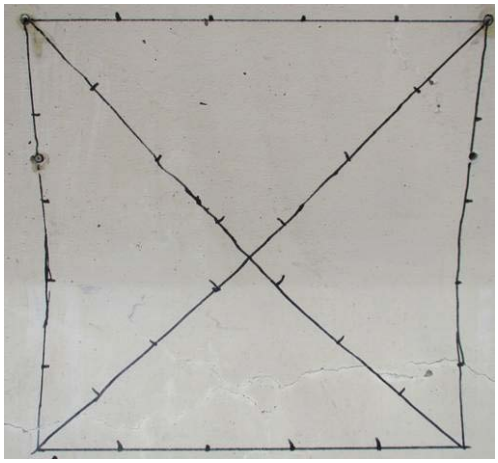

B – Control (site 2: exposed) 2013

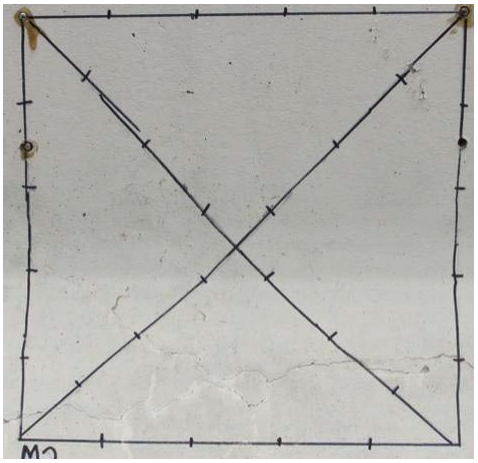

C – Elastomeric coating (site 4: exposed) 2012

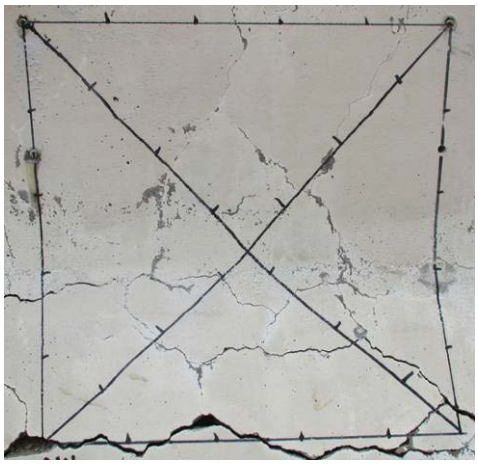

D – Elastomeric coating (site 4: exposed) 2013

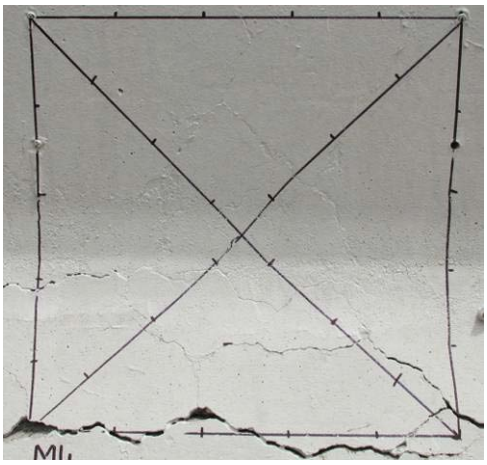

E – 40% silane (site 7: exposed) 2010

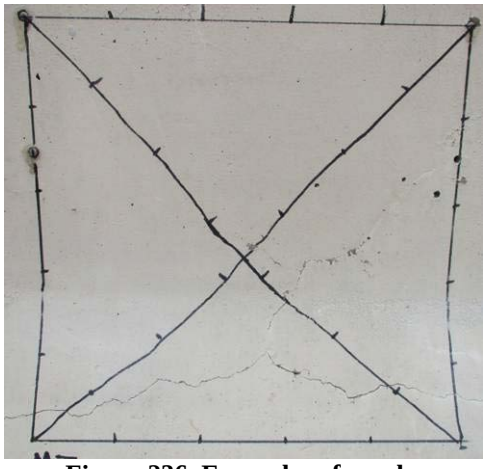

F – 40% silane (site 7: exposed) 2013

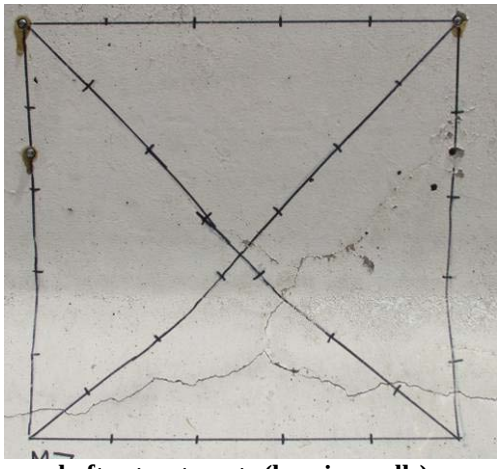

Figure 236. Examples of crack map sections before and after treatments (barrier walls).

11.4 DATA ANALYSES

Considering that ASR was found to be a contributing factor to the deterioration observed in the structures selected for treatment in Warwick, RI, it is important to keep in mind the main objectives of this investigation:

- Main objective: evaluate the long term efficacy of various types of surface treatment, for instance sealers and coating, to control the progress of deterioration in ASR-affected concrete members;
- Secondary objectives: further analyze this efficacy as a function of:
  - Different types of elements (treated vs. control, different types of structural elements – barrier walls, abutment walls, retaining wall),
  - Different exposure conditions (for instance in relation to the exposure conditions, e.g., direct exposure to rain, availability of moisture from backfill material (retaining wall), direct exposure to sun (UV degradation of the sealer), etc.),
  - Different types of products.

First, it should be noted that because of the timing of the applications (June 2012), only limited performance monitoring data are available after treatment (about 12 months). Actually, the June 2012 data served as the initial (or "0") reading. Consequently, in general, it is too early to be able to draw any significant conclusions from the monitoring data accumulated so far.

In concrete members exposed outdoors, internal RH values would be expected to increase with depth, RH values sometimes fluctuating significantly in the “surficial” portion of a concrete element due to local environmental conditions. The use of “breathable” or penetrating sealers are expected to contribute to progressively reducing RH values close to the surface due to their hydrophobic properties. Such a behavior had been measured in ASR-affected barrier walls treated with sealers in Quebec City, Canada (Bérubé et al. 2002a); however, such a trend was established over a six-year monitoring period because significant punctual/seasonal variations were observed due to variations in temperature, humidity, rain, and sun exposure conditions. Bérubé et al. (2002b) also showed that not all surface treatment products had an equivalent efficacy in reducing the internal humidity and controlling expansion due to ASR.

So far, because of the large temperature differences and the limited number of field surveys, there are no consistent/conclusive trends that can be obtained from the RH measurements in the Rhode Island structures investigated. One needs to keep in mind that in the case of the retaining wall, moisture is also available from the backfill material behind the wall. Also, numerous RH values are missing from the October 2012 and June 2013 field surveys. This is due to the fact that some of the holes were filled with water or humid (condensation) to the point that no reliable reading could be taken from those. Also, in the case of the barrier walls, moisture would be available from both sides. This is why the treatment was actually applied on both sides of the barrier walls to try optimizing its efficacy. Finally, in the case of the bridge structure, it will be interesting to determine the differences in the internal concrete moisture contents, and between the different products, for sections exposed to direct moisture and those sheltered from direct moisture (rain) (i.e., under the bridge deck).

Regarding the expansion measurements, no conclusive trends can be extracted from the data so far. A slight expansive behavior seems to be noticeable for the June 2013 data; however, this is likely related to a thermal effect since the average temperature (34 ^{o}C (93 ^{o}F)) on that day was significantly higher than that from the previous field surveys (13 and 12 ^{o}C (55 and 53 ^{o}F)).

Finally, regarding the Cracking Index (CI) values, it is interesting to note that the degree/extent of cracking is actually significantly different between the various monitoring sites. This was particularly the case for the barrier walls, although all were exposed to similar conditions. In the case of the bridge abutment walls, sites exposed to direct moisture (e.g., 1, 6, 7, and 12) showed a higher degree of visual damage and consequently higher CI values than those protected under the bridge deck (e.g., 3, 4, 9, and 10). This can be observed in Figure 233, which illustrates the condition of selected concrete sections (monitoring sites) as a function of exposure conditions. One should also remember that, in addition to the operator, the temperature and moisture state of the concrete can have a significant impact on the CI values. In our case, the CI measurements were made by the same operator, which is minimizing the variations between readings.

No significant differences/progression in the CI values were observed for individual monitoring sites over the one-year monitoring period completed in the case of the abutment walls and barrier walls; this can be noted in Figure 234 to Figure 236 that illustrate the condition, as a function of time (2012 – 2013), of sections that were subjected to various treatments.

It is to be noted that in the case of the sections treated with the elastomeric paint, CI values of "0" were obtained for the measurements carried out following the application of the coating since the product was efficient in bridging the cracks present in the different concrete members.

Significant drops in CI values were however observed from the initial measurement (June 2012) and the following readings (i.e., October 2012 and June 2013) in the case of the retaining wall sections. The exact reason for this behavior is currently unknown; it could perhaps be related to the effect of exposure conditions on this particular structure. This behavior will be further investigated.

11.5 SUMMARY

The results from field survey and laboratory investigations confirmed that ASR was a contributing factor in the deterioration of concrete structures on Post Road in Warwick, RI. It was concluded that these structures would make a suitable test section for the FHWA ASR Development and Deployment Program. The elements selected for treatments include bridge abutment and wing walls, a retaining wall, and barrier walls.

A treatment plan involving the application of different types of surface treatment products (sealers, elastomeric coating) on various elements of the three structures on Post Road was implemented in 2012. In addition to the above treatments, a performance monitoring plan was also developed and implemented to allow quantifying the effects of the various treatments over time. Within each of the structural elements, specific areas were identified for implementation of

a Performance Monitoring Package (PMP), including crack mapping, expansion measurements, and temperature/humidity readings.

With only one year of monitoring data accumulated, it is currently too early to conclude on the efficacy of the above treatments at reducing the deleterious effects of ASR on the structures treated. However, long term monitoring of the above structure is expected to provide data on the effect of various types of surface treatments on different types of structures incorporating a range of reactive aggregates.

11.6 REFERENCES

Bérubé, M.A., Chouinard, D., Pigeon, M., Frenette, J., Rivest, M. and Vézina, D. 2002a. "Effectiveness of Sealers in Counteracting Alkali-Silica Reaction in Highway Median Barriers Exposed to Wetting and Drying, Freezing and Thawing, and Deicing Salts." *Canadian Journal of Civil Engineering*, 29(2): 329-337.

Bérubé, M.A., Chouinard, D., Pigeon, M., Frenette, J., Rivest, M. and Vézina, D. 2002b. "Effectiveness of Sealers in Counteracting Alkali-Silica Reaction in Plain and Air-Entrained Laboratory Concretes Exposed to Wetting and Drying, Freezing and Thawing, and Salt Water." *Canadian Journal of Civil Engineering*, 29(2): 289-300.

12. BARRIER WALLS, NEAR MONTPELIER, VT

On May 12th, 2010, a field visit to twin bridge structures was conducted in the company of representatives from The Vermont Agency of Transportation (VAOT). The structures correspond to two bridges, approximately 300 meters (900 feet) long, consisting of two lanes in the north and south directions along Interstate 89 (I-89) that span the Dog River, U.S. 2/State Street, and Dog River Road (see Figure 237).

The barrier walls display a mixture of map and aligned (longitudinal) cracking with severity ratings ranging from mild to severe (see Figure 238D). During this visit, six cores were taken from different sections of the parapet walls for petrographic examination. Figure 238E and Figure 238F illustrate coring sites showing a moderate-to-severe and mild degree of damage, respectively.

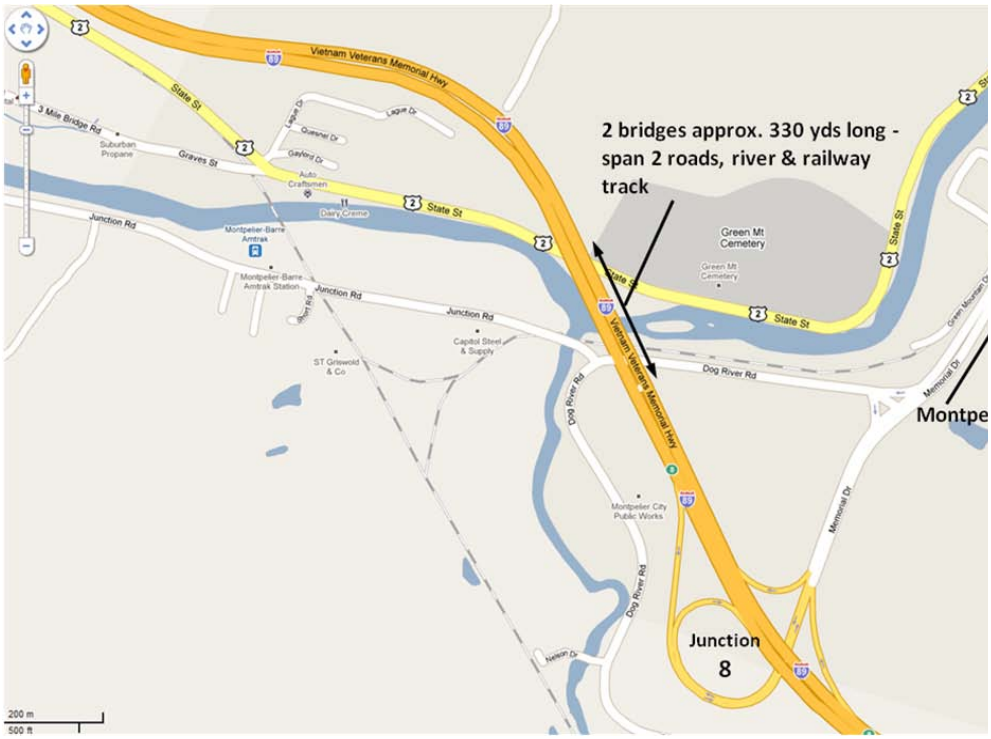

Figure 237. Google map showing location of the structure at the site.

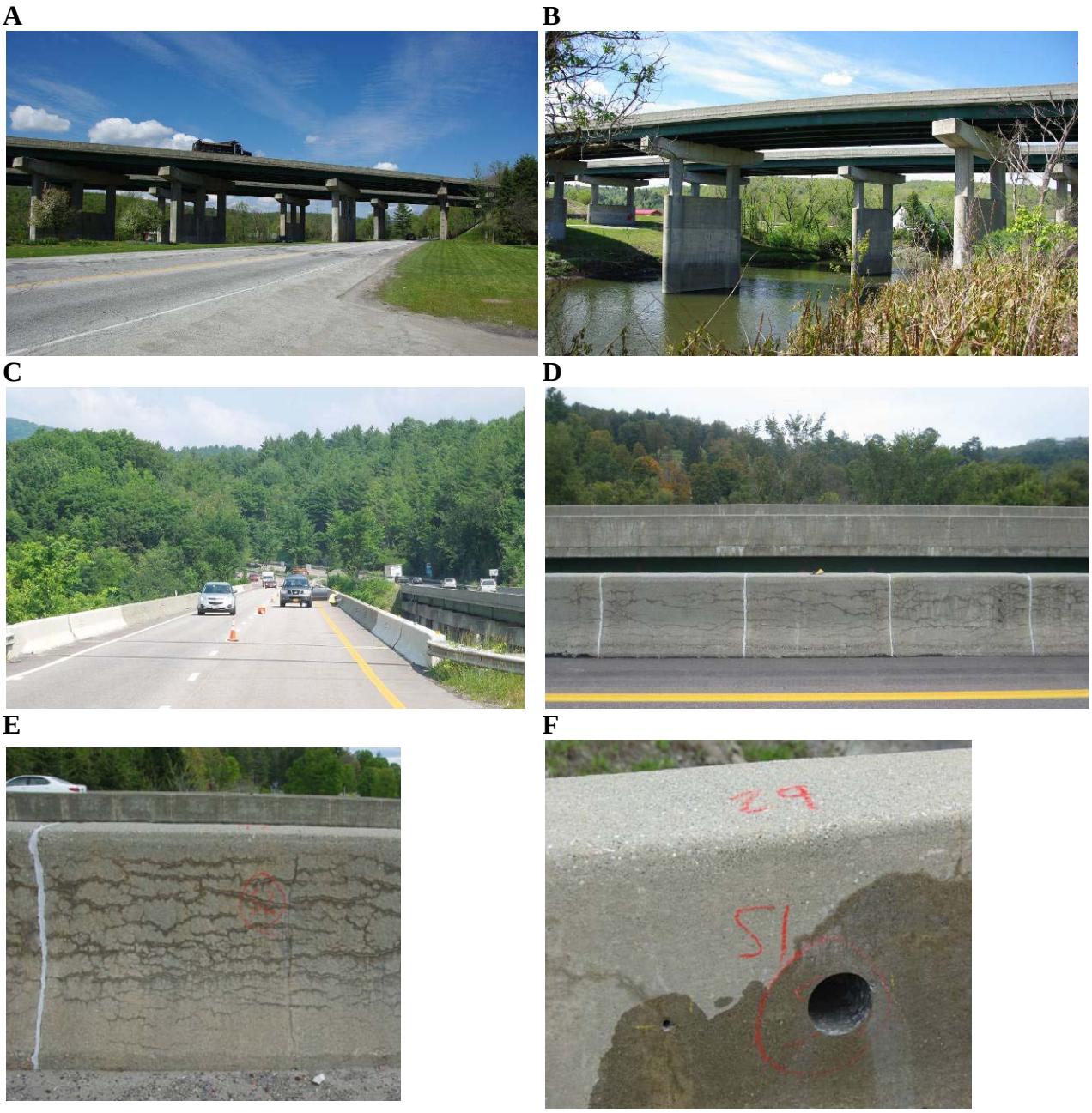

Figure 238. I-89 bridges and barrier walls.
A&B: General views of the I-89 twin bridges over U.S. 2/State St. (A) and Dog River (B) near Montpelier, VT. C: Driving and passing lanes of the southbound bridge. D: General view of barrier walls showing longitudinal and map cracking patterns. E: Section of barrier wall for concrete core S2 showing a moderate degree of deterioration. F: Section of barrier wall for concrete core S1 showing a mild degree of deterioration.

12.1 SUMMARY OF PETROGRAPHIC EVALUATION

Findings of the petrographic examination of the six concrete cores extracted from the barrier walls of the two bridges carrying interstate I-89 over the Dog River near Montpelier, VT were reported to VAOT. The evaluation mainly consisted of the Damage Rating Index (DRI), a method that provides a semi-quantitative assessment of the damage in concrete based on a count of petrographic features of deterioration generally associated with alkali-silica reaction (ASR).

Cores N1 to N3 and S1 were characterized by low to very low degree of deterioration/damage due to ASR (DRIs ranging from 53 to 202). On the other hand, cores S2 and S3 showed moderate to severe degree of deterioration due to ASR (DRIs of 647 and 568, respectively) (Figure 239). For all cores examined, the coarse aggregate consists of a greyish granitic rock that showed no/limited evidence of alkali-reactivity. On the other hand, the sand, which is composed of different rock types (e.g. schist, microquartzite, sandstone, argillite, and other undifferentiated magmatic rocks) showed low to moderate degree of ASR in cores N2, S2, and S3.

The large majority of the counts for *Cracks with reaction products in the coarse aggregate* (Cr+RPCA) in the DRIs of sections S2 and S3 correspond to cracking in the coarse fraction of the sand. Significant cracking is also observed in the cement paste, with and without reaction products; in many cases, cracking extends into the cement paste (with reaction products) connecting "reacted" coarse sand particles (see Figure 240). A fair number of voids in the cement paste of the above cores are lined or filled with secondary reaction products, both alkali-silica gel and ettringite.

In summary, the petrographic evaluation confirmed the presence of ASR in several of the barrier walls that were cored. The extent of ASR and associated damage was found to range from low to high, significant variations in the damage being sometimes observed between adjacent barrier walls.

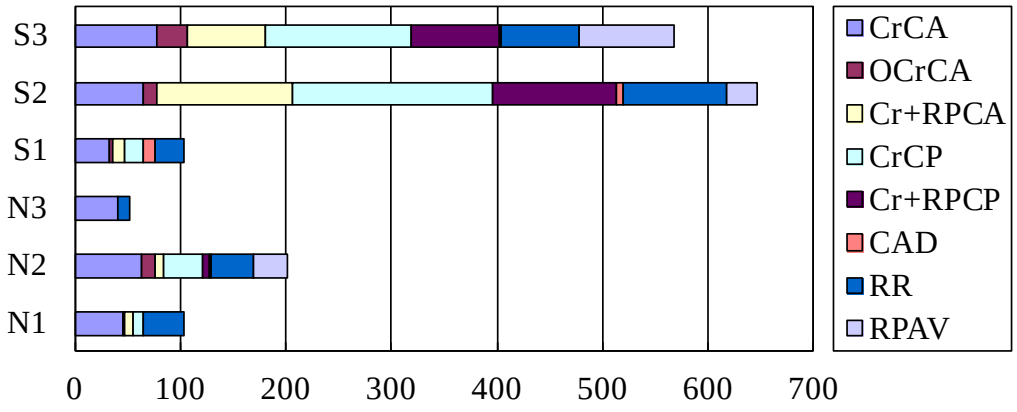

Figure 239. Results of the Damage Rating Index (DRI) for the Vermont cores. The colored cells give the proportions of each petrographic feature to the DRI value. (CrCA: cracking in the coarse aggregate particles; OCrCa: opened cracking in the coarse aggregate particles; Cr+RPCA: cracking in the coarse aggregate particles + reaction product; CrCP: cracking in the cement paste; Cr+RPCP: cracking in the cement paste + reaction product; CAD: coarse aggregate debonded; RR: reaction rim; RPAV: reaction products in air void of the cement paste).

A (distance between vertical lines = 1 cm [0.4 in.])

B (distance between vertical lines = 1 cm [0.4 in.])

Figure 240. Polished concrete surfaces (cores extracted from the barrier walls of two bridges carrying interstate I-89 over Dog River near Montpelier, VT).
A&B: Cracking in particles of the coarse fraction of the fine aggregate, which extends into the cement paste; secondary (ASR) products are observed in the cracks both in the particles and the cement paste. Dark reaction rims are observed surrounding the reactive aggregate particles.

12.2 SUMMARY OF APPLICATION REPORT

Based on the results of the field inspection and laboratory testing (diagnosis), which confirmed that ASR was a contributing factor to the deterioration observed at the site, a treatment plan involving the application of different types of surface treatment products (sealers, elastomeric coating) on the barrier walls of the bridges that span the Dog River, U.S. 2/State Street, and Dog River Road near Montpelier, VT (southbound direction) was implemented in 2011. In addition to the above treatments, a performance monitoring plan was also developed and implemented to allow quantifying the effects of the various treatments over time. Details on the performance monitoring techniques and treatment activities are provided in chapters 2 and 3, respectively.

Within selected barrier walls, specific areas were identified for crack mapping, expansion measurements, and temperature/humidity readings. Figure 241A shows a typical area that is ready for performance monitoring. In the case of the barrier walls, the distance from the top of the barrier to the chamfered base was too short for 500-mm (20-in.) vertical measurements, so the layout shown in Figure 241B was employed. The dimensions of this layout are 150 mm (6 in.) in the vertical direction and 500 mm (20 in.) in the horizontal direction. This layout was later modified to employ the regular 500 x 500 mm grid system for the determination of the Cracking Index (see Figure 245).

A **B**

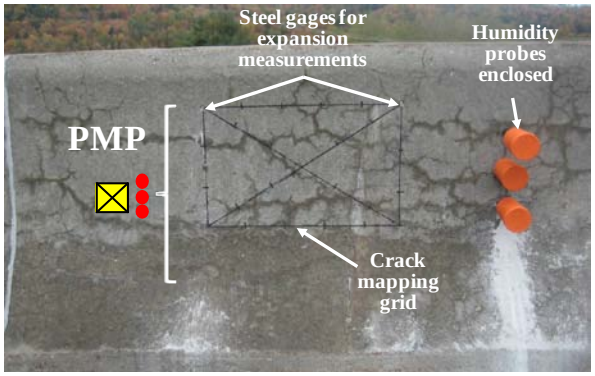

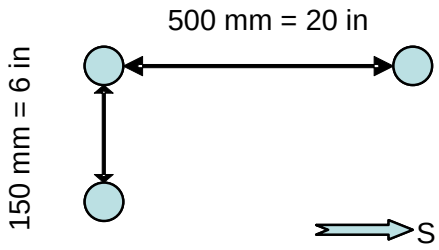

Figure 241. Performance monitoring area.
A: Area within a barrier wall of the bridge instrumented with a crack mapping grid, expansion pins, and humidity sleeves and plugs for data collection. B: Expansion pin layout.

The barrier walls were treated during the spring and fall of 2011. Three sealers were selected for application on separate sections of the above structures. The products correspond to a 100 percent silane, a 40 percent silane (water-based), an alcohol-silane (40 percent solid), and one elastomeric coating. Details on these products are given in chapter 3. Figure 242 and Table 81 give the details of the treatments and monitoring plan for the southbound barrier wall sections.

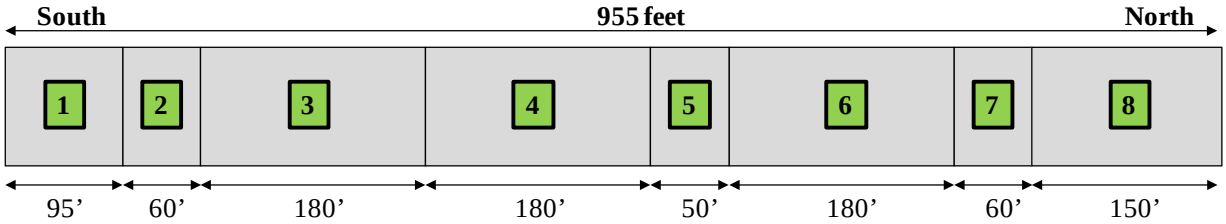

Figure 242. Treatment and monitoring plan for the barrier walls on the bridge structure (southbound lanes, similar layout for both the driving and passing lanes) over the Dog River near Montpelier, VT.

Table 81. Treatment plan details – southbound lanes. Treatment No. 1 begins at the southern end of the bridge, with subsequent treatments progressing northbound. A total of 21 (driving lane) and 24 (passing lane) performance monitoring sites (PMP) were installed on the barrier walls.

Treatment Number	Treatment Type	Length of Treatment, m (ft)	PMP numbers	
			Driving lane	Passing lane
1	100% silane sealer, followed by elastomeric coating	29 (95)	1,2	1-4
2	Control	18 (60)	3,4	5,6
3	40% silane (water-based)	55 (180)	5,6	7-10
4	100% silane	55 (180)	7,8,9	11,12
5	Control	15 (50)	10,11	13-16
6	Elastomeric coating	55 (180)	12-15	17-20
7	Control	18 (60)	16,17	21,22
8	Alcohol-silane (40% solid; used by local contractor conducting bridge repairs)	46 (150)	18-21	23,24
Total			**21**	**24**

The 100 percent silane product was applied using a handheld pressurized container and spray nozzle. It was sprayed onto the surface of the different elements in a left-to-right-to-left pattern. This product was sprayed onto the surface as a clear liquid and dried as a clear coating. The 40 percent silane product was applied in the same way that the 100 percent silane product was applied. The 40 percent silane was sprayed on as a white liquid. While it dried, it became a clear coating. The elastomeric coating product was applied like paint. Rollers and paint brushes were used instead of spray nozzles. Like the above silane products, one coat of material was applied as evenly as possible so that the entire area was covered. The 40 percent silane and 100 percent silane materials were applied at a rate of about 3.7 m^2/L (150 ft^2/gal), while the elastomeric coating was applied with coats at a rate of 2.5m^2/L (100 ft^2/gal). Treatments were applied on both sides of the barrier walls located to the right of the driving lane, while only the inside portion of the barrier walls located to the left of the passing lane was treated. Figure 243 gives examples of the surface treatment procedures.

Figure 243. Application of surface treatments.
A&B: 40 percent silane (left) on the barrier wall of the bridge structure. C&D: Elastomeric coating on the barrier wall of the bridge structure.

12.3 MONITORING DATA

This section presents the data obtained from expansion, crack mapping, and internal relative humidity measurements from the structure under investigation. The treatments and performance monitoring activities were essentially carried out on the southbound bridge structure, i.e., on the barrier walls located to the right of the driving lane, and on the barrier walls located to the left of the passing lane.

In the case of both the driving and passing lane barriers, performance monitoring packages (PMP) were established and "0" readings (for relative humidity/temperature, length change, and Cracking Index) taken in 2010. Since all field activities in 2011 focused on sealing products applications, subsequent performance monitoring readings were taken in July 2012 and May 2013.

Table 82 and Table 83 present the measured temperature and relative humidity values obtained from the performance monitoring sites on the driving lane and passing lane barriers, respectively. The data are grouped in accordance with the type of treatment/ product, i.e., elastomeric coating, silanes, and control sections.

For the various sites, data are reported at 25-mm (~1 in.), 50-mm (~2 in.), and 75-mm (~3 in.) depths below the surface.

One will note that many data are missing from the different survey times. This is due to the fact that many holes were either filled with water or humid (condensation) to the point that no reliable data could be obtained from those holes during the field surveys; also, winter snow removal operations and snow/ice accumulations damaged several measurement points (plastic tubing for RH measurements – see chapter 2) on the barrier walls, so many of those monitoring sites were unfortunately no longer operational at the time of the field visits.

Table 82. Relative humidity and temperature measurements - driving lane barrier walls.

Section	Site	Depth	Data	Sept 2010 12 °C (53 °F)* Before Treatment	July 2012 24 °C (76 °F)*	May 2013 11 °C (52 °F)*
100% silane + Elastomeric coating	1	25 mm (1")	T °C (°F)	15.8 (60.4)	30.7 (87.3)	-
			RH%	88.0	85.7	-
		50 mm (2")	T °C (°F)	15.8 (60.4)	30 (86)	-
			RH%	89.5	91.4	-
		75 mm (3")	T °C (°F)	16.2 (61.2)	29.5 (85.1)	19.3 (66.7)
			RH%	81.2	89.7	81.4
Elastomeric coating	12	25 mm (1")	T °C (°F)	16.4 (61.5)	30.1 (86.2)	23 (73.4)
			RH%	83.6	86	78.5
		50 mm (2")	T °C (°F)	16.1 (61.0)	29.6 (85.3)	20.5 (68.9)
			RH%	90.4	88.8	81.4
		75 mm (3")	T °C (°F)	16.2 (61.2)	29 (84.2)	19.4 (66.9)
			RH%	84.5	88.2	82.6
	14	25 mm (1")	T °C (°F)	15.7 (60.3)	30 (86)	-
			RH%	89.3	90.5	-
		50 mm (2")	T °C (°F)	16.0 (60.8)	29.8 (85.6)	-
			RH%	92.9	87.9	-
		75 mm (3")	T °C (°F)	16.0 (60.8)	34.8 (96.9)	19.3 (66.7)
			RH%	86.9	81.1	86.3
40% silane (water-based)	5	25 mm (1")	T °C (°F)	15.1 (59.2)	31.4 (88.5)	-
			RH%	84.7	79.2	-
		50 mm (2")	T °C (°F)	15.5 (59.9)	31.6 (88.6)	-
			RH%	67.7	85.2	-
		75 mm (3")	T °C (°F)	15.7 (60.3)	30.8 (87.4)	-
			RH%	80.3	87.7	-
	6	25 mm (1")	T °C (°F)	15.1 (59.2)	-	-
			RH%	76.4	-	-
		50 mm (2")	T °C (°F)	15.5 (59.9)	-	-
			RH%	89.4	-	-
		75 mm (3")	T °C (°F)	15.7 (60.3)	-	-
			RH%	87.6	-	-
100% silane	7	25 mm (1")	T °C (°F)	15.9 (60.6)	-	-
			RH%	82.3	-	-
		50 mm (2")	T °C (°F)	16.0 (60.8)	-	-
			RH%	87.8	-	-
		75 mm (3")	T °C (°F)	16.0 (60.8)	35.6 (96.1)	-
			RH%	86.8	80.7	-
	8	25 mm (1")	T °C (°F)	15.9 (60.6)	31.7 (89.1)	25.9 (78.6)
			RH%	78	81.1	70
		50 mm (2")	T °C (°F)	15.9 (60.6)	30.5 (86.9)	22 (71.6)
			RH%	87.6	86.1	79.8
		75 mm (3")	T °C (°F)	15.9 (60.6)	30.3 (86.5)	-
			RH%	90.2	86.2	-
Alcohol-silane (40% solid)	18	25 mm (1")	T °C (°F)	15.8 (60.4)	-	-
			RH%	95.3	-	-
		50 mm (2")	T °C (°F)	15.9 (60.6)	-	22.8 (73)
			RH%	88.6	-	81.2
		75 mm (3")	T °C (°F)	15.9 (60.6)	-	21.7 (71.1)
			RH%	91.7	-	84.7

Table 82 (cont'd). Relative humidity and temperature measurements - driving lane barrier walls.

Section	Site	Depth	Data	Sept 2010 12 °C (53 °F)* Before Treatment	July 2012 24 °C (76 °F)*	May 2013 11 °C (52 °F)*
Control 1	4	25 mm (1")	T °C (°F)	15.8 (60.4)	31.5 (88.7)	-
			RH%	79.6	88.1	-
		50 mm (2")	T °C (°F)	16.0 (60.8)	31.1 (88.7)	-
			RH%	87.0	90.3	-
		75 mm (3")	T °C (°F)	16.5 (61.7)	30.5 (86.9)	-
			RH%	79.0	89.2	-
Control 2	11	25 mm (1")	T °C (°F)	15.9 (60.6)	31 (87.8)	-
			RH%	88.2	94	-
		50 mm (2")	T °C (°F)	16.2 (61.2)	30.8 (87.4)	-
			RH%	91.6	88.4	-
		75 mm (3")	T °C (°F)	16.2 (61.2)	30.5 (86.9)	21.9 (71.4)
			RH%	81.2	89.4	80
Control 3	17	25 mm (1")	T °C (°F)	15.7 (60.3)	-	-
			RH%	92.9	-	-
		50 mm (2")	T °C (°F)	16.0 (60.8)	-	-
			RH%	99.5	-	-
		75 mm (3")	T °C (°F)	16.0 (60.8)	-	-
			RH%	89.7	-	-

*That temperature corresponds to the daily average obtained from http://www.wunderground.com.

Table 83. Relative humidity and temperature measurements - passing lane barrier walls.

Section	Site	Depth	Data	Sept 2010 24 °C (76 °F)* Before Treatment	July 2012 24 °C (76 °F)*	May 2013 11 °C (52 °F)*
100% silane + Elastomeric coating	2	25 mm (1 in.)	T°C (°F)	25.7 (78.3)	24.6 (76.3)	-
			RH%	86.7	89.1	-
		50 mm (2 in.)	T°C (°F)	25.9 (78.6)	24.1 (75.4)	-
			RH%	89.6	86.4	-
		75 mm (3 in.)	T °C (°F)	26 (78.8)	24.5 (76.1)	27 (80.6)
			RH%	90.7	88.5	82.7
Elastomeric coating	15	25 mm (1 in.)	T°C (°F)	30.1 (86.2)	25.7 (78.3)	-
			RH%	87.9	88.7	-
		50 mm (2 in.)	T°C (°F)	29.1 (84.4)	25.2 (77.4)	-
			RH%	91.1	92.5	-
		75 mm (3 in.)	T°C (°F)	28.2 (82.8)	25.1 (77.2)	-
			RH%	85.1	93	-
	17	25 mm (1 in.)	T°C (°F)	33.3 (91.9)	26.1 (79)	-
			RH%	76.7	83.2	-
		50 mm (2 in.)	T°C (°F)	31 (87.8)	25.3 (77.5)	30 (86)
			RH%	86.4	88.7	83.5
		75 mm (3 in.)	T°C (°F)	29.5 (85.1)	25.2 (77.4)	29.8 (85.6)
			RH%	87.6	90.8	79.6

Table 83 (cont'd). Relative humidity and temperature measurements - passing lane barrier walls.

Section	Site	Depth	Data	Sept 2010 24 °C (76 °F)* Before Treatment	July 2012 24 °C (76 °F)*	May 2013 11 °C (52 °F)*
40% silane (water-based)	5	25 mm (1 in.)	T °C (°F)	-	25.1 (77.2)	-
			RH%	-	69.2	-
		50 mm (2 in.)	T°C (°F)	-	24.9 (76.8)	-
			RH%	-	80.4	-
		75 mm (3 in.)	T°C (°F)	-	25 (77)	-
			RH%	-	86.6	-
	6	25 mm (1 in.)	T°C (°F)	26.9 (80.4)	-	-
			RH%	62.9	-	-
		50 mm (2 in.)	T°C (°F)	26.4 (79.5)	-	-
			RH%	80.1	-	-
		75 mm (3 in.)	T°C (°F)	26.5 (79.7)	-	-
			RH%	91.1	-	-
	7	25 mm (1 in.)	T°C (°F)	-	-	-
			RH%	-	-	-
		50 mm (2 in.)	T°C (°F)	-	-	-
			RH%	-	-	-
		75 mm (3 in.)	T°C (°F)	-	-	-
			RH%	-	-	-
	8	25 mm (1 in.)	T°C (°F)	36 (96.8)	-	-
			RH%	72.7	-	-
		50 mm (2 in.)	T°C (°F)	30.9 (87.6)	-	-
			RH%	83.4	-	-
		75 mm (3 in.)	T°C (°F)	29.3 (84.7)	-	-
			RH%	94.4	-	-
100% silane	9	25 mm (1 in.)	T°C (°F)	29.9 (85.8)	25.1 (77.2)	33.1 (91.6)
			RH%	85.7	69.2	84.6
		50 mm (2 in.)	T°C (°F)	28.1 (82.6)	25 (77)	29.7 (85.5)
			RH%	83	88.8	80.8
		75 mm (3 in.)	T°C (°F)	27.4 (81.3)	24.9 (76.8)	28 (82.4)
			RH%	91.7	90.5	83.6
	11	25 mm (1 in.)	T°C (°F)	30.2 (86.4)	-	-
			RH%	77.8	-	-
		50 mm (2 in.)	T°C (°F)	28.3 (82.9)	-	-
			RH%	85.6	-	-
		75 mm (3 in.)	T°C (°F)	27.5 (81.5)	-	29.2 (84.6)
			RH%	89	-	79.6
Alcohol-silane (40% solid)	21	25 mm (1 in.)	T°C (°F)	34.7 (94.5)	-	-
			RH%	78.5	-	-
		50 mm (2 in.)	T°C (°F)	31.8 (89.2)	-	-
			RH%	84.2	-	-
		75 mm (3 in.)	T°C (°F)	28.9 (84)	-	-
			RH%	89.9	-	-

*That temperature corresponds to the daily average obtained from http://www.wunderground.com.

Table 83 (cont'd). Relative humidity and temperature measurements - passing lane barrier walls.

Section	Site	Depth	Data	Sept 2010 24 °C (76 °F)* Before Treatment	July 2012 24 °C (76 °F)*	May 2013 11 °C (52 °F)*
Control 1	4	25 mm (1 in.)	T °C (°F)	25.9 (78.6)	24.7 (76.5)	-
			RH%	89.4	91.9	-
		50 mm (2 in.)	T°C (°F)	25.4 (77.7)	24.6 (76.2)	-
			RH%	86.8	92.3	-
		75 mm (3 in.)	T°C (°F)	26.3 (79.3)	24.7 (76.5)	28.4 (83.1)
			RH%	82.4	88.9	80.4
Control 2	14	25 mm (1 in.)	T°C (°F)	31.6 (88.9)	26.1 (79)	-
			RH%	89.8	89	-
		50 mm (2 in.)	T°C (°F)	28.2 (82.8)	25.4 (77.7)	-
			RH%	90	91	-
		75 mm (3 in.)	T°C (°F)	28.3 (82.9)	25.2 (77.4)	-
			RH%	94.8	92.3	-
Control 3	20	25 mm (1 in.)	T°C (°F)	33.4 (92.1)	27.5 (83.5)	-
			RH%	78.5	83.6	-
		50 mm (2 in.)	T°C (°F)	32.6 (90.7)	26 (78.8)	-
			RH%	73.2	88.6	-
		75 mm (3 in.)	T°C (°F)	29.7 (85.5)	25.7 (78.3)	-
			RH%	90	87.3	-

*That temperature corresponds to the daily average obtained from http://www.wunderground.com.

Table 84 and Table 85 present the length change data for the driving lane and passing lane barriers, respectively. Data are reported for a 500-mm (20-in.) gauge length in the horizontal direction, and a 150-mm (6-in.) gauge length in the vertical direction. The data were not corrected for thermal effects.

Table 84. Expansion results (%) - driving lane barrier walls.

Section	Site	Location	September 2010 12°C (53°F)* Before treatment	July 2012 24°C (76°F)*	May 2013 11°C (52°F)*
100 percent silane + elastomeric coating	1	Vertical	"0" reading	-	0.020
		Horizontal	"0" reading	0.019	0.008
	2	Top	"0" reading	-	-0.090
		Horizontal	"0" reading	0.016	0.006
Elastomeric coating	12	Top	"0" reading	-	0.028
		Vertical	"0" reading	-	-0.004
		Horizontal	"0" reading	0.010	-0.004
	13	Top	"0" reading	-	0.002
		Horizontal	"0" reading	-0.010	-0.043
	14	Horizontal	"0" reading	0.010	-0.003
	15	Vertical	"0" reading	-	-0.010
		Horizontal	"0" reading	0.011	-0.008
40 percent silane (water based)	5	Horizontal	"0" reading	0.021	0.004
	6	Vertical	"0" reading	-	0.011
		Horizontal	"0" reading	-0.039	-0.062
100 percent silane	7	Top	"0" reading	-	0.004
		Vertical	"0" reading	-	0.000
		Horizontal	"0" reading	0.039	0.025
	8	Top	"0" reading	-	0.000
		Vertical	"0" reading	-	0.005
		Horizontal	"0" reading	0.007	-0.007
	9	Horizontal	"0" reading	0.003	-0.003
Alcohol-silane (40% solid)	18	Vertical	"0" reading	-	-0.026
		Horizontal	"0" reading	-0.001	-0.007
	19	Horizontal	"0" reading	0.020	0.003
	20	Top	"0" reading	-	-0.015
		Vertical	"0" reading	-	0.002
		Horizontal	"0" reading	0.006	-0.010
	21	Vertical	"0" reading	-	0.010
		Horizontal	"0" reading	0.002	-0.007
Control 1	3	Vertical	"0" reading	-	0.017
		Horizontal	"0" reading	0.015	-0.003
	4	Vertical	"0" reading	-	0.050
		Horizontal	"0" reading	0.039	0.029
Control 2	10	Top	"0" reading	-	0.010
		Vertical	"0" reading	-	-0.014
		Horizontal	"0" reading	0.016	0.002
	11	Vertical	"0" reading	-	0.010
		Horizontal	"0" reading	0.013	-0.007
Control 3	16	Vertical	"0" reading	-	0.046
		Horizontal	"0" reading	0.023	-0.001
	17	Horizontal	"0" reading	0.010	-0.001

*That temperature corresponds to the daily average obtained from http://www.wunderground.com.

Table 85. Expansion results (%) - passing lane barrier walls.

Section	Site	Location	September 2010 24 °C (76 °F)*	July 2012 24 °C (76 °F)*	May 2013 11 °C (52 °F)*
100% silane + elastomeric coating	1	Vertical	"0" reading	-	0.076
		Horizontal	"0" reading	0.000	0.004
	2	Vertical	"0" reading	-	-
		Horizontal	"0" reading	--	-0.009
Elastomeric coating	15	Vertical	"0" reading	-	0.020
		Horizontal	"0" reading	0.011	-0.002
	16	Vertical	"0" reading	-	0.037
		Horizontal	"0" reading	0.021	0.012
	17	Vertical	"0" reading	-	-0.036
		Horizontal	"0" reading	0.013	0.002
	18	Vertical	"0" reading	-	0.017
		Horizontal	"0" reading	0.005	-0.014
40% silane (water-based)	5	Vertical	"0" reading	-	0.021
		Horizontal	"0" reading	0.004	-0.014
	6	Vertical	"0" reading	-	-0.007
		Horizontal	"0" reading	-0.001	-0.018
	7	Vertical	"0" reading	-	0.023
		Horizontal	"0" reading	-0.006	-0.025
	8	Vertical	"0" reading	-	0.022
		Horizontal	"0" reading	0.007	-0.006
100% silane	9	Vertical	"0" reading	-	0.034
		Horizontal	"0" reading	0.012	0.002
	10	Vertical	"0" reading	-	-0.009
		Horizontal	"0" reading	0.008	-0.009
	11	Vertical	"0" reading	-	-0.043
		Horizontal	"0" reading	-0.004	-0.023
	12	Vertical	"0" reading	-	0.056
		Horizontal	"0" reading	0.012	0.002
Alcohol-silane (40% solid)	21	Vertical	"0" reading	-	-0.017
		Horizontal	"0" reading	0.003	-0.009
	22	Vertical	"0" reading	-	0.094
		Horizontal	"0" reading	0.004	-0.007
	23	Top	"0" reading	-	0.051
		Vertical	"0" reading	-	-0.008
		Horizontal	"0" reading	0.014	0.005
	24	Vertical	"0" reading	-	0.002
		Horizontal	"0" reading	0.013	-0.021

*That temperature corresponds to the daily average obtained from http://www.wunderground.com.

Table 85 (cont'd). Expansion results (%) - passing lane.

Section	Site	Location	September 2010 24 °C (76 °F)*	July 2012 24 °C (76 °F)*	May 2013 11 °C (52 °F)*
Control 1	3	Vertical	"0" reading	-	0.024
		Horizontal	"0" reading	0.011	-0.007
	4	Vertical	"0" reading	-	0.019
		Horizontal	"0" reading	-	0.040
Control 2	13	Vertical	"0" reading	-	0.018
		Horizontal	"0" reading	0.009	-0.005
	14	Vertical	"0" reading	-	-0.007
		Horizontal	"0" reading	0.000	-0.012
Control 3	19	Vertical	"0" reading	-	0.079
		Horizontal	"0" reading	-0.035	-0.055
	20	Vertical	"0" reading	-	0.021
		Horizontal	"0" reading	0.022	0.012

*That temperature corresponds to the daily average obtained from http://www.wunderground.com

Table 86 and Table 87 present the results of Cracking Index measurements for the driving lane and passing lane barriers, respectively.

Table 86. Cracking Index measurements - driving lane.

Section	Site	September 2010 12°C (53°F)* mm/m (in./yd) Before Treatment	July 2012 24°C (76°F)* mm/m (in./yd)	May 2013 11°C (52°F)* mm/m (in./yd)
100 percent silane + Elastomeric coating	1	0.49 (0.017)	0.00 (0.000)	0.00 (0.000)
	2	0.24 (0.009)	0.00 (0.000)	0.11 (0.004)
Elastomeric coating	12	0.09 (0.004)	0.00 (0.000)	0.06 (0.002)
	13	0.41 (0.015)	0.00 (0.000)	0.06 (0.002)
	14	0.53 (0.019)	0.00 (0.000)	0.09 (0.003)
	15	0.15 (0.005)	0.00 (0.000)	0.13 (0.005)
40 percent silane (water baed)	5	0.43 (0.015)	1.18 (0.042)	0.68 (0.024)
	6	0.42 (0.015)	0.76 (0.027)	0.67 (0.024)
100 percent silane	7	0.30 (0.010)	0.59 (0.021)	0.38 (0.014)
	8	0.33 (0.012)	0.57 (0.020)	0.49 (0.018)
	9	0.00 (0.000)	0.35 (0.013)	0.46 (0.017)
Alcohol-silane (40% solid)	18	0.05 (0.002)	0.35 (0.013)	0.35 (0.013)
	19	0.13 (0.005)	0.35 (0.013)	0.25 (0.009)
	20	0.20 (0.008)	0.48 (0.017)	0.43 (0.015)
	21	0.12 (0.004)	0.42 (0.015)	0.28 (0.010)
Control 1	3	0.30 (0.011)	0.95 (0.034)	1.08 (0.039)
	4	0.45 (0.016)	1.14 (0.041)	1.25 (0.045)
Control 2	10	0.24 (0.009)	0.67 (0.024)	0.55 (0.020)
	11	0.20 (0.008)	0.46 (0.017)	0.58 (0.021)
Control 3	16	0.30 (0.010)	0.66 (0.024)	0.79 (0.028)
	17	0.24 (0.009)	0.67 (0.024)	0.79 (0.028)

*That temperature corresponds to the daily average obtained from http://www.wunderground.com.

CI data are given in mm/m (or in./yd) as they correspond to the total crack opening, in mm (in.), averaged over a one-meter (or one-yard) length; from 2012 and after, they are calculated from the measurement of crack widths along a grid system composed of the four lines of a 500-mm (20-in.) square grid and of the two 700-mm (28-in.) diagonal lines (total of 3.4 m (about 11 ft) of lines) of that same grid (see chapter 2). In general, the higher the CI values, the higher the extent of (surface) damage on the concrete element investigated.

Table 87. Cracking Index measurements - passing lane.

Section	Site	September 2010 24°C (76°F)* mm/m (in./yd) Before Treatment	July 2012 24°C (76°F)* mm/m (in./yd)	May 2013 11°C (52°F)* mm/m (in./yd)
Silane + Elastomeric coating	1	0.37 (0.013)	0.00 (0.000)	0.00 (0.000)
	2	0.11 (0.004)	0.00 (0.000)	0.00 (0.000)
Elastomeric coating	15	0.37 (0.013)	0.00 (0.000)	0.00 (0.000)
	16	0.54 (0.019)	0.00 (0.000)	0.03 (0.001)
	17	0.53 (0.019)	0.00 (0.000)	0.10 (0.004)
	18	0.40 (0.014)	0.00 (0.000)	0.00 (0.000)
40% silane (water-based)	5	0.21 (0.008)	0.50 (0.018)	0.26 (0.009)
	6	0.23 (0.009)	0.57 (0.020)	0.38 (0.014)
	7	0.34 (0.012)	0.65 (0.023)	0.34 (0.012)
	8	0.44 (0.016)	0.85 (0.031)	0.56 (0.020)
100% silane	9	0.54 (0.019)	0.98 (0.035)	0.58 (0.021)
	10	0.47 (0.017)	0.74 (0.027)	0.37 (0.013)
	11	0.42 (0.015)	0.64 (0.023)	0.64 (0.023)
	12	0.33 (0.012)	0.60 (0.022)	0.29 (0.010)
Alcohol-silane (40% solid)	21	0.43 (0.015)	0.38 (0.014)	0.17 (0.006)
	22	0.54 (0.019)	0.50 (0.018)	0.33 (0.012)
	23	0.32 (0.011)	0.33 (0.012)	0.27 (0.010)
	24	0.07 (0.003)	0.25 (0.009)	0.11 (0.004)
Control 1	3	0.98 (0.036)	1.36 (0.049)	1.41 (0.051)
	4	0.52 (0.019)	0.88 (0.042)	0.84 (0.030)
Control 2	13	0.61 (0.022)	1.02 (0.037)	0.90 (0.032)
	14	0.46 (0.017)	0.73 (0.026)	0.60 (0.022)
Control 3	19	0.36 (0.013)	0.80 (0.029)	0.46 (0.017)
	20	0.61 (0.022)	0.63 (0.023)	0.51 (0.018)

*That temperature corresponds to the daily average obtained from http://www.wunderground.com.

Figure 244 to Figure 250 show the condition of the barrier walls as well as crack maps, both before and after treatment.

A

B

C

D

E

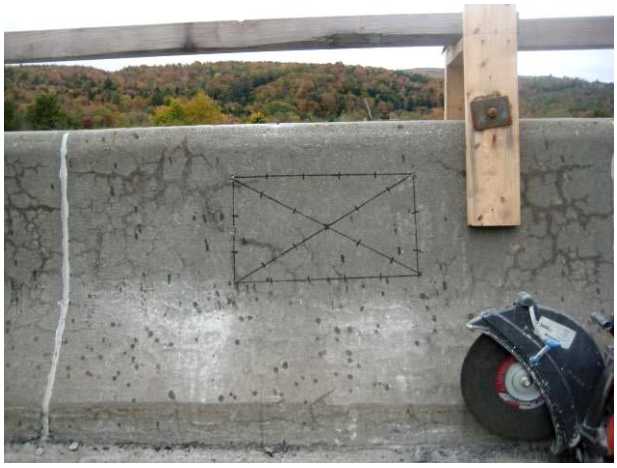

F

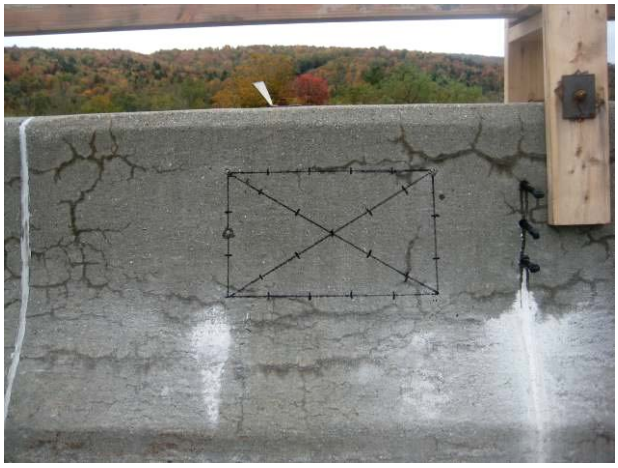

Figure 244. Examples of the "original" condition of barrier walls (driving lane).

A – Control (Site 3) 2010

B – Control (Site 3) 2013

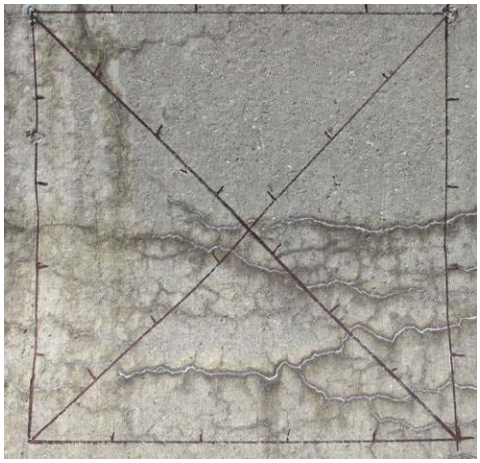

C – 40% silane (Site 5) 2010

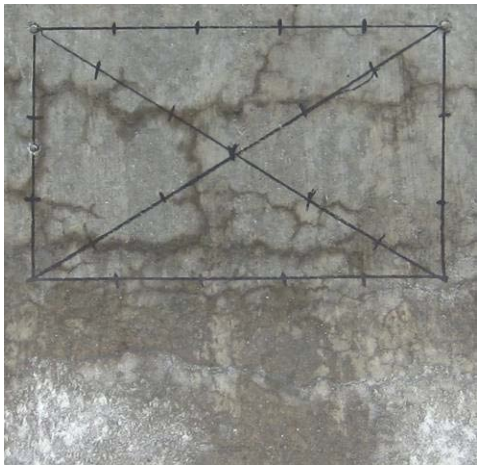

D – 40% silane (Site 5) 2013

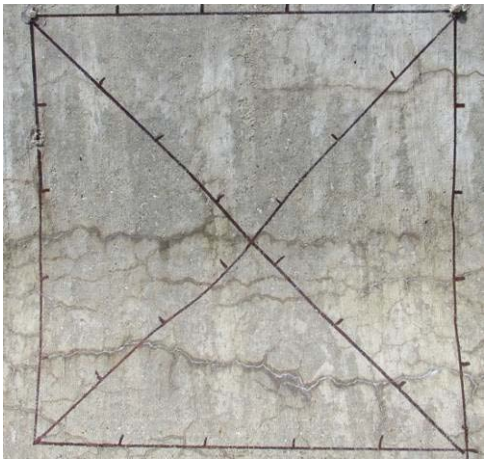

E – 100% silane (Site 7) 2010

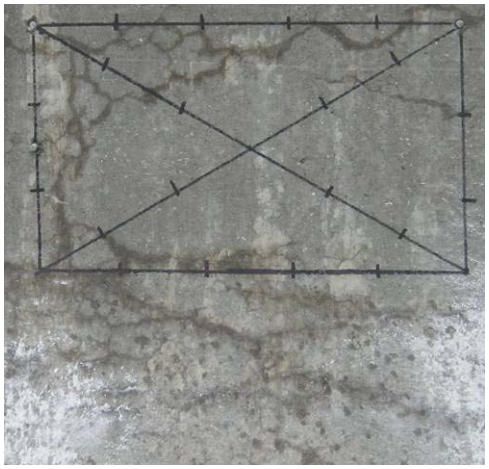

F – 100% silane (Site 7) 2013

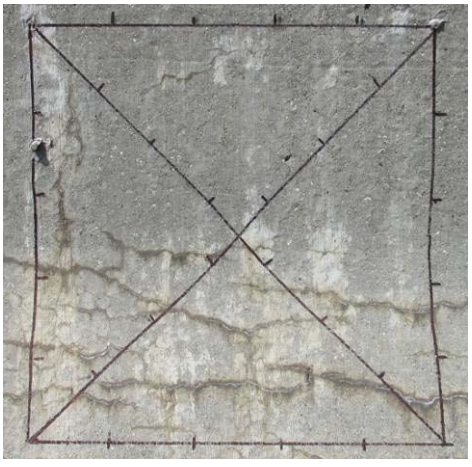

Figure 245. Examples of crack map sections before (2010) and after (2013) treatments (driving lane).

A – Alcohol-silane (40% solid) (Site 20) 2010

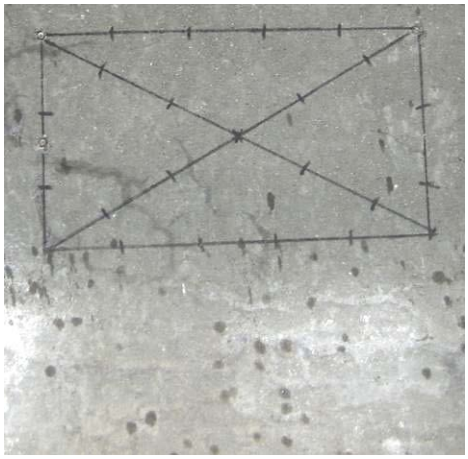

B – Alcohol-silane (40% solid) (Site 20) 2013

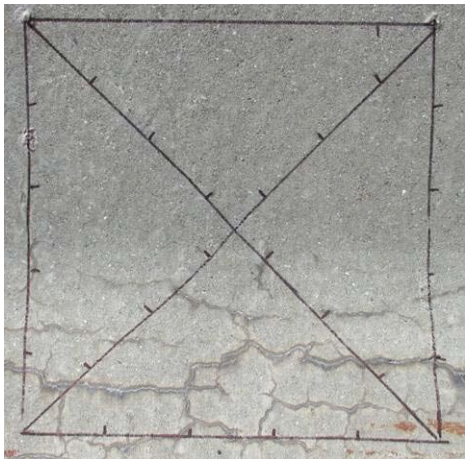

C – Elastomeric coating (Site 14) 2010

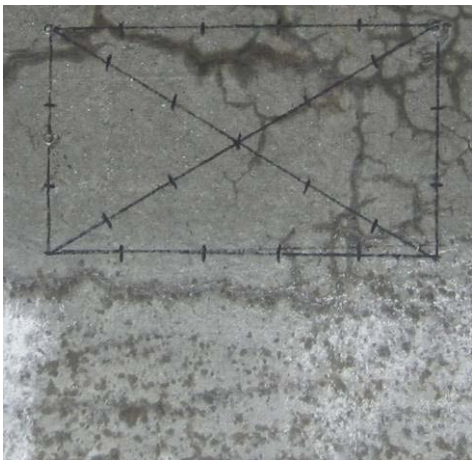

D – Elastomeric coating (Site 14) 2013

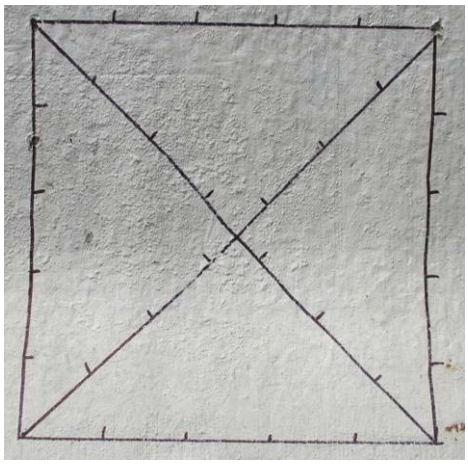

E – Elastomeric coating + 100% silane (Site 2) 2010

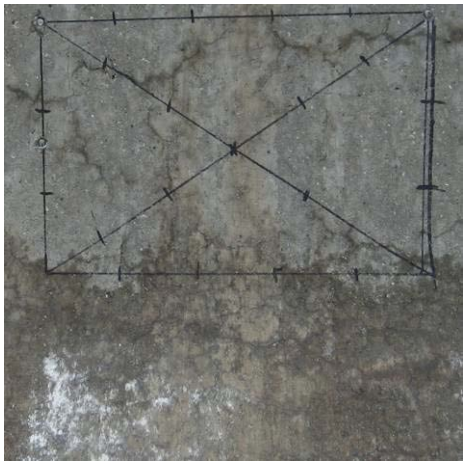

F – Elastomeric coating + 100% silane (Site 2) 2013

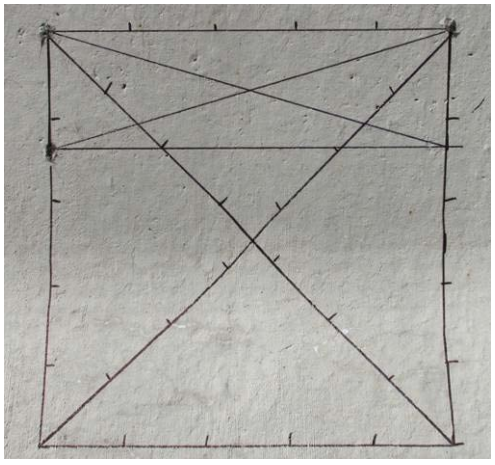

Figure 246. Examples of crack map sections before (2010) and after (2013) treatments (driving lane).

A – Control 2013

B – Control 2013

C – 40% silane 2013

D – 40% silane 2013

E – 100% silane 2013

F – 100% silane 2013

Figure 247. Typical examples of the condition of control and treated barrier walls (driving lane).

A – Alcohol-silane (40% solid) 2013

B – Alcohol-silane (40% solid) 2013

C – 100% silane + elastomeric coating 2013

D – 100% silane + elastomeric coating 2013

E – Elastomeric coating 2013

F – Elastomeric coating 2013

Figure 248. Typical examples of the condition of treated barrier walls (driving lane).

A – Control 2013

B – Control 2013

C – 40% silane 2013

D – 40% silane 2013

E – 100% silane 2013

F – 100% silane 2013

Figure 249. Typical examples of the condition of control and treated barrier walls (passing lane).

A – Alcohol-silane (40% solid) 2013

B – Alcohol-silane (40% solid) 2013

C – 100% silane + elastomeric coating 2013

D – 100% silane + elastomeric coating 2013

E – Elastomeric coating 2013

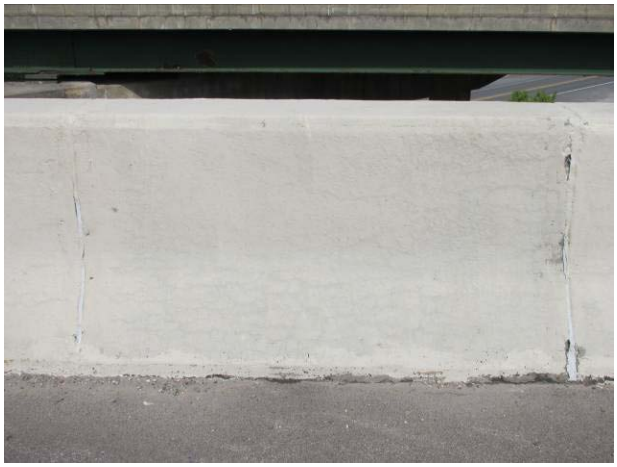

F – Elastomeric coating 2013

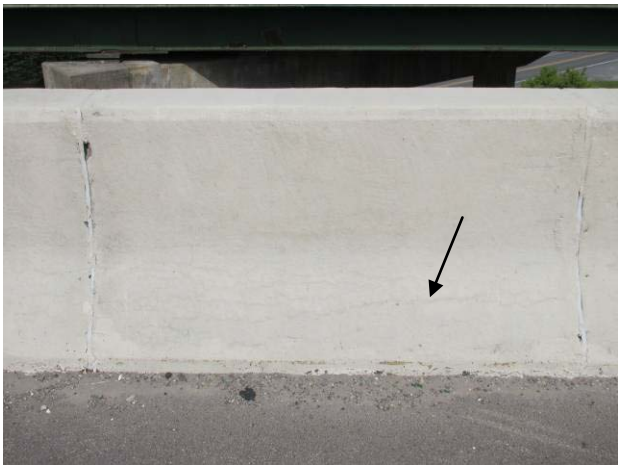

Figure 250. Typical examples of the condition of treated barrier walls (passing lane).

12.4 DATA ANALYSES

Considering that ASR was found to be a contributing factor to the deterioration observed in the barrier walls of the two bridges carrying interstate I-89 over the Dog River near Montpelier, VT, it is important to keep in mind the main objective of this investigation, which is to evaluate the long term efficacy of various types of surface treatment, for instance penetrating sealers and coating, to control the progress of deterioration in ASR-affected concrete members.

First, it should be mentioned that because of the timing of the applications (summer of 2011), only limited performance monitoring data are available after treatment (about 24 months). Consequently, in general, it is too early to be able to draw any significant conclusions from the monitoring data accumulated so far. However, trends/observations can be made from the data accumulated to date.

In concrete members exposed outdoors, internal RH values would be expected to increase with depth, although RH values are often fluctuating significantly in the "surficial" portion of a concrete element due to local environmental conditions. The use of "breathable" or penetrating sealers is expected to contribute at progressively reducing RH values close to the surface due to their hydrophobic properties. Such a behavior had been measured in ASR-affected barrier walls treated with sealers in Quebec City, Canada (Bérubé et al. 2002a); however, such a trend was established over a six-year monitoring period because significant punctual/seasonal variations were observed due to changes in temperature, humidity, rainfall, and sun exposure conditions. Bérubé et al. (2002b) also showed that not all surface treatment products had an equivalent efficacy in reducing the internal humidity and controlling expansion due to ASR.

So far, because of the temperature differences and the limited number of field surveys, no definite conclusions can be drawn from the RH measurements in the barrier walls investigated. However, lower RH values are observed in the surficial portion of several barrier walls treated with sealers and the elastomeric coating in the 2012 (and 2013) data (see Table 82 and Table 83), while such a trend does not seem to be so pronounced in the control sections (see Figure 251 and Figure 252). This suggests a beneficial effect of surface treatments at reducing the progress of cracking; future site readings will be critical at confirming that trend.

One needs to keep in mind that in the case of barrier walls, moisture is available from both sides of the concrete element. Treatments were consequently applied on both sides of the driving lane barriers to try optimizing their efficacy. In parallel, treatments were applied only on the inside portion of the passing lane barriers in order to evaluate the relative efficacy of both types of treatments. So far, there are no significant differences between the RH results obtained for the driving lane and passing lane barriers, although passing lane barriers seem generally in a more advanced stage of deterioration than driving lane barriers. On the other hand, numerous RH values are missing due to moisture effects or breakdown; this lack of data makes interpretations of the effect of surface treatments on internal concrete RH more difficult.

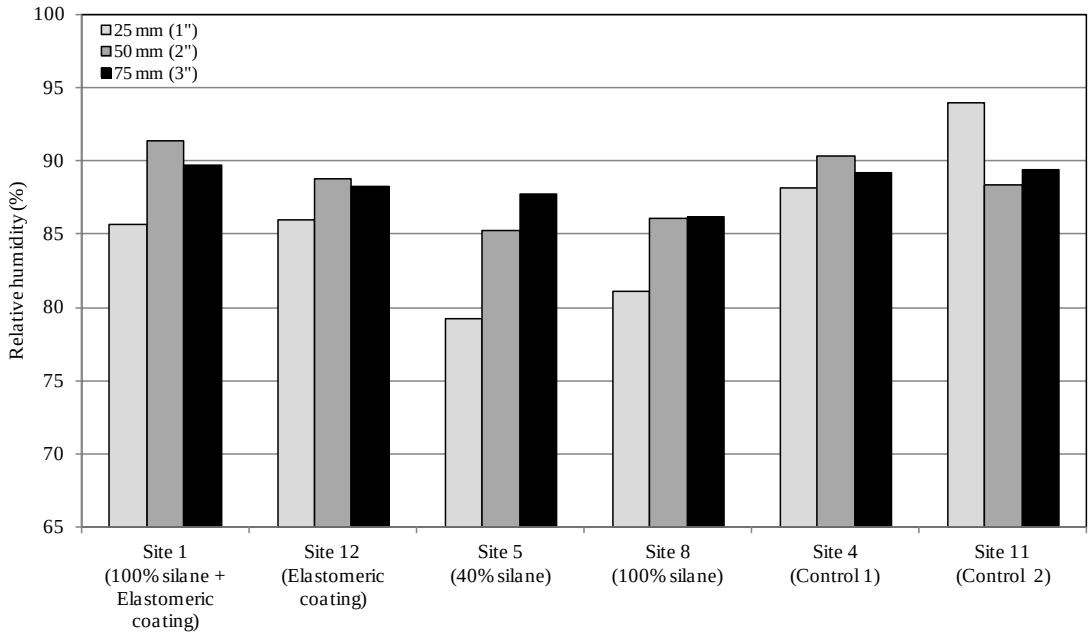

Figure 251. Relative humidity measurements for the driving lane (July 2012).

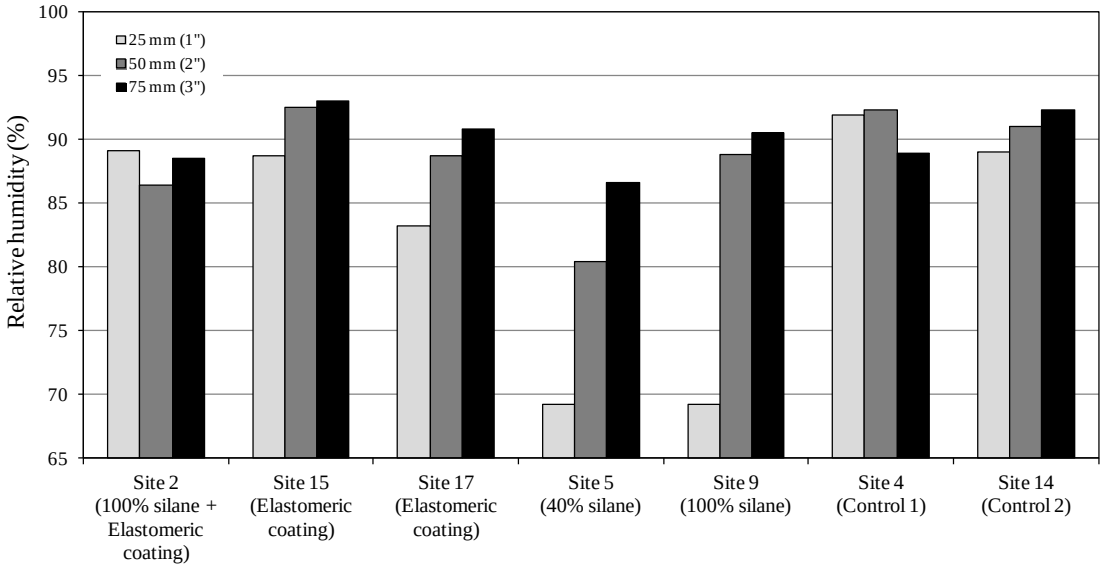

Figure 252. Relative humidity measurements for the passing lane (July 2012).

In the case of the length change data, a significant variation in the "horizontal" and "vertical" measurements can be observed, some barriers showing a contraction ("negative" values) and some an expansion ("positive" values). These variations are likely influenced by thermal effects. It is consequently difficult to recognize significant trends at this stage of the monitoring program as this is based on only a limited set of readings. However, one needs to remember that in the case of the barrier walls, horizontal expansions are likely to be restricted (because of all adjacent barrier walls), while vertical length changes could actually be favored (i.e., showing expansion) because of the horizontal restraint.

Regarding the physical condition (cracking) of the barrier walls, it is important to note that the original degree/extent of cracking varied significantly between the barrier wall sections, although all were exposed to similar conditions. This can be observed in Figure 244, which illustrates the range of damage in the driving lane barrier walls back in 2010, i.e., before treatments. Also, the damage in the barrier walls was generally found to progress during the 2010-2013 time period, as can be visually observed in Figure 245 and Figure 246 which illustrate CI monitoring sites for the driving lane barrier walls.

The data in Table 87, and illustrated in Figure 253 and Figure 254, show a generalized increase in the CI values for both the driving and the passing lane barrier walls over the 2010-2012 monitoring period, followed, however, by a drop in CI values in the May 2013 field survey for most barrier walls; the latter is likely caused by the difference in temperature during the site visits. The temperature and moisture state of the concrete can indeed have a significant impact on the CI values since the above conditions will influence crack widths. It is interesting to note, however, that the drop between 2012 and 2013 was generally less important for the control sections compared to the treated sections on the passing lane (Figure 254); this suggests that expansion/cracking is actually progressing more readily in the control sections. This is supported by the data obtained for the driving lane sections, where CI values generally dropped between 2012 and 2013 for the treated sections (once again due likely to thermal effect) (Figure 253B), but actually increased over the same period for the control sections (Figure 253C). This suggests a beneficial effect of the penetrating silane treatments. This is suggested also by the differences in the physical appearance of the barrier walls, as illustrated in Figure 247 and Figure 248 for the driving lane barriers, and in Figure 249 and Figure 250 for the passing lane barriers.

In the case of the sections treated with the elastomeric coating, CI values of "0" were obtained for the measurements carried out in 2012, i.e., following the application of the coating, since the product has been efficient in bridging the cracks present in the different concrete members. However, cracking was found to start reappearing, especially in the bottom portion of some coated barrier walls in 2013, as indicated by increasing CI values for those sections (see Figure 248, Figure 250, Figure 253, and Figure 254).

Finally, the passing lane barrier walls seem to be generally more severely cracked than the driving lane barrier walls. This might be partially related to the fact that the driving lane barriers were treated on both sides while the passing lane barriers were treated on only one side.

A

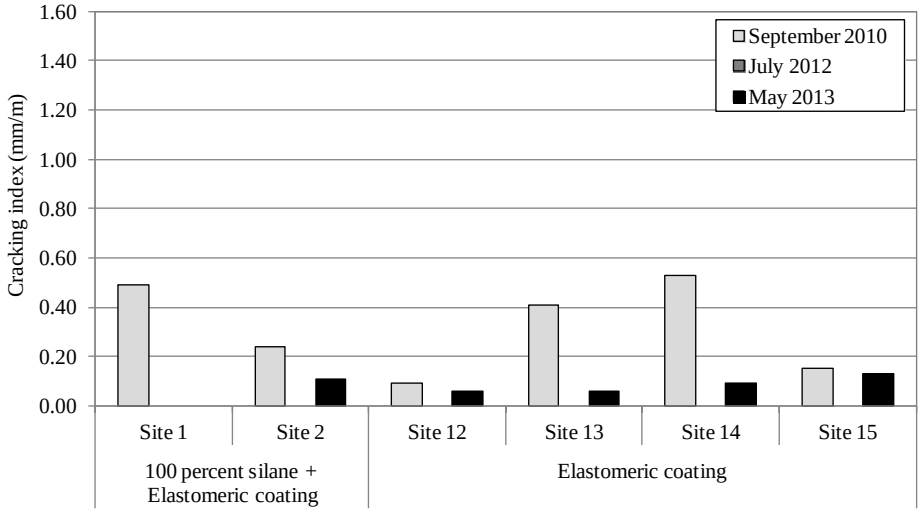

B

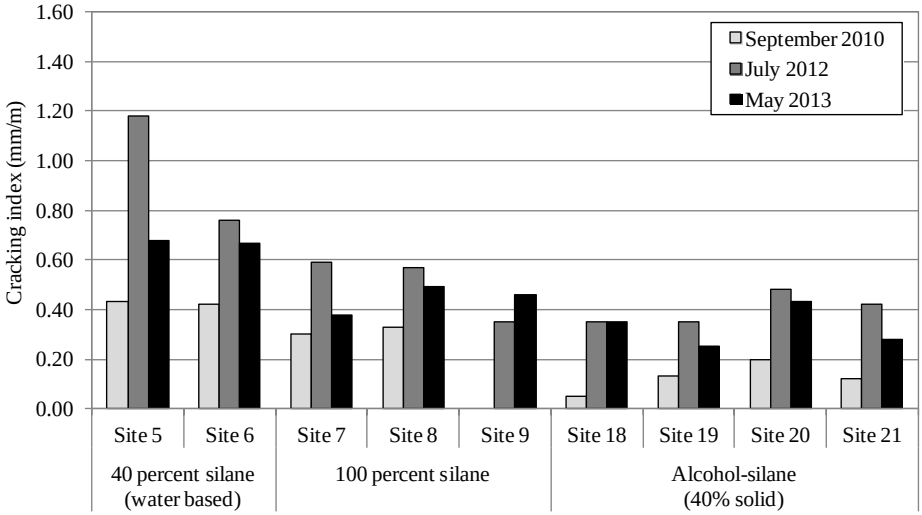

C

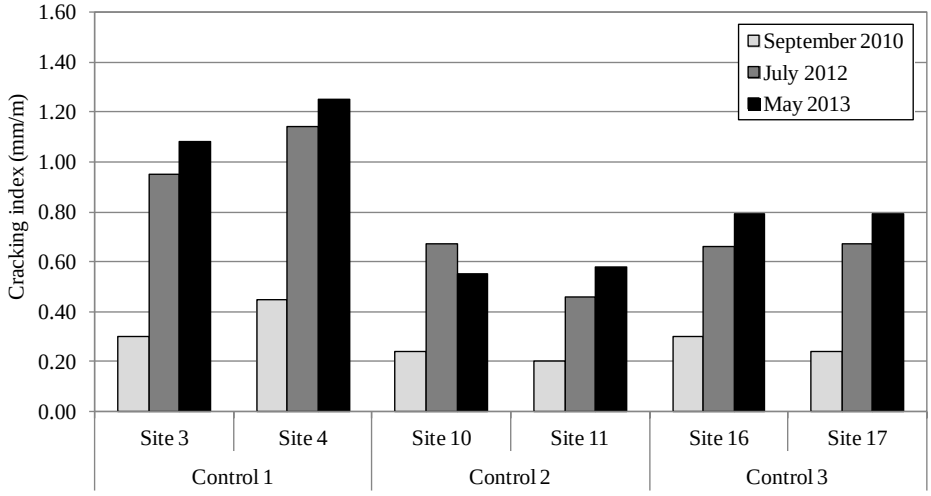

Figure 253. Evolution in the Cracking Index data for the driving lane barrier walls.

A

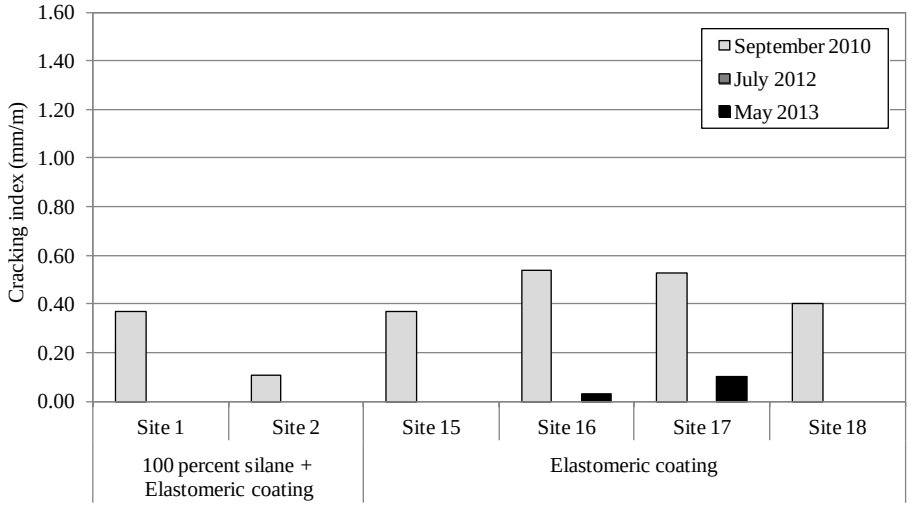

B

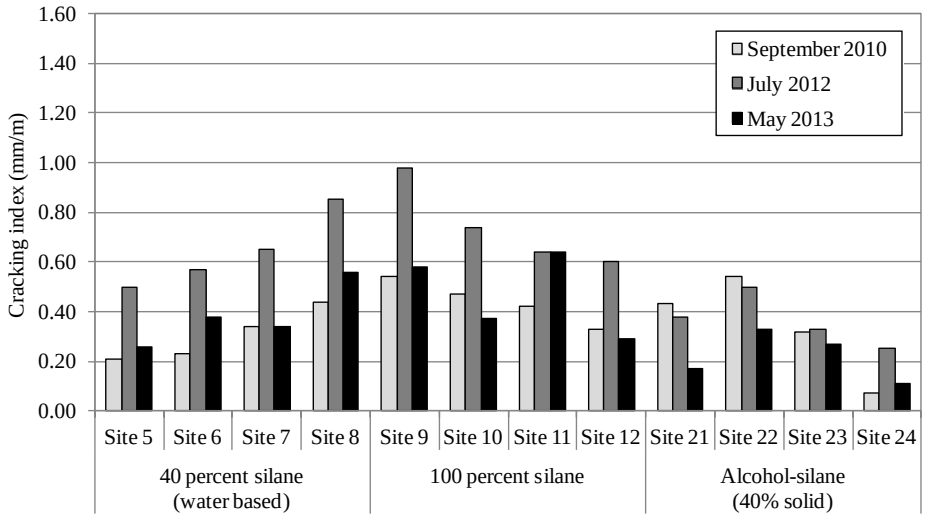

C

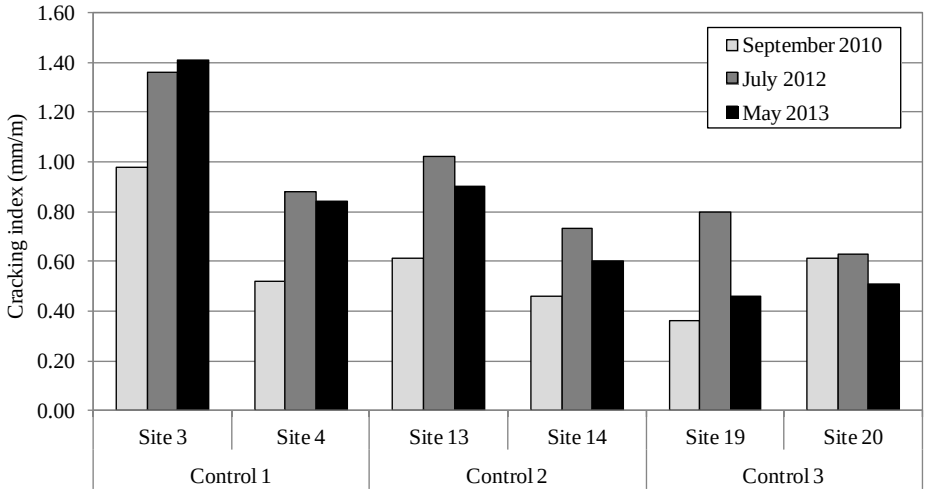

Figure 254. Evolution in the Cracking Index data for the passing lane barrier walls.

12.5 SUMMARY

The results from field survey and laboratory investigations confirmed that ASR was a contributing factor in the deterioration of the barrier walls of the two bridges carrying I-89 over the Dog River near Montpelier, VT. It was consequently concluded that they would make a suitable test section for the FHWA ASR Development and Deployment Program.

A treatment plan involving the application of different types of surface treatment products (sealers, elastomeric coating) on the barrier wall sections was implemented in 2011. In addition to the above treatments, a performance monitoring plan was also developed and implemented to allow quantifying the effects of the various treatments over time. Within selected barrier wall sections, specific areas were identified for crack mapping, expansion measurements, and temperature/humidity readings.

With only two years of monitoring data accumulated, it is currently too early to conclude on the efficacy of the above treatments at reducing the deleterious effects of ASR on the barrier walls treated. However, interesting trends seemed to established themselves, for instance possible reductions in the relative humidity values in the surficial portions of the barrier walls treated with penetrating sealers and elastomeric coating, and a general better visual appearance of the treated barrier walls compared to the control sections. Long term monitoring is expected to provide data on the effect of various types of surface treatments on the progress of ASR-related damage in the above elements.

12.6 REFERENCES

Bérubé, M.A., Chouinard, D., Pigeon, M., Frenette, J., Rivest, M. and Vézina, D. 2002a. "Effectiveness of Sealers in Counteracting Alkali-Silica Reaction in Plain and Air-Entrained Laboratory Concretes Exposed to Wetting and Drying, Freezing and Thawing, and Salt Water." *Canadian Journal of Civil Engineering*, 29(2): 289-300.

Bérubé, M.A., Chouinard, D., Pigeon, M., Frenette, J., Rivest, M. and Vézina, D. 2002b. "Effectiveness of Sealers in Counteracting Alkali-Silica Reaction in Highway Median Barriers Exposed to Wetting and Drying, Freezing and Thawing, and Deicing Salts." *Canadian Journal of Civil Engineering*, 29(2): 329-337.

FHWA-HIF-14-0003